US Army Corps of Engineers

AD-A145 974

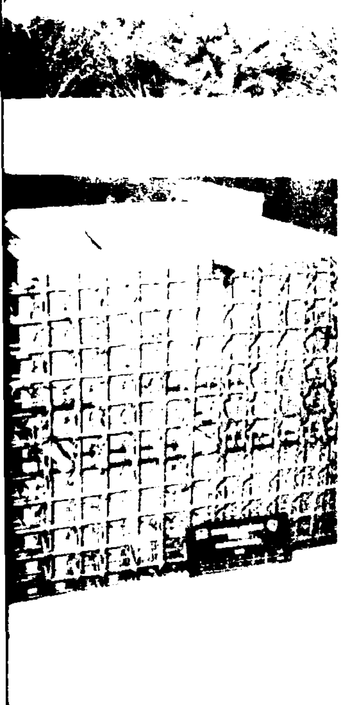

TECHNICAL REPORT SL-84-7

12

DYNAMIC SHEAR FAILURE OF SHALLOW-BURIED FLAT-ROOFED REINFORCED CONCRETE STRUCTURES SUBJECTED TO BLAST LOADING

by

T. R. Slawson

Structures Laboratory
U. S. Army Engineer Waterways Experiment Station
P. O. Box 631, Vicksburg, Miss. 39180

US ARMY ENGINEER WATERWAYS EXPERIMENT STATION

April 1984

Final Report

Approved For Public Release, Distribution Unlimited

DTIC FILE COPY

DTIC
ELECTE
SEP 2 6 1984
S D
A

Prepared for Defense Nuclear Agency
Washington, D. C. 20305

Under Subtask Y99QAXSC062, Work Unit 42

and Office, Chief of Engineers, U. S. Army
Washington, D. C. 20314

Under Project 4A762719AT40, Task AO, Work Unit 008

STRUCTURES LABORATORY

84 09 25 022

Destroy this report when no longer needed. Do not return
it to the originator.

The findings in this report are not to be construed as an official
Department of the Army position unless so designated
by other authorized documents.

The contents of this report are not to be used for
advertising, publication, or promotional purposes.
Citation of trade names does not constitute an
official endorsement or approval of the use of
such commercial products.

Unclassified

SECURITY CLASSIFICATION OF THIS PAGE (When Data Entered)

REPORT DOCUMENTATION PAGE		READ INSTRUCTIONS BEFORE COMPLETING FORM
1. REPORT NUMBER Technical Report SL-84-7	2. GOVT ACCESSION NO. AD-A145974	3. RECIPIENT'S CATALOG NUMBER
4. TITLE (and Subtitle) DYNAMIC SHEAR FAILURE OF SHALLOW-BURIED FLAT-ROOFED REINFORCED CONCRETE STRUCTURES SUBJECTED TO BLAST LOADING		5. TYPE OF REPORT & PERIOD COVERED Final report 6. PERFORMING ORG. REPORT NUMBER
7. AUTHOR(s) T. R. Slawson		8. CONTRACT OR GRANT NUMBER(s)
9. PERFORMING ORGANIZATION NAME AND ADDRESS U. S. Army Engineer Waterways Experiment Station Structures Laboratory P. O. Box 631, Vicksburg, Miss. 39180		10. PROGRAM ELEMENT, PROJECT, TASK AREA & WORK UNIT NUMBERS Subtask Y99QAXSC062, Work Unit 42 and Project 4A762719AT40, Task AO, Work Unit 008
11. CONTROLLING OFFICE NAME AND ADDRESS Defense Nuclear Agency, Washington, D. C. 20305, and Office, Chief of Engineers, U. S. Army, Washington, D. C. 20314		12. REPORT DATE April 1984 13. NUMBER OF PAGES 315
14. MONITORING AGENCY NAME & ADDRESS(if different from Controlling Office)		15. SECURITY CLASS. (of this report) Unclassified 15a. DECLASSIFICATION/DOWNGRADING SCHEDULE

16. DISTRIBUTION STATEMENT (of this Report)

Approved for public release; distribution unlimited.

17. DISTRIBUTION STATEMENT (of the abstract entered in Block 20, if different from Report)

18. SUPPLEMENTARY NOTES

Available from National Technical Information Service, 5285 Port Royal Road, Springfield, Va. 22161.

19. KEY WORDS (Continue on reverse side if necessary and identify by block number)

Airblast simulation	Nuclear explosion simulation
Box structures	Shallow-buried structures
Concrete structures	Soil-structure interaction
Dynamic shear	Underground structures
Dynamic tests	

20. ABSTRACT (Continue on reverse side if necessary and identify by block number)

Five box structures with span-to-depth (L/d) ratios of 10, 1 percent reinforcement in each face, and concrete strengths of approximately 4000 and 6000 psi, and six box structures with L/d ratios of 7, concrete strength of approximately 7000 psi and steel percentages of 1.2 and 0.75 percent, were tested dynamically at depth of burial equal to L/5. The dynamic overpressure simulated the peak overpressure, rate of pressure decay, and load duration

(Continued)

DD FORM 1 JAN 73 1473 EDITION OF 1 NOV 65 IS OBSOLETE

Unclassified

SECURITY CLASSIFICATION OF THIS PAGE (When Data Entered)

20. ABSTRACT (Continued).

associated with nuclear detonation and was generated using high-explosive primacord in a Foam HEST charge cavity configuration placed over the structure at the ground surface.

Results of these tests indicate that current dynamic shear failure criteria significantly underpredict the dynamic shear strength of these structures.

PREFACE

The research reported herein was sponsored by the Defense Nuclear Agency (DNA) under Subtask Y99QAXSC062, Work Unit 42, "Shallow-Buried Structures," and by the Office, Chief of Engineers, U. S. Army, under R&D Project 4A762719AT40, Task AO, Work Unit 008, "Target Response from Low-Yield Nuclear Surface and Subsurface Bursts." Dr. K. L. Goering, DNA, was Technical Monitor.

The construction and testing were conducted by personnel of the Structures Laboratory (SL), U. S. Army Engineer Waterways Experiment Station (WES), under the general supervision of Messrs. Bryant Mather, Chief, SL; W. J. Flathau, Assistant Chief, SL; J. T. Ballard, Chief, Structural Mechanics Division (SMD), SL; and under the direct supervision of Dr. S. A. Kiger of the Research Group, SMD. This report was prepared by Mr. T. R. Slawson of the Research Group, SMD, and is essentially the same as his thesis which was submitted to Mississippi State University in 1983 in partial fulfillment of the requirements for the Master of Science Degree.

COL Tilford C. Creel, CE, was Commander and Director of WES during this study and the preparation and publication of this report. Mr. F. R. Brown was Technical Director.

Accession For
NTIS GRA&I
DTIC TAB
Unannounced
Justification
By
Distribution/
Availability Codes
Dist | Avail and/or Special
A-1

CONTENTS

LIST OF TABLES

LIST OF ILLUSTRATIONS

CONVERSION FACTORS, METRIC (SI) TO U. S. CUSTOMARY (NON-SI) AND U. S. CUSTOMARY TO METRIC UNITS OF MEASUREMENT

Units of measurement used in this report can be converted as follows:

Multiply	By	To Obtain
	Metric (SI) to U. S. Customary (Non-SI)	
centimetres	0.3937007	inches
centimetres per second	0.3937007	inches per second
grams per metre	4.7037828	grains per foot
kilograms per cubic metre	0.06243	pounds (mass) per cubic foot
kilonewton-metres per metre	224.80892	pound (force)-inches per inch
kilonewtons per metre	5.7101483	pounds (force) per inch
kilopascals	0.1450377	pounds (force) per square inch
kilowatts	1.3404826	horsepower (electric)
megapascals	145.0377	pounds (force) per square inch
metres	3.280839	feet
metres	39.37007	inches
metres per second	3.280839	feet per second
terajoules	0.2390	kilotons (nuclear equivalent of TNT)
	U. S. Customary (Non-SI) to Metric (SI)	
feet	0.3048	metres
feet per second	0.3048	metres per second
g's (standard free fall)	9.806650	metres per second squared
grains per foot	0.212594849	grams per metre
inch-pounds	0.113	joules
inches	2.54	centimetres
inches per second	0.0254	metres per second
kips (force) per square inch	6894757.0	pascals
microinches per inch	1.0	millionths
pounds	0.4535	kilograms
pounds (force) per square inch	6.894757	kilopascals
pounds (mass) per cubic foot	16.01846	kilograms per cubic metre
tons (force) per square feet	95.76052	kilopascals

DYNAMIC SHEAR FAILURE OF SHALLOW-BURIED FLAT-ROOFED REINFORCED CONCRETE STRUCTURES SUBJECTED TO BLAST LOADING

CHAPTER 1: INTRODUCTION

Background

1. A great many shallow-buried reinforced concrete military command centers exist both in the United States and in Eastern Europe and the Soviet Union; therefore, a data base to evaluate and improve analytical models used for the design of protective structures and for vulnerability predictions fo targeting purposes is needed. The data base for the response of shallow-buried box-type structures to high explosives is limited. Studies of the response of buried box structures to the effects of localized explosions have been conducted by Mayer and Dahl (1944) for the National Research Council and Fuehrer and Keeser (1977) for the Air Force Armament Laboratory. Hossley and Albritton (1979) and Kiger and Albritton (1980) also conducted such studies for the Defense Nuclear Agency.

2. Since the Nuclear Test Ban Treaty of 1963 prohibited the atmospheric detonation of nuclear devices, the investigation of the response of shallow-buried structures to nuclear airblast effects has had to depend on airblast simulation techniques. Techniques using chemical explosives have been developed to simulate various characteristics of the airblast from nuclear detonations. These simulation techniques include: the Dynamic Airblast Simulator (DABS) geometry described by Martens and Bradshaw (1976) which simulates dynamic air (drag) forces due to nuclear airblasts, the High Explosive Simulation Technique (HEST) geometry described by Wampler, et al. (1978) which simulates the overpressure generated by a nuclear airblast, and the Direct Induced High Explosive Simulation Technique (DIHEST) described by Schlater (1974) which simulates the crater induced horizontal ground shock motions that occur near the nuclear blast.

3. Using the HEST geometry, the U. S. Army Engineer Waterways Experiment Station has conducted a series of nine dynamic tests in the Shallow-Buried Structures (SBS) Test Program for the Defense Nuclear Agency to investigate

the vulnerability of shallow-buried, flat-roofed, box-type structures in sand and clay backfills. Seven tests, referred to as Foam HEST 1-7, were conducted using 1/4-scale shallow-buried box-type structures as described by Kiger and Getchell (1980, 1982) and by Getchell and Kiger (1980, 1981a, 1981b). Two tests, referred to as Element Tests 4 and 5, were conducted using smaller earth-covered slab elements as described by Kiger and Eagles (in publication). The HEST charge cavity designs were identical for the nine tests except for the charge densities. A tabulation of the weapon simulations based on 10 msec of data with zero time at peak pressure for each test is given by Kiger (1981). These weapon simulations were determined by a best fit of the HEST overpressure using the principle of least squares to nuclear overpressure-time histories, as defined by Brode (1970). The least squares fit was determined using a computer code developed by Mlakar and Walker (1980). The SBS Test Program established a data base for the flexural failure mode of the modeled generic structures that was used to evaluate and improve current vulnerability analysis methods.

4. Experimental data from the SBS Test Program have convincingly demonstrated that the structures under consideration are much harder than had been predicted. To fail the structures, very high, short duration, impulsive loads in the 3,000- to 20,000-psi* range are required. Failures for the SBS Test Program were predominantly late time (greater than 1/2 the natural period of the structure) flexural failures rather than early time (less than 1/2 the natural period of the structure) shear failures.

5. Experimental work on reinforced concrete structural elements subjected to short-duration loading is limited. Bucci and Mlakar (1976) conducted tests on earth-covered two-way reinforced concrete roof slabs subjected to contact detonations with effective pulse durations at the slab surfaces ranging from 1/7 to 1/130 times their natural period. However, the dynamic failure mode was still the same as the static failure mode, and a Single Degree of Freedom (SDOF) model was employed to successfully predict the flexural response of the test structures.

6. Keenan (1969a) subjected laced reinforced one-way concrete slabs to uniformly distributed impulsive loads with durations of 0.6 times the natural

---

* A table of factors for converting U. S. customary (non-SI) units of measurement to metric (SI) units is presented on page 6.

period of the slab. Peak pressures of approximately 9/5 times the maximum static collapse pressure were recorded; however, static and dynamic tests again resulted in the same mode of failure. It was concluded that the static mechanism remains operative for peak dynamic pressures up to approximately three times the maximum static pressure that the slab will carry. However, Keenan (1969a) was unable to generate the highly impulsive loads necessary to produce dynamic shear failures in these tests.

7. Keenan (1969b) conducted a theoretical and experimental study of the resistance and behavior of two-way reinforced concrete slabs subjected to static and dynamic uniformly distributed loadings with fixed end restraints. Six slabs were tested statically, and three were tested dynamically with load durations greater than the natural periods of the slabs. The static failure mechanism was found to be operative in the dynamic tests with some shear failures recorded at the supports. The thinner slabs deflected more than 2-1/2 times their thicknesses in the dynamic tests. The theoretical study was based on a square slab, restrained against rotation and longitudinal edge movement. Resistance functions were developed, and methods for calculating the dynamic response were presented. An increase of 40 percent in flexural resistance for slabs tested dynamically as compared with slabs tested statically was noted. This increase was explained by the increase in the material properties of the steel and concrete due to strain rate effects in the dynamic tests. Failure criteria based on limiting deflections were recommended.

8. Peekna (in preparation) concluded from his study of impulsively loaded beams and slabs that the static collapse mechanism (well-defined plastic hinges along the diagonals that divide the beam or slab into nearly flat quadrants) remained operative for impulsive loads with peak pressures up to about three times the maximum static capacity of the beam. The change in the collapse mechanism results in a significant increase in the load capacity of the simply supported beam. Based on the results of this investigation, current flexural failure criteria based on midpoint deflection are not adequate due to the effects of the change in the collapse mechanism. Peekna proposes that the flexural failure criteria for simply supported beams be based on the slope of the deformed shape near the center line of the beam. These criteria proved successful in comparing static and short-duration dynamic loadings in cases where the dynamic collapse mechanism differed from the static failure mechanism.

9. Jones (1981) concurs with Peekna that transverse shear effects for dynamically loaded structures lead to a dramatic reduction in the slopes of the deformed profiles. His review of analytical methods includes small (with respect to structure thickness) transverse shear effects.

10. Keenan (1965) conducted tests on reinforced concrete beams to develop criteria for determining the minimum amount of vertical web reinforcement required to ensure full flexural resistance development without premature shear failure. The tests consisted of nine simply supported beams with static (3) and dynamic (6) application of uniformly distributed loads. Test variables included stirrup spacing, peak load, load duration, and rate of loading Dynamic load durations ranged from 21.2 down to 1.4 times the natural period of the beam. The static failure mode was found to be operative for the dynamic loadings tested. Equations were developed that incorporated the increase in material strengths due to dynamic application of the load to predict dynamic shear resistance corresponding to first yielding of the stirrups and to diagonal tension cracking.

11. Ross, et al. (1974) investigated beam response to impulsive loads of fuel-air explosions. Beam response analysis was based on the classical static plastic hinge mechanism and a traveling plastic hinge mechanism. The static mechanism was found to be operative for peak dynamic overpressures of up to three times the static collapse pressure. At peak blast pressures greater than three times the static collapse pressure the traveling plastic hinge mechanism becomes operative.

12. Menkes and Opat (1973) subjected clamped aluminum beams to short duration, impulsive loads. Three distinct damage modes were identified: (a) large inelastic deformation, (b) tearing (tensile failure) in outer fibers at or over the support, and (c) transverse shear failure at the support with no significant deformation in the severed central section of the beam. It was concluded that for a Mode 1 response the deflection at the midpoint of the span was related to, and generally proportional to, the length of the beam. The threshold impulse intensities for Mode 2 and Mode 3 damage were not dependent upon beam span but were linearly related to beam thickness. Thresholds for Modes 2 and 3 were experimentally correlated as occurring at about 1.36 and 2.0 times the uniform radial impulse intensity required to cause a plastic strain of 5 percent.

13. Jones (1976) employed rigid-plastic methods to predict the large

inelastic deformations of impulsively loaded, fully clamped beams and to predict the threshold velocities for a Mode 2 and a Mode 3 response. The tests performed by Menkes and Opat (1973) gave an adequate correlation to the approximate theoretical methods used by Jones. The equations developed by Jones supported Menkes and Opat's findings that Mode 2 and Mode 3 behavior is independent of beam span.

14. Jones and Gomes de Oliveira (1979) used a rigid-plastic theoretical procedure that includes the effects of transverse shear and rotatory inertia to predict the dynamic plastic behavior of simply supported beams subjected to an impact loading and a uniform impulsive loading. The retention of the effects of transverse shear in the mathematical model resulted in predictions of much smaller slopes in the deflected shape near the beam center than were predicted excluding the effects of transverse shear.

15. Nonaka (1977) employed a rigid-perfectly plastic beam model to predict the permanent deformation and behavior of a simply supported beam subjected to a uniformly distributed blast loading. The analysis ignores elastic deformation, strain rate sensitivity, strain-hardening, and delay time effects of yield. Equations of motion for shear-bending interaction are derived based on an assumed yield polygon.

16. Martin and Ponter (1972) presented equations based on deformation theory of plasticity using minimum work paths to predict plastic deformations of clamped beams subjected to uniformly distributed impulsive loads. The procedure was compared to data from experimental tests on aluminum and steel beams performed by Humphreys (1966). The equations were found to predict an upper bound to the test data.

17. Haltiwanger (1979) submitted equations that approximate the load-deflection behavior of two-way slabs using a multilinear resistance function. The resistance function consists of: (a) a linear rise from zero to maximum resistance, (b) a short horizontal segment for which resistance is constant at its maximum value, (c) a linear decay segment, and (d) a straight line that represents the development of increased strength as the slab responds in tensile membrane action under large deflections. The proposed equations were compared with test data which were recovered by Brotchie, et al. (1965) in tests on simply supported, square, reinforced concrete slabs subjected to a uniformly distributed static load. It was concluded that the proposed scheme reasonably approximated the actual load-deflection behavior of a two-way slab

except for the tensile membrane region for slabs with a span-to-depth ratio of 20. The calculated slope for this region checked exactly with experimental results, but the experimental values were displaced vertically from the theoretical function by a distance that was not explained in the text.

18. Sewell and Kinney (1968) investigated the feasibility of using a new criterion for blast damage based on a blast wave impulse delivered within a critical time. The critical time of 1/4 the natural period of the simple system is based on a study of the amplitude and velocity of the swing of a simple system capable of harmonic motion subjected to a given impulse with various durations. Amplitudes and velocities begin to significantly decrease with durations greater than 1/4 the natural period of the system. Also, a simple harmonic oscillator travels from zero to maximum displacement in 1/4 of its natural period. The critical impulse is given as a function of material density, material thickness, and critical velocity or as a function of material thickness, velocity of sound in the material, and dynamic yield strength of the material. Applicability of this damage criterion has been demonstrated for aircraft skin failure, aircraft wing failure, and structural panel failure.

19. Kingery, et al. (1981) performed tests on simply supported wide aluminum alloy beams using uniformly distributed airblast loadings. The dynamic shear forces near the supports were measured. After experiencing difficulty in simulating simply supported end restraints, the authors decided that fixed end conditions gave a closer approximation to actual test conditions than simple supports. REPSIL (a finite difference elastoplastic structural response program) calculations were performed to compare with test results. However, comparison of experimental results to REPSIL predictions were very inconclusive due to the uncertainties in the test beam support conditions and unknown dynamic material properties.

20. Keenan (1977) developed a procedure for calculating the maximum dynamic shear for one-way reinforced concrete slabs subjected to blast loads. The technique includes calculating a Dynamic Increase Factor (DIF), which depends on the slab properties and the characteristics of the blast load. A nondimensionalized design chart was generated to find the DIF given the load duration to fundamental period and the peak overpressure to ultimate slab resistance ratios. Once the DIF has been obtained, the dynamic shear can be calculated as the product of the shear due to a static application of the loading and the DIF. It was concluded that the proposed method of calculating

dynamic shear gives a more realistic shear value to be used in design than the unconservative method of calculating shear based on the static application of ultimate flexural resistance of the slab.

21. Murtha and Crawford (1981) examined existing static shear failure criteria and proposed modifications to account for the increase in material strengths due to strain rate effects so that the criteria are applicable to dynamic loading conditions. Based on test data, a 50 percent dynamic increase factor was proposed. The finite element program ADINA, as described by Bathe (1977), was used to construct a DIF chart that was more accurate for highly impulsive loads than the one developed by Keenan (1977). Calculations were performed using Foam HEST 1 and 2 test configurations from the SBS test program to evaluate current shear failure criteria and analysis procedures. No failure was predicted for Foam HEST 1, which agrees with experimental results. A diagonal tension failure but no direct shear failure was predicted for Foam HEST 2. Failure in Foam HEST 2 was very early (less than 1/4 the natural period of the roof slab), and the failure planes were essentially vertical. The failure plane indicated either a direct shear failure or a tensile membrane failure. Posttest examination of the roof slab indicated no hinge formation at midspan. This fact and the time of failure exclude membrane failure; therefore, it is concluded that the Foam HEST 2 structure probably failed in direct shear.

22. Karagozian and Case (1973) conducted tests to determine the shear strength and slip characteristics of reinforced concrete construction joints subjected to blast loadings. Test elements were 3 ft long by 10 in. square with a shear plane construction joint to resist an axial load. The construction joints tested were sandblasted, washed, or cast monolithically. Test variables included joint type, concrete strength, percentages of dowel steel, and normal pressures. As expected, the monolithic and sandblast joints were significantly stronger than the washed joint. The sandblast joint approached the strength of the monolithic joint with about a 20 percent degradation in strength. Strength and load-slip characteristics of reinforced concrete construction joints were determined as a result of these tests. Static failure criteria were proposed that could be modified, by increasing the material properties of the dowel steel and the concrete, for dynamic applications. A 20 to 30 percent increase in material properties was proposed to account for the increase in material strength due to dynamic application of the load.

Objectives

23. The objective of the dynamic shear tests was to investigate the possibility of a relatively high-frequency dynamic shear failure in shallow-buried structures with length to effective depth (L/d) ratios of 7 and 10. Specifically, the objectives were as follows: (a) to investigate the dependence of dynamic shear failure on concrete strength, structural stiffness, and steel reinforcement ratio; (b) to evaluate available dynamic shear failure criteria; (c) to establish a data base for evaluating dynamic shear stress computational methods; (d) to document, with high-speed photography, the dynamic shear failure mode; and (e) to obtain a measure of the ductility associated with dynamic shear failures.

24. The primary objective of this report is to evaluate current dynamic shear failure criteria using data from the dynamic shear tests.

Scope

25. Eleven approximately 1:4-scale reinforced concrete box elements were tested dynamically in a sand backfill at a depth of burial (DOB) of L/5. The elements were designed to model a section from a single rectangular bay of a shallow-buried, multiple-bay structure with span-to-effective-depth (L/d) ratios of 7 and 10 and with principal steel ratios of 0.0075, 0.01, and 0.012 in each face. Grade 60 reinforcing bars were used.

26. The parameters varied in the tests were concrete strength, structural stiffness, steel ratio, and charge density. Three models with an L/d of 10, 4000-psi concrete and 1 percent steel (each face), were tested using charge densities of 1.37 pcf, 1.83 pcf, and 0.91 pcf for elements DS1, DS2, and DS3, respectively. Two models with an L/d of 10, 6000-psi concrete and 1 percent steel (each face), were tested using charge densities of 1.37 pcf and 1.83 pcf for elements DS4 and DS5, respectively. Three models with an L/d of 7, 7000-psi concrete and 0.75 percent steel (each face), were tested using charge densities 2.29 pcf, 1.83 pcf, and 1.14 pcf for elements DS2-1, DS2-2, and DS2-3, respectively. Three models with an L/d of 7, 7000-psi concrete and 1.2 percent steel (each face), were tested using charge densities of 2.29 pcf, 1.60 pcf, and 1.14 pcf for elements DS2-4, DS2-5, and DS2-6, respectively. The test on element DS3 was to ensure that the element test configuration (using a

box element placed on a reaction structure) simulated the test conditions of previous shallow-buried tests (in particular, Foam HEST 4 of the SBS Test Program) which were performed on complete rectangular, single, and multiple bay scale models.

27. The elements were tested using a HEST that simulated the peak overpressure, rate of pressure decay, and overpressure duration associated with a nuclear detonation. This procedure involved distributing a high explosive over a relatively large surface area and using a soil overburden to momentarily confine the blast. The HEST test used in this test program was more specifically a Foam HEST test because a low density Styrofoam is used to displace the required charge cavity volume. A more detailed description of the HEST test development and use was given by Wampler, et al. (1978). The charge cavity used in the HEST tests is described in Chapter 2.

CHAPTER 2: TEST DESCRIPTION

Test Date, Location, and General Description

28. Eleven approximately 1:4-scale reinforced concrete box elements were tested dynamically from 15 July to 6 August 1981 and from 10 May to 15 June 1982 at Range 37, Fort Polk, La.

29. Test element construction, test configuration, charge cavity description, instrumentation, test procedure, and material properties are described in the following sections.

Test Element Construction Details

30. The five box elements tested in the FY 81 dynamic shear tests were constructed as detailed in Figure 2-1 in May and June 1981. The elements had inside dimensions of 4 ft high by 4 ft wide by 4 ft long with overall roof, floor, and wall thicknesses of 5.6 in. The effective depth (d) was 4.8 in., and the span-to-effective depth (L/d) ratio was 10 for each element. Principal steel reinforcement was 1 percent in each face.

31. The six box elements tested in the FY 82 dynamic shear tests were constructed as detailed in Figures 2-2 and 2-3 in March and April 1982. The elements had inside dimensions of 3.73 ft high by 3.73 ft wide by 4 ft long with overall roof, floor, and wall thicknesses of 7.25 in. The effective depth (d) was 6.44 in., and the span-to-effective depth (L/d) ratio was 7 for each element. Principal steel reinforcement was 0.75 percent in each face for three test elements (DS2-1,2,3) and 1.2 percent in each face for three test elements (DS2-4,5,6).

32. All elements were cast monolithically at the Structures Laboratory of the Waterways Experiment Station.

33. Construction photographs (Figures 2-4 and 2-5) were made to document the steel reinforcement placement before pouring the concrete.

Reaction Structure Construction Details

34. The reinforced concrete reaction structure for the dynamic shear tests was constructed as detailed in Figure 2-6 in April and May 1981 at the

test site at Range 37, Fort Polk, La. The reaction structure consisted of an approximately 16-ft- by 11-ft- by 4-ft-thick base slab with an approximately 5-ft cubic monolith projecting upward from one end of the base slab as shown in Figure 2-6. A vertical 2-in.-thick steel plate was embedded in the reaction structure to close one end of the test element. A horizontal 2-in.-thick steel plate was embedded on the base slab to form a base to which the 4-ft by 4-ft (inside) by 7-ft-long steel tunnel was welded. The 7-ft-long tunnel was constructed of 6-in.-thick steel plate. The tunnel allowed the conventional high speed movie camera to be removed from the catastrophic test environment. Reaction structure construction is shown in Figure 2-7.

Test Configuration

35. The test configuration for the five element tests is shown in Figures 2-8 and 2-9. The test element was placed on a 1-ft-deep sand pit that was cast into the reaction structure. One end of the test element was blocked off by the vertical 2-in.-thick steel plate embedded in the concrete reaction structure. The other end of the test element opened into a 7-ft-long steel tunnel. Sand backfill was placed in 6-in. lifts from the top of the base slab of the reaction structure until the DOB of L/5 (9.6 in. for FY 81 tests and 9.0 in. for FY 82 tests) was reached. Each 6-in. lift was compacted with gasoline-powered earth tampers. Sand backfill extended for a minimum of 3 ft to either side of the test element.

36. The charge cavity for each test was constructed on the ground surface as shown in Figure 2-10. The 12-ft by 12-ft charge cavity consisted of three layers of Styrofoam as follows: (a) the 1-1/2-in.- by 1-1/2-in.- by 12-ft-long strips spaced 3 in. on center bottom layer; (b) the 12-ft- by 12-ft- by 1-1/2-in.-thick solid middle layer; and (c) 2-1/2-in.- by 1-1/2-in.- by 12-ft-long strips spaced 4 in. on center top layer. The high explosive primacord was placed in the gaps between the Styrofoam strips of the top layer. A 1/2-in.-thick plywood top covered the charge cavity, and a 32-in.-deep uncompacted sand overburden was placed over the charge cavity and extended a distance of 3 ft beyond the edges of the charge cavity to contain the blast and simulate the overpressure duration of a low-yield nuclear weapon. This charge cavity design ensured that the explosive was uniformly distributed, that the charge cavity overlapped the test element far enough to minimize edge effects,

and that the structure loading was due to the propagation of a planar wave.

37. The explosive used was pentaerthritoltetranitrate (PETN) which was made into 200- and 400-grain/ft detonating cord (primacord). The charge cavities for the five tests were identical except for charge density which changed the peak pressure for the test. The charge densities were varied by changing the number of strands of detonating cord in each gap in the top layer of the charge cavity. In tests DS1 and DS4 there were three strands of 400-grain/ft detonating cord in each of the 36 gaps in the top layer of the charge cavity which gave a charge density of 1.37 pcf. In tests DS2, DS5, and DS2-2 there were four strands of 400-grain/ft detonating cord per gap which gave a charge density of 1.83 pcf. Test DS3 used two strands of 400-grain/ft detonating cord per gap which yielded a charge density of 0.91 pcf. Tests DS2-1 and DS2-4 used five strands of 400-grain/ft detonating cord per gap which yielded a charge density of 2.29 pcf. Tests DS2-3 and DS2-6 used two strands of 400 grain/ft and one strand of 200-grain/ft detonating cord per gap which yielded a charge density of 1.14 pcf. Test DS2-5 used three strands of 400 grain/ft and one strand of 200-grain/ft detonating cord which yielded a charge density of 1.60 pcf. An 8-ft length of 100-grain/ft detonating cord was spliced to the end of each bundle of 200- and/or 400-grain/ft detonating cord. The pieces of 100-grain/ft detonating cord were then spliced together in one bundle which enclosed the blasting cap that initiated the detonation of the charge. This provided a simultaneous detonation of the rows of detonating cord beginning at one end of the charge cavity.

Instrumentation

38. The data for each test were recorded on a 32-channel Sangamo Sabre III FM magnetic tape recorder, which was located in the instrumentation trailer about 800 ft from the test site. Data, summarized in Table 2-1, were recorded at the tape speeds of 120 in./sec and later digitized at 200 kHz. A zero-time channel to establish a common time reference for the data records was included in each test.

39. Gages for the dynamic shear tests included airblast pressure, interface pressure, active strain, passive strain, soil stress, and acceleration. Acceleration gages were used only in tests DS3, DS4, and DS5. Soil stress measurements were made only in the FY 82 tests (DS2-1 through DS2-6). Gages

were located as shown in Figures 2-11 and 2-12. Gage ranges were as listed in Table 2-1.

Table 2-1. Instrumentation Summary, Dynamic Shear Tests

Gage	Location	Range	Manufacturer	Model
Airblast pressure	BP-1 BP-2 BP-3 BP-4	10,000 psi	Kulite	HKS-375
Interface pressure	IF-1 IF-2 IF-3 IF-4 IF-5	5,000 psi		VM-750
Strain	EO-1 EI-1 EO-2 EI-2 EO-3 EI-3 EO-4 EI-4 EO-6 EI-6	10,000 μin./in.	Micro-Measurements	EA-06-250BF-350-W
Acceleration	A-1	50,000 g's	Endevco	2264A
Soil stress	S-1	20,000 psi	Kulite	LQV-080-8U

40. Kulite Model HKS-375 airblast pressure (BP) gages were used to measure the overpressure-time history. They were located at ground level directly beneath the Foam HEST charge cavity. The airblast gage configuration (Figure 2-13) used a baffle, designed by the Air Force Weapons Laboratory (AFWL), to prevent destruction of the gage by high frequency and high pressure spikes.

41. Five interface pressure (IF) gages (Kulite Model VM-750) were used to measure the soil-structure interface pressure-time histories.

42. Twelve single-axis, metal-film, 0.25 in. long, 350 ohm, temperature-compensated strain gages were installed on the inside (EI) and on the outside (EO) principal steel reinforcement bars located at mid-length of

the roof slab of each test element. The gages used were Micro-Measurements Model EA-06-250BF-350-W.

43. Permanent strain was measured along the length of two outside and two inside principal steel reinforcement bars located near mid-length of the roof slab of each test element. Four rebars, located on either side of the strain gaged rebars, were scored with a 2-in.-gage length knife edge punch. The distance between punch marks was measured after the tests, and the data were reduced to percent permanent strain.

44. Accelerations were measured at midspan of the roof slab on tests DS3, DS4, and DS5 with Endevco Model 2264A gages.

45. Soil stress measurements were made on either side of the test element as shown in Figure 2-13 at the top of the roof slab elevation on the FY 82 tests (DS2-1 through DS2-6) using Kulite SE Model VQV-080-V gages.

Photographic Data

46. High-speed photography for the FY 81 dynamic shear tests (Tests DS1 through DS5) consisted of conventional high-speed photography (Figure 2-14) looking down the steel tunnel at the bottom of the test element roof slab and high-speed photography using a fiber optics device (Figure 2-15) looking up at the bottom of the test element roof slab from a vantage point 1 ft inside the steel tunnel from the test element. Fiber optics allowed an up-close view of the failure with little risk of damage to the remote mounted delicate high-speed camera. As a roof slab displacement measurement reference, 1/2-in.-wide lines were painted on the 2-in.-thick vertical steel plate that closed one end of the test element. These lines were spaced 2-1/2 in. on center with the top edge of the first line located 1 in. below the bottom edge of the roof slab. Lighting for the high-speed photography was supplied by four banks of nine floodflash lamps located on the floor slab of the test element. For the FY 82 tests the fiber optics setup was deleted.

47. The 12-ft fiber optics cable (part No. IS-810-144) was manufactured by Galileo Electro-Optics Co., located in Sturbridge, Mass. It had a 16mm motion picture format with 60-μ fiber sizes. The fiber optics cable used was a flexible imagescope comprised of thousands of cladded optical fibers perfectly aligned to transmit a high resolution image. The imagescope reduced the image into thousands of minute parts, transmitted each part separately within the

individual fibers, and then reassembled them for recovery by the high-speed movie camera. The use of the fiber optics cable allowed the removal of the delicate high-speed movie camera from the catastrophic test environment and accomplished the goal of filming the roof slab failure from a very close vantage point not attainable with conventional photography. The camera used in conjunction with the fiber optic cable was a Hycam Model 42 16mm high-speed rotating prism camera manufactured by Redlake Co., located in Campbell, Calif. The frame rate used was approximately 9000 frames per second.

48. The camera used as shown in Figure 2-14 for the conventional high-speed photography setup was a Nova Model 16-3, 16-mm high-speed rotating prism camera for tests DS1, DS2, and DS3, while a Fastax Model 48, 16mm high-speed rotating prism camera was used for tests DS4 and DS5. The Nova was manufactured by Photo-Kinetics, Inc., located in Bronx, N. Y., and the Fastax was manufactured by the Redlake Co., located in Campbell, Calif. The frame rates attained by these cameras during the tests ranged from 7000 to 9000 frames per second.

49. For tests DS2-1 through DS2-6 a Fastax Model 48 and a Photec high-speed rotating prism camera manufactured by Photonics Systems, Inc., located in Santa Clara, Calif, were used. Frames rates ranged from 6000 to 10000 frames per second. Both cameras were located as shown in Figure 2-14 with the Photec located at the center line of the tunnel and the Fastax located 1 ft to the right of the center line from a line of sight looking towards the test element from the camera location. All cameras used a 115-volt AC power source and 400 ft of 7241 Extachrome Daylight Film manufactured by Kodak.

Sequence of Events

50. The timing for turning on the high-speed cameras and firing the flood-flash lamps was critical for this series of tests. The high-speed movie cameras required about 1-3/4 sec to attain maximum frame rate. With 400 ft of film, the cameras average about 2-1/2 sec of run time. The flood flash lamps had a duration of 1-3/4 sec and a 50-msec lag time to attain maximum luminosity. Therefore, the cameras were started 1.8 sec before the blast was initiated, and the floodflash lamps were started 0.7 sec before the blast was initiated to insure that the cameras were up to speed and that there was ample lighting during the event.

Material Properties

51. Determining the effects of concrete strength on dynamic shear failure was one objective of the FY 81 dynamic shear tests. To study these effects the concrete mix for the first three test elements (DS1, DS2, and DS3) was designed to have a 28-day compressive strength of 4000 psi, and the concrete mix for the last two test elements (DS4 and DS5) was designed to have a 28-day compressive strength of 6000 psi. DS1, DS2, and DS3 were cast from one batch of concrete, and DS4 and DS5 were cast from a second batch of concrete. The concrete was composed of a Type I Portland Cement and was obtained from a local commercial supplier. The fine aggregate was a natural siliceous sand, and the coarse aggregate was pea gravel with a 3/8-in.-maximum diameter. Four test cylinders, cured in the same environment as the test elements, were cast for each test element. Two cylinders were tested at 28 days and two at the day of the test for each element except as noted in Table 2-2. Generally, the 28-day compressive strengths were about 300 psi lower than the design strengths, while the cylinders tested on the day of the dynamic test were within 100 psi of the design strength as shown in Table 2-2.

Table 2-2. Dynamic Shear Test Concrete Strengths

Test Element	Concrete Pour	28-Day Compressive Strength, psi	Day of Test Compressive Strength, psi	Element Age When Tested, days
DS1	1	3710	3930	62
		3710	3850	
DS2	1	3820	4030	67
		3710	3800	
DS3	1	3820	4010	70
		3630	4070	
DS4	2	5680	5850	65
		5730	*	
DS5	2	5680	6150	71
		*	5850	
DS2-1**	3	7000	6970	43
		7020	7000	

(Continued)

* One cylinder from DS4 and one cylinder from DS5 tested at 4800 psi at 7 days.

** DS2-1 had approximately the same strength at 28 days as at the day of the test.

Table 2-2. (Concluded)

Test Element	Concrete Pour	28-Day Compressive Strength, psi	Day of Test Compressive Strength, psi	Element Age when Tested, days
DS2-2	4	7360	7800	50
		7640	7680	
DS2-3	5	7340	7450	53
		7090	7600	
DS2-4	3	6890	7300	67
		6910	7450	
DS2-5	4	7020	7800	64
		7290	7780	
DS2-6	5	7060	7070	58
		7230	7450	

52. For the FY 82 dynamic shear test, a high strength concrete was required with a minimum 28-day compressive strength of 6000 psi, because failure in the low strength (4000 psi), $L/d = 10$ elements (FY 81) included considerable concrete crushing at the support which allowed reinforcement steel pullout (i.e., premature failure). Since an objective of the FY 82 tests on $L/d = 7$ elements was to evaluate the effect of steel reinforcement ratio on dynamic shear failure, a higher strength concrete was required to resist crushing of the support and reinforcement pullout at higher test levels. The coarse and fine aggregates and cement were identical to the FY 81 tests. The six test elements were cast in three batches with DS2-1 and DS2-4 cast from the first batch, DS2-2 and DS2-5 cast from the second batch, and DS2-3 and DS2-6 cast from the third batch. Four cylinders were cast for each test element and were cured in the same environment as the test elements. Two cylinders were tested at 28 days for each element, and two cylinders were tested the day of each element test Generally, 28-day concrete compressive strengths were approximately 7000 psi with day of test strengths ranging from approximately 7000 psi to 7800 psi as shown in Table 2-2.

53. All reinforcing steel bars used in the FY 81 and FY 82 tests were ASTM A615, grade 60 (1969). Shear stirrups and longitudinal steel consisted of No. 3 bars (FY 81) and No. 2 bars (FY 82). Transverse reinforcement consisted of No. 4 bars (FY 81 and 82) or No. 5 bars (FY 82). Average tensile yield strengths were 60,500 psi for the No. 3 bars, 62,750 psi for the No. 4 bars in

FY 81, 79,500 psi for the No. 4 bars in FY 81, 66,055 psi for the No. 2 bars, and 67,340 psi for the No. 5 bars. Tensile tests were performed on a minimum of four random samples from each bar size as shown in Table 2-3.

Table 2-3. Tensile Tests for Steel Reinforcement Bars for the Dynamic Shear Tests

Bar Size	Yield Stress psi	Ultimate Stress psi
No. 3	60,725	92,000
(FY 81)	60,180	91,090
	60,000	92,365
	60,725	92,180
	60,910	92,180
No. 4	62,000	99,500
(FY 81)	63,500	105,000
	62,100	99,600
	63,300	104,850
	62,850	102,300
No. 2	71,430	94,080
(FY 82)	61,835	90,000
	65,100	91,835
	64,080	92,655
	67,345	93,675
	66,530	95,100
No. 4	79,000	117,500
(FY 82)	79,000	118,750
	80,000	119,250
	80,000	119,500
No. 5	66,935	105,645
(FY 82)	67,740	106,615
	66,935	106,935
	67,740	107,095

54. The sand backfill used was obtained from a commercial supplier in the Fort Polk, La., area. The sand backfill was a "flume sand" that was classified as a poorly graded sand (SP) by the Unified Soil Classification System (1968) and had properties similar to the sand backfills used in the Foam HEST Test series of the SBS Test Program.

55. The sand backfill was placed in 6-in. lifts and compacted with three passes of a 7-hp Dynapac Model CM-10 gasoline powered vibrator. Water content and density tests were conducted after each layer of backfill was

placed. Table 2-4 presents average moisture content, wet density, and dry density for the backfill in each test. The uncompacted sand overburden, which was identical to the sand backfill, was placed to a depth of 32 in. over the charge cavity.

Table 2-4. Average Moisture Content, Wet Density, and Dry Density for the Backfill in the Dynamic Shear Tests

Test	Average Moisture Content, %	Wet Density, pcf	Dry Density, pcf
DS1	4.6 (3.8-5.7)*	106.0 (103.3-108.6)	101.1 (98.5-103.8)
DS2	4.3 (3.4-5.9)	108.7 (105.7-111.3)	104.1 (102.2-106.3)
DS3	4.6 (3.8-6.7)	109.3 (107.9-111.5)	104.3 (102.2-106.2)
DS4	5.4 (4.7-5.9)	110.8 (108.9-114.5)	104.8 (102.2-108.1)
DS5	4.1 (3.7-4.7)	107.1 (106.2-109.4)	102.7 (101.8-104.5)
DS2-1	6.6 (5.0-8.9)	106.7 (105.6-109.7)	100.1 (98.7-101.9)
DS2-2	5.9 (4.6-7.3)	106.2 (105.2-107.3)	100.4 (98.3-102.5)
DS2-3	5.3 (4.5-6.3)	107.2 (105.3-113.4)	101.9 (100.4-106.6)
DS2-4	4.3 (3.9-4.9)	105.7 (105.2-106.3)	101.3 (100.3-102.1)
DS2-5	4.3 (3.8-5.3)	106.1 (104.5-107.5)	101.8 (99.3-102.9)
DS2-6	5.2 (4.2-5.7)	105.1 (103.4-106.9)	100.0 (98.5-101.7)

* Minimum and maximum values in parentheses.

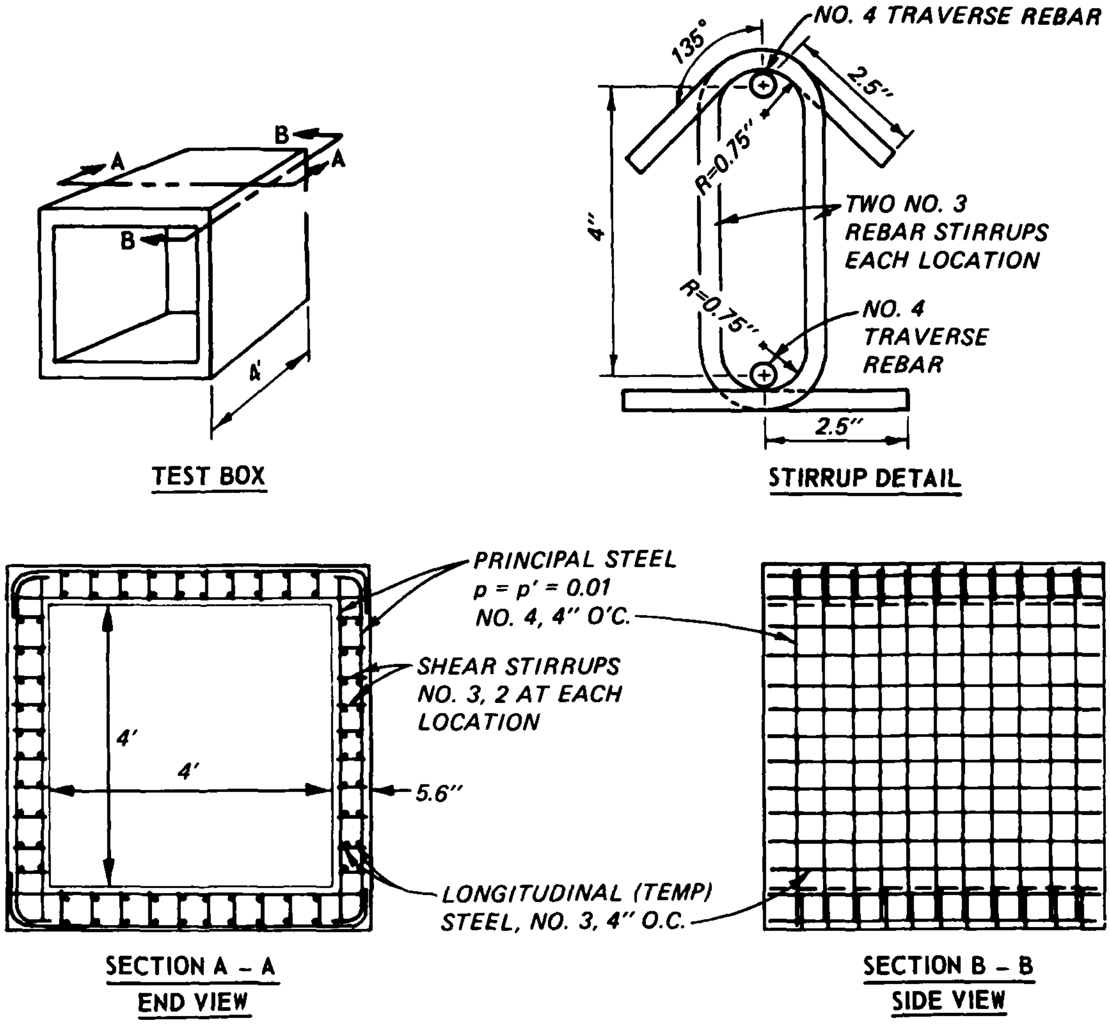

Figure 2-1. FY 81 Dynamic Shear Test Element Construction Details.

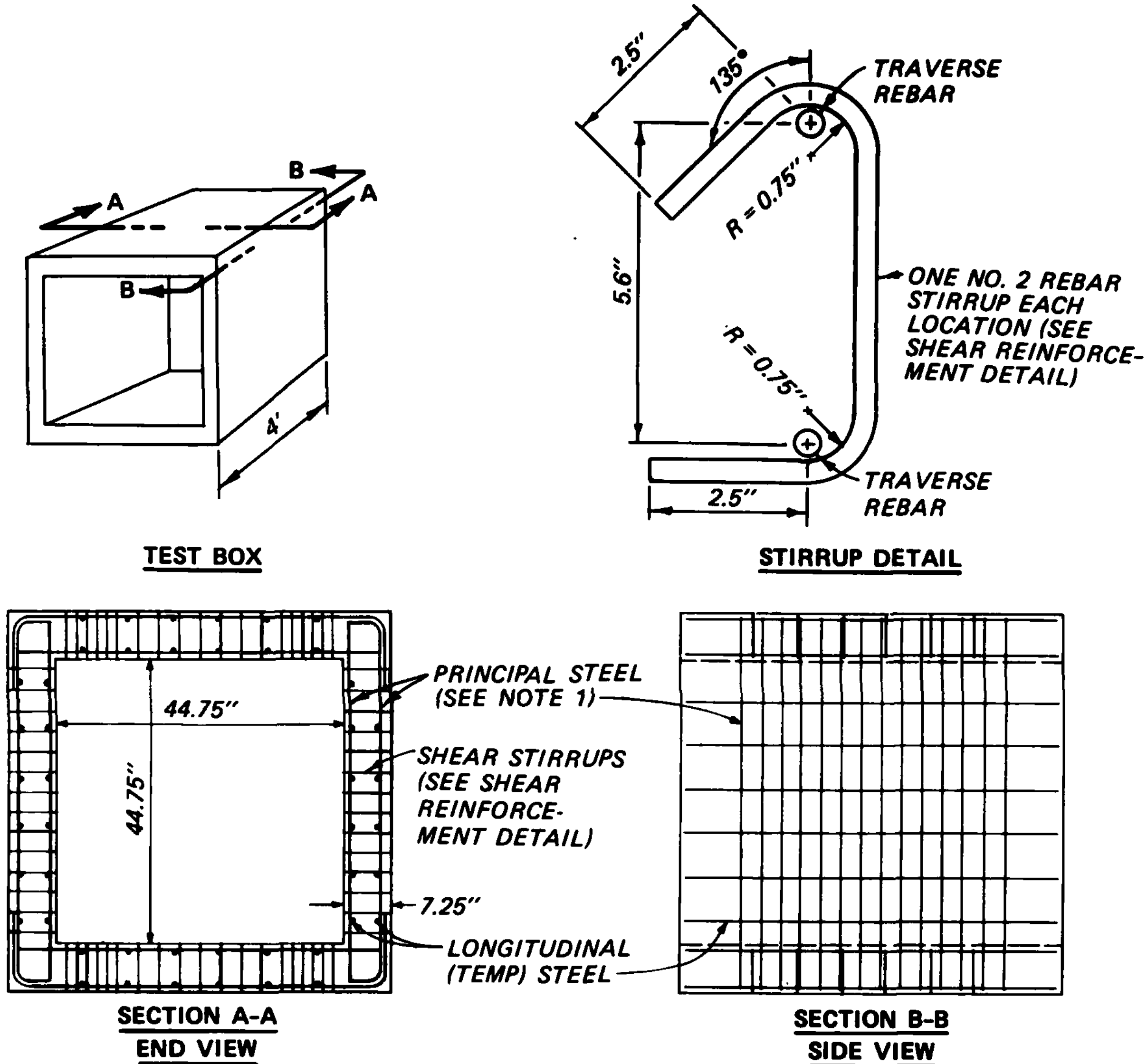

NOTES: 1 - FOR ρ = 0.012, #5 ~ 4" O.C. (INSIDE AND OUTSIDE FACE)
FOR ρ = 0.075, #4 ~ 4" O.C. (INSIDE AND OUTSIDE FACE)
2 - LONGITUDINAL STEEL ~ #2 ~ 7.5" O.C. (INSIDE AND OUTSIDE FACE)

Figure 2-2. FY 82 Dynamic Shear Test Element Construction Details.

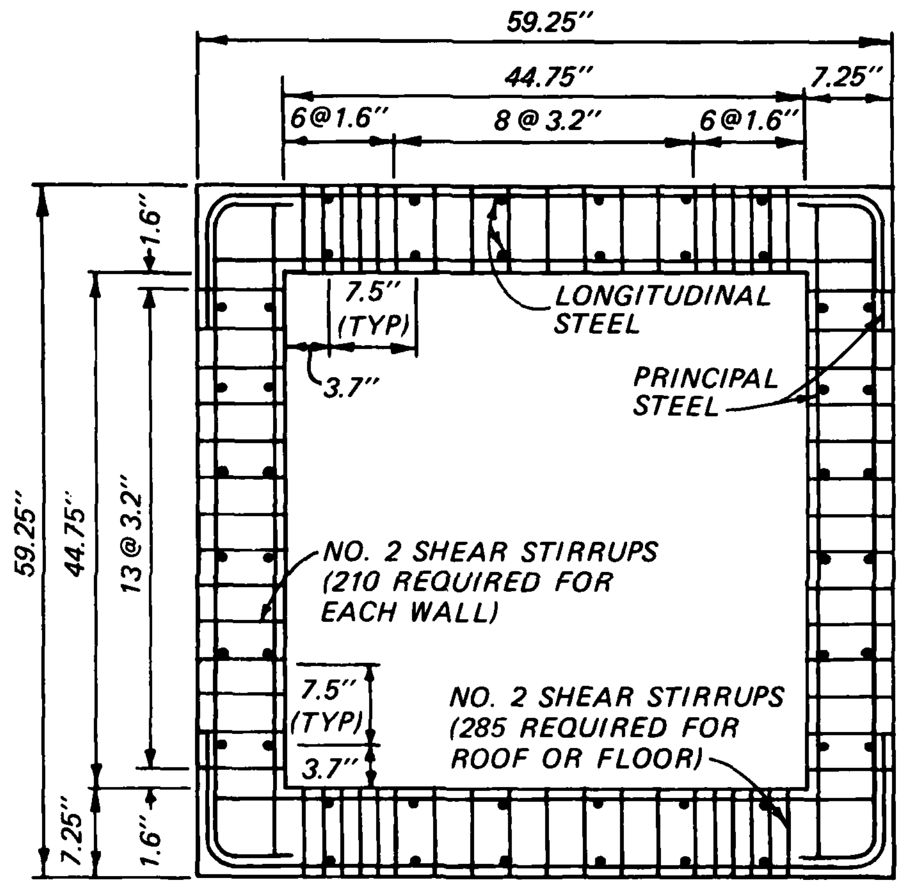

SHEAR REINFORCEMENT DETAILS

Figure 2-3. FY 82 Dynamic Shear Test Shear Reinforcement Details.

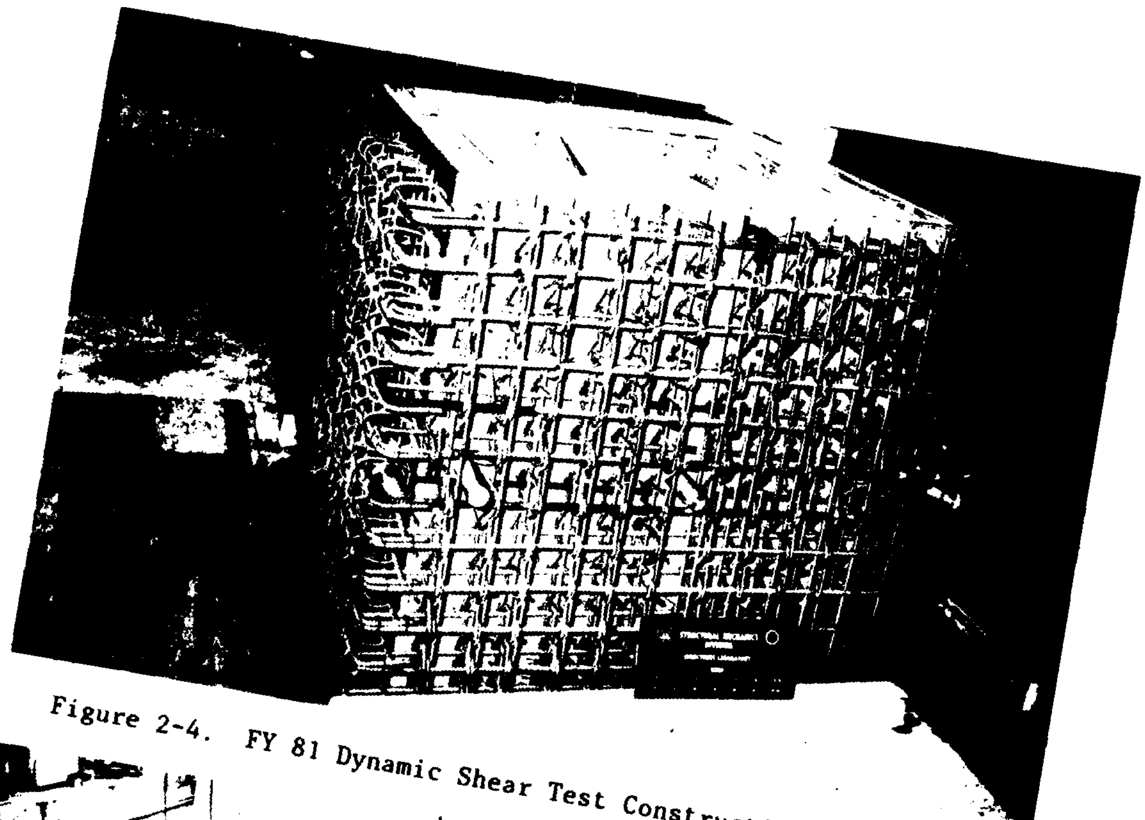

Figure 2-4. FY 81 Dynamic Shear Test Construction Photograph.

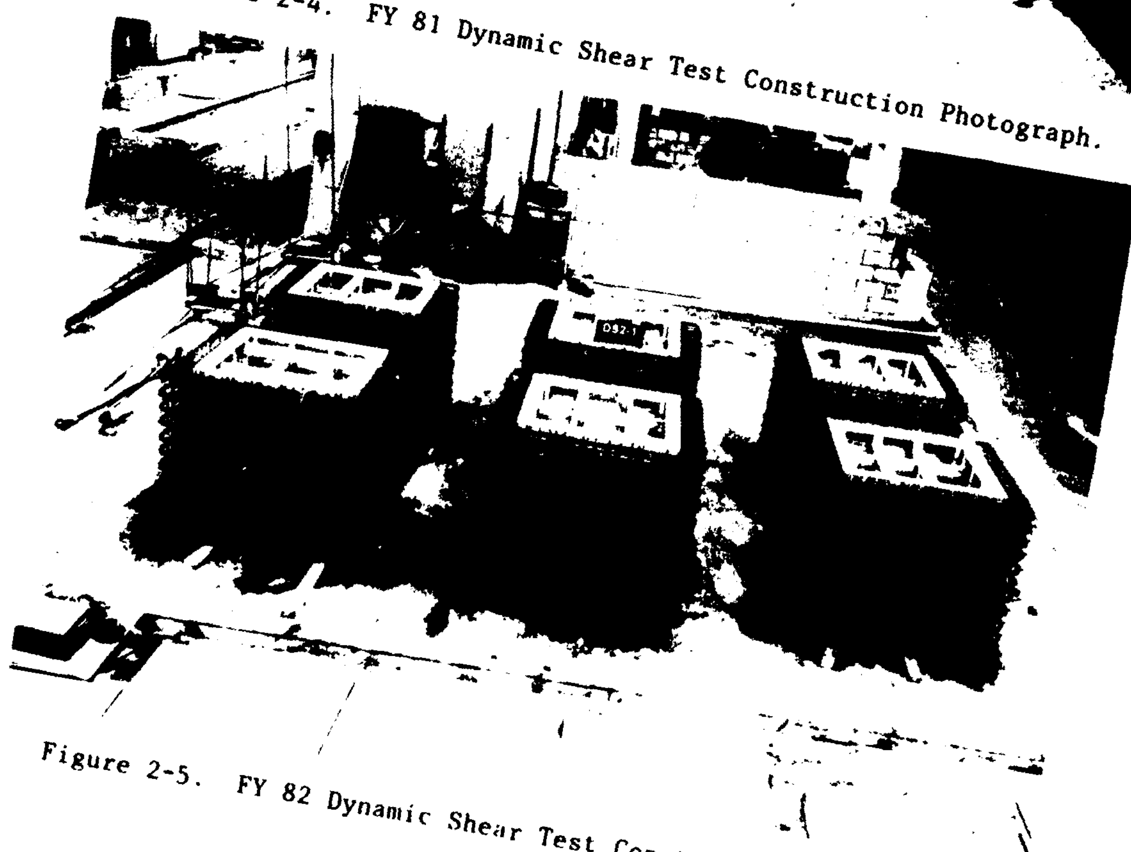

Figure 2-5. FY 82 Dynamic Shear Test Construction Photograph.

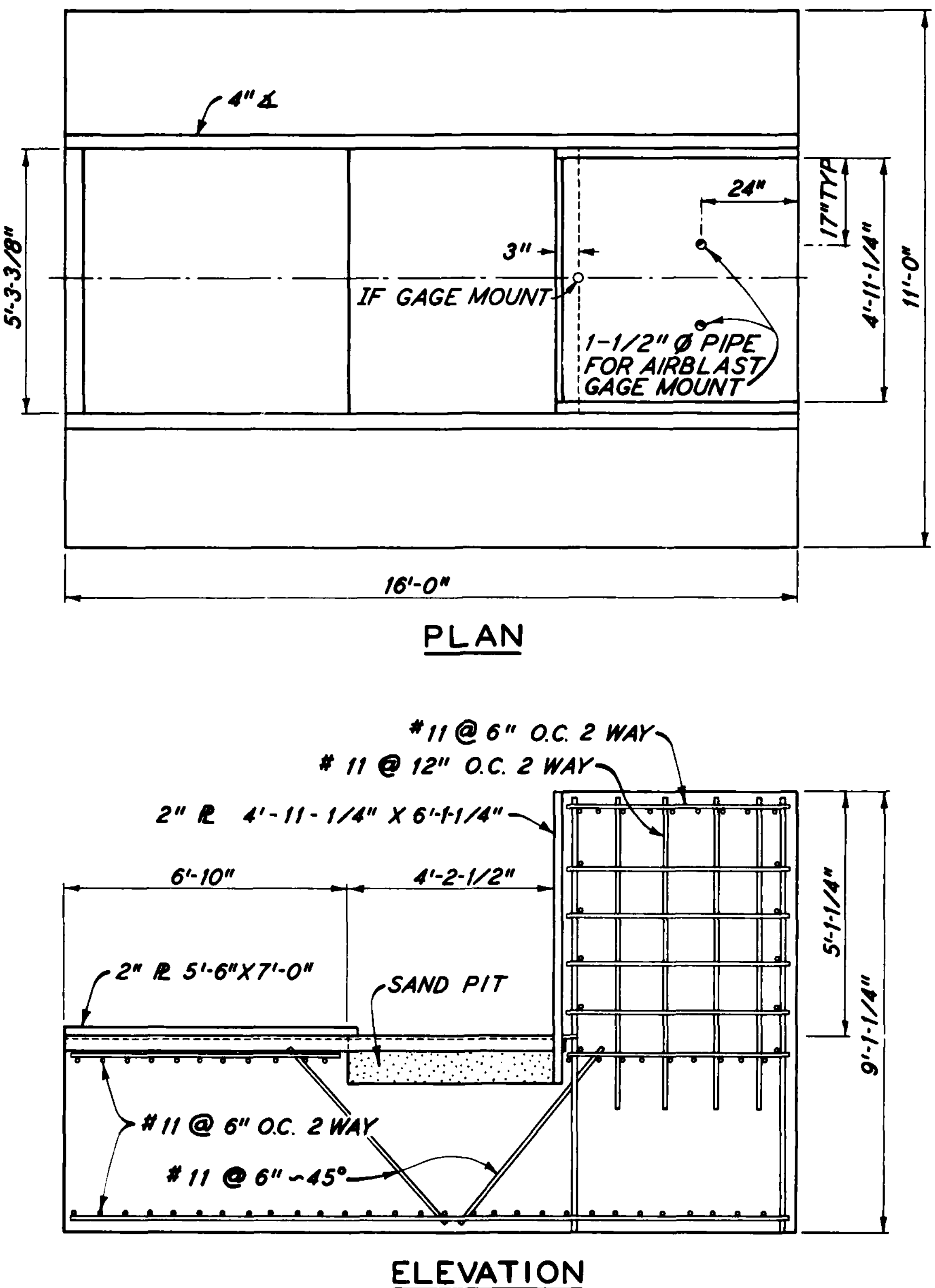

Figure 2-6. Dynamic Shear Concrete Reaction Structure Details.

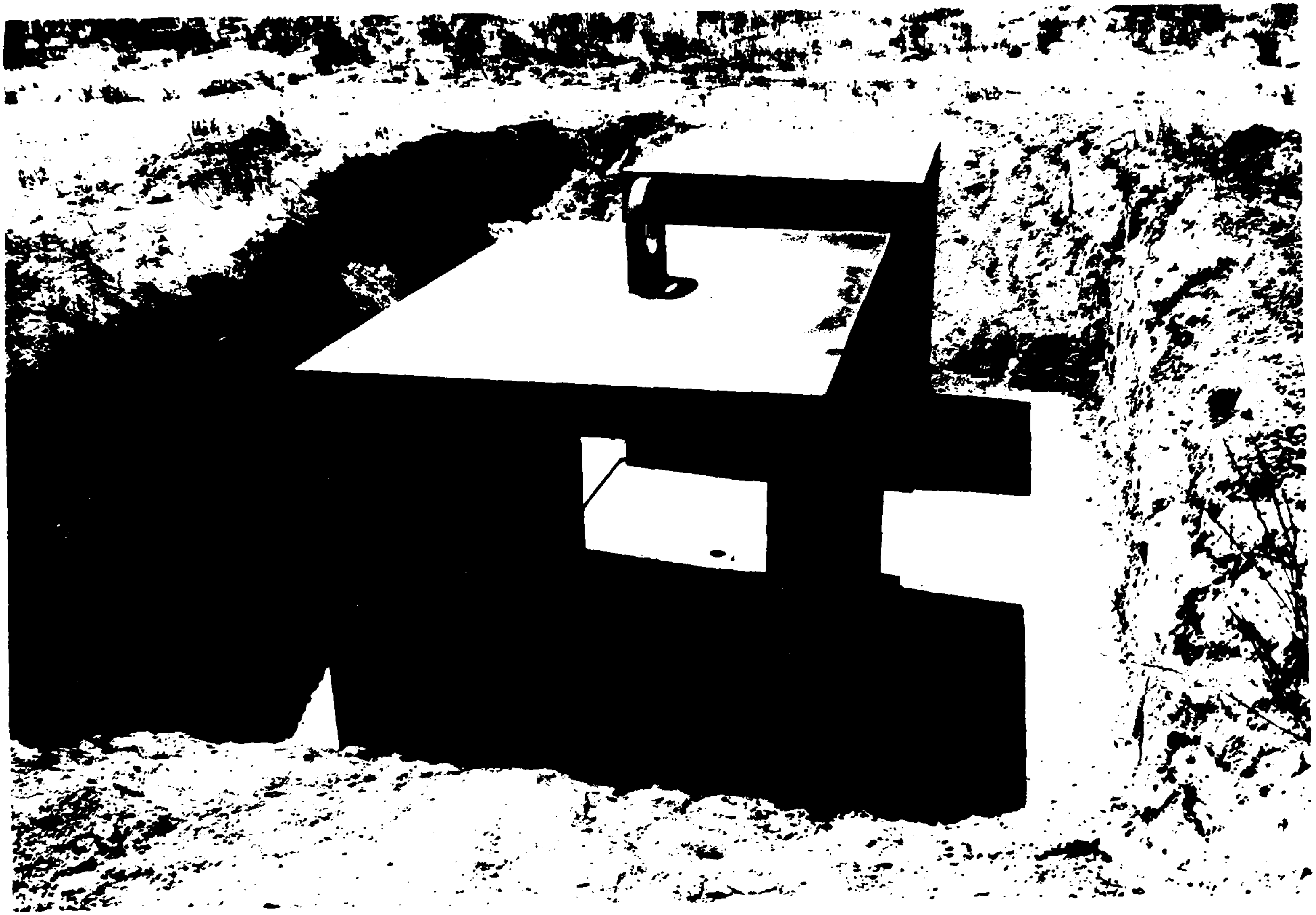

Figure 2-7. Dynamic Shear Test Reaction Structure Photograph.

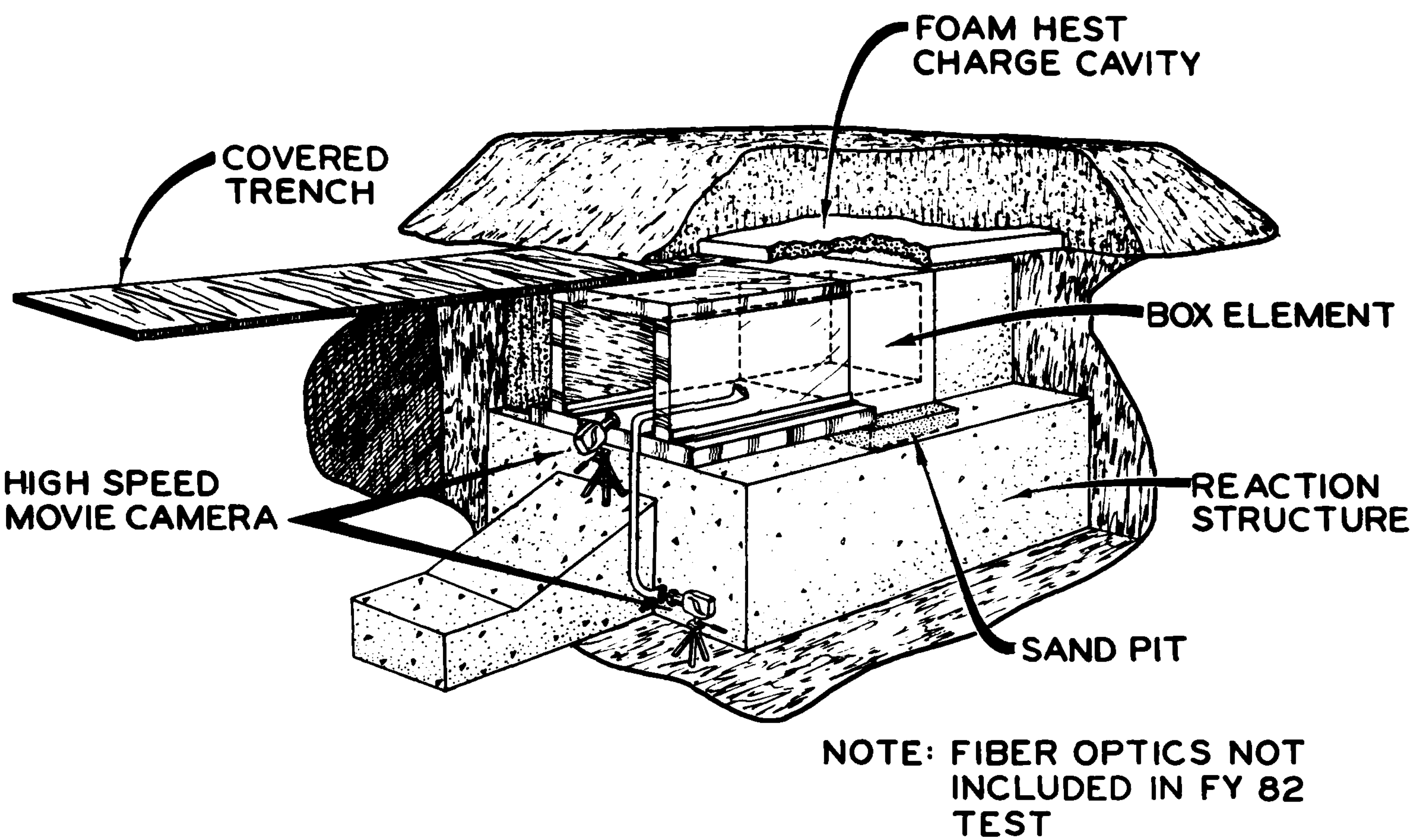

Figure 2-8. Dynamic Shear Test Configuration, Three-Dimensional View.

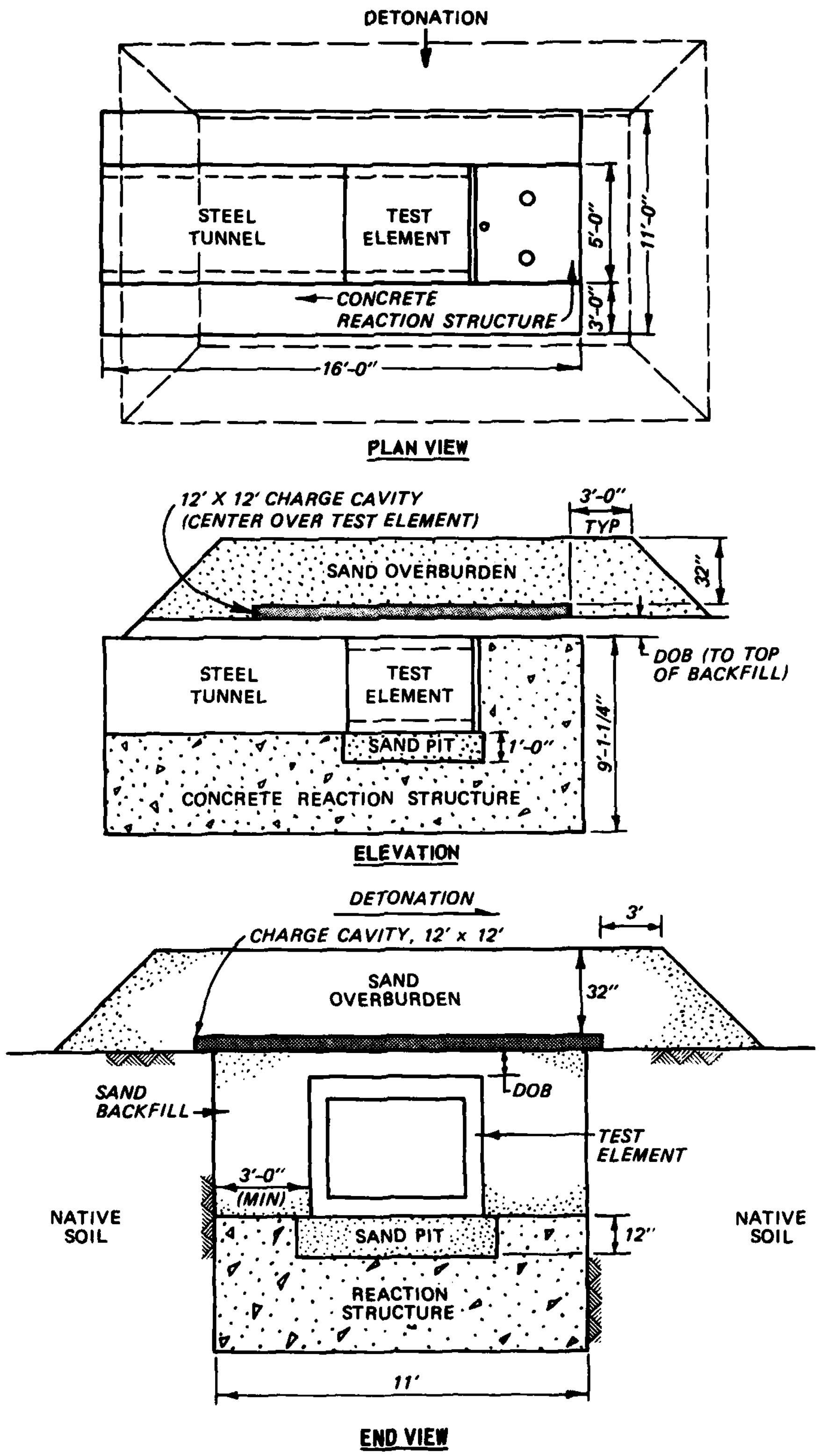

Figure 2-9. Dynamic Shear Test Configuration, Plan View, Elevation, and End View.

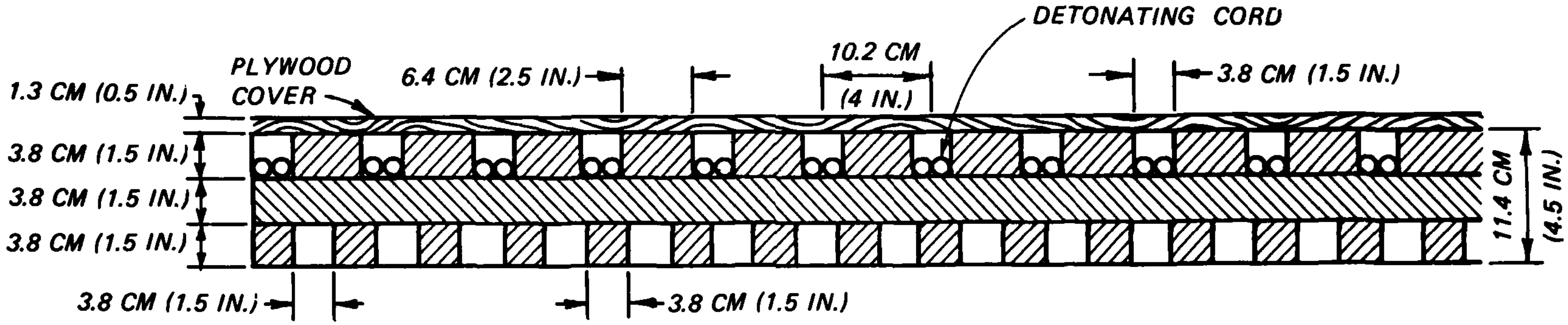

STYROFOAM

CHARGE DENSITY = 21.9 KG/M^3 (1.37 LB/FT^3) FOR DS1 AND DS4
29.2 KG/M^3 (1.83 LB/FT^3) FOR DS2, DS5 AND DS2-2
14.6 KG/M^3 (0.91 LB/FT^3) FOR DS3
36.6 KG/M^3 (2.29 LB/FT^3) FOR DS2-1 AND DS2-4
18.2 KG/M^3 (1.14 LB/FT^3) FOR DS2-3 AND DS2-6
25.6 KG/M^3 (1.60 LB/FT^3) FOR DS2-5

DETONATING CORD = 1312 GRAIN/M (400 GRAIN/FT)
AND/OR 656 GRAIN/M (200 GRAIN/FT)

OVERBURDEN = 81 CM (32 IN.)
AREA = 3.7 M x 3.7 M (12 FT x 12 FT)

Figure 2-10. Dynamic Shear Charge Cavity Details.

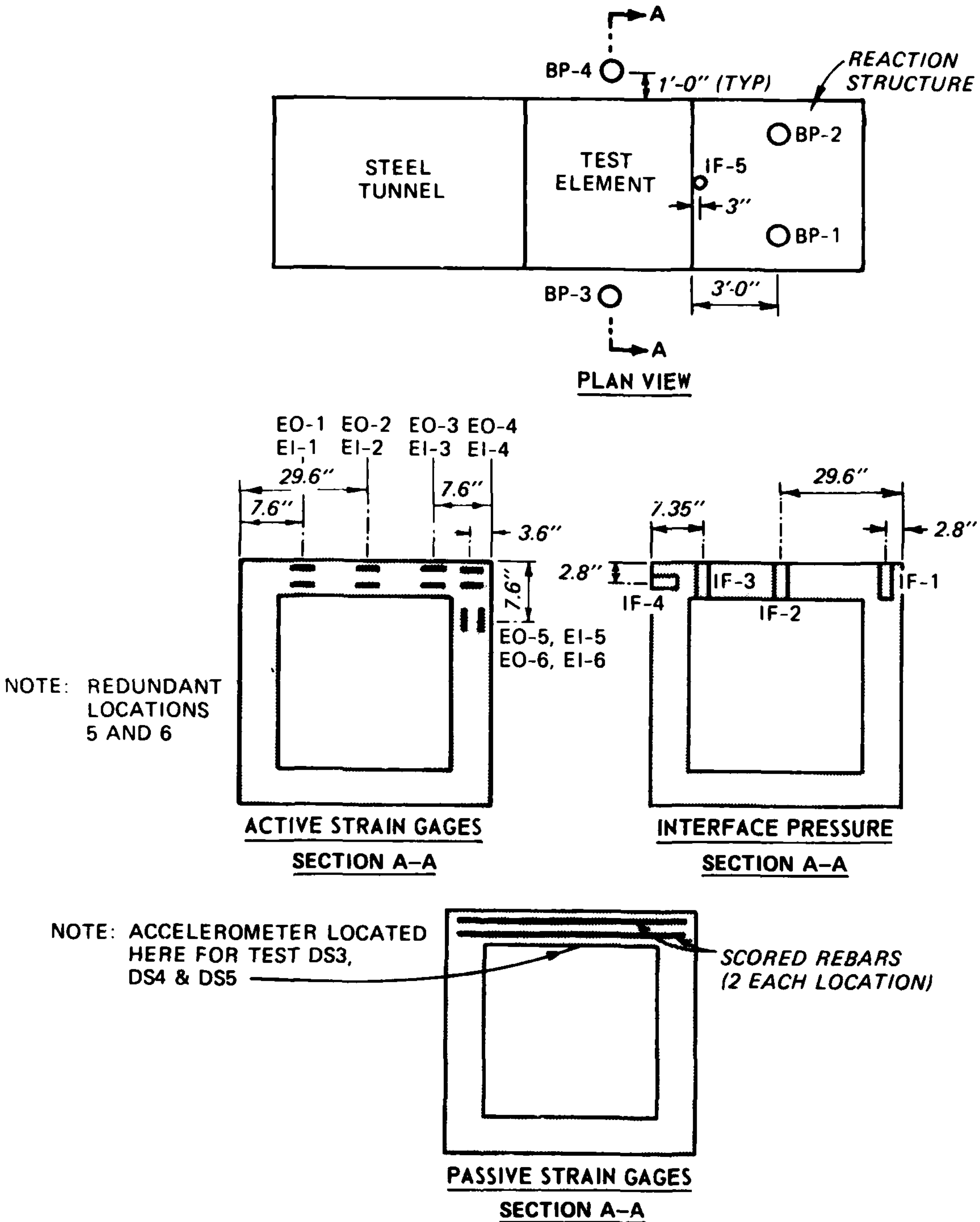

Figure 2-11. FY 81 Dynamic Shear Test Instrumentation Layout.

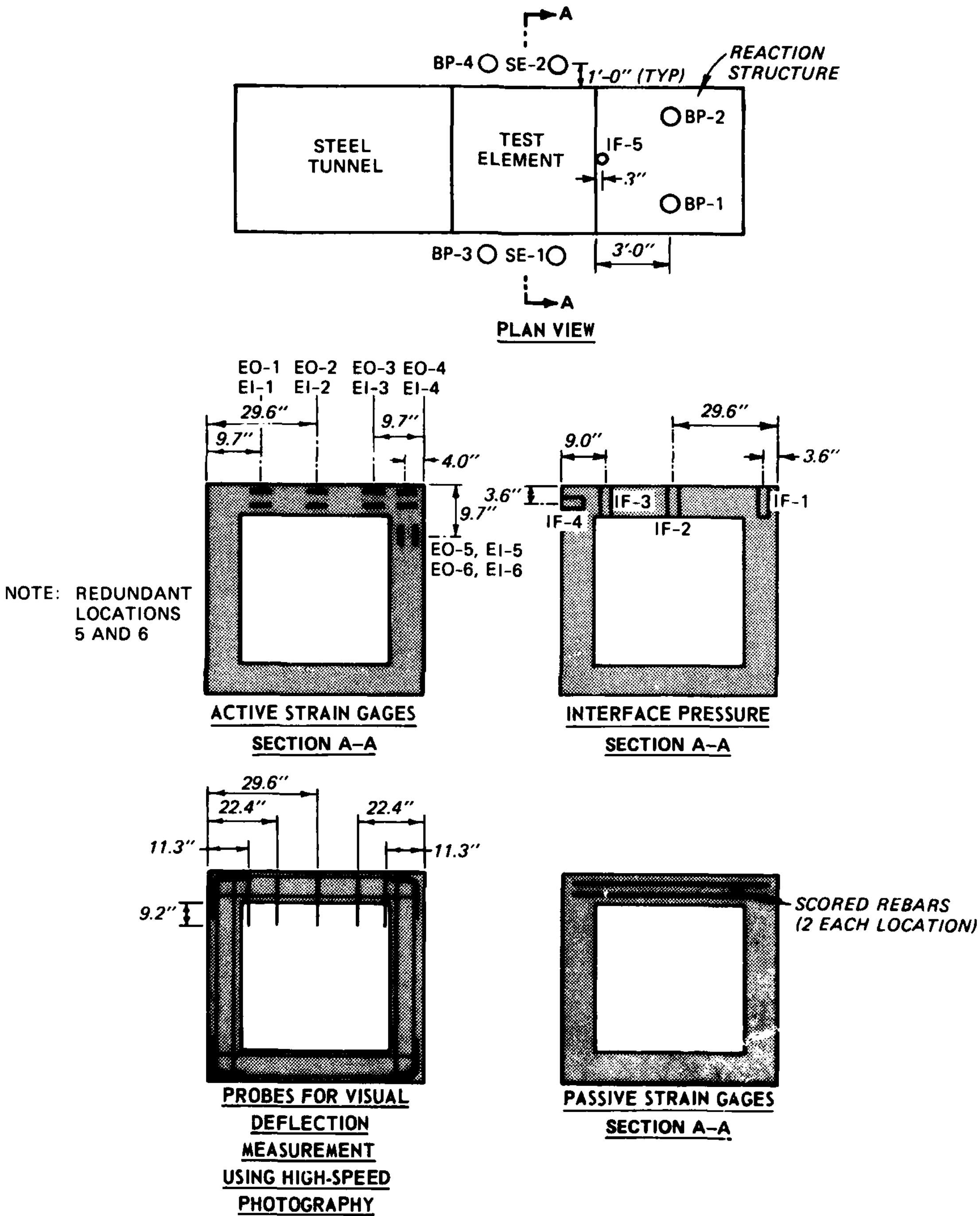

Figure 2-12. FY 82 Dynamic Shear Test Instrumentation Layout.

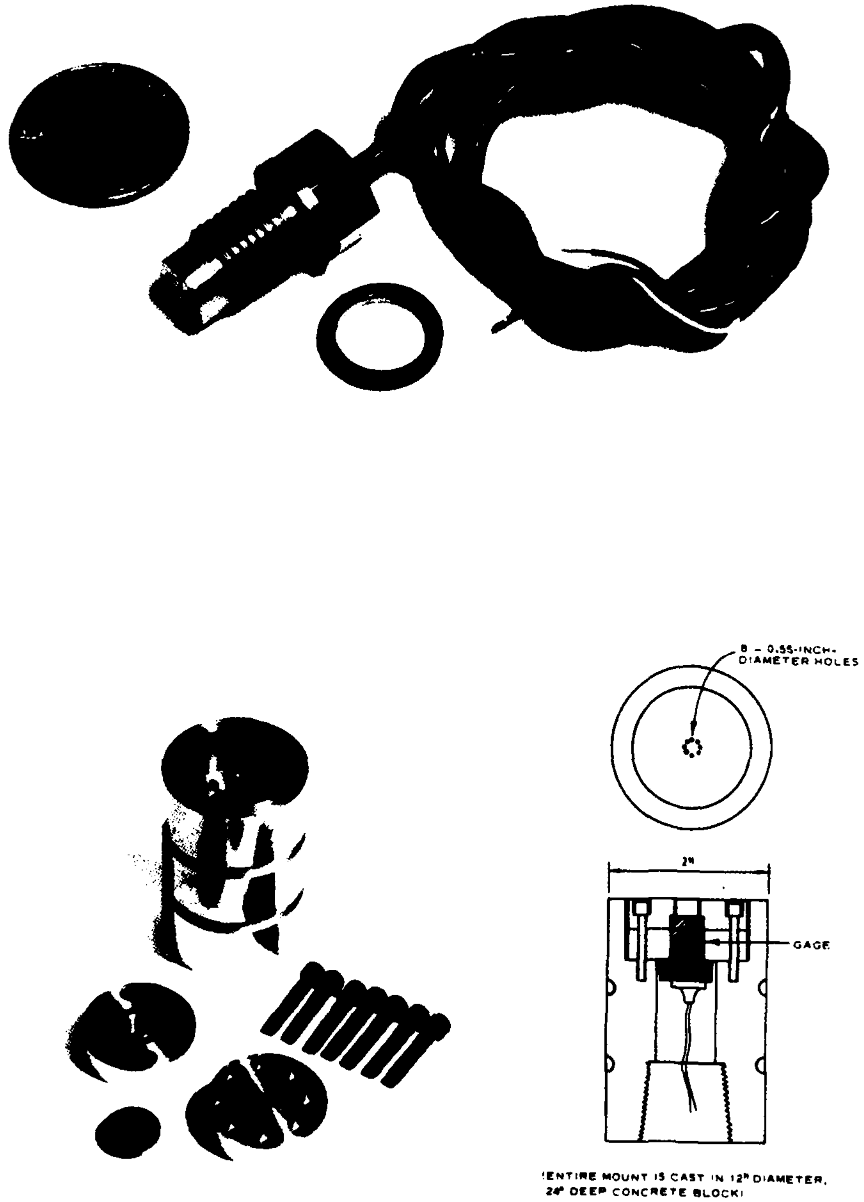

Figure 2-13. Airblast Pressure Gage and Mount.

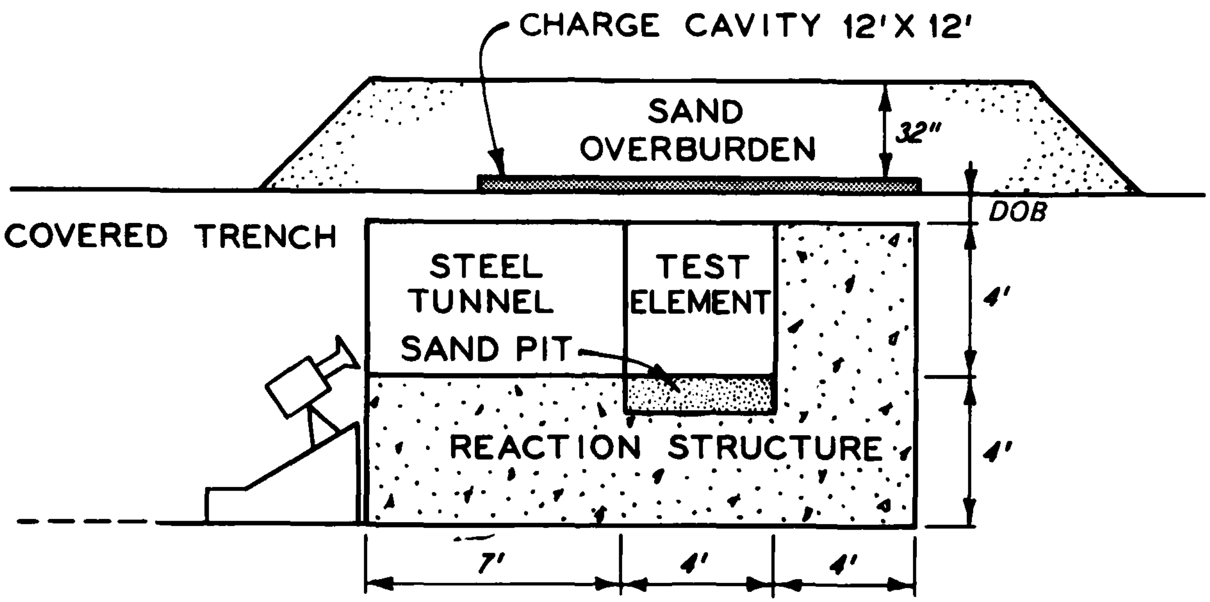

Figure 2-14. Dynamic Shear High-Speed Photography Setup.

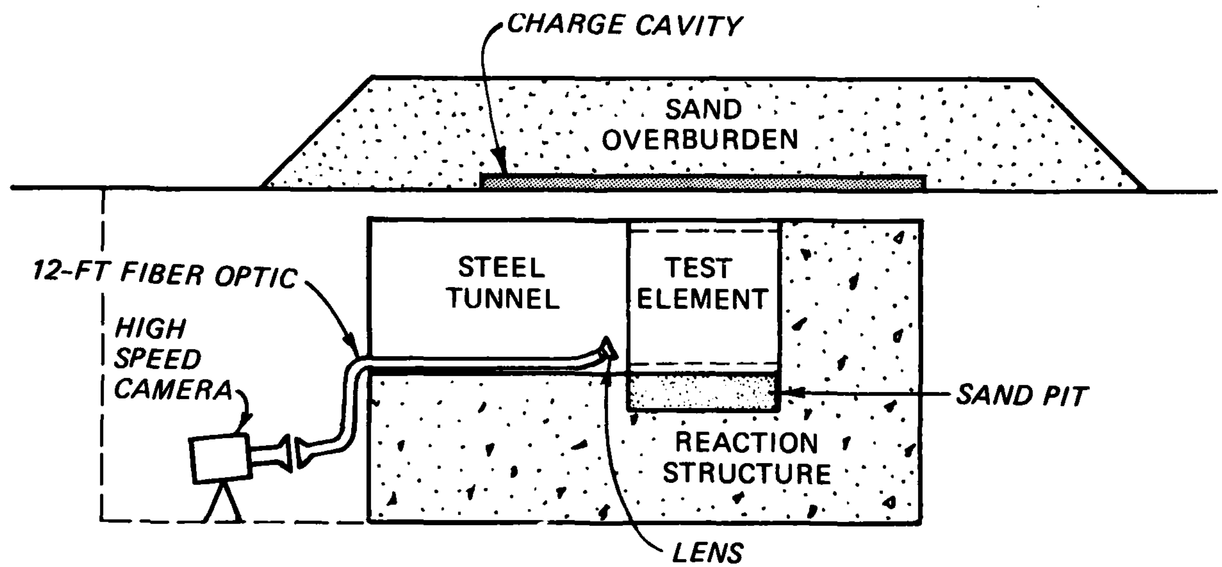

Figure 2-15. Dynamic Shear High-Speed Photography Setup with Fiber Optics.

CHAPTER 3: TEST RESULTS

Damage

56. Inspection of the test site immediately after each test showed that the sand overburden was distributed over the test bed area, making observations about the blast crater very difficult. A typical posttest overview of a structure before excavation is shown in Figure 3-1. Posttest surveys indicated that the reaction structure displaced downward from 1/2 in. to 1-11/16 in. during the tests. Measurements of the relative displacement (the movement of the test element downward into the sand pit on the reaction structure) of the test element and the reaction structure ranged from 1/2 in. to 1-3/8 in. for the tests. The posttest elevation survey results for the dynamic shear tests are presented in Table 3-1.

Table 3-1. Posttest Elevation Survey Results for the Dynamic Shear Tests

Test	Reaction Structure Displacement, in.	Displacement of Test Element into Sand Pit on Reaction Structure, in.
DS1	5/8	7/8
DS2	1-9/16	1-1/8
DS3	1/2	1/2
DS4	13/16	1
DS5	1-1/4	1-1/4
DS2-1	1-11/16	1-3/8
DS2-2	1-7/16	1-1/8
DS2-3	3/4	5/8
DS2-4	5/8	3/4
DS2-5	1-5/16	1
DS2-6	1-9/16	1-1/4

57. An overall view of element DS1 after removal from the reaction structure is shown in Figure 3-2. The roof slab was completely severed from

the walls in vertical failure planes. There were four broken top bars and three broken bottom bars in the west failure plane and two broken bars in the east failure plane (Note: Detonation of the Foam HEST charge was from the west side of the structure in all tests). Slight necking down of broken rebars was noted. The remaining reinforcement bars were pulled out of the concrete during failure. Figure 3-3 shows a typical bar pullout. Only 19 percent of the roof bars was broken. The west wall was pushed in 5 in. from vertical (measured at the top of the wall), and the east wall was pushed in 4 in. Considerable concrete cracking as shown in Figure 3-4 was noted at the base of the walls due to rotation of the walls and at midspan of the floor slab due to flexure. Upon removal of the roof slab from test element DS1 it was noted that the concrete was crushed such that it fell away from the rebar except in the center 1-ft section as shown in Figure 3-5.

58. An overall view of element DS2 after removal from the reaction structure is shown in Figure 3-6. The roof slab was completely severed from the walls in vertical failure planes in test DS2. There were only two broken reinforcement bars (both top bars) in the failure planes and a slight necking down of the broken rebar. The remaining roof slab reinforcement bars were pulled out of the wall. Only 4 percent of the roof reinforcement bars was broken. The west wall was pushed in 10 in. from vertical at the top, while the east wall did not rotate. Considerable cracking was noted at the base of the west wall and at midspan of the floor slab as shown in Figure 3-7. Figure 3-8 shows an interior view of the east wall. The degree of concrete spalling on the interior face of the east wall was such that the inside reinforcement steel was exposed for up to 1 ft below the top of the wall. The degradation of the concrete at the top of the walls allowed the roof slab reinforcement bars to pull out rather than break. When the roof slab from test element DS2 was removed, the concrete fell away from the rebar except in the center 20-in. section as shown in Figure 3-9.

59. Overall views of element DS3 before and after its removal are shown in Figure 3-10 and Figure 3-11, respectively. Permanent center-line deflections ranged from 9-1/2 in. at mid-length to 11 in. at the north end. Initial response appeared to be in diagonal tension shear. The center 18 in. of the roof slab remained relatively flat. Figure 3-12 shows the extent of concrete spalling and cracking of the bottom of the roof slab at the west wall.

60. An overall view of element DS4 after removal from the reaction

structure is shown in Figure 3-13. The roof slab was completely severed from the walls in nearly vertical failure planes. From the final position of the roof slab as shown in Figure 3-13, it was determined that the roof slab separated from the west support before it separated from the east support. There were seven top and one bottom reinforcement bars broken in the west failure plane and nine top and nine bottom reinforcement bars broken in the west failure plane. Slight necking down of the broken rebars was noted. The remaining roof slab reinforcement bars were pulled out of the wall. A total of 54 percent of the roof slab reinforcement bars was broken. The west wall was pushed in 2-1/2 in. from vertical at the top, and the east wall was pushed in 3 in. An interior view of the top of the east wall is shown in Figure 3-14. Con siderable cracking was noted at the base of the walls and at midspan of the floor slab.

61. Figure 3-15 shows a top view of element DS5 before its removal from the reaction structure. Figure 3-16 shows element DS5 after its removal from the reaction structure and after the removal of the roof slab. The roof slab was completely severed from the walls in nearly vertical failure planes in test DS5. There were six top and four bottom reinforcement bars broken in the east failure plane, and there were nine top and eight bottom reinforcement bars broken in the west failure plane for a total of 56 percent of the roof slab reinforcement bars broken in the two failure planes. Slight necking down of the broken reinforcement bars was noted. The remaining roof slab reinforcement bars were pulled out of the wall during failure. Figure 3-17 shows an inside view of the top of the east wall of element DS5. The west wall was pushed in 4 in. from vertical at the top, and the east wall was pushed in 3 in. from vertical at the top. Considerable concrete cracking was noted at the base of the walls and at midspan of the floor slab as shown in Figure 3-18. Upon removal of the roof slab from test element DS5, concrete fell away from the rebar except in a section 23 in. wide at midspan along the length of the roof slab.

62. An overall view of element DS2-1 after removal from the reaction structure is shown in Figure 3-19. The roof slab was completely severed from the walls in vertical failure planes. All roof slab reinforcement bars were pulled out of the east wall while eight top and three bottom bars were broken in the west failure plane for a total of 23 percent breakage of the bars crossing failure planes. Failure occurred first at the west wall, followed by

rotation of the roof slab and pull out of the reinforcement bars on the east side of the roof slab. This failure resulted in considerable cracking of the concrete in the top portion of the east wall as shown in Figure 3-20. The east wall was pushed in 2 in. from vertical at the top while the west wall remained essentially vertical. Considerable cracking occurred at the base of the walls, and some cracking occurred at midspan of the floor slab as shown in Figure 3-21. The roof slab of element DS2-1 is shown in Figure 3-22 after its removal from the test element.

63. An overall view of element DS2-2 after removal from the reaction structures is shown in Figure 3-23. The roof slab was severed from the walls. The west failure plane was approximately 35 deg from vertical, and the east failure plane was approximately 22 deg from vertical. There were eight top and five bottom reinforcement bars broken in the west failure plane and five top and one bottom reinforcement bars broken in the east failure plane, for a total principal reinforcing bar breakage of 40 percent. Slight necking down was noted on the broken reinforcement bars. In addition to broken principal reinforcement bars, there were four broken shear stirrups in the west failure plane. Shear stirrup breakage was as shown in Figure 3-24. The east wall was pushed in 1/2 in. from vertical at the top, and the west wall was pushed in 2 in. from vertical at the top. Some cracking was noted at the base of the walls and at midspan of the floor slab. A top view of the walls is shown in Figure 3-25. Very little concrete remained intact in the roof slab after its removal from the test element. Also, very little of the roof slab reinforcement cage was left intact as shown in Figure 3-26.

64. An overall view of element DS2-3 after removal from the reaction structure is shown in Figure 3-27. Structural response was predominantly in shear with approximately 4-1/8 in. of permanent midspan deflection. Figure 3-28 shows the extent of concrete crushing at the walls and midspan flexural cracking. Figure 3-29 shows the extent of cracking on the bottom of the roof slab. Some cracking at the base of the walls and at midspan of the floor slab was noted.

65. An overall view of test element DS2-4 after removal from the reaction structure is shown in Figure 3-30. The roof slab was completely severed from the walls in vertical failure planes. Two top roof reinforcement bars were broken in the west failure plane for a total reinforcing bar breakage of 4 percent. All other roof slab reinforcement bars were pulled out of the

walls during roof failure. The west wall was pushed in 10 in. from vertical at the top, and the east wall was pushed in 1 in. from vertical at the top. Considerable cracking and spalling of concrete was noted at the base of the walls as shown in Figure 3-31. Extensive cracking of concrete was noted on the outside face of the west wall as shown in Figure 3-32. Extensive crushing of concrete occurred at the top of the east wall as shown in Figure 3-33. The concrete in the roof slab was broken up throughout the entire span.

66. An overall view of test element DS2-5 after removal from the reaction structure is shown in Figure 3-34. Permanent deflection at midspan was approximately 12 in. The west wall was pushed in 5-1/2 in. from vertical at the top, and the east wall was pushed in 3 in. from vertical at the top. Concrete was broken up over the entire span, and most of the concrete cover spalled from the bottom of the roof slab exposing the bottom principal reinforcing steel as shown in Figure 3-35. Considerable cracking was noted on the exterior faces of the walls as shown in Figures 3-36 and 3-37. Concrete cracking was noted at the base of the walls and at midspan of the floor as shown in Figure 3-34.

67. An overall view of test element DS2-6 is shown in Figure 3-38. Structural response was in diagonal tension shear with a permanent midspan deflection of 3-1/2 in. The roof slab remained relatively flat with the deflection due to shear deformation at the support. The west wall was pushed in 1-1/2 in. from vertical at the top, while the east wall remained vertical. Some cracking at the base of the walls and at midspan of the floor slab was noted as shown in Figure 3-38. Figure 3-39 shows concrete cracking of the bottom of the roof slab. Concrete cracking on the exterior faces of the walls is shown in Figures 3-40 and 3-41.

Recovered Data

68. A data summary for each test is listed in Tables 3-2 through 3-12, and all recovered electronic data are included in Appendix E. The data for each test are referenced to a common zero time and are displayed with time in milliseconds as the abscissa.

69. Data recovery for airblast pressure, soil-structure interface pressure, soil stress and acceleration was good, as shown in Tables 3-2 through 3-12. In general, strain data were of very short durations. Since the shear

phenomenon studied in the dynamic shear tests occurs early, the strain data are useful.

70. Permanent strain measurements on principal reinforcement steel were made as described in Chapter 2. The data are analyzed in Chapter 4.

71. In the FY 81 dynamic shear tests, high-speed movies were recovered using conventional high-speed photography and fiber optics as described in Chapter 2. In the FY 82 dynamic shear tests two conventional high-speed movie setups were used. A movie recovery summary is listed in Table 3-13 and the data are analyzed in Chapter 4.

Table 3-2. Data Summary, Dynamic Shear Test DS1

Gage	Location	Time Span msec	Comments
Airblast pressure	BP-1	10, 20	
	BP-2	10, 20	
	BP-3	10, 20	
	BP-4	10, 20	
Interface pressure	IF-1	10	
	IF-2	10	
	IF-3	10	
	IF-4	10	
	IF-5	10	
Soil stress	SE-1		*
	SE-2		*
Acceleration	A-1		*
Strain	EO-1	10	Cable break at 3.7 msec
	EI-1	10	Cable break at 4.5 msec
	EO-2	--	Not recovered
	EI-2	10	
	EO-3	10	Range exceeded at 3 msec
	EI-3	10	Cable break at 3.3 msec
	EO-4	10	Range exceeded at 7.5 msec
	EI-4	10	
	EO-5	10	Range exceeded at 2.0 msec
	EI-5	10	Range exceeded at 2.1 msec
	EO-6	10	Range exceeded at 8.5 msec
	EI-6	10	Range exceeded at 2.2 msec

* Not used.

Table 3-3. Data Summary, Dynamic Shear Test DS2

Gage	Location	Time Span msec	Comments
Airblast pressure	BP-1	10, 20	
	BP-2	10, 20	
	BP-3	10, 20	
	BP-4	10, 20	
Interface pressure	IF-1	10	
	IF-2	10	
	IF-3	10	
	IF-4	10	Cable break at 7.8 msec
	IF-5	10	
Soil stress	SE-1		*
	SE-2		*
Acceleration	A-1		*
Strain	EO-1	10	Cable break at 4.3 msec
	EI-1	10	Cable break at 7.3 msec
	EO-2	10	Cable break at 5.6 msec
	EI-2	10	Cable break at 8.0 msec
	EO-3	10	Cable break at 2.9 msec
	EI-3	10	Cable break at 7.2 msec
	EO-4	10	Cable break at 6.3 msec
	EI-4	10	Range exceeded at 7.8 msec
	EO-5	10	
	EI-5	10	Range exceeded at 1.9 msec
	EO-6	10	Range exceeded at 8.8 msec
	EI-6	10	Range exceeded at 1.9 msec

* Not used.

Table 3-4. Data Summary, Dynamic Shear Test DS3

Gage	Location	Time Span msec	Comments
Airblast pressure	BP-1		Not recovered
	BP-2		Not recovered
	BP-3	10, 20	
	BP-4	10, 20	
Interface pressure	IF-1	10	
	IF-2	10	Cable break at 6.5 msec
	IF-3	10	
	IF-4	10	
	IF-5		Not recovered
Soil stress	SE-1		*
	SE-2		*
Acceleration	A-1	10	Cable break at 6 msec
Strain	EO-1	10	Cable break at 4.5 msec
	EI-1	10	Range exceeded at 4.2 msec
	EO-2	10	Cable break at 6.5 msec
	EI-2	10	
	EO-3	10	Cable break at 4.5 msec
	EI-3	10	Cable break at 2.2 msec
	EO-4	10	
	EI-4	10	
	EO-5	10	
	EI-5	10	
	EO-6	10	
	EI-6	10	

* Not used.

Table 3-5. Data Summary, Dynamic Shear Test DS4

Gage	Location	Time Span msec	Comments
Airblast pressure	BP-1	10, 20	
	BP-2	10, 20	
	BP-3		Not recovered
	BP-4	10, 20	
Interface pressure	IF-1	10	
	IF-2	10	
	IF-3	10	
	IF-4	10	
	IF-5	10	
Soil stress	SE-1		*
	SE-2		*
Acceleration	A-1	10	
Strain	EO-1	10	Cable break at 2.9 msec
	EI-1	10	Cable break at 3.4 msec
	EO-2	10	Cable break at 9.6 msec
	EI-2	10	Cable break at 6.9 msec
	EO-3	10	Range exceeded at 3.5 msec
	EI-3	10	Cable break at 3.9 msec
	EO-4	10	Range exceeded at 5.3 msec
	EI-4	10	
	EO-5	10	
	EO-6		Not recovered
	EI-6		Not recovered

* Not used.

Table 3-6. Data Summary, Dynamic Shear Test DS5

Gage	Location	Time Span msec	Comments
Airblast pressure	BP-1		Not recovered
	BP-2	10, 20	
	BP-3	10, 20	
	BP-4		Not recovered
Interface pressure	IF-1	10	
	IF-2	10	Cable break at 5 msec
	IF-3	10	Cable break at 5 msec
	IF-4	10	Cable break at 4.5 msec
	IF-5	10	
Soil stress	SE-1		*
	SE-2		*
Acceleration	A-1	10	Cable break at 6.3 msec
Strain	EO-1	10	Cable break at 2.5 msec
	EI-1	10	Cable break at 2.5 msec
	EO-2	10	
	EI-2	10	
	EO-3	10	Cable break at 3.2 msec
	EI-3	10	Cable break at 2.6 msec
	EO-4	10	Range exceeded at 5.2 msec
	EI-4	10	Range exceeded at 7.6 msec
	EO-5	10	
	EI-5	10	
	EO-6	10	
	EI-6	10	

* Not used.

Table 3-7. Data Summary, Dynamic Shear Test DS2-1

Gage	Location	Time Span msec	Comments
Airblast pressure	BP-1	10, 20	
	BP-2		Not recovered
	BP-3		Not recovered
	BP-4	10, 20	
Interface pressure	IF-1	10	Cable break at 4.0 msec
	IF-2	10	Cable break at 2.8 msec
	IF-3	10	Cable break at 4.0 msec
	IF-4	10	Cable break at 4.0 msec
	IF-5	10	
Soil stress	SE-1	10	Cable break at 1.9 msec
	SE-2	10	
Acceleration	A-1		*
Strain	EO-1	10	Cable break at 3.5 msec
	EI-1	10	Cable break at 2.0 msec
	EO-2		Not recovered
	EI-2		Not recovered
	EO-3	10	Cable break at 3.2 msec
	EI-3	10	Cable break at 3.0 msec
	EO-4	10	Cable break at 3.0 msec
	EI-4	10	Cable break at 3.6 msec
	EO-5	10	Cable break at 2.3 msec
	EI-5	10	Cable break at 4.4 msec
	EO-6	10	Cable break at 2.5 msec
	EI-6	10	Cable break at 2.0 msec

* Not used.

Table 3-8. Data Summary, Dynamic Shear Test DS2-2

Gage	Location	Time Span msec	Comments
Airblast pressure	BP-1	10, 20	
	BP-2	10, 20	
	BP-3	10, 20	
	BP-4	10, 20	
Interface pressure	IF-1	10	Cable break at 6.5 msec
	IF-2	10	Not recovered
	IF-3	10	Cable break at 2.8 msec
	IF-4	10	Cable break at 4.0 msec
	IF-5	10	
Soil stress	SE-1	10	
	SE-2	10	
Acceleration	A-1		*
Strain	EO-1	10	Cable break at 2.7 msec
	EI-1	10	Cable break at 2.4 msec
	EO-2	10	
	EI-2	10	
	EO-3	10	Cable break at 3.5 msec
	EI-3	10	Cable break at 2.7 msec
	EO-4	10	Cable break at 3.5 msec
	EI-4	10	Cable break at 3.0 msec
	EO-5	10	
	EI-5	10	
	EO-6	10	Cable break at 6.5 msec
	EI-6	10	Cable break at 7.2 msec

* Not used.

Table 3-9. Data Summary, Dynamic Shear Test DS2-3

Gage	Location	Time Span msec	Comments
Airblast pressure	BP-1	10, 20	
	BP-2	10, 20	
	BP-3	10, 20	
	BP-4	10, 20	
Interface pressure	IF-1	10	
	IF-2	10	
	IF-3	10	
	IF-4	10	Cable break at 5.0 msec
	IF-5	10	
Soil stress	SE-1	10	
	SE-2	10	
Acceleration	A-1		*
Strain	EO-1	10	Cable break at 4.5 msec
	EI-1	10	Cable break at 5.3 msec
	EO-2	10	
	EI-2	10	Range exceeded at 2.5 msec
	EO-3	10	Cable break at 4.7 msec
	EI-3	10	Cable break at 4.3 msec
	EO-4	10	Cable break at 5.3 msec
	EI-4	10	Cable break at 5.3 msec
	EO-5	10	
	EI-5	10	
	EO-6	10	
	EI-6	10	

* Not used.

Table 3-10. Data S ·mary, Dynamic Shear Test DS2-4

Gage	Location	Time Span msec	Comments
Airblast pressure	BP-1	10, 20	
	BP-2	10, 20	
	BP-3	10, 20	
	BP-4	10, 20	
Interface pressure	IF-1	10	Cable break at 3.3 msec
	IF-2	10	Cable break at 3.4 msec
	IF-3	10	Cable break at 4.7 msec
	IF-4	10	Cable break at 4.2 msec
	IF-5	10	
Soil stress	SE-1	10	
	SE-2	10	
Acceleration	A-1	10	*
Strain	EO-1	10	Cable break at 2.6 msec
	EI-1	10	Cable break at 2.0 msec
	EO-2	10	
	EI-2	10	
	EO-3	10	Cable break at 3.0 msec
	EI-3	10	Cable break at 3.7 msec
	EO-4	10	Cable break at 3.1 msec
	EI-4	10	Cable break at 4.8 msec
	EO-5	10	Cable break at 2.0 msec
	EI-5	10	Cable break at 2.1 msec
	EO-6	10	Cable break at 1.8 msec
	EI-6	10	

* Not used.

Table 3-11. Data Summary, Dynamic Shear Test DS2-5

Gage	Location	Time Span msec	Comments
Airblast pressure	BP-1	10, 20	
	BP-2	10, 20	
	BP-3		Not recovered
	BP-4	10, 20	
Interface pressure	IF-1	10	Cable break at 4.0 msec
	IF-2	10	Cable break at 1.7 msec
	IF-3	10	
	IF-4	10	Cable break at 5.8 msec
	IF-5	10	
Soil stress	SE-1	10	
	SE-2	10	
Acceleration	A-1		*
Strain	EO-1	10	Cable break at 2.8 msec
	EI-1	10	
	EO-2	10	Cable break at 8.0 msec
	EI-2	10	Cable break at 2.7 msec
	EO-3	10	Cable break at 3.8 msec
	EI-3	10	
	EO-4	10	Cable break at 3.8 msec
	EI-4	10	Cable break at 4.2 msec
	EO-5	10	
	EI-5	10	Cable break at 9.2 msec
	EO-6	10	
	EI-6	10	

* Not used.

Table 3-12. Data Summary, Dynamic Shear Test DS2-6

Gage	Location	Time Span msec	Comments
Airblast pressure	BP-1	10, 20	
	BP-2	10, 20	
	BP-3		Not recovered
	BP-4	10, 20	
Interface pressure	IF-1	10	
	IF-2	10	Cable break at 8.7 msec
	IF-3	10	
	IF-4	10	Cable break at 4.3
	IF-5	10	
Soil stress	SE-1	10	
	SE-2	10	Cable break at 1.7 msec
Acceleration	A-1		*
Strain	EO-1	10	Cable break at 3.3 msec
	EI-1	10	Cable break at 2.4 msec
	EO-2		Not recovered
	EI-2	10	Cable break at 6.0 msec
	EO-3	10	Cable break at 5.8 msec
	EI-3	10	Cable break at 7.5 msec
	EO-4	10	Cable break at 6.0 msec
	EI-4	10	
	EO-5	10	
	EI-5		Not recovered
	EO-6	10	
	EI-6	10	

* Not used.

Table 3-13. High-Speed Movie Summary, Dynamic Shear Tests

Test	Camera* Location 1	Camera** Location 2	Camera† Location 3
DS1	Over exposed	Recovered	††
DS2	Recovered	Not recovered	††
DS3	Recovered, but frame partially obscured	Recovered	††
DS4	Not recovered	Recovered	††
DS5	Recovered	Recovered	††
DS2-1	Recovered	††	Not recovered
DS2-2	Recovered	††	Recovered
DS2-3	Recovered	††	Recovered
DS2-4	Recovered	††	Recovered
DS2-5	Recovered	††	Recovered
DS2-6	Not recovered	††	Not recovered

* Conventional high-speed camera located on center line of steel tunnel as shown in Figure 2-14.

** Fiber optics as shown in Figure 2-15.

† Conventional high-speed camera located 9 in. off center line of steel tunnel in the same position as camera 1.

†† Not used.

Figure 3-1. Typical Posttest Overview Before Test Element Excavation.

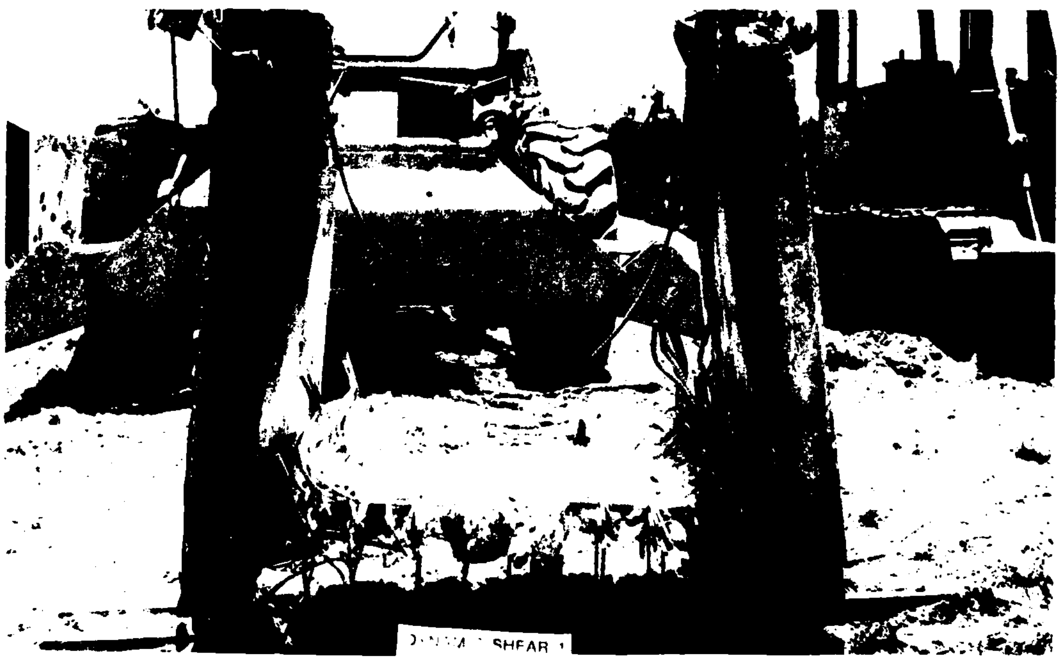

Figure 3-2. Posttest View, DS1.

Figure 3-3. Inside View of the Top of the East Wall, DS1.

Figure 3-4. Top of the Floor Slab, DS1.

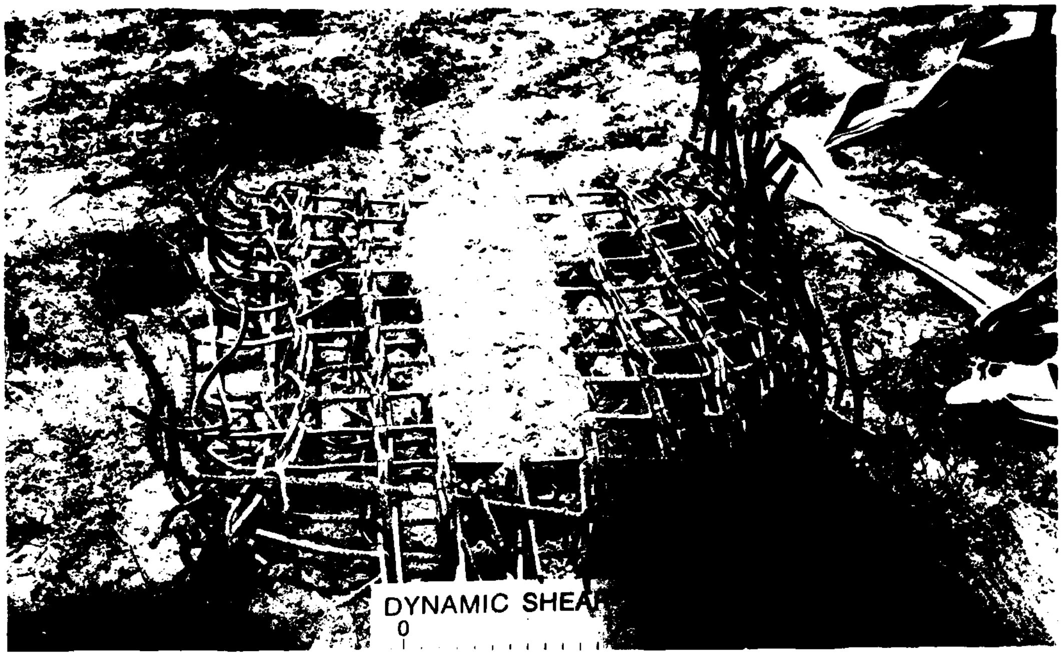

Figure 3-5. Roof Slab, DS1.


Figure 3-6. Posttest View, DS2.

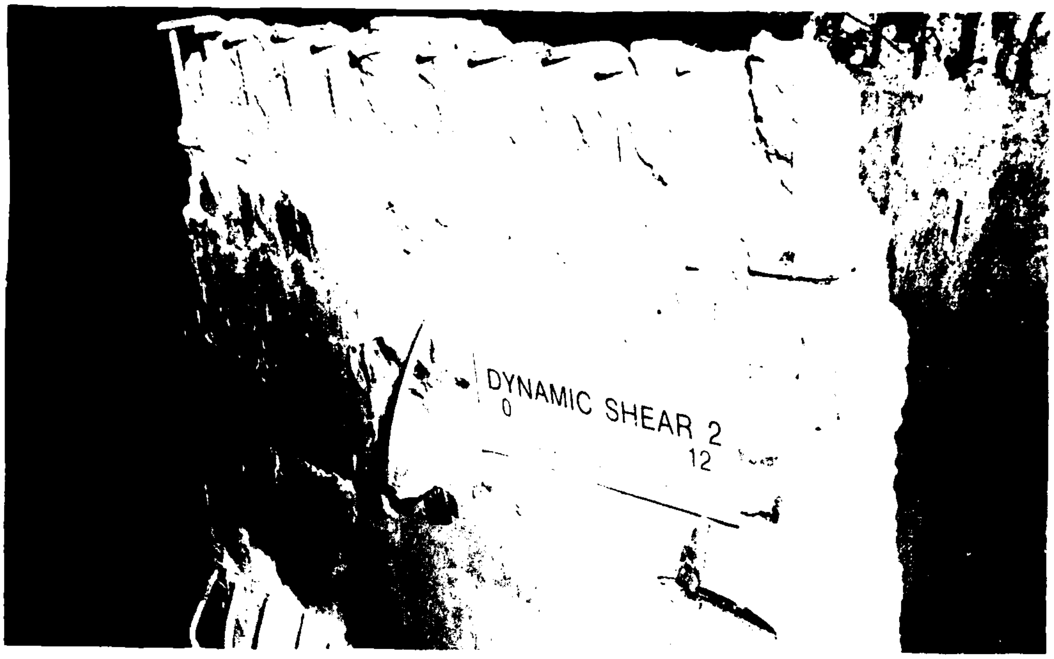

Figure 3-7. Top of the Floor Slab, DS2.

Figure 3-8. Inside View of the Top of the East Wall, DS2.

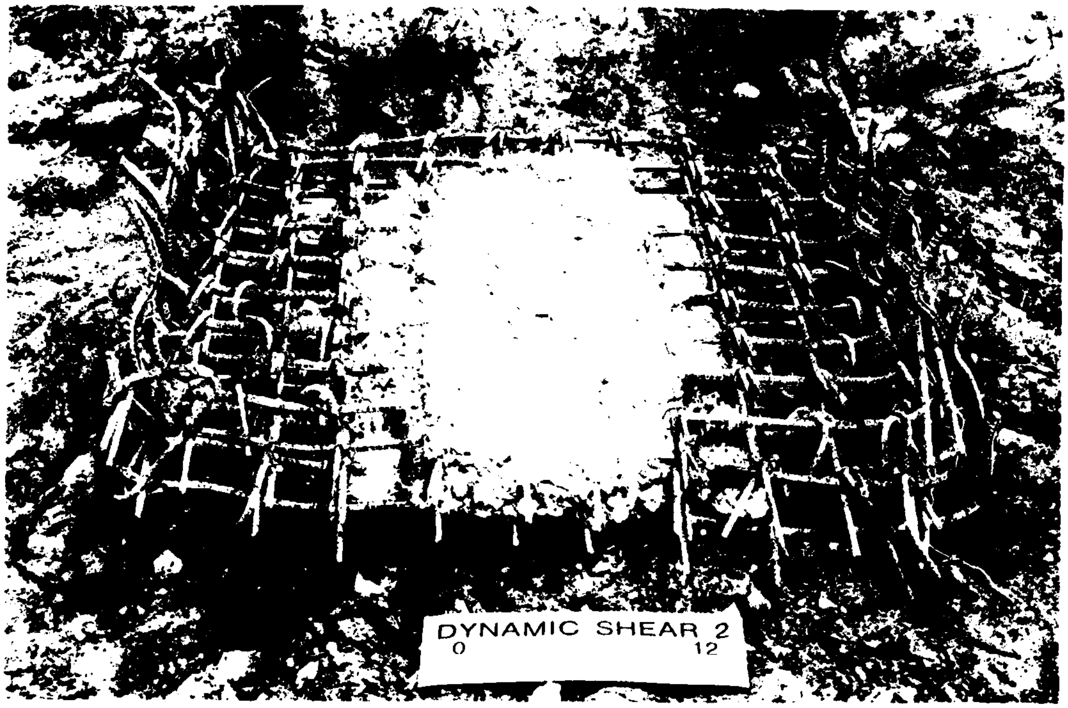

Figure 3-9. Roof Slab, DS2.

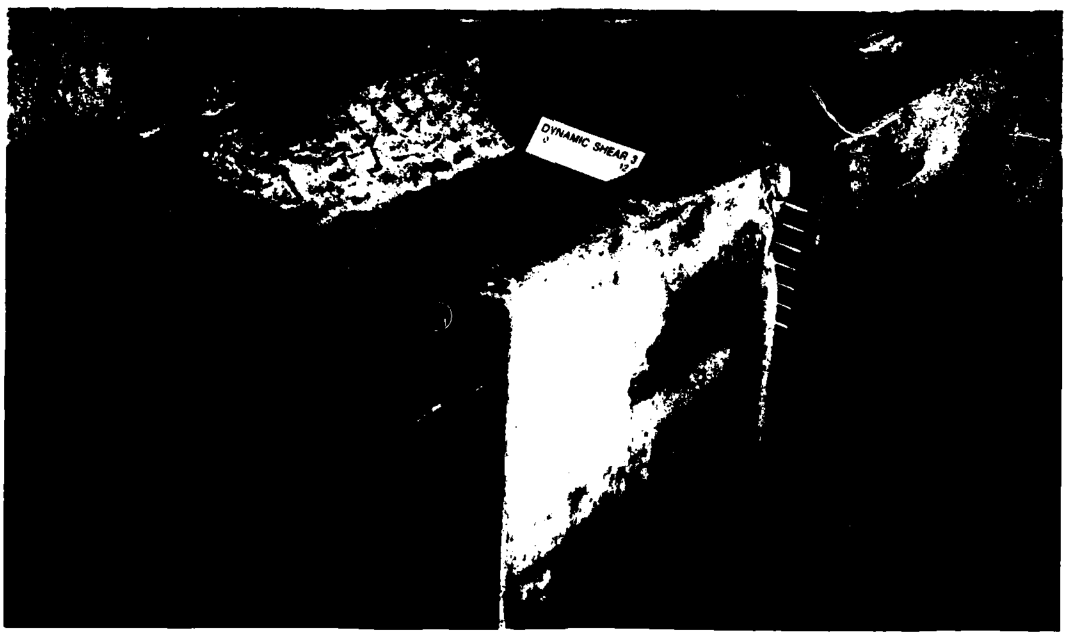

Figure 3-10. Posttest View Before Removal from the Reaction Structure, DS3.

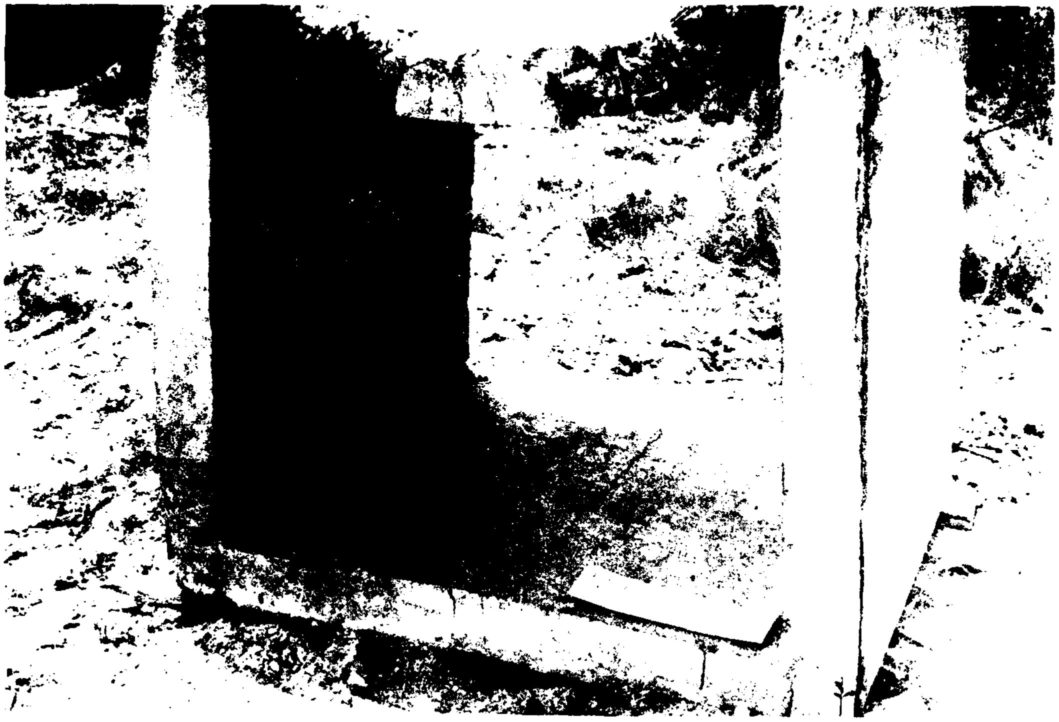

Figure 3-11. Posttest View After Removal from the Reaction Structure, DS3.

Figure 3-12. Bottom of the Roof Slab at the Top of the West Wall, DS3.

Figure 3-13. Posttest View, DS4.

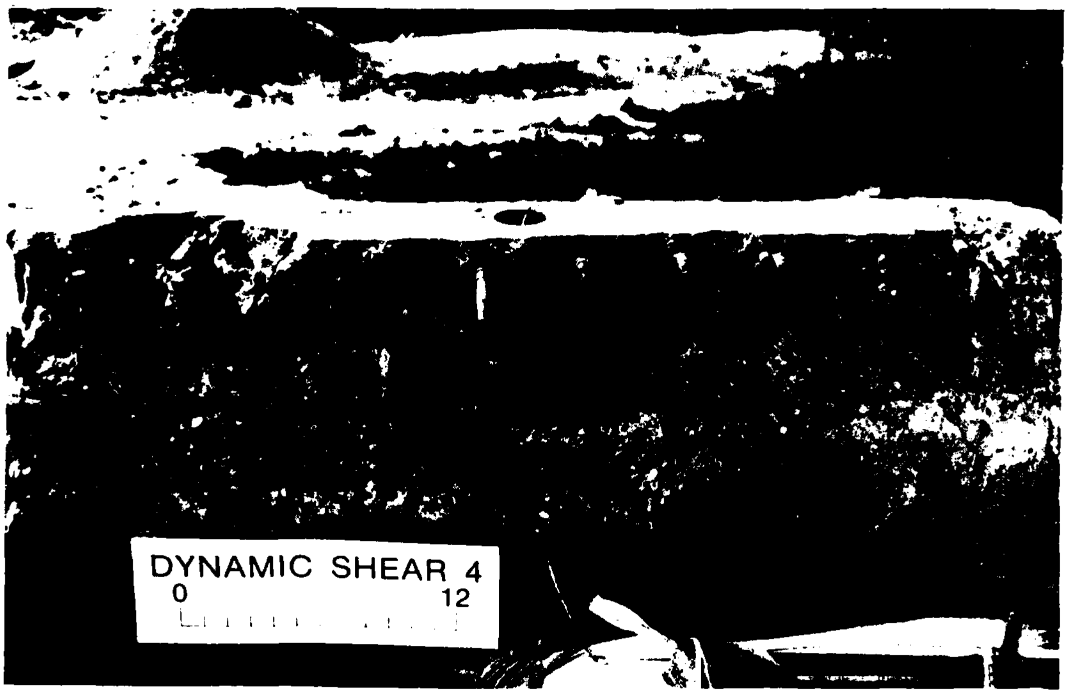

Figure 3-14. Inside View of the Top of the East Wall, DS4.

Figure 3-15. Posttest Top View, DS5.

Figure 3-16. Posttest View, DS5.

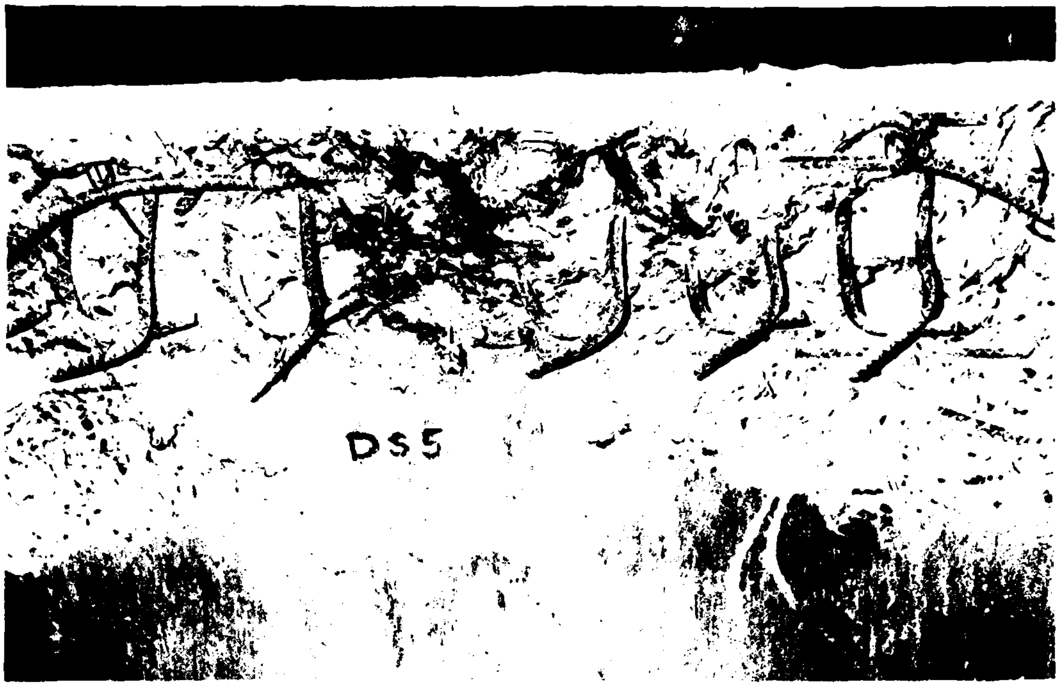

Figure 3-17. Inside View of the Top of the East Wall, DS5.

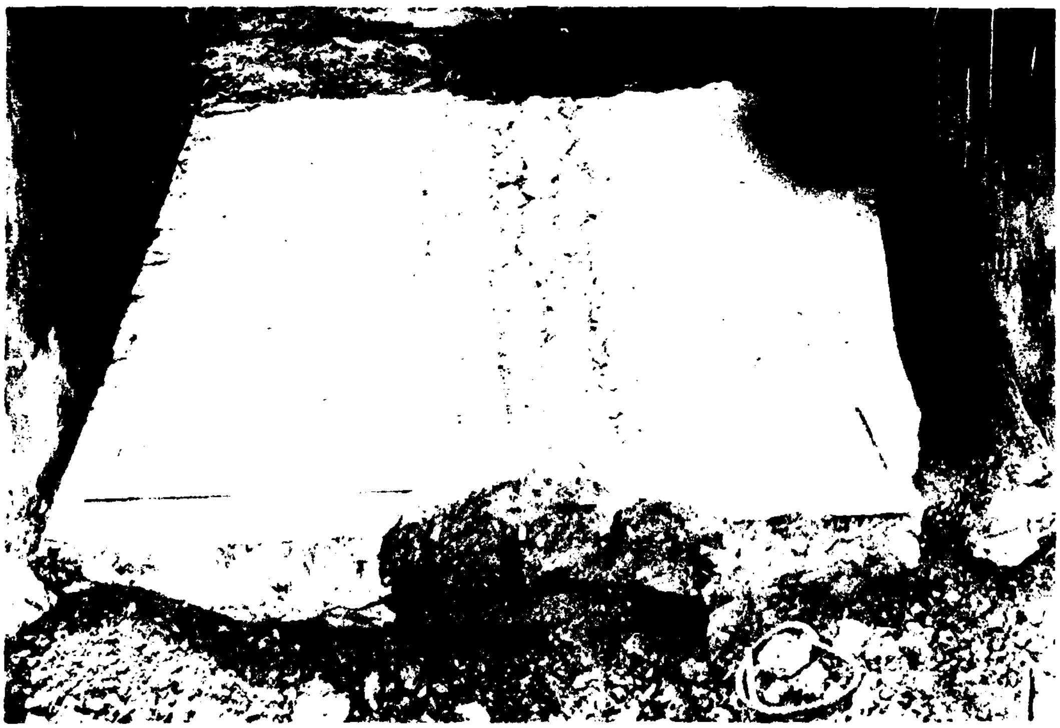

Figure 3-18. Top of the Floor Slab, DS5.

Figure 3-19. Posttest View, DS2-1.

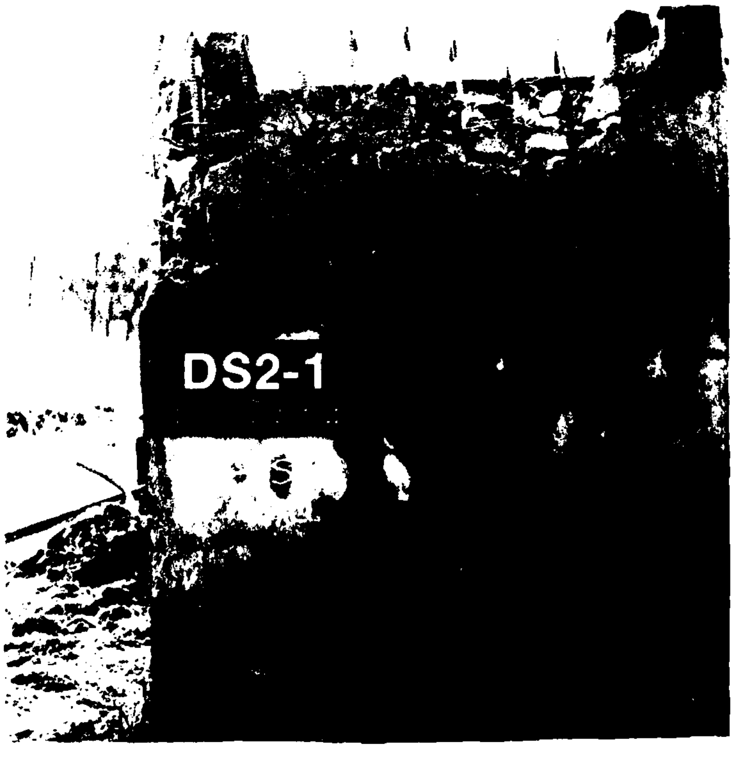

Figure 3-20. Exterior View of the East Wall, DS2-1.

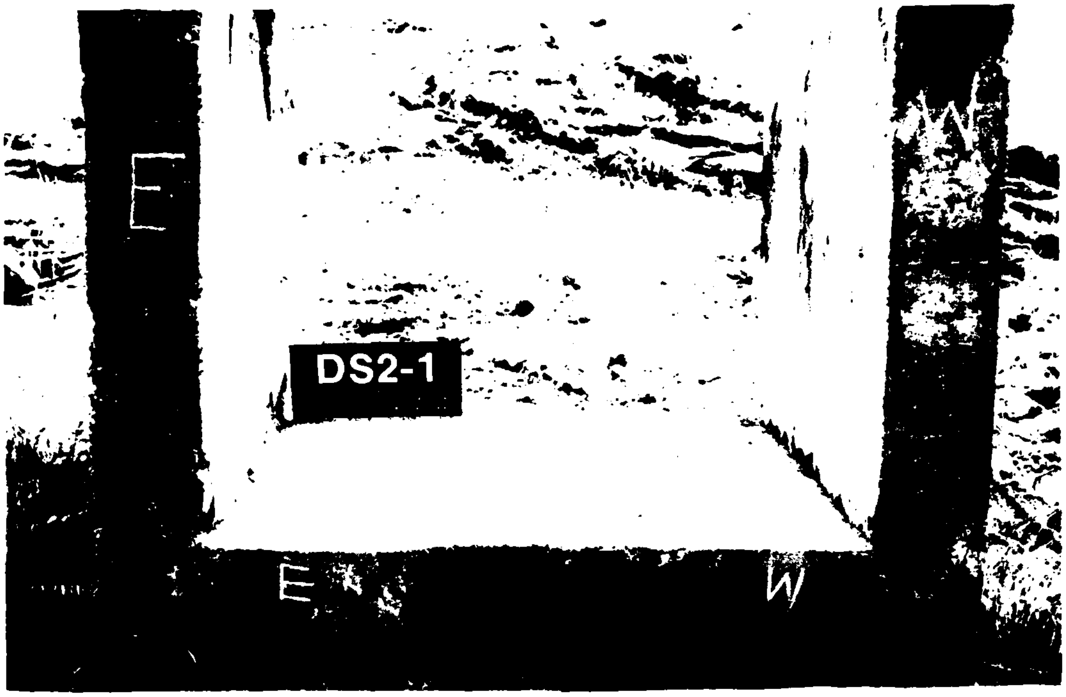

Figure 3-21. Top of the Floor Slab, DS2-1.

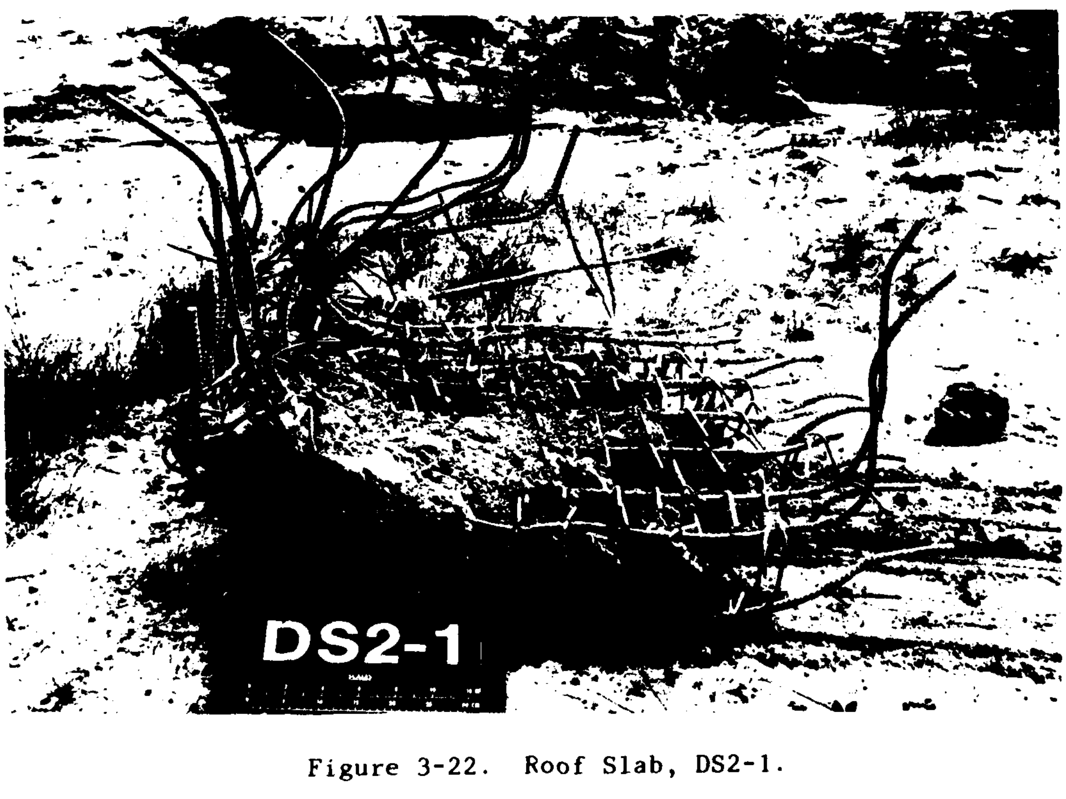

Figure 3-22. Roof Slab, DS2-1.

Figure 3-23. Posttest View, DS2-2.

Figure 3-24. Top of the West Wall, DS2-2
(Arrows Indicate Broken Shear Stirrups).

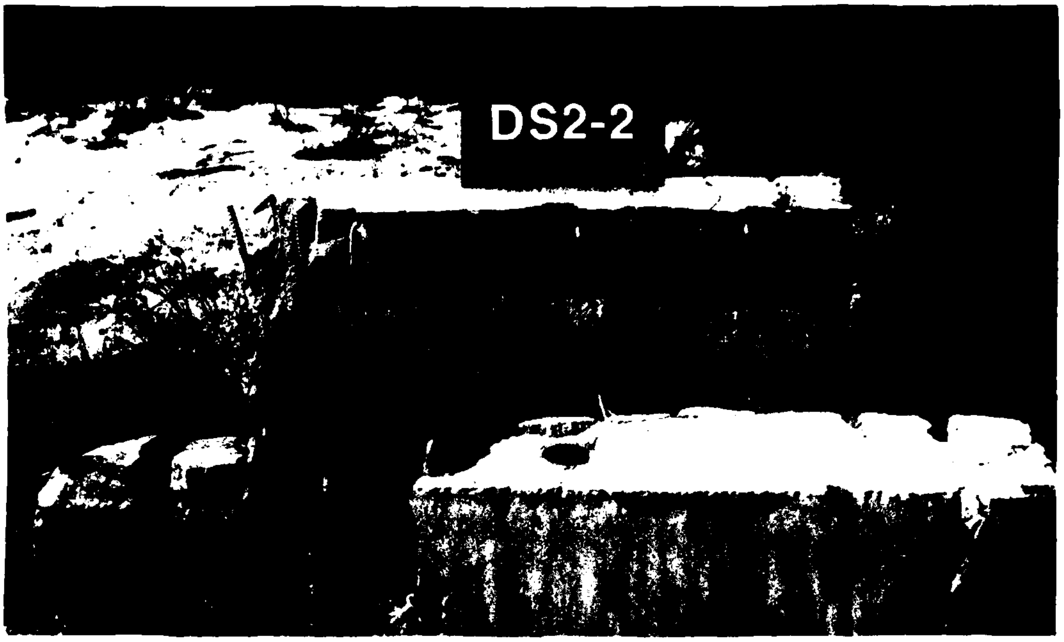

Figure 3-25. Top of the Walls, DS2-2.

Figure 3-26. Roof Slab, DS2-2.

Figure 3-27. Posttest View, DS2-3.

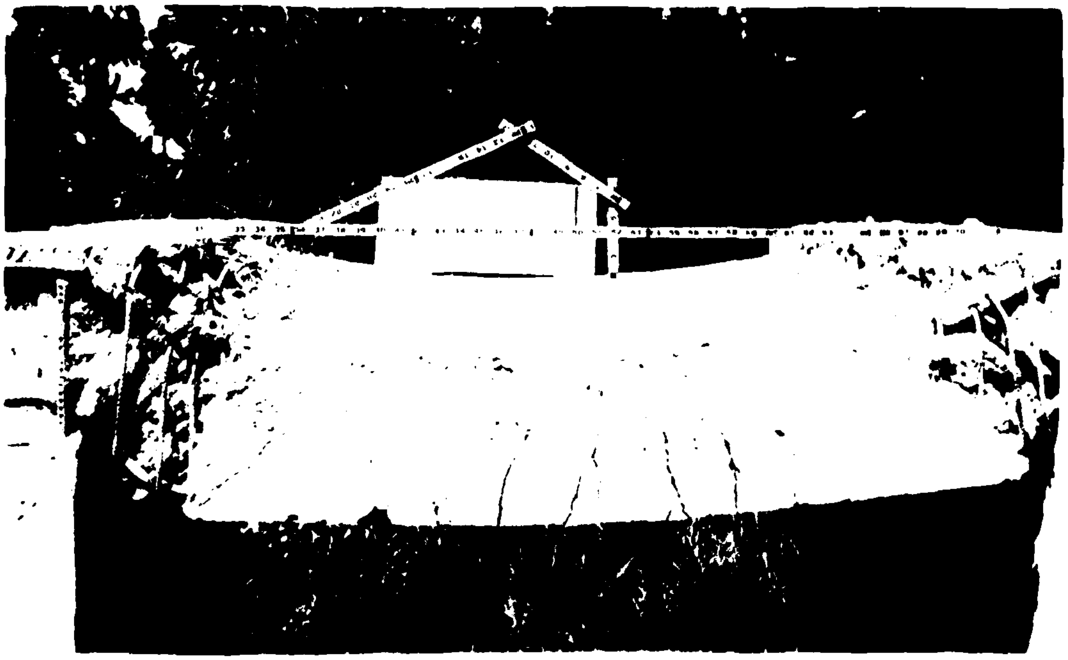

Figure 3-28. End View from South, DS2-3.

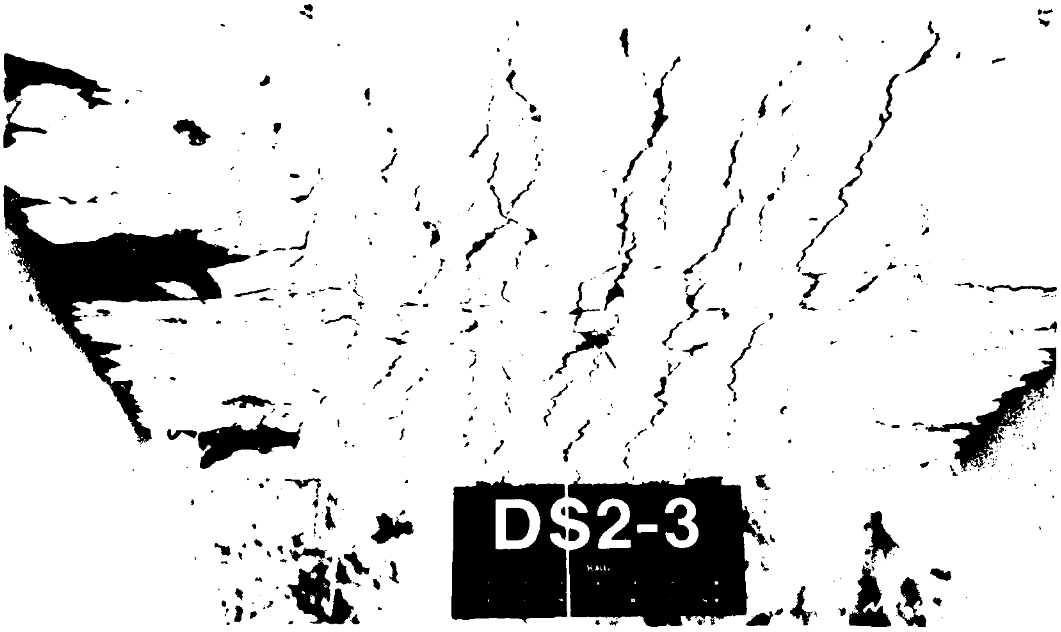

Figure 3-29. Bottom of the Roof Slab from the South, DS2-3.

Figure 3-30. Posttest View, DS2-4.

Figure 3-31. End View After Roof Slab Removal, DS2-4.

Figure 3-32. Exterior View of West Wall, DS2-4.

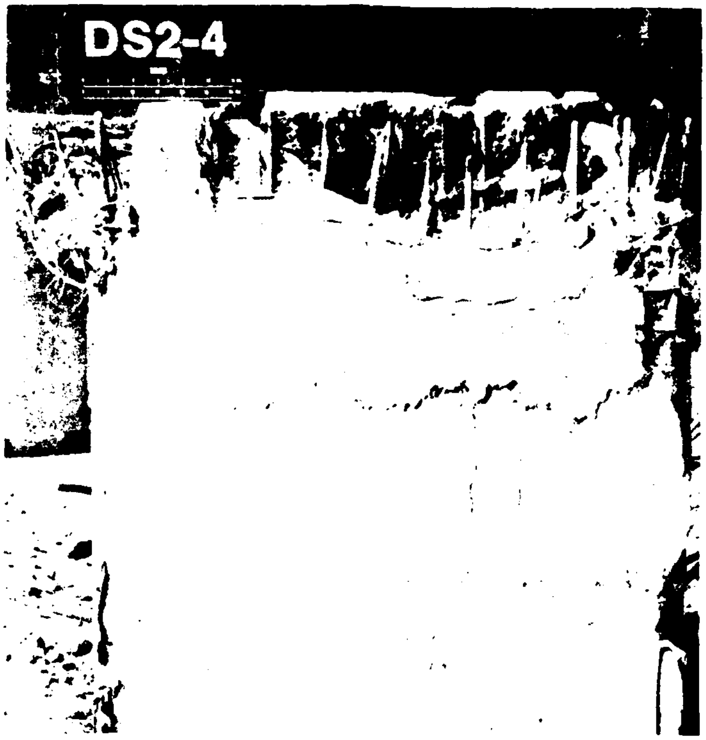

Figure 3-33. Exterior View of the East Wall, DS2-4.

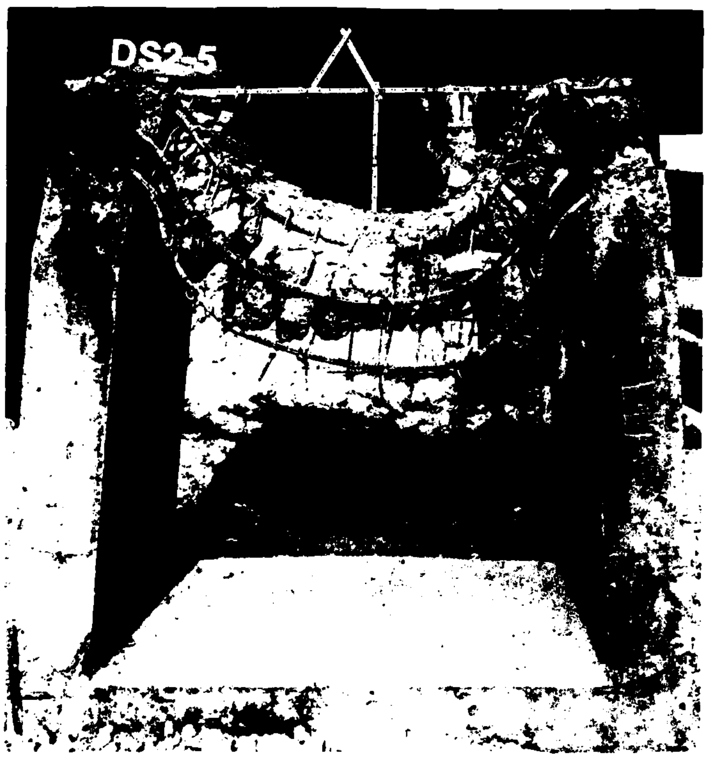

Figure 3-34. Posttest View, DS2-5.

Figure 3-35. Bottom of the Roof, DS2-5.

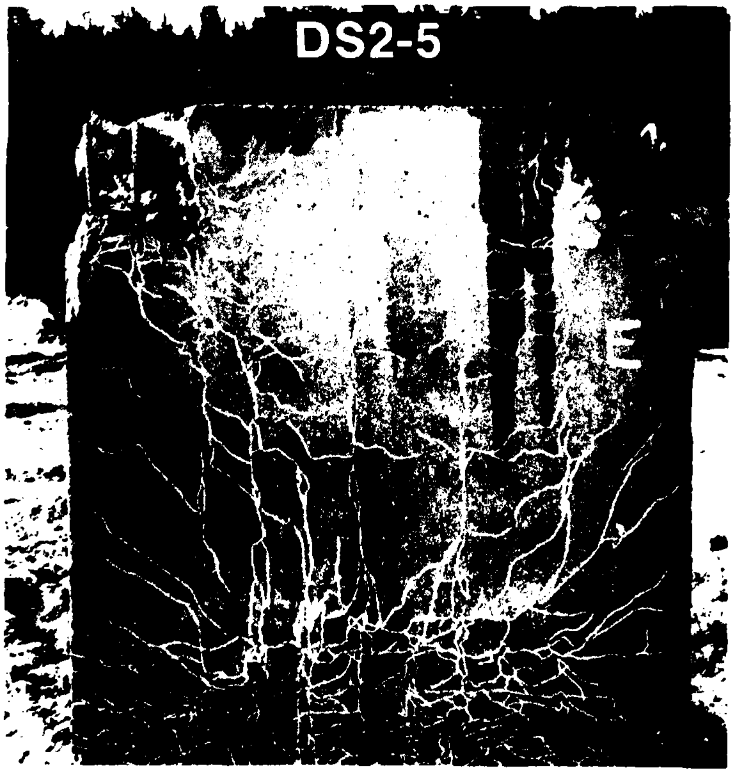

Figure 3-36. Exterior View of East Wall, DS2-5.

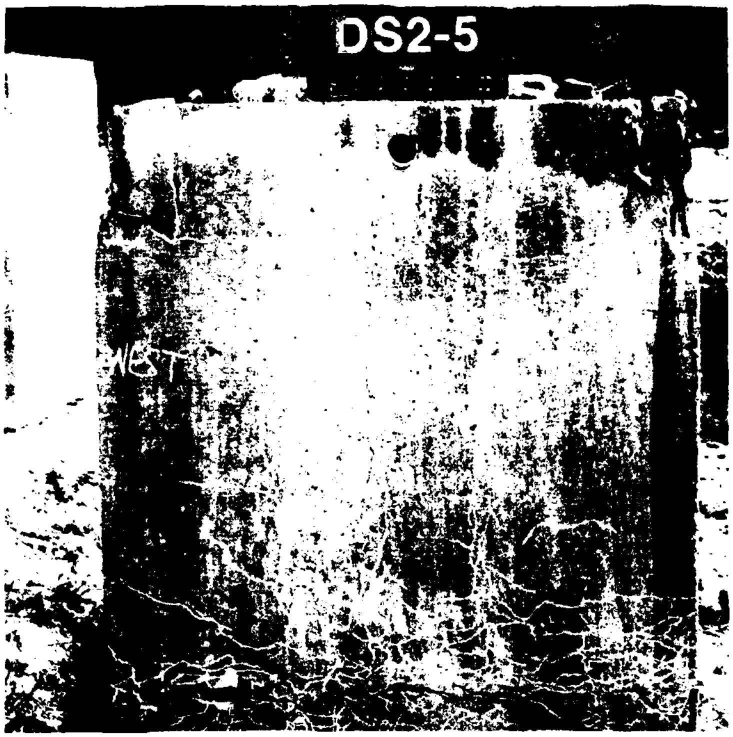

Figure 3-37. Exterior View of the West Wall, DS2-5.

Figure 3-38. Posttest View, DS2-6.

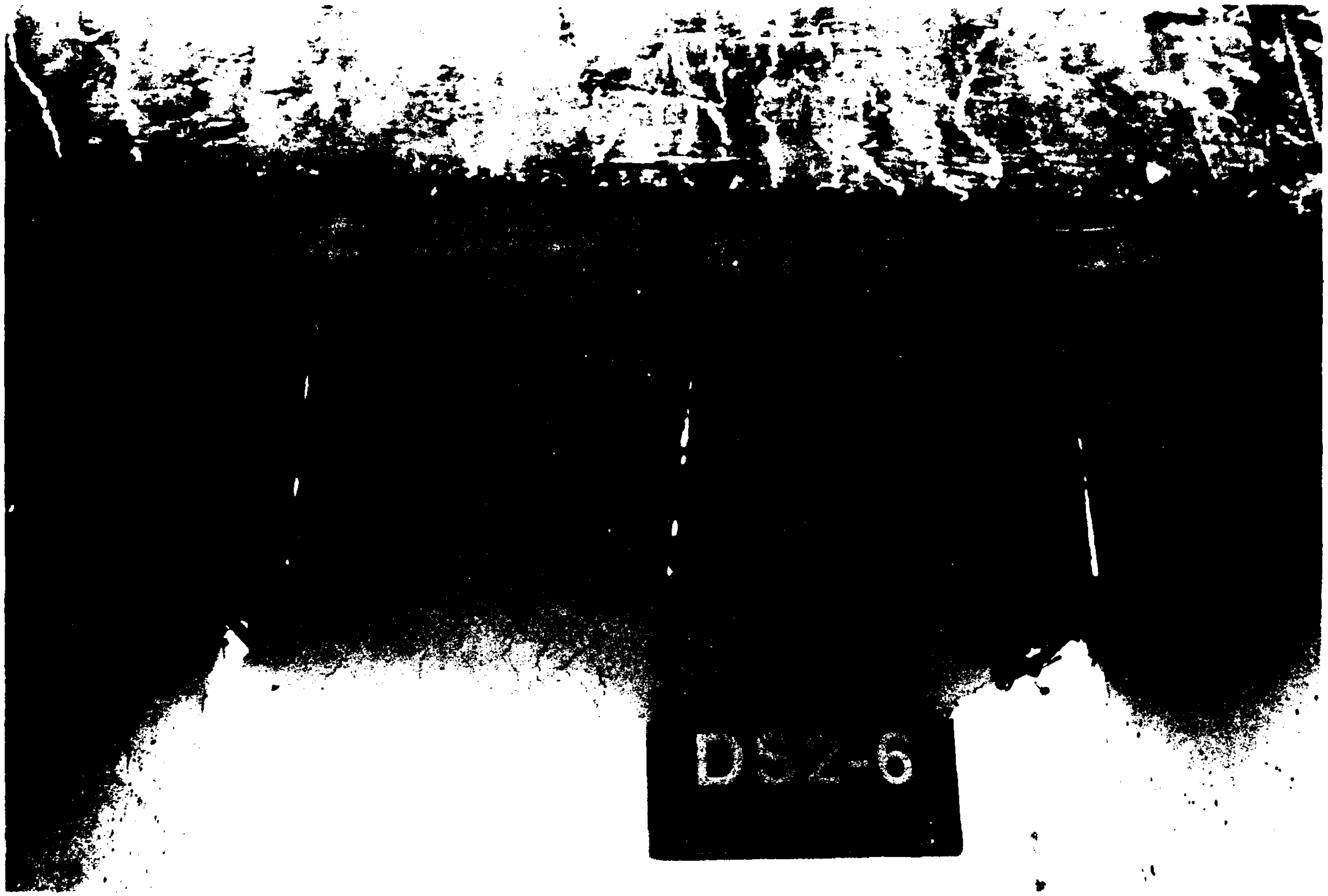

Figure 3-39. Bottom View of the Roof Slab from the North, DS2-6.

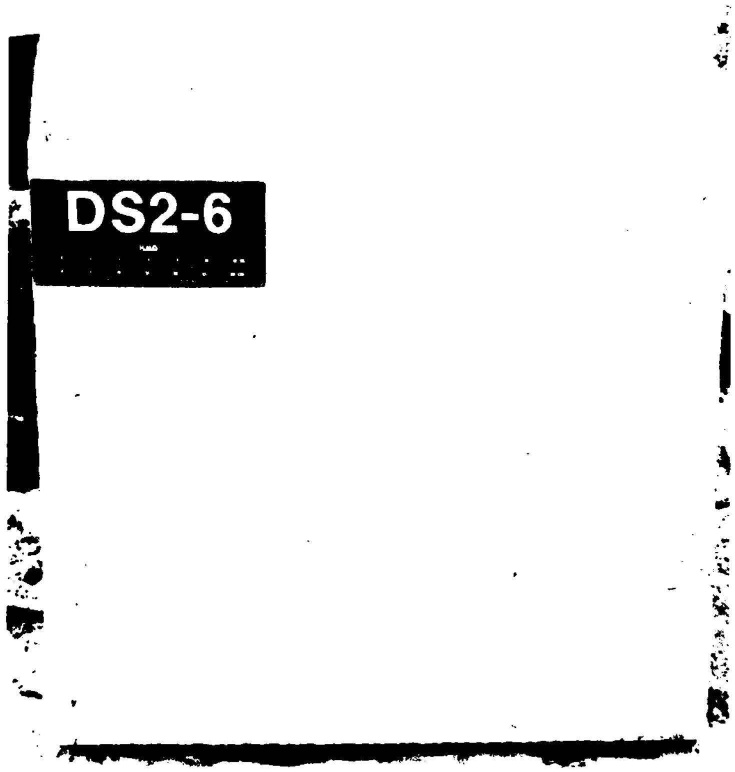

Figure 3-40. Exterior View of East Wall, DS2-6.

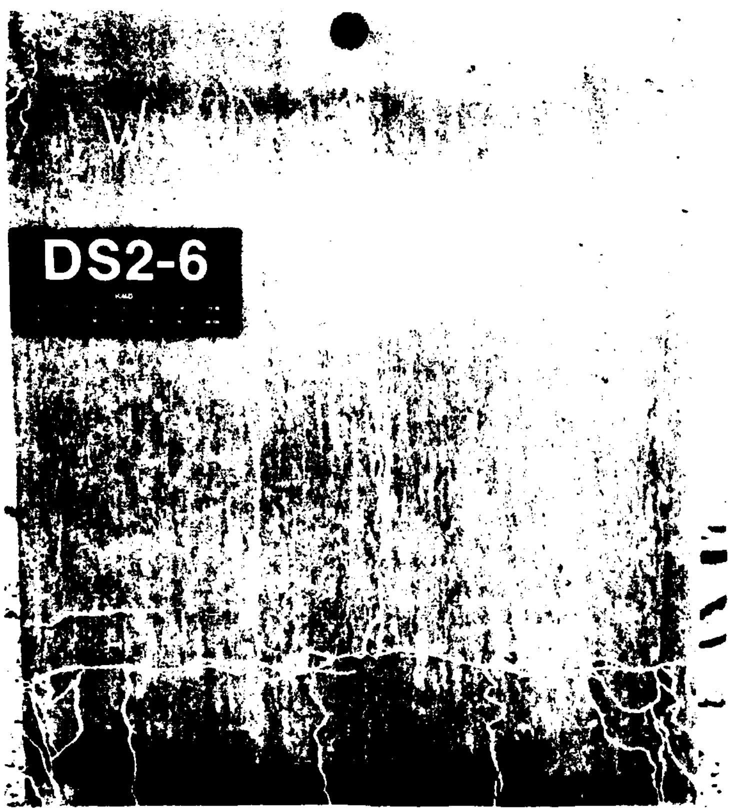

Figure 3-41. Exterior View of the West Wall, DS2-6.

CHAPTER 4: ANALYSIS

72. Chapter 4 includes weapon simulations from the recovered blast pressure records, analysis of the recovered high-speed movies, analysis of the permanent strain recovered from measurements made on the scored reinforcement steel from each test, shear strength calculations from existing failure criteria, hardness analysis of the dynamic hear test structures using a method proposed by Keenan (1977), support shear stress calculations from recovered strain data and interface pressure data for the Dynamic Shear Tests, and support shear stress calculations from a structural analysis code developed in the Shallow Buried Structures Research Program at WES.

Nuclear Weapon Simulations

73. Estimates of the surface burst nuclear yields and overpressures which best correspond to the airblast data records are required to define the loading function. The weapon simulations are determined by a least squares fit of the overpressure data to nuclear overpressure-time histories, as defined by Brode (1970) using a computer code developed by Mlakar and Walker (1980). Since the weapon simulation varies according to the length of data record, a 10-msec fit is used to simulate the weapon for the duration of interest for the dynamic shear tests. The weapon simulations for each recovered airblast data record are listed in Table 4-1. The pressure and impulse data with the best fit nuclear pressure and corresponding impulse time histories superimposed on the data for each recovered airblast pressure record are included as Appendix A.

Table 4-1. Weapon Simulations for the Dynamic Shear Tests

Test	Gage	Weapon, kt	Overpressure, psi
DS1	BP1	1.51	3,890
	BP2	0.64	4,030
	BP3	0.70	4,175
	BP4	1.12	4,345
	(Avg)	(0.99)	(4,110)
DS2	BP1	1.40	5,095
	BP2	1.12	5,310
	BP3	0.38	6,615
	BP4	0.66	5,635
	(Avg)	(0.89)	(5,665)

(Continued)

Table 4-1. (Concluded)

Test	Gage	Weapon, kt	Overpressure, psi
DS3	BP3	0.18	3,605
	BP4	0.28	3,060
	(Avg)	(0.23)	(3,330)
DS4	BP1	0.77	3,555
	BP2	0.60	4,370
	BP4	1.14	4,170
	(Avg)	(0.84)	(4,030)
DS5	BP2	2.28	7,355
	BP3	1.94	4,695
	(Avg)	(2.11)	(6,025)
DS2-1	BP1	2.35	6,690
	BP4	0.71	8,560
	(Avg)	(1.53)	(7,625)
DS2-2	BP1	2.75	5,795
	BP2	1.29	5,980
	BP3	3.81	5,145
	BP4	1.62	5,805
	(Avg)	(2.37)	(5,680)
DS2-3	BP1	0.84	3,065
	BP2	0.34	3,560
	BP3	0.52	3,320
	BP4	0.25	3,850
	(Avg)	(0.49)	(3,450)
DS2-4	BP1	1.90	5,660
	BP2	0.82	8,170
	BP3	0.87	10,815
	BP4	0.59	10,855
	(Avg)	(1.05)	(8,875)
DS2-5	BP1	4.30	4,005
	BP2	1.24	4,750
	BP4	0.64	6,350
	(Avg)	(2.06)	(5,035)
DS2-6	BP1	0.99	3,165
	BP2	0.90	3,310
	BP4	0.51	3,655
	(Avg)	(0.80)	(3,375)

High-Speed Movie Data Reduction

74. High-speed movies were recovered for the dynamic shear tests as described in Chapters 2 and 3. Displacement coordinates were determined from each recovered high-speed movie using a Vanguard Model M-16C Motion Analyzer.

For the FY 81 Dynamic Shear Tests, displacement measurements were made at 1/2-msec intervals at the supports, quarter points, and at midspan. At the supports it was very difficult to track the bottom of the roof slab due to spalling concrete. To overcome this problem, deflection probes (as shown in Figure 2-12) were added in the FY 82 Dynamic Shear Tests, and displacements were made at 1-msec intervals at each deflection probe.

75. Deflection profiles were plotted by passing a spline curve through the deflection coordinates at each time interval. For test DS1 only a centerline deflection versus time curve was plotted (see Figure 4-1) due to the difficulty of determining deflection coordinates near the support. For the remaining tests, deflection profiles were plotted (see Figures 4-2 through 4-10).

Permanent Rebar Strain

76. To determine the ductilities associated with shear failures of the box elements tested, two top reinforcement bars and two bottom reinforcement bars in the roof slab were marked along their full straight lengths using a knife edge punch with a 2-in. gage length. The distance between punch marks was measured after the tests, and the data were reduced to percent permanent strain. Permanent strains were plotted across the roof span for each scored bar from each test. The results are presented in Figures 4-11 through 4-21. Considerable scatter exists in these plots, but these data are an indication of the dowel action occurring at the support during failure of the roof slab. The length of the reinforcement effective in dowel action varied from 4 to 8 in.

Shear Strength

77. ACI (1977), based on experience, test results, and analysis, has proposed shear failure criteria for diagonal tension shear failure and direct shear failure. The diagonal tension shear failure criterion is:

$$V_n = V_c + V_s \tag{4-1}$$

where

V_n = nominal shear strength

V_c = nominal shear strength provided by concrete

V_s = nominal shear strength provided by shear reinforcement

Murtha and Crawford (1981) concluded that for beams with high shear reinforcement ratios static diagonal tension shear strength is predicted by:

$$V_n = 14.4 \sqrt{f'_c} \tag{4-1a}$$

The nominal shear strength provided by the steel is given by:

$$V_s = \frac{A_{vs} f_y}{bs} \leq 8 \sqrt{f'_c} \tag{4-2}$$

where

A_{vs} = area of vertical shear reinforcement within a distance s

f_y = yield strength of steel

b = width of the compression face

s = shear reinforcement spacing

For members subject to shear and flexure only:

$$V_c = 1.9 \sqrt{f'_c} + 2500\rho \frac{Vd}{M} \leq 3.5 \sqrt{f'_c} \tag{4-3}$$

where

$\frac{Vd}{M} \leq 1$

f'_c = concrete compressive strength

ρ = tension reinforcement ratio

V = shear force at section

d = distance from extreme compression fiber to the centroid of the longitudinal tension reinforcement

M = moment at section

78. For members subject to axial compression, Equation 4-3 may be used to compute V_c provided M_m is substituted for M and Vd/M is not limited to 1. M_m is given by:

$$M_m = M - N \frac{(4h - d)}{8} \tag{4-4}$$

where

N = axial load normal to cross section occurring simultaneously with V

h = member thickness

Also, for a member subject to axial load, the nominal shear stress provided by the concrete is limited to:

$$V_c \leq 3.5 \sqrt{f'_c} \sqrt{1 + \frac{N}{500bh}} \tag{4-5}$$

ACI proposed a criterion for direct static shear stress (shear-friction stress) to prevent failure due to the propagation of a vertical crack through the depth of the member at the location where the maximum shear stress occurs, usually at the supports. The criterion, limited to $0.2f'_c$ and 800 psi, is given by:

$$V_n = \frac{A_v f_y \mu}{bh} \tag{4-6}$$

where

A_v = area of shear-friction reinforcement

f_y = yield strength of shear-friction reinforcement

μ = coefficient of friction (1.4 for concrete cast monolithically)

79. The degree of conservatism of Equation 4-6 is shown to be a factor of 1.5 to 2.0 as a result of static tests performed by Balsara, et al. (1973) on shear keys with principal steel reinforcement ratios of 0.0072 to 0.0144. Direct shear failure was found to occur when shear stress reaches $0.3f'_c$ to $0.4f'_c$.

80. Karagozian and Case (1973) proposed a direct shear failure criterion for construction joints cast monolithically and subjected to static loadings. Construction joint strength is given by:

$$V_n = 0.16f'_c + 1.4 \left(\sigma_n + \frac{A_v f_y}{bh} \right) \leq 0.51f'_c \tag{4-7}$$

where σ_n is the applied normal stress (psi).

In Equation 4-7, the limiting strength is due to a lack of experimental data for

$$\left(\sigma_n + \frac{A_v f_y}{bh} \right) > 0.25f'_c \tag{4-8}$$

81. Murtha and Crawford (1981) proposed that a 50 percent dynamic increase factor be applied to Equations 4-1, 4-6, and 4-7 to predict shear failures due to diagonal tension and direct shear.

82. Equation 4-1a and Equation 4-7 are evaluated as dynamic shear failure criteria in the remainder of this chapter since they are upper bounds of the equations presented for diagonal tension shear failure and direct shear failure, respectively. The shear strengths for the dynamic shear tests are given in Table 4-2 (σ_n is calculated using Equation 4-14).

Table 4-2. Shear Strength Predictions for the Dynamic Shear Tests

Test	Diagonal Tension* (Eq. 4-1a, psi)	Direct Shear* (Eq. 4-7, psi)
DS1	1347	2976
DS2	1352	2995
DS3	1373	3091
DS4	1652	4475
DS5	1673	4590
DS2-1	1805	5344
DS2-2	1900	5921
DS2-3	1874	5757
DS2-4	1855	5642
DS2-5	1906	5959
DS2-6	1840	5554

* A 50 percent increase factor is used to account for increased material strengths due to dynamic application of the load.

Shear Stress Analysis

83. The purpose of this section is to use a procedure based on the method proposed by Keenan (1977) to compute diagonal tension shear stress and direct shear stress. The chart used in Keenan's procedure is based on a solution of the partial differential equation of motion of the roof (treated as a one-way beam) for various values of peak stress. Murtha and Crawford (1981) updated Keenan's Maximum Dynamic Increase Factor Chart (DIF_m). The updated

chart shown in Figure 4-25 can be used to compute the maximum dynamic shear stress. (Figure 4-24 should be used if values of t_d/T are greater than 0.9). To use the DIF_m chart, the ultimate resistance (r_u) of the roof slab, the fundamental period (T) of the roof slab, the peak applied stress (B) of the blast loading, and the duration (t_d) of the blast loading must be found. The following approach is used to determine the required parameters.

84. The peak applied stress is determined by the method used by Kiger, Slawson, and Hyde (1984). First, the peak overpressure P_{so} (an average of the peak overpressures of the nuclear weapon simulations from airblast data) is reduced by an attenuation factor (α_z) which is a function of the soil properties weapon yield, overpressure, and depth of burial. Figure 4-22 from the Air Force Systems Command (1976) is used to determine α_z for a sand backfill using a loading wave speed (C_L) in the backfill of 1500 ft/sec from Kiger, Slawson, and Hyde. The pressure is then increased by a reflection factor of 1.6 from Kiger, Slawson, and Hyde which yields the peak structure loading.

$$B = 1.6\alpha_z P_{so} \tag{4-9}$$

85. The duration of the peak reflecting pressure is given by Kiger, Slawson, and Hyde as:

$$t_d = \frac{12h}{C_c} \leq (\sqrt{r} + 1)\frac{z}{C_L} \tag{4-10}$$

where

- h = slab thickness, ft
- C_c = compression wave speed in the slab (10,000 fps)
- r = strain recovery ratio in backfill (0.1 for sand)
- z = depth of burial, ft
- C_L = loading wave speed in backfill

86. This duration is used in the idealization of the structural loading since dynamic shear failure is an early time phenomenon and is dependent upon the reflected pressure. For the dynamic shear tests the duration of the reflected pressure correlates very well with the duration t_{oo}, as suggested by Crawford, et al. (1974). The duration that fixes the slope of the equivalent

triangular load such that it is tangent to the actual overpressure-time history curve at time equals zero is t_{oo}.

87. The fundamental period of the roof slab is calculated as suggested by Biggs (1964).

$$T = 2\pi\sqrt{\frac{K_{LM}m}{k}} \qquad (4\text{-}11)$$

where

K_{LM} = load mass factor for a fixed-fixed beam

m = total mass, lb-sec^2/in.^{2}

k = stiffness of the roof slab, lb/in.

The stiffness of the roof slab is given by:

$$k = \frac{307EI}{L^3} \qquad (4\text{-}12)$$

where

E = modulus of elasticity of concrete from ACI (1977)

$E = 57{,}000\sqrt{f'_c}$, psi

I = moment of inertia, in.^{4}

The moment of inertia is taken as the average of the uncracked and cracked transformed sections which is approximated by Biggs (1964):

$$I = bd^3\left(\frac{5.5\rho + 0.083}{2}\right) \qquad (4\text{-}13)$$

88. The ultimate resistance of the roof slab is a function of the inplane thrust on the slab. The inplane thrust (P_n) and stress (σ_n) for the duration, t_d , are calculated by:

$$P_n = K_oP_{so}\alpha_z{}'t_dC_L \text{ , lb}$$

$$\sigma_n = \frac{P_n}{h} \text{ , psi} \qquad (4\text{-}14)$$

where

K_o = lateral earth pressure coefficient (0.5 for sand)

α'_z = attenuation factor from Figure 4-5 at depth, z'

$z' = z + t_d C_L/2$

The ultimate moment capacity is calculated using Figure 4-23. Equilibrium of forces yields the distance to the neutral axis, c. The ultimate moment capacity is determined by equilibrium of moments. The ultimate moment capacity of the roof slab increases from M_o (ultimate moment capacity with no inplane thrust) up to a maximum capacity M_b when the inplane thrust reaches P_b, the thrust in the balance condition (i.e., the concrete begins crushing just as the tension steel yields). Since uncertainties exist in predicting the inplane stress, the ultimate moment capacity is taken as M_b if the inplane stress is greater than or equal to the stress at the balanced condition.

89. The static collapse load (w, lb/in.) for the roof acting as a fixed-fixed beam is:

$$w = \frac{16M}{L^2} \tag{4-15}$$

90. The dynamic ultimate resistance (r_u) is taken as the static collapse load with a 50 percent dynamic increase factor as suggested by Murtha and Crawford (1981).

$$r_u = 1.5w \tag{4-16}$$

91. A Dynamic Increase Factor (DIF_m) is determined using Figures 4-24 and 4-25 and the parameters B/r_u and t_d/T. The maximum dynamic support shear stress is calculated using Equation 4-17.

$$V = (DIF_m)\ \frac{r_u L}{2h} \tag{4-17}$$

92. A sample analysis is presented in Appendix B for test DS1. The structural details of the test elements are summarized below in Table 4-3. Determination of structure and load parameters for all dynamic shear tests are presented in Table 4-4. Maximum dynamic support shear stresses for dynamic shear tests are presented in Table 4-5.

Table 4-3. Roof Properties for the Dynamic Shear Test Elements

Property*	DS1/5	DS2-1/3	DS2-4/6
Effective depth, d (in.)	4.8	6.44	6.44
Roof thickness, h (in.)	5.6	7.25	7.25
Section width, b (in.)**	1.0	1.0	1.0
Clear span, L (in.)	48.0	44.75	44.75
Mass, m ($lb\text{-}sec^2/in.^2$)	0.06275	0.07510	0.07642
Tensio steel ratio, ρ	0.01	0.0075	0.012
Compression steel ratio, ρ'	0.01	0.0075	0.012
Stirrup ratio, A_v/b_s	0.014	0.0077	0.0077

* See Chapter 2 for material properties.
** For analysis purposes.

Calculation of Dynamic Support Shear from Strain and Interface Pressure Data

93. In this section the support shear stresses are calculated from the Dynamic Shear Test data.

94. Strain data for the dynamic shear tests were recorded from gages located at the top of the walls on the inside and outside rebar as described in Chapter 2. Also, interface pressure data from Gage IF1 were recorded directly over the wall. Gage locations are shown in Figure 4-26.

95. The support shear is calculated by satisfying equilibrium of vertical forces in the free-body diagram shown in Figure 4-27.

96. To calculate the axial wall thrust from strain gage data, constitutive equations for steel and concrete are required. For steel an elastic-plastic-strain hardening model as shown in Figure 4-28 is used as suggested by Mahin and Bertero (1977). The model is elastic in tension and compression until the steel yields, plastic from the yield point until the strain reaches ±10,000 μin./in., and strain hardening until stress equals 1.6 times the yield stress at strain values of ±100,000 μin./in. Stress is constant ($1.6f_y$) at strain magnitudes greater than 100,000 μin./in. The stress-strain relation in the strain hardening region is given by:

Table 4-4. Determination of Slab and Loading Parameters

Test	T msec	t_d msec	w kt	P_{so} psi	α_z	B psi	α_z	σ_n psi	σ_{nb} psi	M in.-lb	r_u lb/in.
DS1	4.66	0.56	0.99	4109	0.75	4931	0.63	2330	1393	24,640	257
DS2	4.65	0.56	0.89	5664	0.72	6525	0.57	2906	1402	24,720	258
DS3	4.61	0.56	0.23	3333	0.62	3306	0.53	1590	1444	25,120	262
DS4	4.21	0.56	0.83	4031	0.74	4773	0.61	2213	1870	30,300	316
DS5	4.18	0.56	2.11	6025	0.78	7519	0.67	3633	1899	30,690	320
DS2-1	2.69	0.66	1.53	7624	0.75	9149	0.58	3623	1842	54,040	648
DS2-2	2.62	0.66	2.37	5682	0.81	7364	0.68	3166	1935	56,630	679
DS2-3	2.64	0.66	0.49	3448	0.72	3972	0.56	1582	1911	52,000	623
DS2-4	2.44	0.66	1.04	8875	0.69	9798	0.48	3490	2143	66,220	794
DS2-5	2.41	0.66	2.06	5034	0.81	6524	0.68	2805	2195	67,710	811
DS2-6	2.45	0.66	0.80	3377	0.77	4160	0.61	1688	2127	61,000	731

$$\sigma = A + B\varepsilon + C\varepsilon^2 + D\varepsilon^3 \tag{4-18}$$

where

σ = stress, psi

ε = strain, μin./in.

A,B,C,D = constants

The constants are determined from the following boundary conditions:

1. $\sigma = f_y$ when ε = 10,000 μin./in.
2. $\sigma = 1.6f_y$ when ε = 100,000 μin./in.
3. The initial strain hardening modulus equals 1.5×10^6 psi.
4. The final strain hardening modulus equals 0.

The concrete model can be represented by the family of curves from Wang and Salmon (1979) shown in Figure 4-29. The stress-strain relationship for concrete will be approximated by a parabola of the general form:

$$\sigma_c = -b(\varepsilon_o - \varepsilon_c)^2 + a \tag{4-19}$$

Table 4-5. Maximum Dynamic Support Shearing Stress and Shearing Stress at a Distance d from the Face of the Support

Test	B/r_u	t_d/T	DIF_m	V, psi	V_d, psi
DS1	19.2	0.12	3.4	3745	3495
DS2	25.3	0.12	4.1	4533	4231
DS3	12.6	0.12	2.7	3032	2830
DS4	15.1	0.13	3.1	4198	3918
DS5	23.5	0.13	4.0	5486	5120
DS2-1	14.1	0.25	3.4	6800	5452
DS2-2	10.8	0.25	2.8	5867	4704
DS2-3	6.4	0.25	1.9	3653	2929
DS2-4	12.3	0.27	3.2	7841	6287
DS2-5	8.0	0.27	2.4	6007	4816
DS2-6	5.7	0.27	1.7	3835	3075

where

σ_c = concrete stress, psi

ε_o = constant, the strain at which the tangent to the stress-strain diagram is horizontal, in./in.

ε_c = concrete strain, in./in.

$a = 0.9f'_c + 300$, psi (for $f'_c \geq 3000$ psi)

From Figure 4-29 a value of ε_o equal to 0.0019 is appropriate. From the boundary condition, σ_c must equal zero when ε_c equals zero:

$$b = \frac{a}{(0.0019)^2} \tag{4-20}$$

Therefore, by substitution of Equation 4-18 into Equation 4-17 the constitutive equation for the concrete model may be written as:

$$\sigma_c = \frac{-(0.9f'_c + 300)(0.0019 - \varepsilon_c)^2}{(0.0019)^2} + (0.9f'_c + 300) \tag{4-21}$$

The concrete model is shown in Figure 4-30. Concrete stress, σ_c, remains constant at strains greater than 0.003 in./in.

97. Plasticity effects on the stress-strain relations are considered for loading, unloading, and reloading for both the steel and concrete models. For the steel model the unloading and reloading slope is equal to E, Young's Modulus, which is taken as 29×10^6 psi. For the concrete model the unloading and reloading slope is taken as the slope of the tangent to the stress-strain curve (DC in Figure 4-11) at zero strain and is given by:

$$DC = \frac{2a}{0.0019} \tag{4-22}$$

For concrete stresses less than 30 percent of f'_c unloading is along the initial loading curve (elastic). The loading histories for the inside steel, the outside steel, and 100 equal increments of concrete across the wall section are considered in conjunction with the constitutive equations in calculating stresses.

98. As the first step in calculating the axial thrust in the wall the strain is determined from the known strains on the inside rebar (ε'_s) and the outside rebar (ε_s) as shown in Figure 4-31. The concrete strain at any

location, X , from the outside face of the wall is given by:

$$\varepsilon_c = -[\varepsilon_{of} + XK(X)] \tag{4-23}$$

where

$XK = (\varepsilon_s' - \varepsilon_s)/(d - d')$

$\varepsilon_{of} = \varepsilon_s' - XK(d)$

The average concrete strain (ε_c) for each of 100 increments across the wall section is determined, and the corresponding stress (σ_c) is found from the concrete constitutive equations. The concrete compressive force (FC) is found by summing the incremental concrete forces over the thickness (h) of the wall section.

$$FC = \int_0^h \sigma_c b dx = \frac{h}{100} \sum_{i=1}^{100} \sigma_{c_i} b \tag{4-24}$$

where b is a unit width. The stresses (σ_s and σ_s') in the reinforcing steel are determined using the known strain data and the steel constitutive equations. The forces in the outside rebar (FS) and the inside rebar (FSP) are calculated as the product of the stresses and the reinforcement steel areas. The axial wall thrust (T_w) is then given by:

$$T_w = (FC + FS + FSP) \tag{4-25}$$

Satisfying equilibrium of vertical forces in Figure 4-27 yields the support shear.

$$V_R = T_w - P - S + m\ddot{y} \tag{4-26}$$

The contribution of the frictional force (S) may be neglected due to relatively small magnitude as compared with the force (P) due to overwall stresses. Since rigid body motion of the test element walls is small the acceleration, $\ddot{y}$, will be taken as zero (see Figure 4-27). Therefore, the support shear is the axial thrust in the wall (T_w) minus the overwall force (P). P is calculated as the interface pressure at the top of the wall times the thickness of the wall (h) times a unit width (b). The average support shearing stress may

then be calculated by dividing the support shear by the roof slab thickness (h) and a unit width (b).

$$V = \frac{V_R}{h} \tag{4-27}$$

99. A computer code (SHEAR) using this procedure is included in Appendix C. The results of analysis of the dynamic shear test data using the SHEAR code are presented in Figures 4-32 through 4-41.

100. To account for the increase in material strengths due to the dynamic application of the structure loading, the static compressive strength of the concrete and the static tensile yield strength of the reinforcing steel is increased by 50 percent as suggested by Murtha and Crawford (1981). Also, unloading and reloading in the plastic region is not considered in these runs since it does not affect the early time results. Results of these analyses are summarized in Table 4-6. The analysis for test DS2 is not included since the data appear to be bad. For tests DS1 and DS2-1 the durations of recovered data are not long enough to reach the time of maximum shear; therefore, the results are not the absolute maximum shearing stresses (V_{max}) but are the maximum shearing stresses for the given data durations. For this reason V_{max} for test DS1 is lower than V_{max} for test DS3, and V_{max} for test DS2-1 is lower than V_{max} for tests DS2-2 and DS2-3. This is inconsistent with the expected results since test DS3 was at a lower pressure level than test DS1, and tests DS2-2 and DS2-3 were at lower pressure levels than test DS2-1. Analysis results are inconsistent for tests DS4 and DS5. As far as test pressure levels are concerned, test DS5 should result in higher support shearing stresses than test DS4. Analysis of tests DS4 and DS5 neglecting the interface pressure over the wall yields maximum support shear stresses of 7467 psi and 9062 psi, respectively. This is consistent with the strain data (Appendix E) which shows larger strains and higher strain rates for test DS5. Also, test DS3 is inconsistent with tests DS4 and DS5. Both tests DS4 and DS5 should yield higher support shear stress than test DS3 since the test pressure levels are higher. For the FY 82 dynamic shear tests (DS2-1 through DS2-6) the data analysis results are consistent with the expected results based on test pressure levels.

101. There exists considerable scatter in the results of the data analyses shown in Table 4-6. Some of the scatter is due to the extremely high pressure levels producing rebar strains that are at the upper limits of the

Table 4-6. Results of SHEAR Analysis of Data
from the Dynamic Shear Tests

Test	Computed Shear Stress, V, psi
DS1	2855*
DS2	**
DS3	4755
DS4	4698
DS5	4037
DS2-1	5451*
DS2-2	6339
DS2-3	6005
DS2-4	9656
DS2-5	5910
DS2-6	5715

* Data durations did not extend to time of maximum shearing stress.
** Data for test DS2 were bad.

range of the strain gages. Even though scatter exists, the shear stress calculations are useful. These calculations confirm that the DIF method used to predict shearing stresses in the preceding section (Table 4-5) gives results that are comparable to the stresses in Table 4-6.

Comparison of Analysis

102. Table 4-7 compares the results of the direct shear strength calculations (Equation 4-7) with the shear stress calculations using the DIF method as described in this chapter and with the shear stress calculations using data from the FY 82 dynamic shear tests. Also included in this comparison are shear stress calculations by an existing vulnerability program (VSBS) as described by Kiger, Slawson, and Hyde which uses the DIF method for calculating shear stress but uses different methods from those presented in this chapter for calculating the parameters r_u, t_d, and T.

103. There is a very good correlation between the shear stress calculations using the DIF method and the VSBS program, as might be expected.

Table 4-7. Comparison of Computed Direct Shear Strength, Predicted Shear Stresses, and Shear Stresses Calculated from Test Data

Test	Shear Strength (Eq. 4-7) psi	Shear Stress (DIF Method) psi	Shear Stress* (VSBS) psi	Shear Stress (SHEAR Program) psi
DS1	2976	3745	4084	**
DS2	2995	4533	4948	**
DS3	3091	3032	3247	**
DS4	4475	4198	4321	**
DS5	4590	5486	5853	**
DS2-1	5344	6800	6607	5451†
DS2-2	5921	5867	5913	6339
DS2-3	5757	3653	3612	6005
DS2-4	5642	7841	7841	9656
DS2-5	5959	6007	6027	5910
DS2-6	5554	3835	4017	5715

* The VSBS code uses a variation of Keenan's (1977) DIF method in predicting shear stresses.
** Results were inconsistent based on test pressure levels.
† Data duration did not extend to peak shearing stress.

Comparing the shear strength predictions (Equation 4-7) to the shear stress values using the DIF method results in direct shear failures for tests DS1, DS2, DS5, DS2-1, DS2-4, and DS2-5 with tests DS3 and DS2-2 resulting in impending direct shear failures. Based on test data and high-speed movies, only tests DS2-1 and DS2-4 are considered direct shear failures. A comparison of shear stress calculations from the DIF method and from the code SHEAR using FY 82 test data reveals that the DIF method does not overpredict the support shearing stresses. Thus, a revision of the shear strength failure criteria (Equation 4-7) is in order. Since the pressure levels for tests DS2-1 and DS2-4 are above the threshold loading for direct shear failure tests, DS2, DS5, and DS2-2 are included in the determination of an increase factor to modify Equation 4-7 since these three tests are considered to be just below the threshold loading for direct shear failure. If the calculations for tests DS2, DS5, DS2-1, DS2-2, and DS2-4 are used, a mean increase factor of 1.27 is

determined with a range of 0.52 and a standard deviation of 0.20. It is suggested that the increase factor of 1.27 be applied to the upper bound on Equation 4-7, in addition to the 50 percent increase factor for dynamic loading. The increase factor was determined using the upper bound, therefore Equation 4-7 should be increased by 50 percent. Equation 4-28 should be used to predict shear strength.

$$V_n = 0.24f'_c + 2.1\left(\sigma_n + \frac{A_v f_y}{bh}\right) \leq 0.97f'_c \qquad (4\text{-}28)$$

104. Table 4-8 compares the diagonal tension shear strength (Equation 4-1a) with the shear stress calculations using the DIF method. Tests DS1,

Table 4-8. Comparison of Computed Diagonal Tension Shear Strength and Shear Stresses

Test	Shear Strength (Eq. 4-1a) psi	Shear Stress (DIF Method) psi
DS1	1347	3495
DS2	1352	4231
DS3	1373	2830
DS4	1652	3915
DS5	1673	5120
DS2-1	1805	5452
DS2-2	1900	4704
DS2-3	1874	2929
DS2-4	1855	6287
DS2-5	1906	4816
DS2-6	1840	3075

DS4, and DS2-2 are used as upper bounds for diagonal tension failure while tests DS3, DS2-3, and DS2-5 are used as lower bounds to bracket the threshold of diagonal tension shear failure. From a comparison of the shear stresses computed using the DIF method for these tests to the shear strength as predicted by Equation 4-1a, a mean increase factor of 2.27 is determined with a range of 1.03 and a standard deviation of 0.39. Using an increase factor

of 2.27 and a 50 percent increase to account for the increase in material strengths due to dynamic load application (Equation 4-1a) gives the dynamic diagonal tension shear strength for members with high shear reinforcement ratio. Equation 4-29 is the modified diagonal tension shear failure criterion.

$$V_n = 49\sqrt{f'_c} \qquad (4\text{-}29)$$

105. It is proposed, therefore, that Equations 4-28 and 4-29 be used as direct shear and diagonal tension shear failure criteria, respectively.

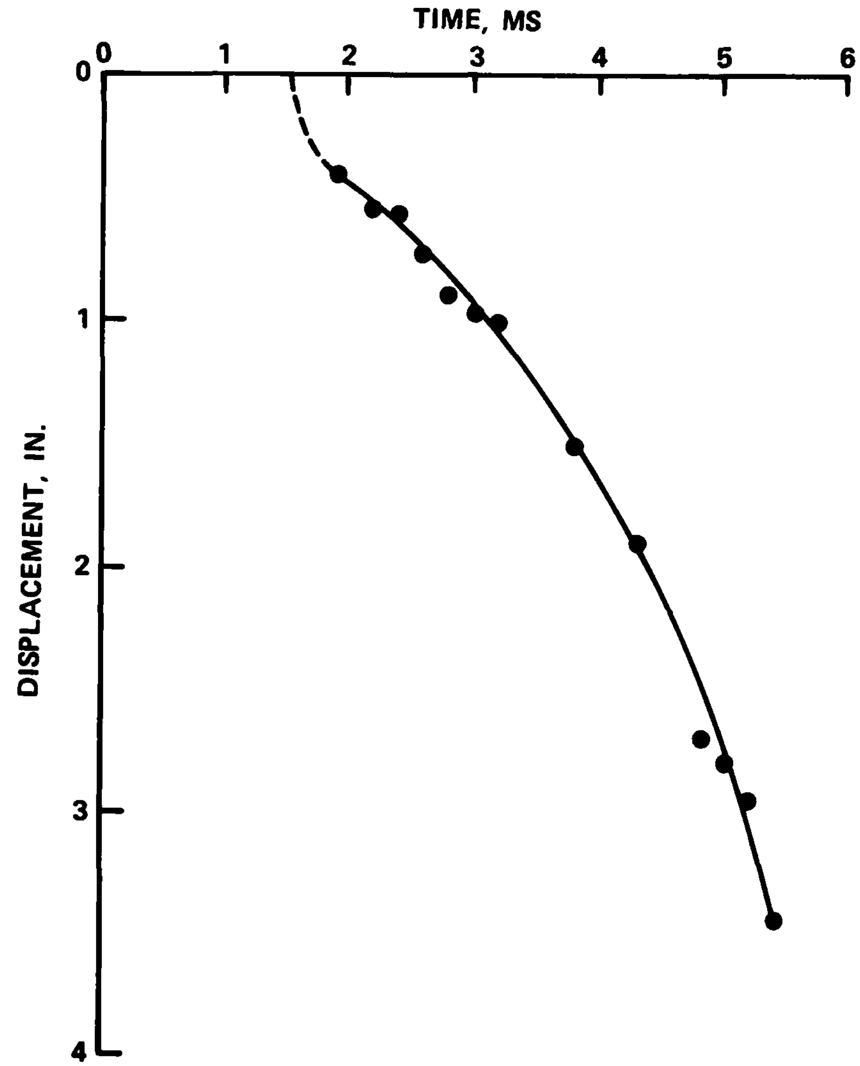

Figure 4-1. Center-Line Displacement Versus Time Plot for DS1.

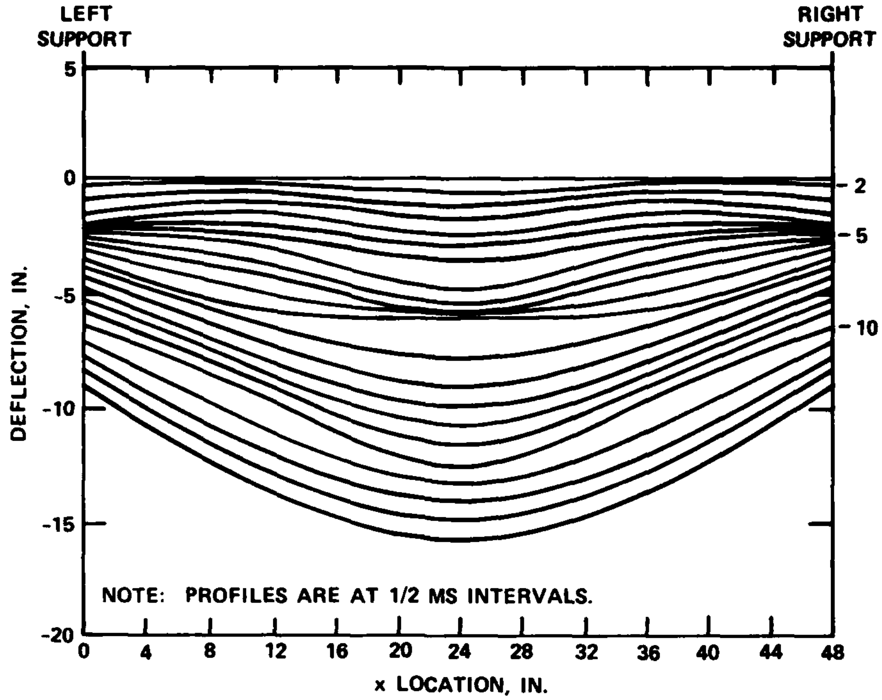

Figure 4-2. DS3 Roof Deflection Profiles.

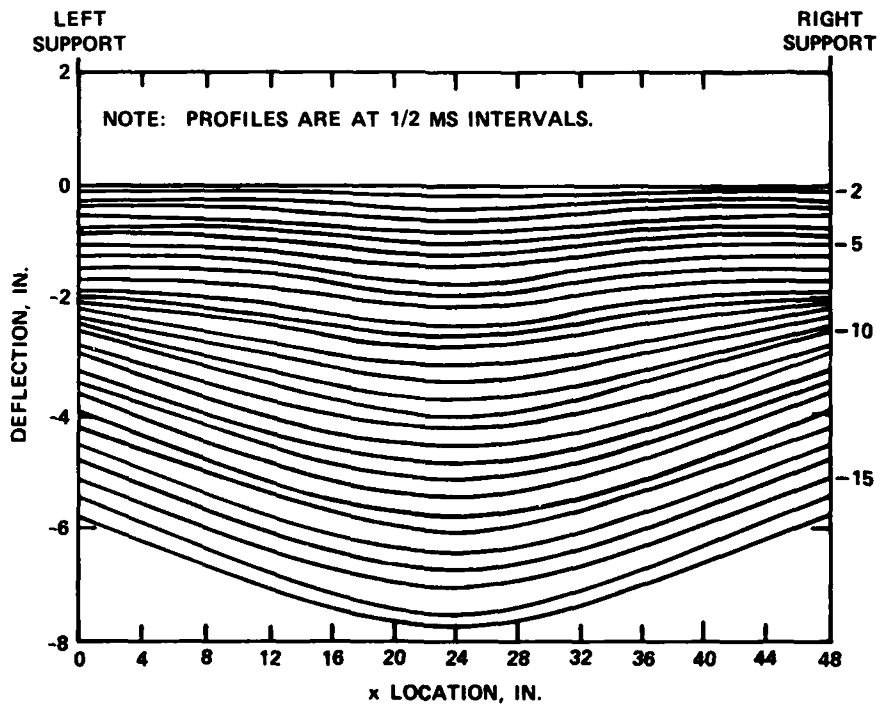

Figure 4-3. Permanent Strain of Rebar for DS2-1.

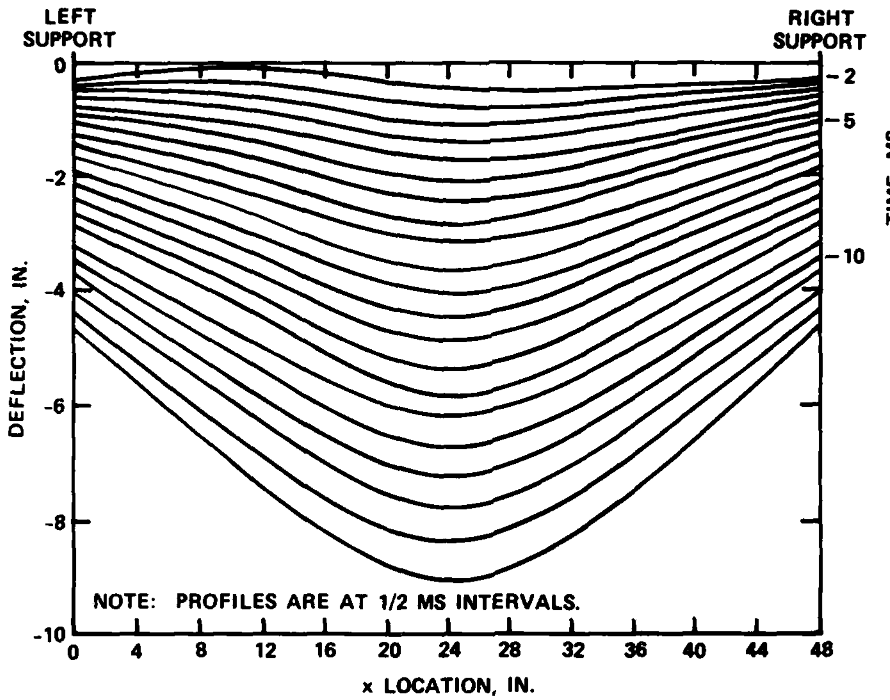

Figure 4-4. DS4 Roof Deflection Profiles.

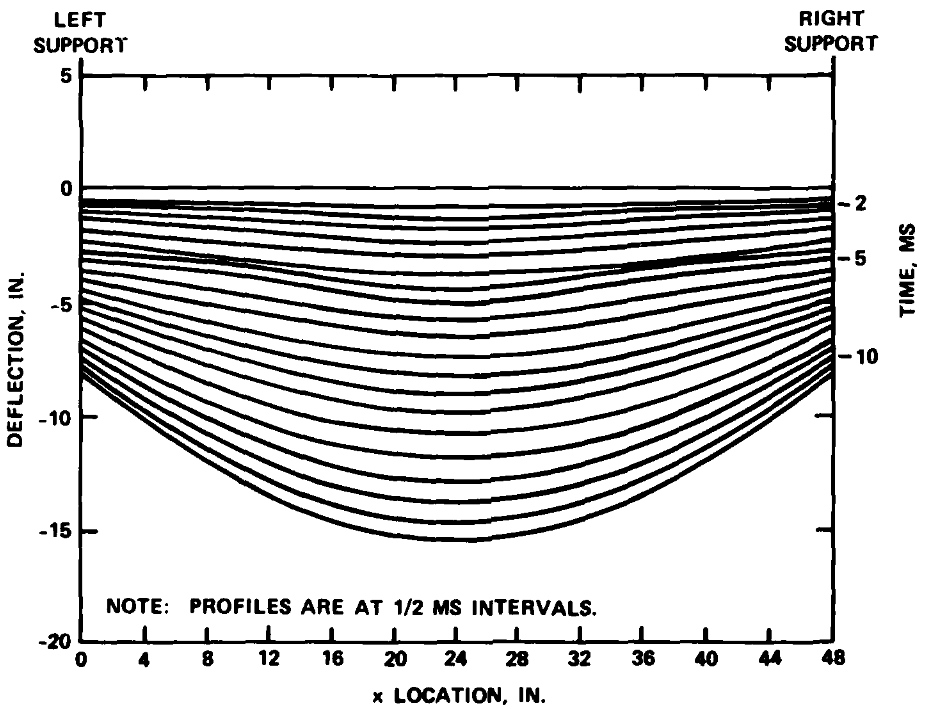

Figure 4-5. DS5 Roof Deflection Profiles.

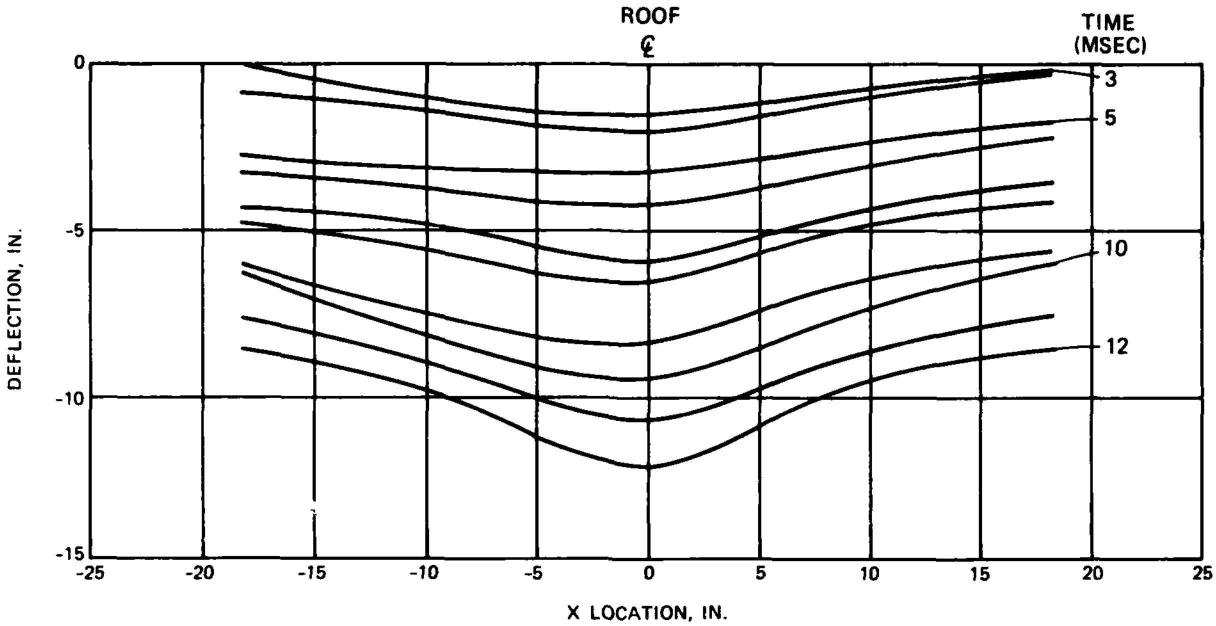

Figure 4-6. DS2-1 Roof Deflection Profiles.

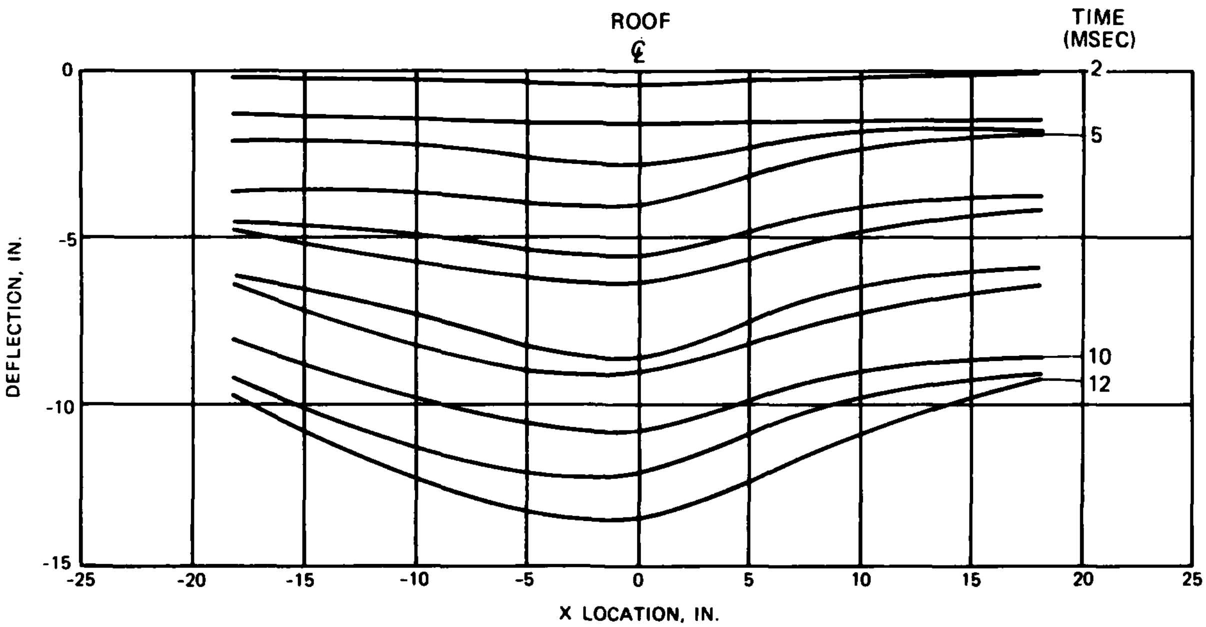

Figure 4-7. DS2-2 Roof Deflection Profiles.

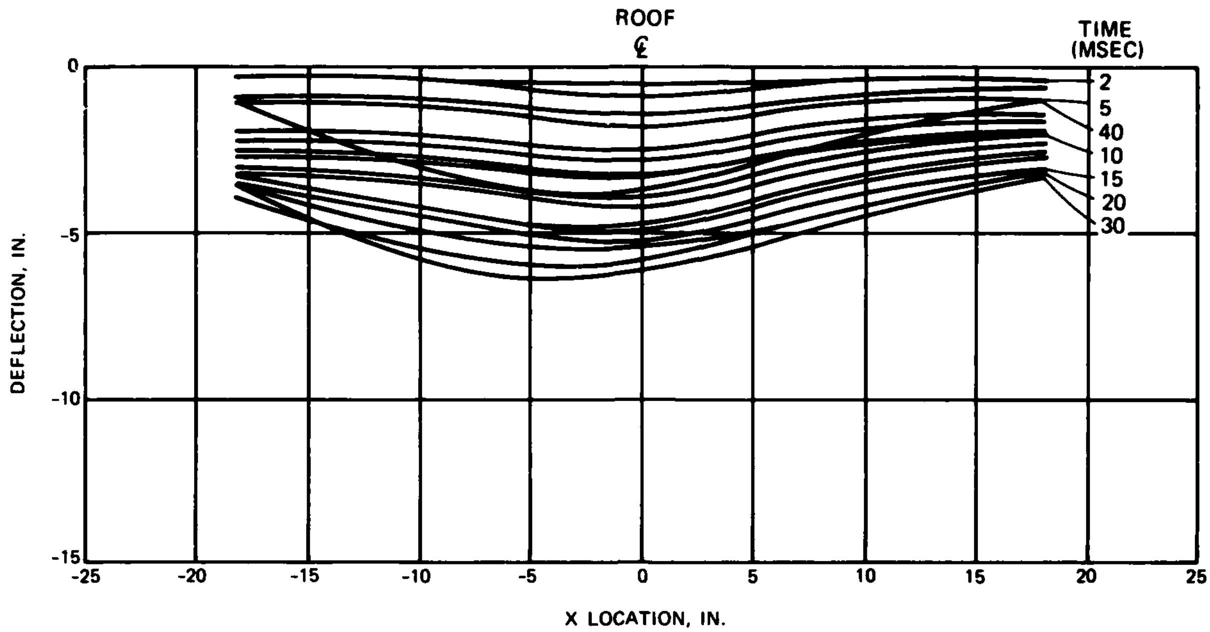

Figure 4-8. DS2-3 Roof Deflection Profiles.

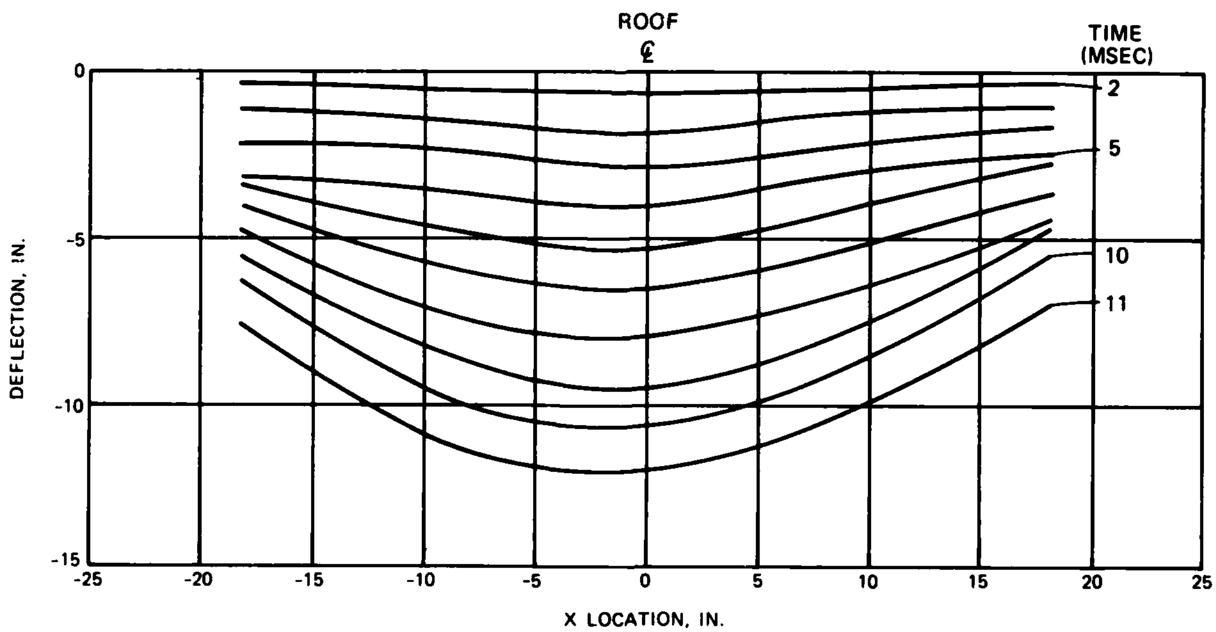

Figure 4-9. DS2-4 Roof Deflection Profiles.

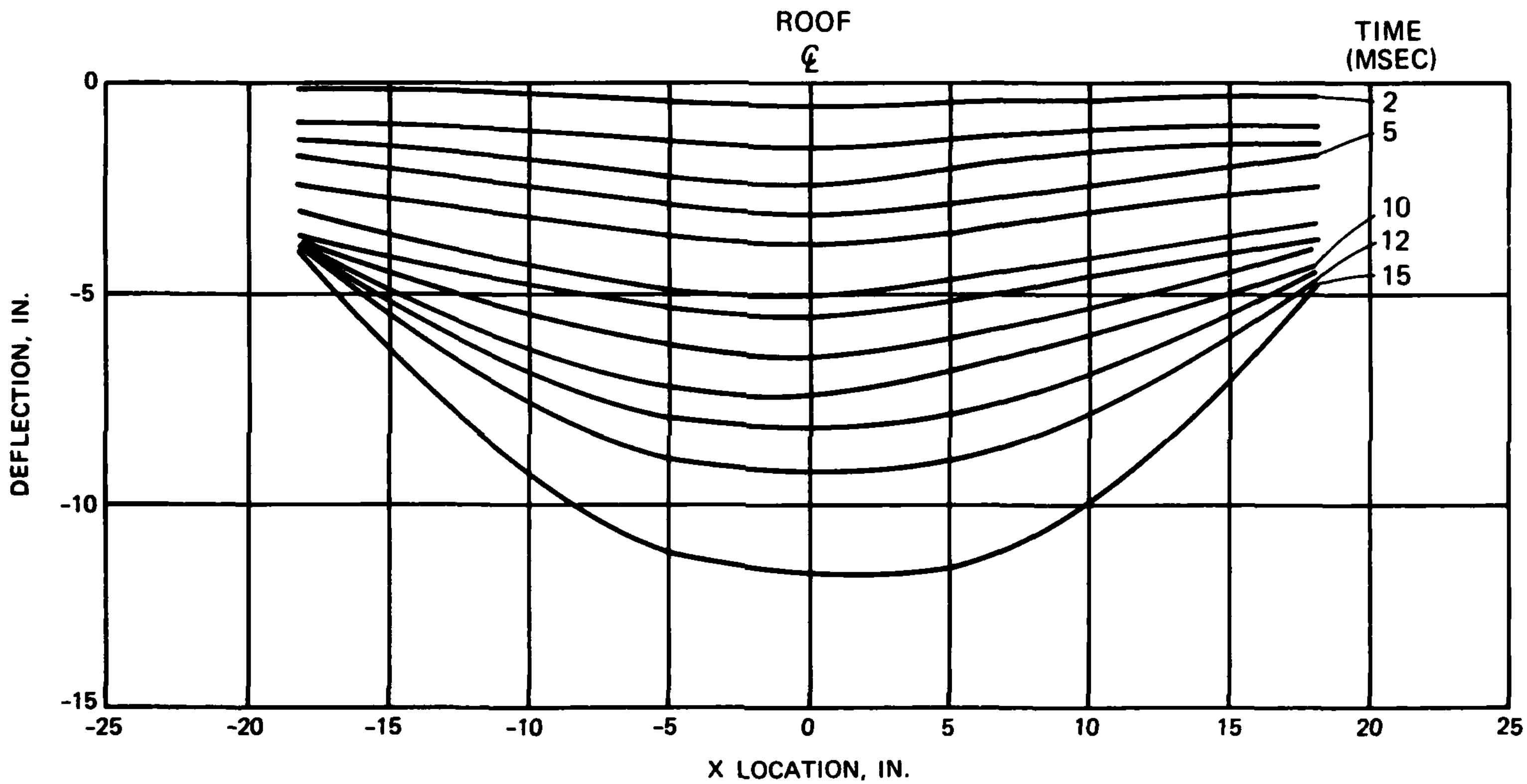

Figure 4-10. DS2-5 Roof Deflection Profiles.

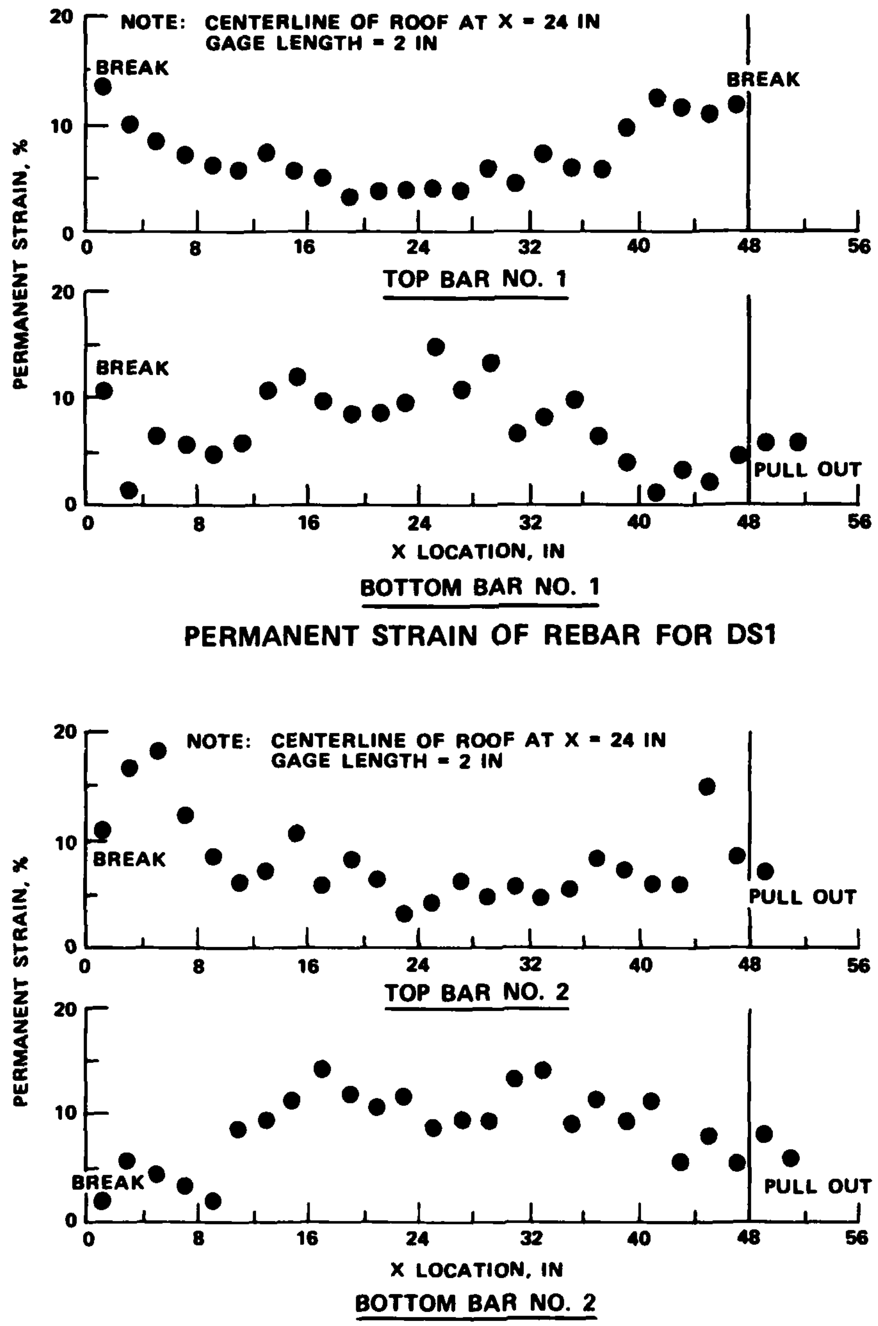

Figure 4-11. Permanent Strain of Rebar for DS1.

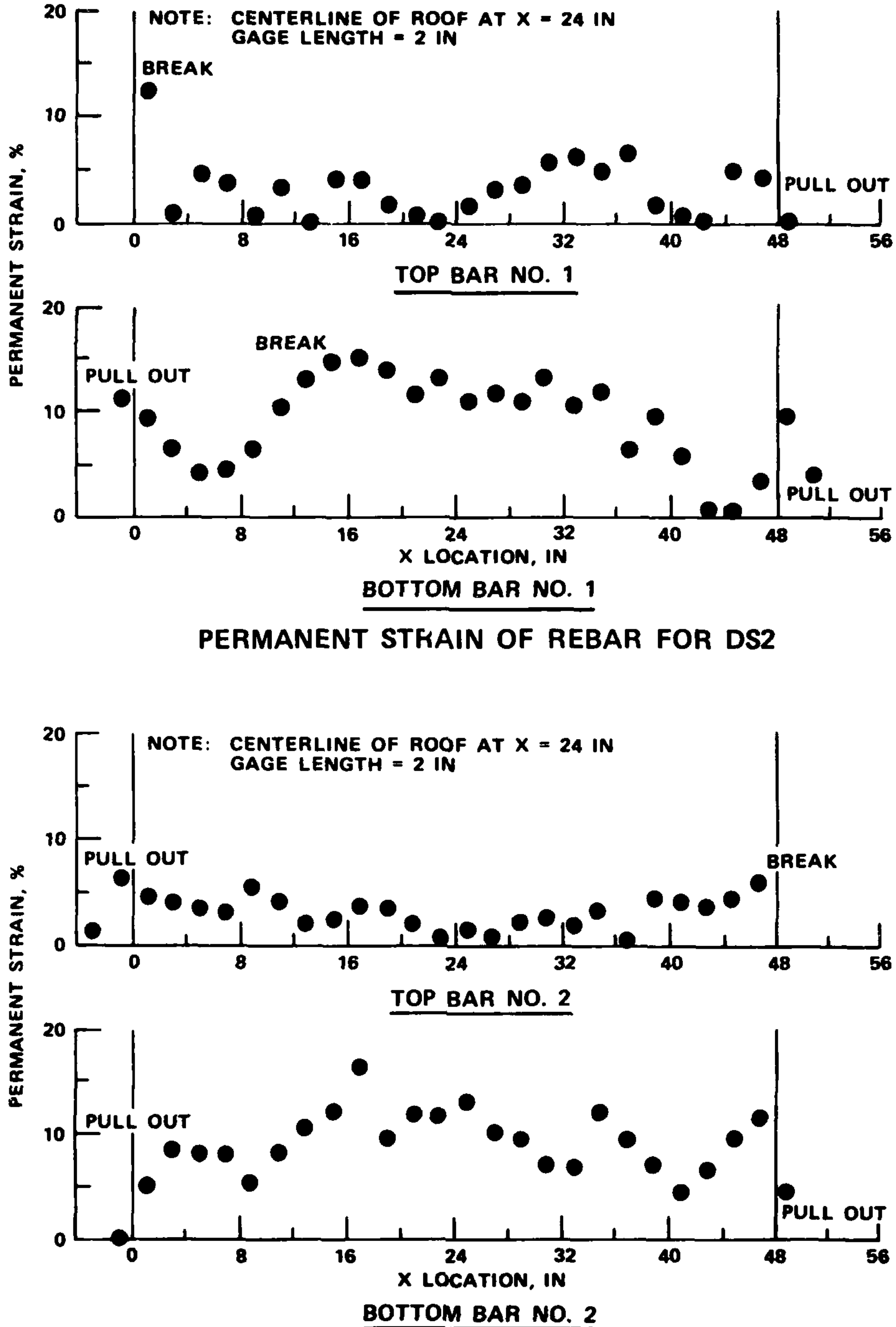

Figure 4-12. Permanent Strain of Rebar for DS2.

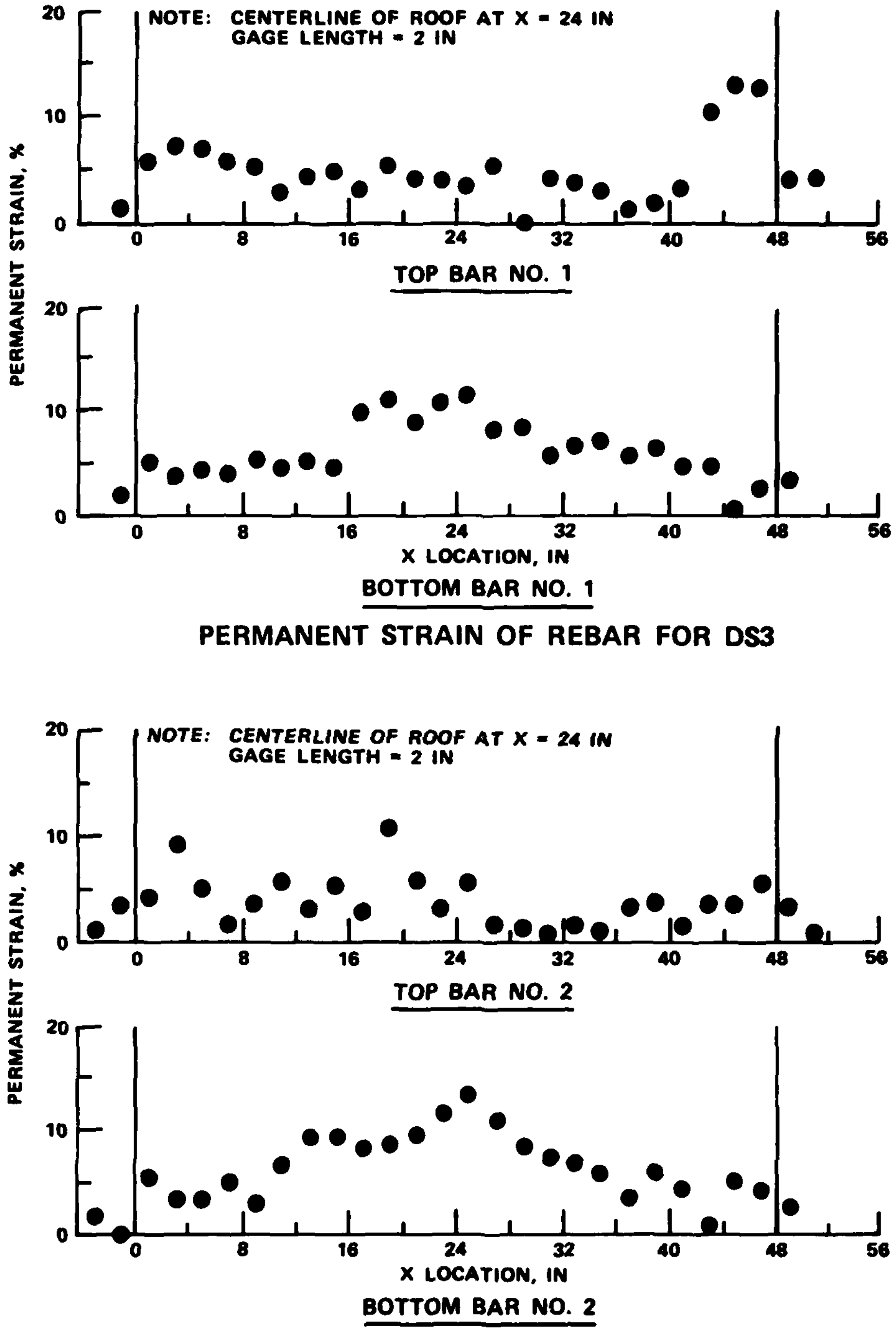

Figure 4-13. Permanent Strain of Rebar for DS3.

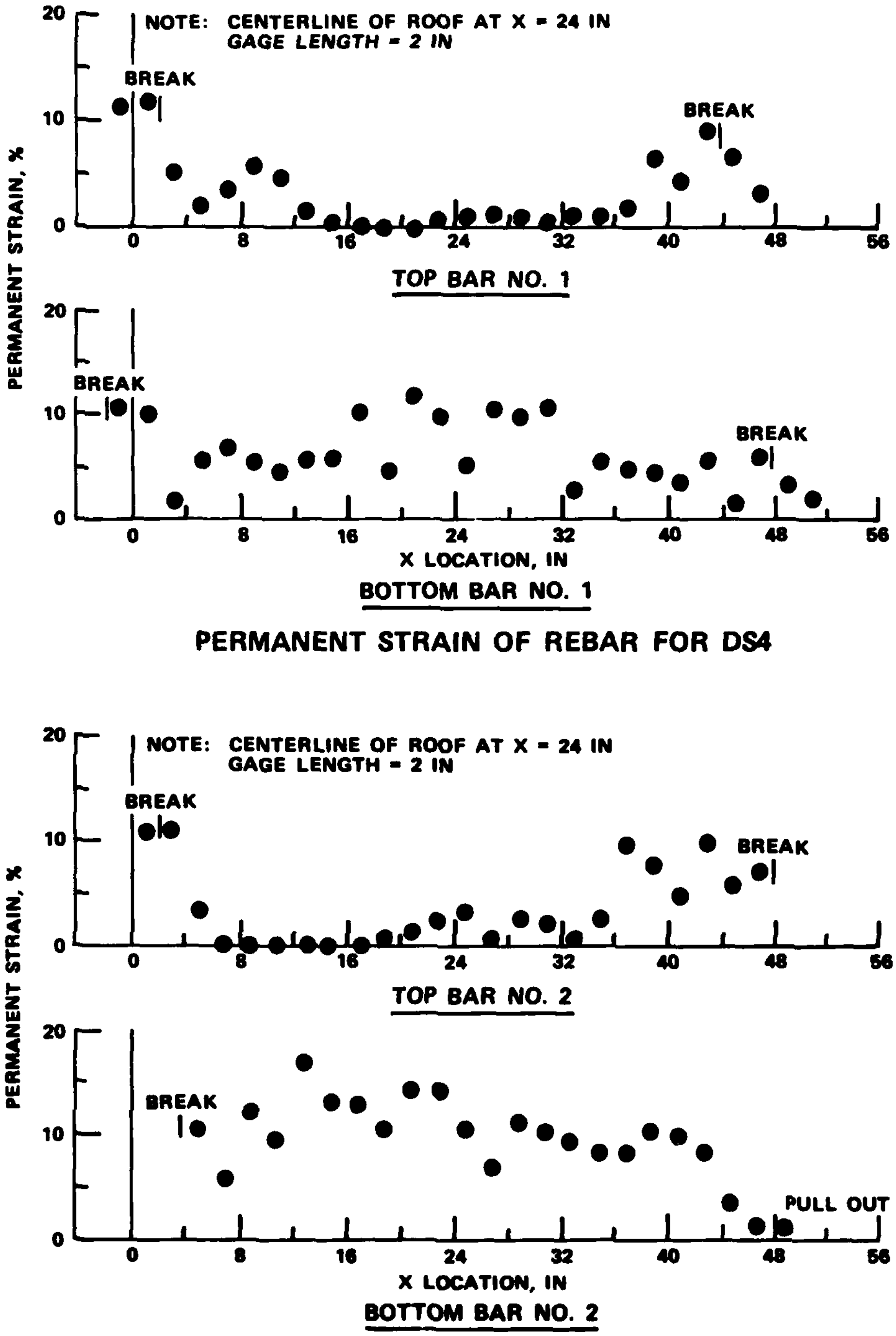

Figure 4-14. Permanent Strain of Rebar for DS4.

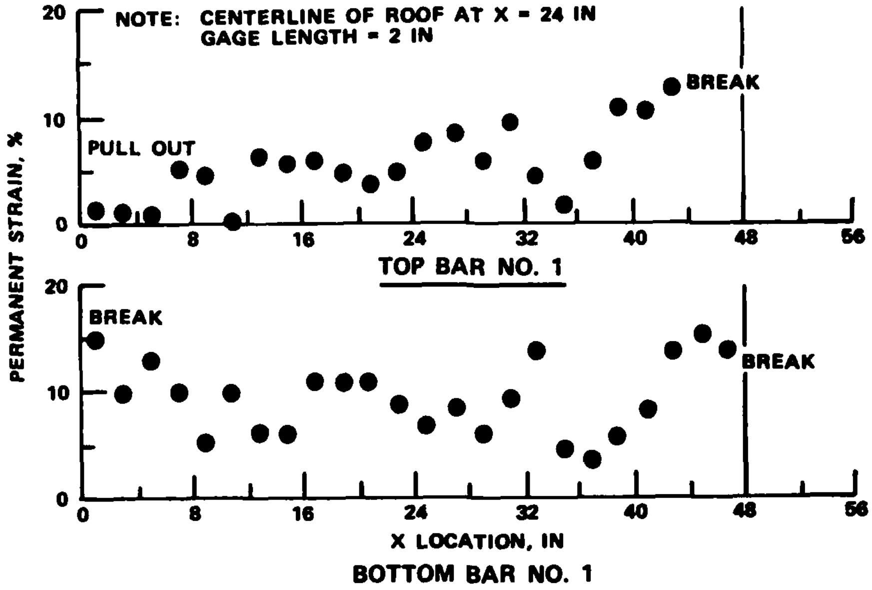

PERMANENT STRAIN OF REBAR FOR DS5

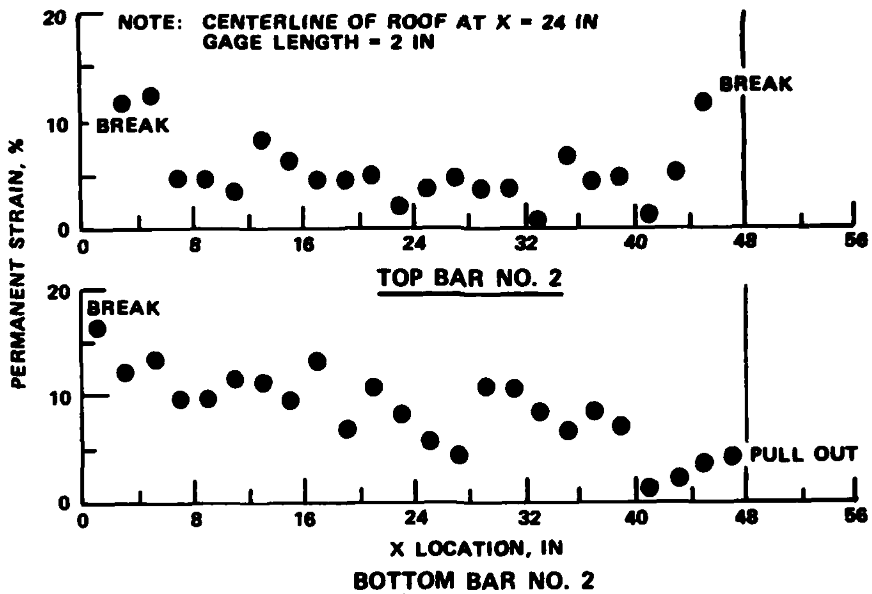

Figure 4-15. Permanent Strain of Rebar for DS5.

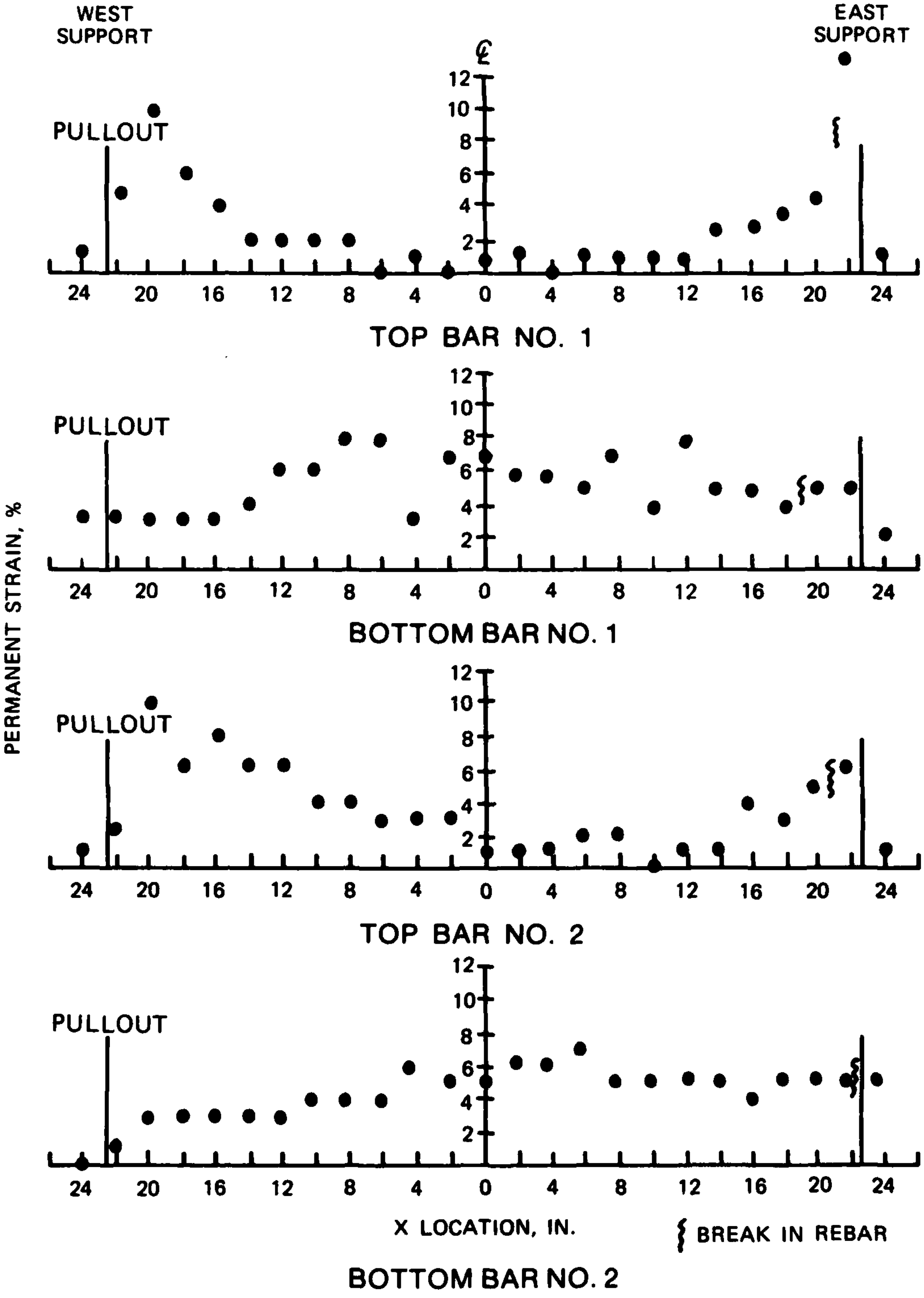

Figure 4-16. Permanent Strain of Rebar for DS2-1.

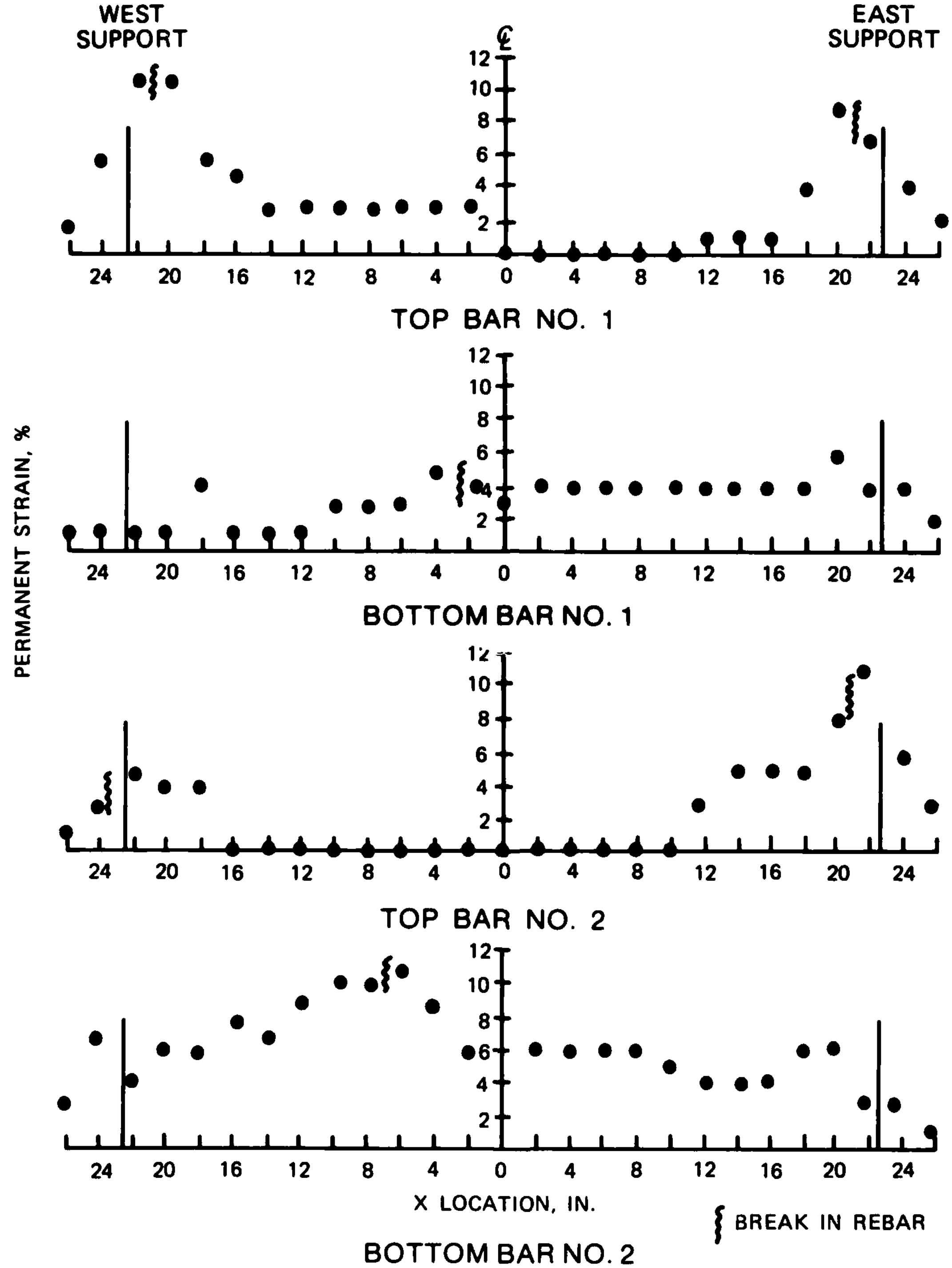

Figure 4-17. Permanent Strain of Rebar for DS2-2.

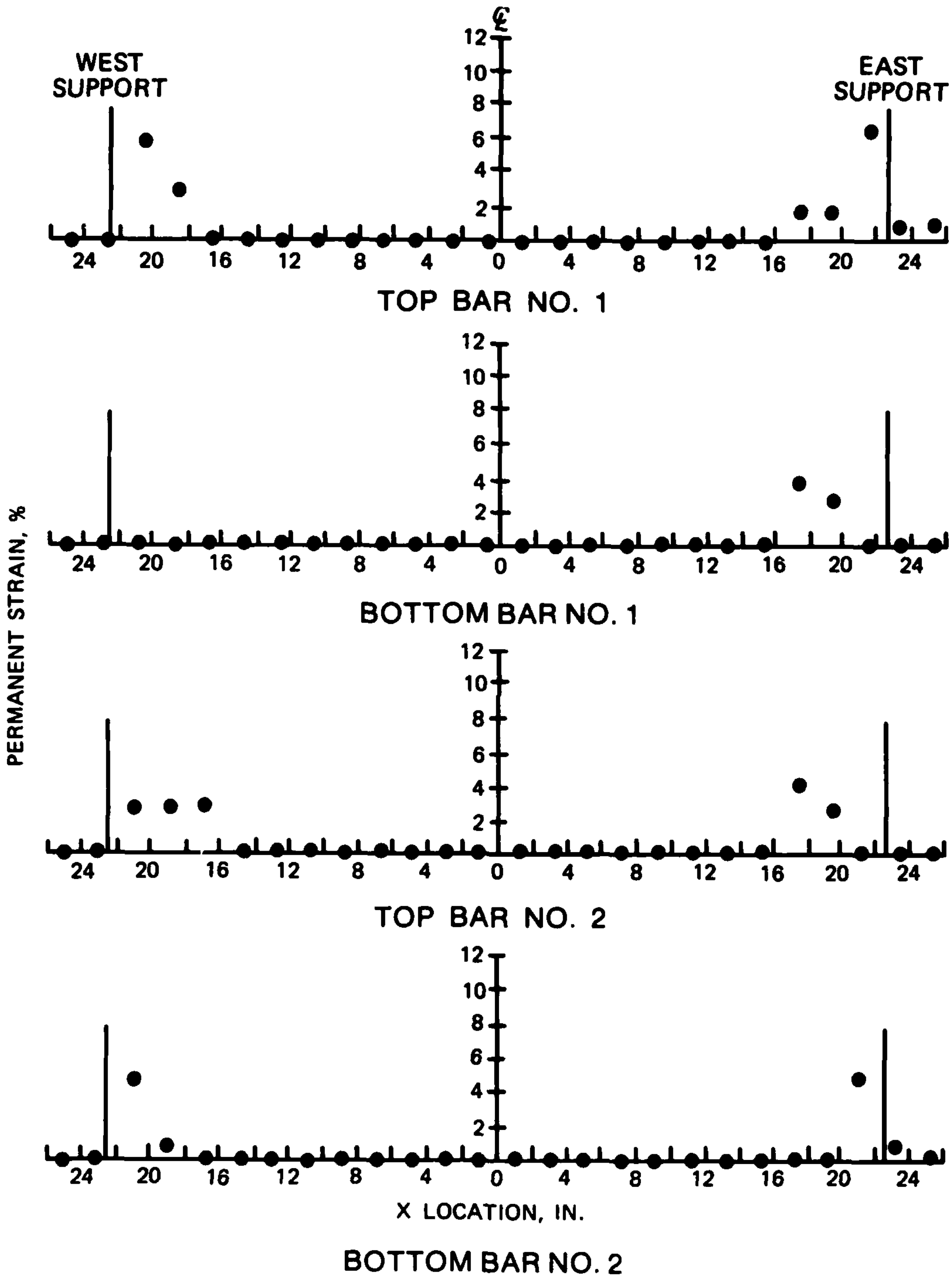

Figure 4-18. Permanent Strain of Rebar for DS2-3.

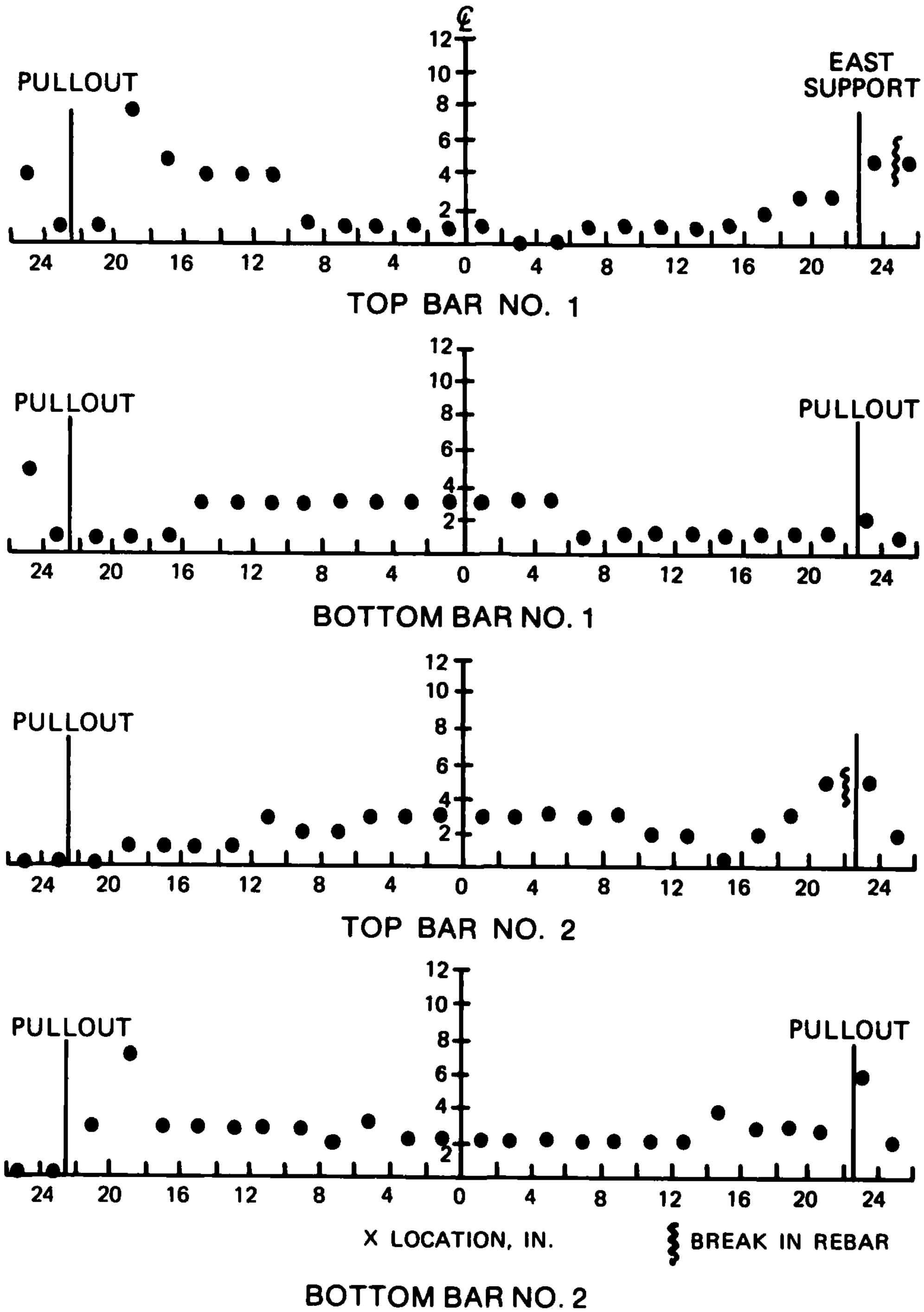

Figure 4-19. Permanent Strain of Rebar for DS2-4.

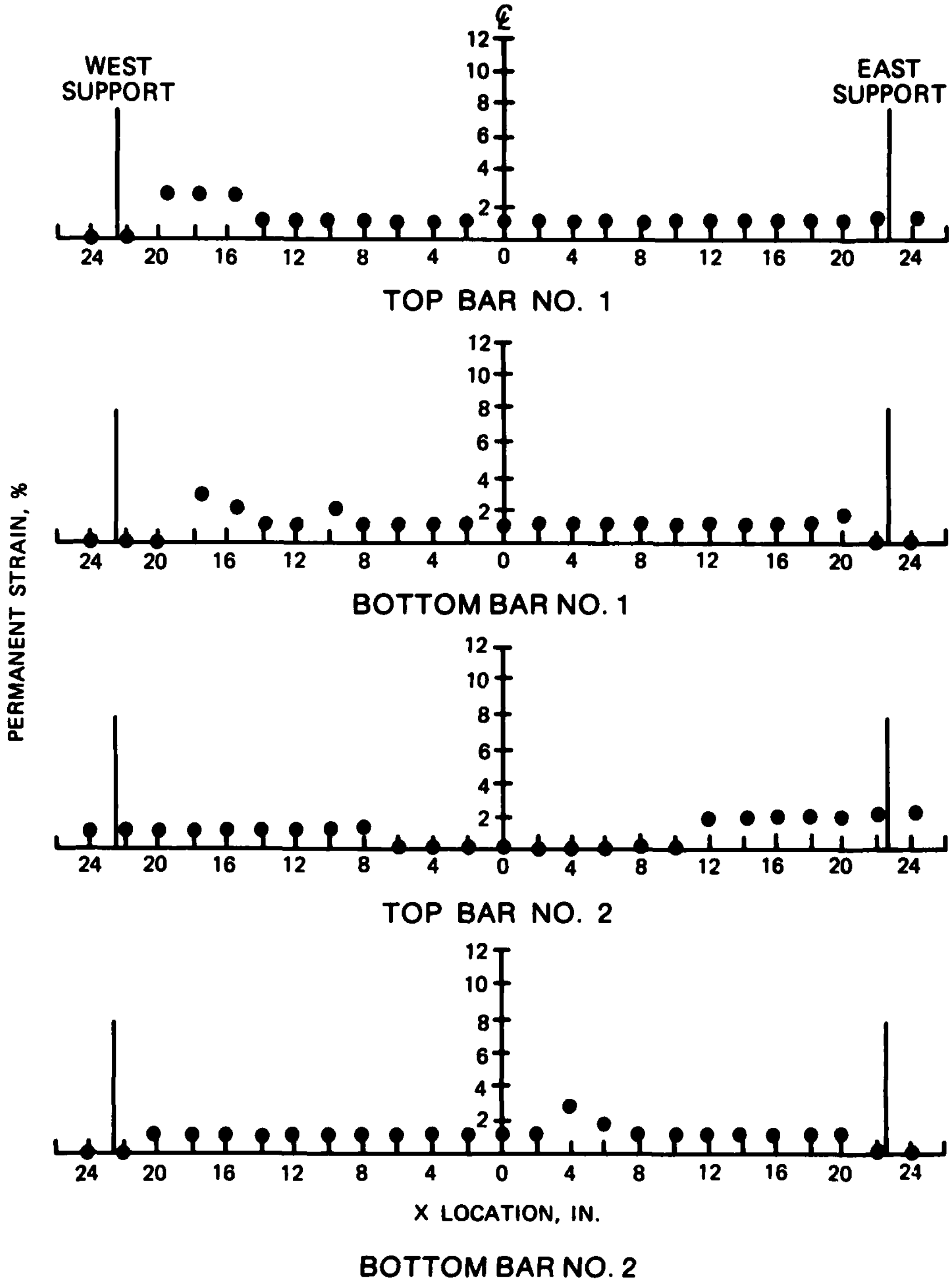

Figure 4-20. Permanent Strain of Rebar for DS2-5.

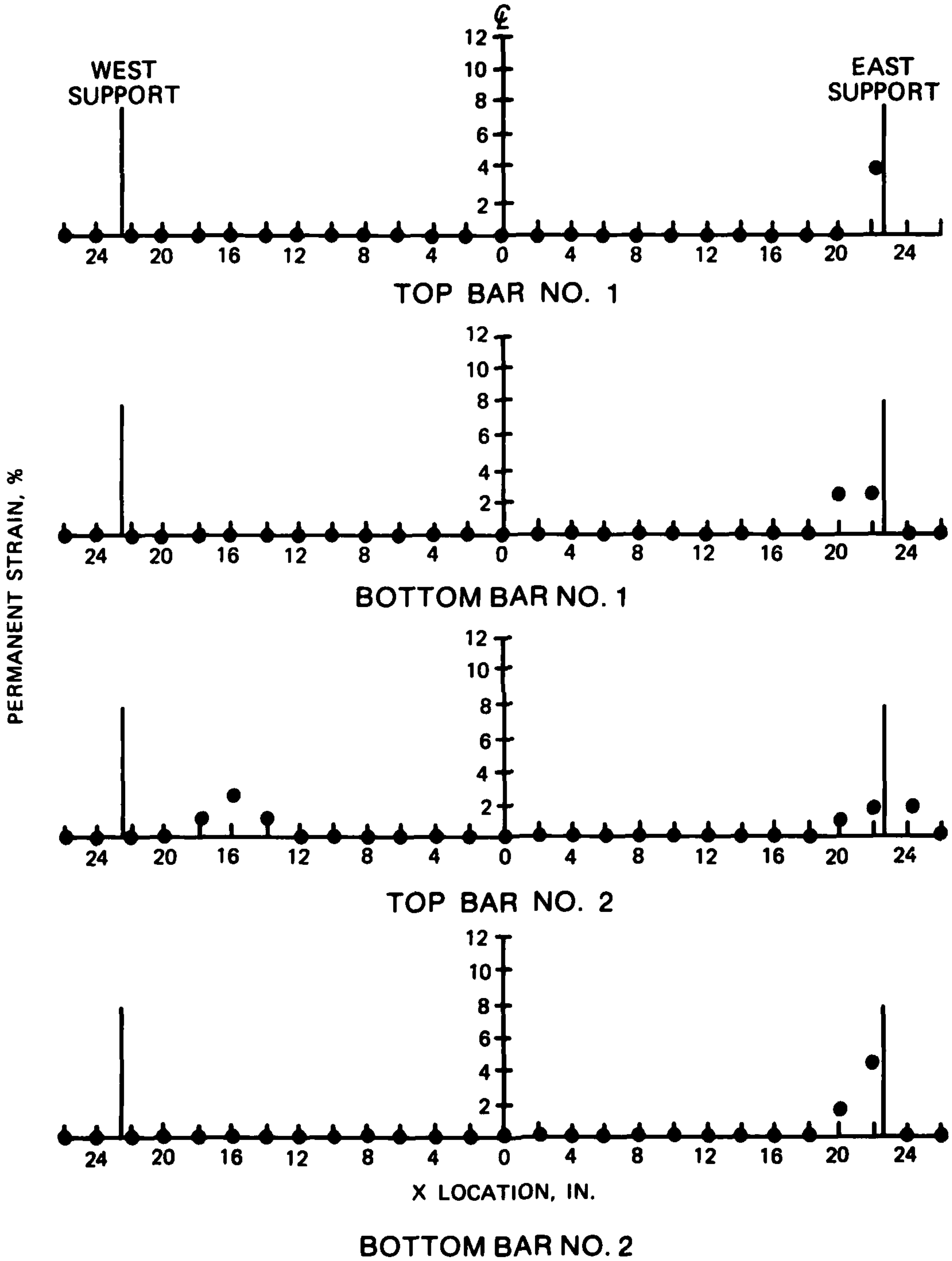

Figure 4-21. Permanent Strain of Rebar for DS2-6.

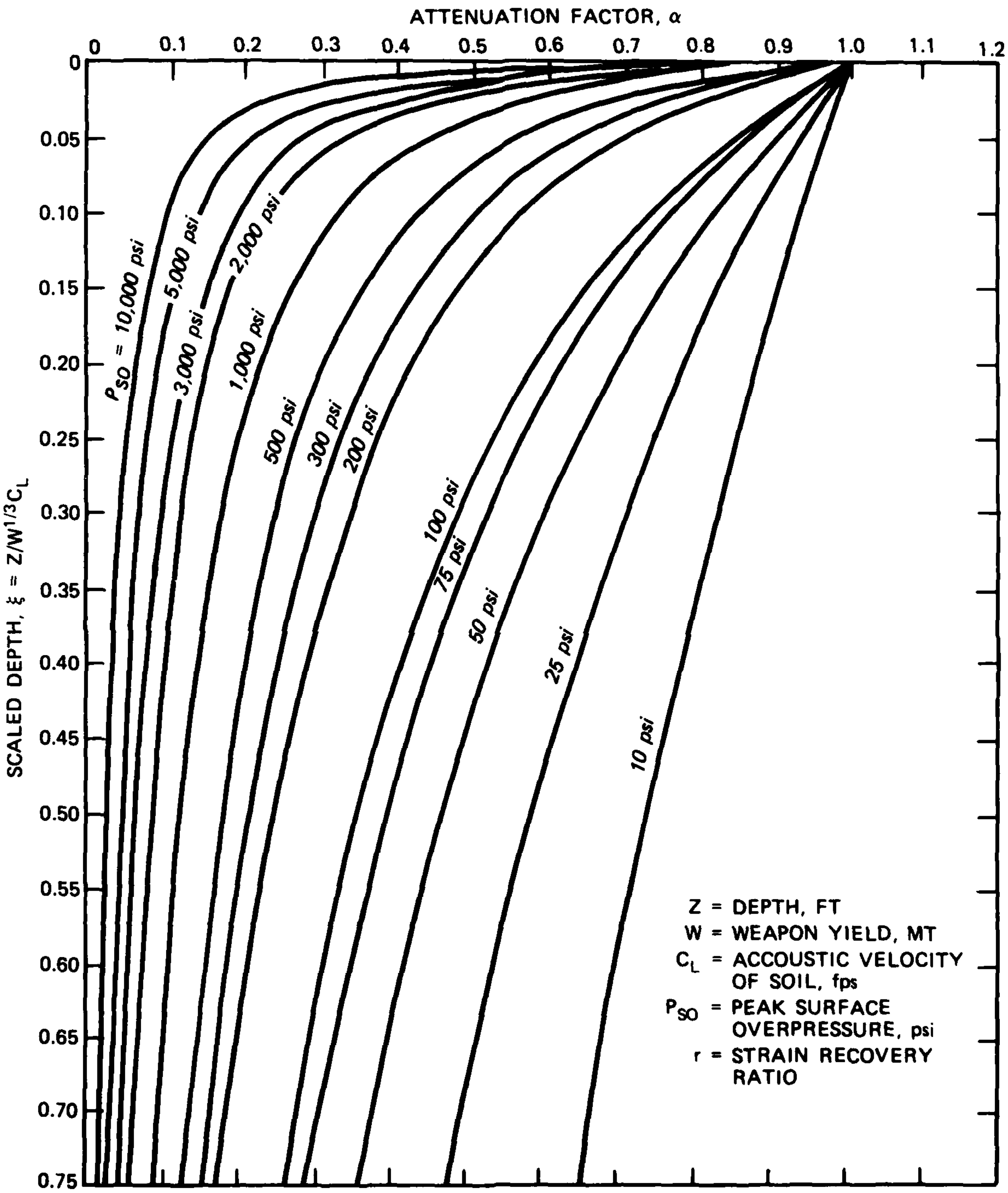

Figure 4-22. Attenuation Factor Versus Scaled Depth (Air Force Systems Command).

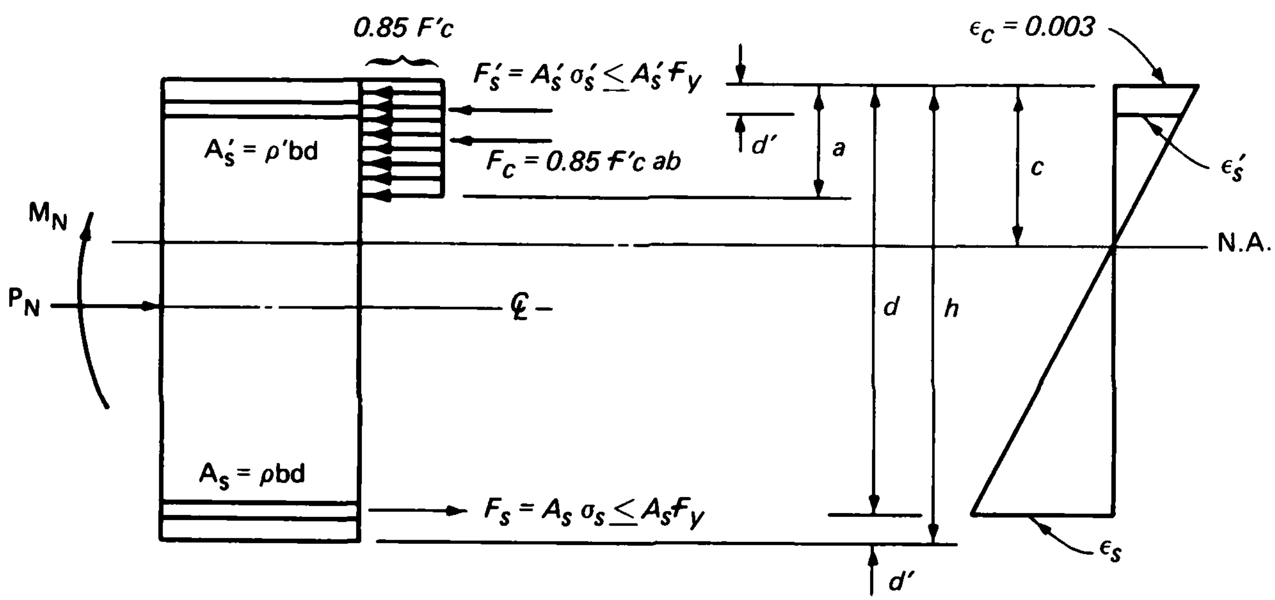

$a = \beta_1 c$

$\beta_1 = 0.85 - (F'c - 4{,}000)/20{,}000$ (ACI, 1977)

$0.65 \leq \beta_1 \leq 0.85$

Figure 4-23. Free Body Diagram and Strain Distribution.

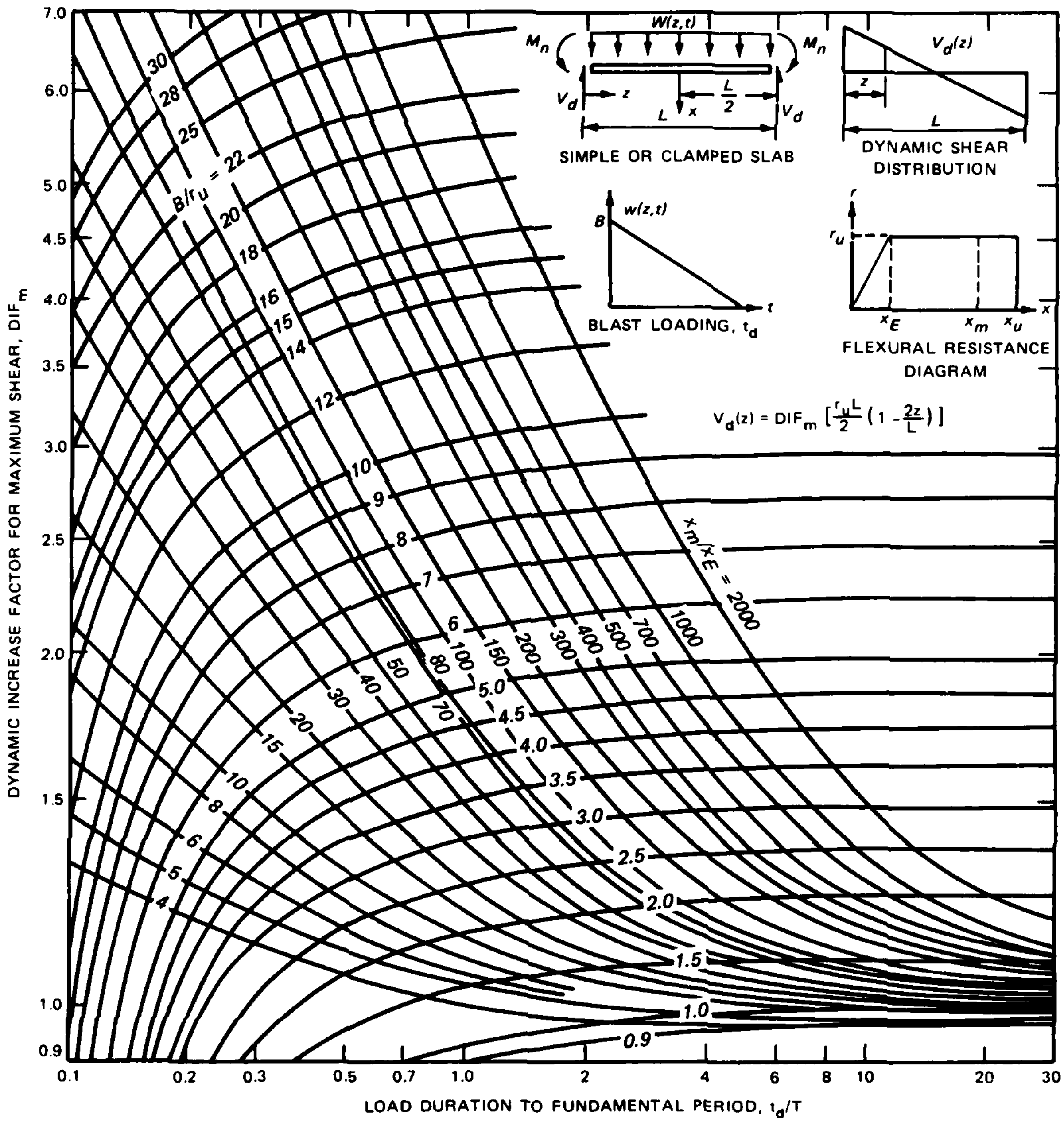

Figure 4-24. Design Chart for Maximum Dynamic Shear in a One-Way Slab (Keenan, 1977).

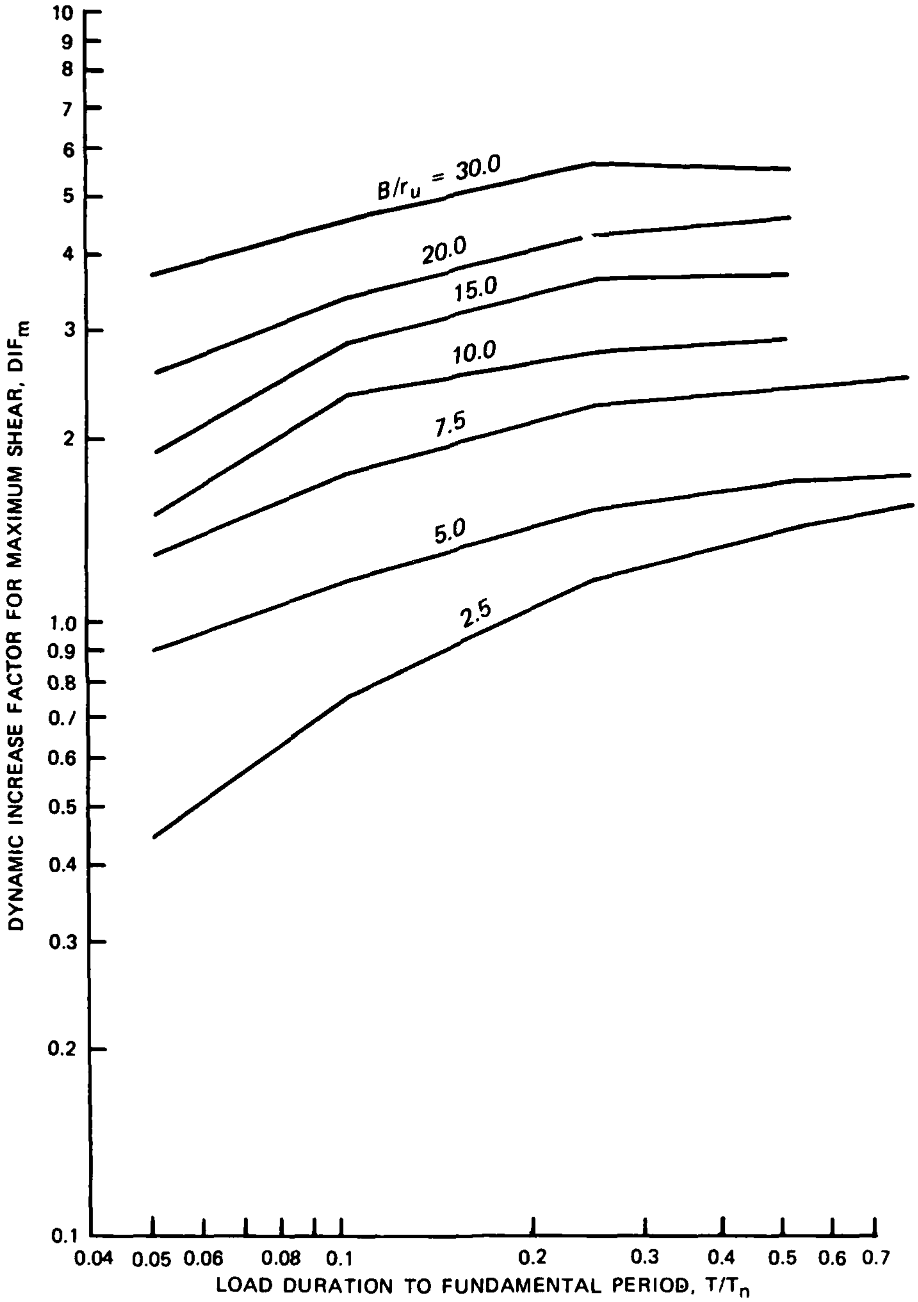

...ure 4-25. Maximum Dynamic Increase Factors for Support Shears ...imply Supported Beams (from R. N. Murtha, CEL, in a Letter to Dr. Kent Goering, DNA, Dated 28 April 1980).

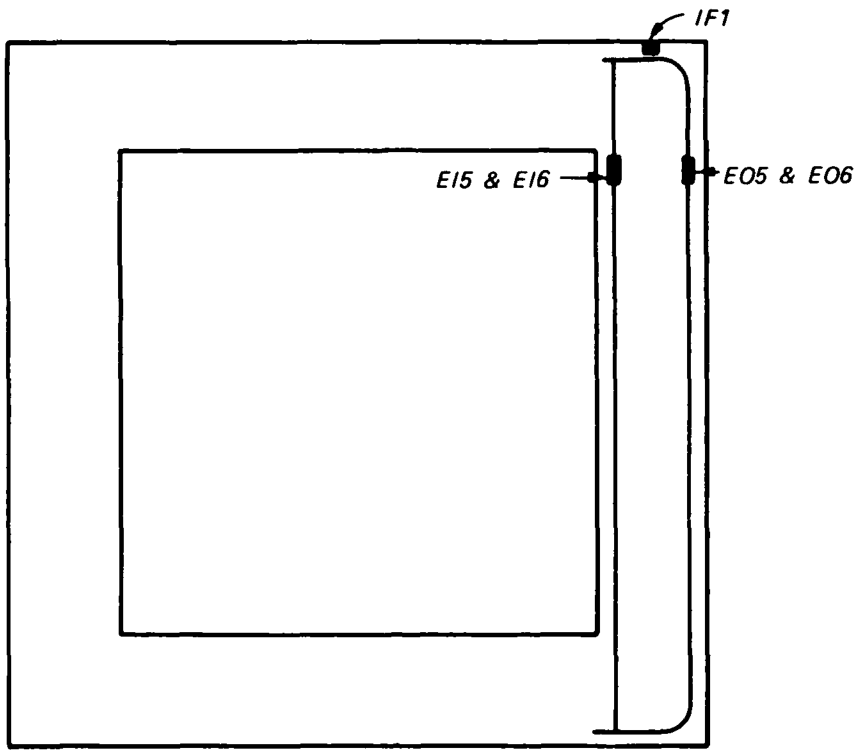

Figure 4-26. Instrumentation Locations Used in Support Shear Calculations.

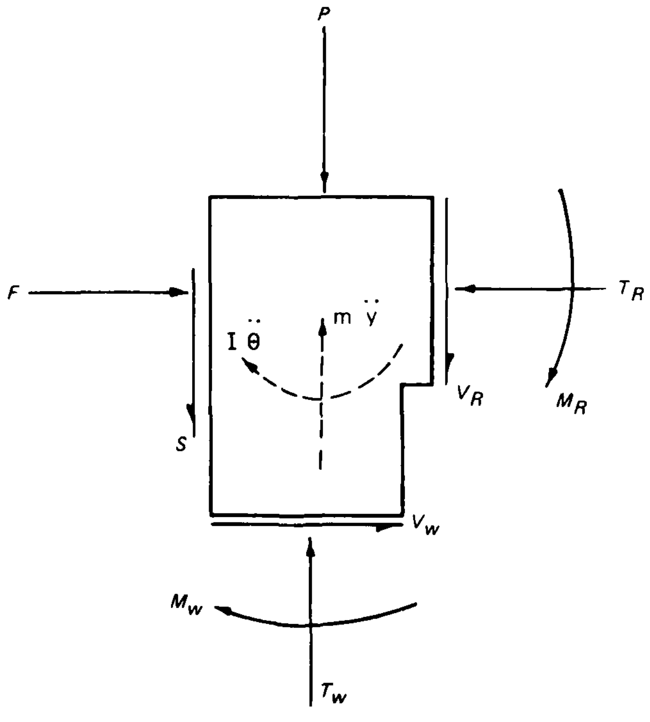

Figure 4-27. Free Body Diagram at the Top of the Wall.

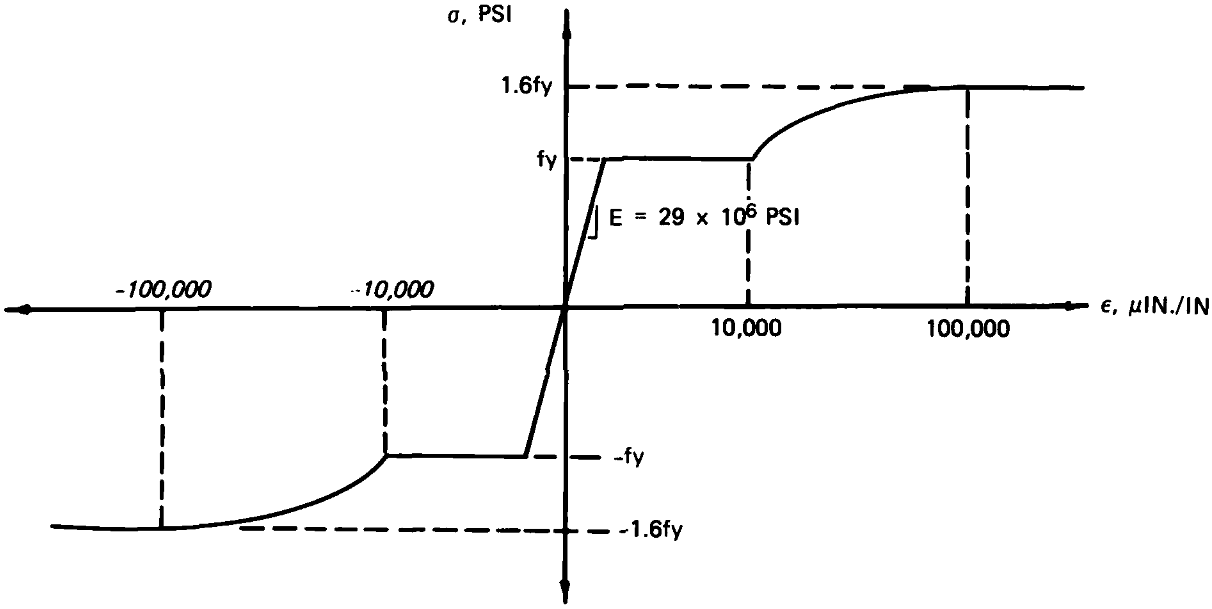

Figure 4-28. Stress-Strain Curve for Reinforcement Steel.

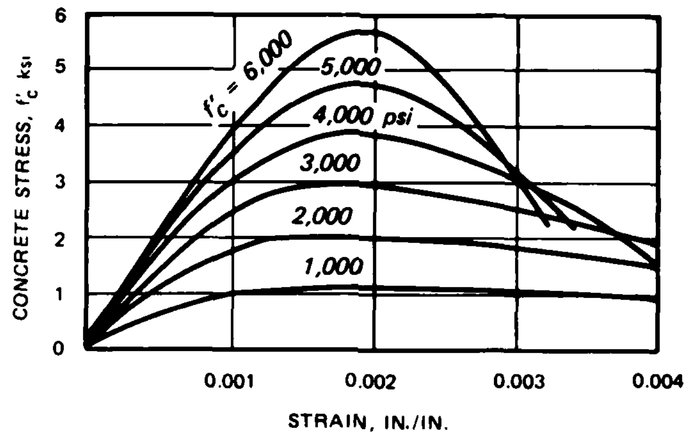

Figure 4-29. Typical Stress-Strain Curves for Concrete Under Short-Time Compressive Loading (Wang and Salmon 1979).

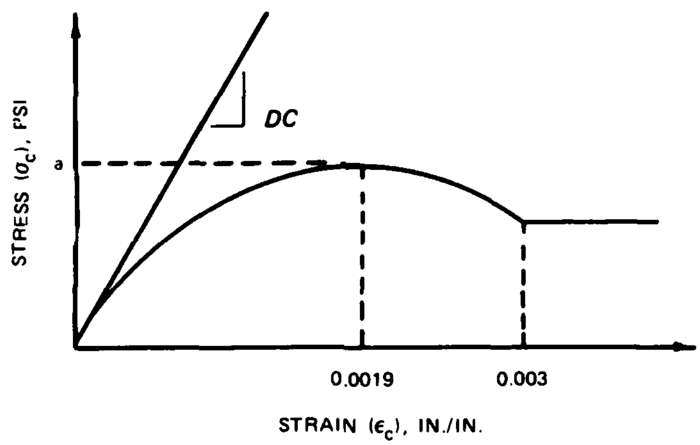

Figure 4-30. Stress-Strain Curve for Concrete.

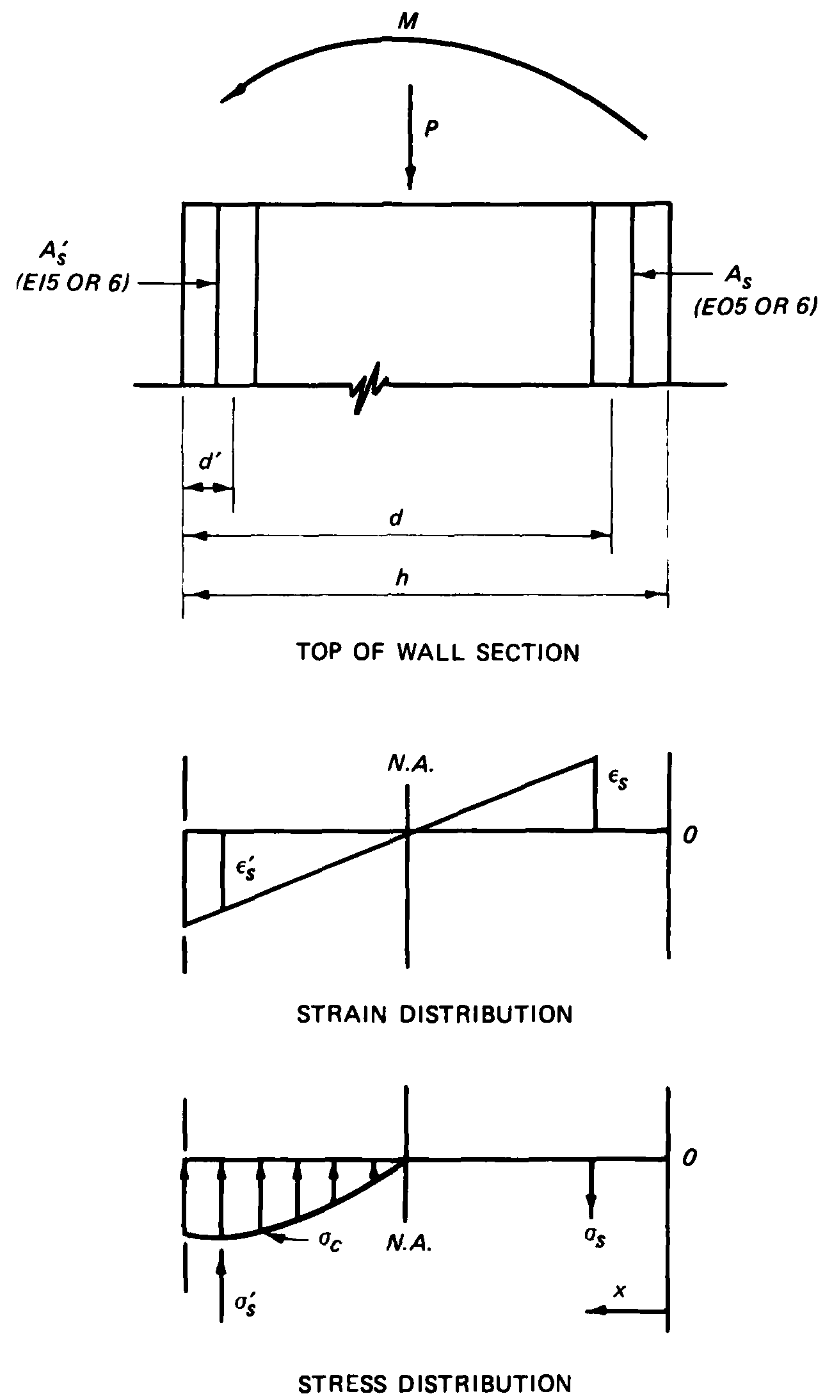

Figure 4-31. Stress and Strain Distributions at the Top of the Wall.

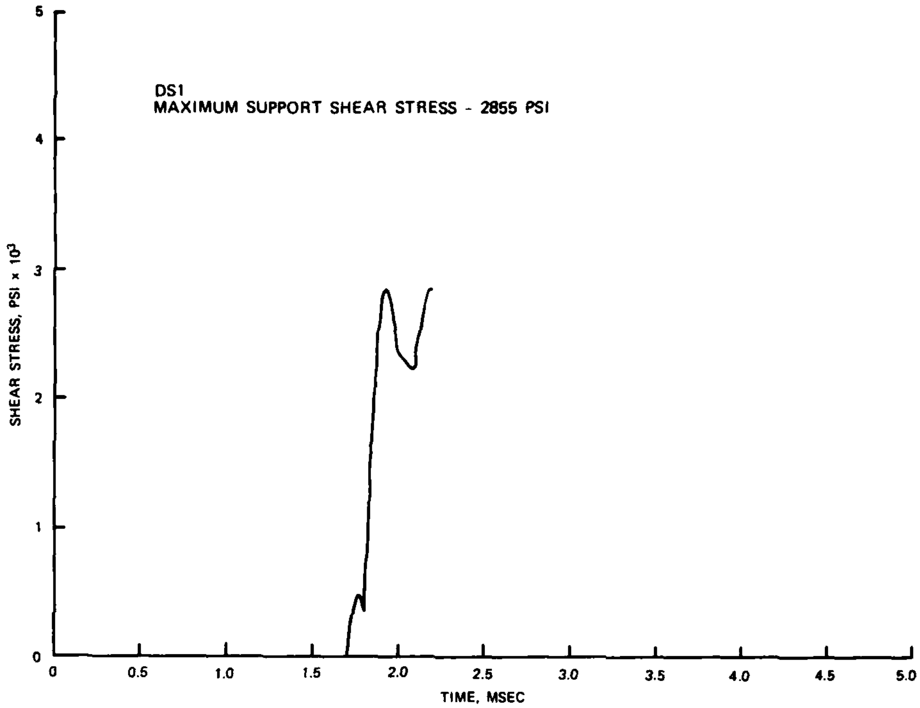

Figure 4-32. Support Shear Stress for DS1.

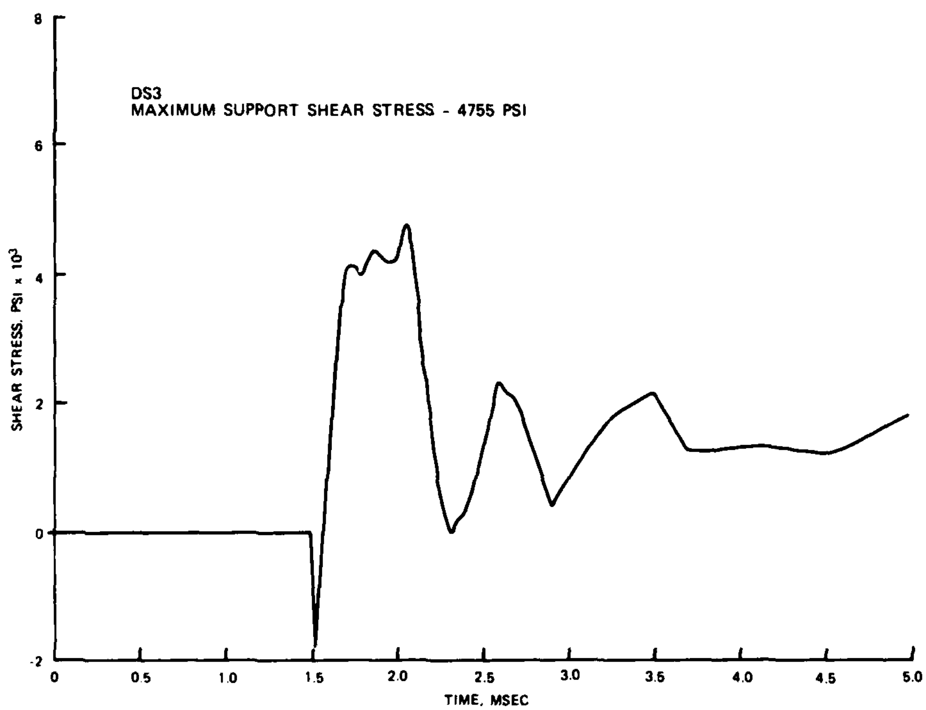

Figure 4-33. Support Shear Stress for DS3.

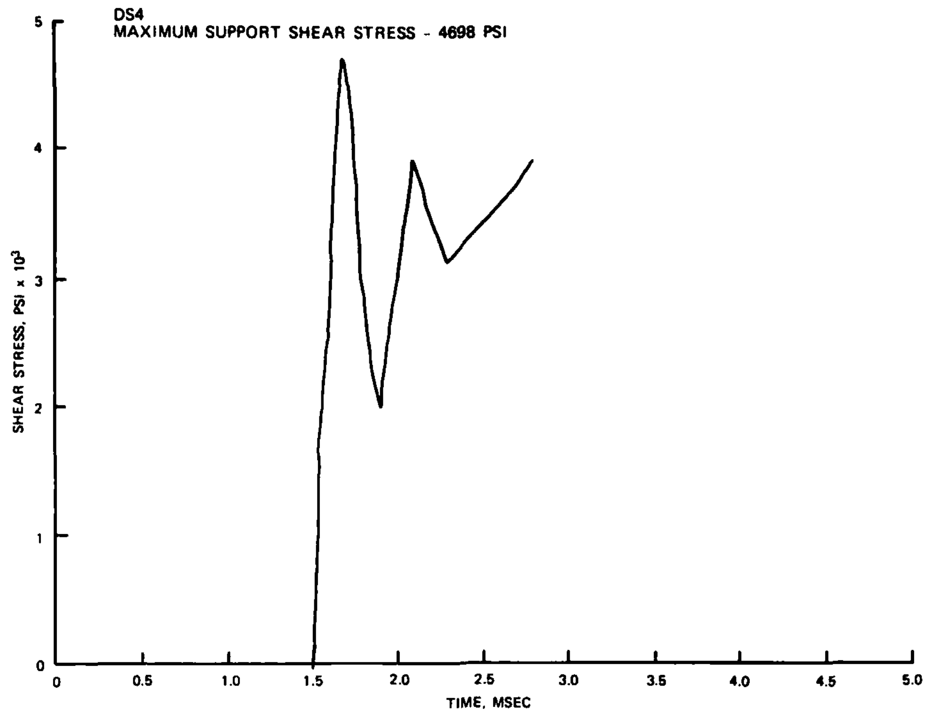

Figure 4-34. Support Shear Stress for DS4.

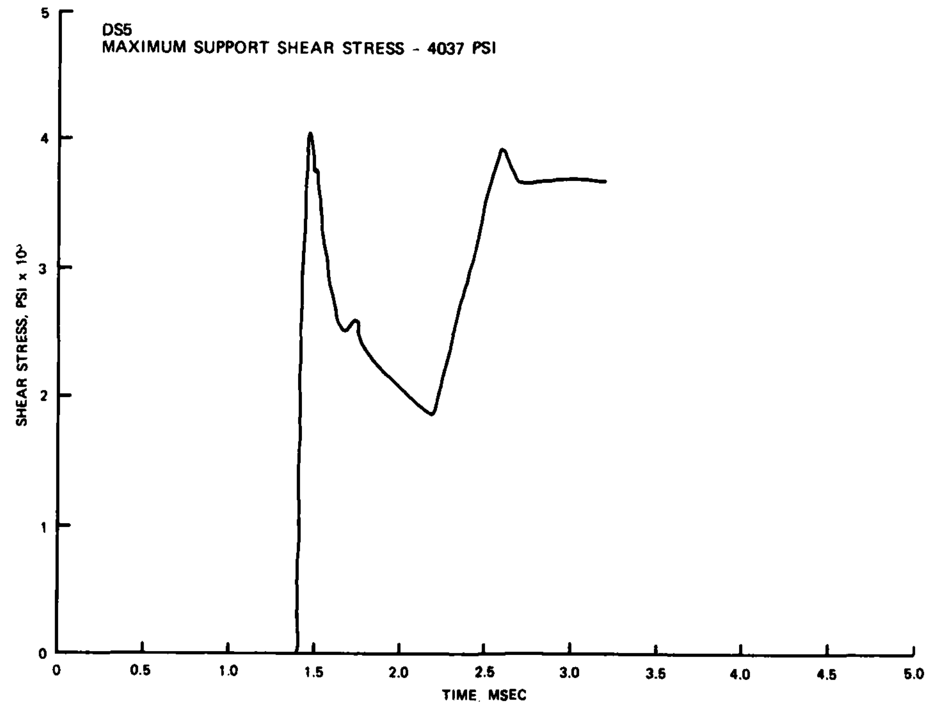

Figure 4-35. Support Shear Stress for DS5.

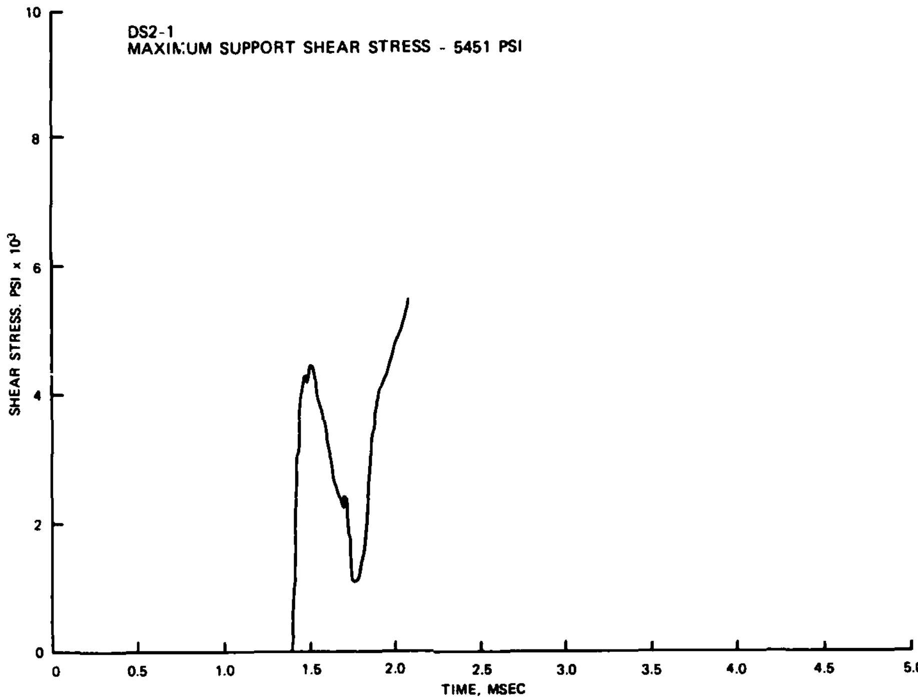

Figure 4-36. Support Shear Stress for DS2-1.

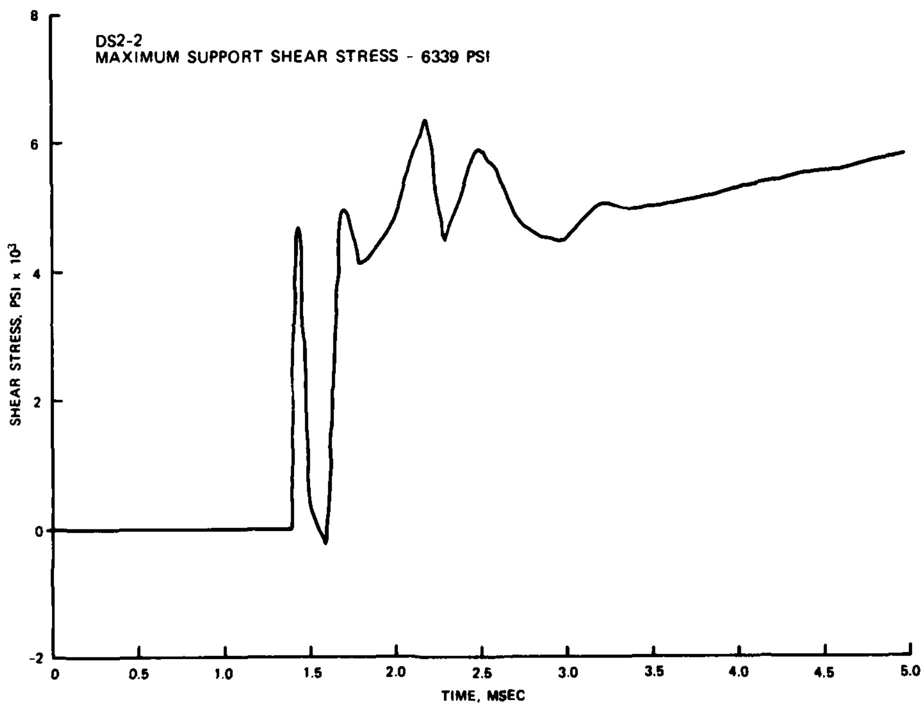

Figure 4-37. Support Shear Stress for DS2-2.

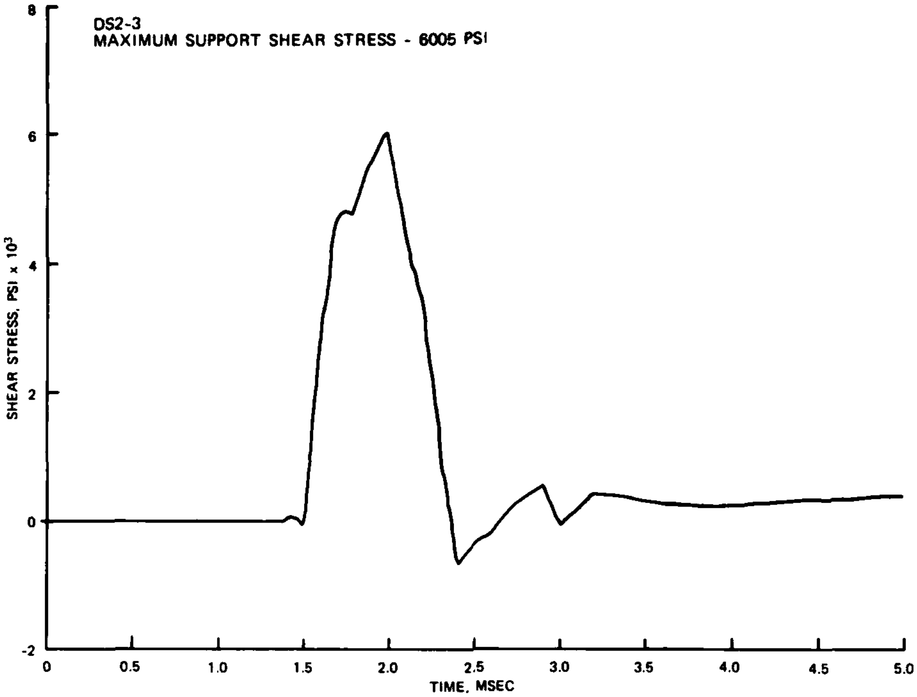

Figure 4-38. Support Shear Stress for DS2-3.

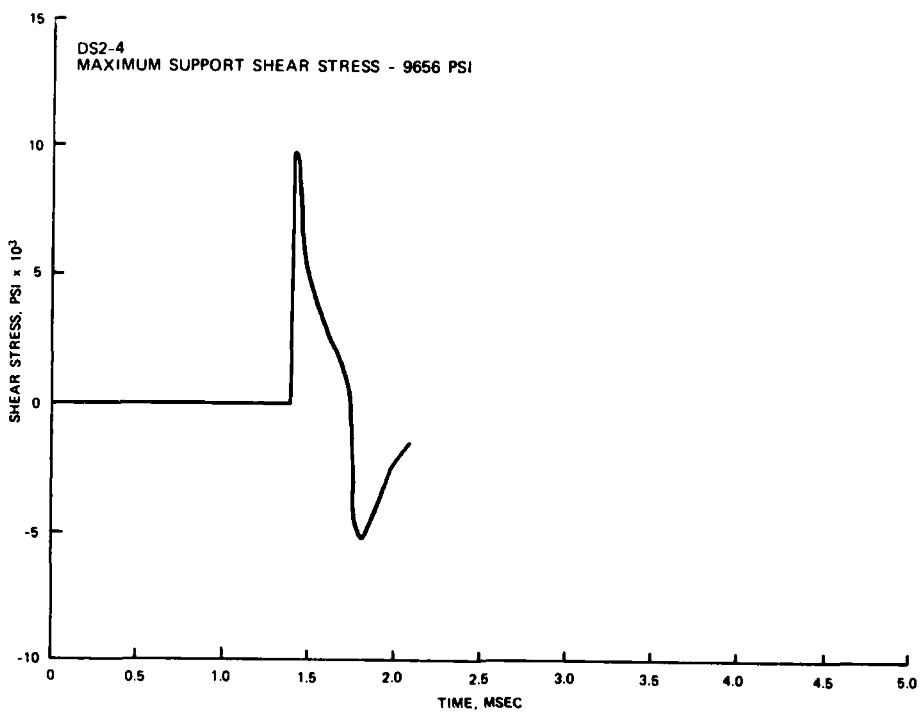

Figure 4-39. Support Shear Stress for DS2-4.

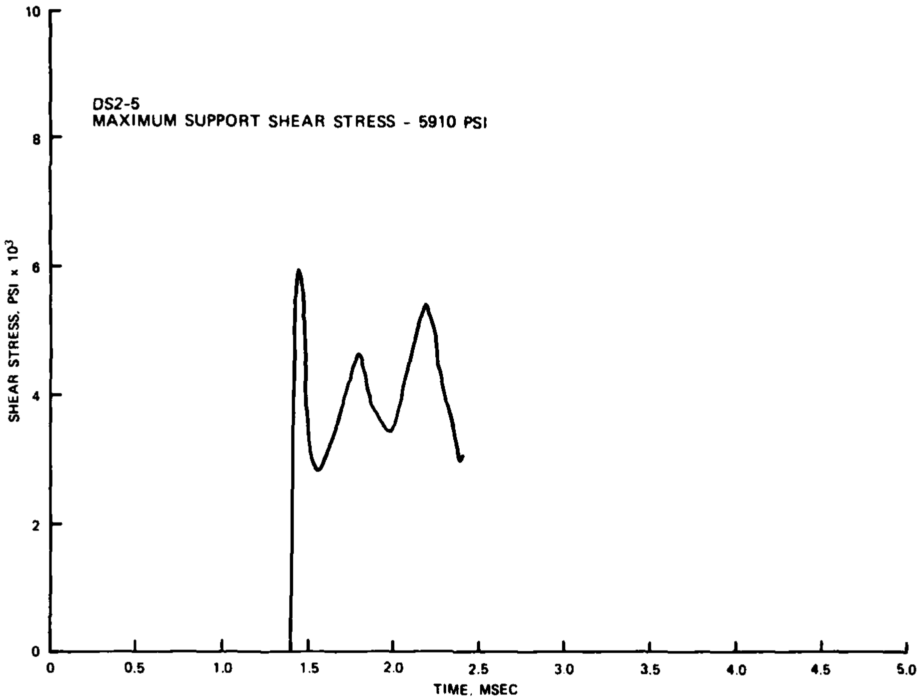

Figure 4-40. Support Shear Stress for DS2-5.

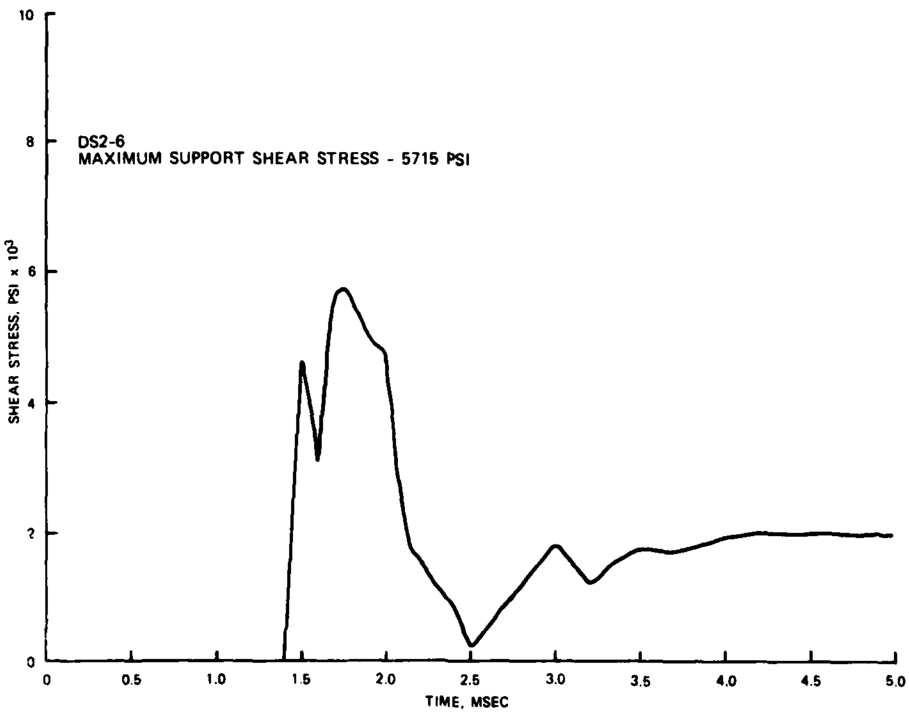

Figure 4-41. Support Shear Stress for DS2-6.

CHAPTER 5: CONCLUSIONS AND RECOMMENDATIONS

Conclusions

106. It is concluded that a relatively high frequency dynamic shear failure in shallow-buried structures with L/d ratios of seven and ten may be induced. For the structures and test configurations used, the threshold overpressure level that will generate shear failure is much greater than the flexural failure overpressure.

107. The FY 81 tests showed that the failure mode is dependent on concrete strength in that the lower strength concrete (4000 psi) was crushed at the supports, allowing premature failure of the roof slab by roof reinforcement pullout.

108. The FY 82 tests showed almost identical response of L/d of seven structures with steel ratios of 0.0075 and 0.012 at the overpressure levels of the tests. However, the data are not extensive enough to conclude that there is no dependence of dynamic shear failure on steel reinforcement ratio.

109. Each test except test DS2-6 is documented with high-speed photography. The high-speed movies clearly show the roof slab response for each test and help to determine the failure mode for each test. The high-speed movies confirm that tests DS2-1 and DS2-4 are dynamic direct shear failures.

110. A data base for evaluating dynamic shear stress computational methods is established for structures having an L/d ratio of 10 with concrete strengths ranging from 4000 to 6000 psi and steel ratios of 0.01 as well as for structures having an L/d ratio of 7 with concrete strength of 7000 psi and steel ratios of 0.0075 and 0.012.

111. The measurement of permanent rebar strains gives an indication of the amount of dowel action occurring at the support during roof slab failure. Even though considerable scatter exists in the data, it is concluded that the length of the reinforcement effective in dowel action ranges from 4 to 8 in. for the dynamic shear tests. Permanent rebar strains in the 10 to 15 percent range are noted for the Dynamic Shear Tests.

112. Upper bound failure criteria are proposed for dynamic direct and diagonal tension shear. The dynamic diagonal tension shear failure criterion (Equation 4-29) is based on an upper bound equation proposed by Murtha and Crawford (1981). The dynamic direct shear failure criterion (Equation 4-28)

is based on an equation proposed by Karagozian and Case (1973). These equations can be used to estimate the dynamic shear strength under highly impulsive loading conditions.

Recommendations

113. Additional tests are required to establish the dependence of dynamic direct shear failure upon principal steel reinforcement ratio. Tests with a steel ratio range greater than those tested in the FY 82 tests are required to address this subject. Also, tests with variable shear reinforcement ratio would be interesting from a diagonal tension shear failure standpoint.

114. Additional tests with the Dynamic Shear Test configuration are required in order that the threshold shear stress levels for direct and diagonal tension shear failure can be more accurately established. Several tests with an L/d ratio of 10 are required to get an upper bound for dynamic direct shear failure.

115. The shear failure criteria proposed in Chapter 4 are applicable to the structures tested and should be validated using tests on structures of various L/d ratios, steel ratios, and concrete strengths.

REFERENCES

Air Force Systems Command. 1976 (Jan). "Effects of Airblast, Cratering, Ground Shock, and Radiation on Hardened Structures," AFSCM 500-8, Norton AFB, Calif.

American Concrete Institute. 1977. "ACI 318-77: Building Code Requirements for Reinforced Concrete," Detroit, Mich.

American Society for Testing and Materials. 1969. "Standard Specification for Deformed and Plain Billet Steel Bars for Concrete Reinforcement," Designation: A-615-68, 1969 Book of ASTM Standards, Part 4, Philadelphia, Pa.

Balsara, J. P., and Hossley, J. R. 1973 (Dec). "Evaluation of SAFEGUARD System Perimeter Acquisition Radar Building Shear Key Connection," Technical Report N-73-9, U. S. Army Engineer Waterways Experiment Station, CE, Vicksburg, Miss.

Bathe, K. J. 1977 (May). "User's Manual for ADINA, a Finite Element Program for Automatic Dynamic Incremental Nonlinear Analysis," Report 82448-1, Massachusetts Institute of Technology, Cambridge, Mass.

Biggs, J. M. 1964. Introduction to Structural Dynamics, McGraw-Hill, New York.

Brode, H. L. 1970 (Jul). "Heights of Burst Effects at High Overpressures," RM-6301-DASA, Revised 1979, The Rand Corporation, Santa Monica, Calif.

Brotchie, J. F., Jacobson, A., and Okubo, S. 1965 (Aug). "Effect of Membrane Action on Slab Behavior," U. S. Naval Civil Engineering Laboratory Report No. R65-25, Revised in 1979, Massachusetts Institute of Technology, Cambridge, Mass.

Bucci, D. R., and Mlakar, P. F. 1976 (Jun). "Design of Earth-Covered Structures to Defeat Contact Burst Rounds," Technical Report No. N-76-7, U. S. Army Engineer Waterways Experiment Station, CE, Vicksburg, Miss.

Crawford, R. E., Higgins, C. J., and Bultmann, E. H. 1974 (Oct). "The Air Force Manual for Design and Analysis of Hardened Structures," Technical Report AFWL-TR-74-102, Air Force Weapons Laboratory, Kirtland Air Force Base, N. Mex.

Fuehrer, H. R., and Keeser, J. W. 1977. "Response of Buried Concrete Slabs to Underground Explosions," Report No. AFATL-TR-77-115, Orlando Technology, Inc., for Air Force Armament Laboratory, Orlando, Fla.

Getchell, J. V., and Kiger, S. A. 1980 (Oct). "Vulnerability of Shallow-Buried Flat-Roof Structures, Foam HEST 4," Technical Report SL-80-7, Report 2, U. S. Army Engineer Waterways Experiment Station, CE, Vicksburg, Miss.

__________. 1981a (Feb). "Vulnerability of Shallow-Buried Flat-Roof Structures; Foam HEST 5," Technical Report SL-80-7, Report 3, U. S. Army Engineer Waterways Experiment Station, CE, Vicksburg, Miss.

Getchell, J. V., and Kiger, S. A. 1981b (Dec). "Vulnerability of Shallow-Buried Flat-Roof Structures; Foam HEST 3 and 6," Technical Report SL-80-7, Report 4, U. S. Army Engineer Waterways Experiment Station, CE, Vicksburg, Miss.

Haltiwanger, J. D. 1979 (Feb). "Behavior of Restrained Two-Way Slabs," DNA 49592, N. M. Newmark Consulting Engineering Services, Urbana, Ill.

Hossley, J. R., and Albritton, G. E. 1979 (Nov). "ESSEX-Diamond Ore Research Program; Hardened Structure Response, Project ESSEX V," Technical Report SL-79-11, U. S. Army Engineer Waterways Experiment Station, CE, Vicksburg, Miss.

Humphreys, J. S. 1966. "Plastic Deformation of Impulsively Loading Straight Clamped Beams," Journal of Solids and Structures, Vol 2.

Jones, N. 1976. "Plastic Failure of Ductile Beams Loaded Dynamically," Journal of Engineering for Industry, Trans. ASME 98(1).

__________. 1981 (Oct). "Recent Progress in the Dynamic Plastic Behavior of Structures, Part III," The Shock and Vibration Digest, Volume 13, No. 10, The Shock and Vibration Information Center, Naval Research Laboratory, Washington, D. C.

Jones, N., and Gomes de Oliveira, J. 1979 (Jun). "The Influence of Rotatory Inertia and Transverse Shear on the Dynamic Plastic Behavior of Beams," Journal of Applied Mechanics, Trans. ASME 46(2).

Karagozian and Case, Structural Engineers. 1973 (Jan). "Construction Joint Test Program" (Final Report), Air Force Systems Command, Space and Missile Systems Organization Contract F0701-72-C-0358, Los Angeles, Calif.

Keenan, W. A. 1965 (Dec). "Dynamic Shear Strength of Reinforced Concrete Beams, Part I," Technical Report No. R395, Naval Civil Engineering Laboratory, Port Hueneme, Calif.

__________. 1969a (Apr). "Strength and Behavior of Laced Reinforced Concrete Slabs Under Static and Dynamic Load," Technical Report No. R620, Naval Civil Engineering Laboratory, Port Hueneme, Calif.

__________. 1969b (Apr). "Strength and Behavior of Restrained Reinforced Concrete Slabs Under Static and Dynamic Loading," Technical Report No. R621, Naval Civil Engineering Laboratory, Port Hueneme, Calif.

__________. 1977 (Aug). "Shear Stress in One-Way Slabs Subjected to Blast Load," Technical Memorandum M-51-77-10, Civil Engineering Laboratory, Naval Construction Battalion Center, Port Hueneme, Calif.

Kiger, S. A. 1981. "Use of a Foam HEST to Simulate Low Yield Nuclear Overpressures," Proceedings of the Seventh International Symposium on Military Applications of Blast Simulation, 13-17 July 1981, Medicine Hat, Alberta, Canada.

Kiger, S. A., and Albritton, G. E. 1980 (Mar). "Response of Buried Hardened Box Structures to the Effects of Localized Explosions," Technical Report SL-80-1, U. S. Army Engineer Waterways Experiment Station, CE, Vicksburg, Miss.

Kiger, S. A., and Eagles, P. E. (in publication). "Effects of Earth Cover on the Ultimate Capacity of Reinforced Concrete Slabs," U. S. Army Engineer Waterways Experiment Station, CE, Vicksburg, Miss.

Kiger, S. A., and Getchell, J. V. 1980 (Sep). "Vulnerability of Shallow-Buried Flat-Roof Structures; Foam HEST 1 and 2," Technical Report SL-80-7, Report 1, U. S. Army Engineer Waterways Experiment Station, CE, Vicksburg, Miss.

__________. 1982 (Jan). "Vulnerability of Shallow-Buried Flat-Roof Structures; Foam HEST 7," Technical Report SL-80-7, Report 5, U. S. Army Engineer Waterways Experiment Station, CE, Vicksburg, Miss.

Kiger, S. A., Slawson, T. R., and Hyde, D. W. 1984 (Apr). Classified reference. Bibliographic material for the classified reference will be furnished to qualified agencies upon request.

Kingery, C. N., Huffington, N. J., and Wortman, J. D. 1981. "Response of Beams to Airblast Loading," Civil Engineering Laboratory, Port Hueneme, Calif.

Mahin, S. A., and Bertero, V. V. 1977. "RCCOLA: A Computer Program for Reinforced Concrete Column Analysis," University of California, Berkeley, Calif.

Martens, D. P., and Bradshaw, J. C. 1976. "Dynamic Airblast Simulator Parametric Test Series, Events I-A, I-B, I-C, I-D, and I-E Data Report," AFWL-TR-76-018, Air Force Weapons Laboratory, Kirtland Air Force Base, N. Mex.

Martin, J. B., and Ponter, A. R. S. 1972 (Feb). "Bounds for Impulsively Loaded Plastic Structures," Journal of the Engineering Mechanics Division, Proceedings, American Society of Civil Engineers, Vol 98, No. EM1.

Mayer, D., and Dahl, N. C. 1944. "Effects of Underground Explosions, Volume III: Resulting Damage to Structures," No. 26, National Research Council, Washington, D. C.

Menkes, S. B., and Opat, H. J. 1973 (Nov). "Broken Beams," Experimental Mechanics, Vol 13, No. 11.

Mlakar, P. F., and Walker, R. E. 1980 (Sep). "Statistical Estimation of Simulated Yield and Overpressure," The Shock and Vibration Bulletin, Bulletin 50, Part 2, The Shock and Vibration Information Center, Naval Research Laboratory, Washington, D. C.

Murtha R., and Crawford, J. 1981 (May). "Dynamic Shear Failure Predictions of Shallow-Buried Reinforced-Concrete Slabs," Technical Memorandum M-51-81-04, Civil Engineering Laboratory, Naval Construction Center, Port Hueneme, Calif.

Nonaka, T. 1977. "Shear and Bending Response of a Rigid-Plastic Beam to

Blast-Type Loading," Ingenieur-Archiv, Vol 46, No. 1.

Peekna, A. (in preparation). "Review of the Response of Beams and Slabs to Nearly Impulsive Loads," U. S. Army Engineer Waterways Experiment Station, CE, Vicksburg, Miss.

Ross, C. A., Sierakowski, R. L., and Malvern, L. E. 1974 (Jul). "Dynamic Response of Structures and Materials to Impulsive Loads," AFATL-TR-74-120; University of Florida, Gainesville, Fla.

Schlater, D. R. 1974. "DIEHEST Improvement Program TEST DIP IIIA," AFWL-TR-74-16, Air Force Weapons Laboratory, Kirtland Air Force Base, N. Mex.

Sewell, R. G. S., and Kinney, F. G. 1968 (Jun). "Response of Structures to Blast: A New Criterion," Naval Weapons Center Report No. 4422, China Lake, Calif.

U. S. Department of Defense. 1968 (Jun). "Unified Soil Classification System for Roads, Airfields, Embankments, and Foundations," Military Standard MIL-STD-619B, Washington, D. C.

Wampler, H. W., Leigh, G. G., and Furbee, M. E. 1978. "A Status and Capability Report on Nuclear Airblast Simulation Using HEST," Proceedings of the Nuclear Blast and Shock Simulation Symposium, 28-30 November 1978, Vol 1, General Electric-TEMPO, Santa Barbara, Calif.

Wang, C., and Salmon, C. G. 1979. Reinforced Concrete Design, Harper and Row, New York, N. Y.

APPENDIX A: NUCLEAR WEAPON SIMULATIONS

(From Dynamic Shear Test Air Blast Pressure Data)

PRESSURE COMPARISON
DYNAMIC SHEAR 1
BP1
W(KT) = 1.507
P(PSI) =3866.
01/29/83 7405E

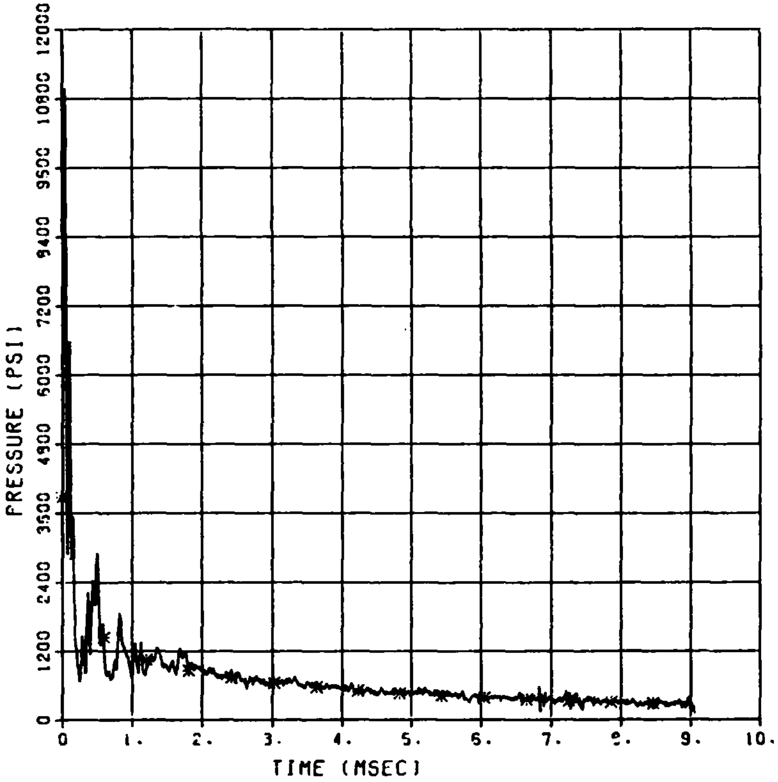

IMPULSE COMPARISON
DYNAMIC SHEAR 1
BP1
W(KT) = 1.507
P(PSI) =3868.
01/29/83 7405E

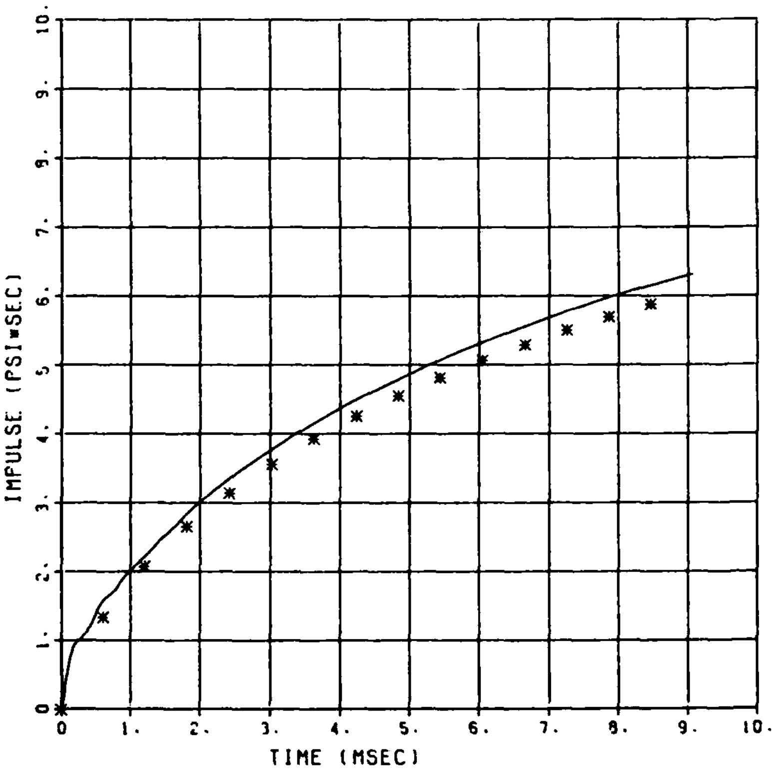

PRESSURE COMPARISON
DYNAMIC SHEAR 1
BP2
W(KT) = 0.644
P(PSI) =4032.
01/29/93   7405E

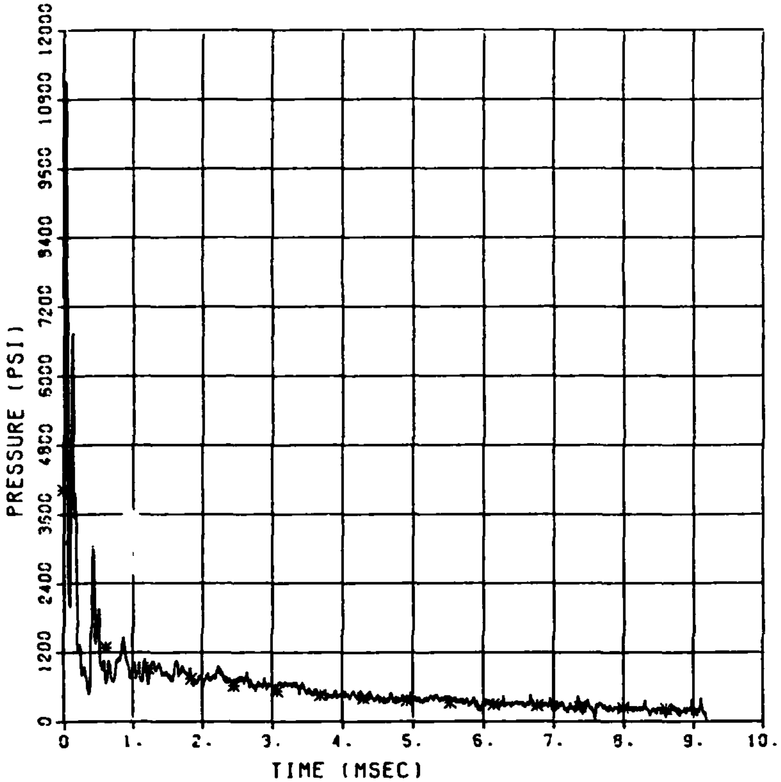

IMPULSE COMPARISON
DYNAMIC SHEAR 1
BP2
W(KT) = 0.644
P(PSI) =4032.
01/28/93   7405E

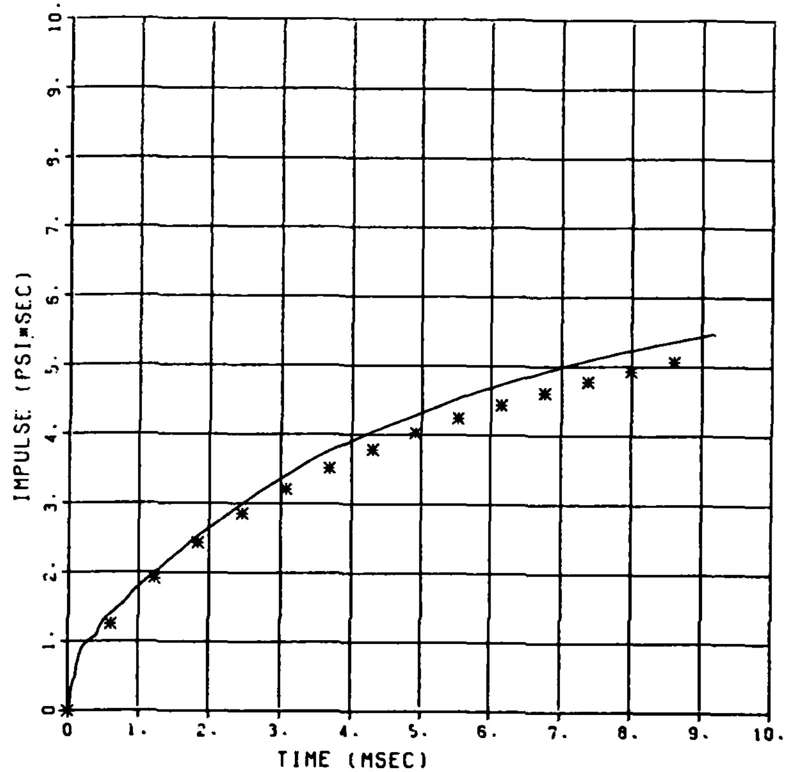

PRESSURE COMPARISON
DYNAMIC SHEAR 1
BP3
W(KT) = 0 697
P(PSI) =4174.
01/28/93 7405E

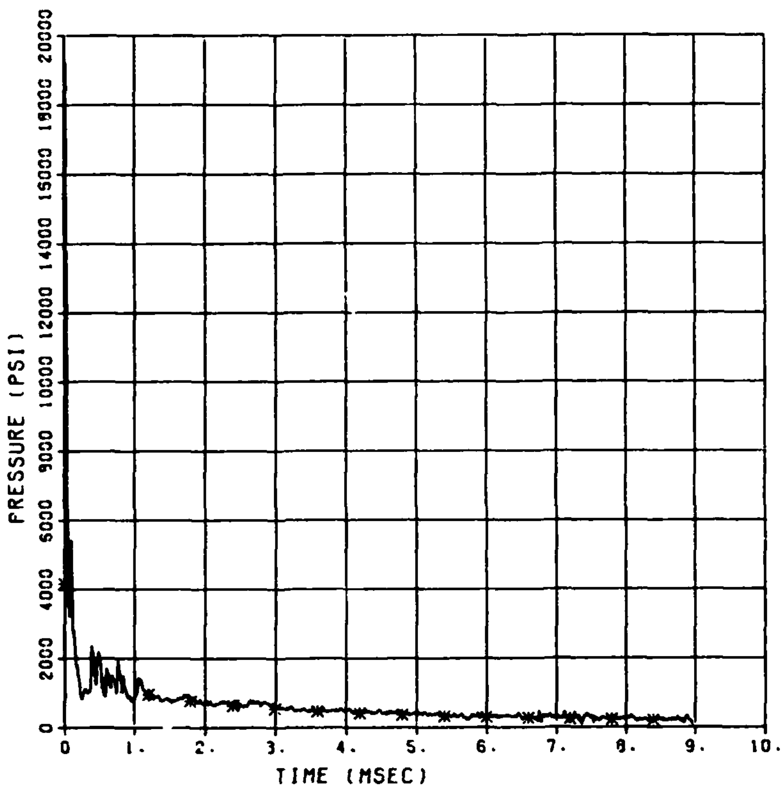

IMPULSE COMPARISON
DYNAMIC SHEAR 1
BP3
W(KT) = 0 697
P(PSI) =4174.
01/28/93 7405E

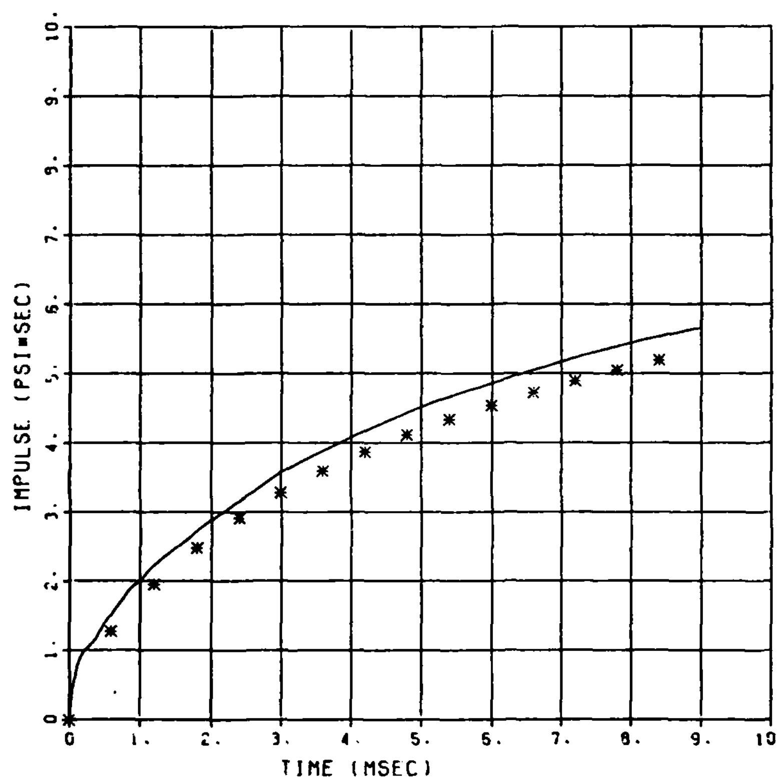

PRESSURE COMPARISON
DYNAMIC SHEAR 1
BP4
W(KT) = 1 115
P(PSI) =4343.
01/29/93 7405E

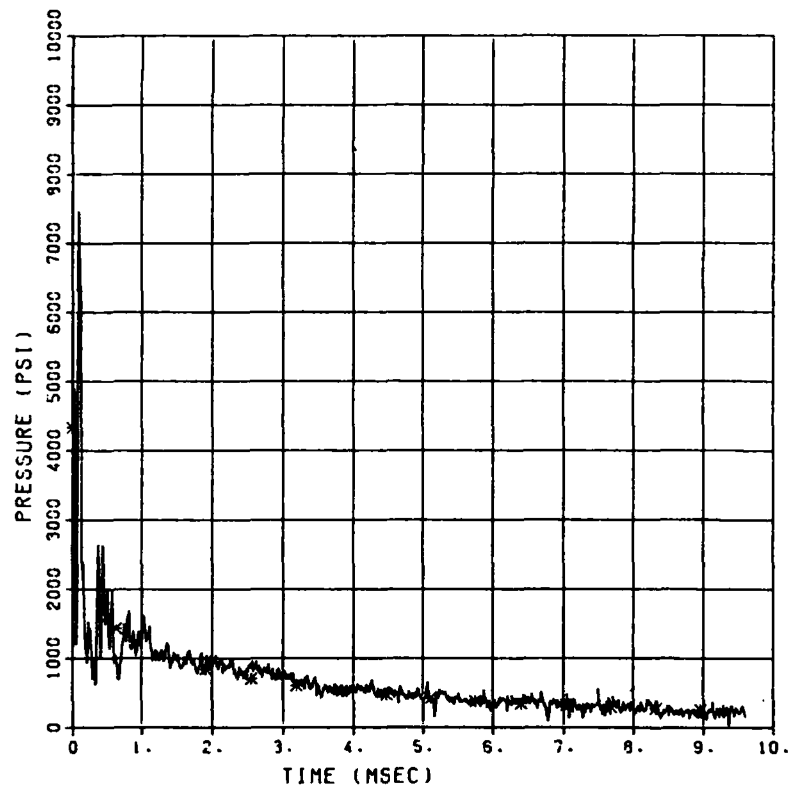

IMPULSE COMPARISON
DYNAMIC SHEAR 1
BP4
W(KT) = 1.115
P(PSI) =4343.
01/29/83 7405E

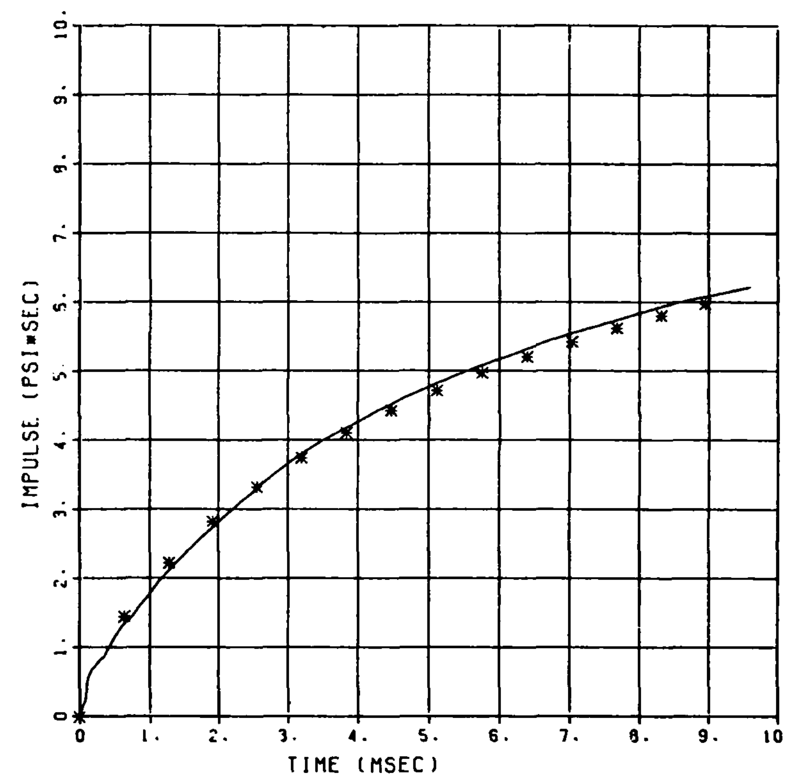

PRESSURE COMPARISON
DYNAMIC SHEAR 2
BP1
W(KT) = 1.403
P(PSI) =5094.
01/29/85 7359E

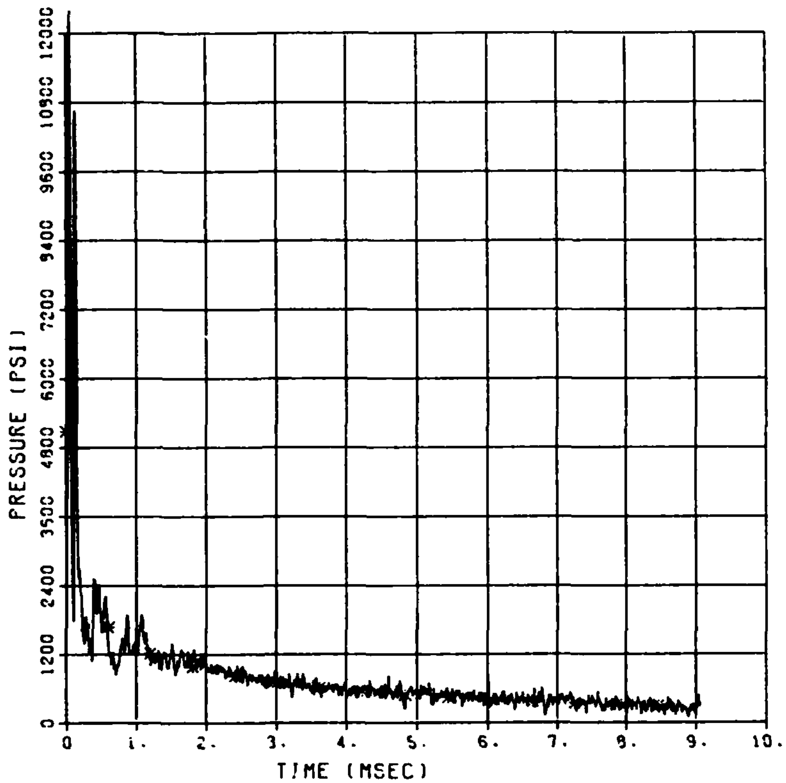

IMPULSE COMPARISON
DYNAMIC SHEAR 2
BP1
W(KT) = 1.403
P(PSI) =5094.
01/29/85 7359E

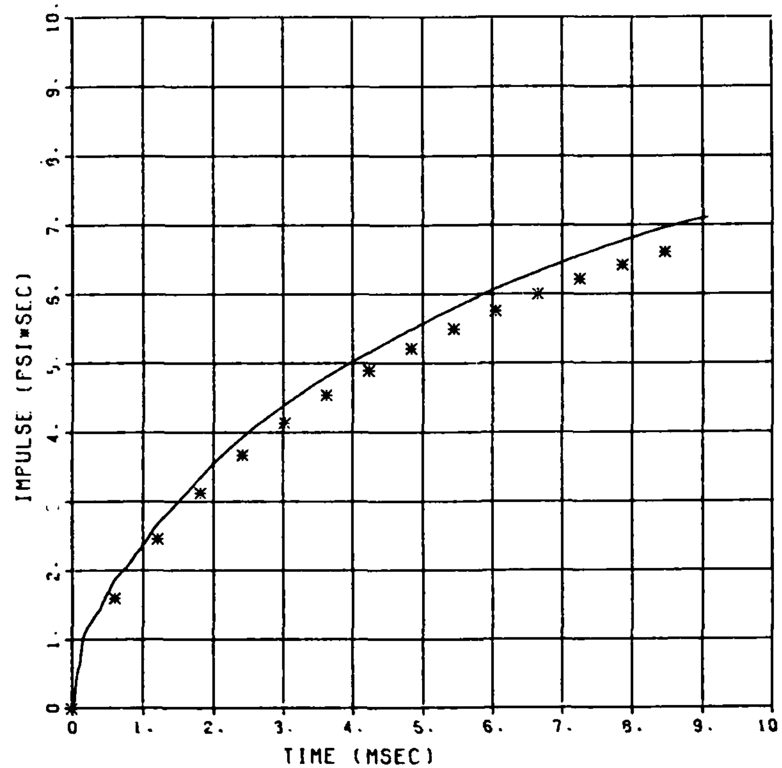

PRESSURE COMPARISON
DYNAMIC SHEAR 2
BP2
W(KT) = 1 115
P(PSI) =5312
01/28/83 7353E

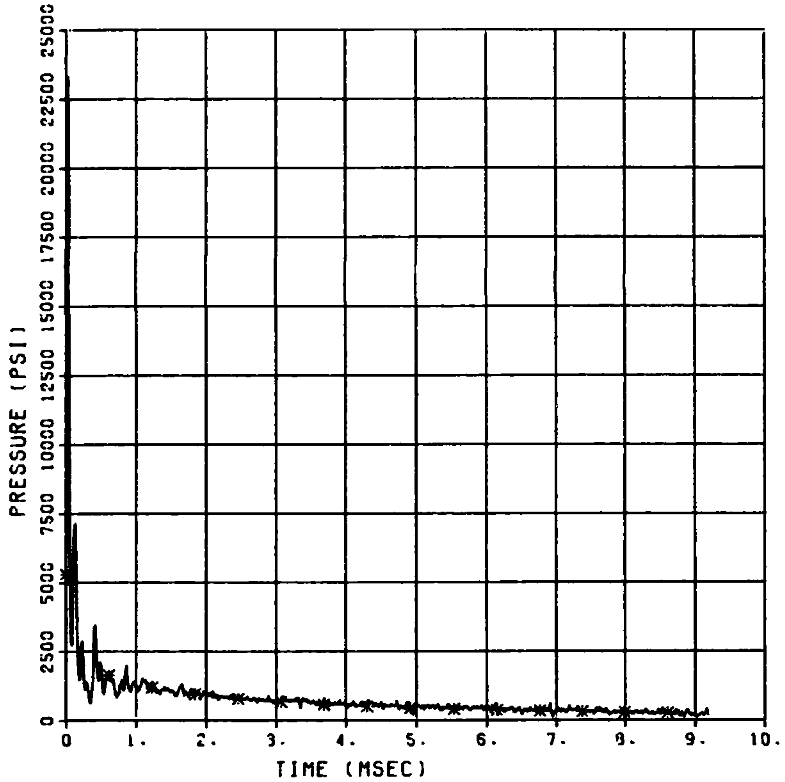

IMPULSE COMPARISON
DYNAMIC SHEAR 2
BP2
W(KT) = 1 115
P(PSI) =5312
01/28/83 7353E

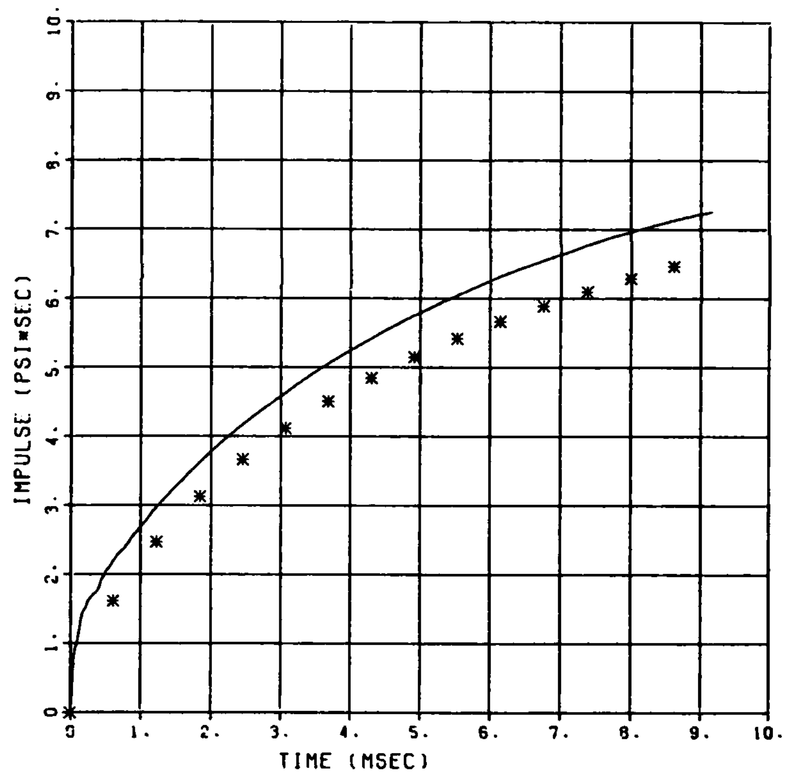

PRESSURE COMPARISON
DYNAMIC SHEAR 2
BF3
W(KT) = 0.392
P(PSI) =6614.
01/28/83 7359E

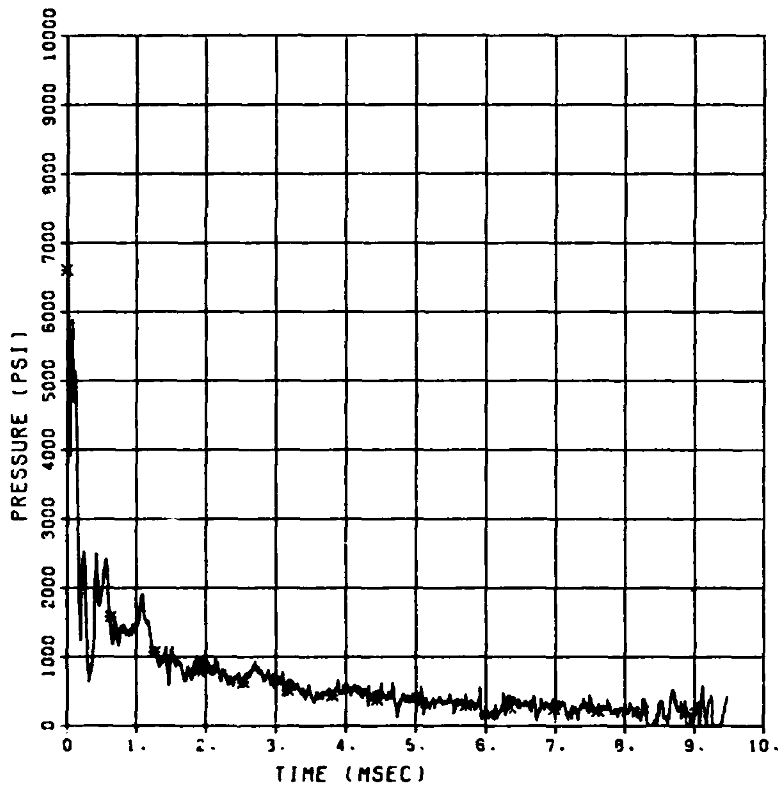

IMPULSE COMPARISON
DYNAMIC SHEAR 2
BF3
W(KT) = 0 382
P(PSI) =6614.
01/28/83 7353E

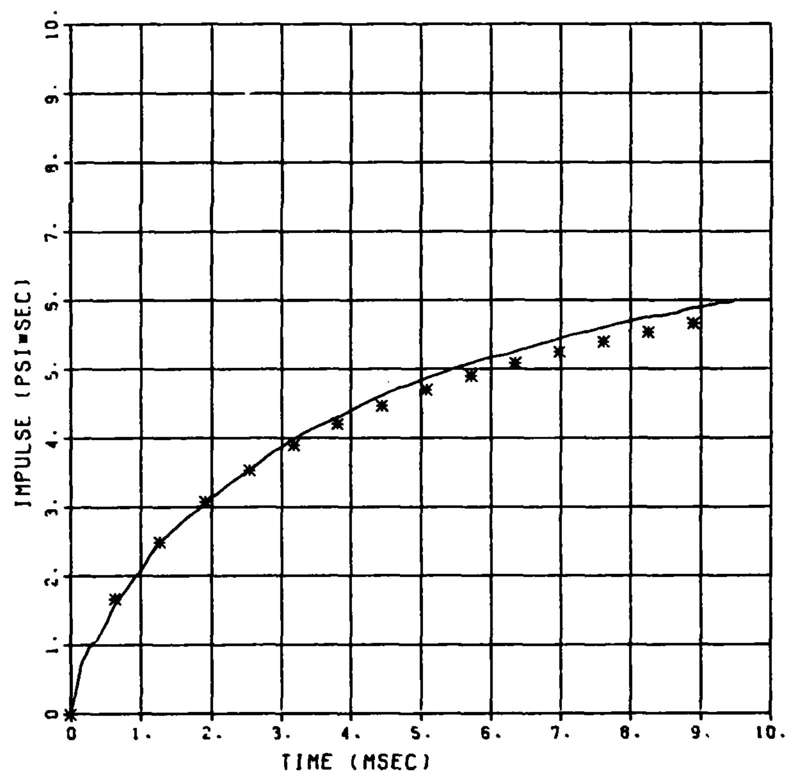

PRESSURE COMPARISON
DYNAMIC SHEAR 2
BP4
W(KT) = 0.657
P(PSI) =5637.
01/28/83 7359E

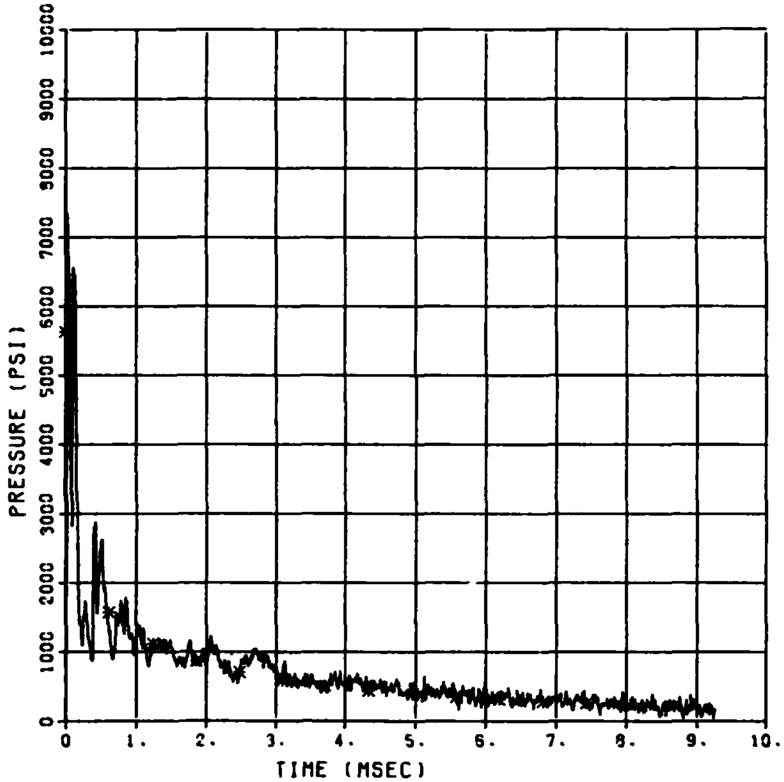

IMPULSE COMPARISON
DYNAMIC SHEAR 2
BP4
W(KT) = 0.657
P(PSI) =5637.
01/28/83 7359E

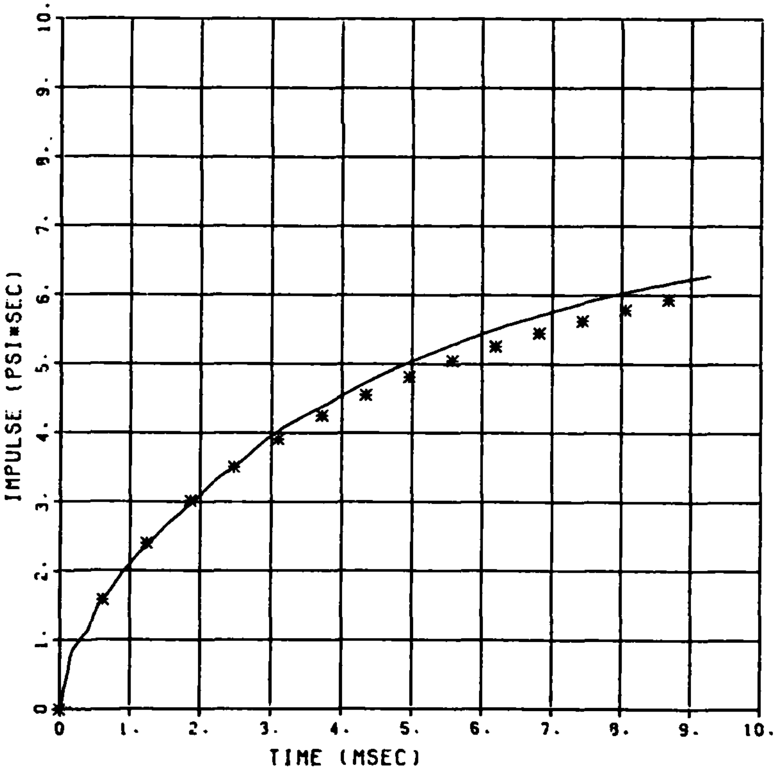

PRESSURE COMPARISON
DYNAMIC SHEAR 3
BP3
W(KT) = 0.177
P(PSI) =3607.
02/04/83 2663E

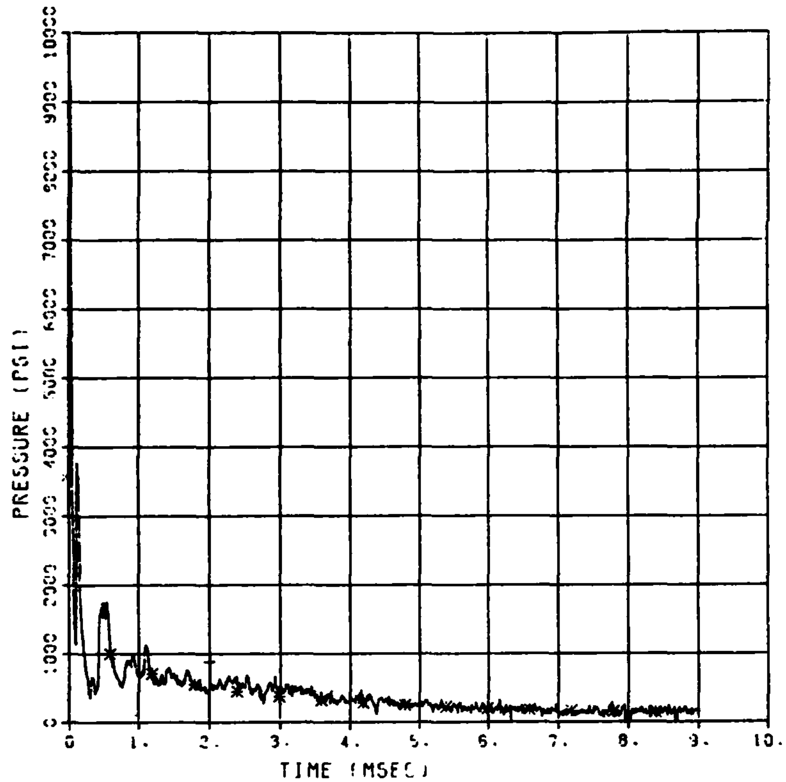

IMPULSE COMPARISON
DYNAMIC SHEAR 3
BP3
W(KT) = 0.177
P(PSI) =3607.
02/04/83 2663E

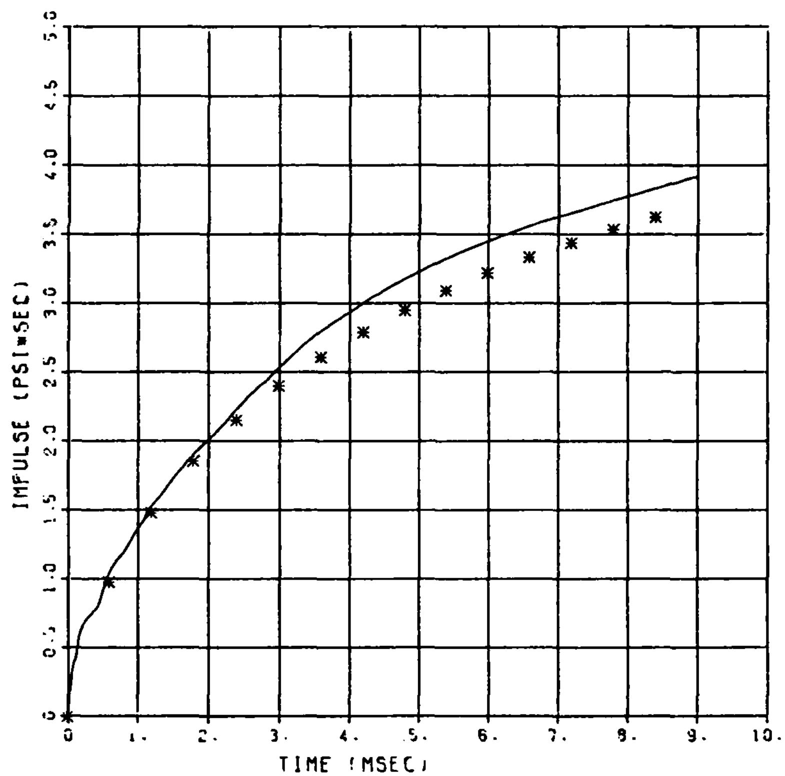

PRESSURE COMPARISON
DYNAMIC SHEAR 3
BP4
W(KT) = 0.276
P(PSI) =3058.
01/28/83 7783E

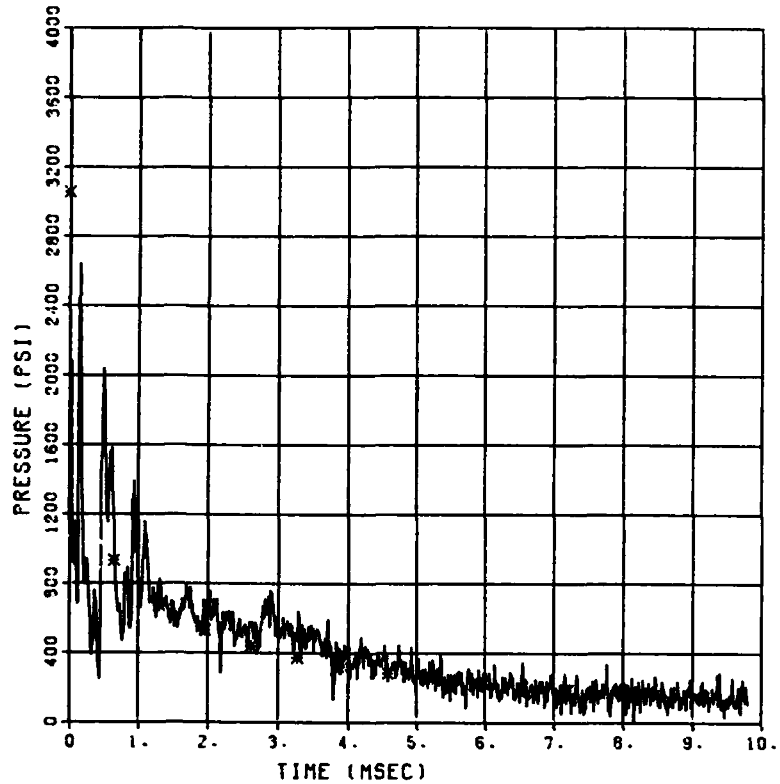

IMPULSE COMPARISON
DYNAMIC SHEAR 3
BP4
W(KT) = 0.276
P(PSI) =3058.
01/28/83 7783E

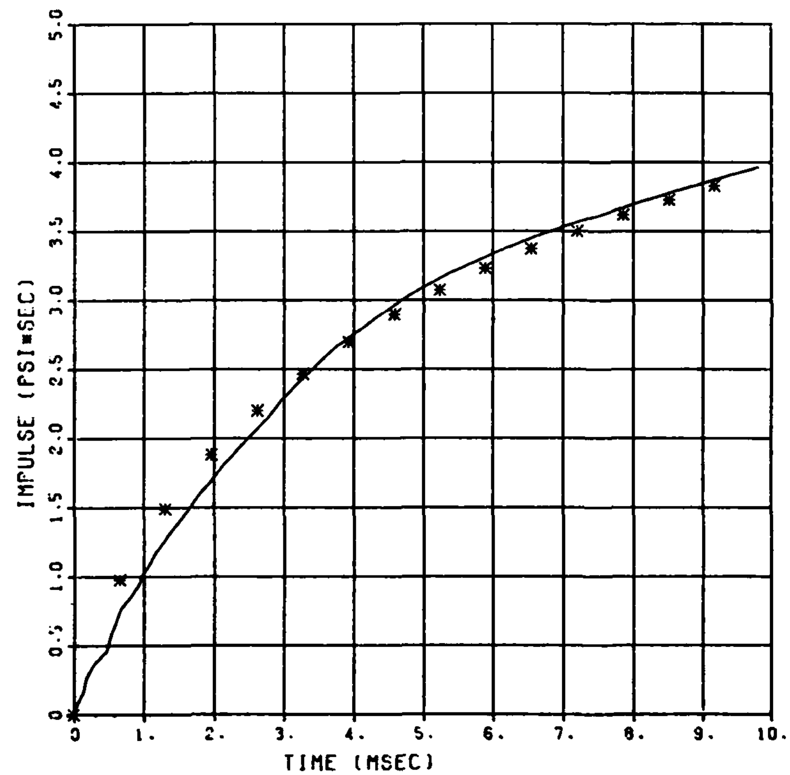

PRESSURE COMPARISON
DYNAMIC SHEAR 4
BP1
W(KT) = 0 766
P(PSI) =3554.
01/28/83 7754E

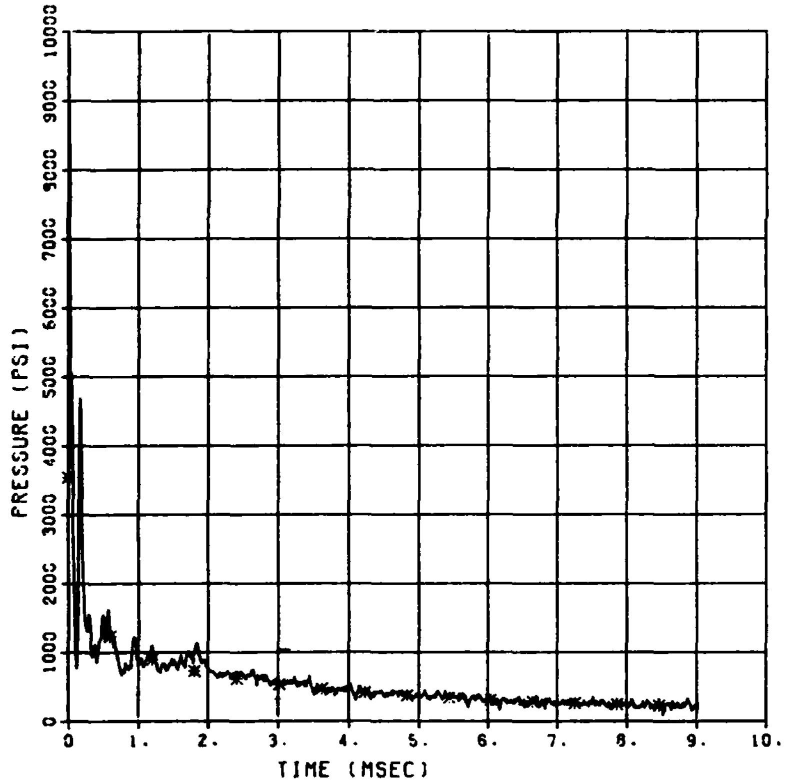

IMPULSE COMPARISON
DYNAMIC SHEAR 4
BP1
W(KT) = 0.766
P(PSI) =3554.
01/29/83 7754E

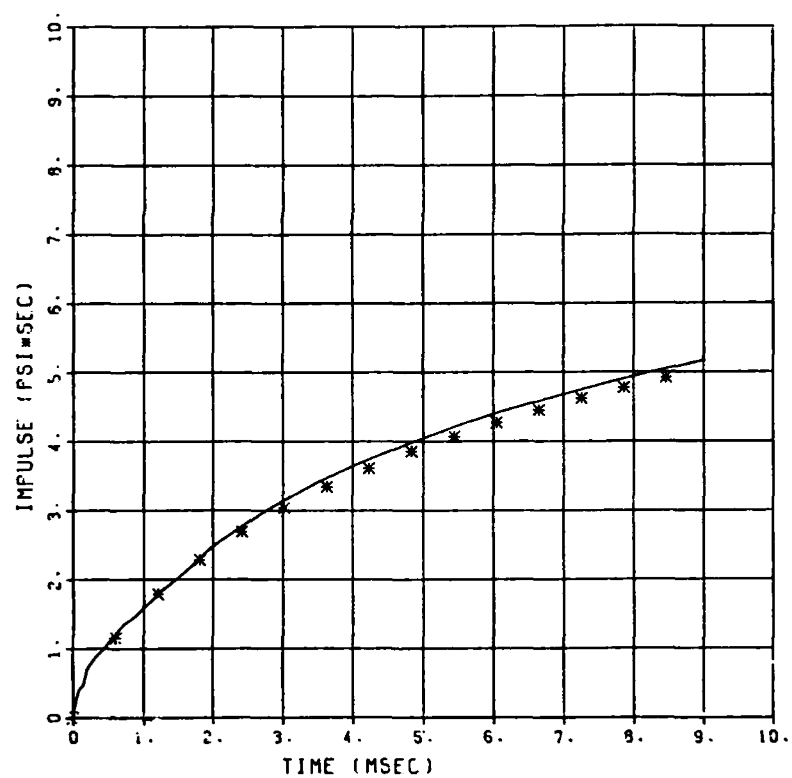

PRESSURE COMPARISON
DYNAMIC SHEAR 4
BP2
W(KT) = 0.595
P(PSI) =4359.
01/28/93 7754E

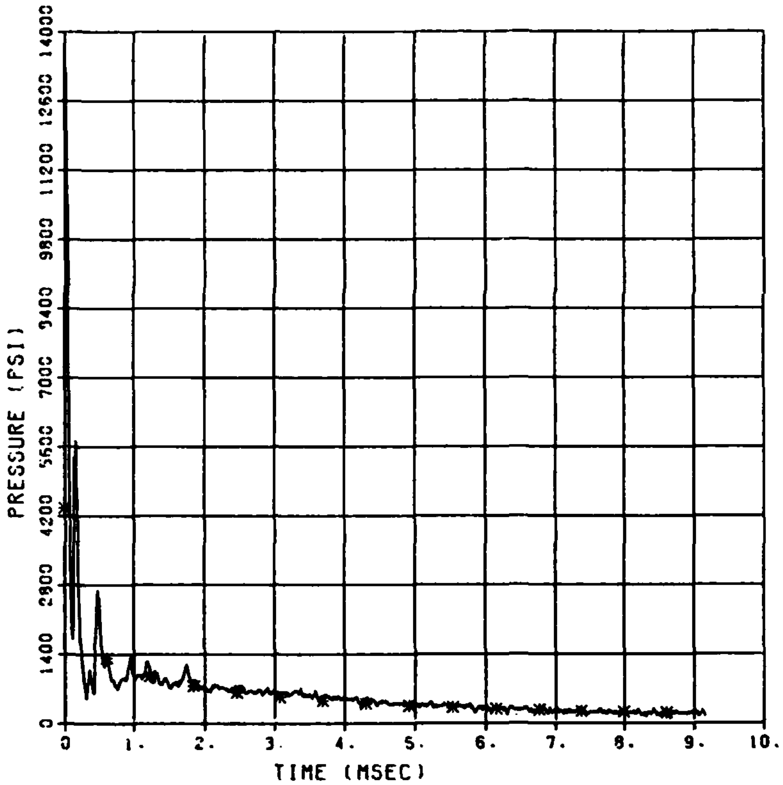

IMPULSE COMPARISON
DYNAMIC SHEAR 4
BP2
W(KT) = 0.595
P(PSI) =4363.
01/28/93 7754E

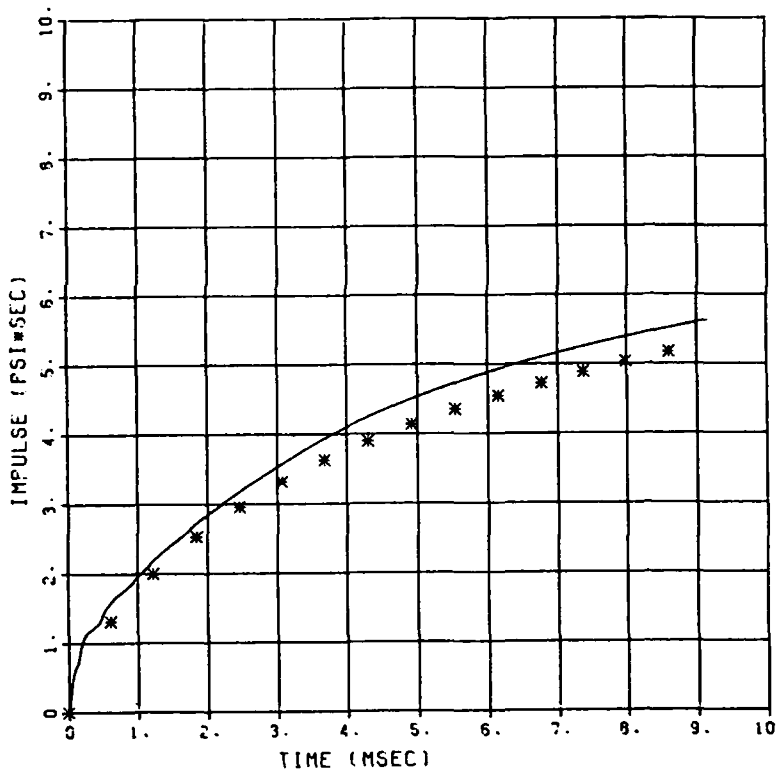

PRESSURE COMPARISON
DYNAMIC SHEAR 4
BP4
W(KT) = 1.137
P(PSI) =4169.
01/29/83 7754E

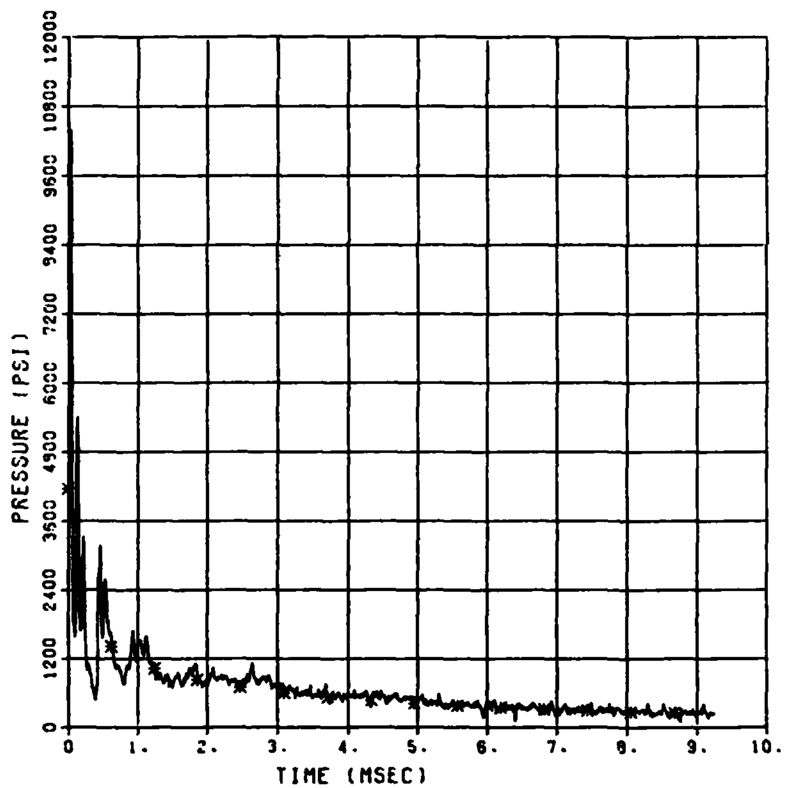

IMPULSE COMPARISON
DYNAMIC SHEAR 4
BP4
W(KT) = 1.137
P(PSI) =4169.
01/28/83 7754E

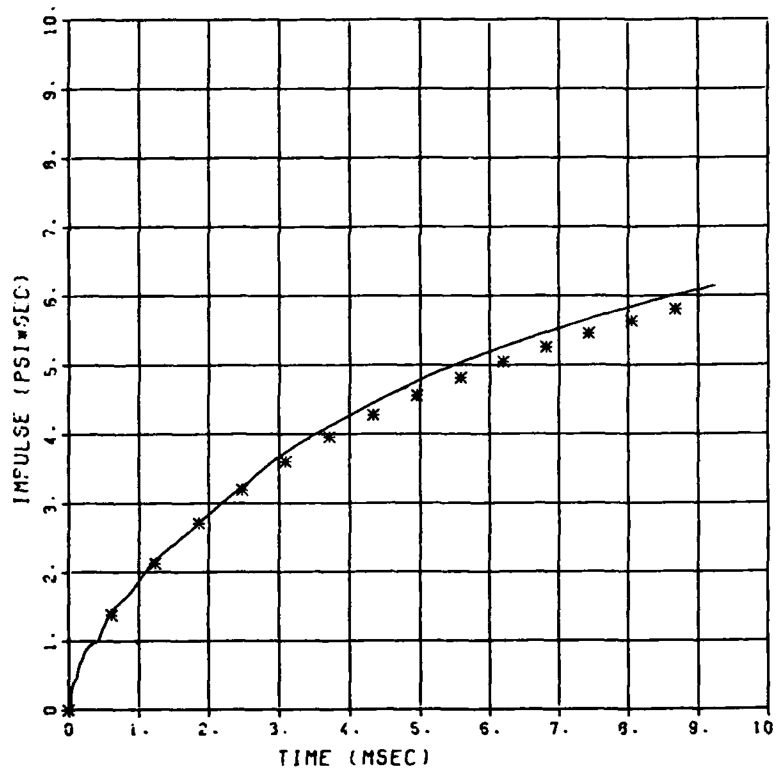

PRESSURE COMPARISON
DYNAMIC SHEAR 5
BP2
W(KT) = 2.277
P(PSI) =7354.
01/29/85 7754E

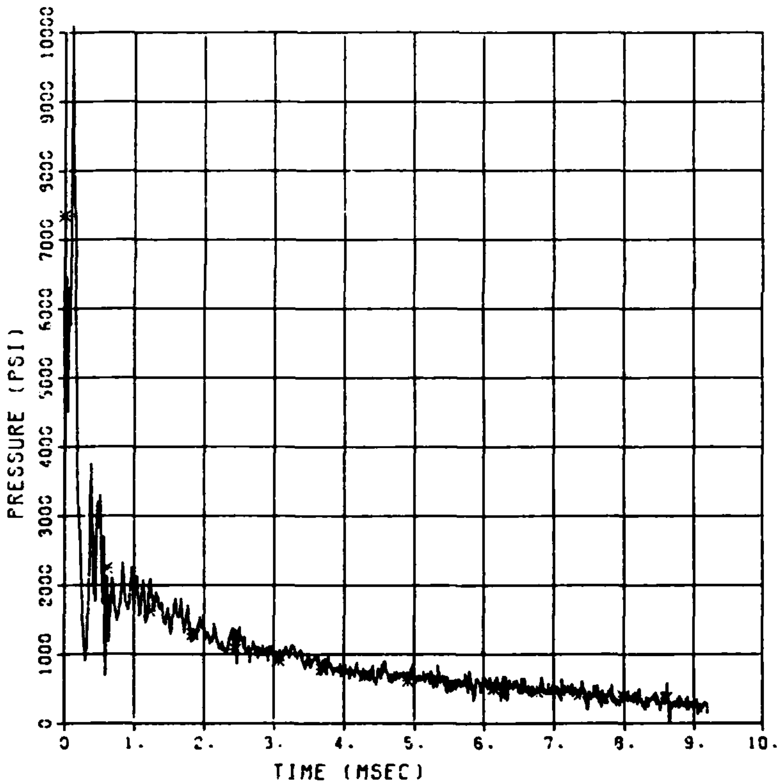

IMPULSE COMPARISON
DYNAMIC SHEAR 5
BP2
W(KT) = 2.277
P(PSI) =7354.
01/28/85 7754E

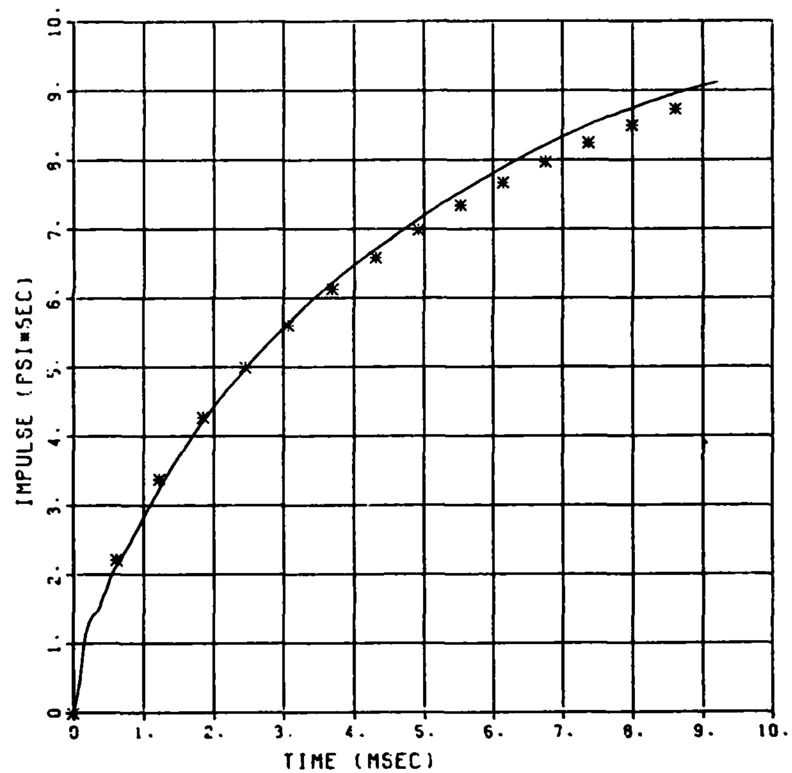

PRESSURE COMPARISON
DYNAMIC SHEAR 5
BP3
W(KT) = 1.942
P(PSI) =4696.
01/28/93 7754E

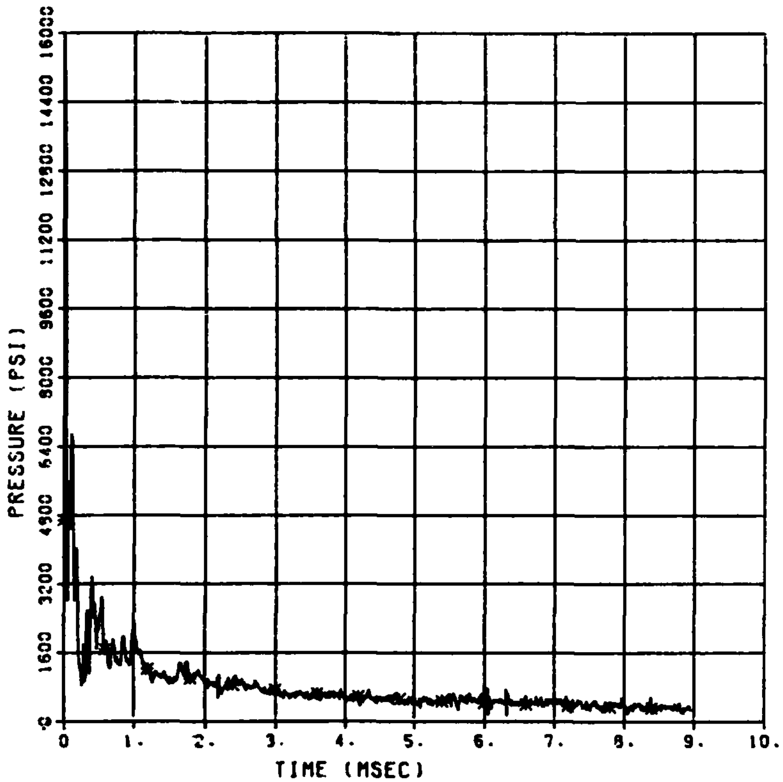

IMPULSE COMPARISON
DYNAMIC SHEAR 5
BP3
W(KT) = 1.942
P(PSI) =4696
01/28/93 7754E

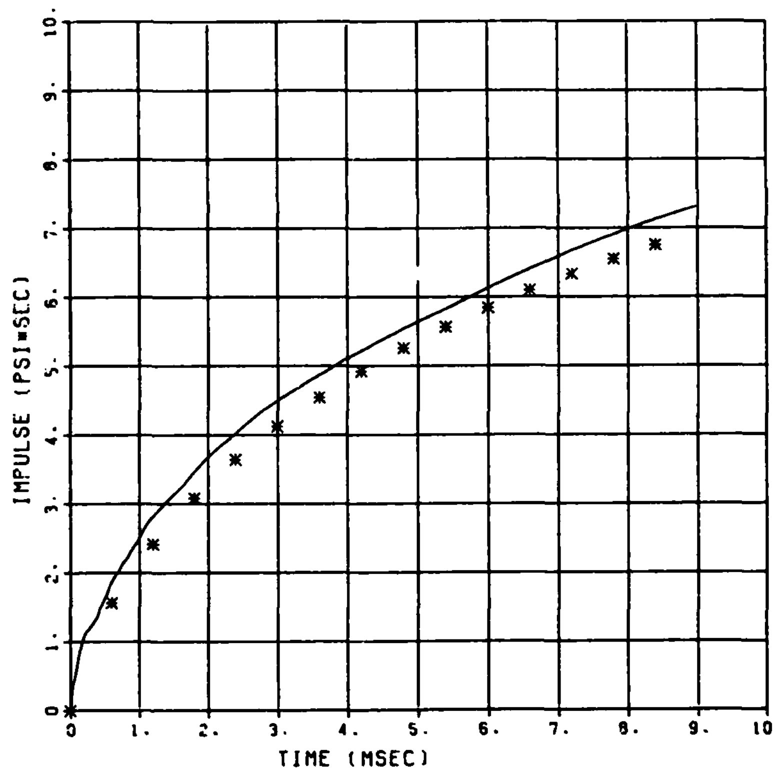

PRESSURE COMPARISON
DYN SH II TEST 1
BP1
W(KT) = 2.347
P(PSI) =6690.
06/30/82 2435C

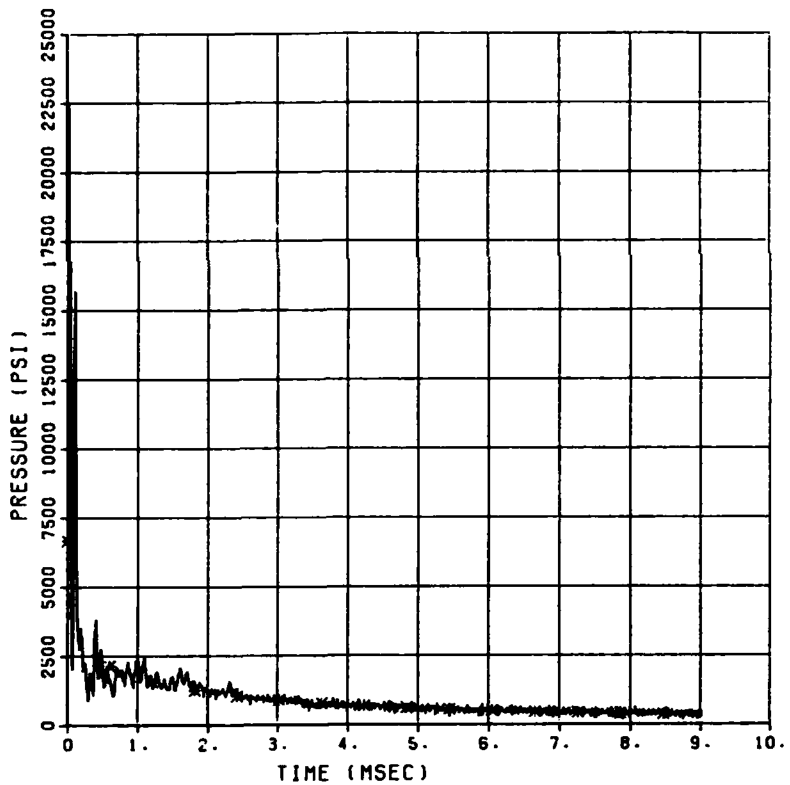

IMPULSE COMPARISON
DYN SH II TEST 1
BP1
W(KT) = 2.347
P(PSI) =6690.
06/30/82 2435C

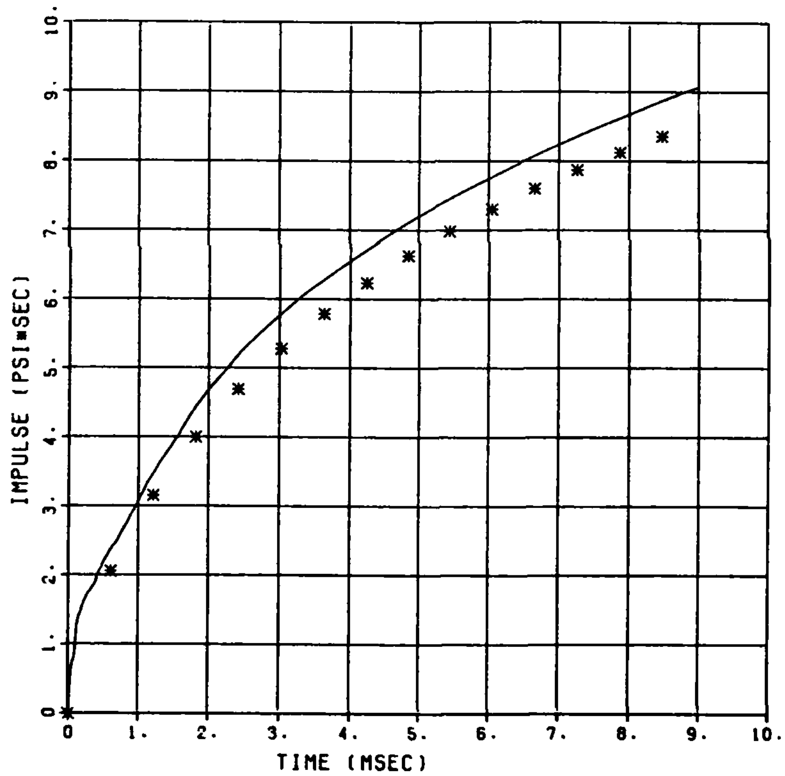

PRESSURE COMPARISON
DYN SH II TEST 1
BP4
W(KT) = 0.713
P(PSI) =9556.
06/30/82 2435C

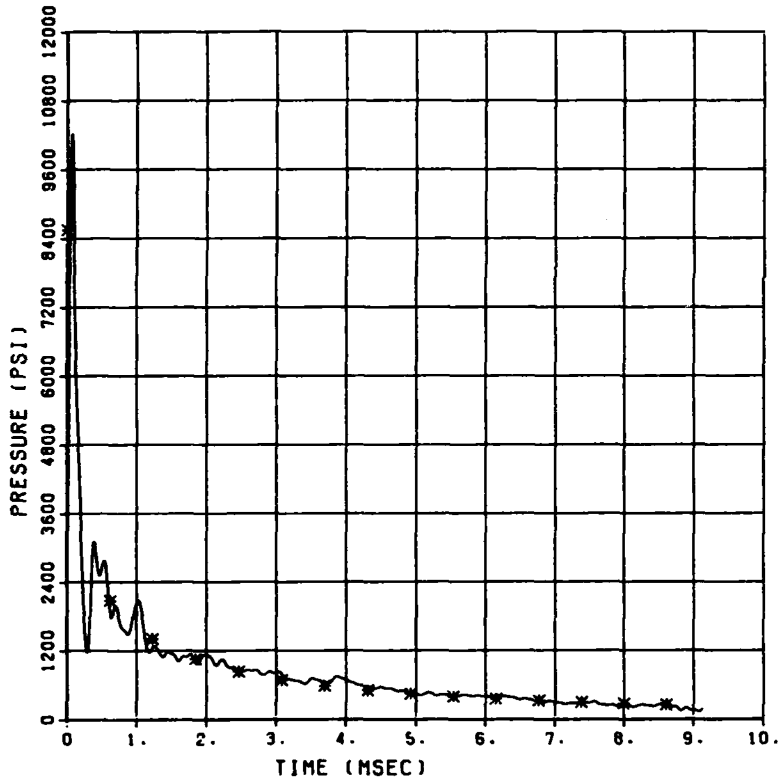

IMPULSE COMPARISON
DYN SH II TEST 1
BP4
W(KT) = 0.713
P(PSI) =9558.
06/30/82 2435C

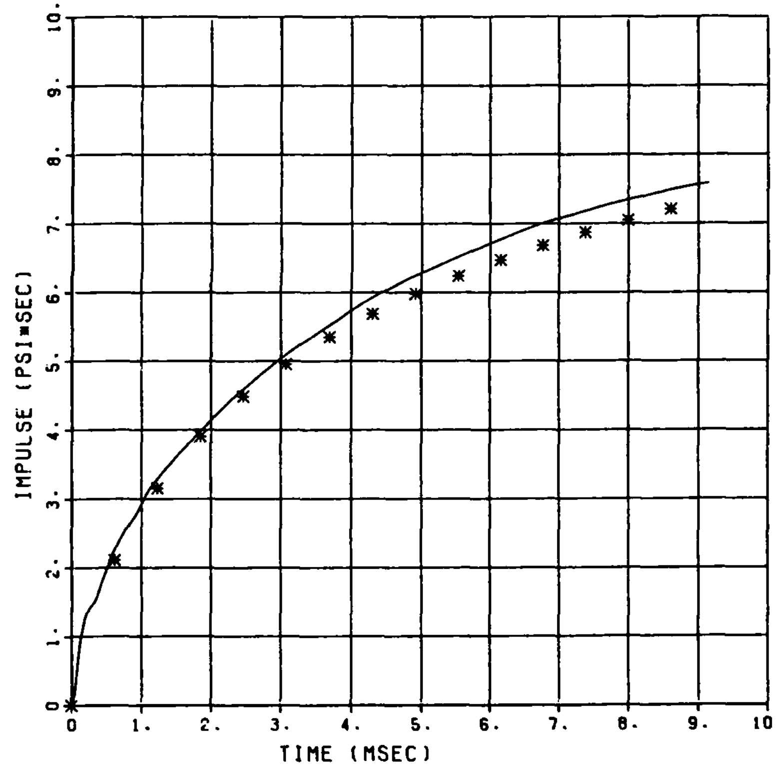

PRESSURE COMPARISON
DYN SH II TEST 2
BP1
W(KT) = 2 754
P(PSI) =5795.
07/01/82 70290

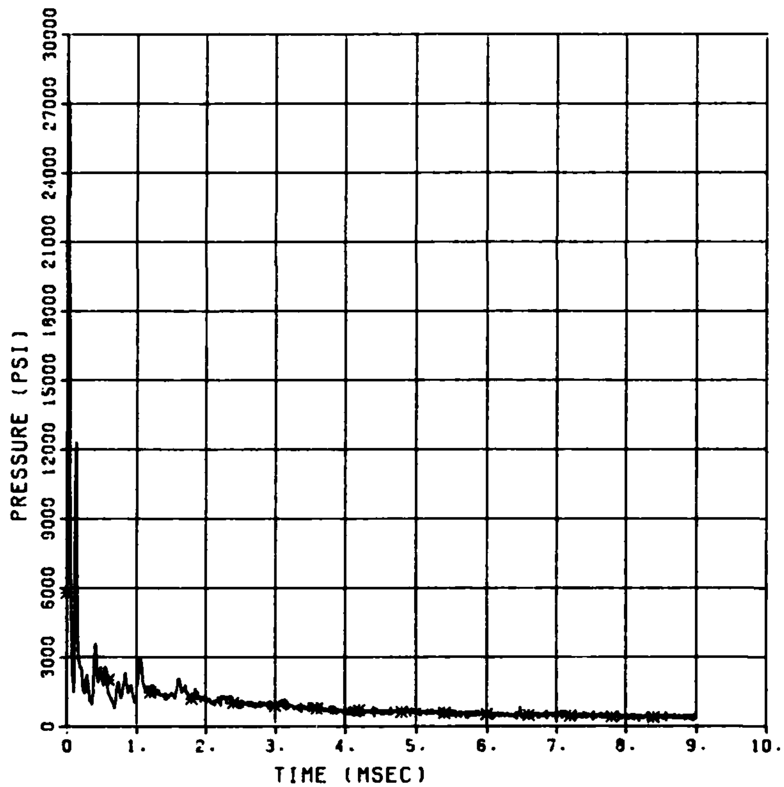

IMPULSE COMPARISON
DYN SH II TEST 2
BP1
W(KT) = 2.754
P(PSI) =5795.
07/01/82 70290

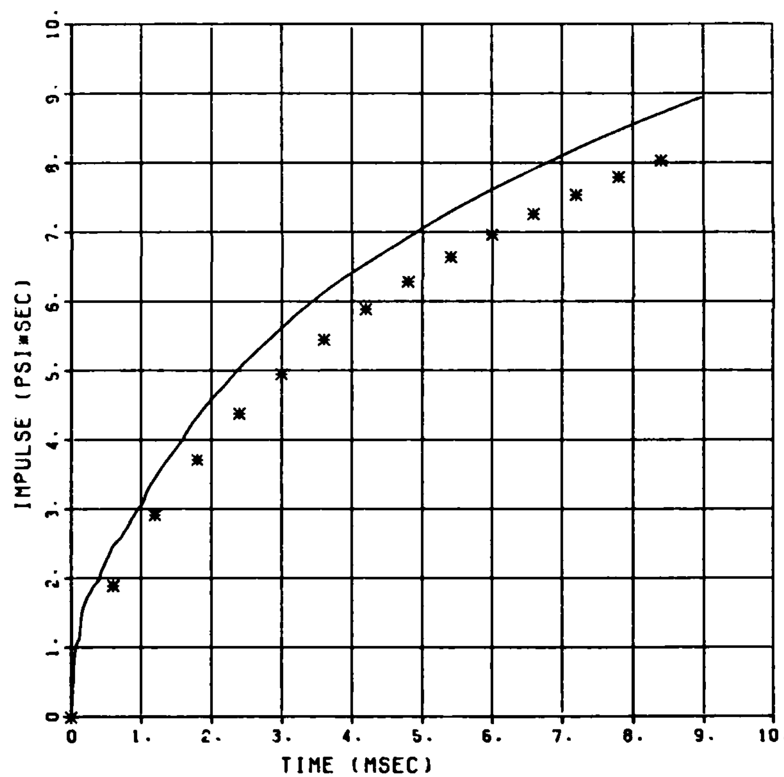

PRESSURE COMPARISON
DYN SH II TEST 2
BP2
W(KT) = 1.293
P(PSI) =5982.
07/01/82 70290

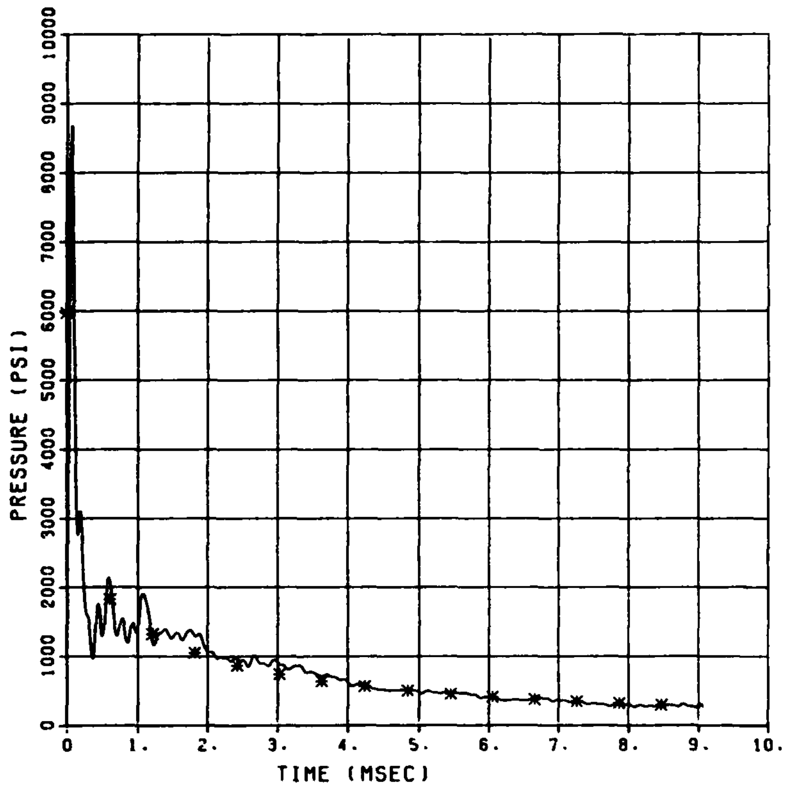

IMPULSE COMPARISON
DYN SH II TEST 2
BP2
W(KT) = 1.293
P(PSI) =5982.
07/01/82 70290

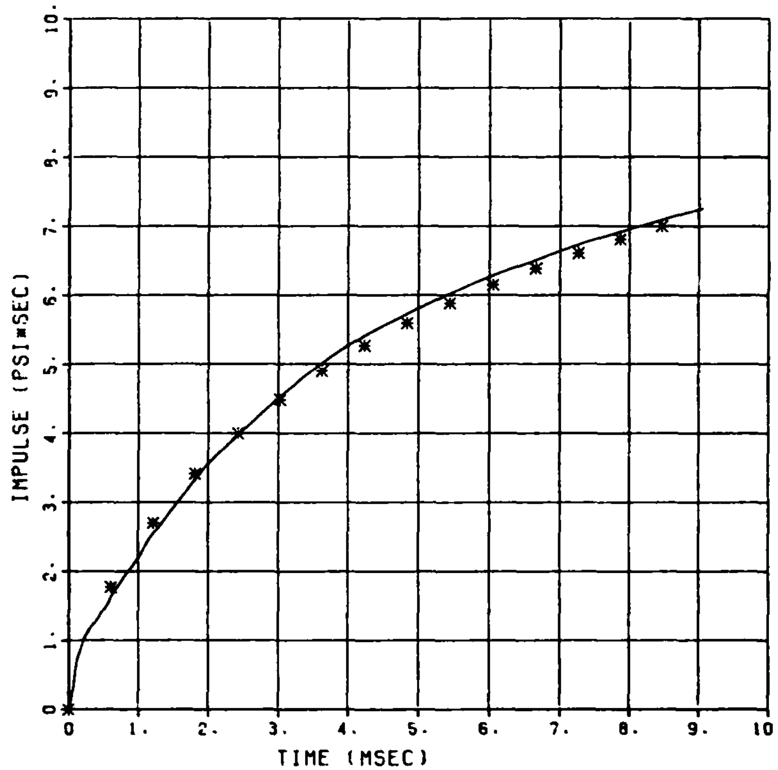

PRESSURE COMPARISON
DYN SH II TEST 2
BP4
W(KT) = 1.617
P(PSI) =5806.
07/01/82 70290

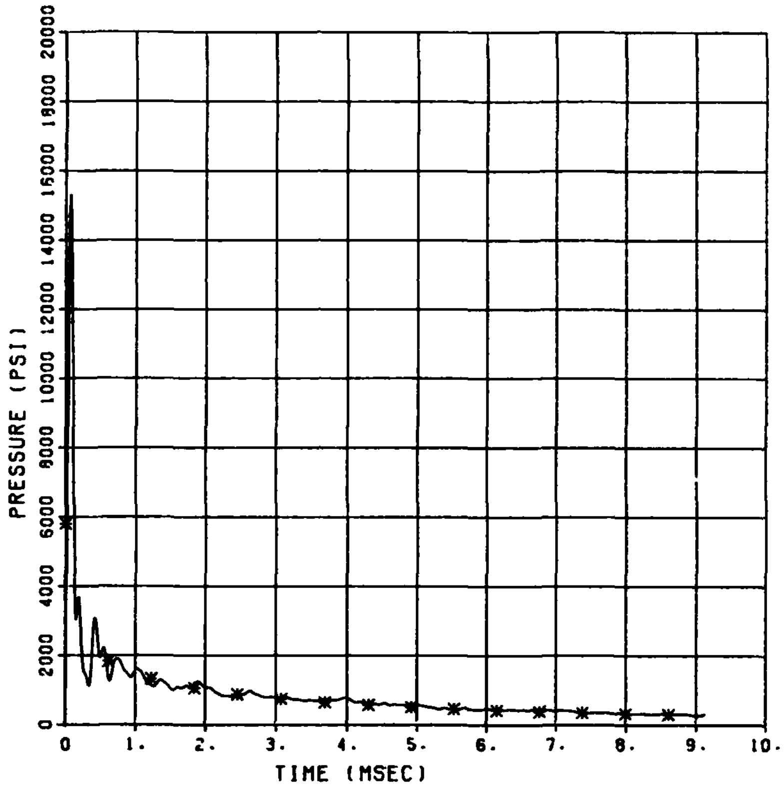

IMPULSE COMPARISON
DYN SH II TEST 2
BP4
W(KT) = 1.617
P(PSI) =5806.
07/01/82 70290

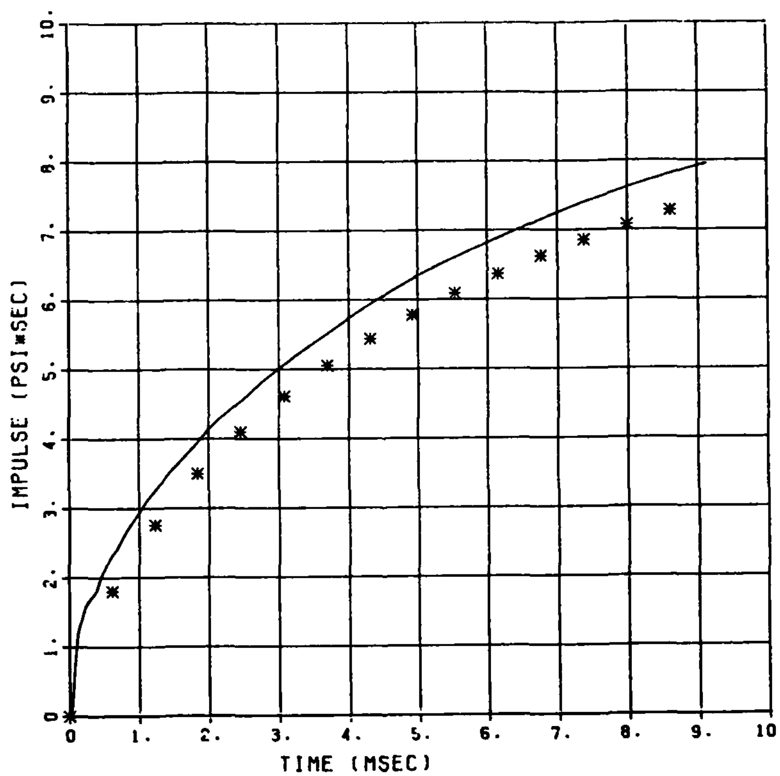

PRESSURE COMPARISON
DYN SH II TEST 3
BP1
W(KT) = 0.837
P(PSI) =3064.
01/17/83 2940B

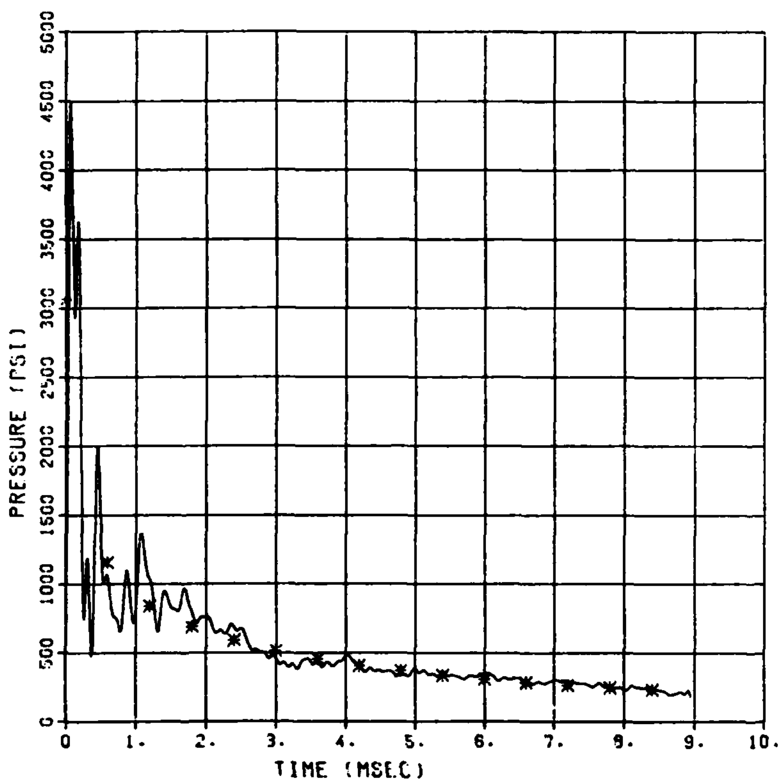

IMPULSE COMPARISON
DYN SH II TEST 3
BP1
W(KT) = 0.837
P(PSI) =3064.
01/17/83 2940A

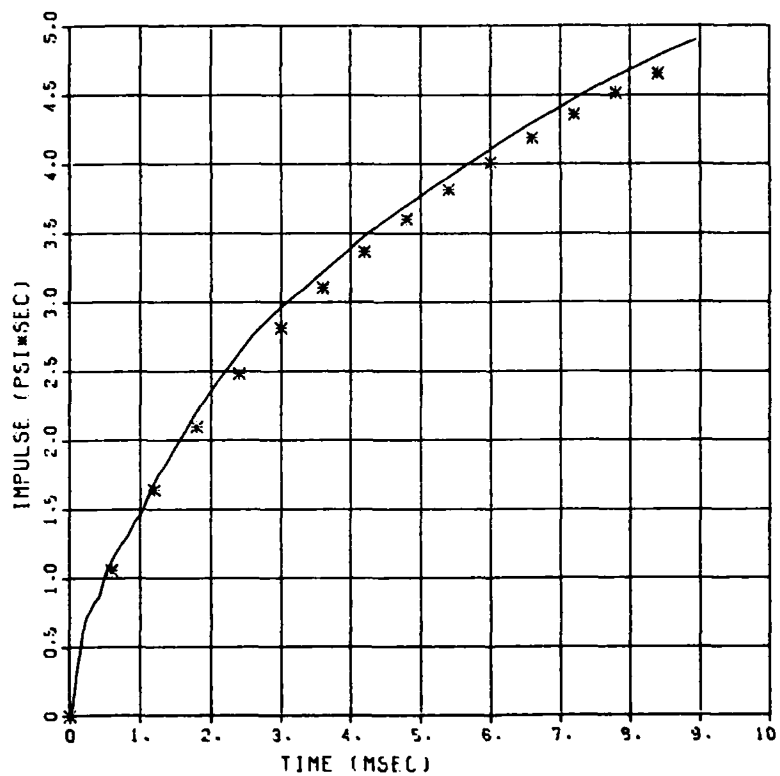

PRESSURE COMPARISON
DYN SH II TEST 3
BP2
W(KT) = 0 342
P(PSI) =3553.
07/01/82 70230

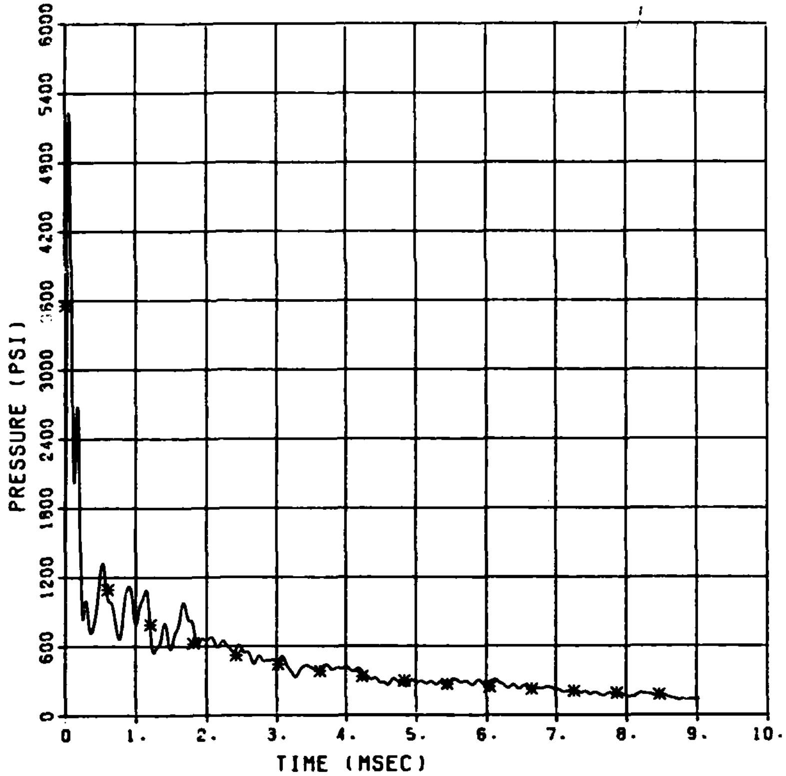

IMPULSE COMPARISON
DYN SH II TEST 3
BP2
W(KT) = 0.342
P(PSI) =3559.
07/01/82 70230

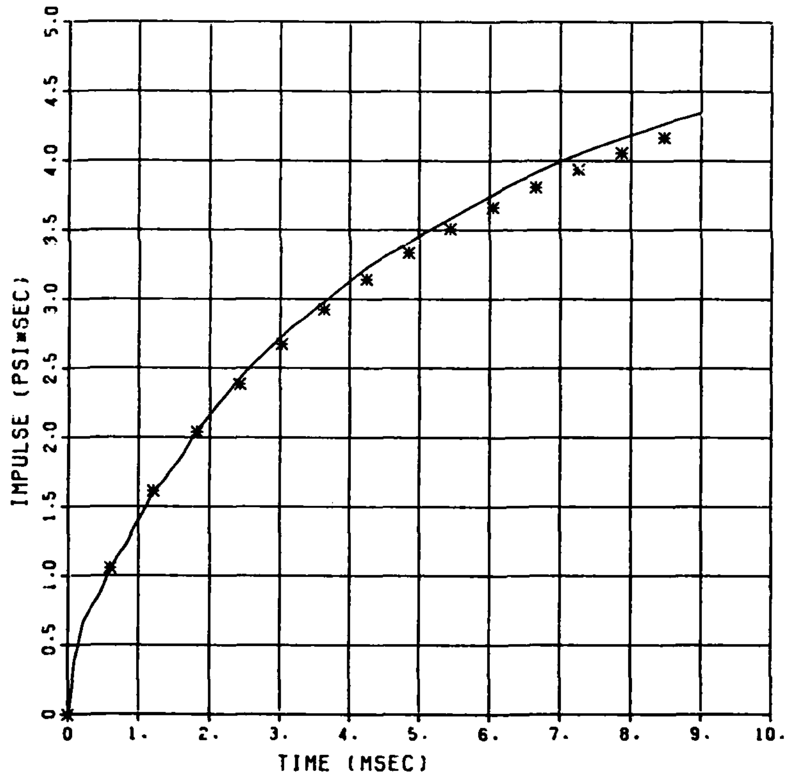

PRESSURE COMPARISON
DYN SH II TEST 3
BP4
W(KT) = 0.249
P(PSI) =3848.
07/01/82 70290

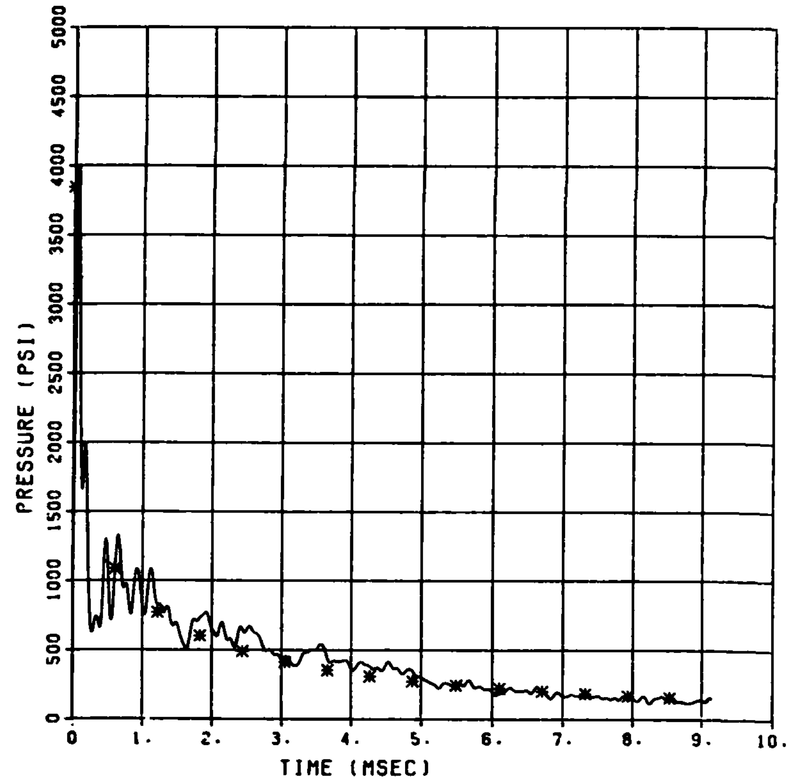

IMPULSE COMPARISON
DYN SH II TEST 3
BP4
W(KT) = 0.248
P(PSI) =3848.
07/01/82 70290

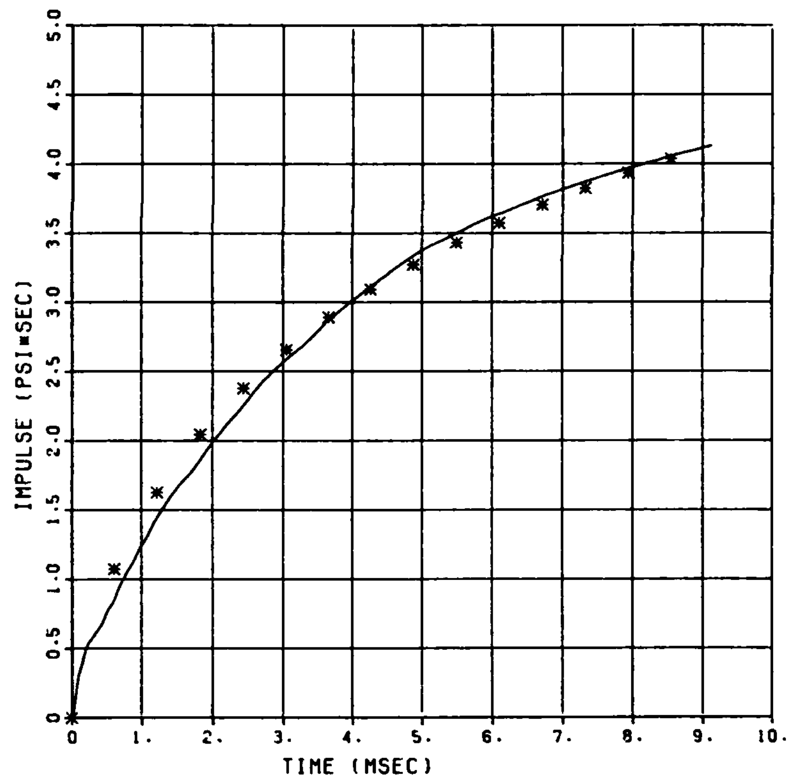

PRESSURE COMPARISON
DYN SH II TEST 4
BP1
W(KT) = 1.900
P(PSI) =5658.
07/01/82 7481D

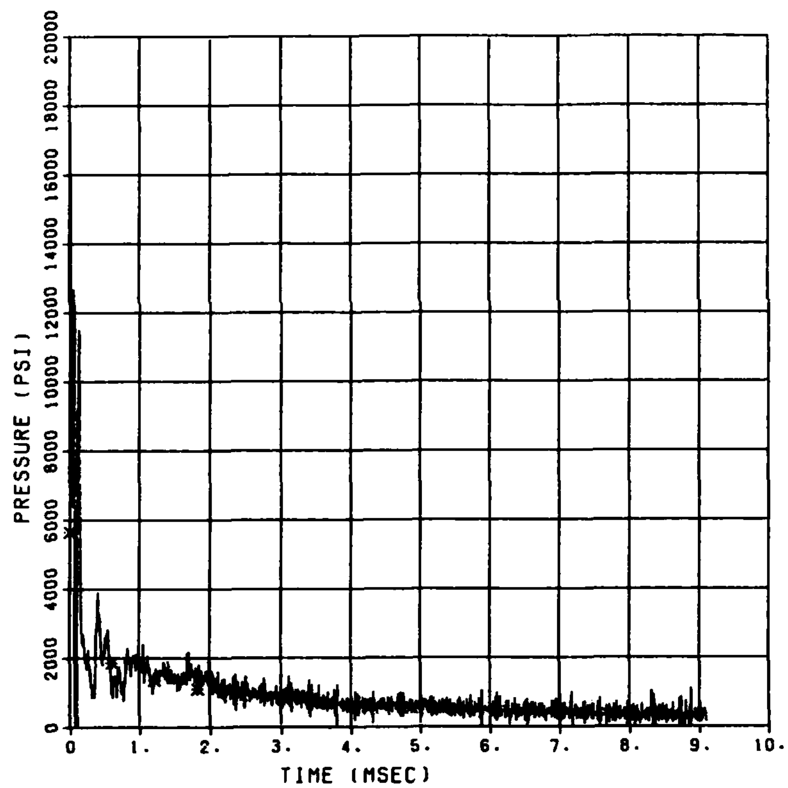

IMPULSE COMPARISON
DYN SH II TEST 4
BP1
W(KT) = 1.900
P(PSI) =5658.
07/01/82 7481D

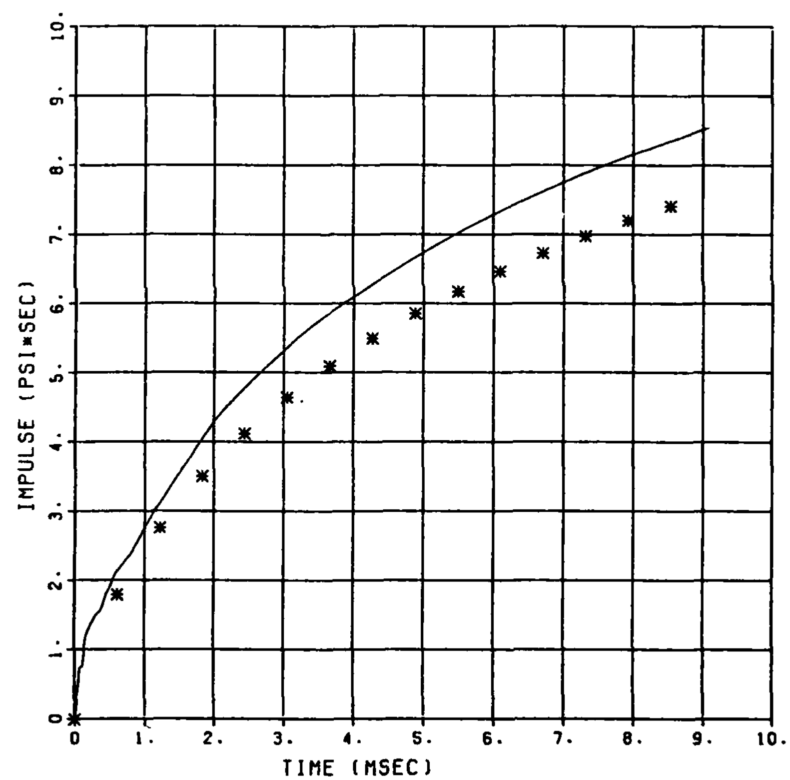

PRESSURE COMPARISON
DYN SH II TEST 4
BP3
W(KT) = 0.869
P(PSI) =10813.
07/01/82 74810

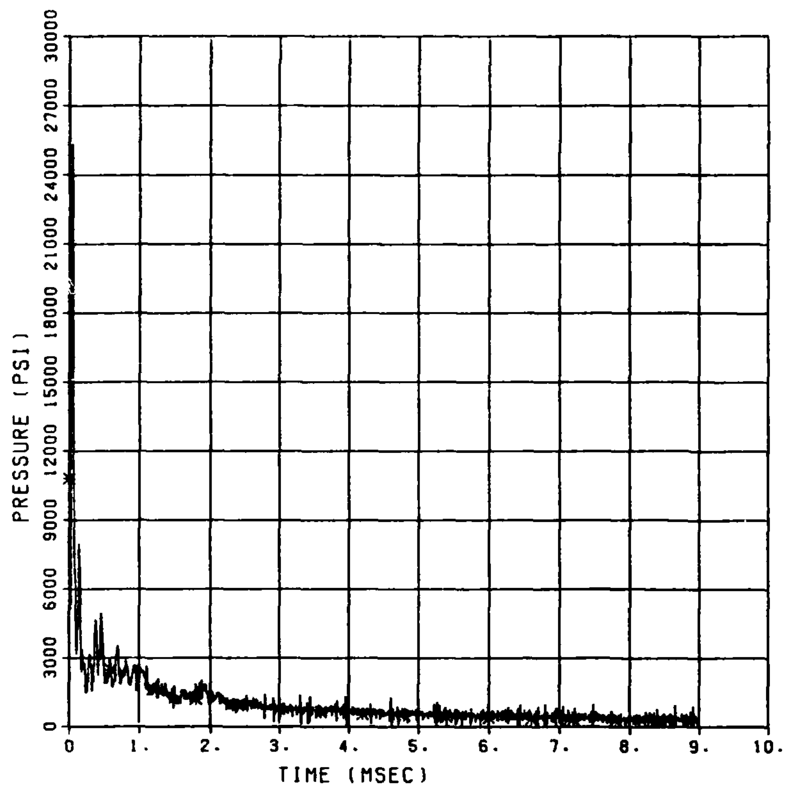

IMPULSE COMPARISON
DYN SH II TEST 4
BP3
W(KT) = 0.869
P(PSI) =10813.
07/01/82 74810

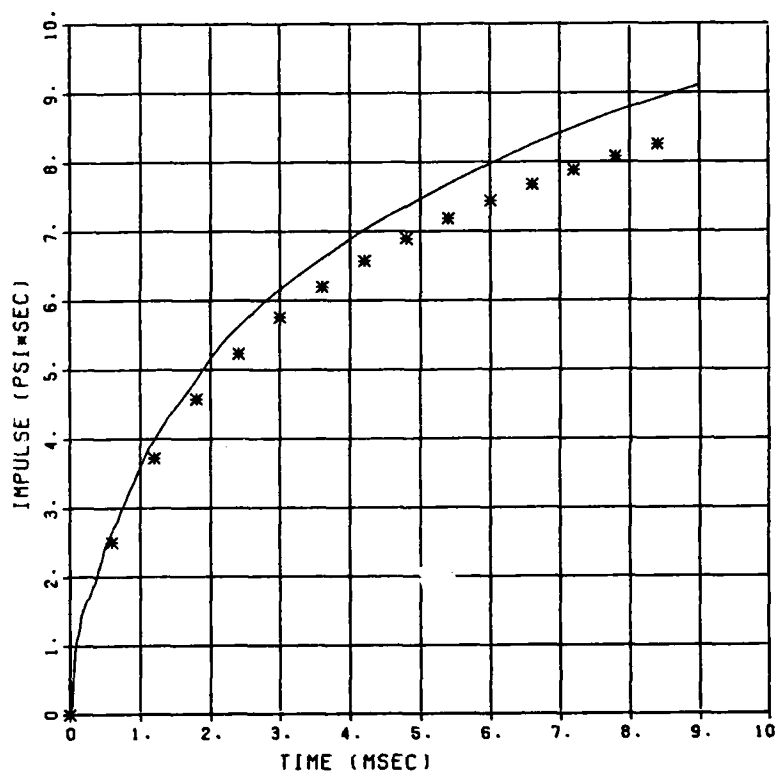

PRESSURE COMPARISON
DYN SH II TEST 4
BP2
W(KT) = 0.820
P(PSI) =8170.
01/17/93 2941A

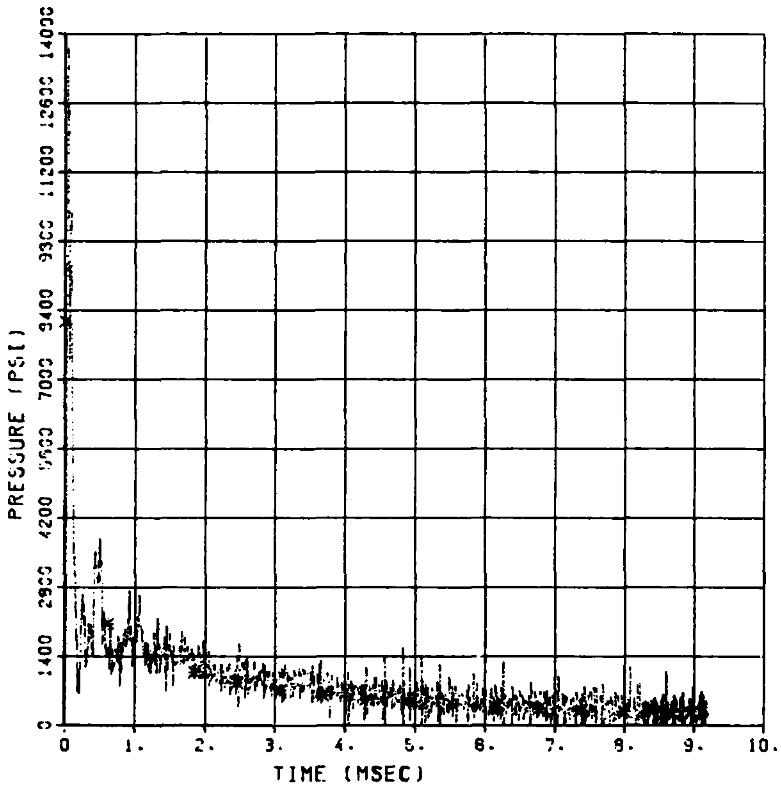

IMPULSE COMPARISON
DYN SH II TEST 4
BP2
W(KT) = 0.820
P(PSI) =8170.
01/17/93 2941A

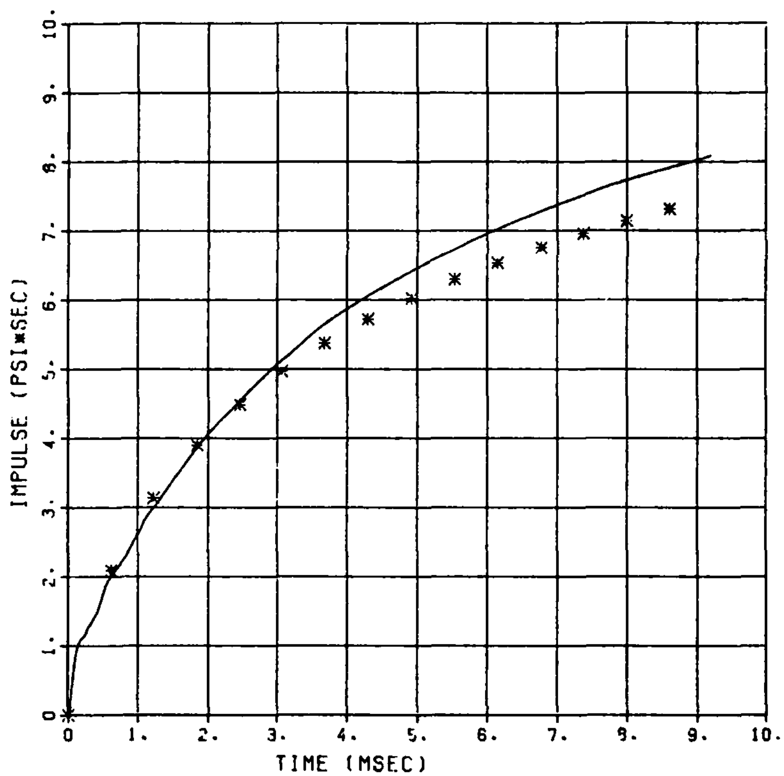

PRESSURE COMPARISON
DYN SH II TEST 4
BP4
W(KT) = 0.566
P(PSI) =10857.
07/01/82 74810

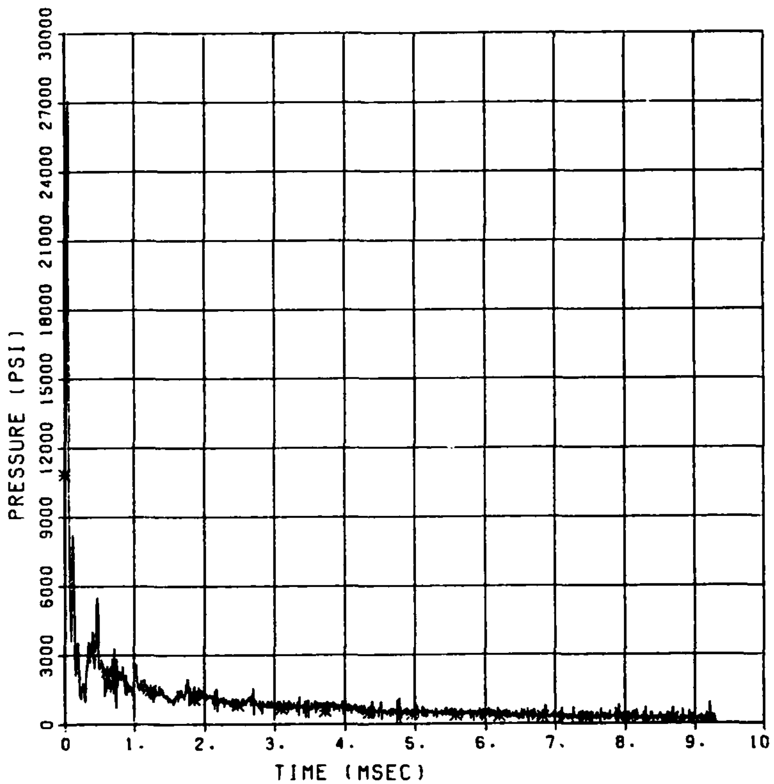

IMPULSE COMPARISON
DYN SH II TEST 4
BP4
W(KT) = 0.568
P(PSI) =10857.
07/01/82 74810

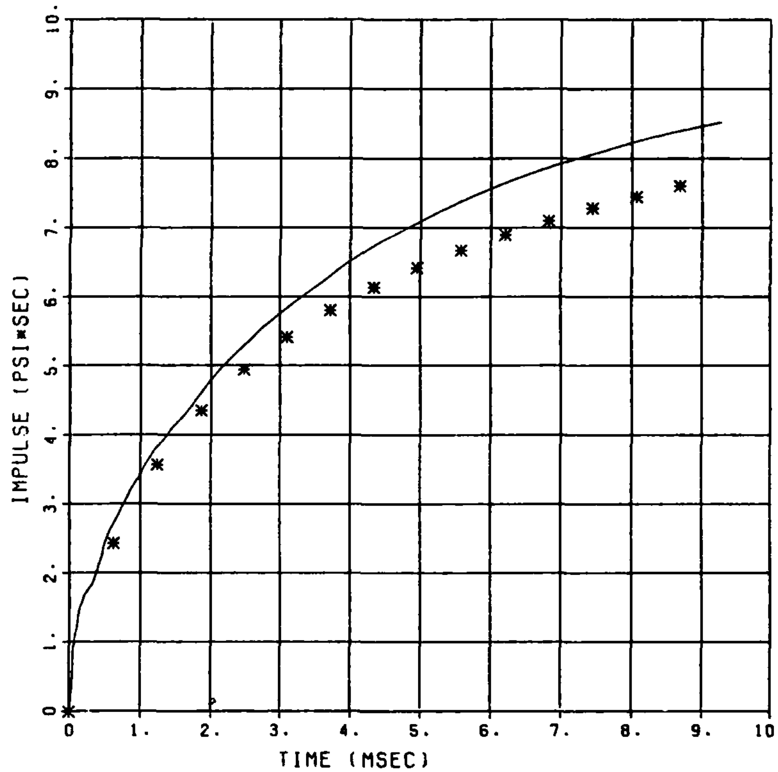

PRESSURE COM ?RISON
DYN SH II TEST 5
BP1
W(KT) = 4.298
P(PSI) =4003.
07/01/82 70640

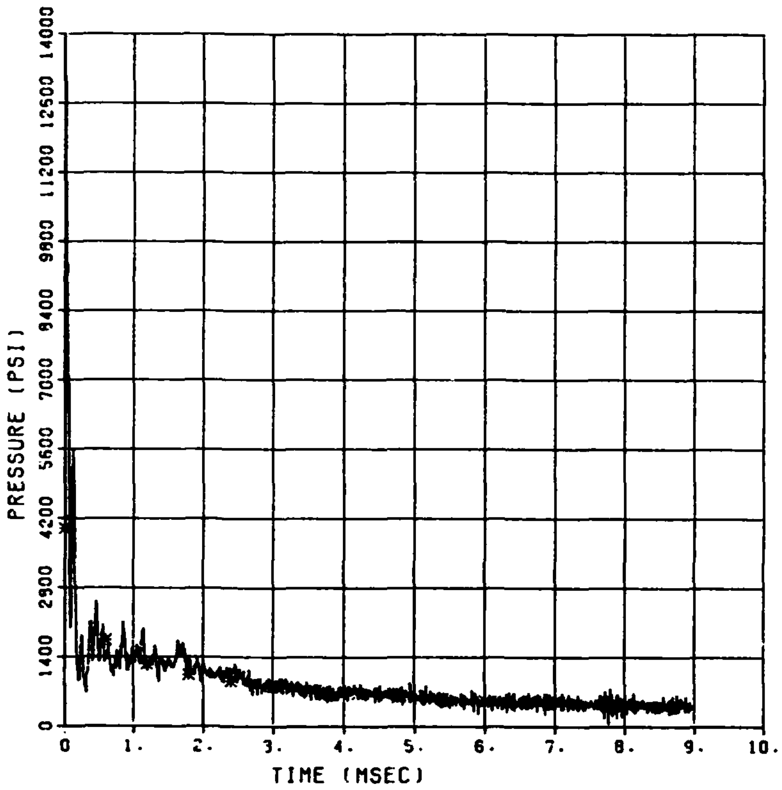

IMPULSE COMPARISON
DYN SH II TEST 5
BP1
W(KT) = 4.298
P(PSI) =4003.
07/01/82 70640

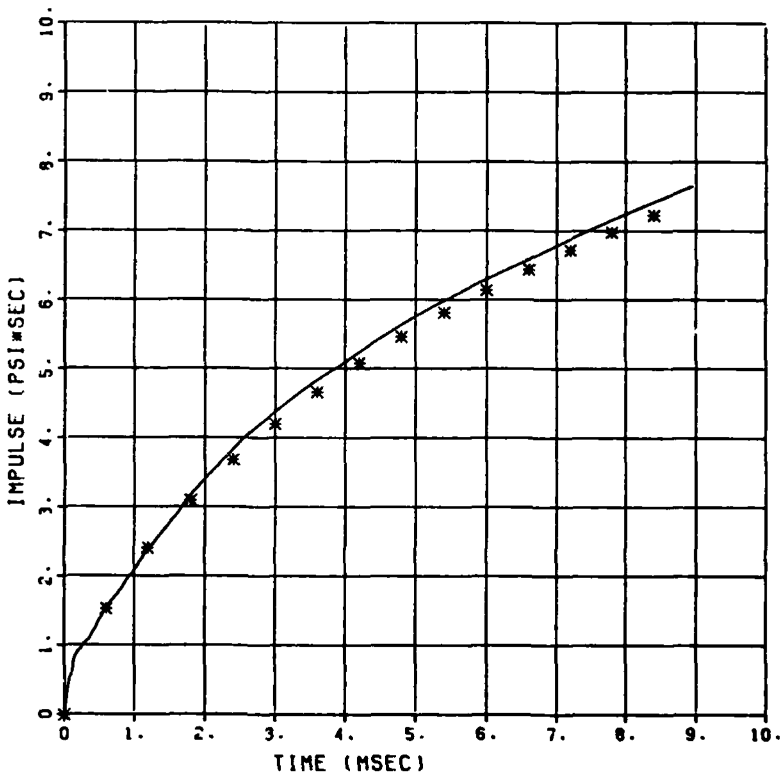

PRESSURE COMPARISON
DYN SH II TEST 5
BP2
W(KT) = 1.236
P(PSI) =4751.
07/01/82 70640

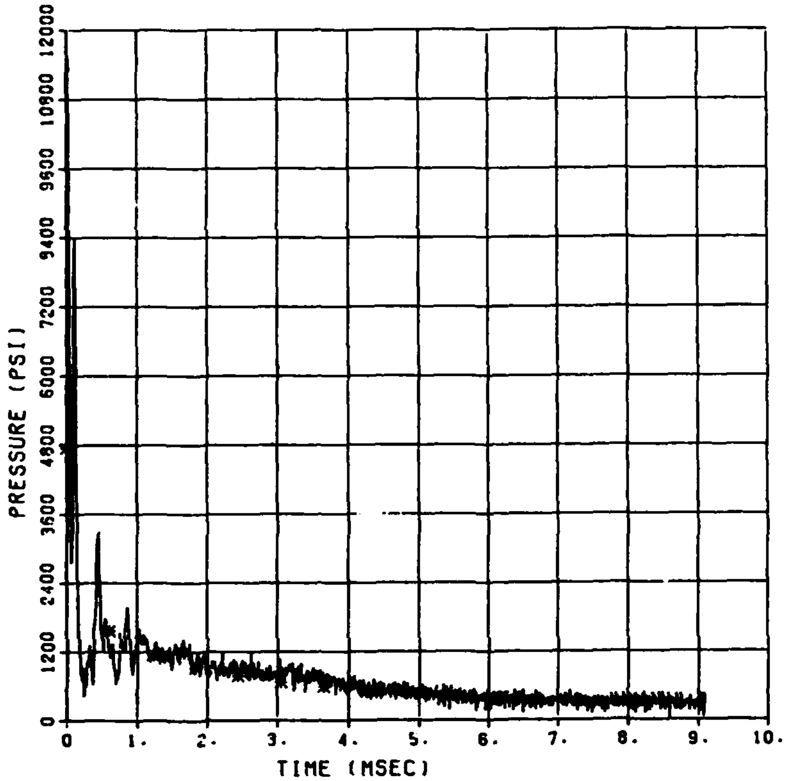

IMPULSE COMPARISON
DYN SH II TEST 5
BP2
W(KT) = 1.236
P(PSI) =4751.
07/01/82 70640

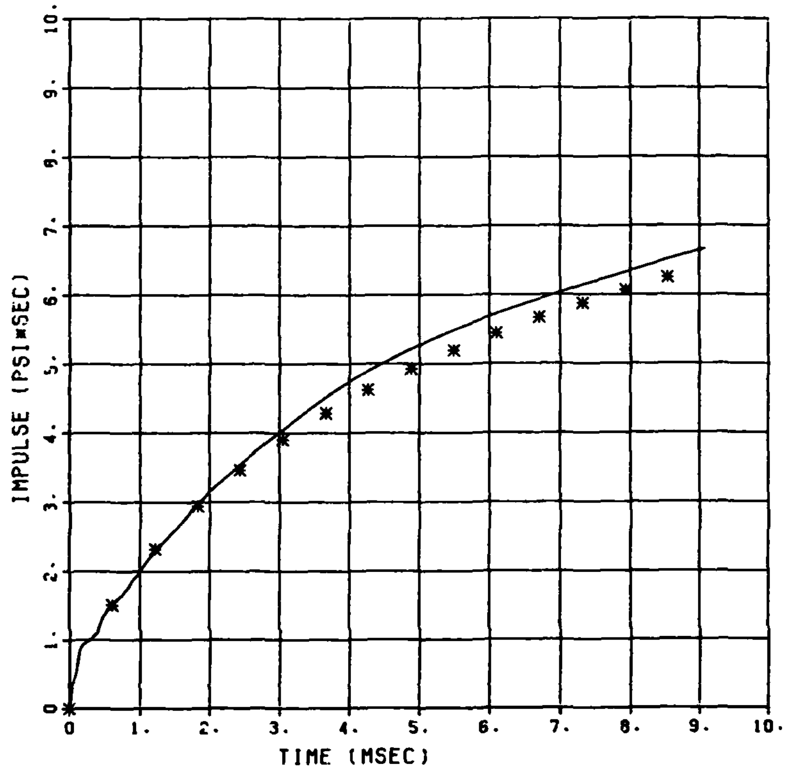

PRESSURE COMPARISON
DYN SH II TEST 5
BP4
W(KT) = 0.644
P(PSI) =6349.
07/01/82 70640

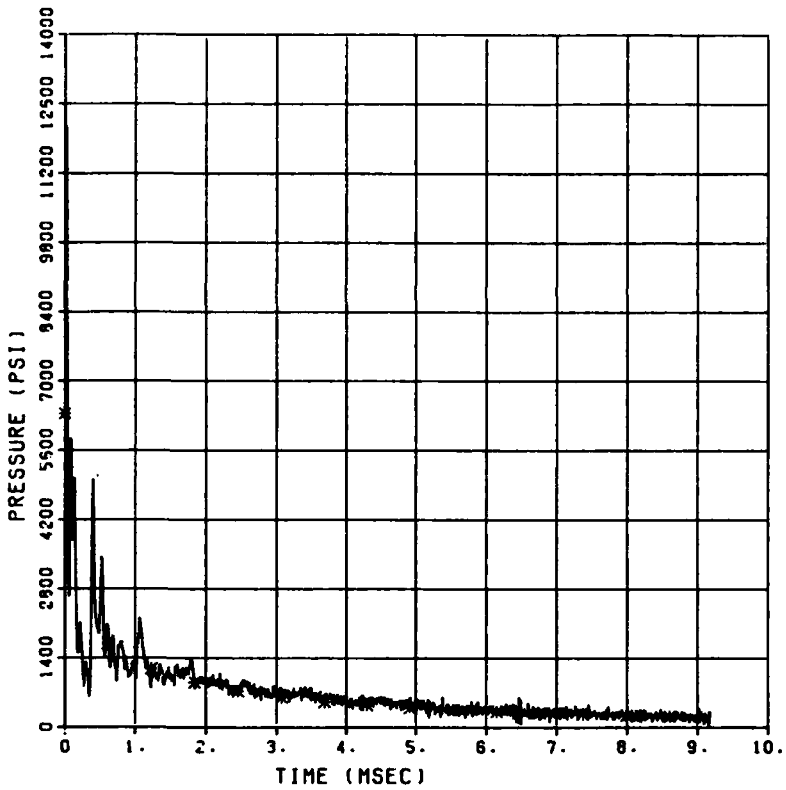

IMPULSE COMPARISON
DYN SH II TEST 5
BP4
W(KT) = 0.644
P(PSI) =6349.
07/01/82 70640

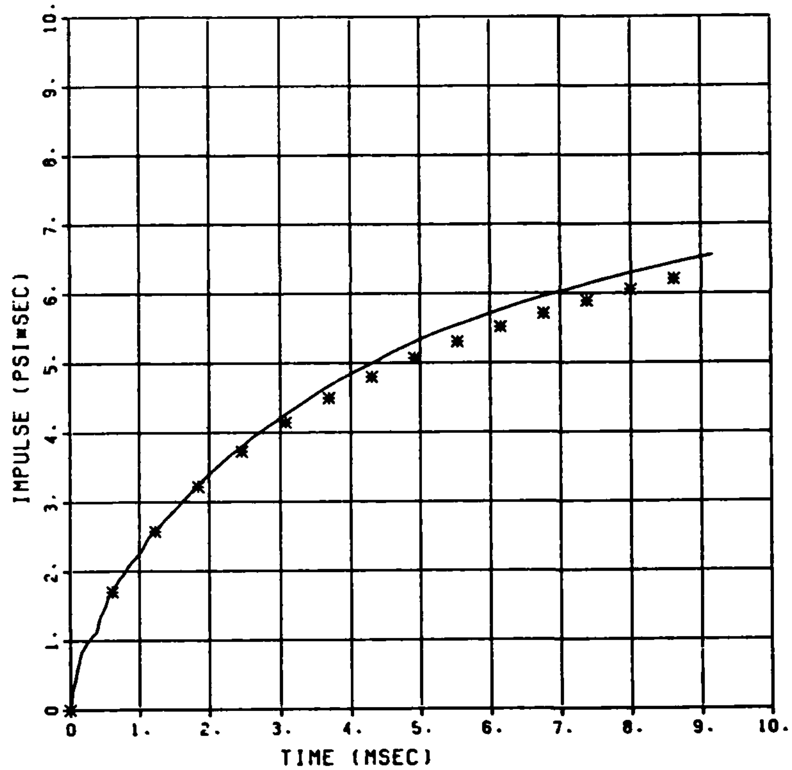

PRESSURE COMPARISON
DYN SH II TEST 6
BP1
W(KT) = 0.985
P(PSI) =3164.
07/01/82 7095D

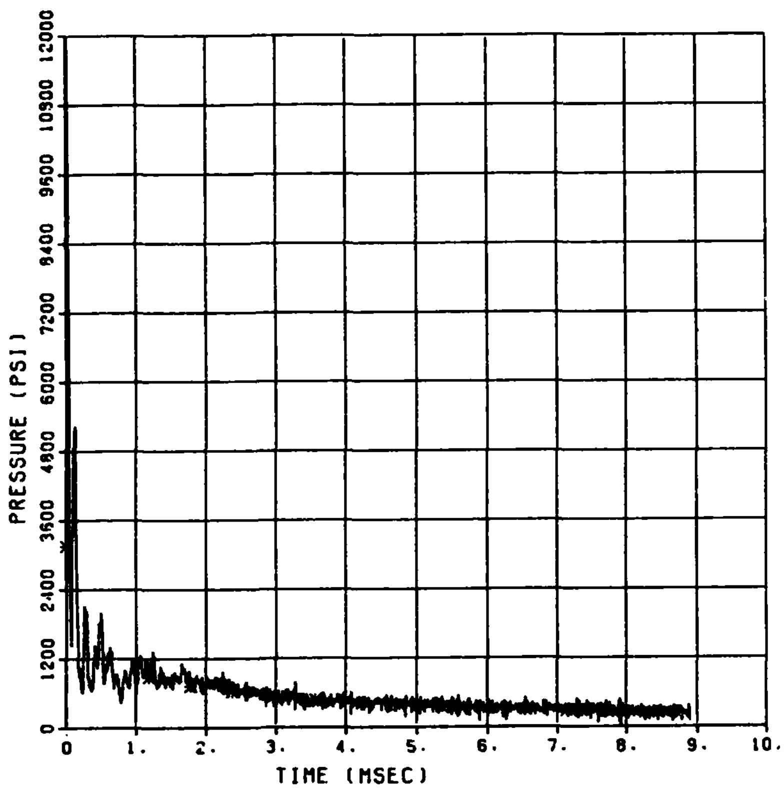

IMPULSE COMPARISON
DYN SH II TEST 6
BP1
W(KT) = 0.985
P(PSI) =3164.
07/01/82 7095D

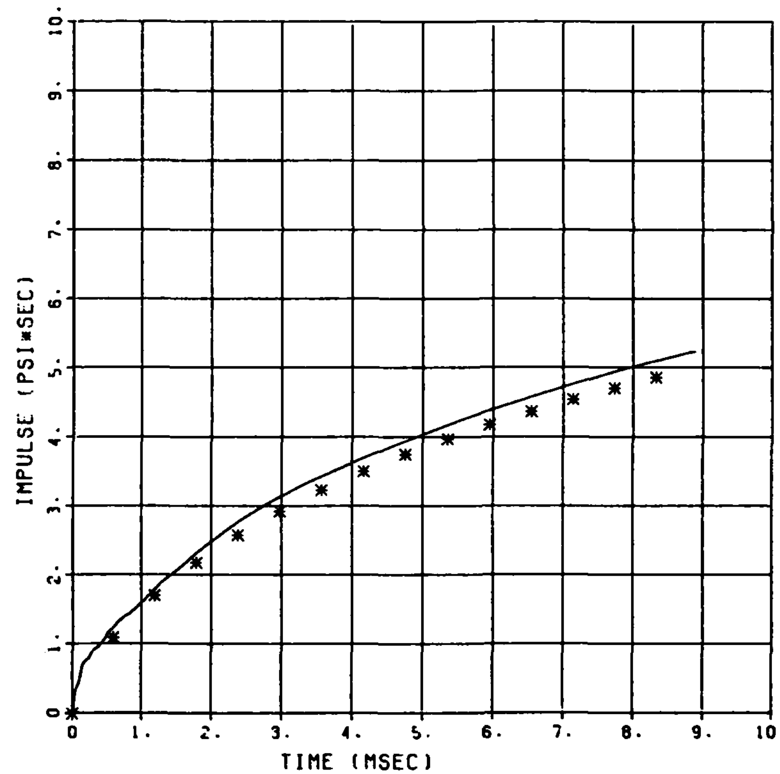

PRESSURE COMPARISON
DYN SH II TEST 6
BP2
W(KT) = 0 896
P(PSI) =3310
01/17/85 23428

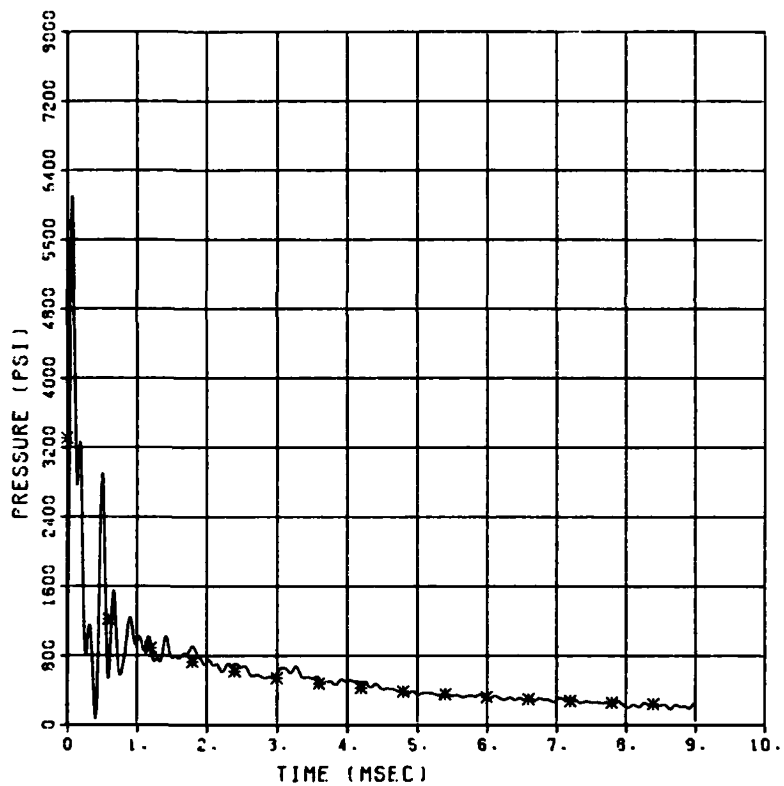

IMPULSE COMPARISON
DYN SH II TEST 6
BP2
W(KT) = 0.896
P(PSI) =3310
01/17/83 23426

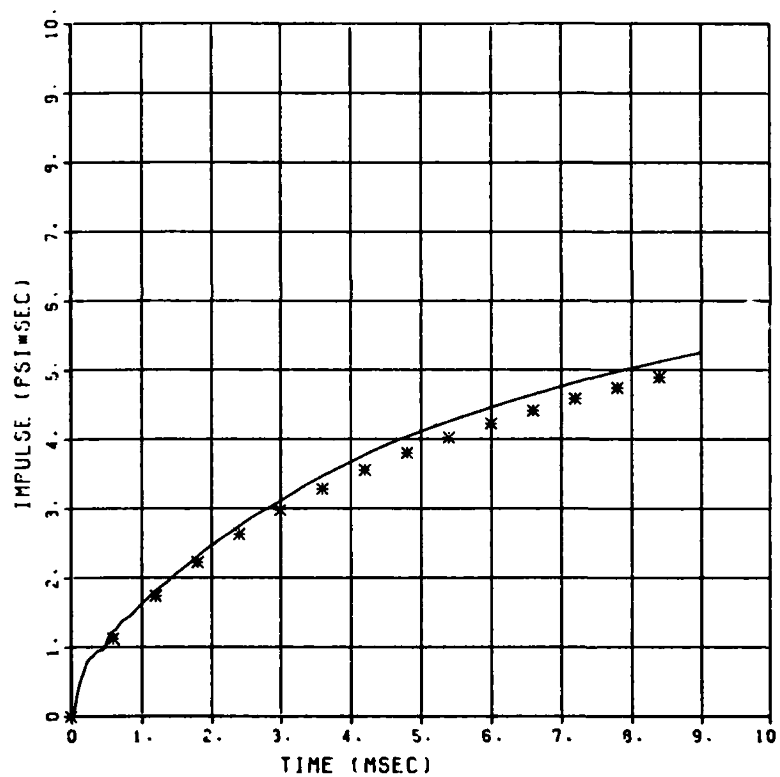

PRESSURE COMPARISON
DYN SH II TEST 6
BP4
W(KT) = 0.510
P(PSI) =3658.
07/01/82 70950

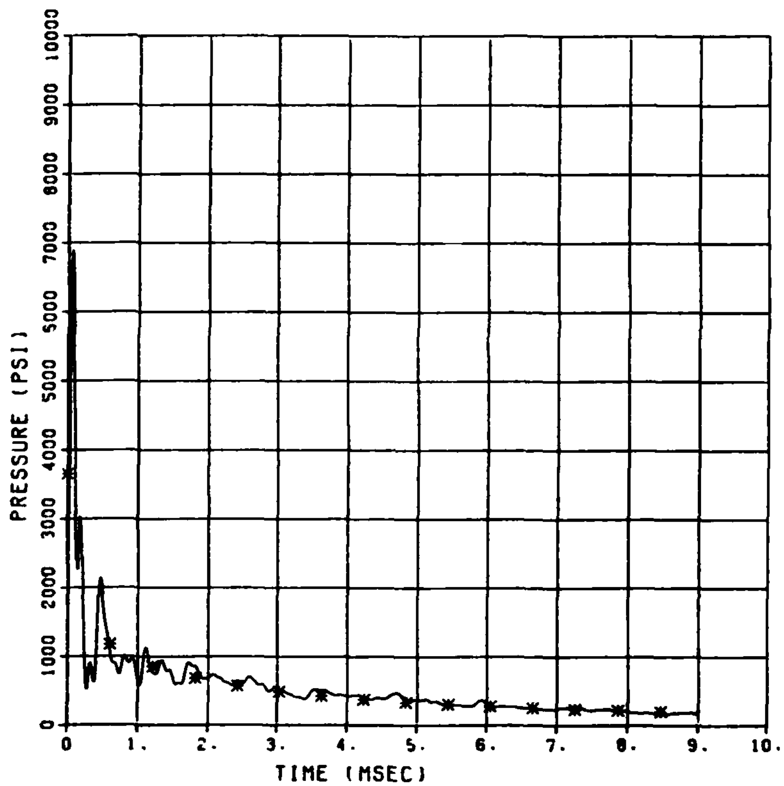

IMPULSE COMPARISON
DYN SH II TEST 6
BP4
W(KT) = 0.510
P(PSI) =3656.
07/01/82 70950

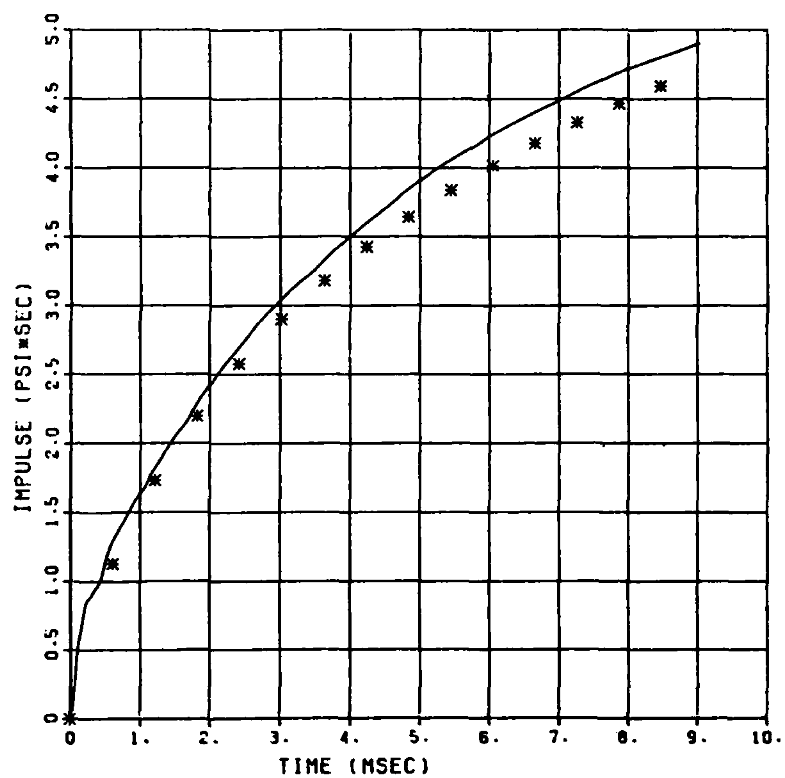

APPENDIX B: CALCULATION OF MAXIMUM DYNAMIC SUPPORT SHEAR STRESS AND SHEAR STRENGTH FOR TEST DS1

1. Find peak structure loading, B .

$B = 1.6\alpha_z P_{so}$

From Figure 4-22: $\alpha_z = 0.75$ for $z = 9.6$ in.

$B = 1.6(0.75)4109 = 4931$ psi

2. Find duration, t_d .

$t_d = 12h/C_c \leq (\sqrt{r} + 1)z/C_L$

$t_d = 12(5.6)/12(10{,}000) \leq (\sqrt{0.1} + 1)9.6/12(1500)$

$t_d = 0.00056 \leq 0.000702$

$t_d = 0.00056$ sec

3. Find fundamental period of roof slab, T .

$E = 57{,}000\sqrt{f'_c} = 57{,}000\sqrt{3{,}890} = 3{,}555{,}082$ psi

$I = bd^3(5.5\rho + 0.083)/2$

$I = (1)(4.8)^3(5.5(0.01) + 0.083)/2$

$I = 7.63 \text{ in.}^4$

$k = 307EI/L^3 = 307(3{,}555{,}082)(7.63)/48^3$

$k = 75{,}299$ lb/in.

$m = \gamma_c(bh - 2\rho bd)L + 2\gamma_s\rho bdL$

$m = 0.0002247[(1)(5.6) - 2(0.01)(1)(4.8)]\ 48 + 2(0.0007339)\ (0.01)(1)(4.8)(48)$

$m = 0.06275$

$T = 2\pi\sqrt{K_{LM}m/k}$

$T = 2\pi\sqrt{0.66(0.06276)/75{,}299}$

$T = 0.00466$ sec

4. Find inplane stress, σ_n .

$\sigma_n = K_o P_{so}\alpha'_z t_d C_L/h$

From Figure 4-22:

$\alpha'_z = 0.63$ for $z' = z + t_d C_L/2 = 14.64$ in.

$\sigma_n = 0.5(4109)(0.63)(0.00056)(1500)(12)/5.6$

$\sigma_n = 2330$ psi, $P_N = 13{,}047$ lb

5. Find thrust at the balanced condition

Using Figure B-1

Depth of the Whitney Stress Block, $a = c\beta_1$

$$\beta_1 = 0.85 - 0.2(f'_c - 4000)/4000 \leq 0.85$$
$$\geq 0.65$$

$\beta_1 = 0.85$ for $f'_c = 3890$ psi

By proportion from the strain diagram:

$c = 0.003[4.8/(0.003 + 62.75/29{,}000)] = 2.789$ in.

$a = 2.37$ in.

$FC = 2.37(0.85)(3890) = 7837.6$ lb

$FS = \rho b d f_y = 0.01(1)(4.8)(62{,}750) = 3012$ lb

$\varepsilon'_s = (2.789 - 0.8)0.003/2.789 = 0.00214 \leq \varepsilon_y = 0.00216$

$FSP = 0.01(1)(4.8)(29{,}000{,}000)(0.00214) = 2978$ lb

$\Sigma F = 0$

$P_b = FC + FSP - FS$

$P_b = 7837.6 + 2978 - 3012$

$P_b = 7803.6$ lb

6. Find ultimate moment capacity, M .

Since $P_n > P_b$, $M = M_b$ to be conservative

Using Figure B-1 and summing moments about A_s:

$M_b = FSP(d - d') + FC(d - a/2) - P_b(d - h/2)$

where h = total thickness of slab

$M_b = 2978(4) + 7837.6(3.615) - 7803.6(2)$

$M_b = 24{,}640$ in.-lb

7. Find the static collapse load for the roof acting as a fixed-fixed beam.

$w = 16M/L^2 = 16(24{,}640)/48^2$

$w = 171$ lb/in.

8. Find the dynamic ultimate flexural resistance.

$r_u = 1.5w = 1.5(171)$

$r_u = 257$ lb/in.

9. Find DIF values.

$B/r_u = 4931/257 = 19.2$

$t_d/T = 0.56/4.66 = 0.12$

Using Figure 4-4 DIF = 3.4

10. Calculate maximum dynamic support shear stress.

$V = DIF(r_u L)/(2h)$

$V = 3.4(257)(48)/2(5.6)$

$V = 3745$ psi

11. Calculate maximum dynamic shear stress at a distance d from the face of the wall.

$V_d = (Vh/bd)[(L/2 - d)]/(L/2)$

$V_d = [3745(5.6)/1(4.8)][(24 - 4.8)]/24$

$V_d = 3495$ psi

12. Find diagonal tension shear strength.

Since V_s is greater than the ACI limit of $8\sqrt{f'_c}$ Equation 4-1a is used with a 50% dynamic increase factor.

$V_n = 1.5(14.4)\sqrt{f'_c} = 1.5(14.4)\sqrt{3890}$

$V_n = 1347$ psi $< V_d = 3495$ psi $\therefore$ diagonal tension shear failure is predicted

13. Find direct shear strength.

Using Equation 4-6:

$V_n = 1.5A_v f_y \mu/bh = 1.5(2)(0.01)(1)(4.8)(62{,}750)(1.4)/(1)(5.6)$

$V_n = 2259$ psi $< V = 3745$ psi $\therefore$ direct shear failure is predicted

Using Equation 4-7:

$\sigma_n = 2330$ psi from step 4

$V_n = 1.5[0.16f'_c + 1.4(\sigma_n + A_v f_y/bh)] \leq 1.5(0.51f'_c)$

$V_n = 1.5[0.16(3890) + 1.4[2330 + 2(0.01)(4.8)(62{,}750)/5.6]]$

$V_n = 8086 \leq 2976$

$\therefore V_n = 2976$ psi $< V = 3745$ $\therefore$ A direct shear failure is predicted if V_n is limited to $1.5(0.51f'_c)$. High-speed movies show that test DS1 did not fail in direct shear. This shows that Equations 4-6 and 4-7 underpredict the direct shear strength.

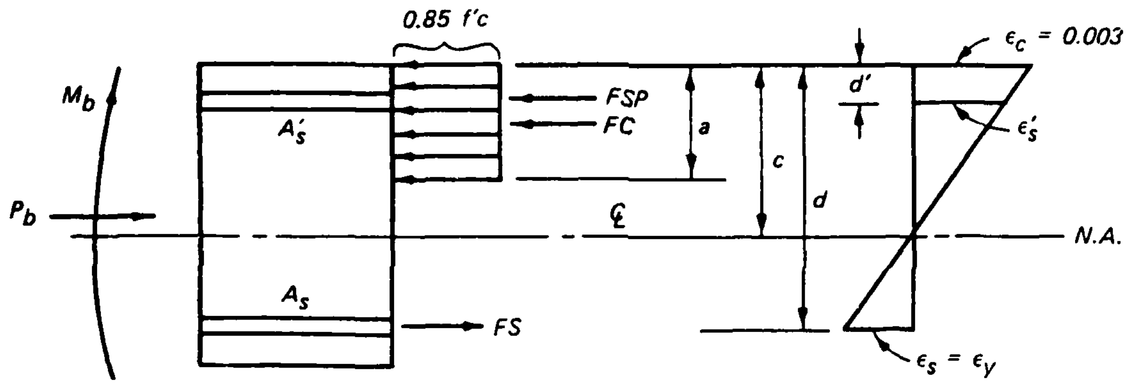

Figure B-1. Free Body Diagram and Strain Distribution for Balanced Condition

APPENDIX C: COMPUTER CODE SHEAR: CODE TO CALCULATE DYNAMIC SUPPORT SHEARING STRESS FROM STRAIN AND INTERFACE PRESSURE DATA

```
C SHEAR MAIN PROGRAM  13 JAN 83
      IMPLICIT INTEGER *2 (I-N,#)
      INTEGER *1  FLNM1(6),FLNM2(6),FLNM3(6)
      DIMENSION T(500),V(500),M(500),TIF(10),PIF(10),TEO(10),
     & SEO(10),TEI(10),SEI(10),XINTC(100)
      DATA  IOP/2/, LUI/2/,NPTS/500/
C  REQUEST USER INPUT
   10 CALL INPUT(DUR,FPC,FY,H,D,DP,RHO,IFLAG)
C  INPUT DATA
   20 CALL DATA(TIF,PIF,TEO,SEO,TEI,SEI)
C  ECHO DATA
      WRITE(6,*)' TIF,MS   PIF,PSI   TEO,MS  SEO,MI/I  TEI,MS  SEI,MI/I'
      WRITE(6,*)' '
      DO 21 I=1,10
   21 WRITE(6,*)TIF(I),PIF(I),TEO(I),SEO(I),TEI(I),SEI(I)
      WRITE(6,*)' '
C CALCULATE AXIAL THRUST, MOMENT IN WALL & SUPPORT SHEAR
      DO 30 I=1,100
   30 XINTC(I)=0.0
      XIS=0.0
      XISP=0.0
      VMAX=0.0
      MMAX=0.0
      MMIN=0.0
      DO 100 I=1,NPTS
      T(I) = (I-1)*DUR/NPTS
      CALL INTER(T(I),TIF,PIF,P)
      CALL INTER(T(I),TEO,SEO,ES)
      CALL INTER(T(I),TEI,SEI,ESP)
      XK=(ESP-ES)/1000000./(D-DP)
      EO=ESP/1000000.-XK*D
      IF(ES .EQ. 0.0 .AND. ESP .EQ. 0.0) XK=0.0
      IF(ES .EQ. 0.0 .AND. ESP .EQ. 0.0) EO=0.0
      CALL STEEL(IFLAG,FY,ESP,RHO,D,XISP,FSP)
      CALL STEEL(IFLAG,FY,ES,RHO,D,XIS,FS)
      CALL SUM(IFLAG,XK,EO,FPC,H,XINTC,FC,MC)
      THRUST=-(FC+FSP+FS)
      V(I)=(THRUST-P*H)/H
C     M(I)=-(MC+FSP*D+FS*DP)
      IF(V(I) .GE. VMAX) VMAX=V(I)
  100 CONTINUE
      WRITE(6,*)'VMAX=',VMAX
      WRITE(6,*)' '
      CALL PFILE(NPTS,T,V,VMAX)
      WRITE(6,*)'ENTER 1 TO RUN NEW PROBLEM, 2 TO STOP'
      READ(5,*) IRUN
      IF(IRUN .EQ. 1) GO TO 10
      CALL EXIT
      END
```

```
      SUBROUTINE CONC(FFC,EC,XINT,IFLAG,SIGC)
      IMPLICIT INTEGER *2(I-N,#)
      DATA  E0/0.0019/, EMAX/0.003/
      A = 0.9 * FPC + 300.
      B = A / E0 / E0
      DC=2.*A/E0
      IF(EC.LT.EMAX) GO TO 10
      SIGC= -B * (E0 - EMAX) * (E0 - EMAX) + A
      IF(IFLAG .EQ. 1) RETURN
      GO TO 15
   10 SIGC = -B * (E0 - EC) * (E0 - EC) + A
      IF(IFLAG .EQ. 1) RETURN
   15 EC = EC-XINT
      STRESS=EC*DC
      IF(STRESS .GT. 0.0) GO TO 20
      SIGC=0.0
      RETURN
   20 IF(STRESS .GT. SIGC) GO TO 30
      SIGC=STRESS
      RETURN
   30 P3FPC=0.3*FPC
      IF(XINT.EQ.0.0 .AND. SIGC.LE.P3FPC) RETURN
      XINT=XINT+EC-SIGC/DC
      RETURN
      END


      SUBROUTINE DATA(TIF,PIF,TEO,SEO,TEI,SEI)
      IMPLICIT INTEGER *2 (A-Z,#)
      INTEGER *1 FLNM1(10),FLNM2(10),FLNM3(10)
      REAL TIF,PIF,TEO,SEO,TEI,SEI
      DIMENSION TIF(10),PIF(10),TEO(10),SEO(10),TEI(10),SEI(10)
      DATA IOP/2/,LUI/1/
C
C   SUBROUTINE TO READ EO, EI & IF DATA FILES
C
      READ(5,20)
   10 WRITE(6,*)'ENTER IF GAGE FILE NAME'
      READ(5,20) FLNM1
   20 FORMAT(10A1)
      CALL FILE(FLNM1,LUI,IOP,ISTA)
      IF(ISTA .EQ. 8) STOP 'IF FILE NOT ATTACHED'
      DO 30 I=1,10
   30 READ(LUI,*) TIF(I),PIF(I)
C
   40 WRITE(6,*)'ENTER EO FILE NAME'
      READ(5,20) FLNM2
      CALL FILE(FLNM2,LUI,IOP,ISTA)
      IF(ISTA .EQ. 8) STOP 'EO FILE NOT ATTACHED'
      DO 50 I=1,10
   50 READ(LUI,*) TEO(I),SEO(I)
C
   60 WRITE(6,*)'ENTER EI FILE NAME'
      READ(5,20) FLNM3
      CALL FILE(FLNM3,LUI,IOP,ISTA)
      IF(ISTA .EQ. 8) STOP 'EI FILE NOT ATTACHED'
      DO 70 I=1,10
   70 READ(LUI,*) TEI(I),SEI(I)
      RETURN
      END
```

```
SUBROUTINE INPUT(DUR,FPC,FY,H,D,DP,RHO,IFLAG)
IMPLICIT INTEGER *2 (I-N,#)
WRITE(6,*)'  '
WRITE(6,*)'CODE TO CALCULATE SHEAR STRESS AT THE FACE OF '
WRITE(6,*)'THE SUPPORT FROM WALL STRAINS & OVERWALL PRESSURES'
WRITE(6,*)'               13 JAN. 1983'
WRITE(6,*)'  '
WRITE(6,*)'ENTER: H(IN),D(IN),RHO,FPC(PSI),FY(PSI),DUR(MSEC)'
READ(5,*) H,D,RHO,FPC,FY,DUR
WRITE(6,*)'.'
DP=H-D
WRITE(6,*)'ENTER 1 FOR ELASTIC MATERIAL MODELS, 2 FOR PLASTIC'
READ(5,*) IFLAG
WRITE(6,*)' '
WRITE(6,*)'ENTER DYNAMIC INCREASE FACTOR'
READ(5,*)DIF
WRITE(6,*)' '
FPC=FPC*DIF
FY=FY*DIF
RETURN
END
```

```
      SUBROUTINE INTER(X,XRAY,YRAY,Y)
      IMPLICIT INTEGER *2 (I-N,#)
      DIMENSION XRAY(10),YRAY(10)
C
C   SUBROUTINE TO LINEAR INTERPOLATE FOR Y AT X FOR
C   10 GIVEN POINTS(XRAY(I),YRAY(I));I=1,10
C
      N=0
      DO 10 I=1,10
      N=N+1
      IF(X .GE. XRAY(I) .AND. X .LT. XRAY(I+1)) GO TO 20
   10 CONTINUE
C
      IF(X .GT. XRAY(10)) STOP 'RANGE OF DATA EXCEEDED IN INTER'
   20 Y=YRAY(N)+(X-XRAY(N))*(YRAY(N+1)-YRAY(N))/(XRAY(N+1)-XRAY(N))
      RETURN
      END
```

```
      SUBROUTINE PFILE(NP,T,V,VMAX)
C.....CREATES (X,Y) PLOT DATA FILE FOR PROGRAM PSHEAR
      IMPLICIT INTEGER *2 (I-N,#)
      INTEGER *1 FLNM(16), HED(72)
      DIMENSION T(NP), V(NP)
      DATA IOP/3/, LUO/3/
C
      WRITE(6,*)'ENTER GRAPHICS OUTPUT DATA FILE NAME'
      READ(5,100) FLNM
  100 FORMAT(16A1)
      CALL FILE(FLNM, LUO, IOP, ISTA)
      IF(ISTA .EQ. 8) STOP 'FILE NOT OPEN FOR INPUT'
      WRITE(6,*)'ENTER HEADING FOR OUTPUT DATA FILE'
      READ(5,110) HED
  110 FORMAT(72A1)
C
      WRITE(LUO,110) HED
      WRITE(LUO,*) IPLOT, NP
      WRITE(LUO,*) VMAX
C
      DO 140 I = 1, NP
      WRITE(LUO,*) T(I), V(I)
  140 CONTINUE
C
      CALL CLOSE(LUO)
      RETURN
      END


      SUBROUTINE STEEL(IFLAG,FY,E,RHO,DEPTH,XINT,F)
      IMPLICIT INTEGER *2 (I-N,#)
      EY=FY/29.
      ABSE=ABS(E)
      IF(ABSE .LE. EY) STRESS=29.*ABSE
      IF(ABSE .GT. EY .AND. ABSE .LE. 10000.) STRESS=FY
C
C  CALCULATE PARAMETERS FOR NONLINEAR PORTION
      D=(0.75-FY/150000.)/4.05/10.**9
      C=-(165000.*D+1./120000.)
      B=FY/150000.+7.05*10.**9*D+11./12.
      A=FY-10000.*B-10000.*10000.*C-10000.**3*D
C
      STRES2=A+ABSE*B+ABSE*ABSE*C+ABSE**3*D
      IF(ABSE.GT.10000.0 .AND. ABSE.LT.100000.) STRESS=STRES2
      IF(ABSE .GE.100000.) STRESS=1.6*FY
      IF(E .LT. 0.0) STRESS=-STRESS
      IF(IFLAG .EQ. 1) GO TO 100
C
C  USING PLASTIC STEEL MODEL
      STRES3=(E-XINT)*29.
      IF(STRES3 .LT. 0.0 .AND. STRESS .LT. 0.0) GO TO 10
      IF(STRES3 .LT. 0.0 .AND. STRESS .GE. 0.0) GO TO 20
      IF(STRES3 .GE. 0.0 .AND. STRESS .LT. 0.0) GO TO 30
      IF(STRES3 .LT. STRESS) STRESS=STRES3
      GO TO 40
   10 IF(STRES3 .GT. STRESS) STRESS=STRES3
      GO TO 40
   20 IF(STRES3 .GT. -FY) STRESS=STRES3
      IF(STRES3 .LE. -FY) STRESS=-FY
      GO TO 40
   30 IF(STRES3 .LT. FY) STRESS=STRES3
      IF(STRES3 .GE. FY) STRESS=FY
   40 XINT=E-STRESS/29.
  100 F=RHO*DEPTH*STRESS
      RETURN
      END
```

```
      SUBROUTINE SUM(IFLAG,XK,EO,FPC,H,XINTC,FC,MC)
      IMPLICIT INTEGER *2 (I-N,#)
      DIMENSION XINTC(1)
      N=0
      DX=H/100.
      SUM1=0.
      SUM2=0.
      DO 100 I=1,199,2
      X=I*DX/2.
      N=N+1
      EC=-(EO+XK*X)
      IF(EC.GT.0.0) GO TO 10
      SIGC=0.0
      GO TO 20
   10 CALL CONC(FPC,EC,XINTC(N),IFLAG,SIGC)
   20 SUM1=SUM1+SIGC
      SUM2=SUM2+X*SIGC
  100 CONTINUE
      FC=-SUM1*DX
      MC=-SUM2*DX
      RETURN
      END
```

```
CODE TO CALCULATE SHEAR STRESS AT THE FACE OF
THE SUPPORT FROM WALL STRAINS & OVERWALL PRESSURES
               13 JAN  1983

ENTER  H(IN),D(IN),RHO,FPC(PSI),FY(PSI),DUR(MSEC)
7 25 6 44 2 012 7262  67000  5

ENTER 1 FOR ELASTIC MATERIAL MODELS, 2 FOR PLASTIC
1

ENTER DYNAMIC INCREASE FACTOR
1 S

ENTER IF GAGE FILE NAME
D26IF
ENTER EO FILE NAME
D26EO
ENTER EI FILE NAME
D26EI
 TIF,MS    PIF,PSI    TEO,MS   SEO,MI/I   TEI,MS   SEI,MI/I

 0 00000   0 20000   0 00000   0 00000   0 00000   0 00000
   1 5000  0 00000    1 4000   0 00000    1 4000   0 00000
   1 6000   5200 0    1 7000   -1000 0    2 0000   -3700 0
   2 4000   620 00    2 0000   0 00000    2 2000   -3700 0
   3 0000   400 00    2 5000    11600     2 5000   -1400 0
   3 2000   1300 0    3 4000   9000 0     3 5000   -5600 0
   4 0000   700 00    3 8000    10500     3 7000   -5300 0
   7 0000   650 00    4 2000    10000     7 0200   -5300 0
   9 0000   400 00    7 0000    10300     8 0200   -4800 0
  10 000    200 00    8 0000    14000    10 000    -4900 0

VMAX=   5715 0

ENTER GRAPHICS OUTPUT DATA FILE NAME
```

APPENDIX D: LIST OF SYMBOLS

a	Depth of stress block
A_s	Area of tension steel
A'_s	Area of compression steel
A_v	Area of shear-friction reinforcement
A_{vs}	Area of vertical shear reinforcement within a distance s
b	Width of the compression face
B	Peak applied stress of the blast loading
c	Distance from compression face of the slab to neutral axis
C_c	Compression wave speed in the slab
C_L	Loading wave velocity
d	Depth from the compression face of the slab to the centroid of the tension steel (effective depth)
d'	Distance from the compression face of the slab to the centroid of the compression steel
DC	Slope of the tangent to the concrete stress-strain curve at zero strain
DIF_m	Dynamic Increase Factor for shear
E	Modulus of elasticity
f'_c	Compressive strength of concrete
f_y	Yield strength of steel
F	External force acting perpendicular to wall
FC	Concrete compressive force
FS	Force in tension steel
FSP	Force in compression steel
h	Member thickness
I	Moment of inertia
$I\ddot{\theta}$	Moment due to rotational inertia
k	Roof slab stiffness
K_o	Lateral earth pressure coefficient
K_{LM}	Load mass factor
L	Clear span
L/d	Clear span-to-effective depth ratio
m	Mass
$m\ddot{y}$	Wall axial force due to vertical acceleration
M	Moment at a section
M_b	Balanced moment capacity
M_m	Moment at a section of a member subjected to axial compression

M_n	Moment capacity
M_o	Moment capacity with no inplane thrust
M_R	Roof moment
M_W	Wall moment
N	Inplane thrust
P	Vertical wall force
P_b	Balanced thrust
P_n	Inplane thrust
P_{so}	Peak overpressure
r	Strain recovery ratio
r_u	Ultimate resistance of the roof slab
s	Shear reinforcement spacing
S	Wall frictional force
t_d	Duration of the peak reflecting pressure
t_{oo}	Duration of the equivalent triangular load that is fixed by a line tangent to the actual nuclear overpressure-time history curve at zero time
T	Fundamental period of the roof slab
T_r	Roof axial force
T_w	Wall axial force
V	Shear at a section
V_c	Nominal shear strength provided by concrete
V_d	Roof shear stress at a distance, d, from the face of the support
V_n	Nominal shear strength
V_R	Roof shear
V_s	Nominal shear strength provided by shear reinforcement
V_w	Wall shear
V_{max}	Maximum shearing stress
w	Static collapse load
XK	Slope of the concrete strain distribution
z	Depth of burial
z'	Attenuation depth for inplane thrust calculation
α_z	Attenuation factor to roof level
α'_z	Attenuation factor at depth z'
β_1	Factor defined by ACI (1977)
ε	Strain

ε_c	Concrete strain
ε_o	Constant, the strain at which the tangent to the stress-strain diagram is horizontal
ε_s	Tension steel strain
ε'_s	Compression steel strain
ε_{of}	Concrete strain at the compression face
μ	Coefficient of friction
π	3.14159
ρ	Tension reinforcement ratio
ρ'	Compression steel ratio
σ	Stress
σ_c	Concrete stress
σ_n	Applied normal stress
σ_s	Stress in tension steel
σ'_s	Stress in compression steel
σ_{nb}	Inplane stress at balance thrust

APPENDIX E: DYNAMIC SHEAR TEST DATA

Complete data (analog) records obtained for the free field and the structures of the Dynamic Shear Tests are presented in this appendix. Positive measurements of acceleration and velocity indicate motions vertically down. Positive values of interface pressure indicate soil pressures toward the structure. Positive values of airblast pressure indicate pressure in the charge cavity. Tensile strains are positive, whereas compressive strains are negative. Labels on the plots are explained as follows:

1. First line: test name
2. Second line: gage number
3. Third line: digitization rate, baseline shift, and calibration peak
4. Fourth line: filter option (blank implies no filter)
5. Fifth line: bookkeeping data

DYNAMIC SHEAR 1
BP1
200000. HZ CAL= 12132.

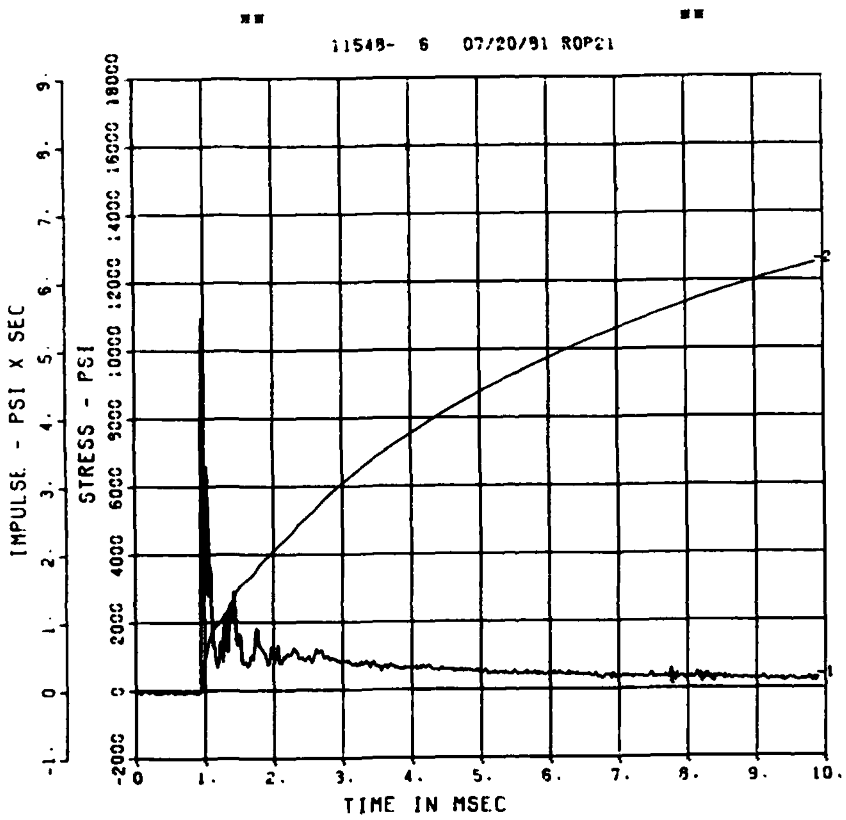

DYNAMIC SHEAR 1
BP1
200000. HZ CAL= 12132.

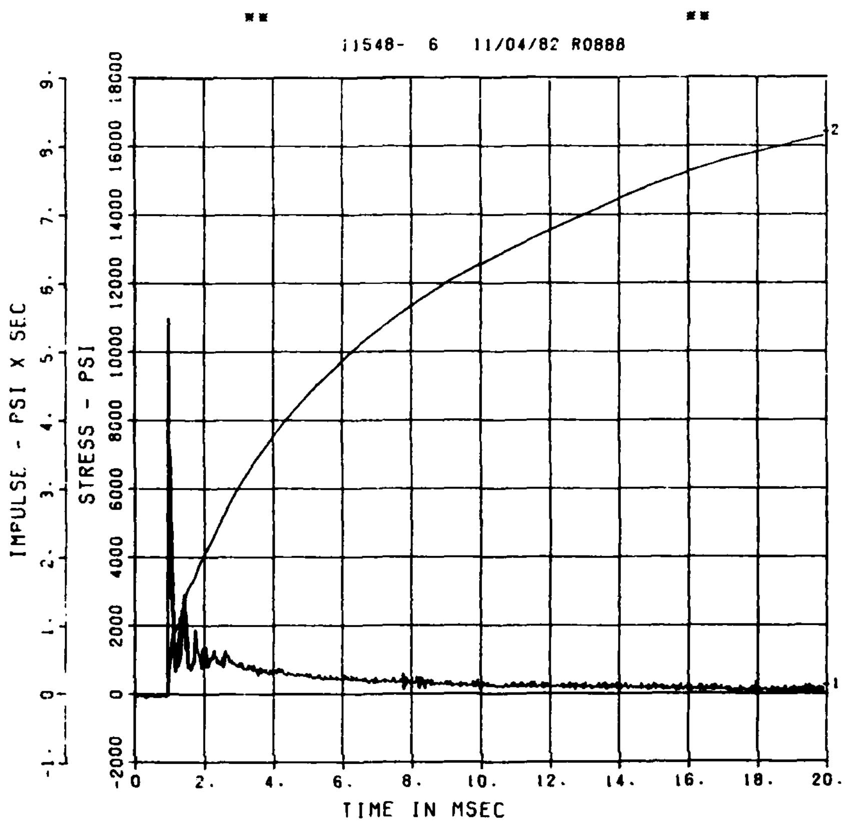

DYNAMIC SHEAR 1
BP2
200000. HZ CAL= 14915.

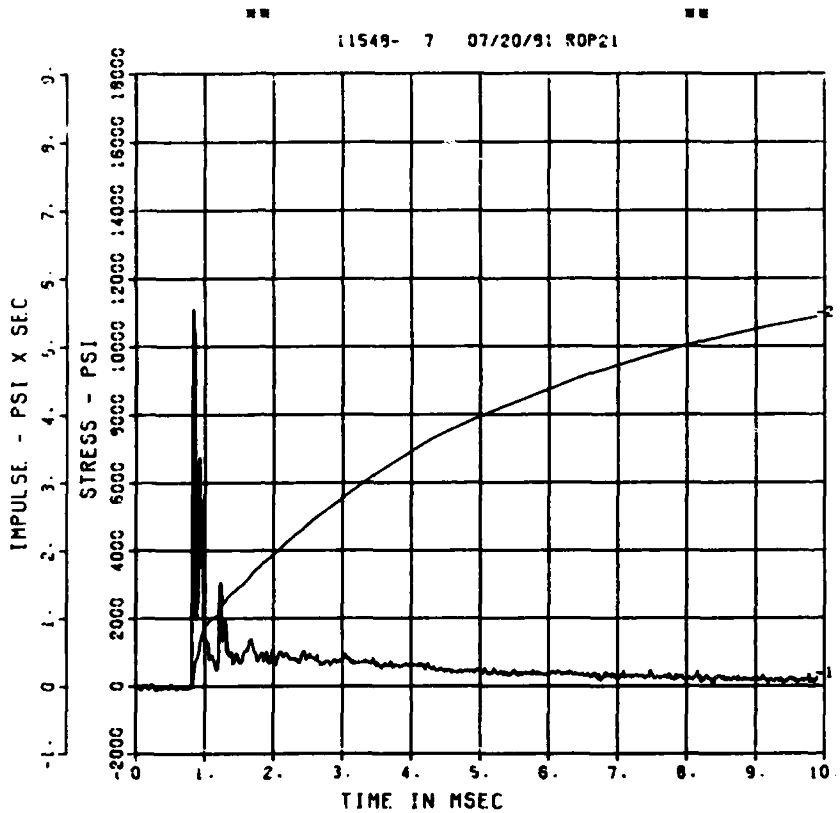

DYNAMIC SHEAR 1
BP2
200000. HZ CAL= 14915.

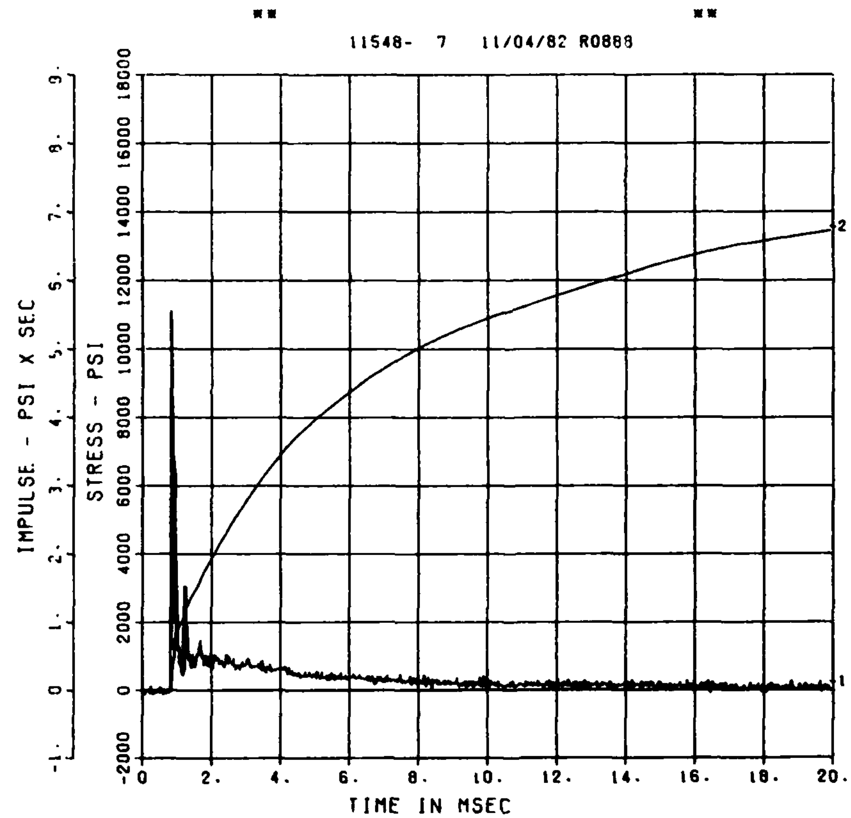

DYNAMIC SHEAR 1
BP3
200000. HZ CAL= 14298.

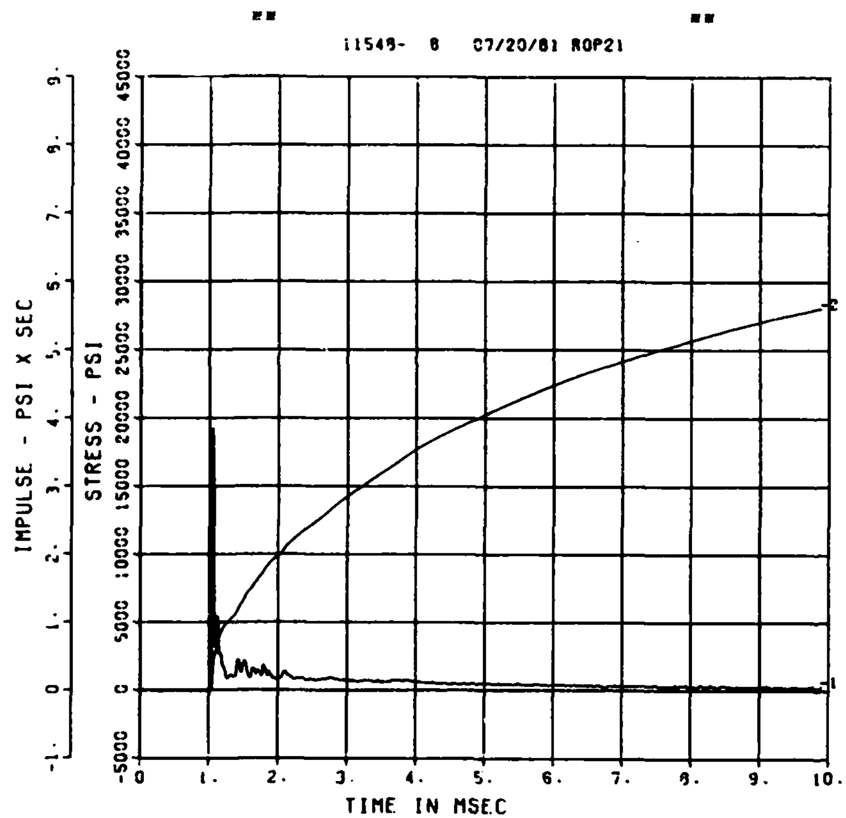

** PEAK VALUE IS 34 % OVER CALIBRATION **

DYNAMIC SHEAR 1
BP3
200000. HZ CAL= 14298.

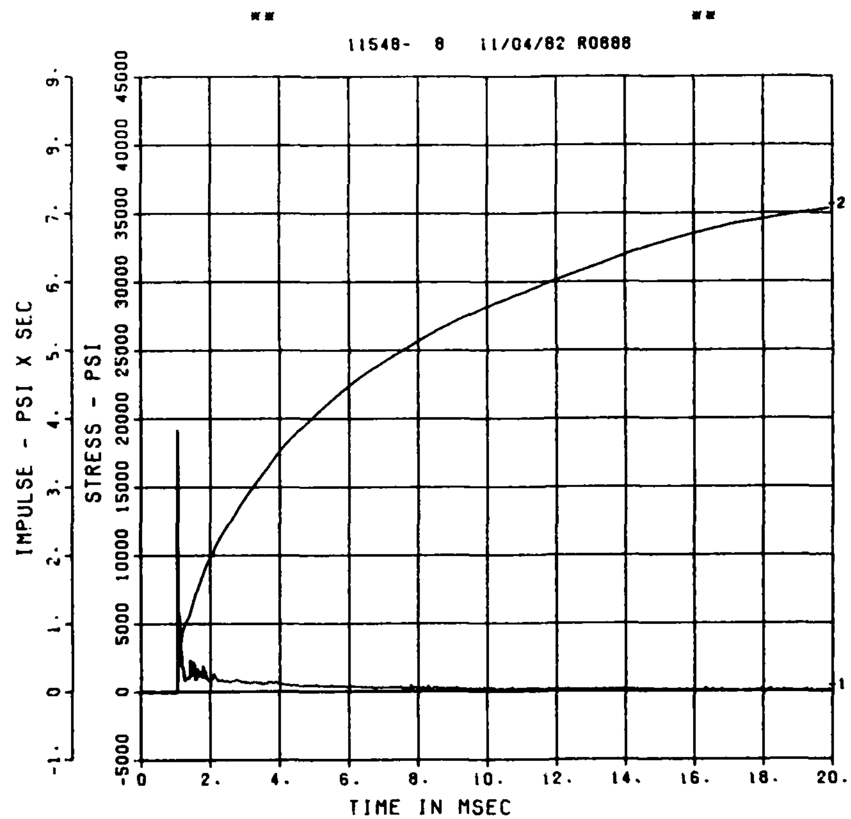

** PEAK VALUE IS 34 % OVER CALIBRATION **

DYNAMIC SHEAR 1
BP4
200000. HZ CAL= 14785..

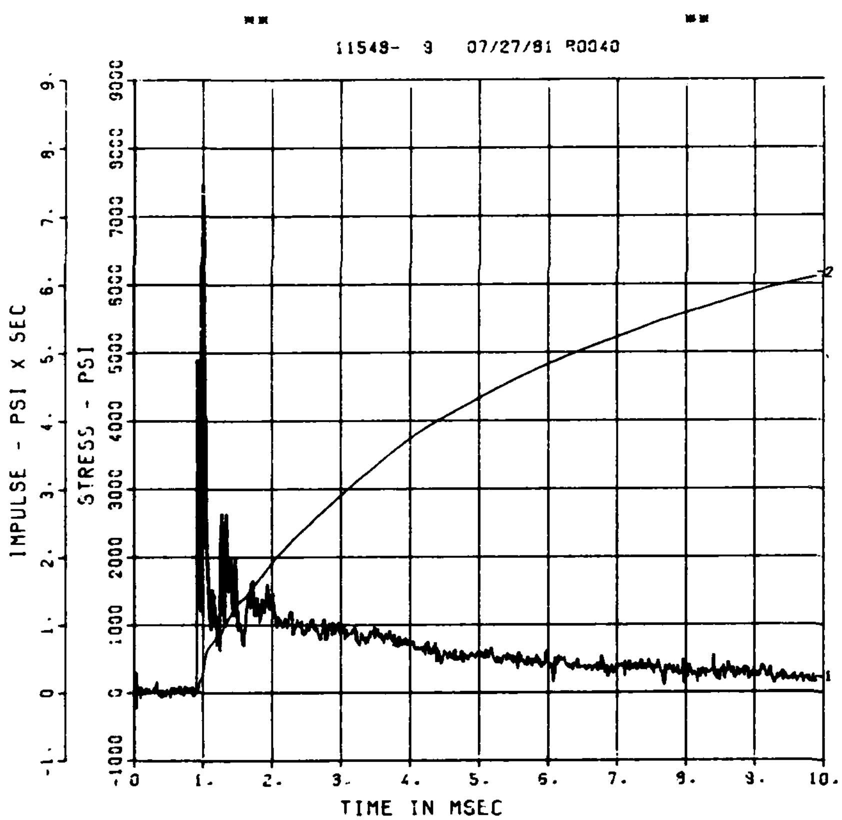

DYNAMIC SHEAR 1
BP4
200000. HZ CAL= 14785.

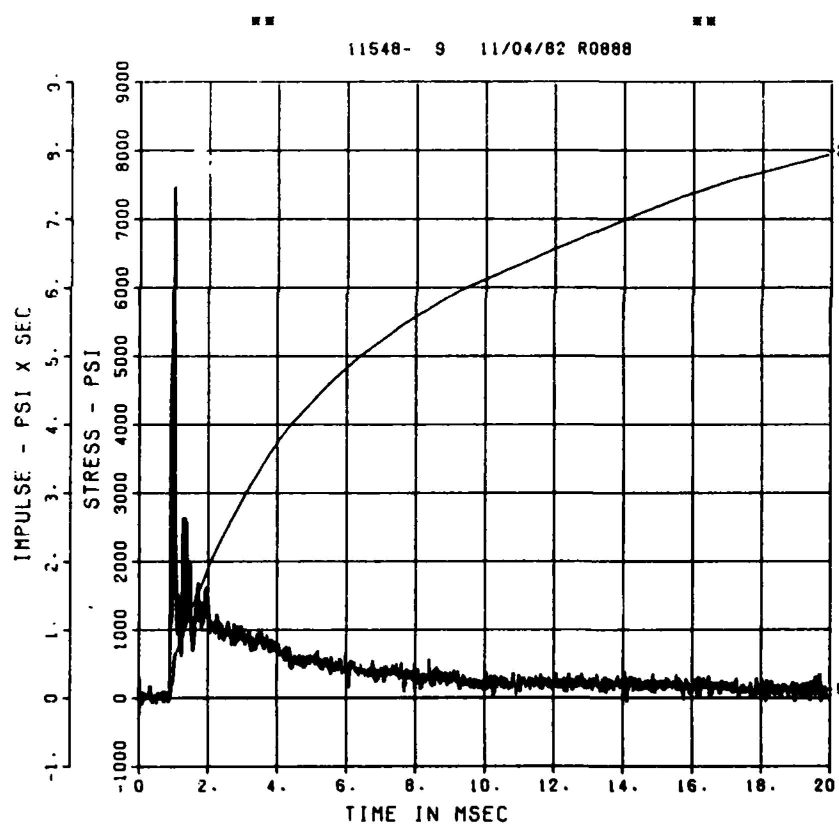

DYNAMIC SHEAR 1
IF1
200000. HZ CAL= 6271.

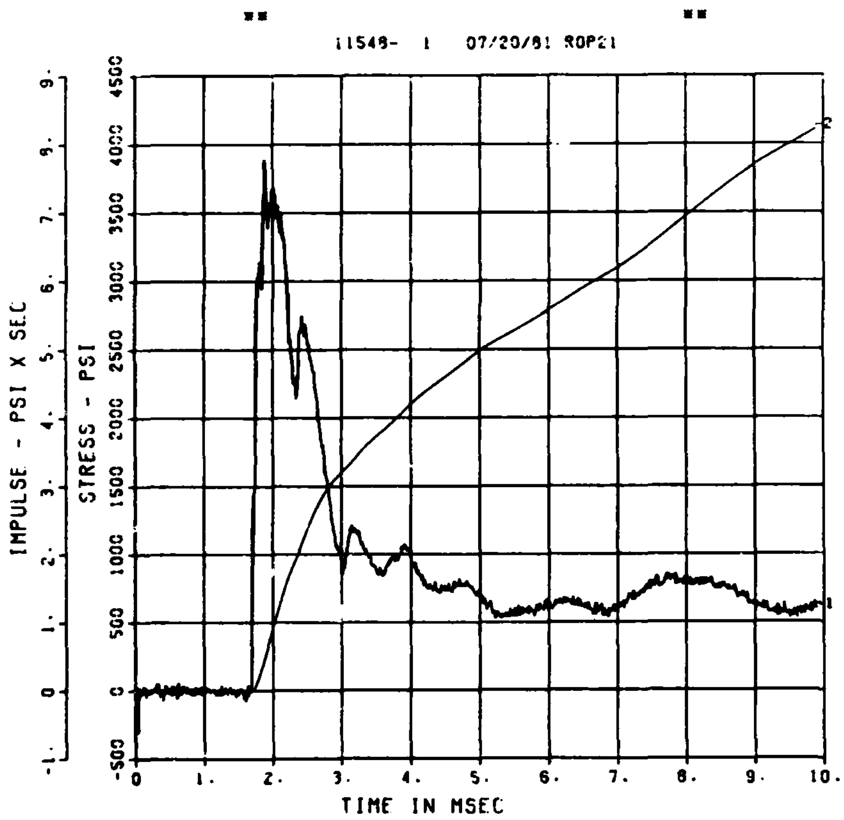

DYNAMIC SHEAR 1
IF2
200000. HZ CAL= 10562.

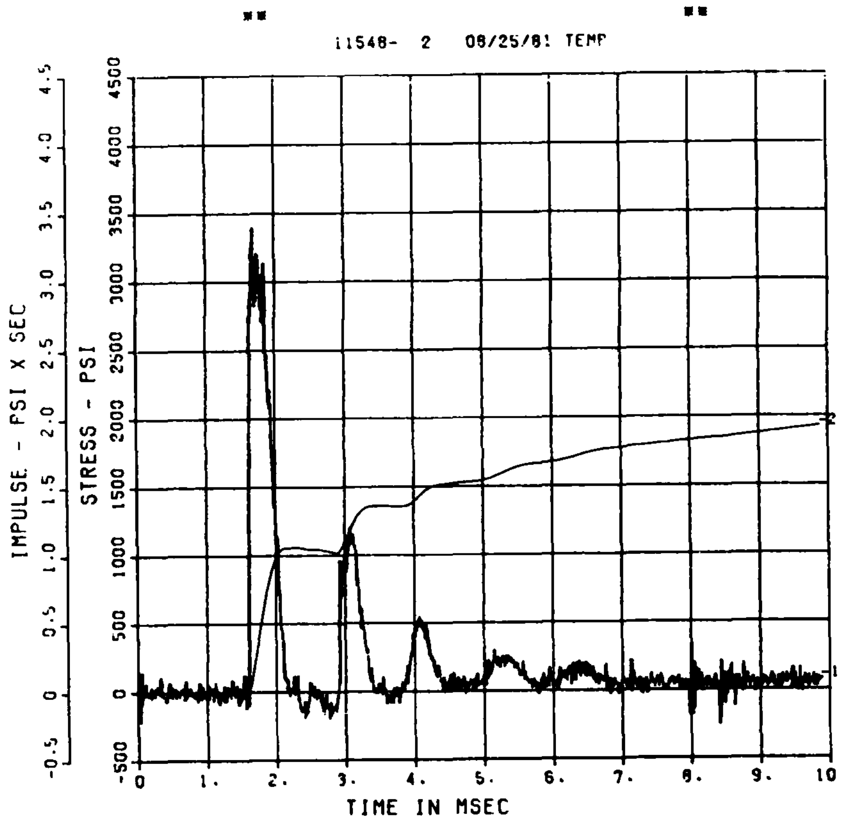

DYNAMIC SHEAR 1
IF3
200000. HZ CAL= 6152.

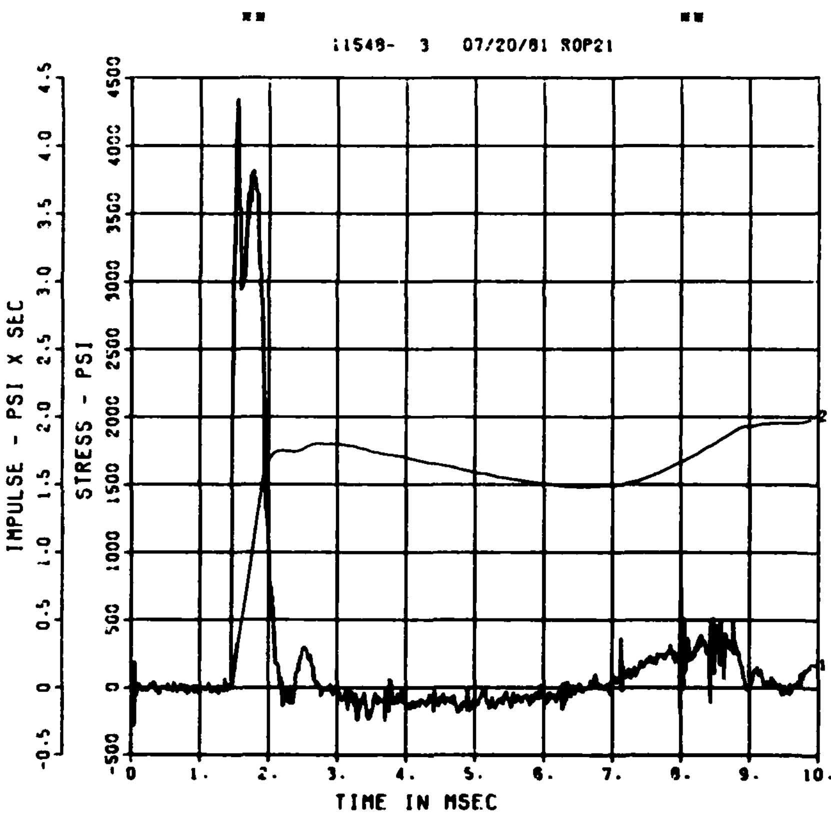

DYNAMIC SHEAR 1
IF4
200000. HZ CAL= 4340.

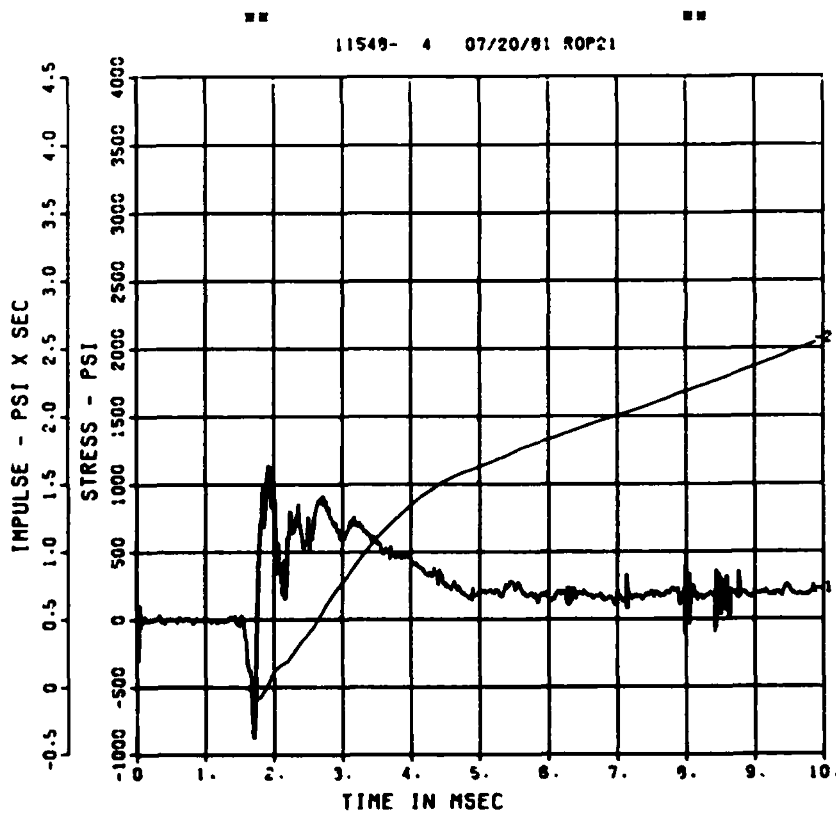

DYNAMIC SHEAR 1
IF5
200000. HZ CAL= 5719.

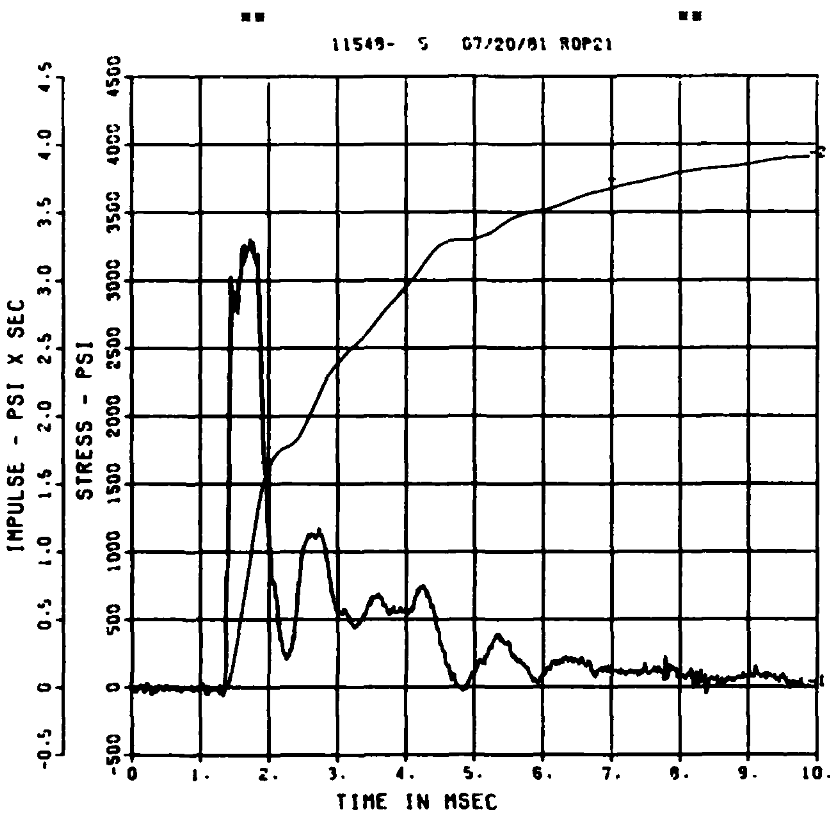

DYNAMIC SHEAR 1
E01
200000. HZ CAL= 11170.
LP4 70% CUTOFF= 9000. HZ

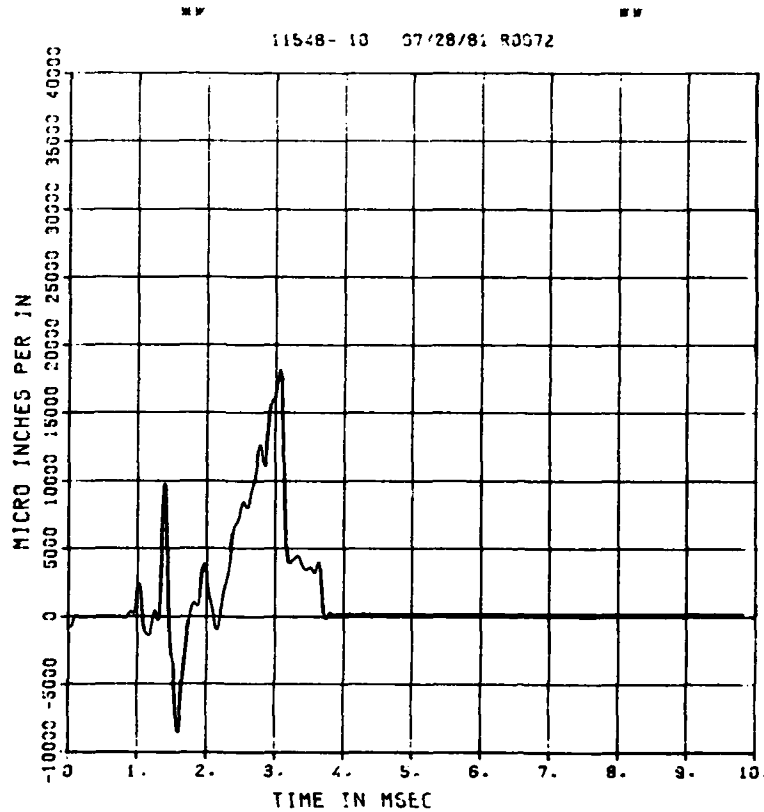

** PEAK VALUE IS 63 % OVER CALIBRATION **

DYNAMIC SHEAR 1
EI1
200000. HZ CAL= 11170.
LP4 70% CUTOFF= 9000. HZ

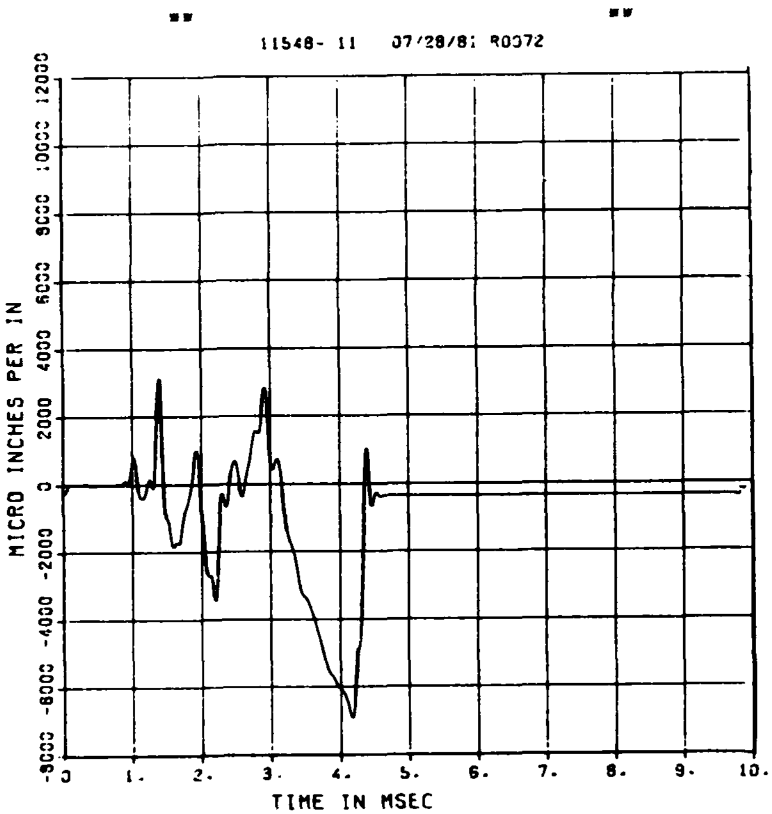

DYNAMIC SHEAR 1
EI2
200000. HZ CAL= 11170.
LP4 70% CUTOFF= 9000. HZ

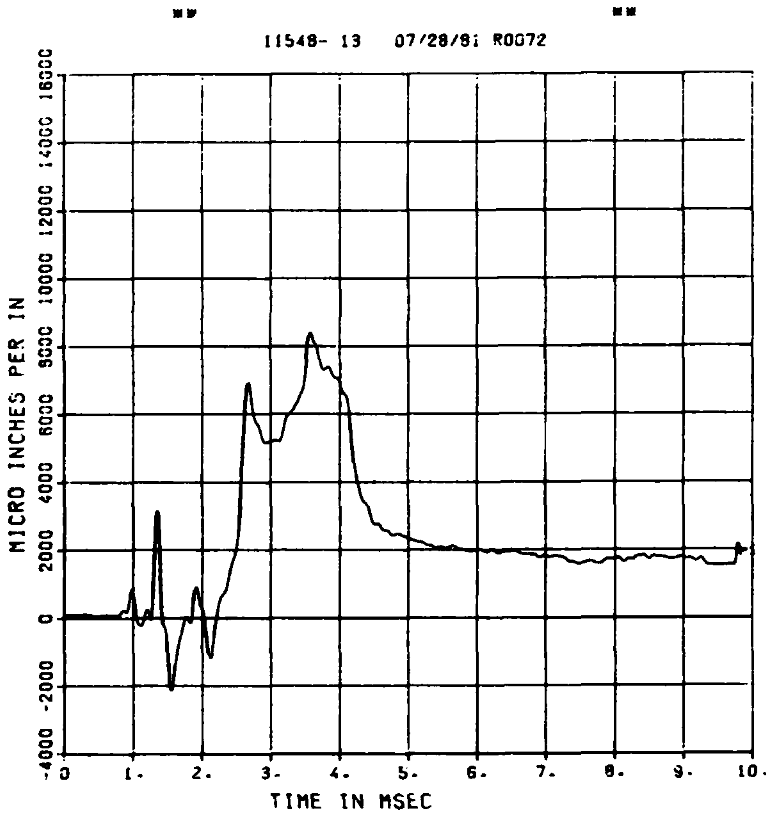

DYNAMIC SHEAR 1
E03
200000. HZ CAL= 11170.
LP4 70% CUTOFF= 9000. HZ

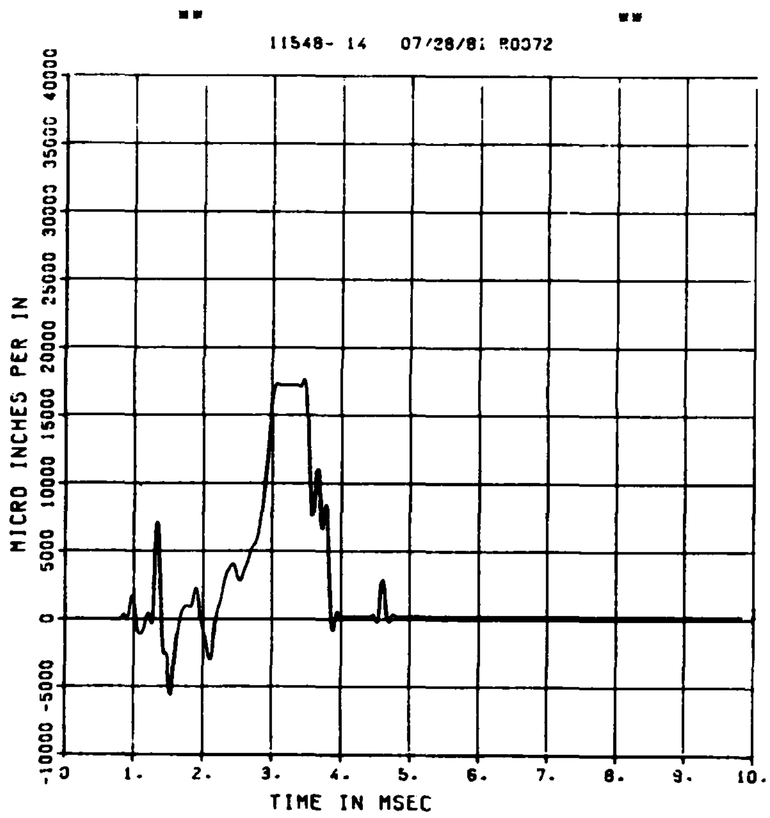

** PEAK VALUE IS 59 % OVER CALIBRATION **

DYNAMIC SHEAR 1
E13
200000. HZ CAL= 11170.
LP4 70% CUTOFF= 9000. HZ

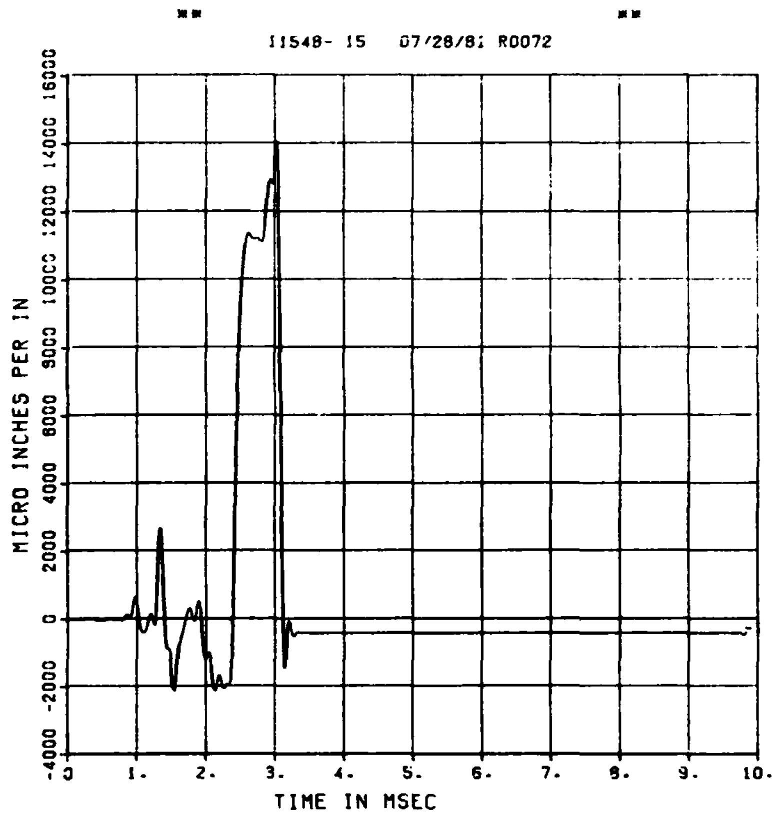

** PEAK VALUE IS 26 % OVER CALIBRATION **

DYNAMIC SHEAR 1
E04
200000. HZ CAL= 11170.
LP4 70% CUTOFF= 9000. HZ

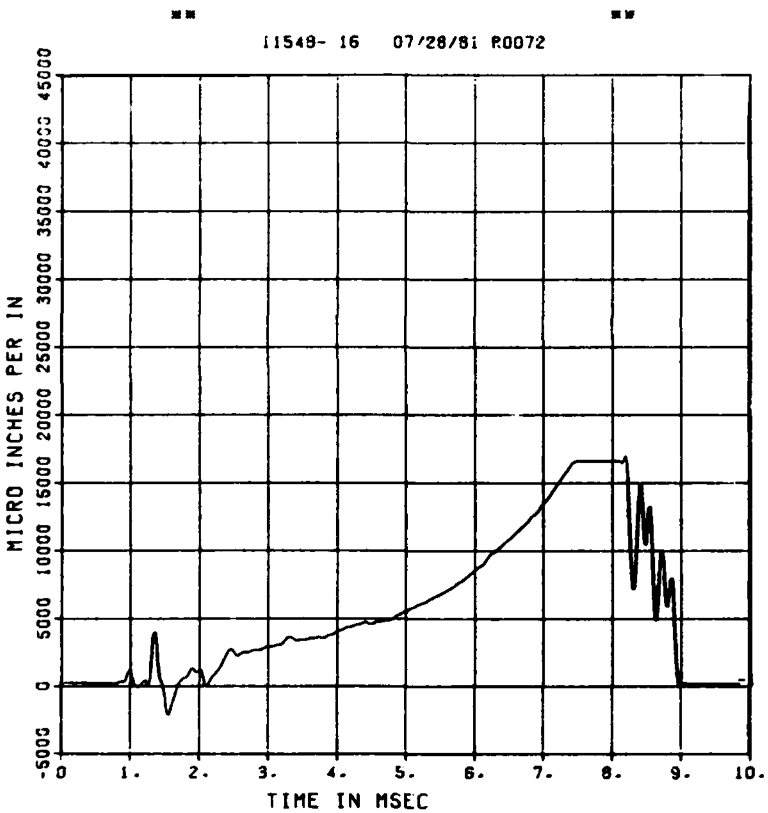

** PEAK VALUE IS 52 % OVER CALIBRATION **

DYNAMIC SHEAR 1
EI4
200000. HZ CAL= 11170.
LP4 70% CUTOFF= 9000. HZ

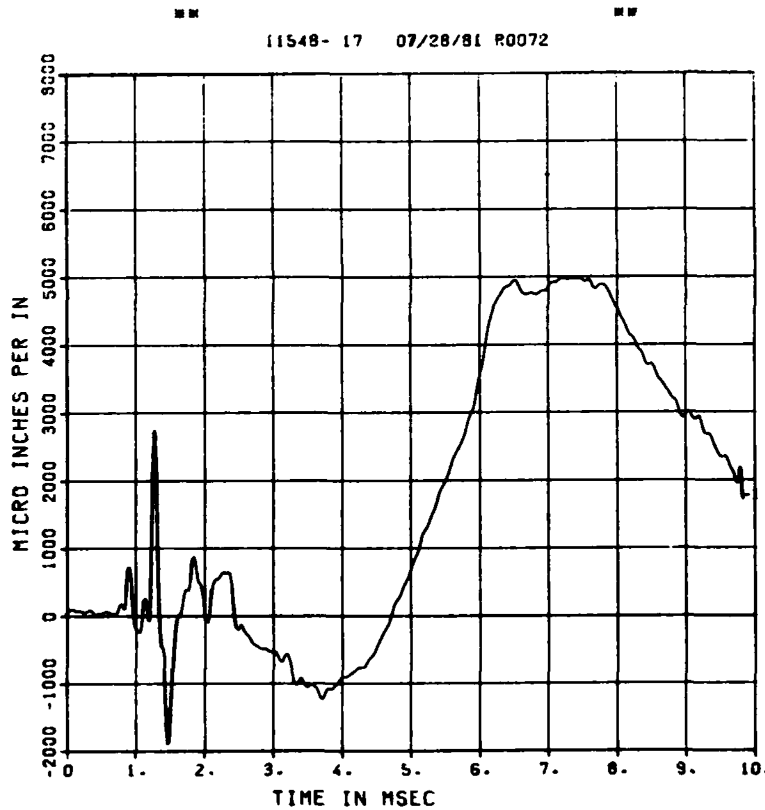

DYNAMIC SHEAR 1
E05
200000. HZ CAL= 11170.
LP4 70% CUTOFF= 9000. HZ

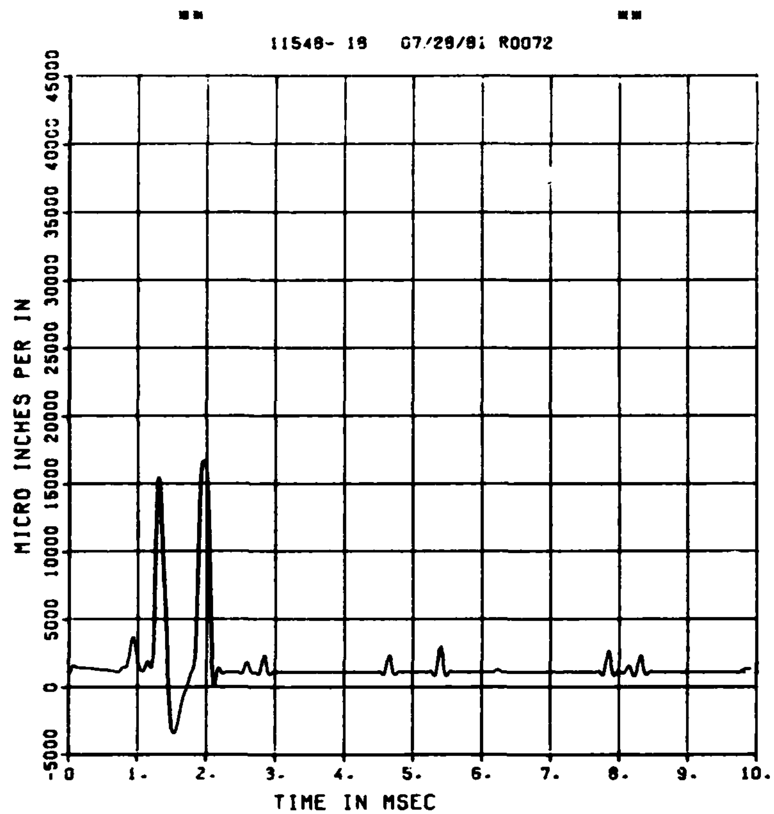

** PEAK VALUE IS 50 % OVER CALIBRATION **

DYNAMIC SHEAR 1
E15
200000. HZ CAL= 11170.
LP4 70% CUTOFF= 9000. HZ

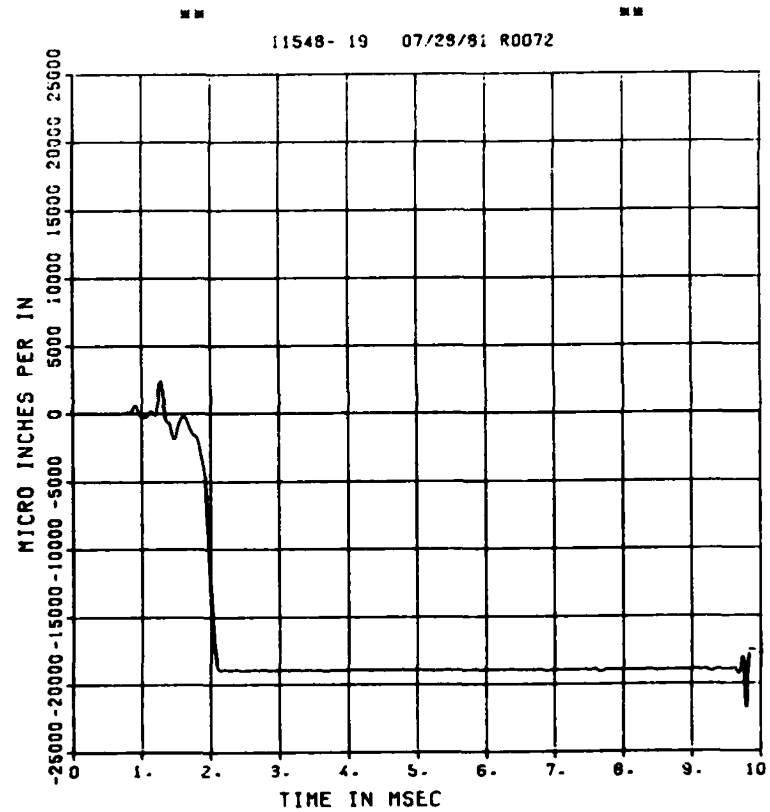

** PEAK VALUE IS 95 % OVER CALIBRATION **

DYNAMIC SHEAR 1
E06
200000. HZ CAL= 11170.
LP4 70% CUTOFF= 9000. HZ

** **

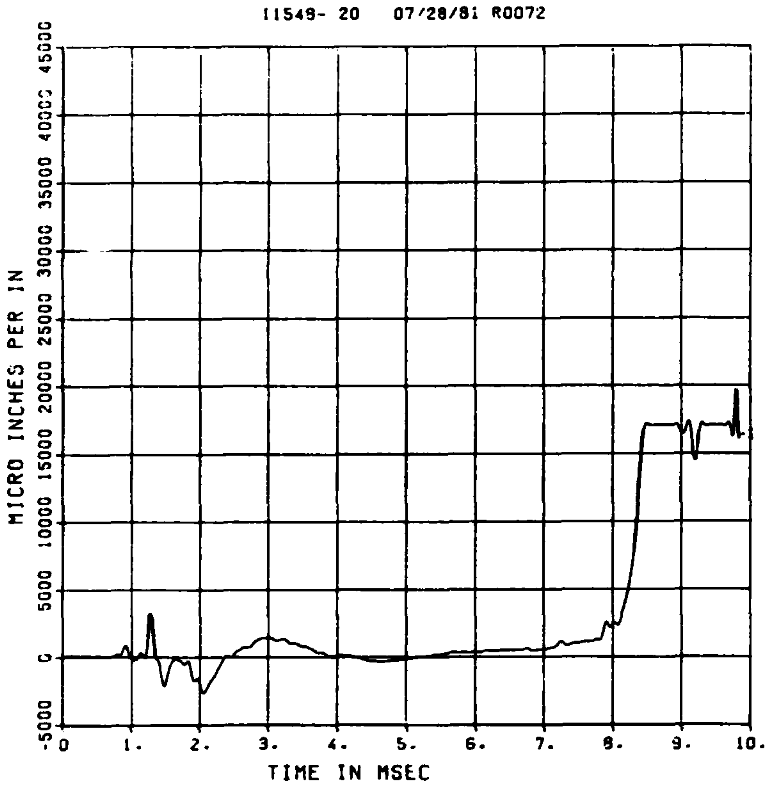

** PEAK VALUE IS 76 % OVER CALIBRATION **

DYNAMIC SHEAR 1
EI6
200000. HZ CAL= 11170.
LP4 70% CUTOFF= 9000. HZ

** **

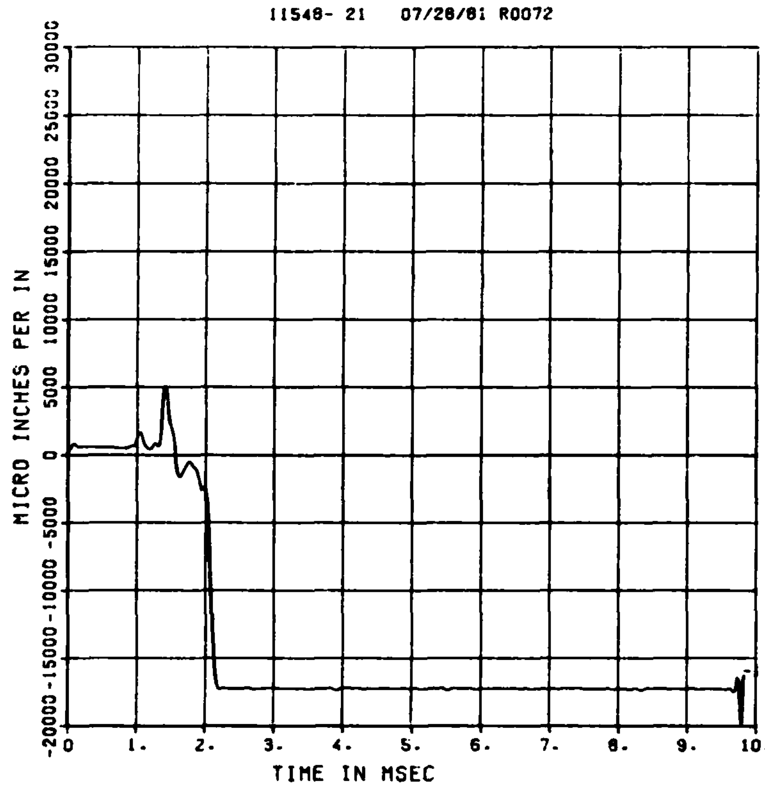

** PEAK VALUE IS 78 % OVER CALIBRATION **

DYNAMIC SHEAR 2
BP1
200000. HZ CAL= 23470.

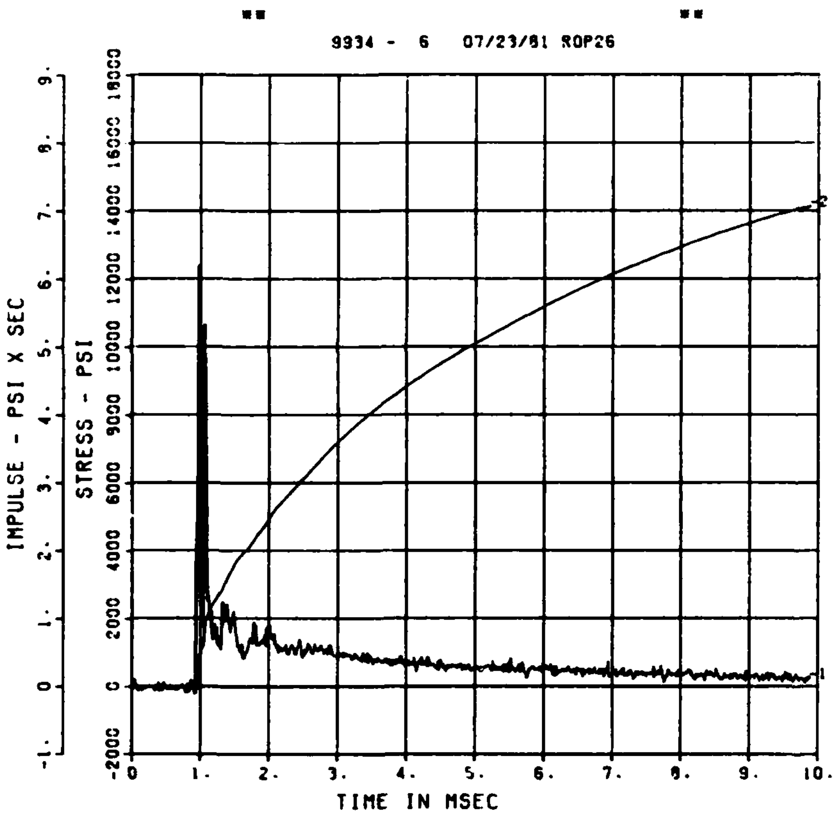

DYNAMIC SHEAR 2
BP1
200000. HZ CAL= 23470.

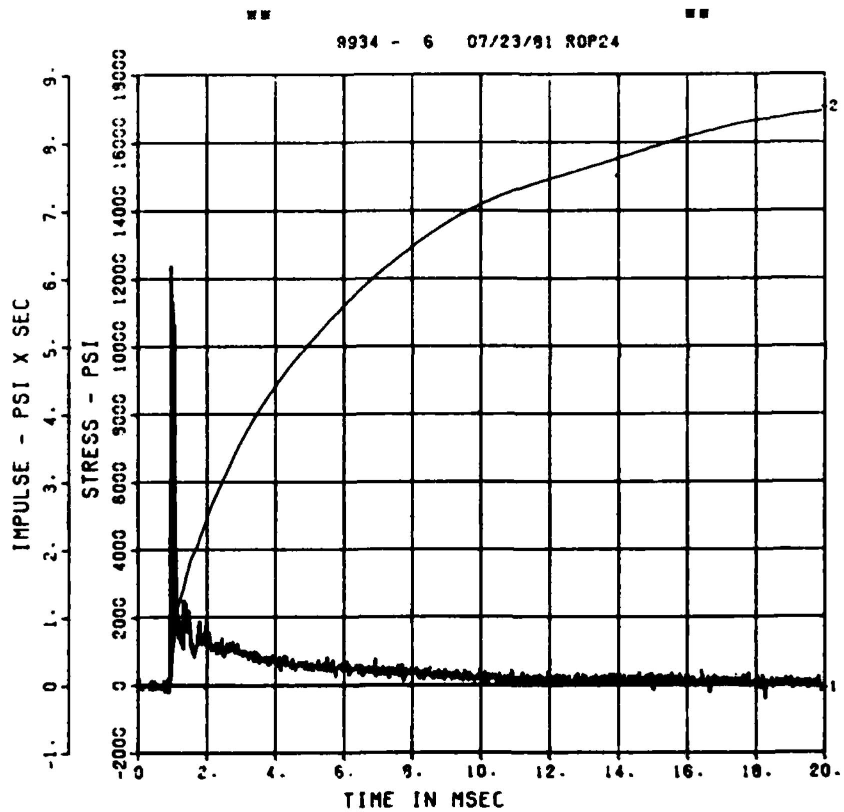

DYNAMIC SHEAR 2
BP2
200000. HZ CAL= 20491.

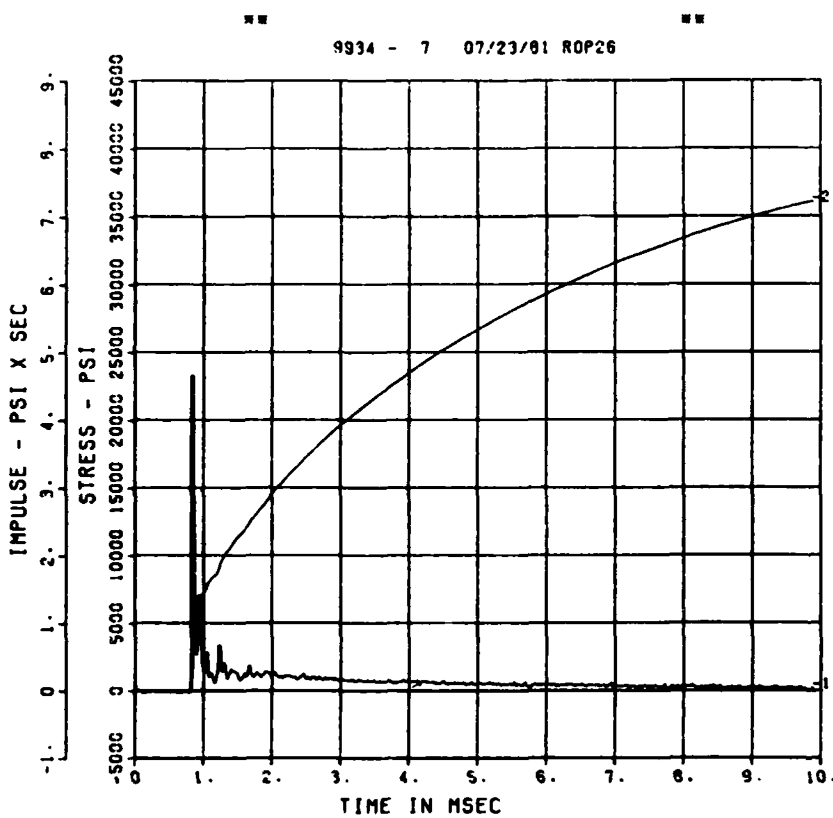

** PEAK VALUE IS 14 % OVER CALIBRATION **

DYNAMIC SHEAR 2
BP2
200000. HZ CAL= 20491.

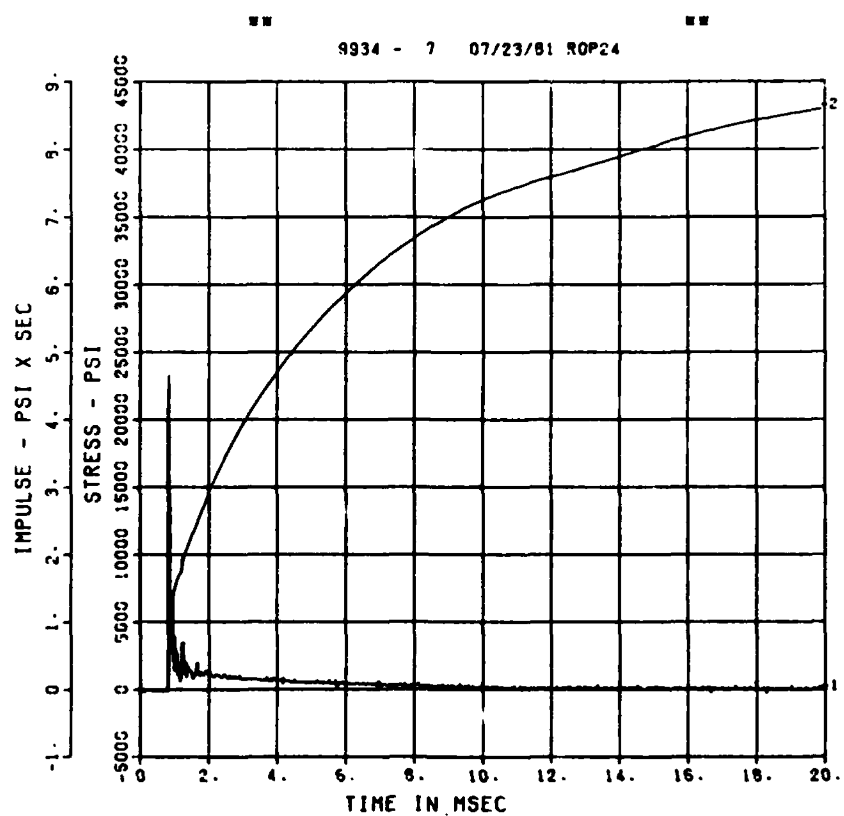

** PEAK VALUE IS 14 % OVER CALIBRATION **

DYNAMIC SHEAR 2
BP3
200000. HZ CAL= 20270.

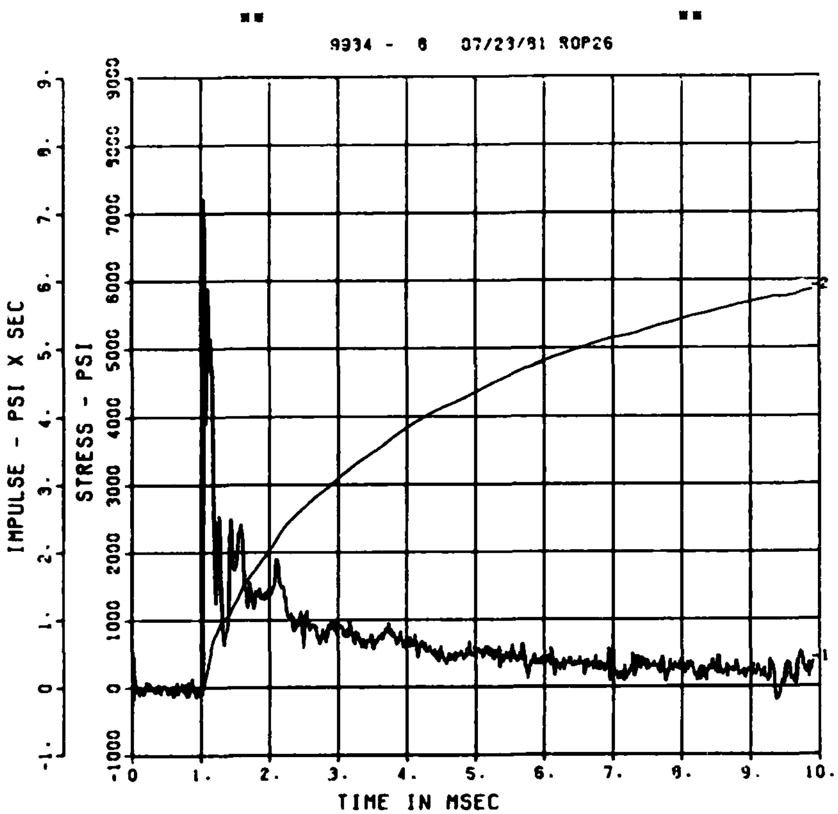

DYNAMIC SHEAR 2
BP3
200000. HZ CAL= 20270.

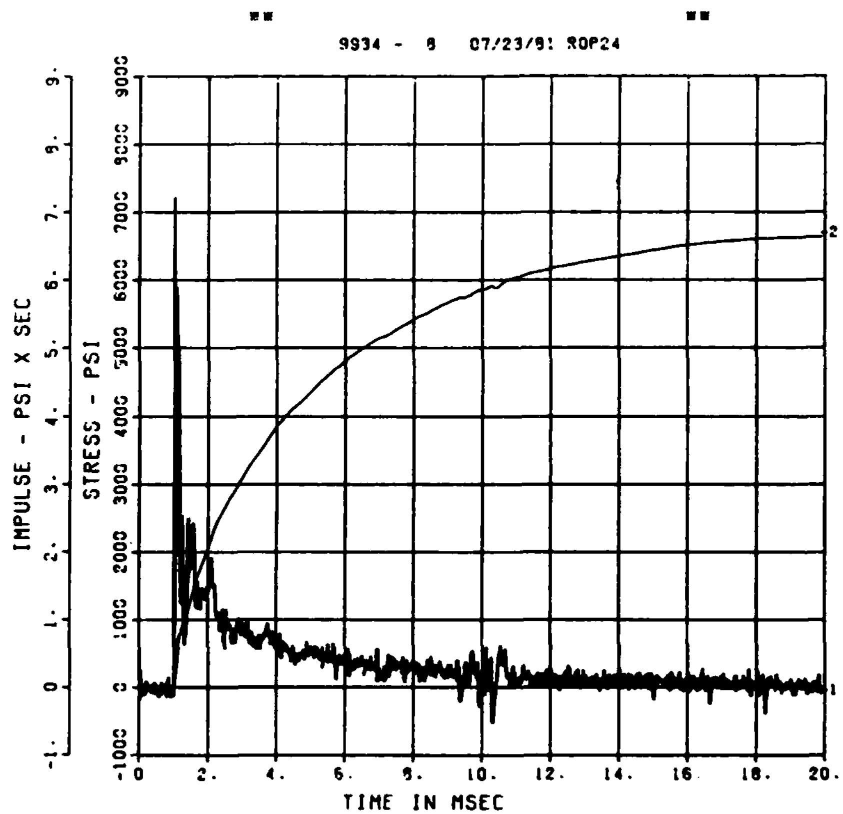

DYNAMIC SHEAR 2
BP4
200000. HZ CAL= 20312.

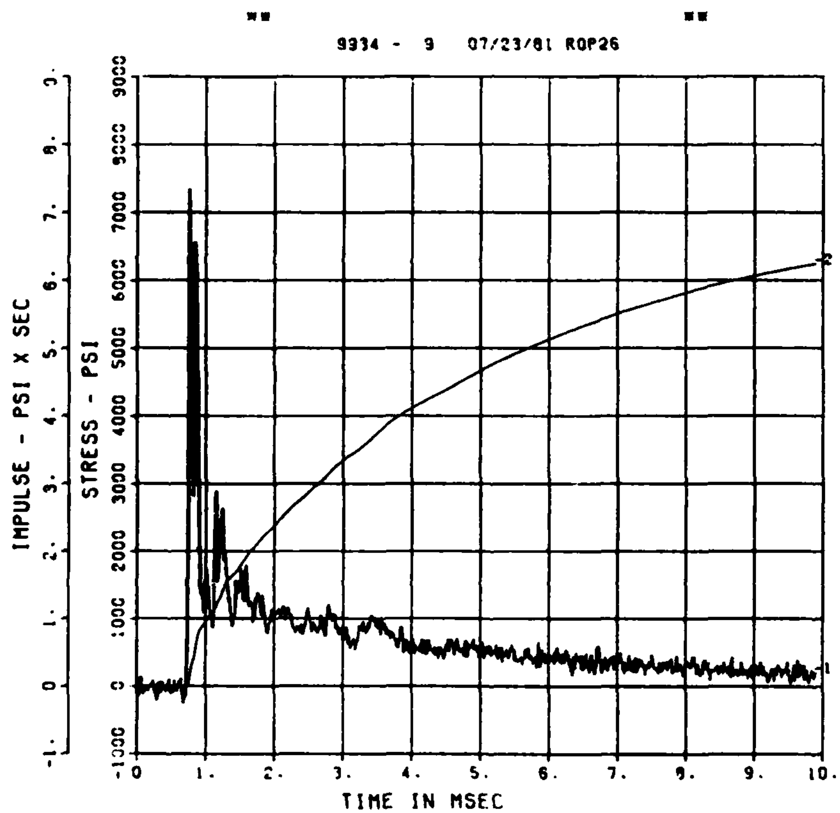

DYNAMIC SHEAR 2
BP4
200000. HZ CAL= 20312.

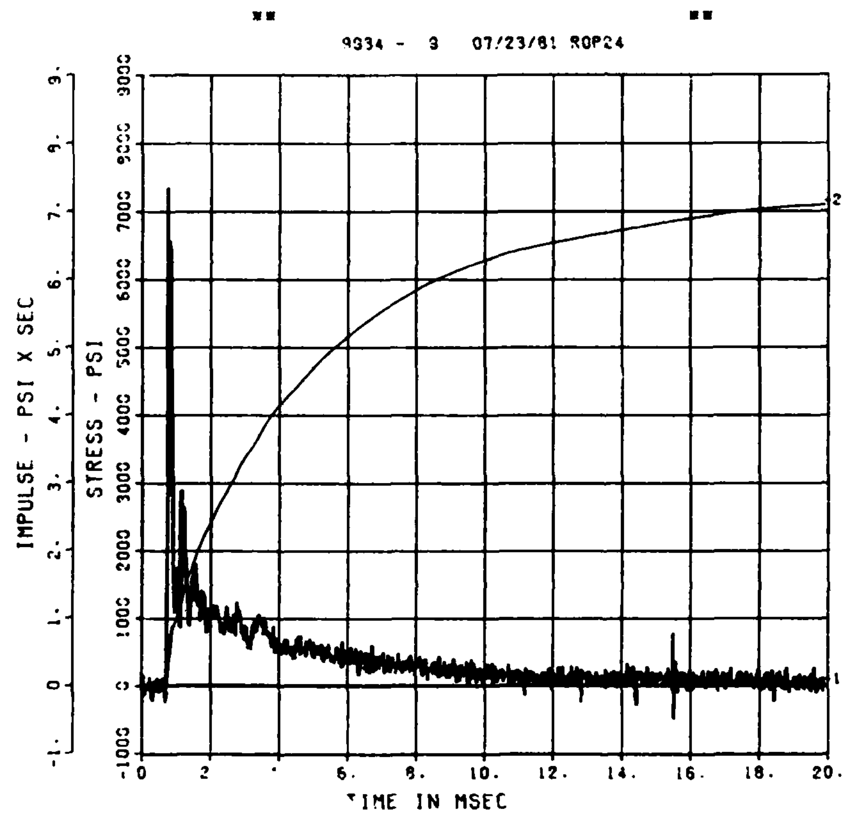

DYNAMIC SHEAR 2
IF1
200000. HZ CAL= 12056.

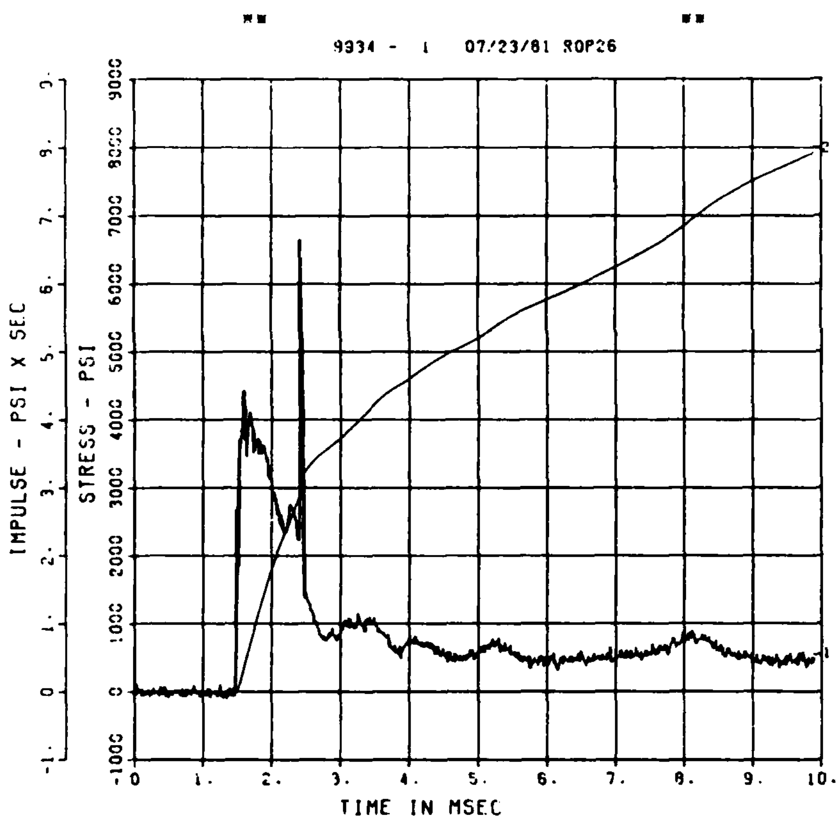

DYNAMIC SHEAR 2
IF2
200000. HZ CAL= 20304.

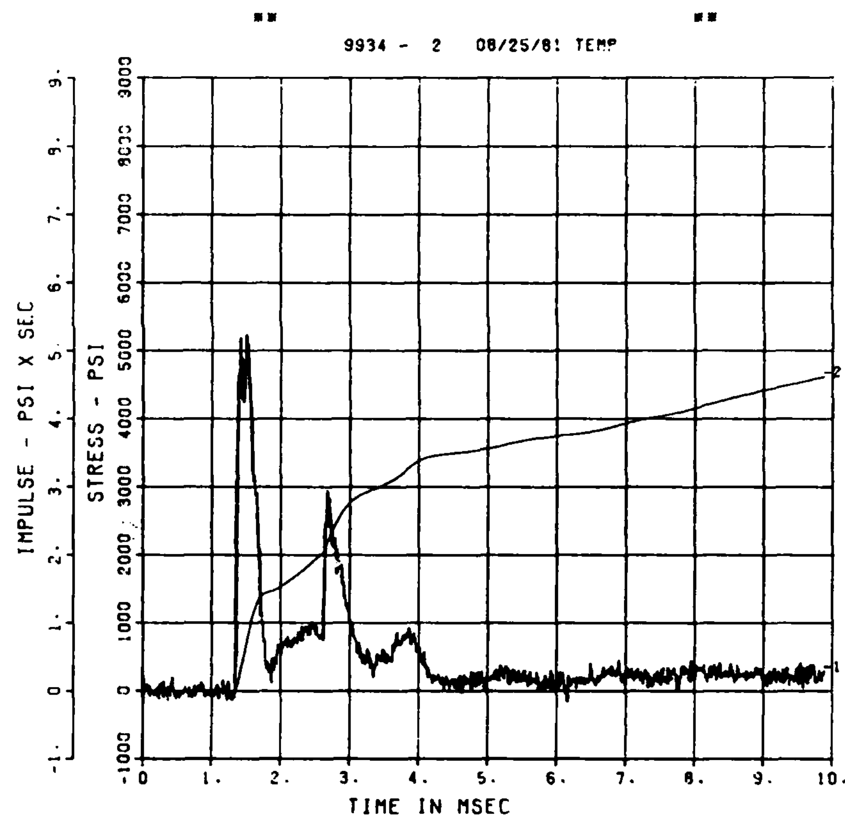

DYNAMIC SHEAR 2
IF3
200000. HZ CAL= 9104.

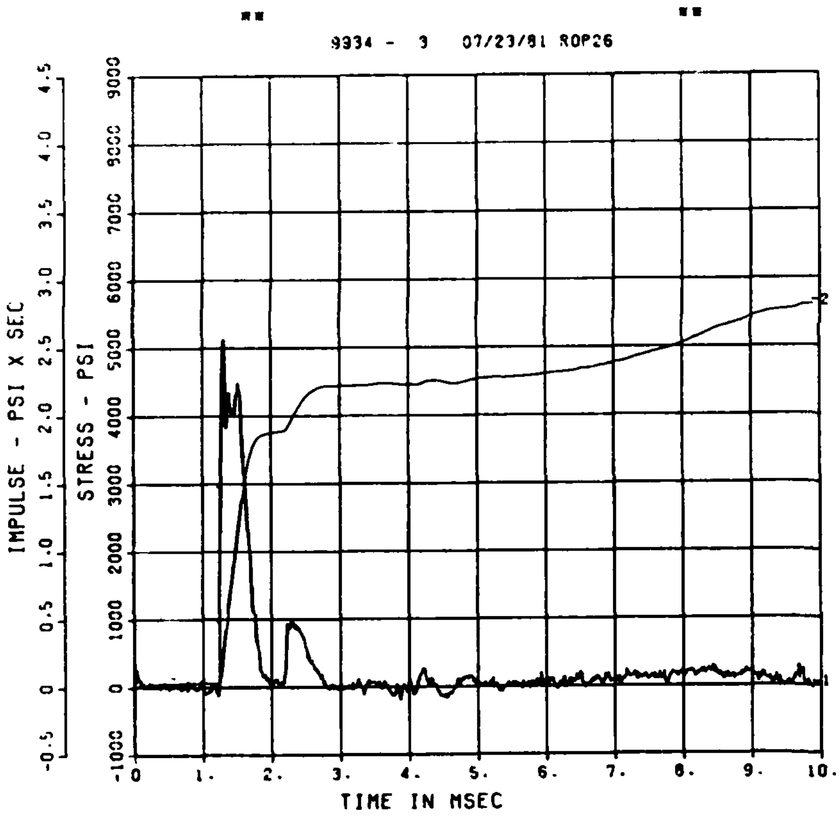

DYNAMIC SHEAR 2
IF4
200000. HZ CAL= 10587.

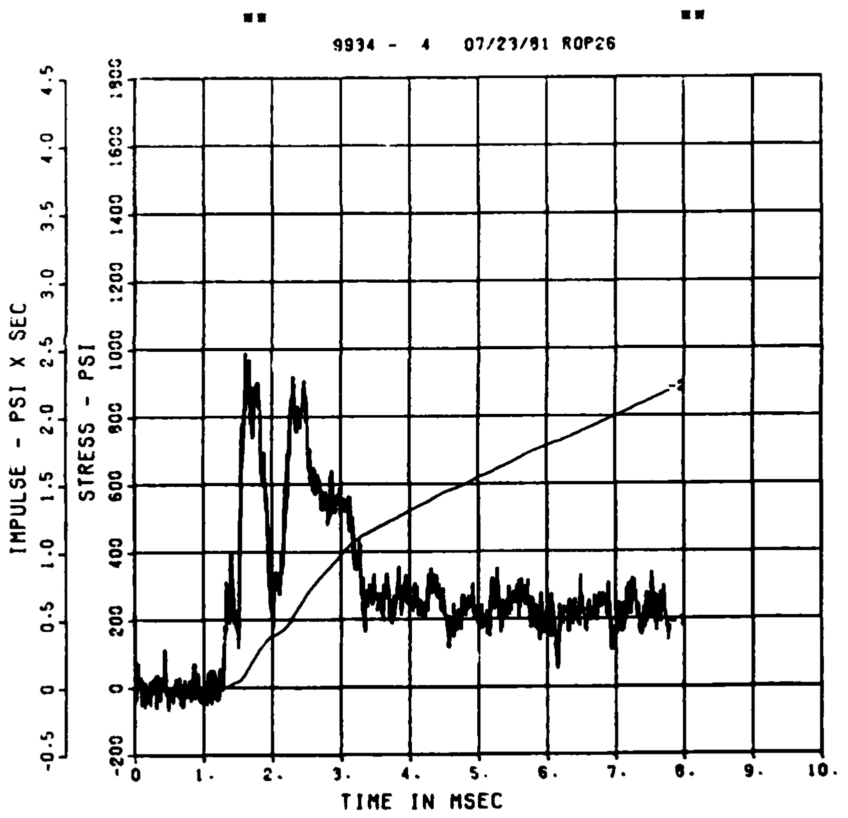

** PEAK VALUE IS 91 % UNDER CALIBRATION **

DYNAMIC SHEAR 2
IF5
200000. HZ CAL= 11885.

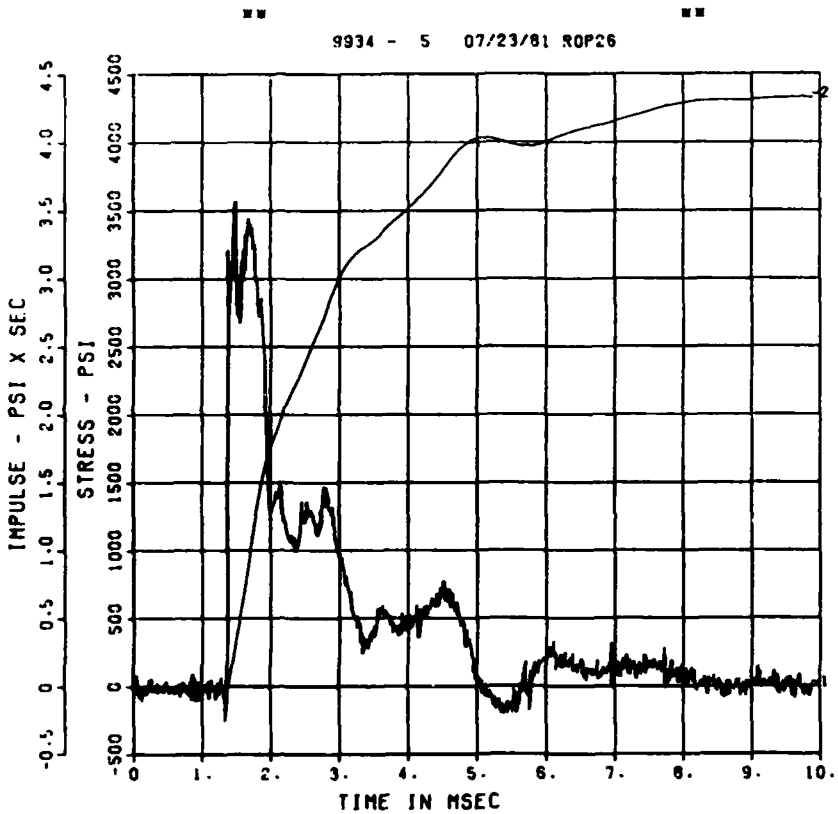

DYNAMIC SHEAR 2
E01
200000. HZ CAL= 11170.
LP4 70% CUTOFF= 9000. HZ

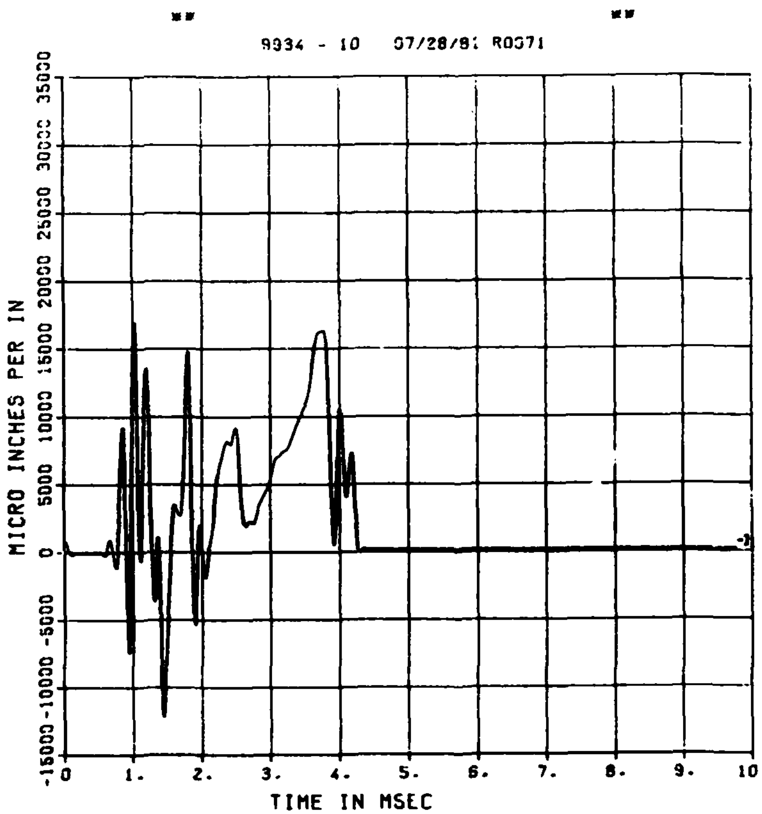

** PEAK VALUE IS 51 % OVER CALIBRATION **

DYNAMIC SHEAR 2
EI1
200000. HZ CAL= 11170.
LP4 70% CUTOFF= 9000. HZ

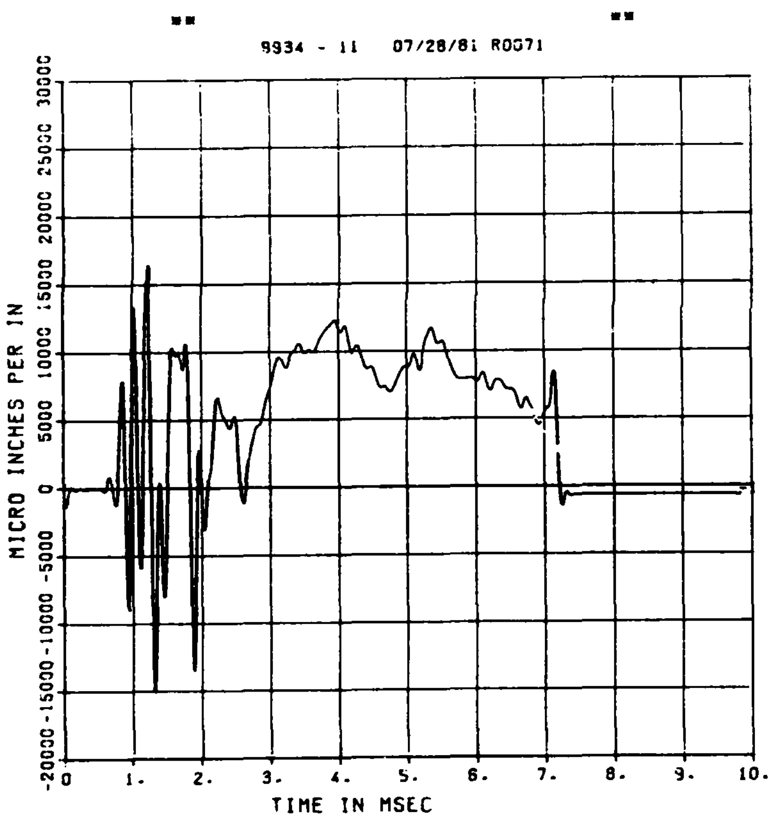

** PEAK VALUE IS 47 % OVER CALIBRATION **

DYNAMIC SHEAR 2
E02
200000. HZ CAL= 11170.
LP4 70% CUTOFF= 9000. HZ

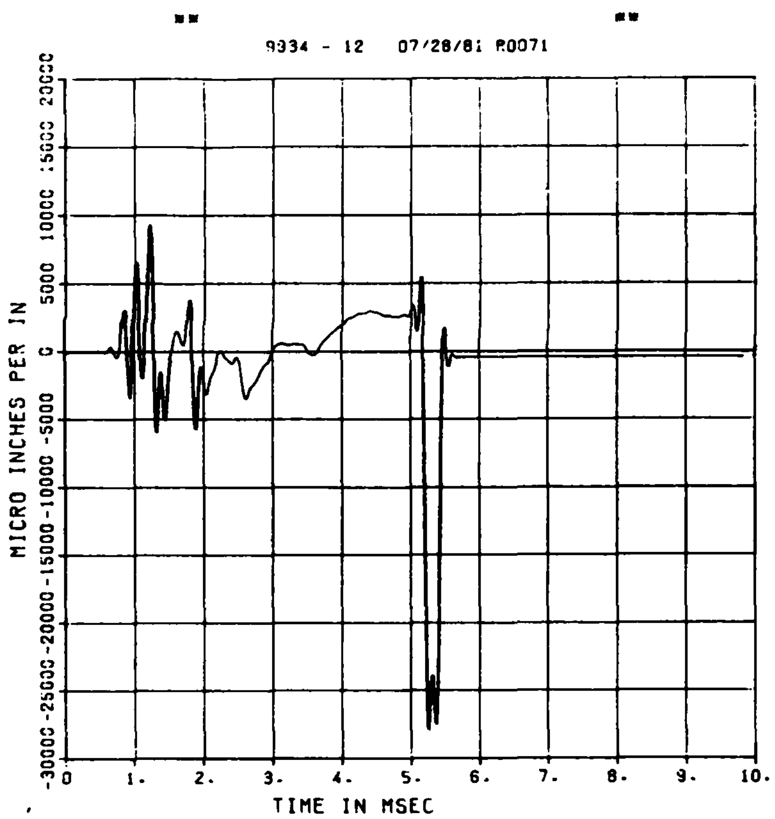

** PEAK VALUE IS 150 % OVER CALIBRATION **

DYNAMIC SHEAR 2
E12
200000. HZ CAL= 11170.
LP4 70% CUTOFF= 9000. HZ

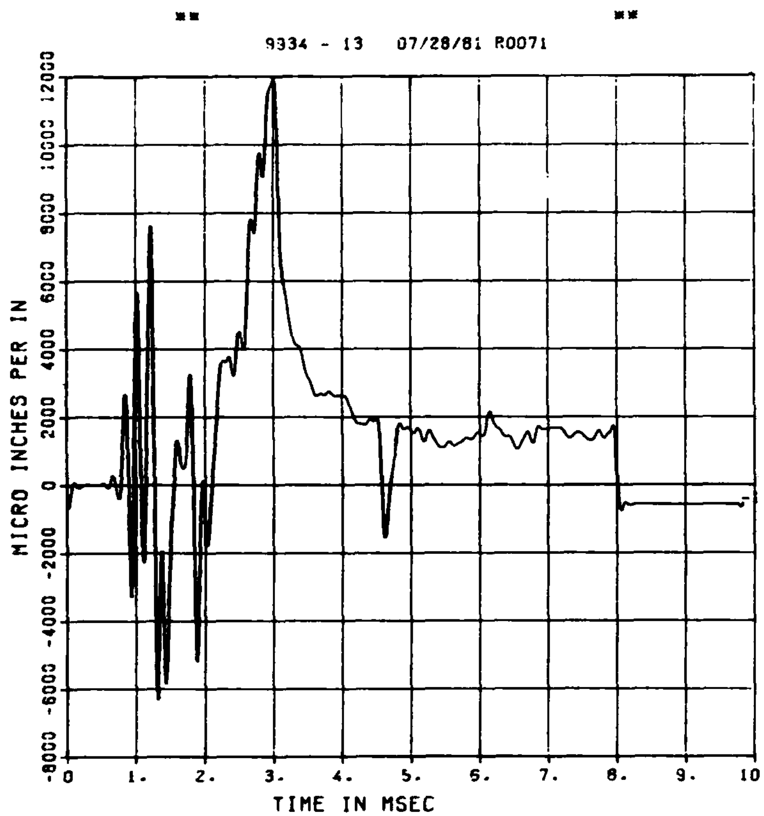

** PEAK VALUE IS 7 % OVER CALIBRATION **

DYNAMIC SHEAR 2
E03
200000. HZ CAL= 11170.
LP4 70% CUTOFF= 9000. HZ

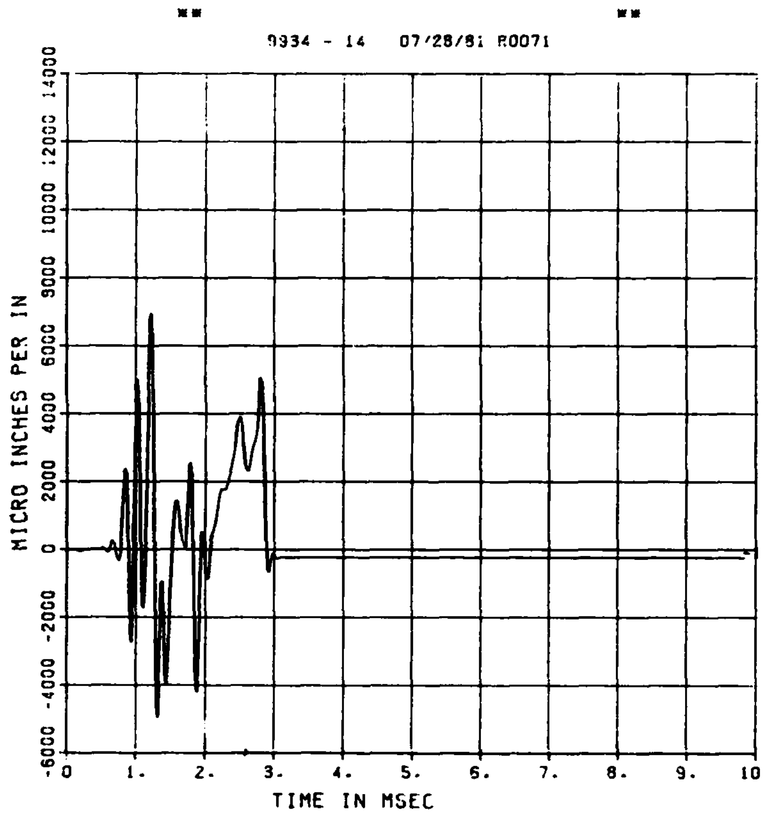

DYNAMIC SHEAR 2
EI3
200000. HZ CAL= 11170.
LP4 70% CUTOFF= 9000. HZ

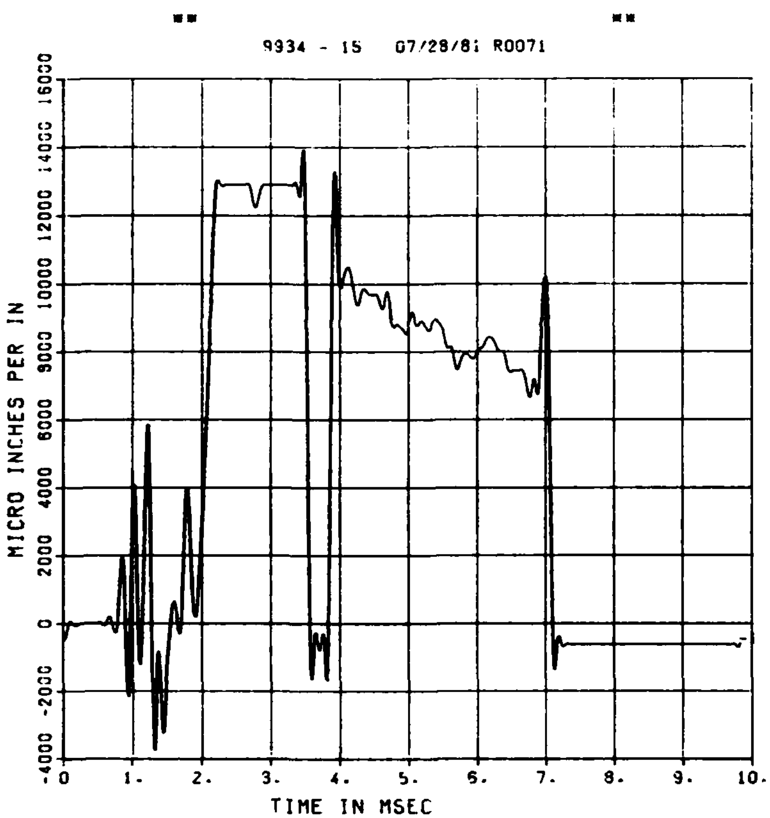

DYNAMIC SHEAR 2
E04
200000. HZ CAL= 11170.
LP4 70% CUTOFF= 9000. HZ

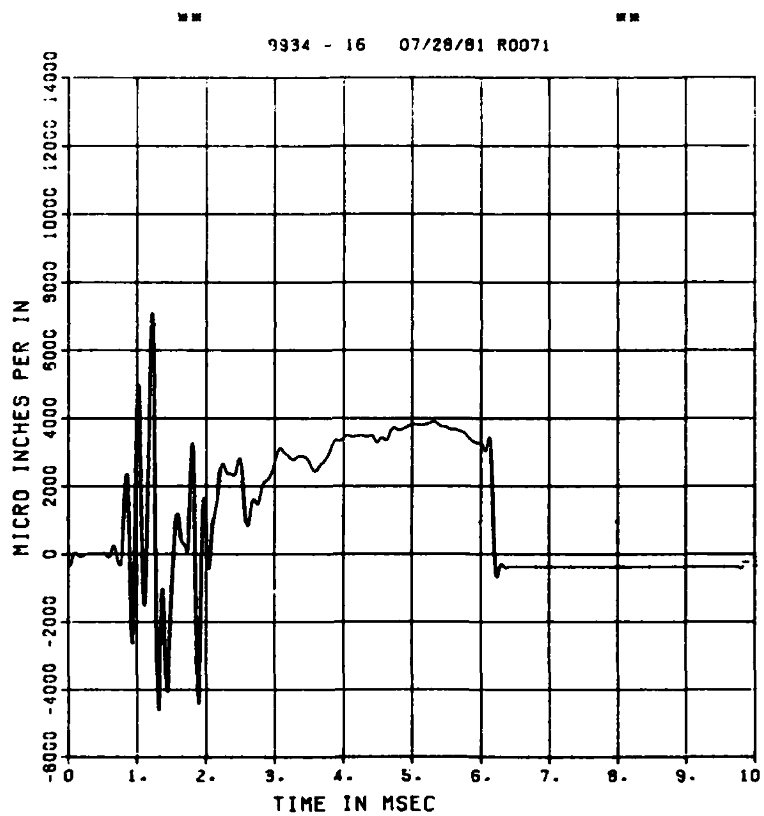

** PEAK VALUE IS 25 % OVER CALIBRATION **

DYNAMIC SHEAR 2
EI4
200000. HZ CAL= 11170.
LP4 70% CUTOFF= 9000. HZ

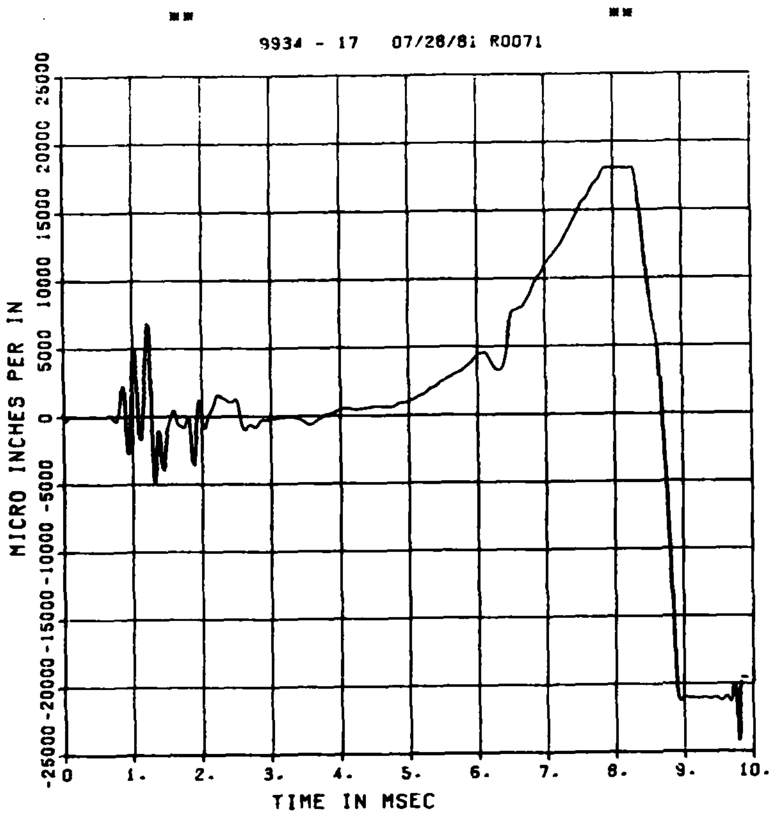

** PEAK VALUE IS 117 % OVER CALIBRATION **

DYNAMIC SHEAR 2
E05
200000. HZ CAL= 11170.
LP4 70% CUTOFF= 9000. HZ

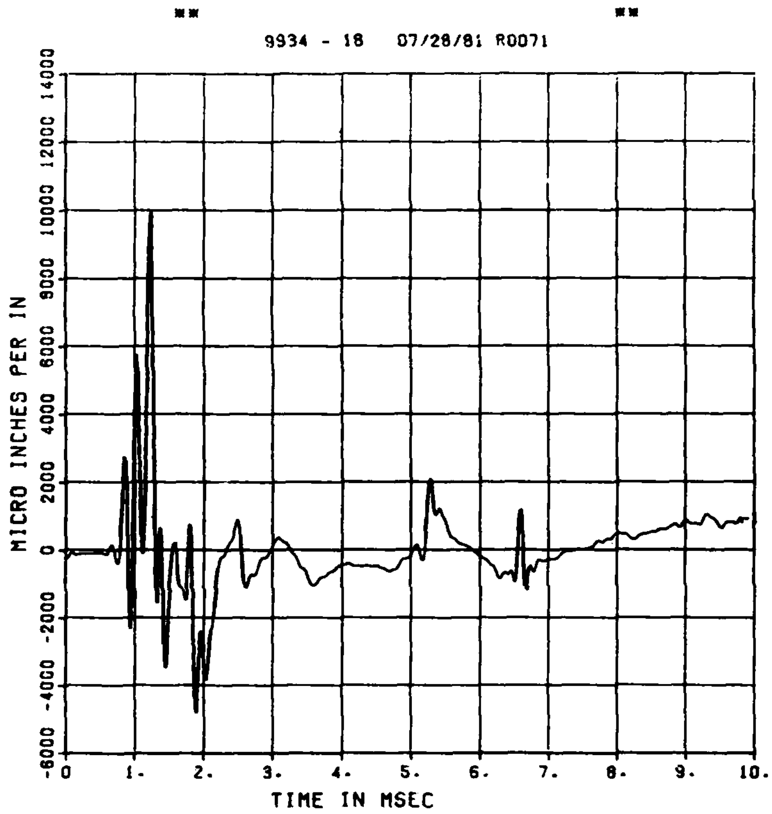

DYNAMIC SHEAR 2
E15
200000. HZ CAL= 11170.
LP4 70% CUTOFF= 9000. HZ

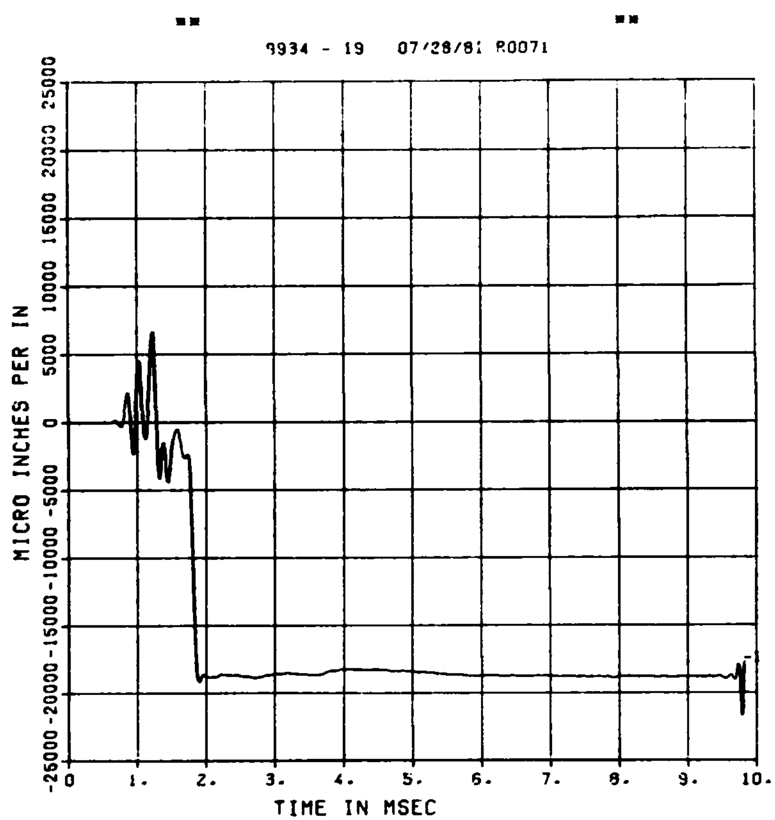

** PEAK VALUE IS 94 % OVER CALIBRATION **

DYNAMIC SHEAR 2
E06
200000. HZ CAL= 11170.
LP4 70% CUTOFF= 9000. HZ

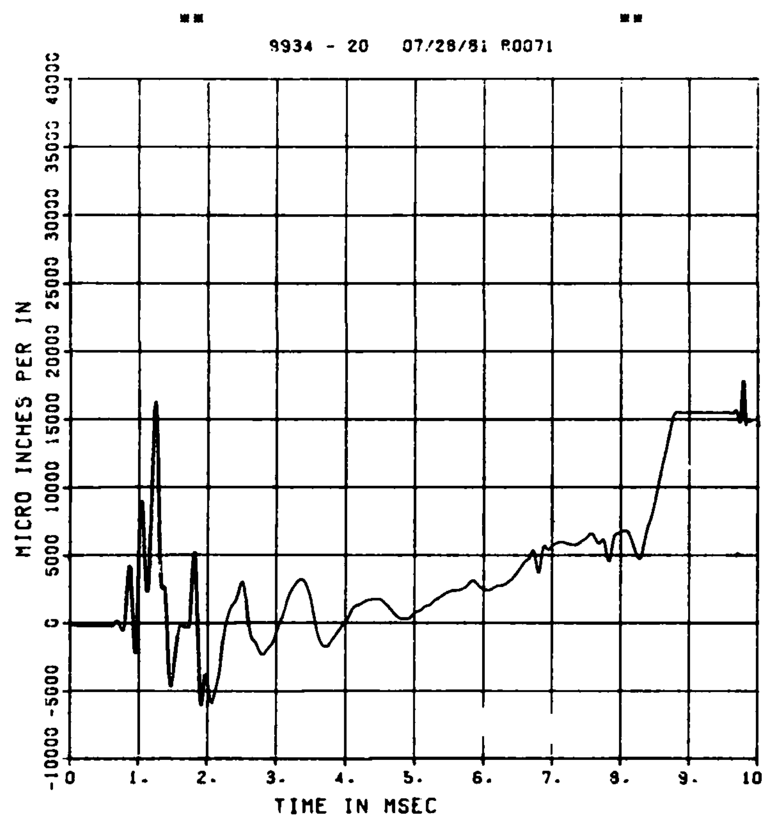

** PEAK VALUE IS 60 % OVER CALIBRATION **

DYNAMIC SHEAR 2
EI6
200000. HZ CAL= 11170.
LP4 70% CUTOFF= 9000. HZ

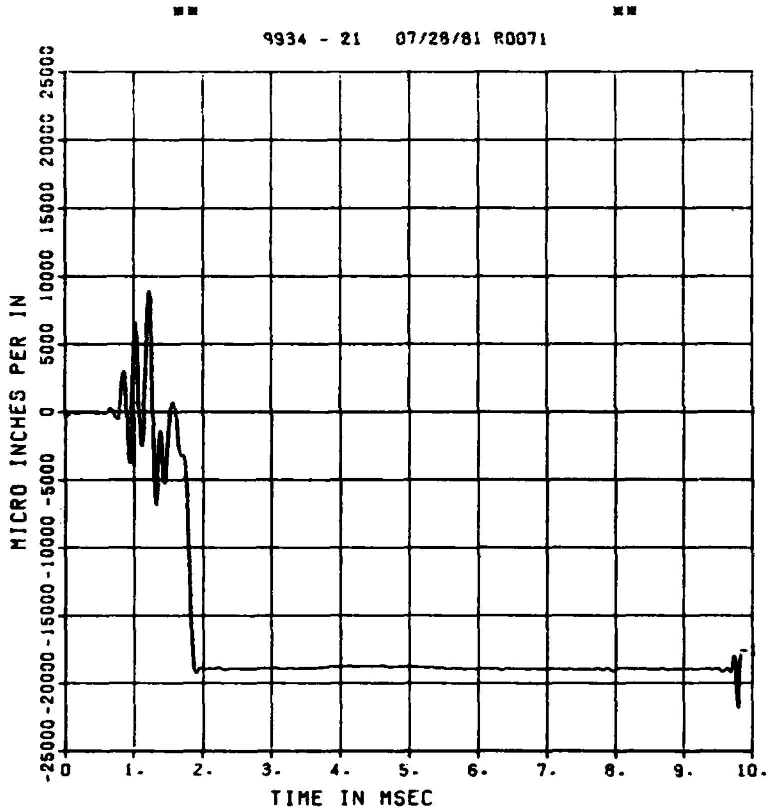

** PEAK VALUE IS 95 % OVER CALIBRATION **

DYNAMIC SHEAR 3
BP3
200000. HZ CAL= 14298.

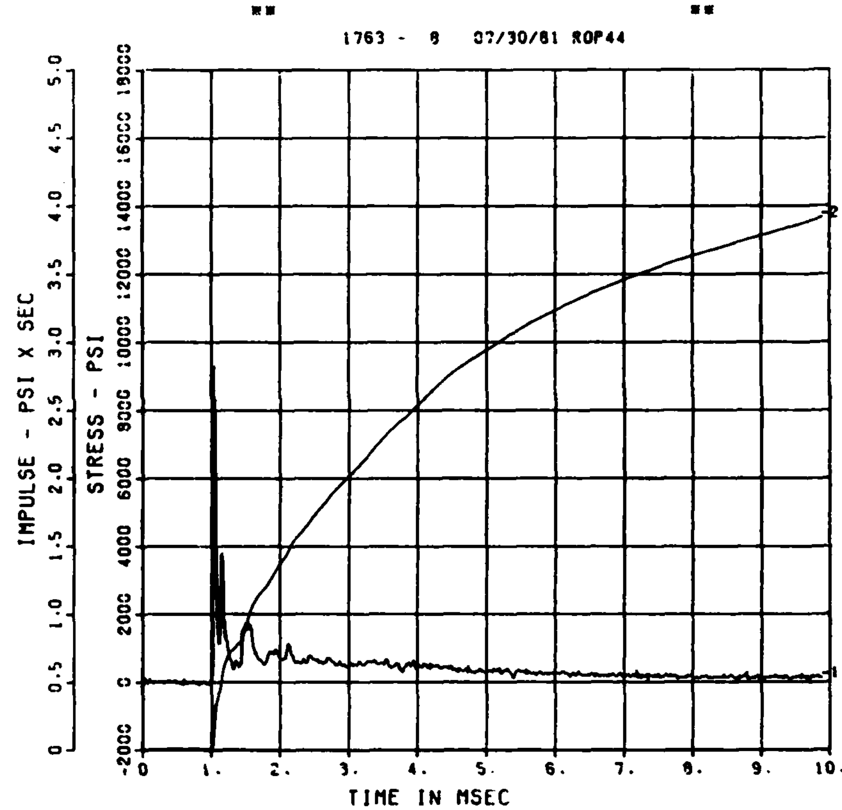

DYNAMIC SHEAR 3
BP3
200000. HZ CAL= 14298.

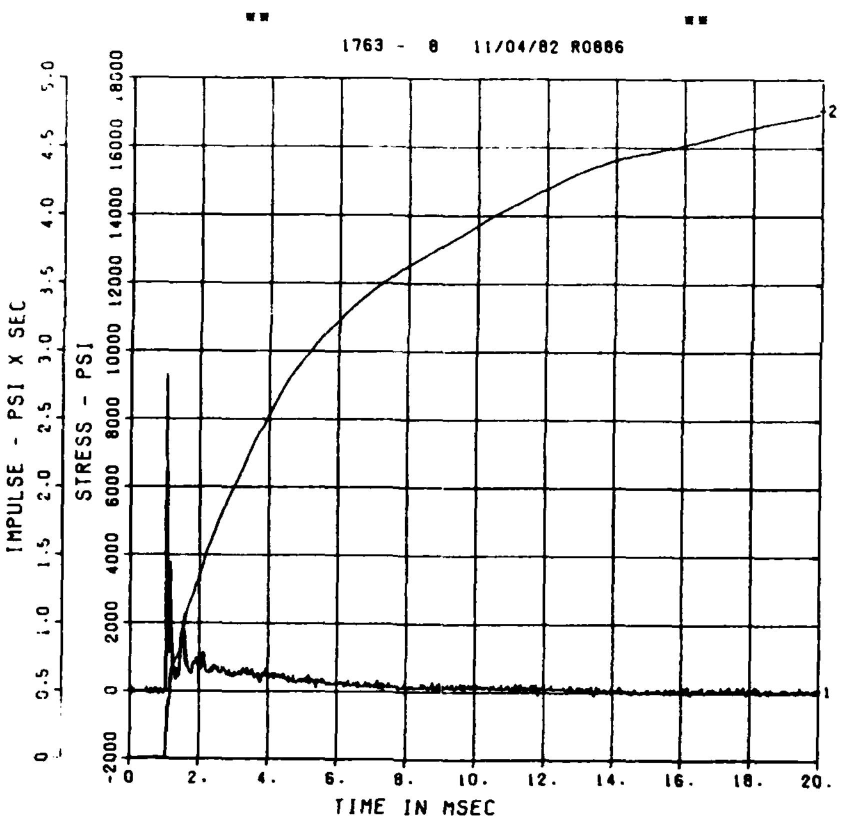

DYNAMIC SHEAR 3
BP4
200000. HZ CAL= 14785.

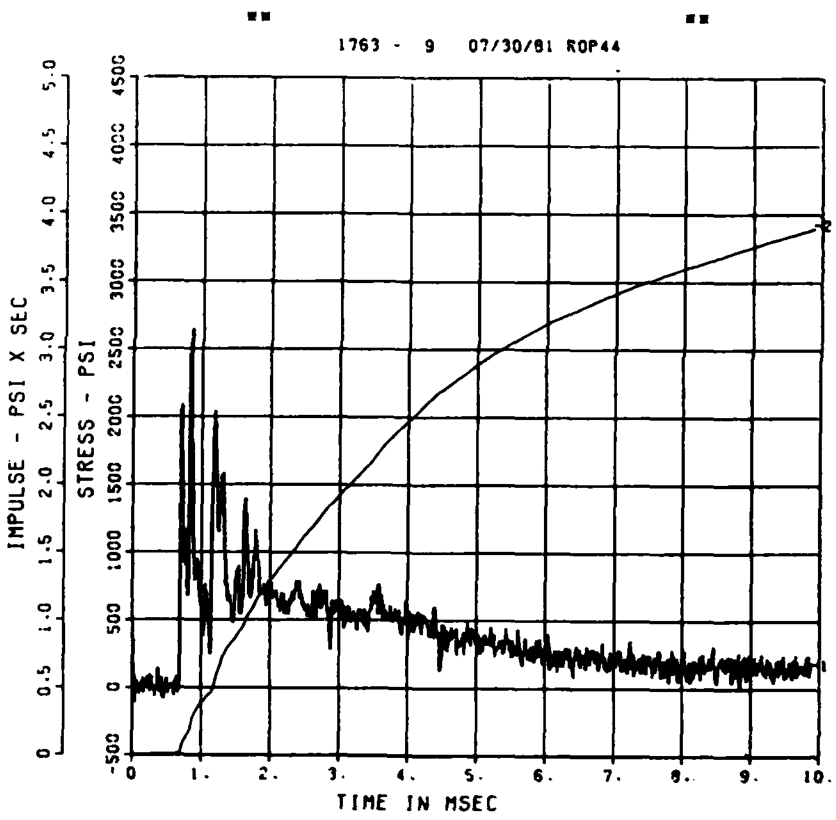

** PEAK VALUE IS 82 % UNDER CALIBRATION **

DYNAMIC SHEAR 3
BP4
200000. HZ CAL= 14785.

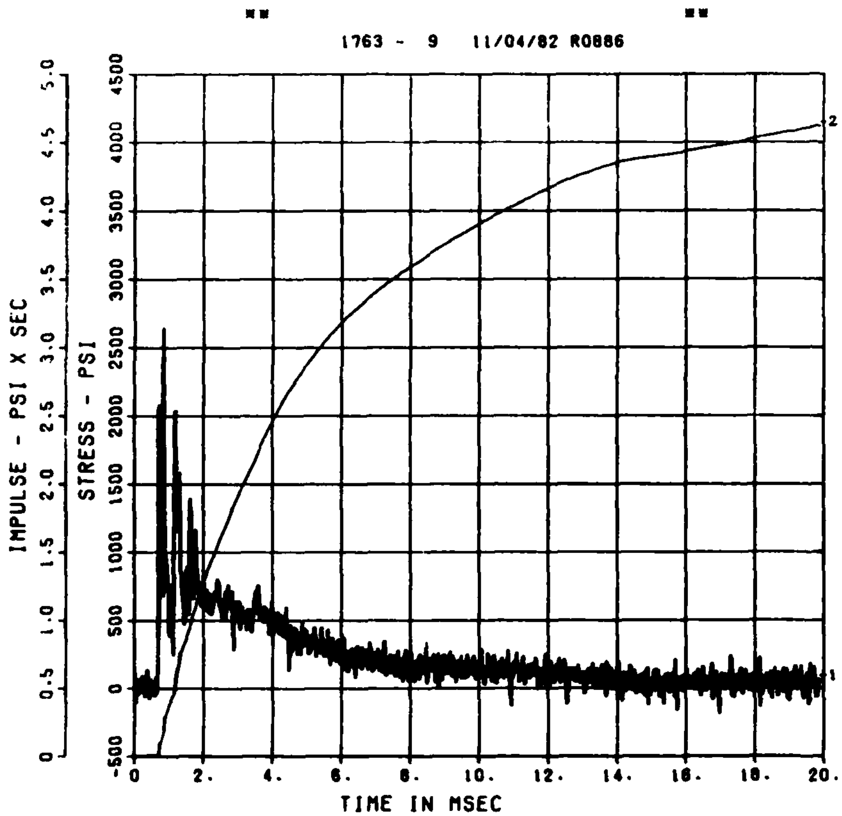

** PEAK VALUE IS 82 % UNDER CALIBRATION **

DYNAMIC SHEAR 3
IF1
200000. HZ CAL= 6271.

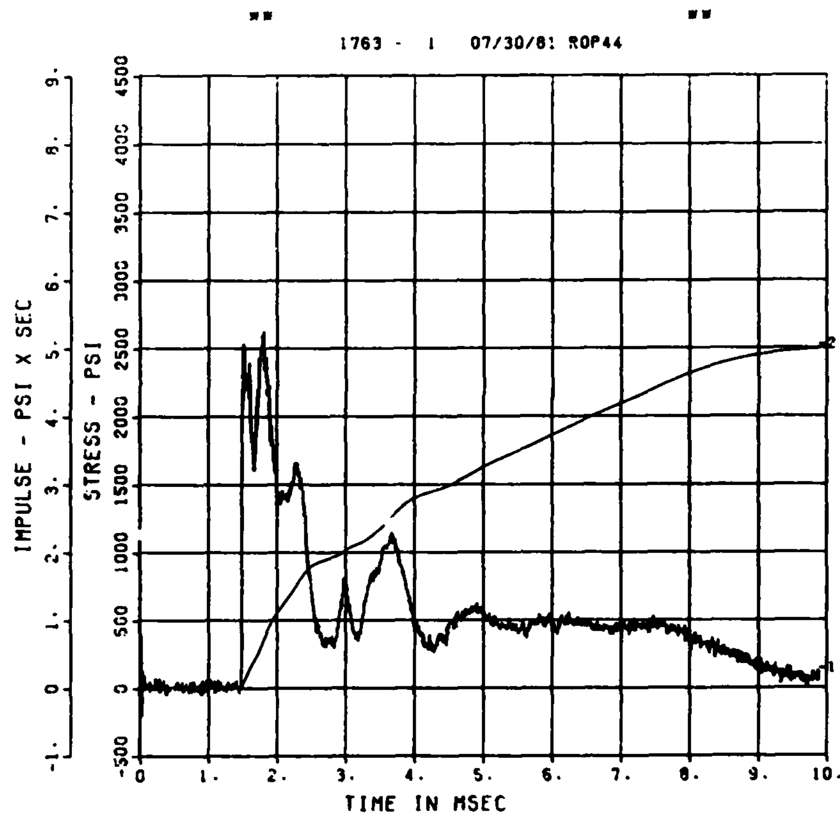

DYNAMIC SHEAR 3
IF2
200000. HZ CAL= 6542.

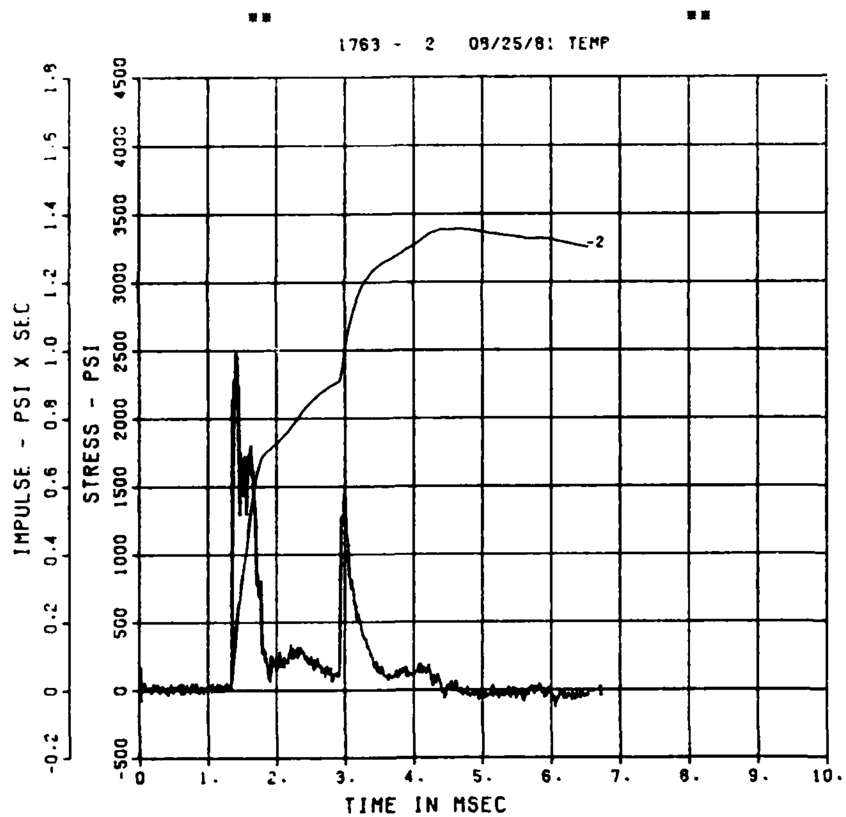

DYNAMIC SHEAR 3
IF3
200000. HZ CAL= 4263.

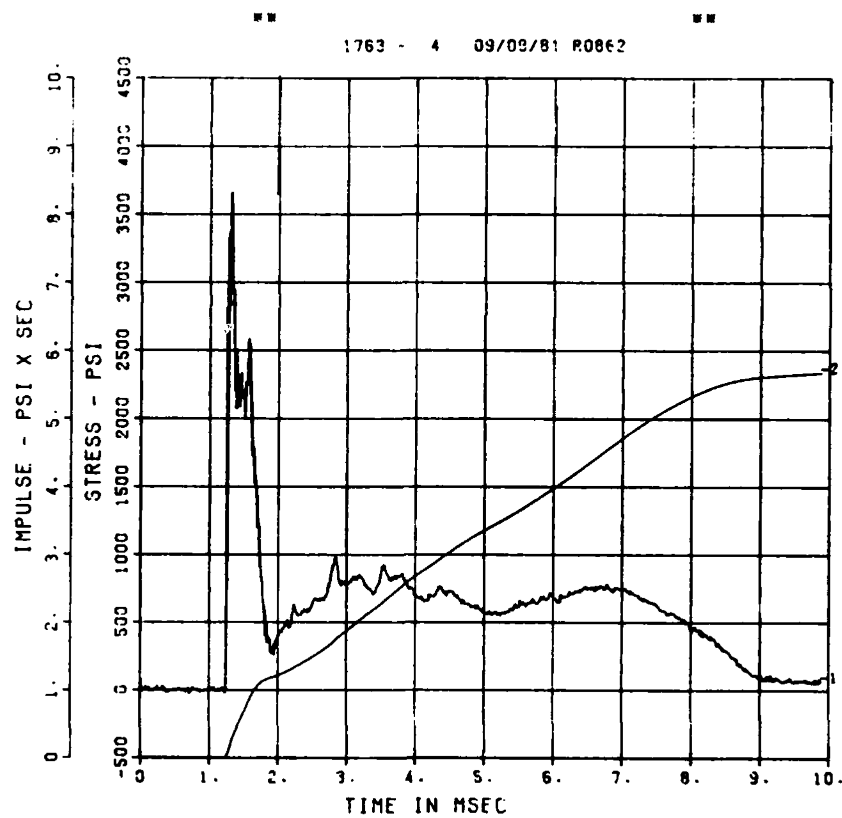

DYNAMIC SHEAR 3
IF4
200000. HZ CAL= 6366.

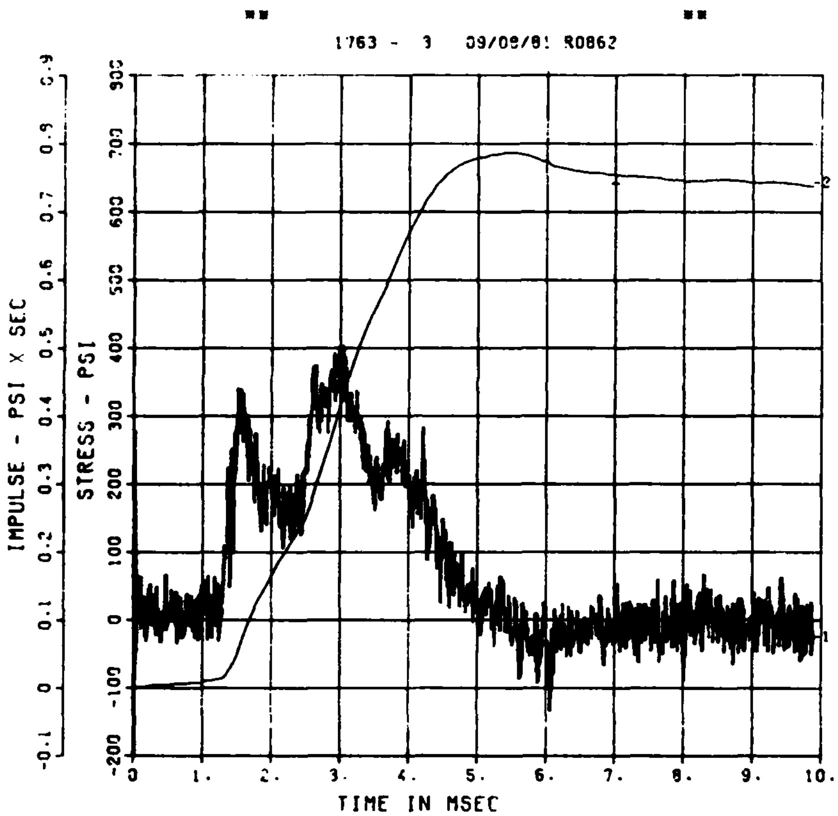

** PEAK VALUE IS 94 % UNDER CALIBRATION **

DYNAMIC SHEAR 3
A1
200000. HZ CAL= 23593.

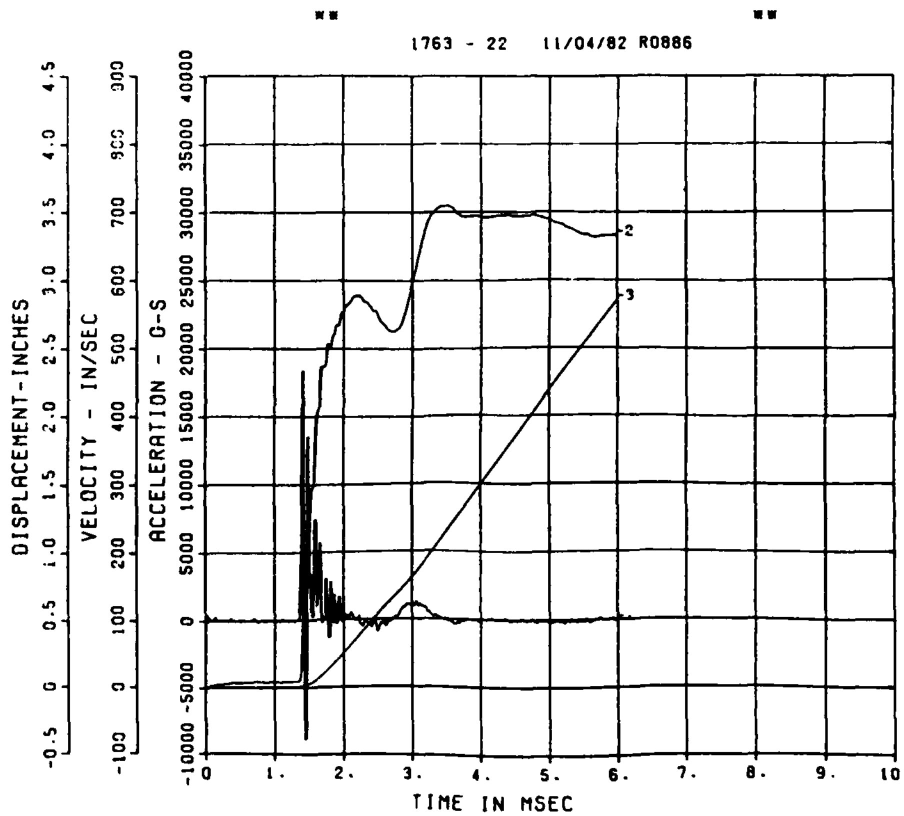

DYNAMIC SHEAR 3
E01
200000. HZ CAL= 11170.

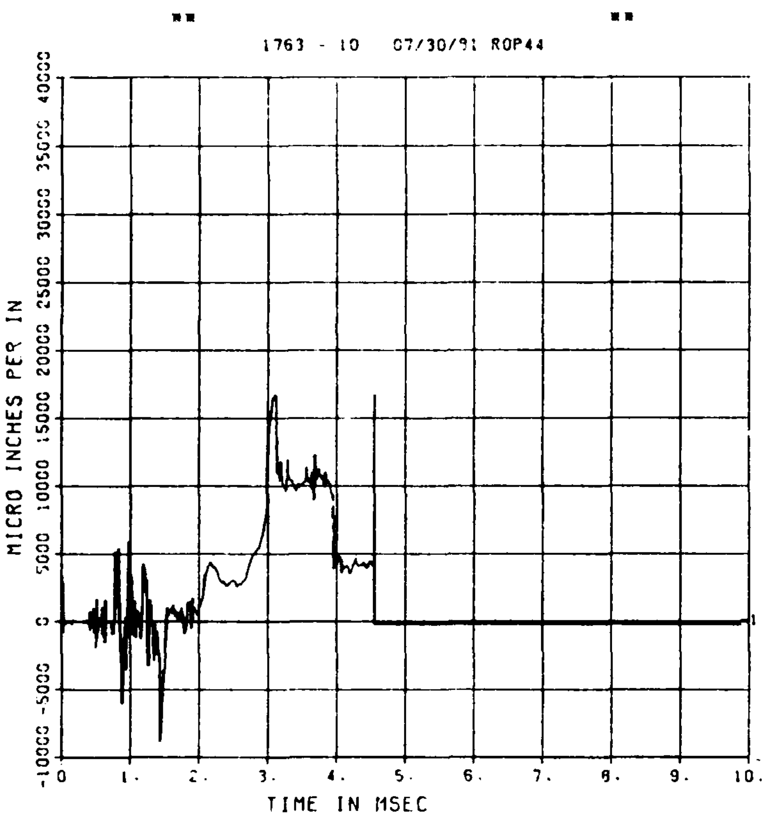

** PEAK VALUE IS 50 % OVER CALIBRATION **

DYNAMIC SHEAR 3
EI1
200000. HZ CAL= 11170.

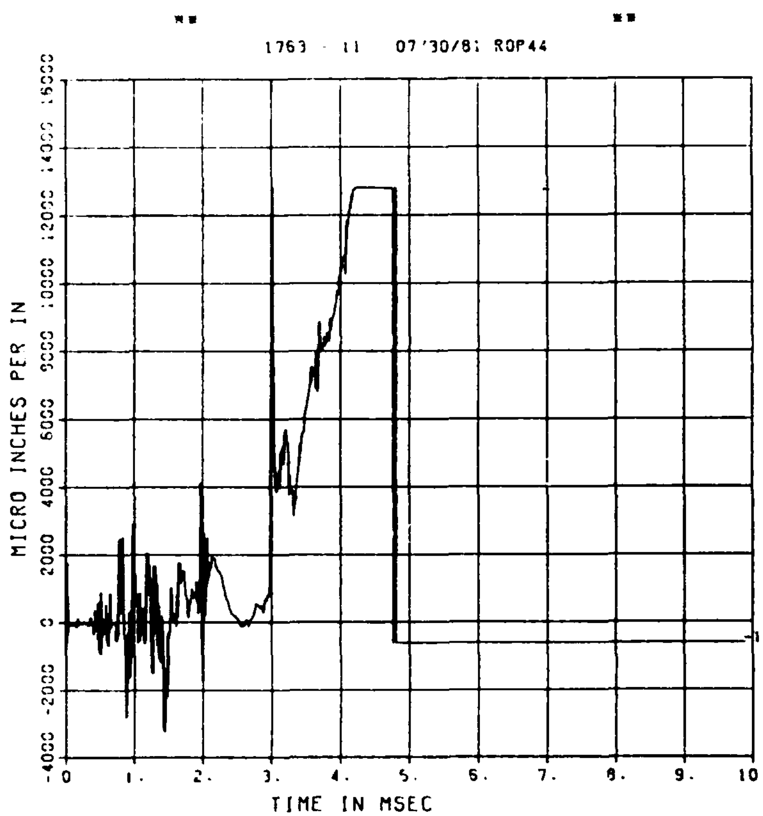

** PEAK VALUE IS 15 % OVER CALIBRATION **

DYNAMIC SHEAR 3
E02
200000. HZ CAL= 11170.
LP4/0 70% CUTOFF= 9000. HZ

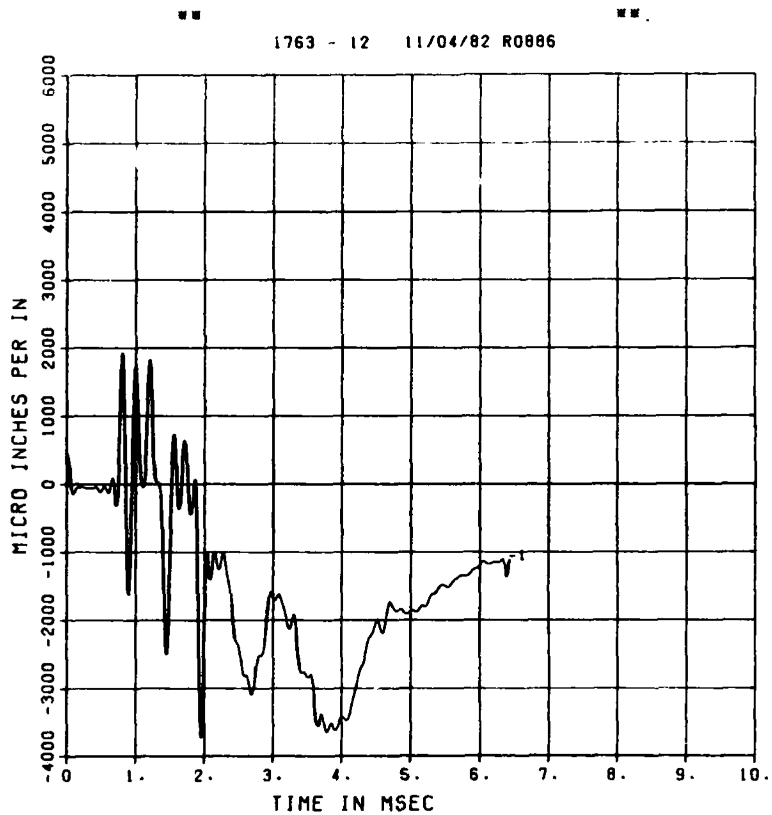

DYNAMIC SHEAR 3
EI2
200000. HZ CAL= 11170.

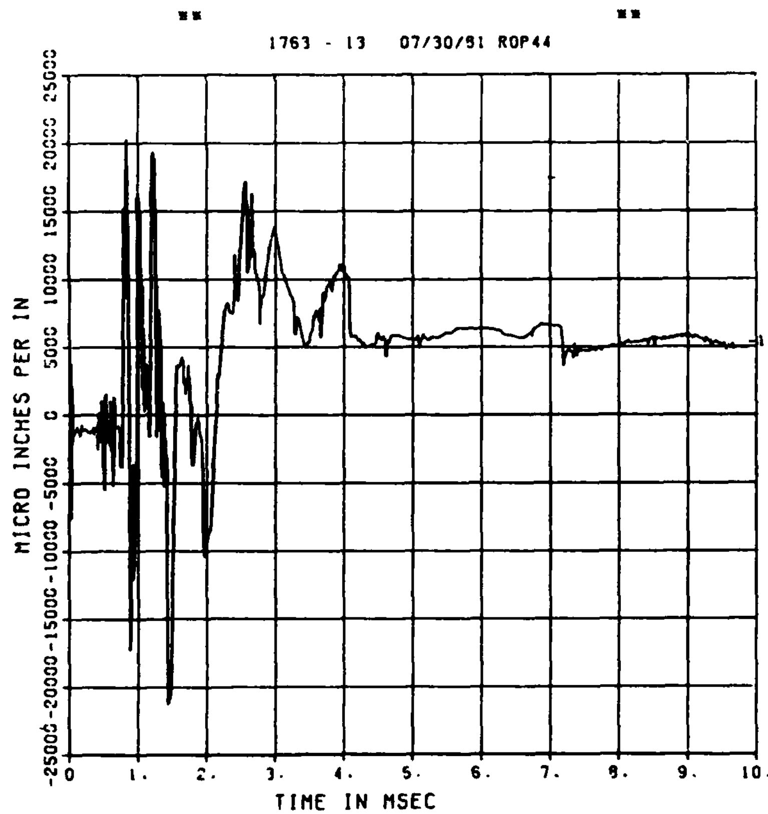

** PEAK VALUE IS 90 % OVER CALIBRATION **

DYNAMIC SHEAR 3
E03
200000. HZ CAL= 11170.
LP4/0 70% CUTOFF= 9000. HZ

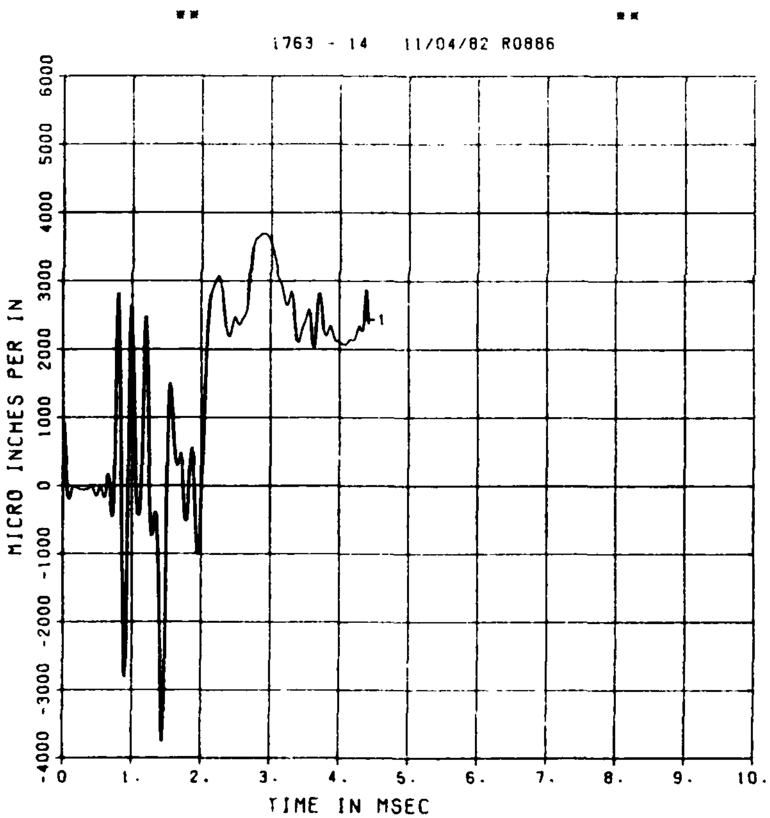

DYNAMIC SHEAR 3
EI3
200000. HZ CAL= 11170.
LP4/0 70% CUTOFF= 9000. HZ

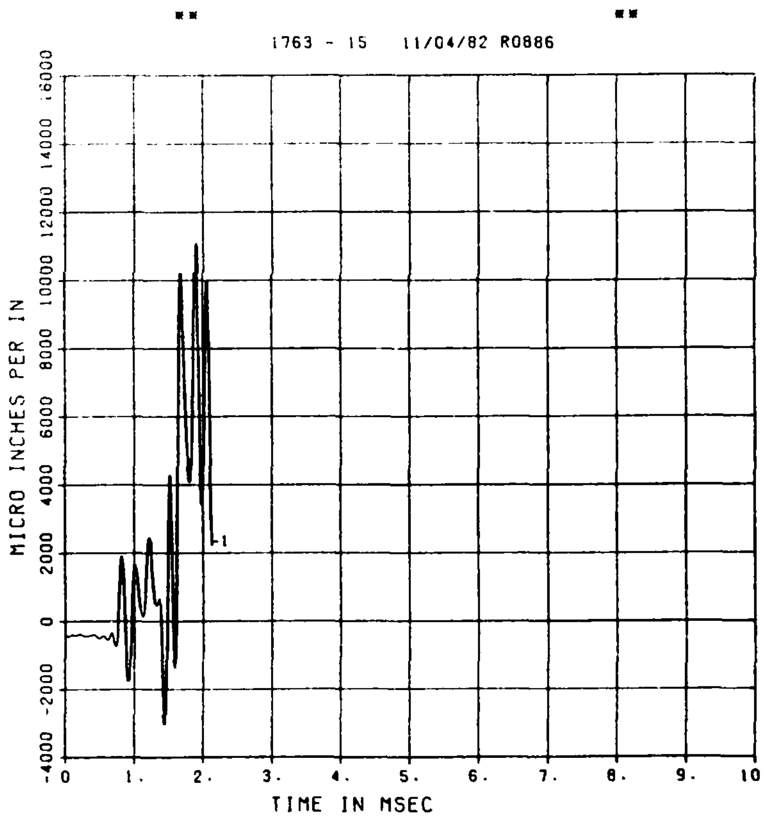

DYNAMIC SHEAR 3
E04
200000. HZ CAL= 11170.

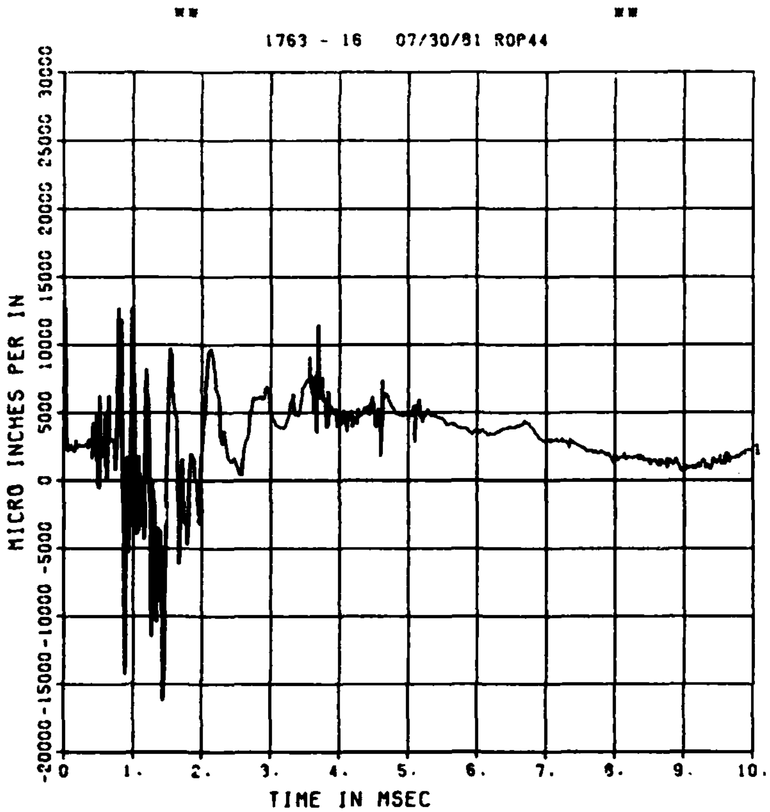

DYNAMIC SHEAR 3
EI4
200000. HZ CAL= 11170.

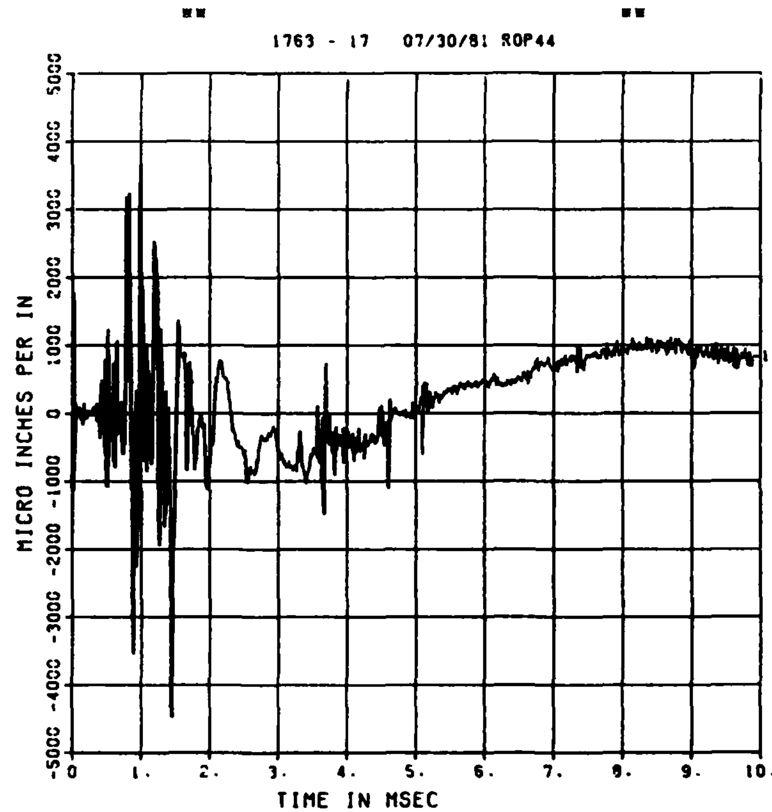

** PEAK VALUE IS 46 % OVER CALIBRATION **

DYNAMIC SHEAR 3
E05
200000. HZ CAL= 42490.

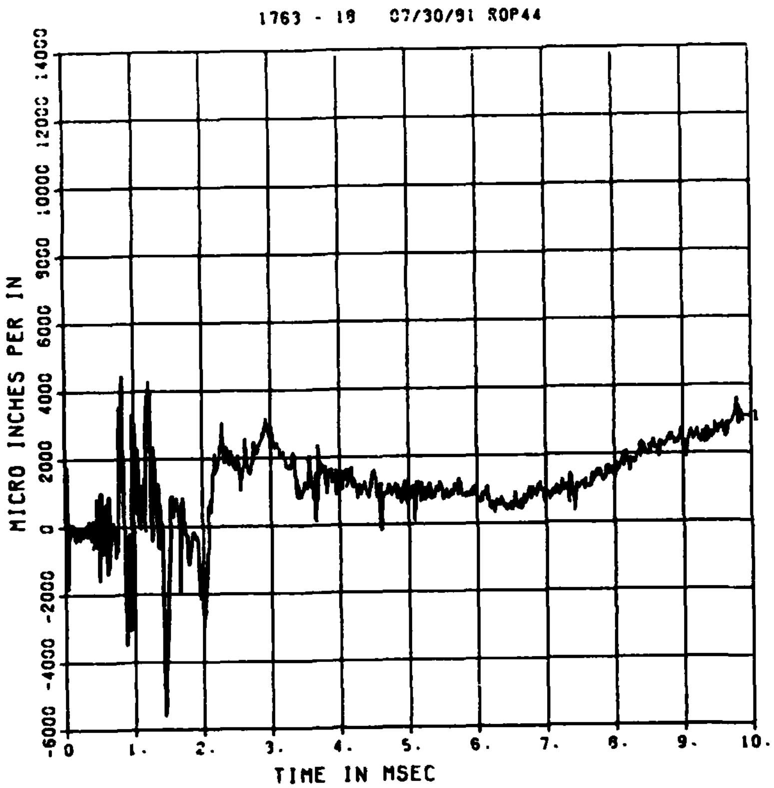

** PEAK VALUE IS 87 % UNDER CALIBRATION **

DYNAMIC SHEAR 3
E15
200000. HZ CAL= 42490.

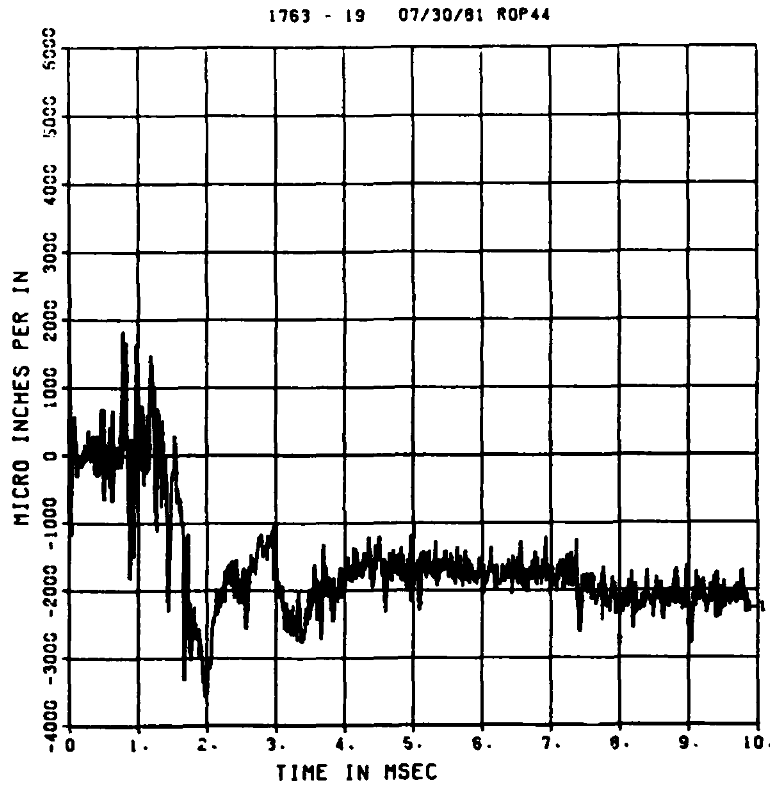

** PEAK VALUE IS 92 % UNDER CALIBRATION **

DYNAMIC SHEAR 3
E06
200000. HZ CAL= 42490.

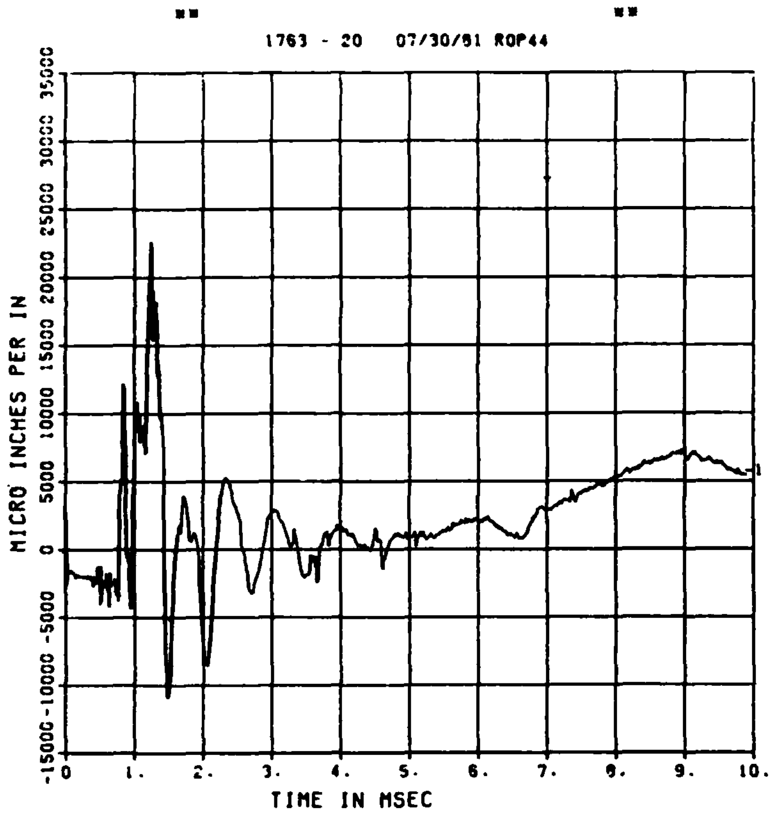

DYNAMIC SHEAR 3
EI6
200000. HZ CAL= 42490.

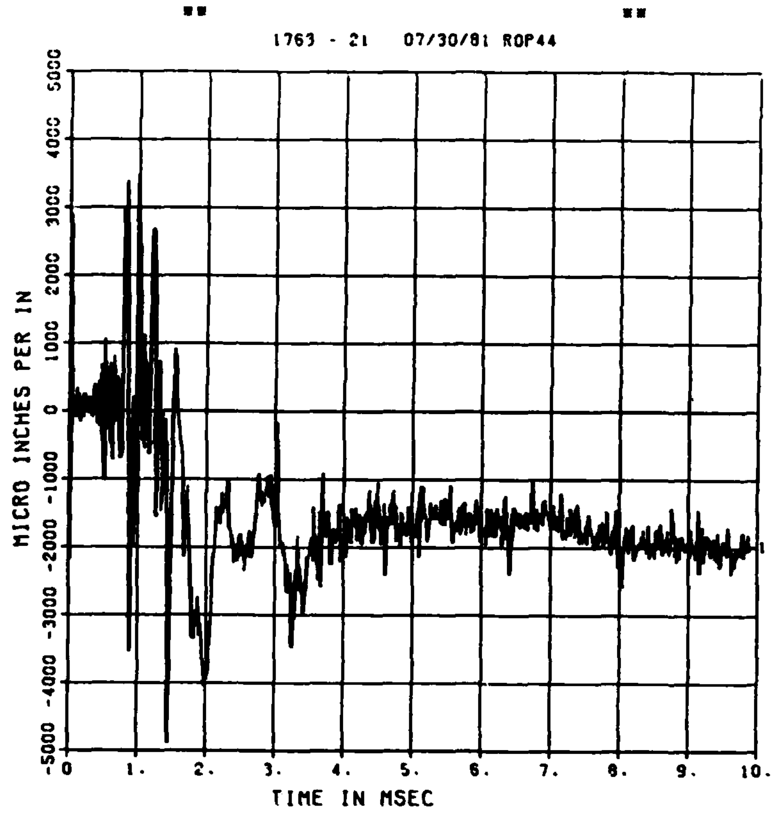

** PEAK VALUE IS 88 % UNDER CALIBRATION **

DYNAMIC SHEAR 4
BP1
200000. HZ CAL= 10795.

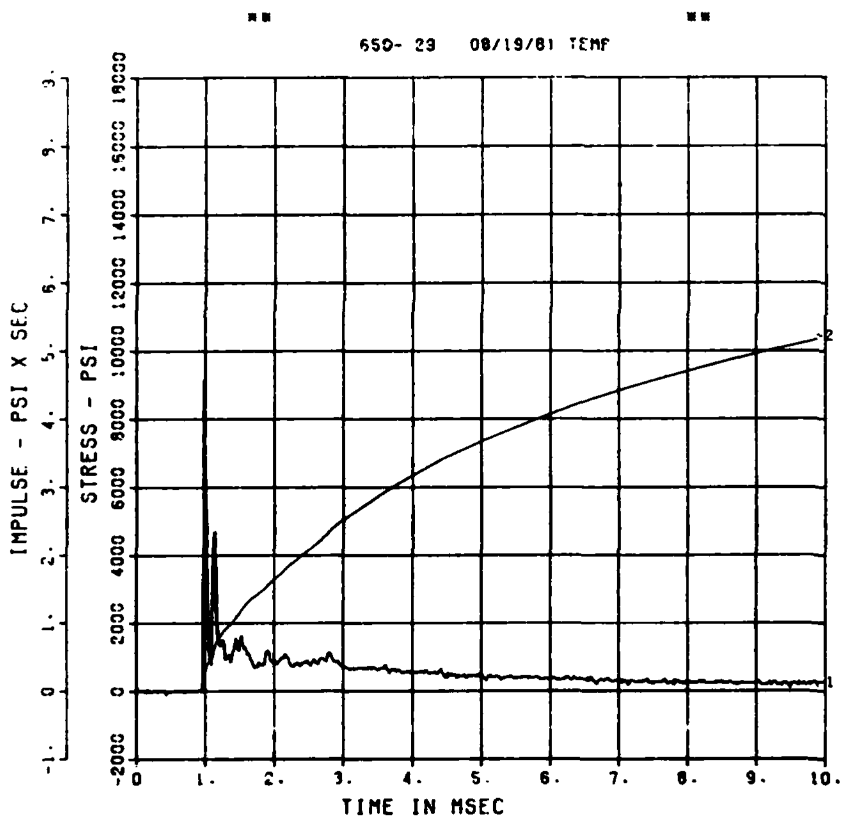

DYNAMIC SHEAR 4
BP1
200000. HZ CAL= 10795.

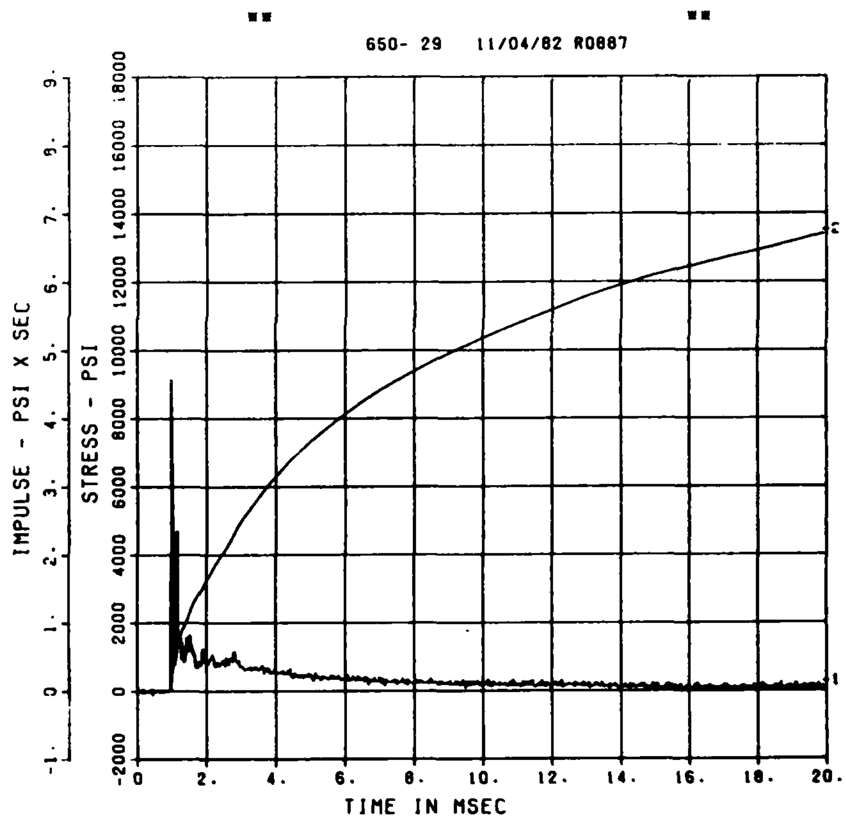

DYNAMIC SHEAR 4
BP2
200000. HZ CAL= 9603.

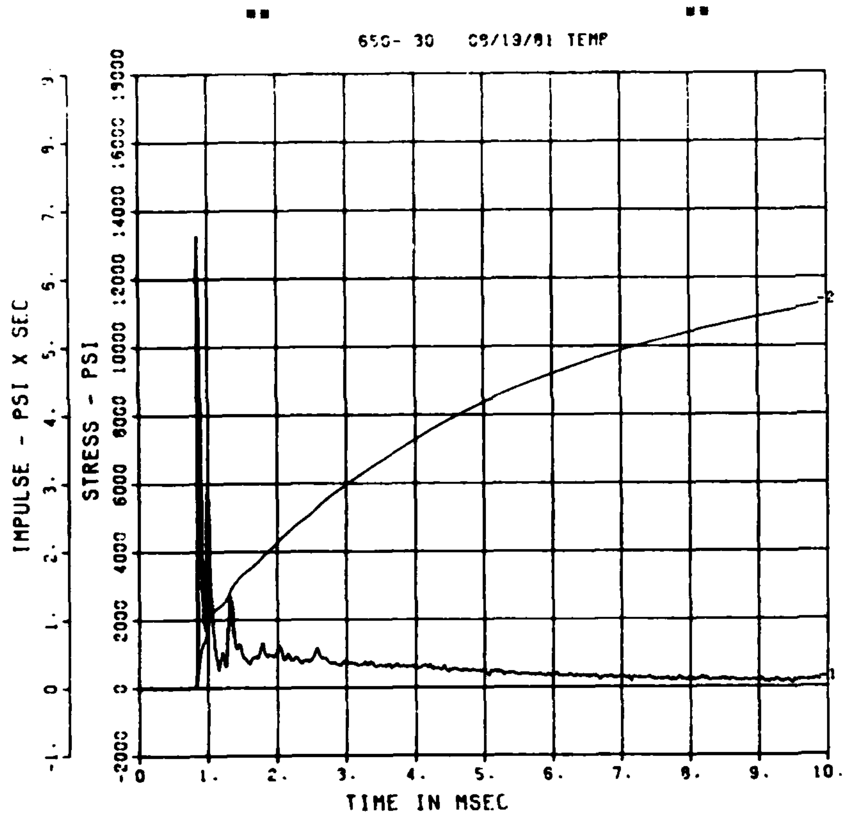

** PEAK VALUE IS 38 % OVER CALIBRATION **

DYNAMIC SHEAR 4
BP2
200000. HZ CAL= 9603.

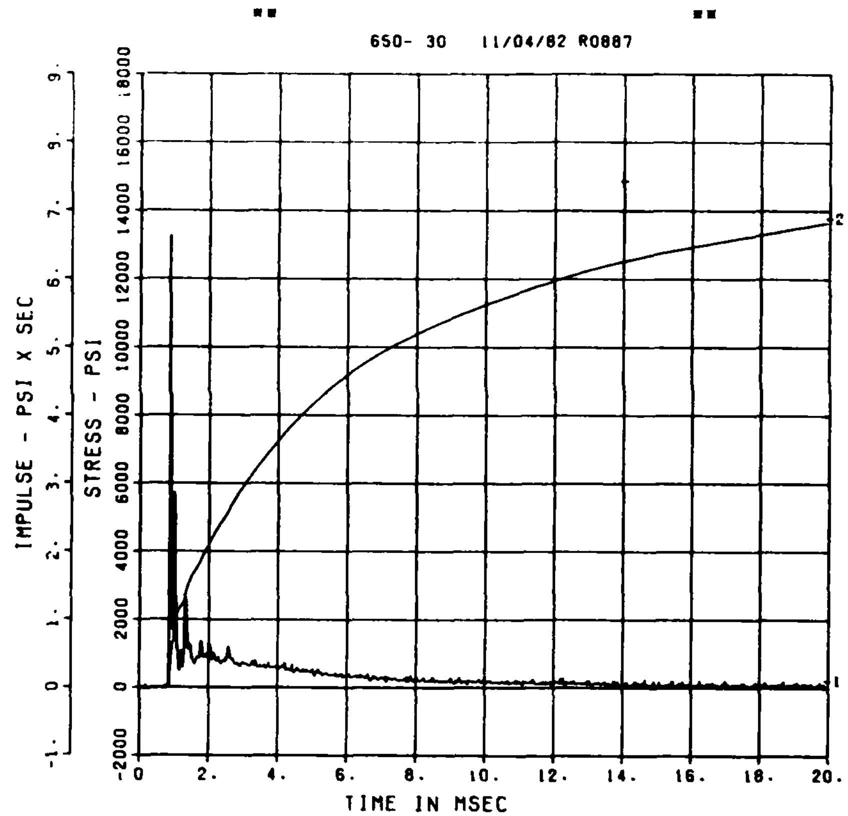

** PEAK VALUE IS 38 % OVER CALIBRATION **

DYNAMIC SHEAR 4
BP4
200000. HZ CAL= 14785.

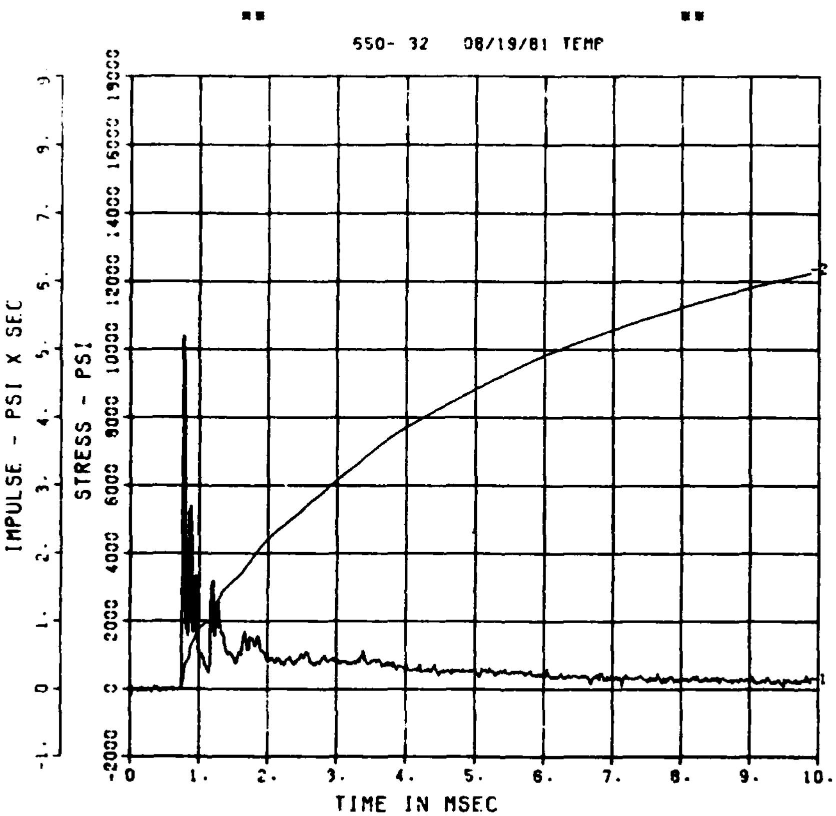

DYNAMIC SHEAR 4
BP4
200000. HZ CAL= 14785.

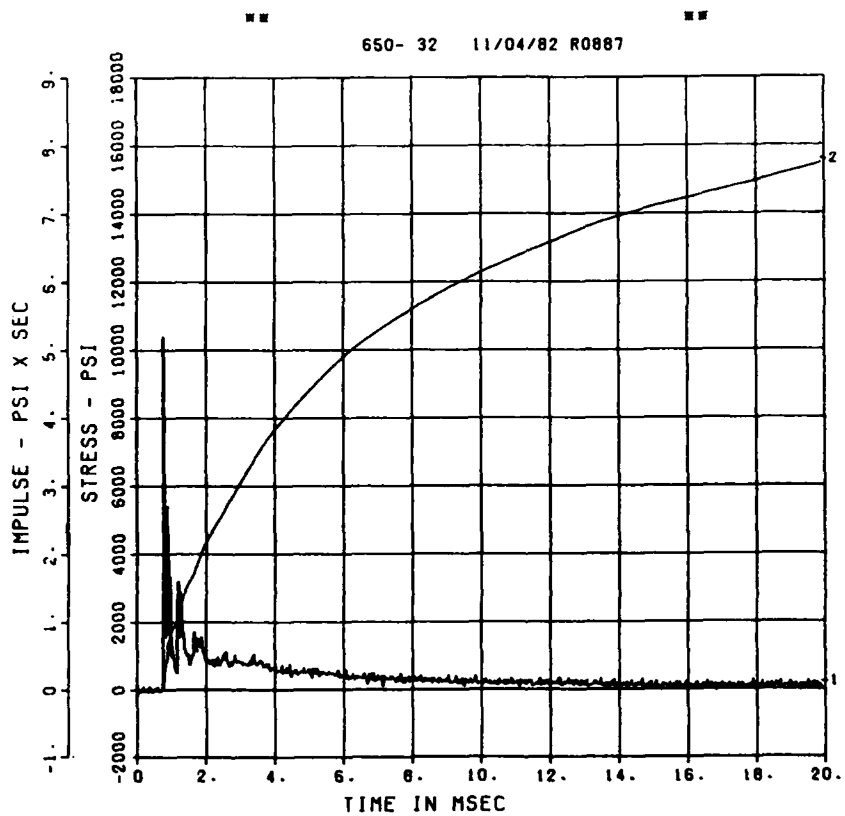

DYNAMIC SHEAR 4
IF1
200000. HZ CAL= 6271.

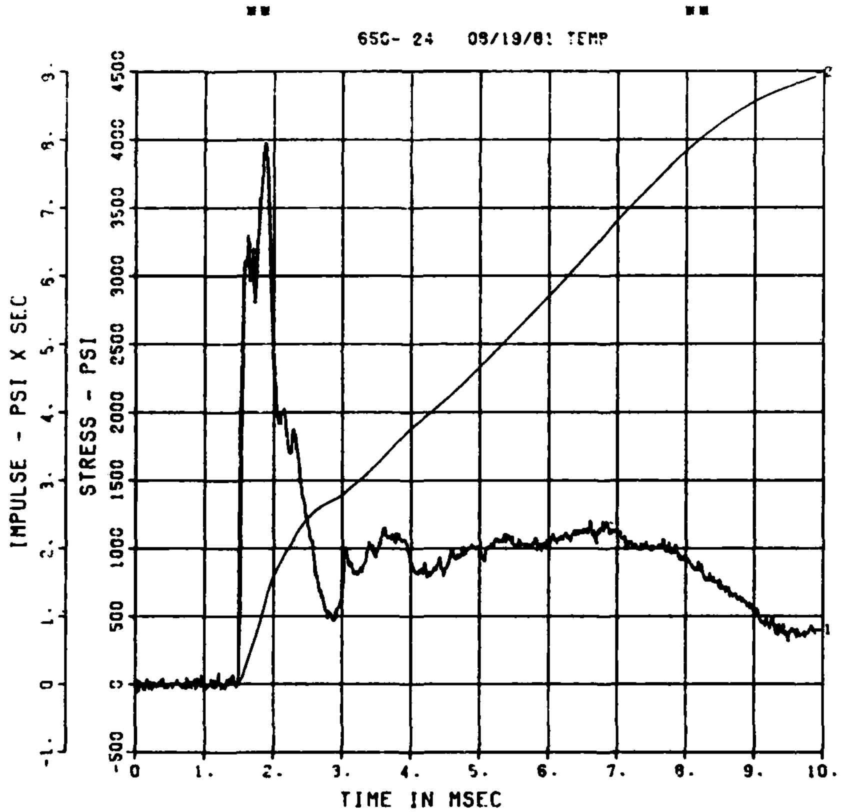

DYNAMIC SHEAR 4
IF2
200000. HZ CAL= 5270.

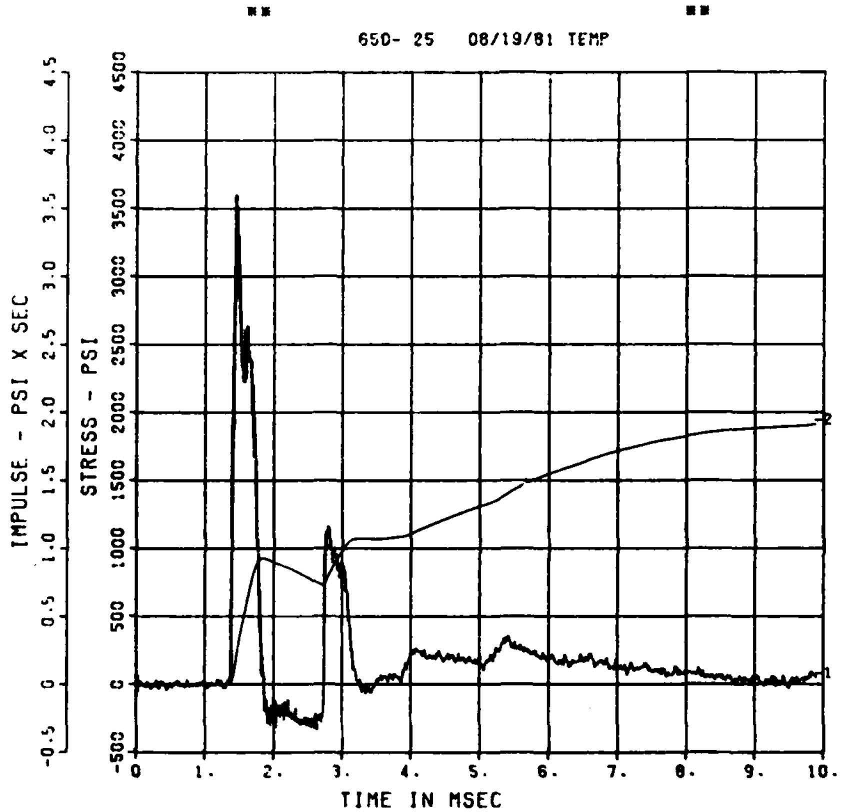

DYNAMIC SHEAR 4
IF3
200000. HZ CAL= 7454.

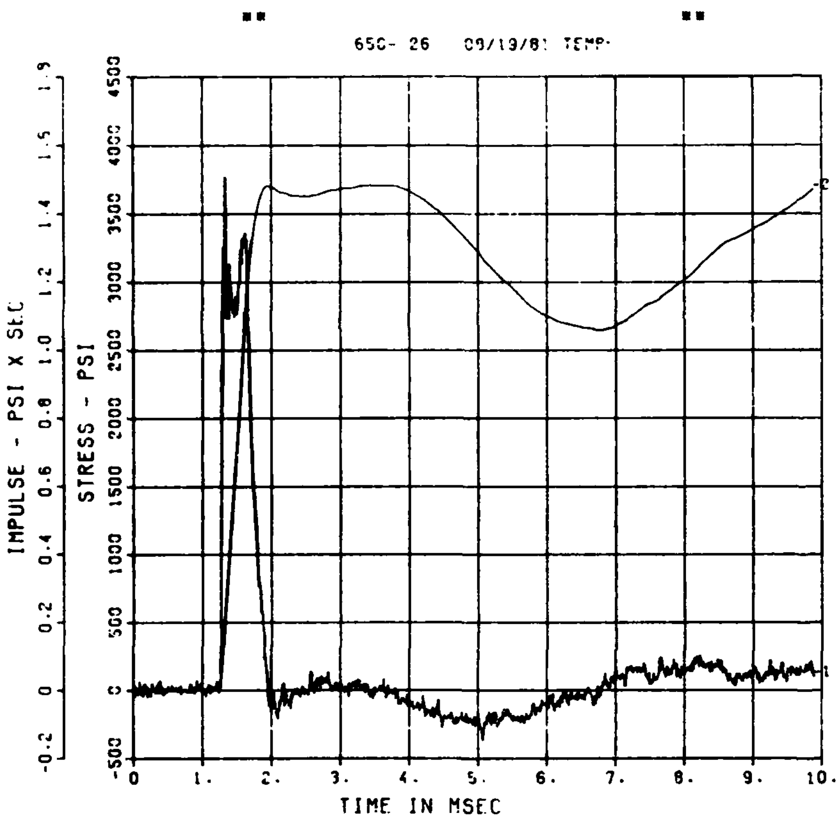

DYNAMIC SHEAR 4
IF4
200000. HZ CAL= 4340.

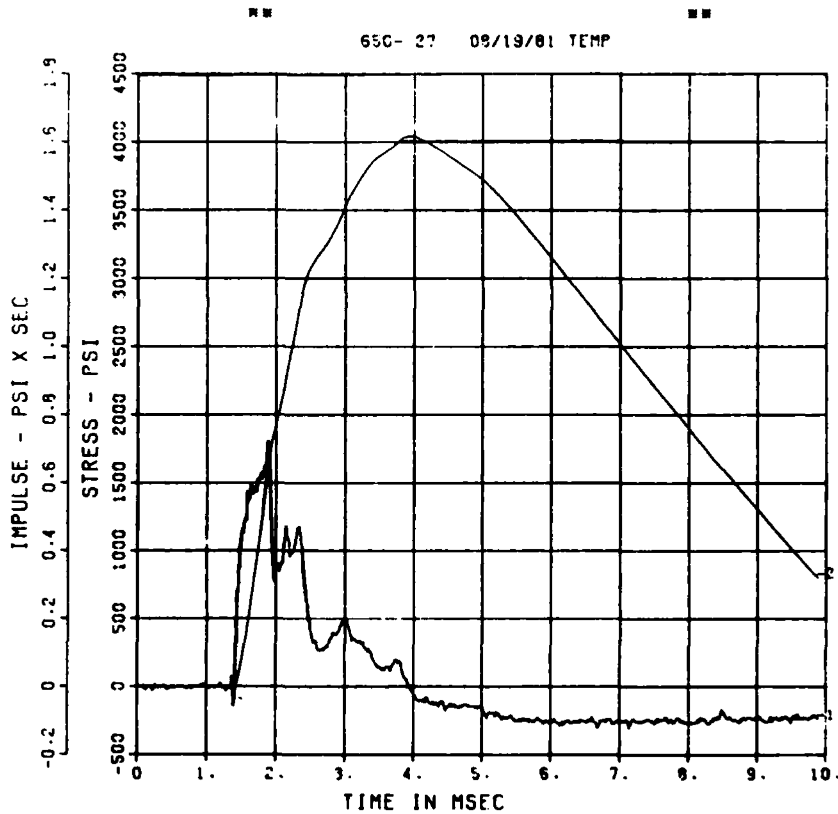

DYNAMIC SHEAR 4
IF5
200000. HZ CAL= 5103.

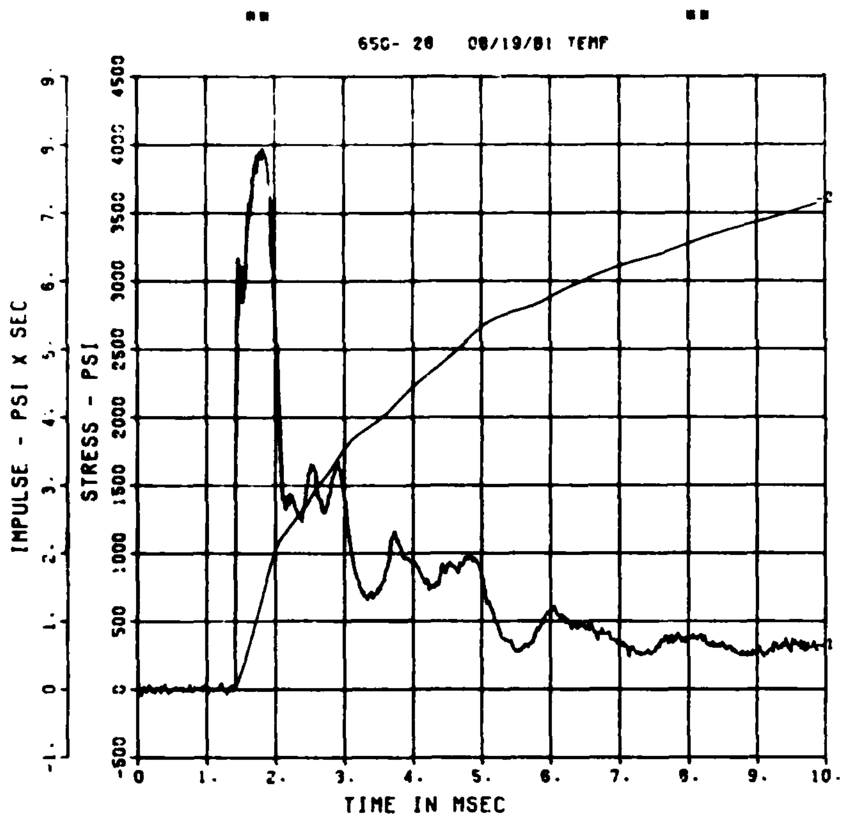

DYNAMIC SHEAR 4
A1
200000. HZ CAL= 23593.

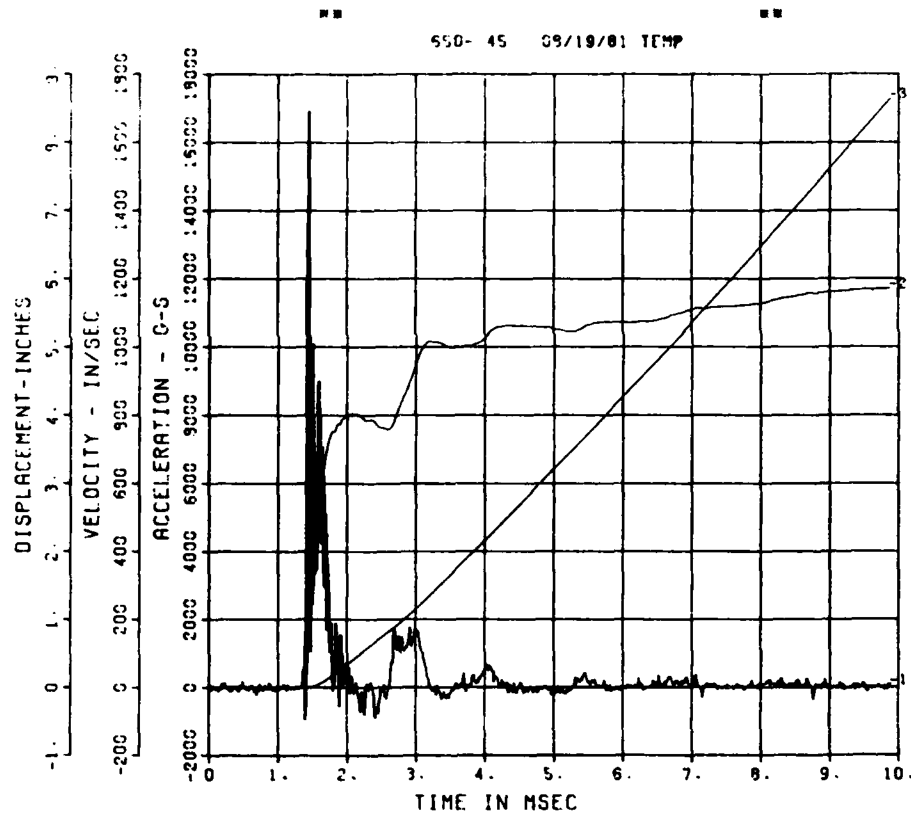

DYNAMIC SHEAR 4
EO1
200000. HZ CAL= 11170.

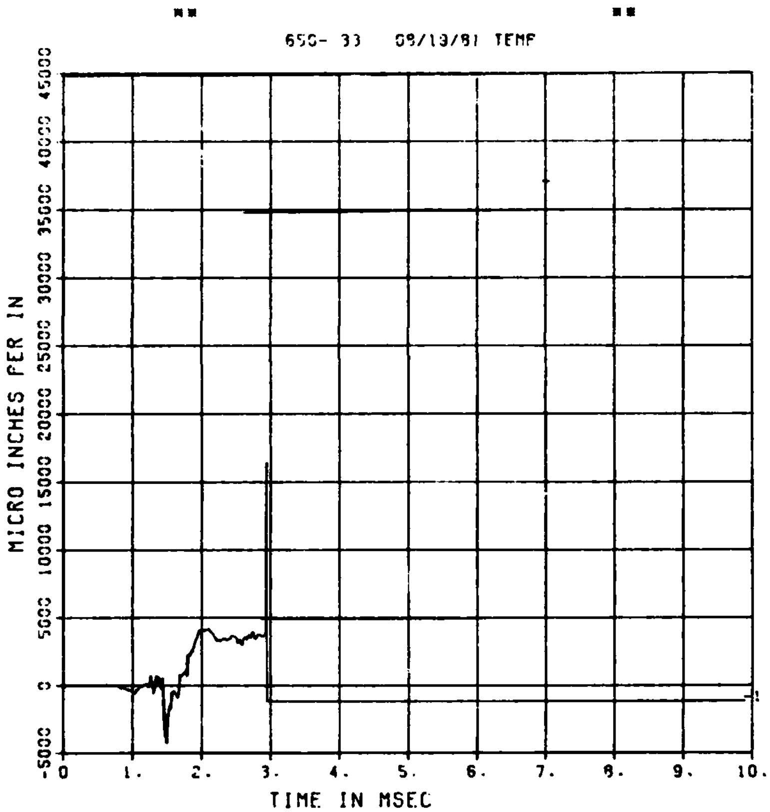

** PEAK VALUE IS 47 7 OVER CALIBRATION **

DYNAMIC SHEAR 4
EI1
200000. HZ CAL= 11170.
LP4/0 70% CUTOFF= 9000. HZ

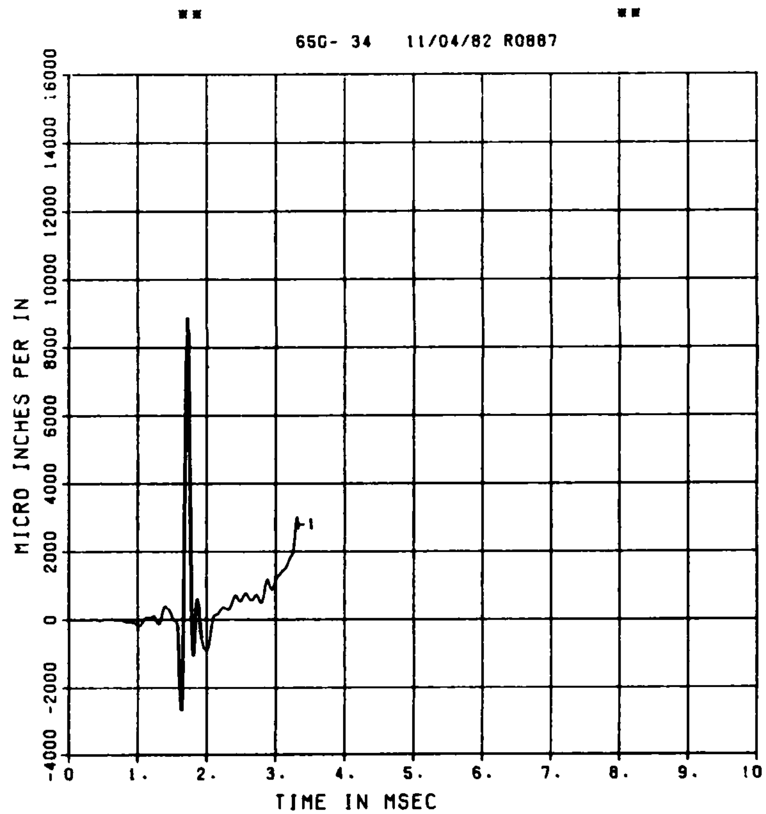

DYNAMIC SHEAR 4
E02
200000. HZ CAL= 11170.
LP4/0 70% CUTOFF= 9000. HZ

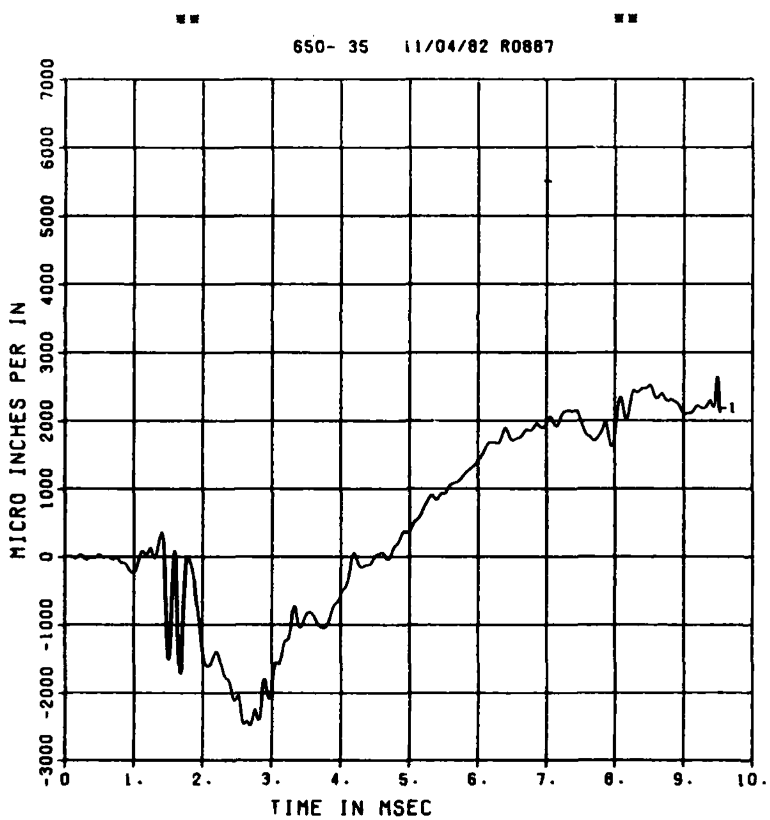

DYNAMIC SHEAR 4
EI2
200000. HZ CAL= 11170.
LP4/0 70% CUTOFF= 9000. HZ

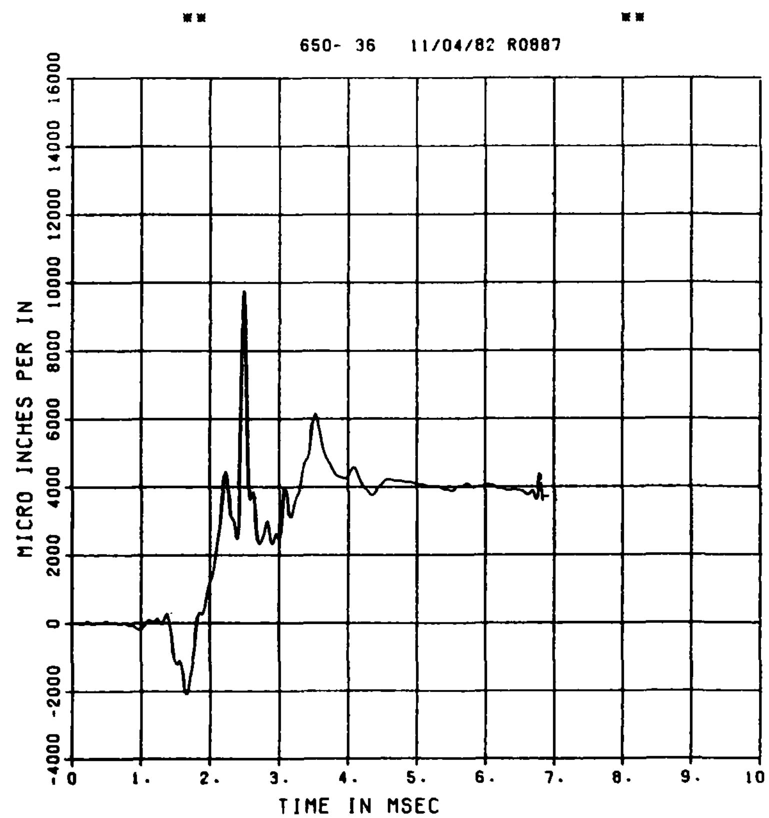

DYNAMIC SHEAR 4
E03
200000. HZ CAL= 11170.
LP4/0 70% CUTOFF= 9000. HZ

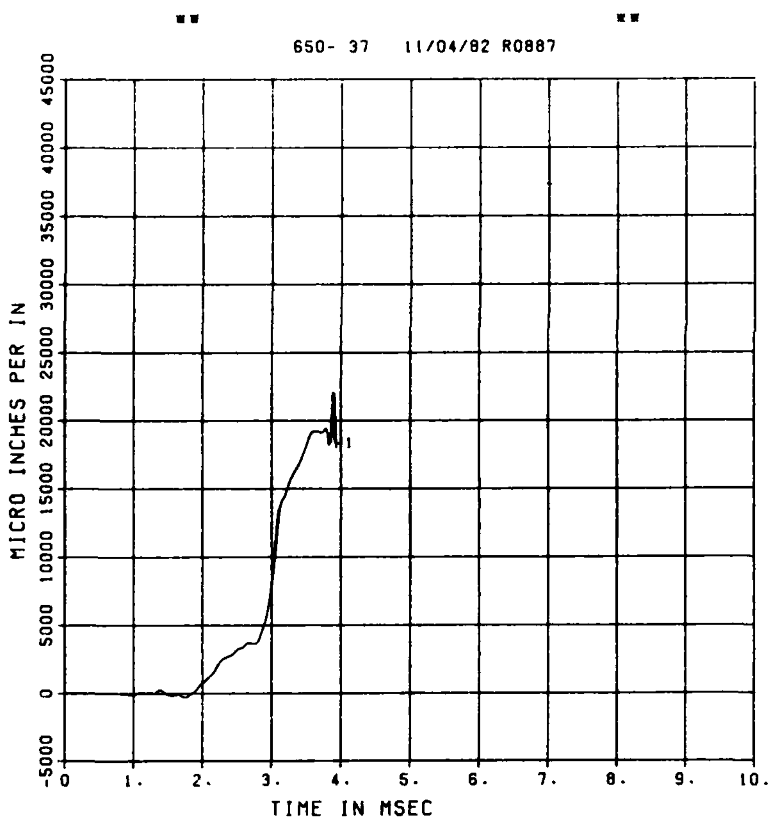

** PEAK VALUE IS 98 % OVER CALIBRATION **

DYNAMIC SHEAR 4
EI3
200000. HZ CAL= 11170.

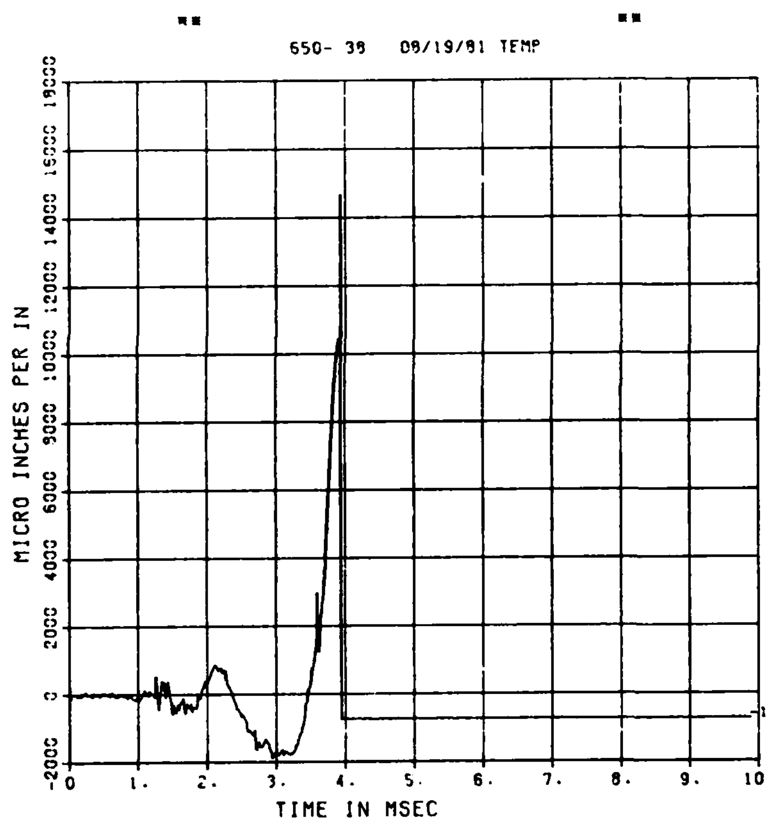

** PEAK VALUE IS 31 % OVER CALIBRATION **

DYNAMIC SHEAR 4
E04
200000. HZ CAL= 11170.
LP4/0 70% CUTOFF= 9000. HZ

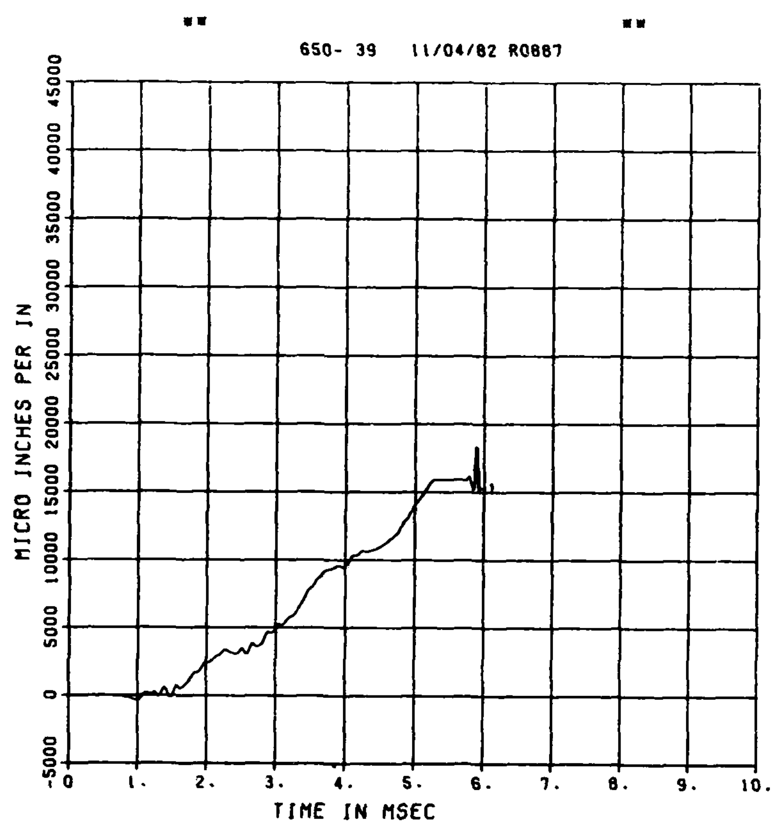

** PEAK VALUE IS 54 % OVER CALIBRATION **

DYNAMIC SHEAR 4
EI4
200000. HZ CAL= 11170.

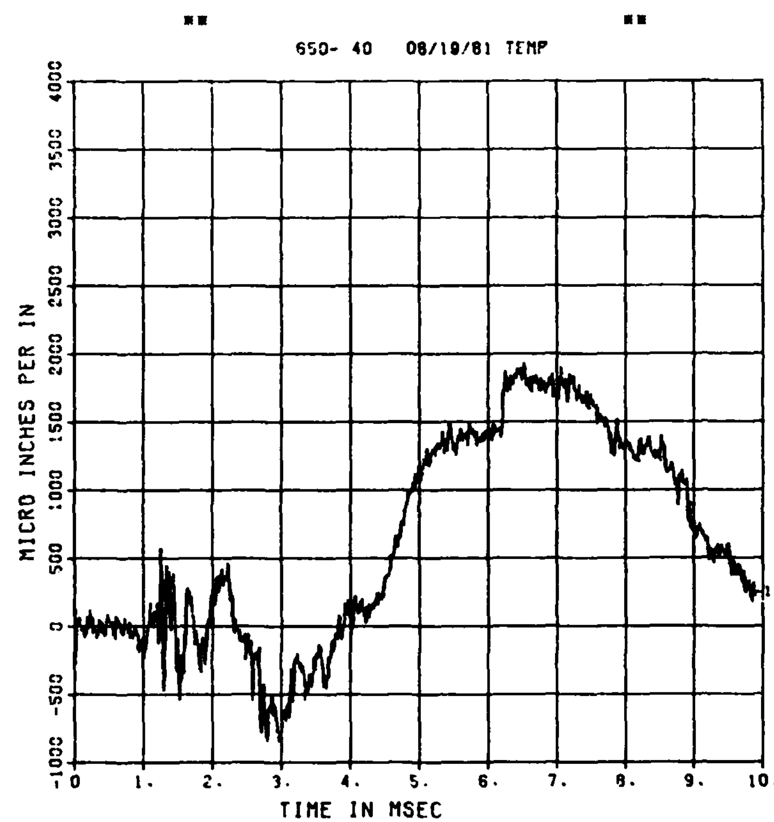

** PEAK VALUE IS 83 % UNDER CALIBRATION **

DYNAMIC SHEAR 4
E05
200000. HZ CAL= 42490.

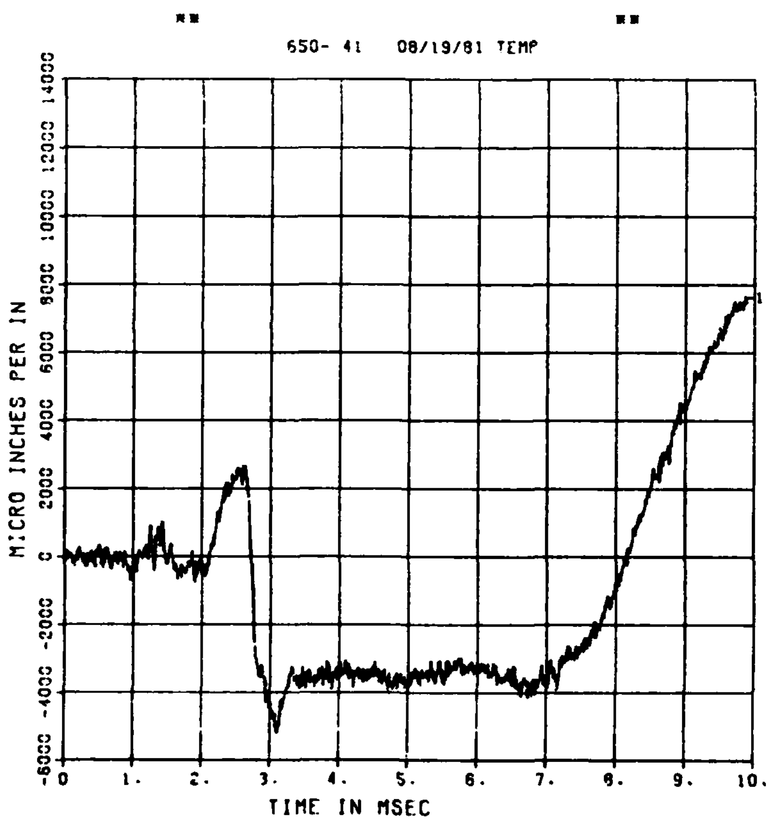

** PEAK VALUE IS 82 % UNDER CALIBRATION **

DYNAMIC SHEAR 4
EI5
200000. HZ CAL= 42490.

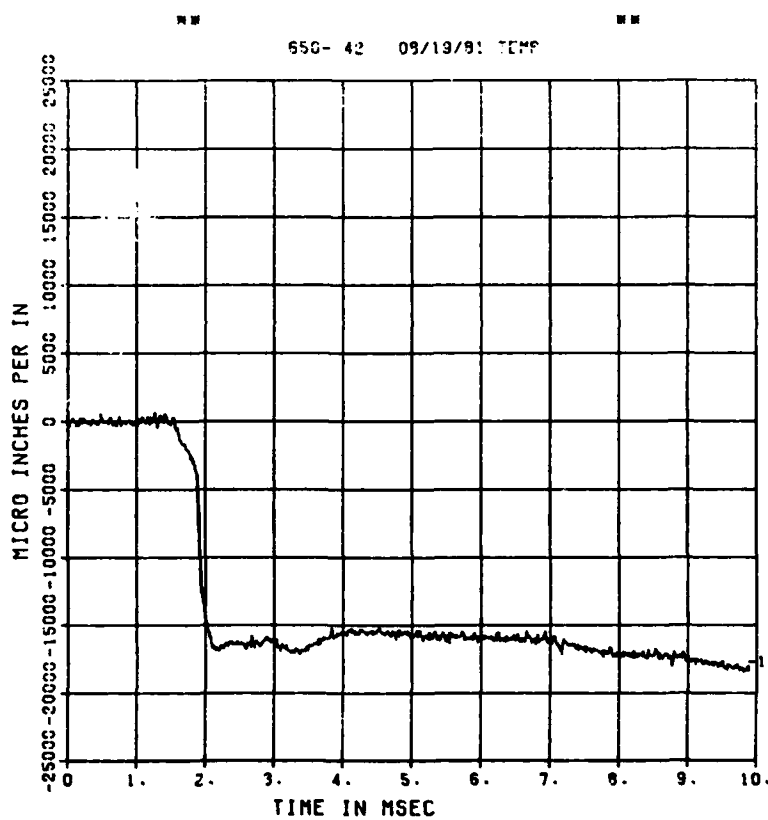

DYNAMIC SHEAR 5
BP2
200000. HZ CAL= 18577.

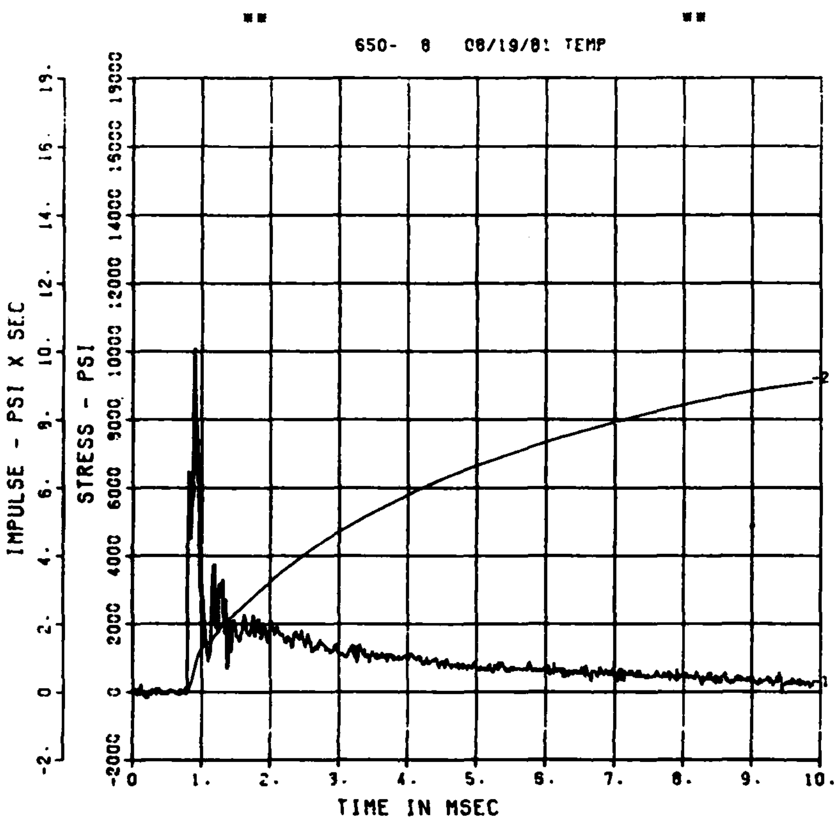

DYNAMIC SHEAR 5
BP2
200000. HZ CAL= 18577.

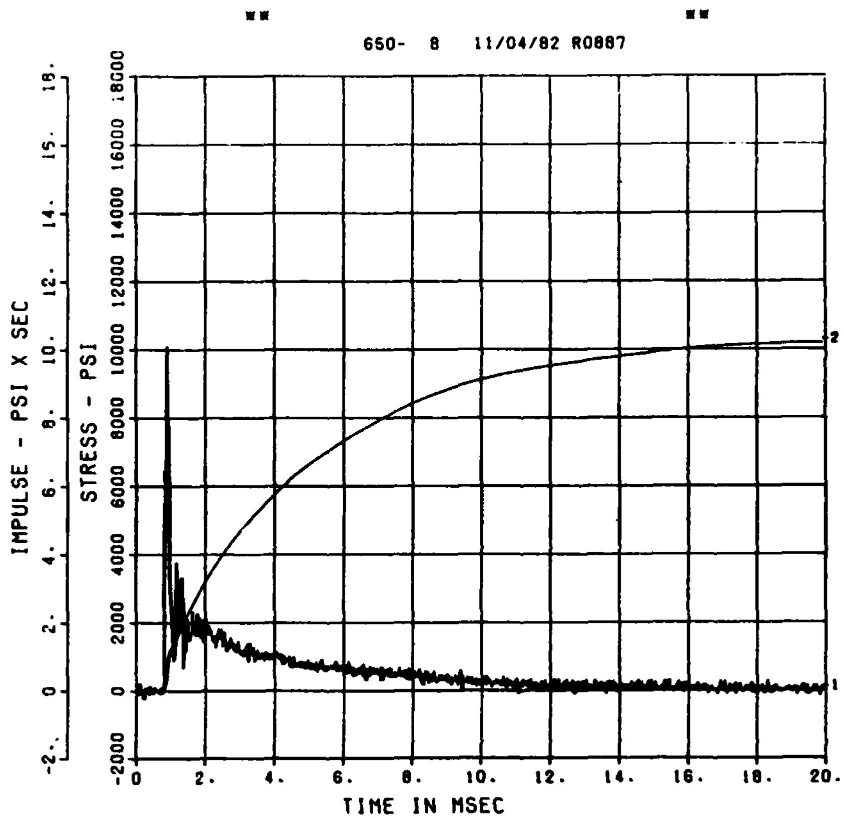

DYNAMIC SHEAR 5
BP3
200000. HZ CAL= 18768.

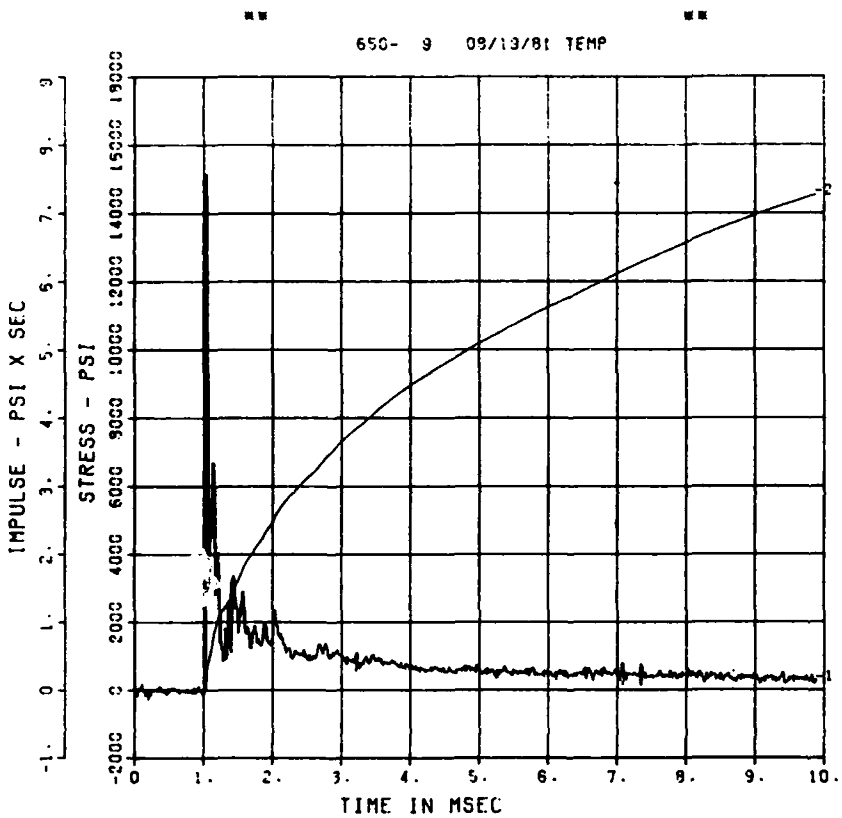

DYNAMIC SHEAR 5
BP3
200000. HZ CAL= 18768.

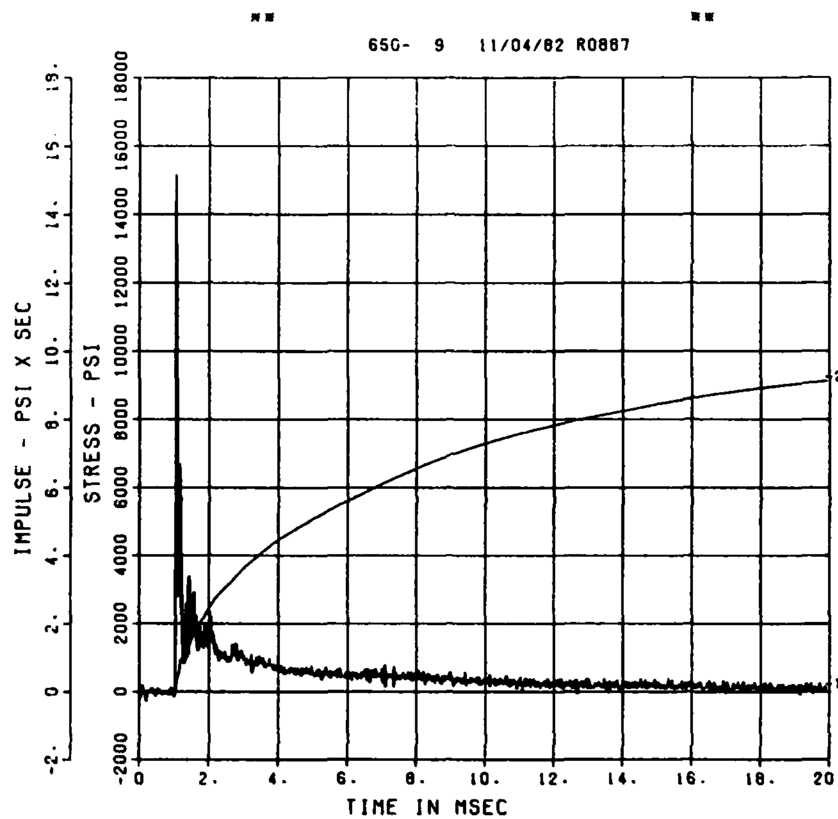

DYNAMIC SHEAR 5
IF1
200000. HZ CAL= 12056.

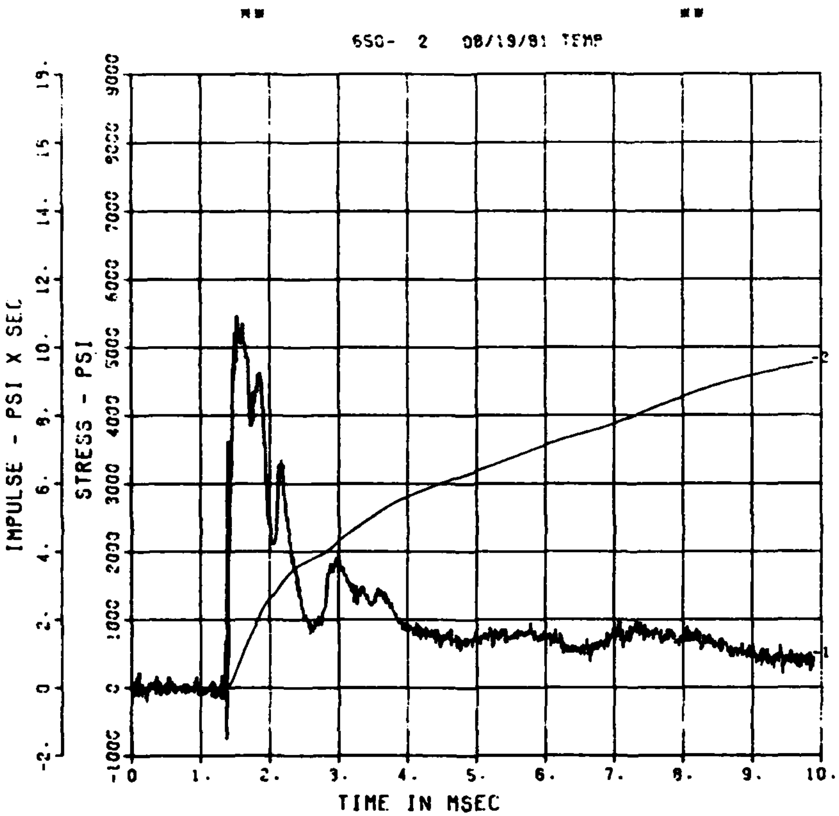

DYNAMIC SHEAR 5
IF2
200000. HZ CAL= 10951.

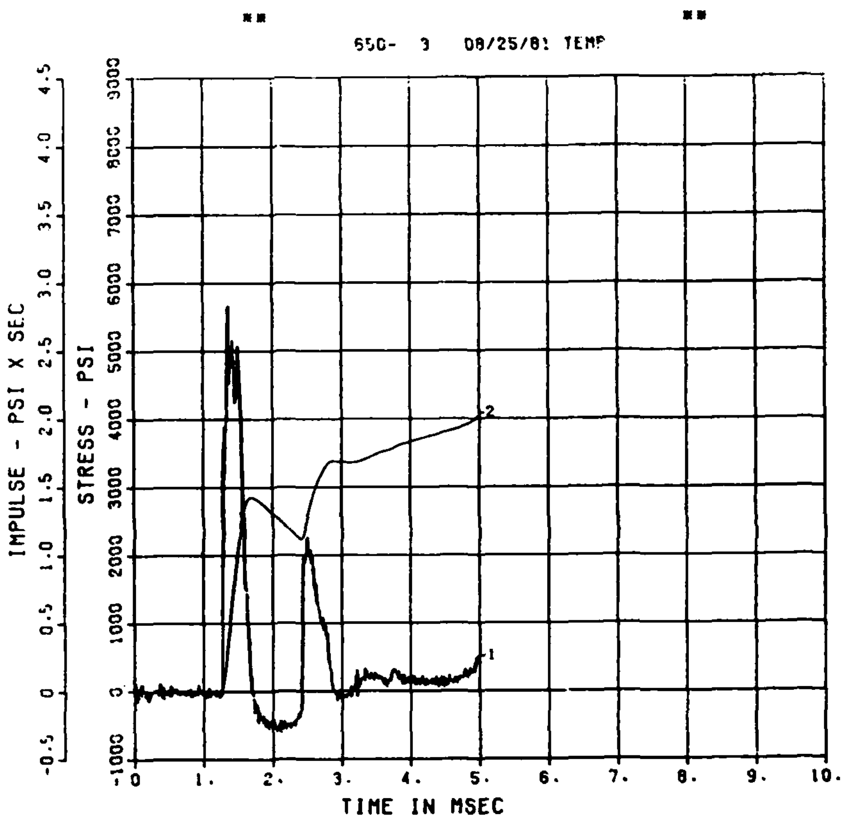

DYNAMIC SHEAR 5
IF3
200000. HZ CAL= 10468.

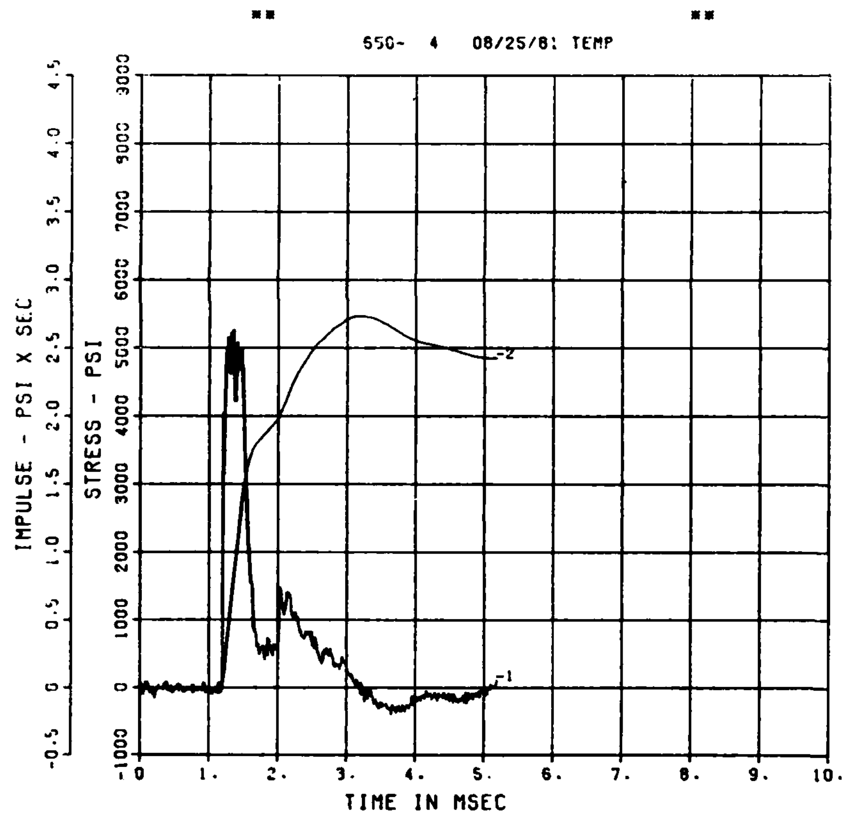

DYNAMIC SHEAR 5
IF4
200000. HZ CAL= 10587.

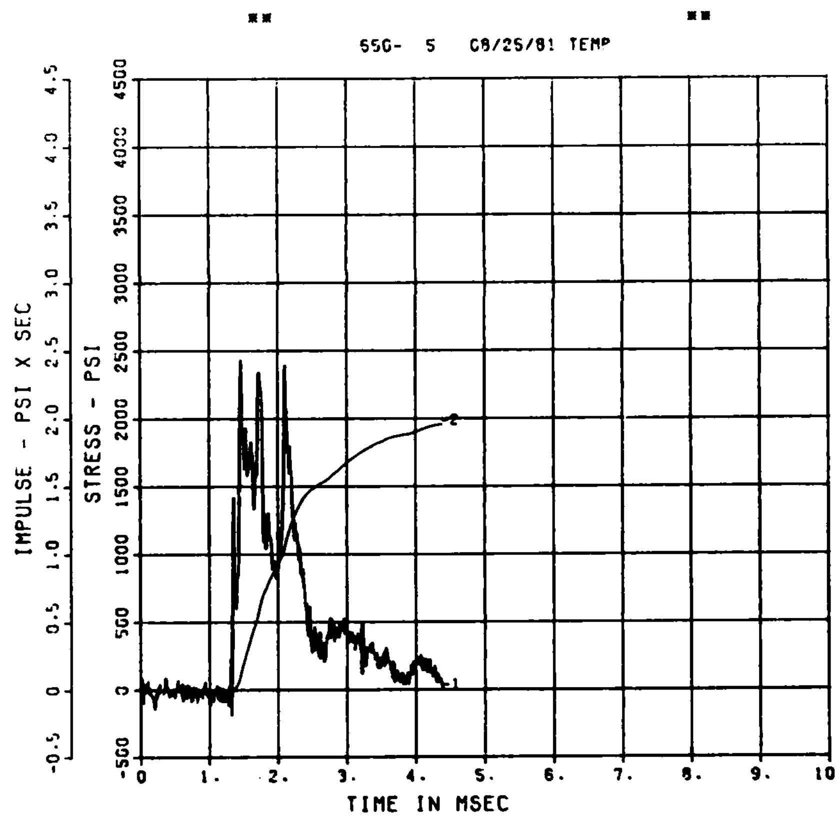

DYNAMIC SHEAR 5
IF5
200000. HZ CAL= 10605.

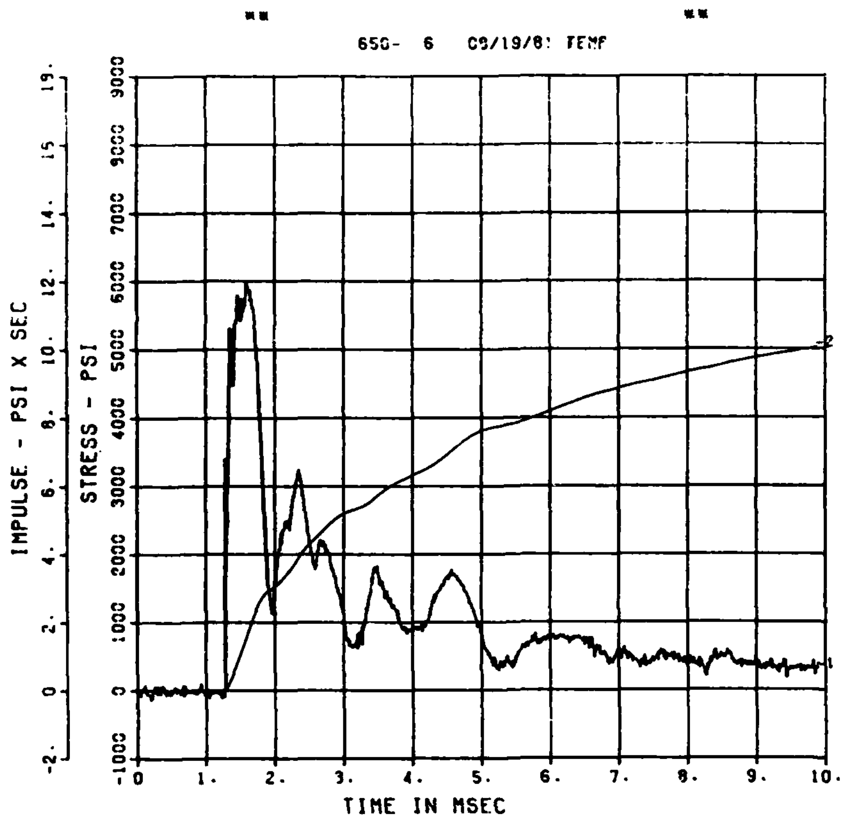

DYNAMIC SHEAR 5
A1
200000. HZ CAL= 20490.

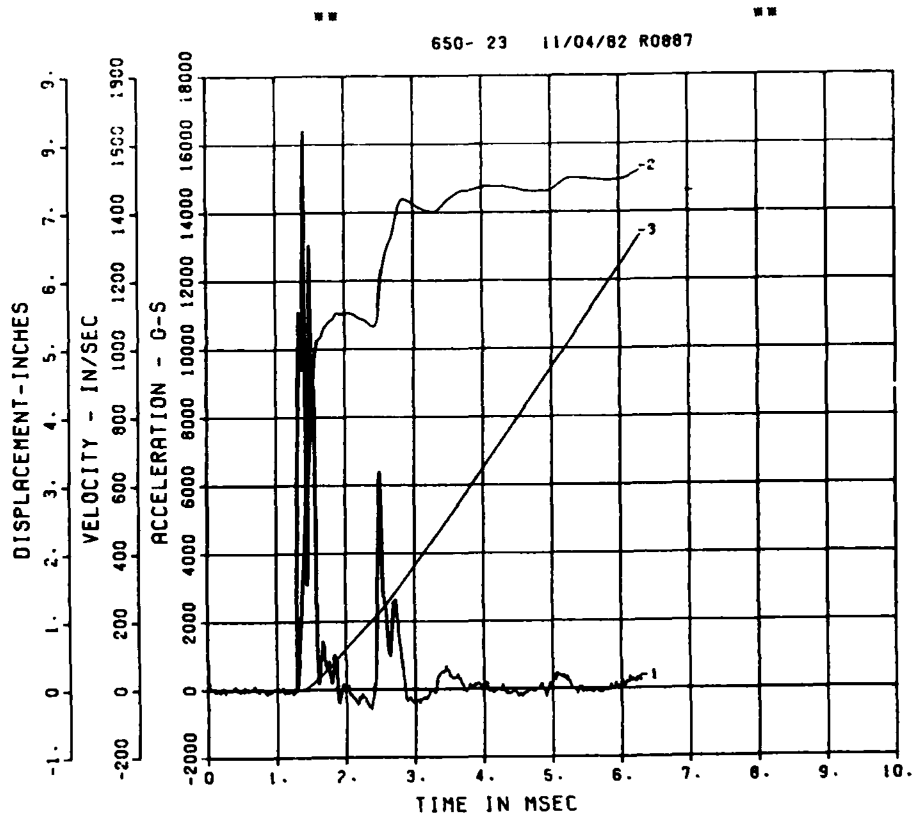

DYNAMIC SHEAR 5
E01
200000. HZ CAL= 11170.
LP4/0 70% CUTOFF= 9000. HZ

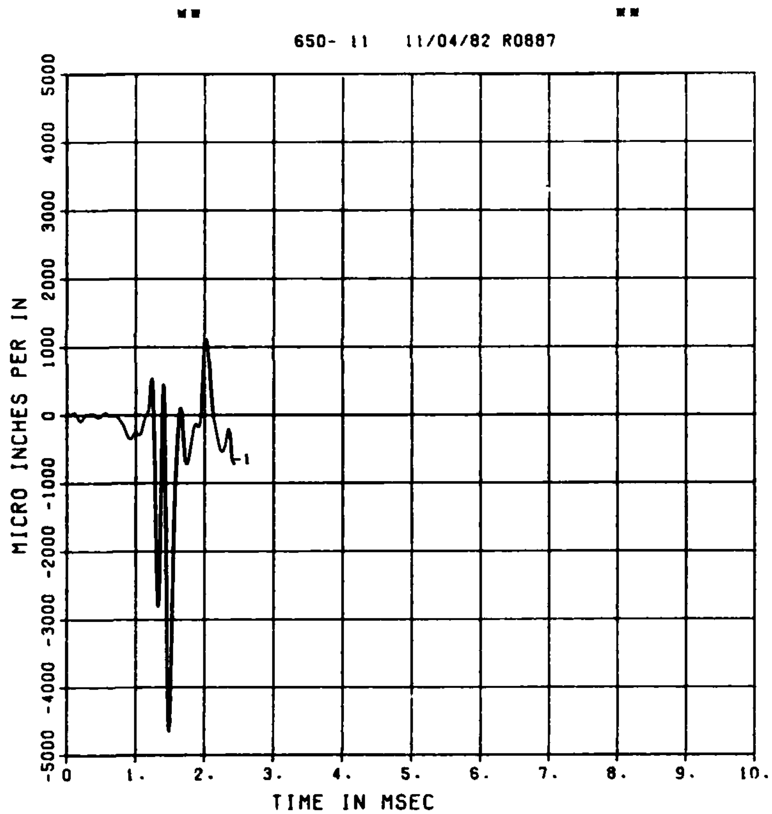

DYNAMIC SHEAR 5
EI1
200000. HZ CAL= 11170.
LP4/0 70% CUTOFF= 9000. HZ

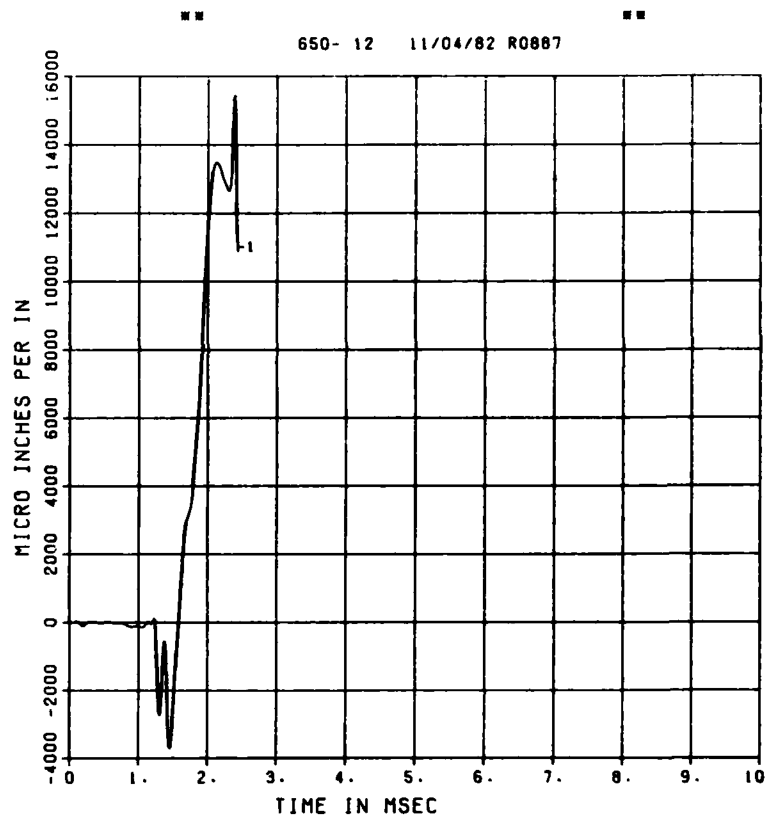

** PEAK VALUE IS 38 % OVER CALIBRATION **

DYNAMIC SHEAR 5
E02
200000. HZ CAL= 11170.

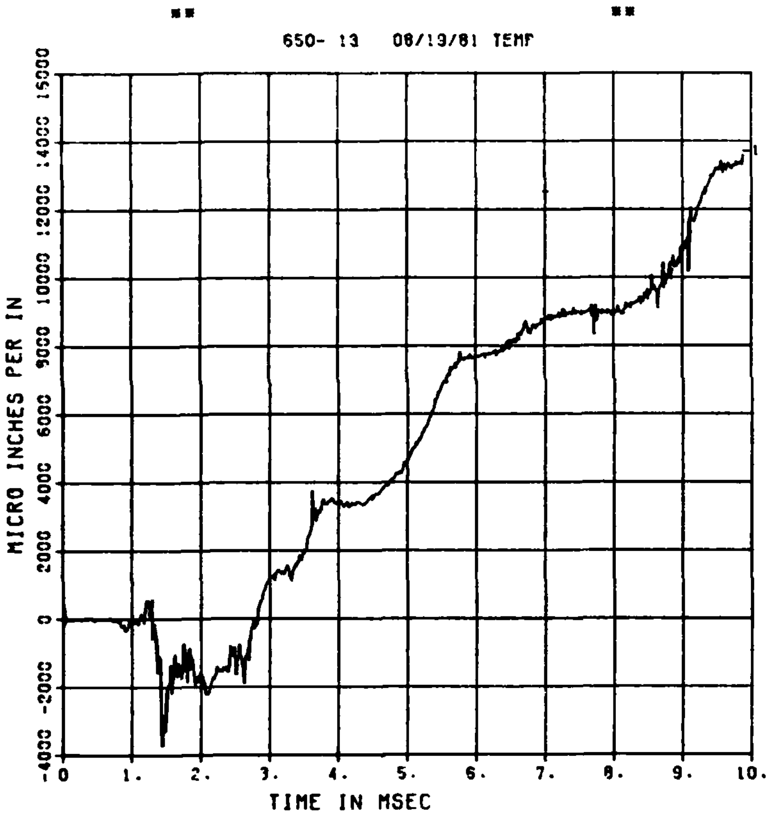

** PEAK VALUE IS 22 % OVER CALIBRATION **

DYNAMIC SHEAR 5
E12
200000. HZ CAL= 11170.

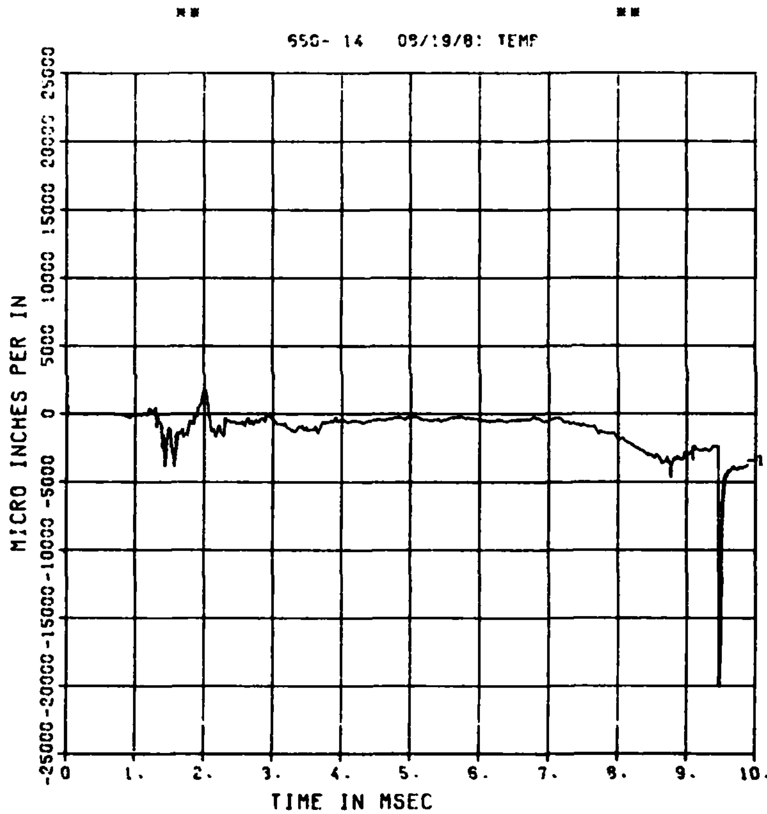

** PEAK VALUE IS 79 % OVER CALIBRATION **

DYNAMIC SHEAR 5
E03
200000. HZ CAL= 11170.

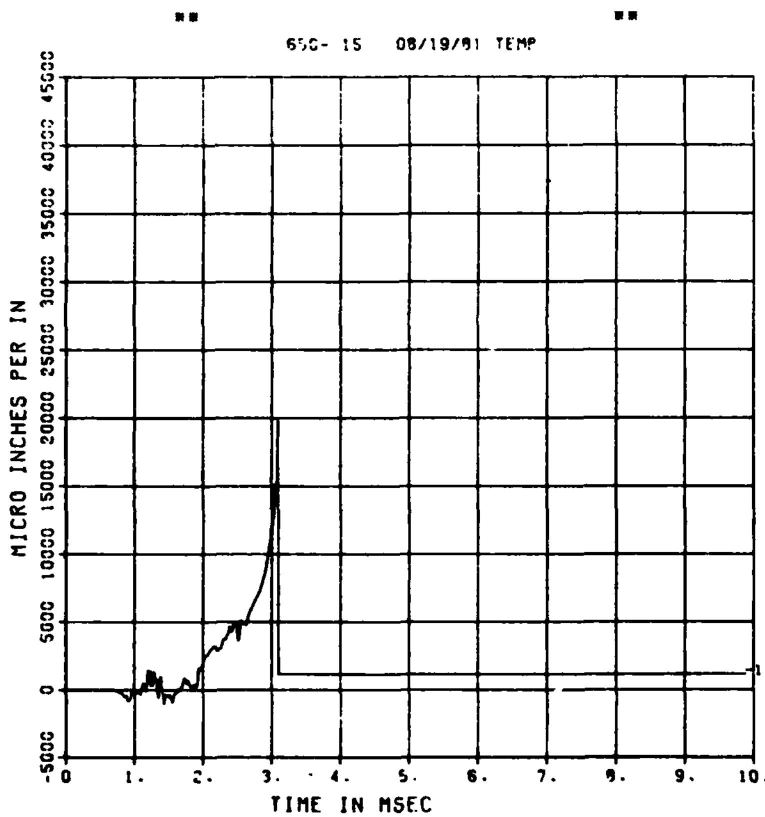

** PEAK VALUE IS 77 % OVER CALIBRATION **

DYNAMIC SHEAR 5
E13
200000. HZ CAL= 11170.

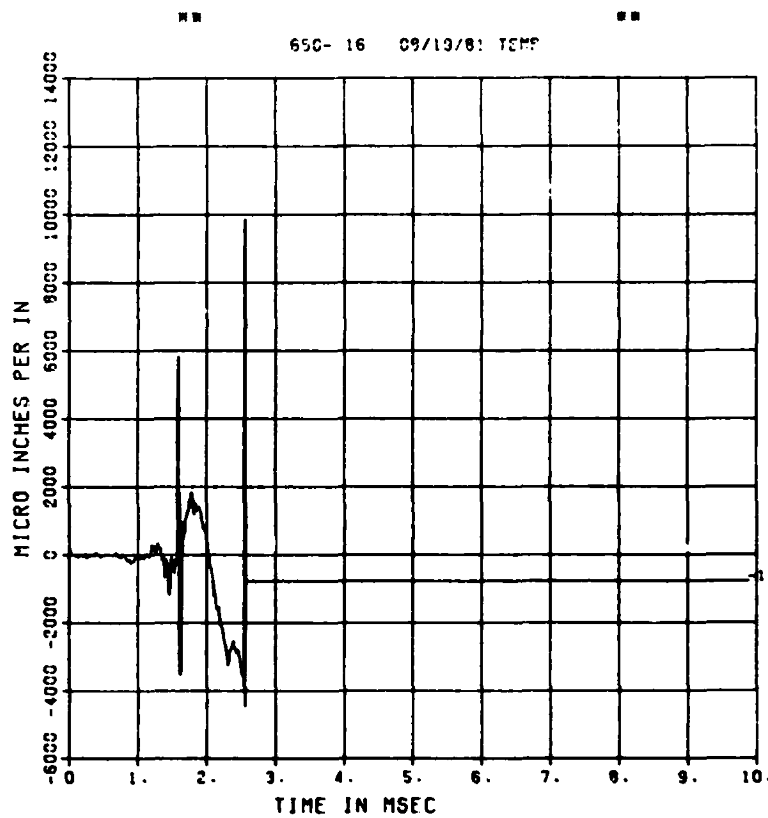

DYNAMIC SHEAR 5
E04
200000. HZ CAL= 11170.

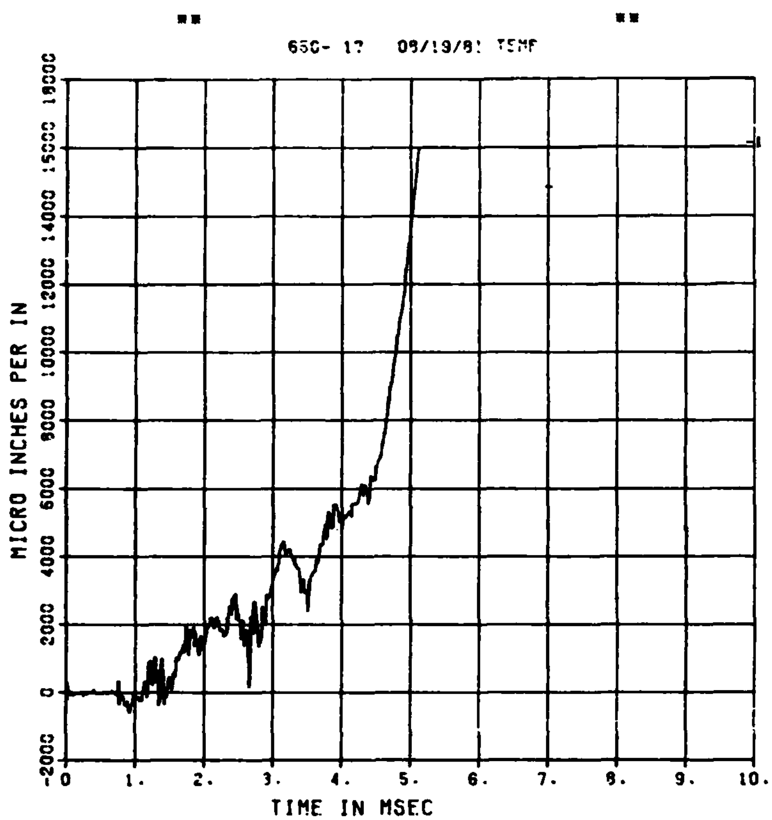

** PEAK VALUE IS 43 % OVER CALIBRATION **

DYNAMIC SHEAR 5
E14
200000. HZ CAL= 11170.

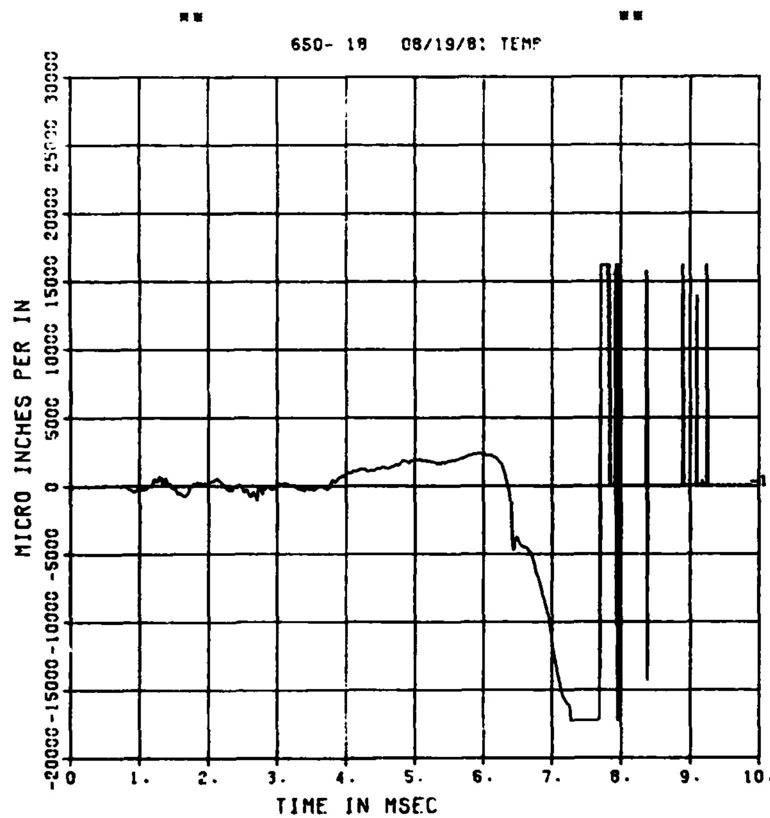

** PEAK VALUE IS 54 % OVER CALIBRATION **

DYNAMIC SHEAR 5
E05
200000. HZ CAL= 42495.

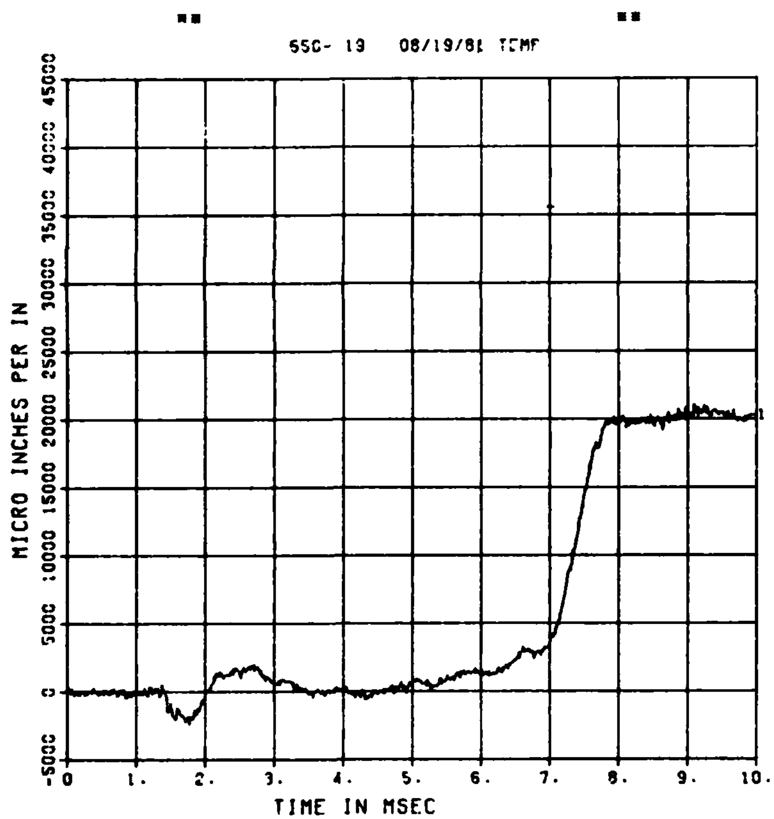

DYNAMIC SHEAR 5
E15
200000. HZ CAL= 42495.

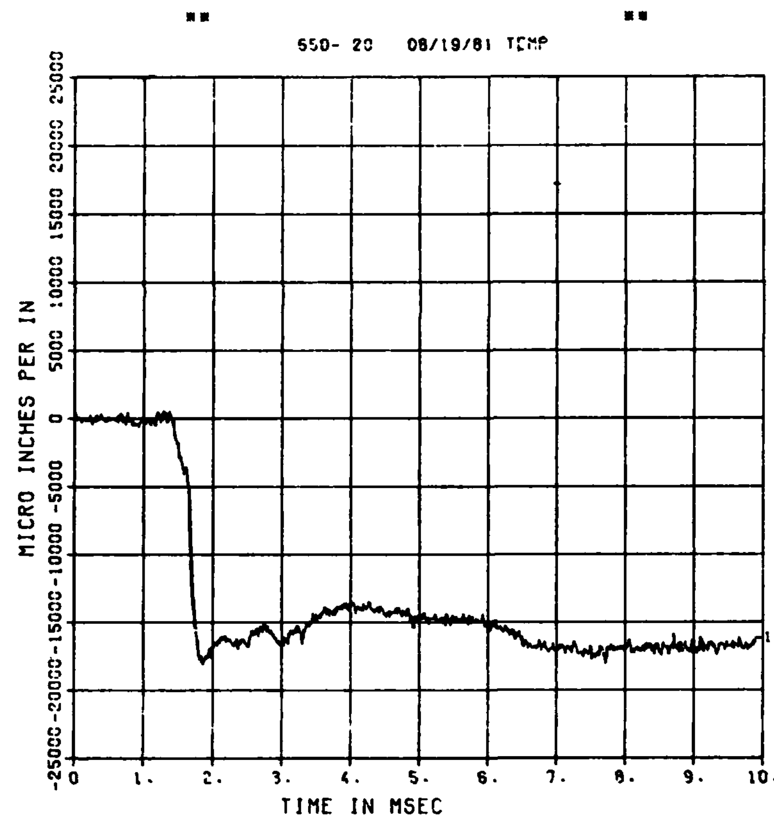

DYNAMIC SHEAR 5
E06
200000. HZ CAL= 42495.

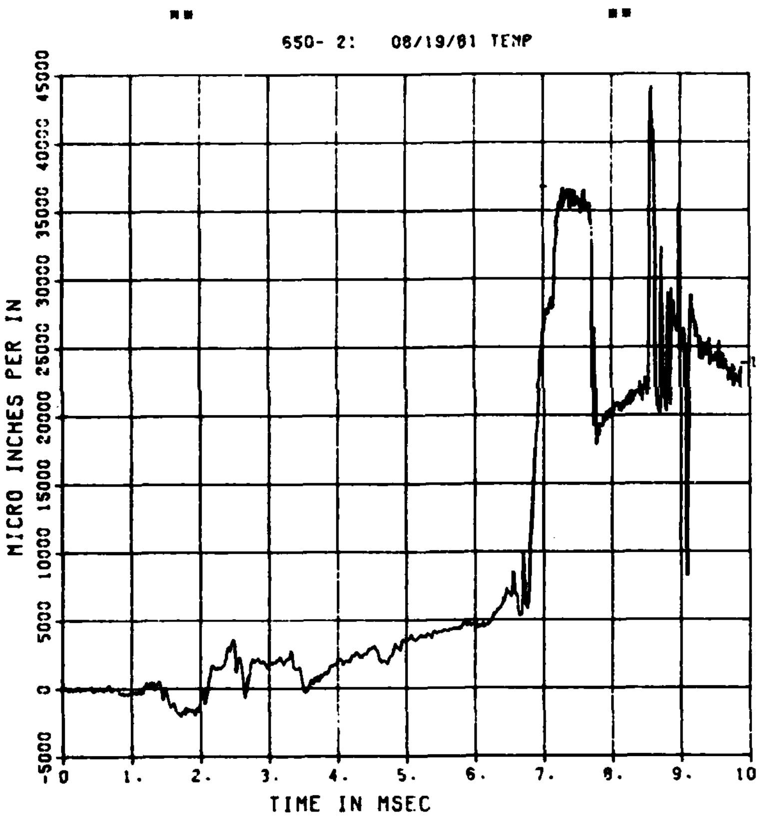

** PEAK VALUE IS 4 % OVER CALIBRATION **

DYNAMIC SHEAR 5
EI6
200000. HZ CAL= 42495.

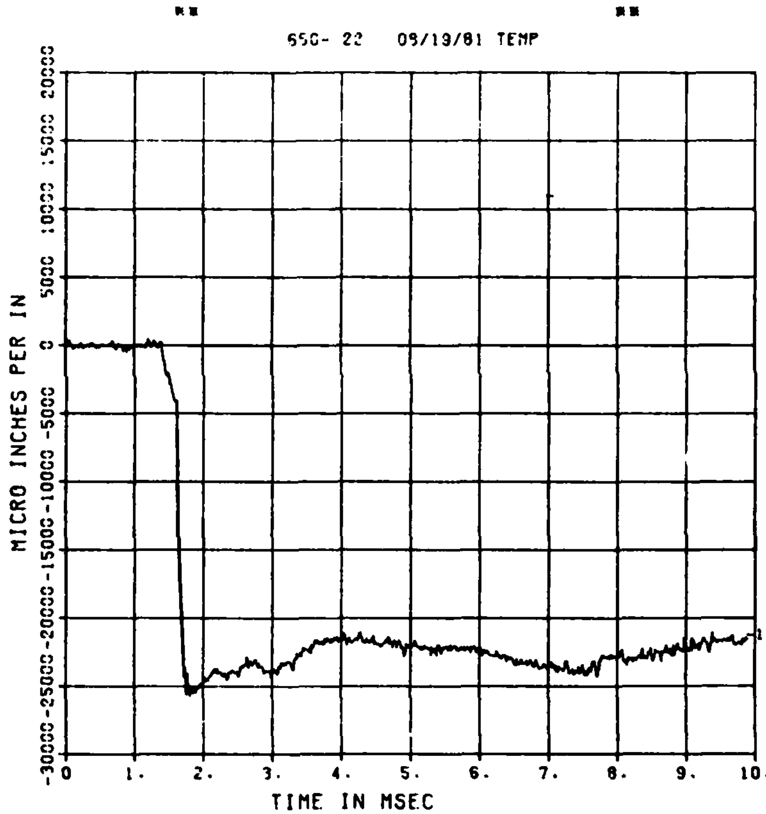

DYN SH II TEST 1
BP1
200000. HZ CAL= 20825.

** **

18458- 16 11/08/82 R0037

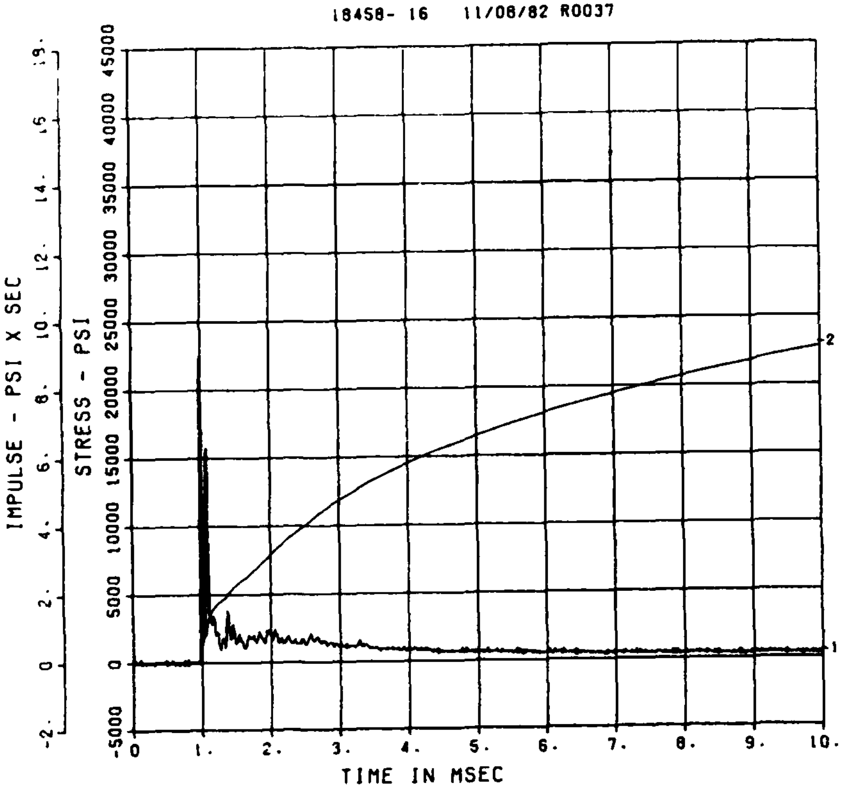

** PEAK VALUE IS 8 % OVER CALIBRATION **

DYN SH II TEST 1
BP1
200000. HZ CAL= 20825.

** **

18458- 16 06/08/82 ROP78

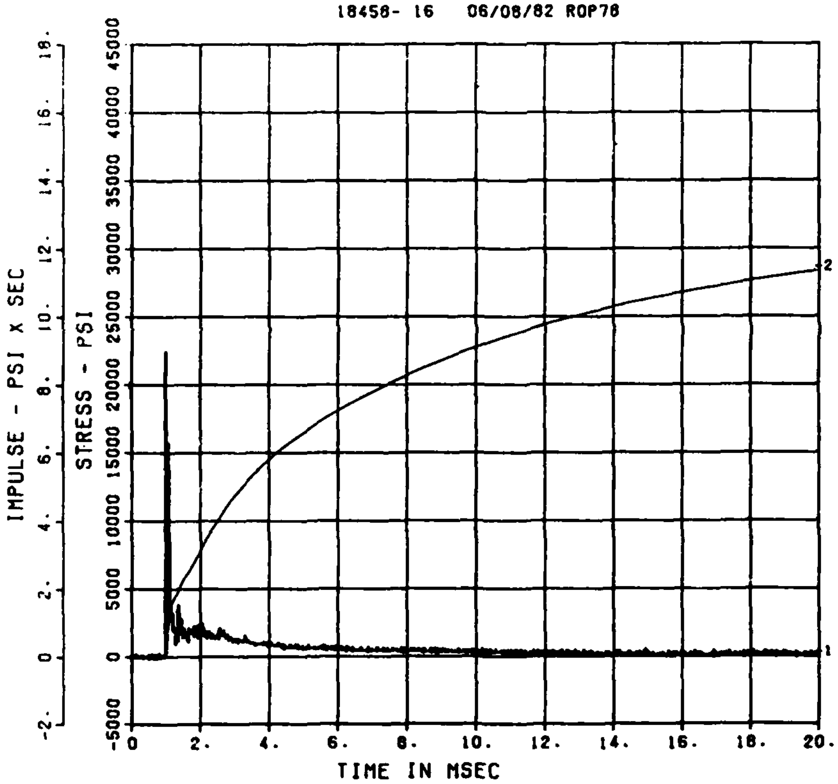

** PEAK VALUE IS 8 % OVER CALIBRATION **

DYN SH II TEST 1
BP4
200000. HZ CAL= 24163.
LP4/0 70% CUTOFF= 9000. HZ

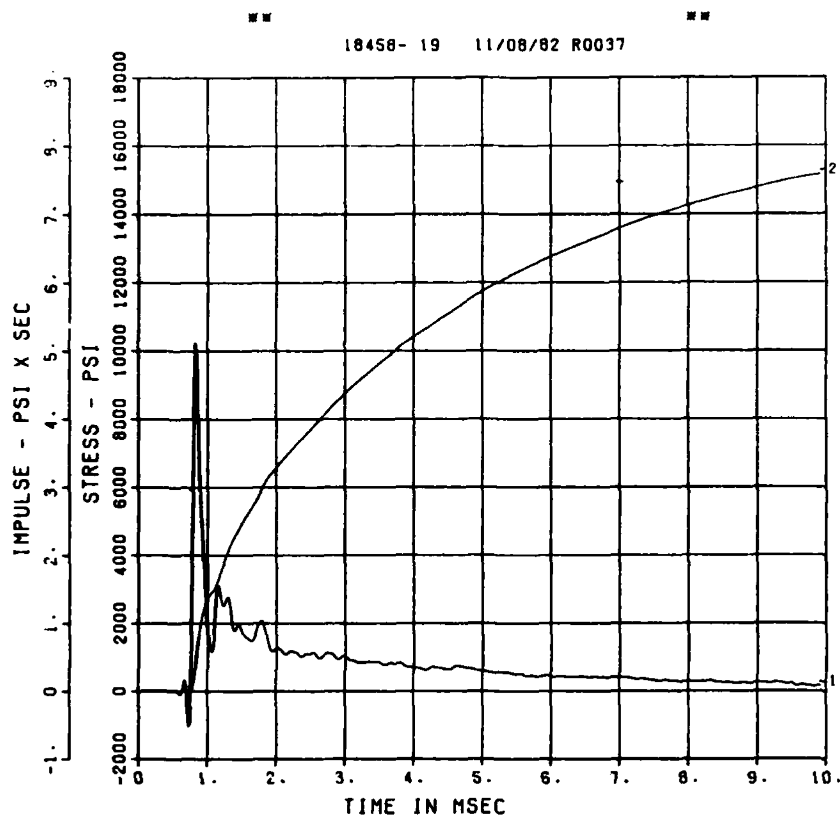

DYN SH II TEST 1
BP4
200000. HZ CAL= 24163.
LP4/0 70% CUTOFF= 9000. HZ

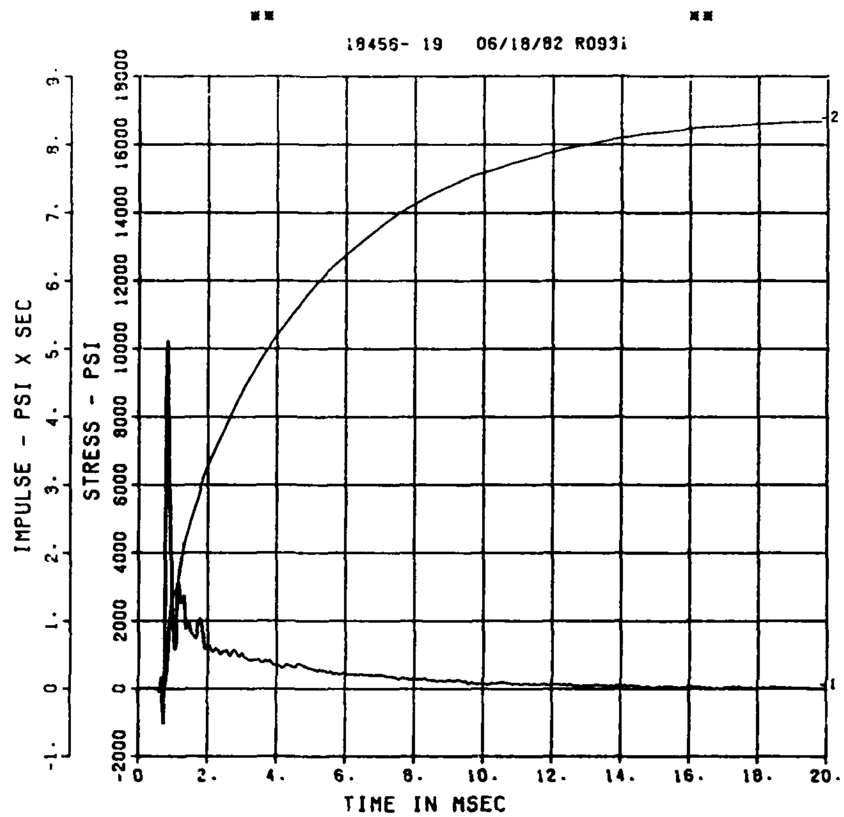

DYN SH II TEST 1
IF1
200000. HZ CAL= 11828.

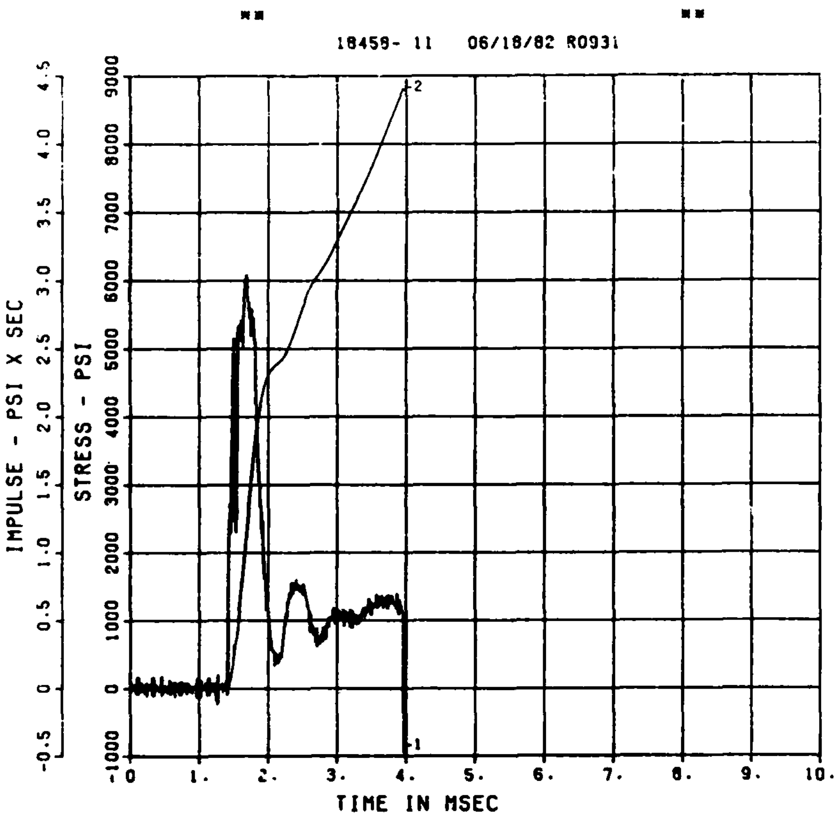

DYN SH II TEST 1
IF2
200000. HZ CAL= 12249.

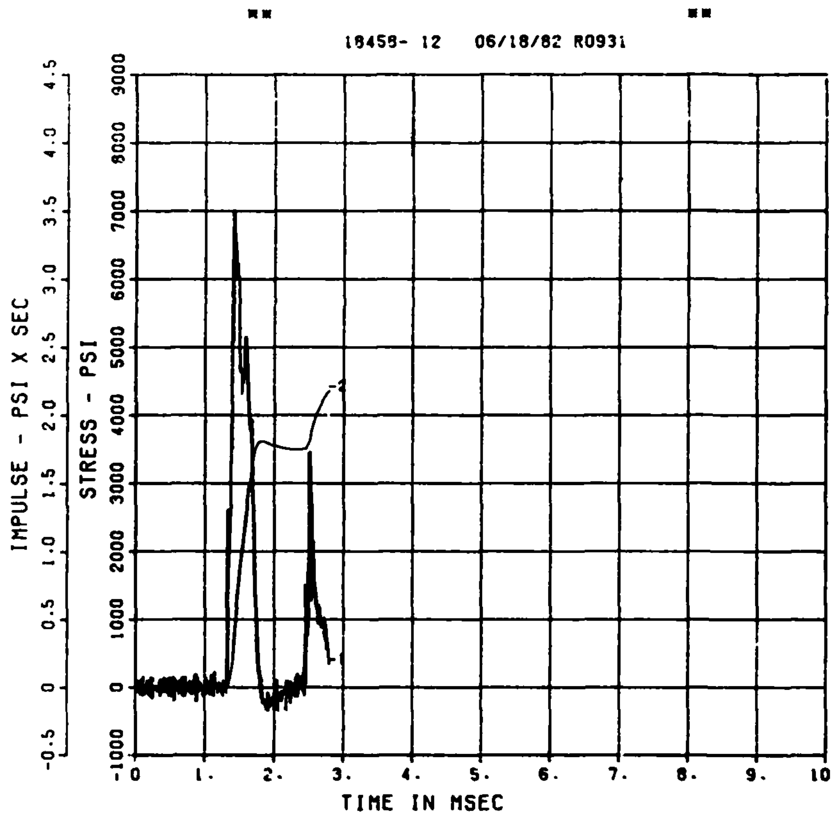

DYN SH II TEST 1
IF3
200000. HZ CAL= 12100.

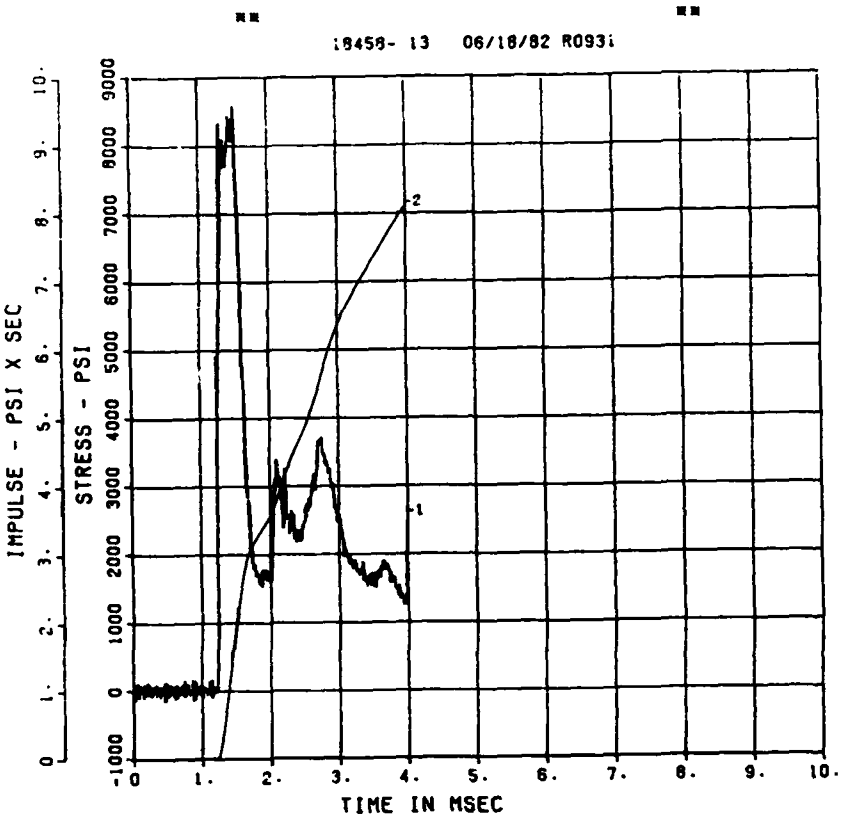

DYN SH II TEST 1
IF4
200000. HZ CAL= 8181.

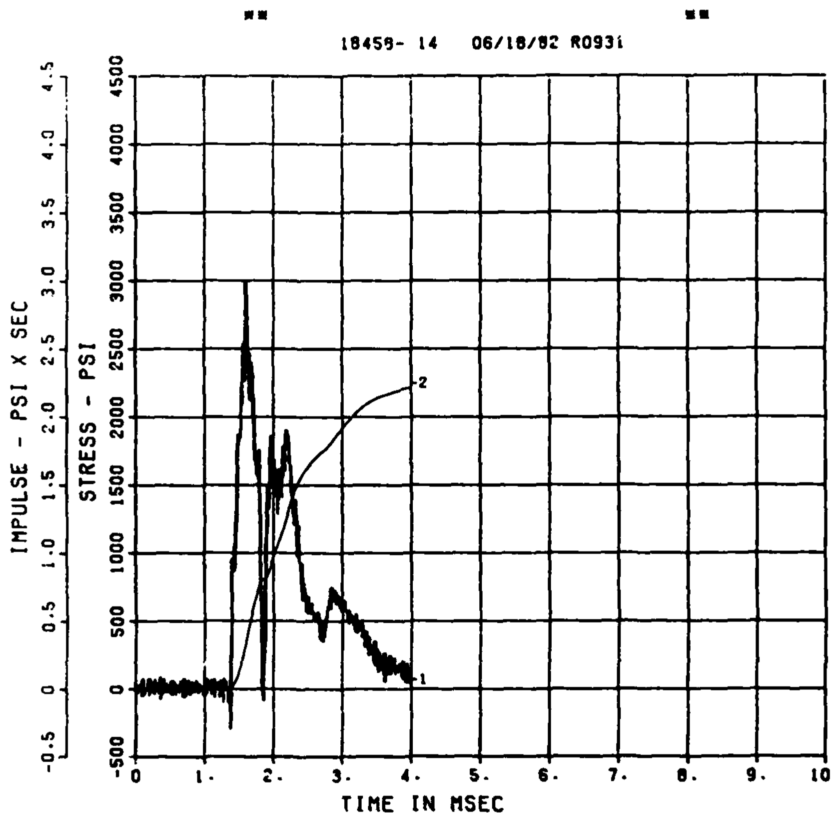

DYN SH II TEST 1
IF5
200000. HZ CAL= 11417.
LP4/0 70% CUTOFF= 9000. HZ

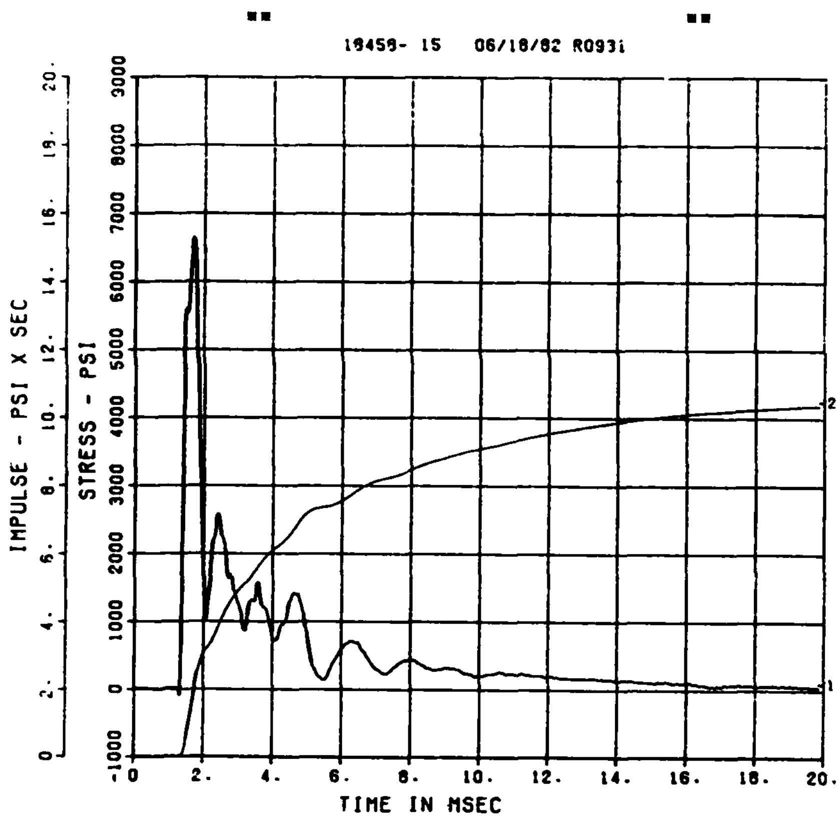

DYN SH II TEST 1
SE1
200000. HZ CAL= 13845.

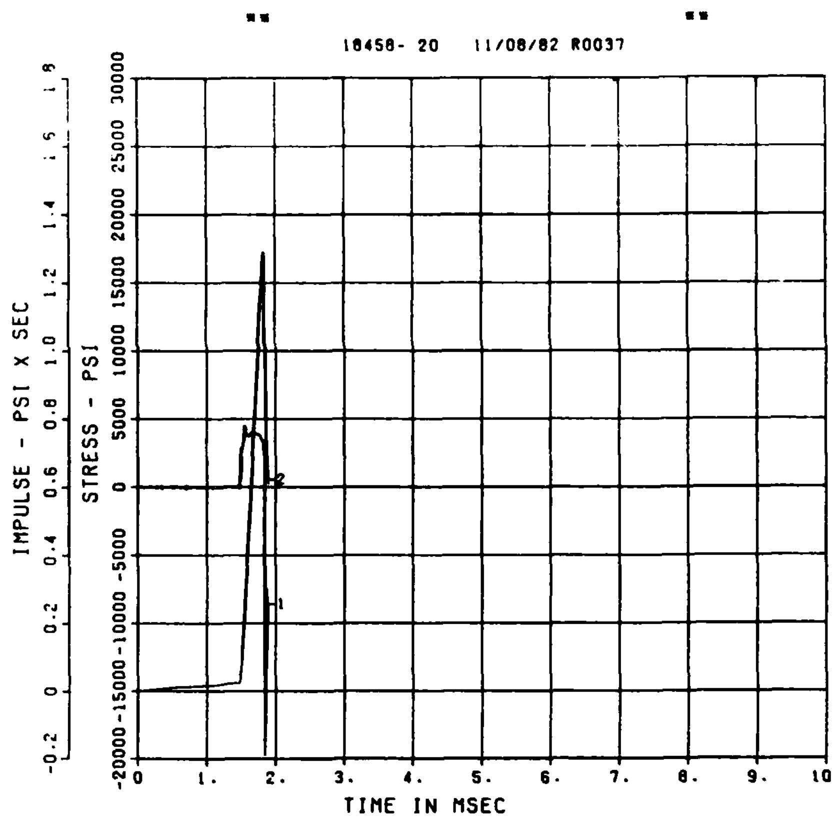

** PEAK VALUE IS 43 % OVER CALIBRATION **

DYN SH II TEST 1
SE2
200000. HZ CAL= 10474.
LP4/0 70% CUTOFF= 9000. HZ

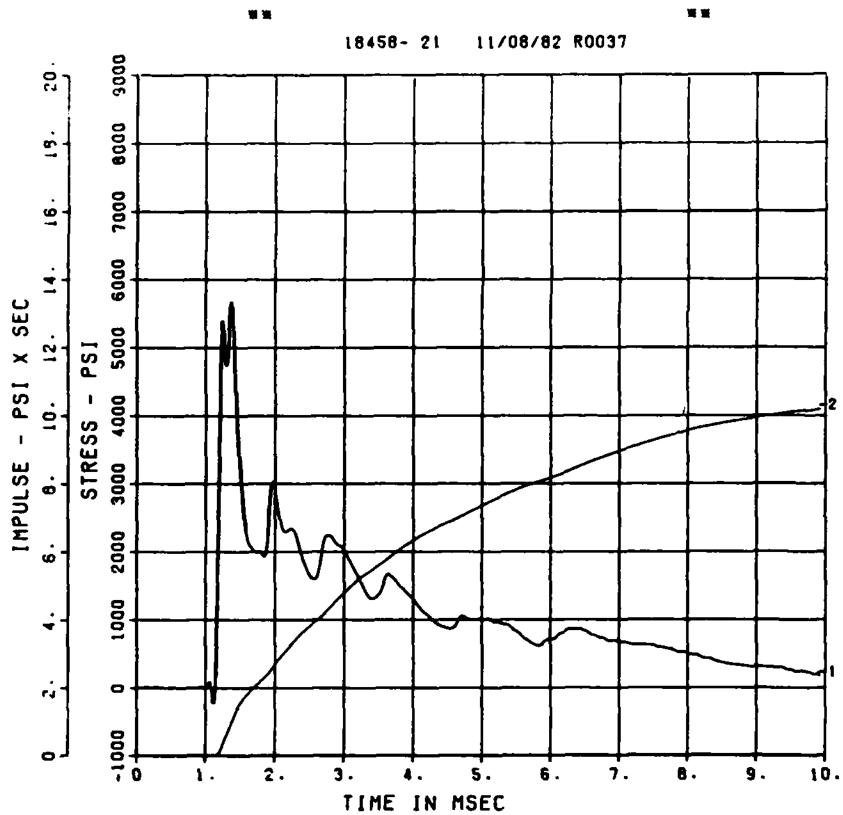

DYN SH II TEST 1
E01
200000. HZ CAL= 21625.

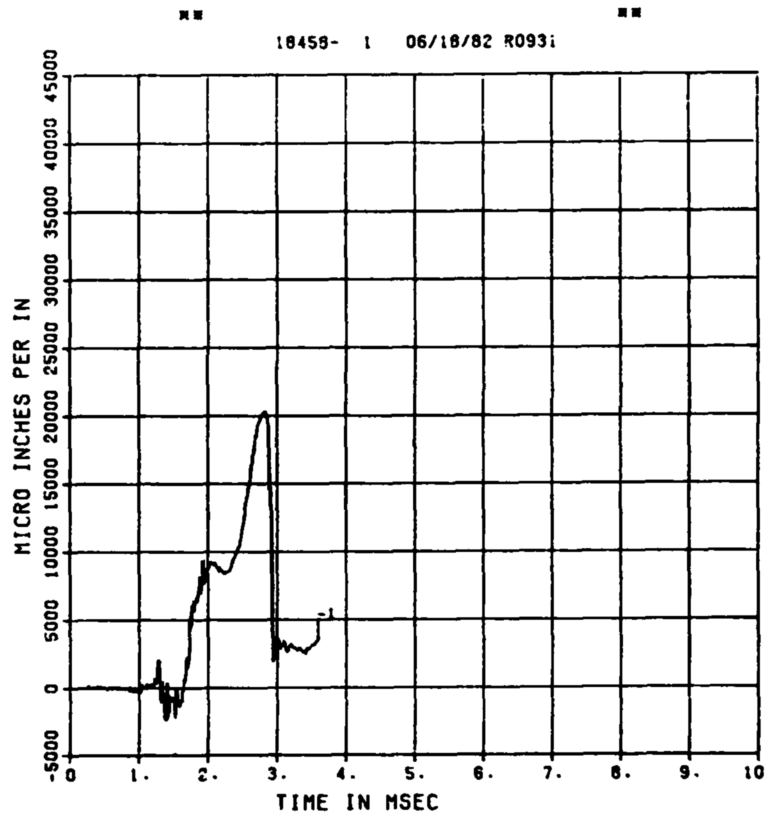

DYN SH II TEST 1
EI1
200000. HZ CAL= 21625.

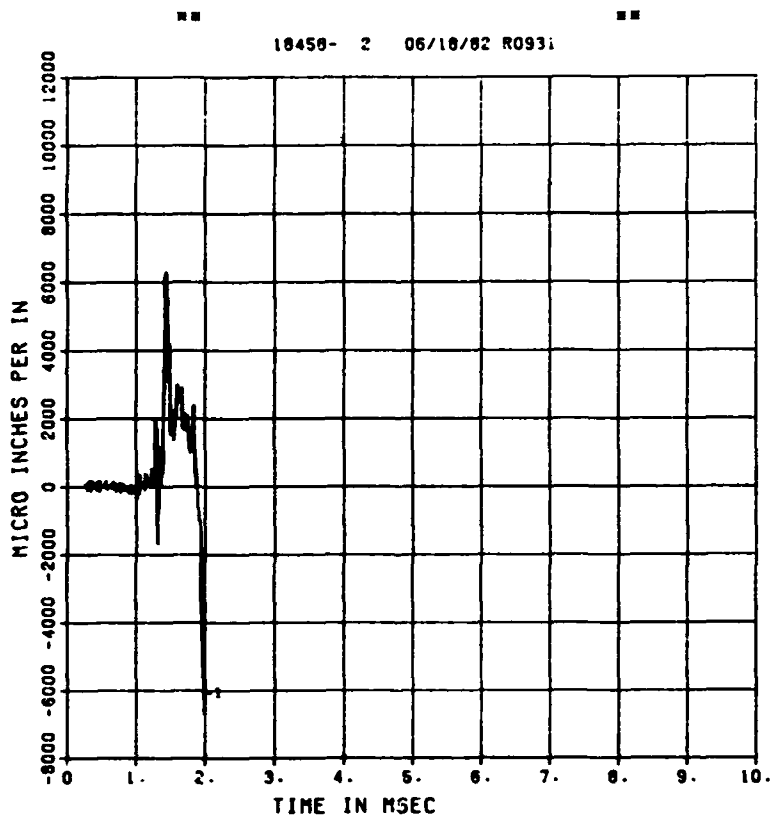

DYN SH II TEST 1
E03
200000. HZ CAL= 21625.

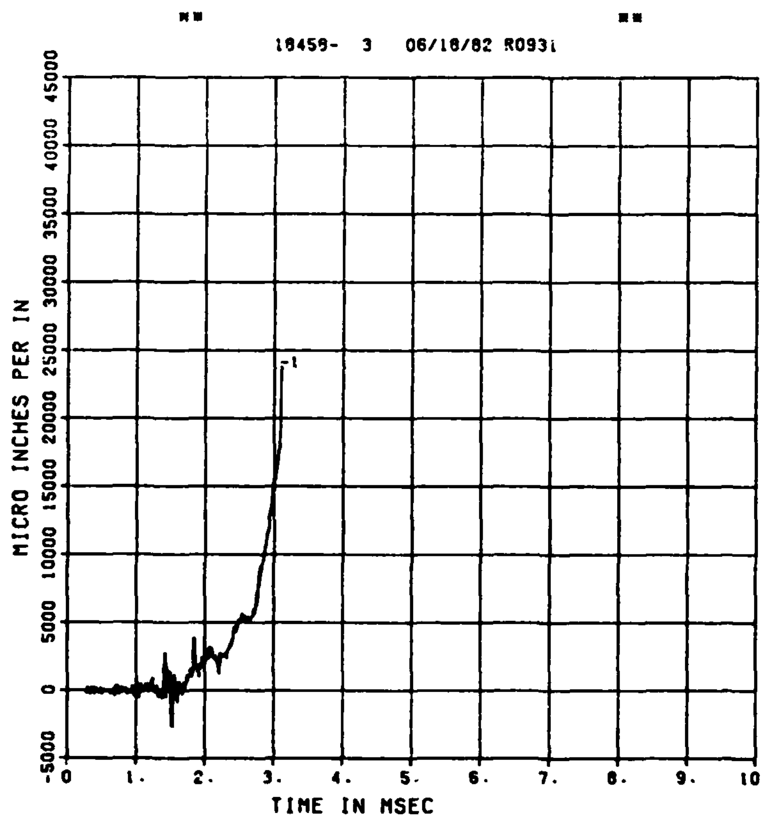

** PEAK VALUE IS 10 % OVER CALIBRATION **

DYN SH II TEST 1
EI3
200000. HZ CAL= 21625.

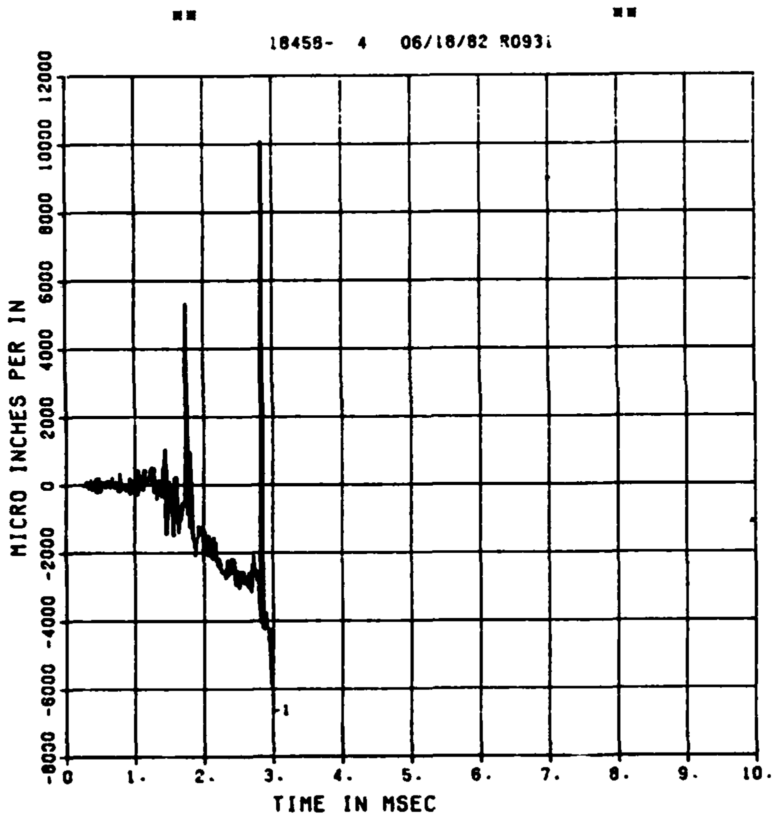

DYN SH II TEST 1
E04
200000. HZ CAL= 21625.

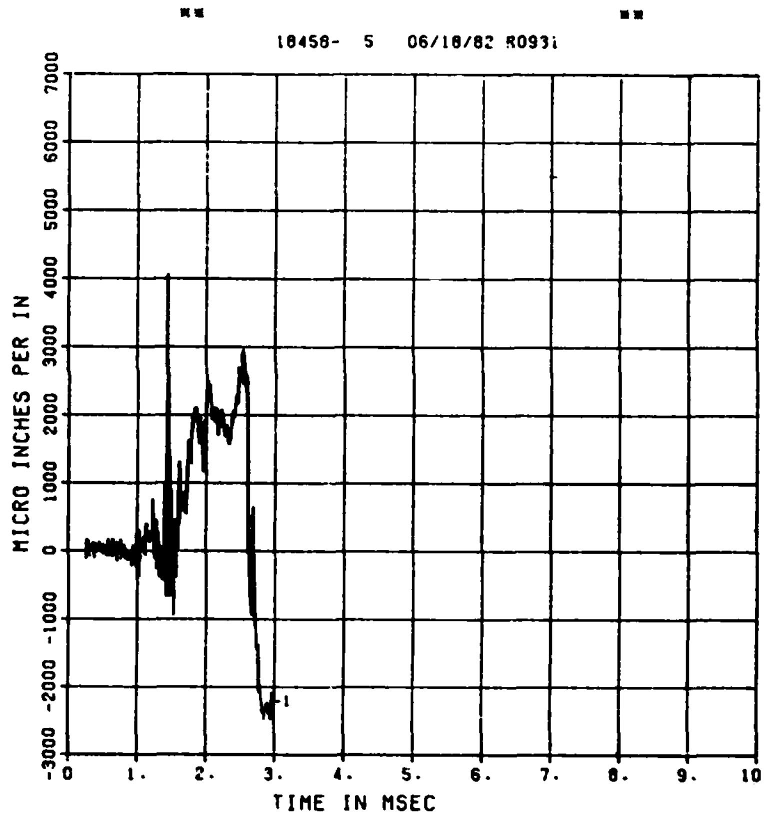

** PEAK VALUE IS 81 % UNDER CALIBRATION **

DYN SH II TEST 1
EI4
200000. HZ CAL= 21625.

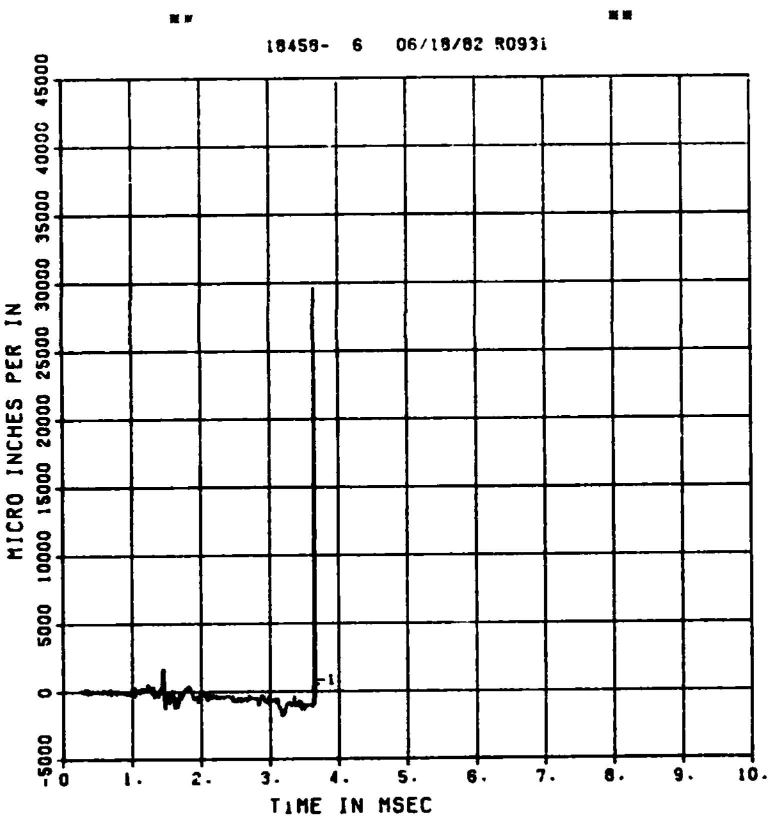

** PEAK VALUE IS 37 % OVER CALIBRATION **

DYN SH II TEST 1
E05
200000. HZ CAL= 21625.

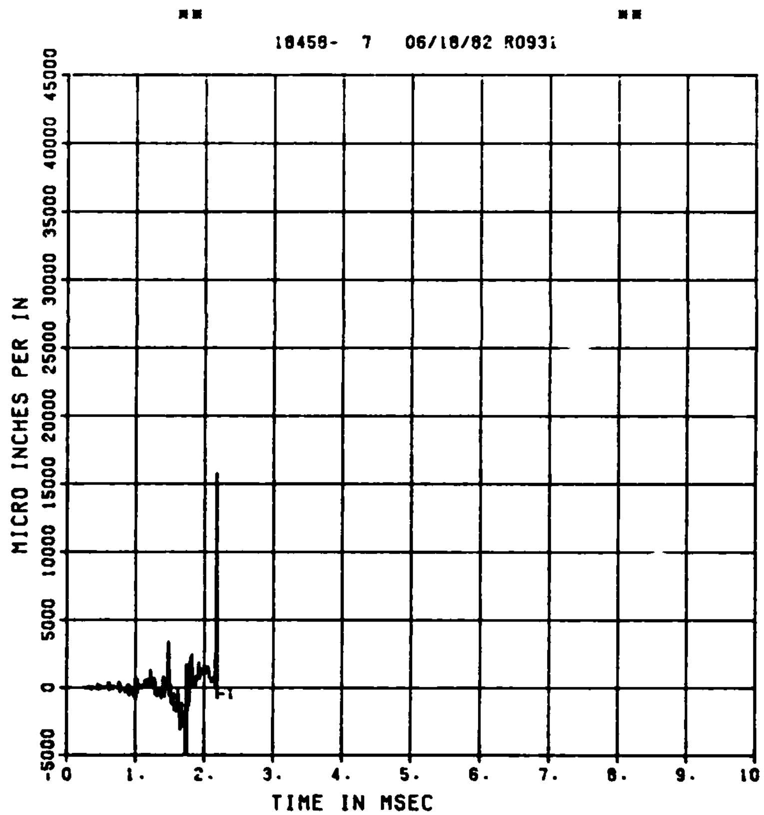

DYN SH II TEST 1
EI5
200000. HZ CAL= 43705.

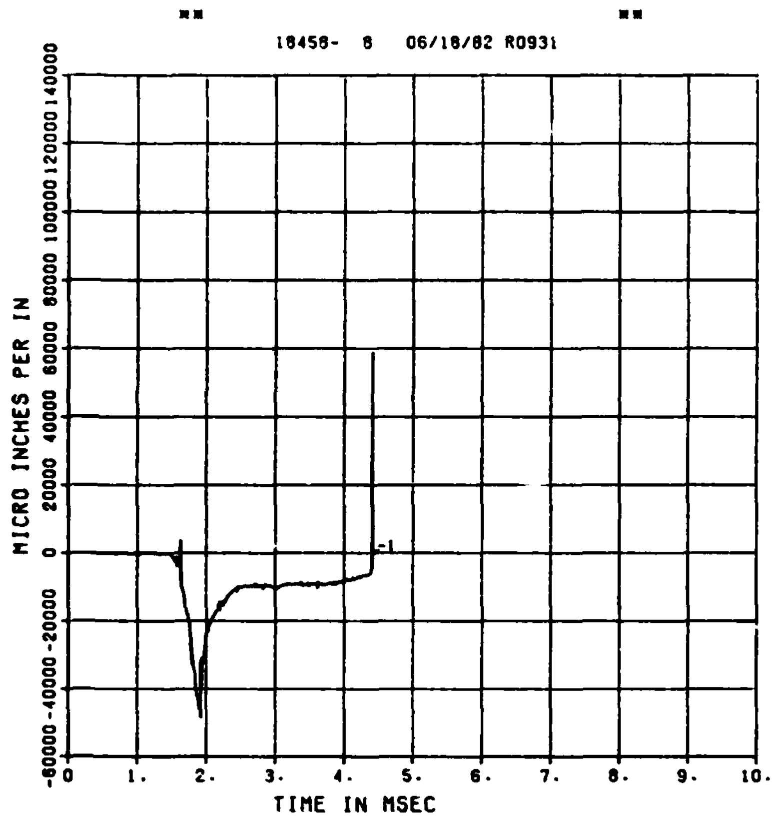

** PEAK VALUE IS 35 % OVER CALIBRATION **

DYN SH II TEST 1
E06
200000. HZ CAL= 21625.

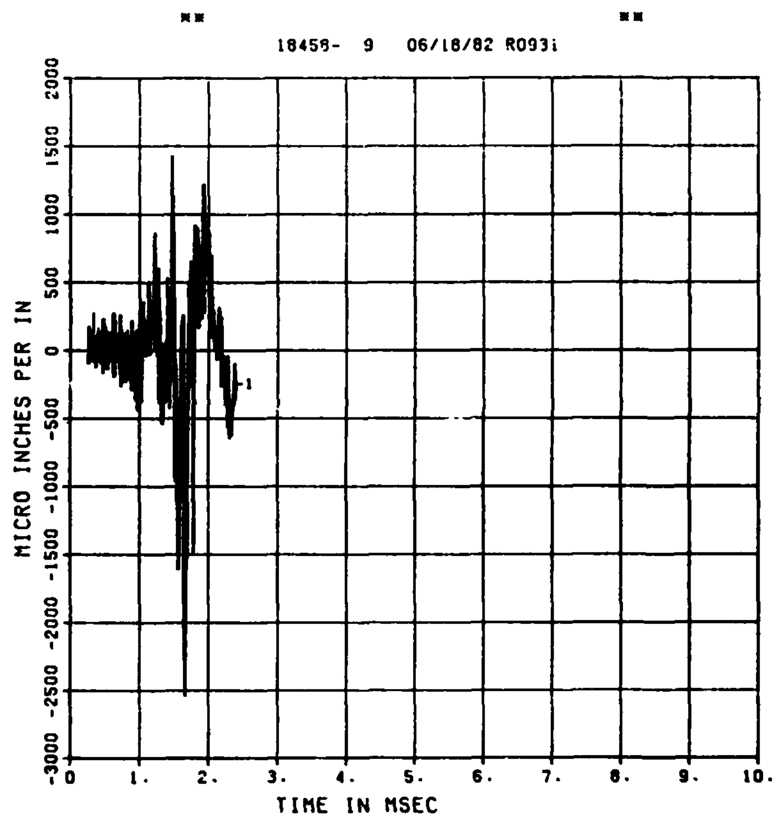

** PEAK VALUE IS 88 % UNDER CALIBRATION **

DYN SH II TEST 1
EI6
200000. HZ CAL= 43705.

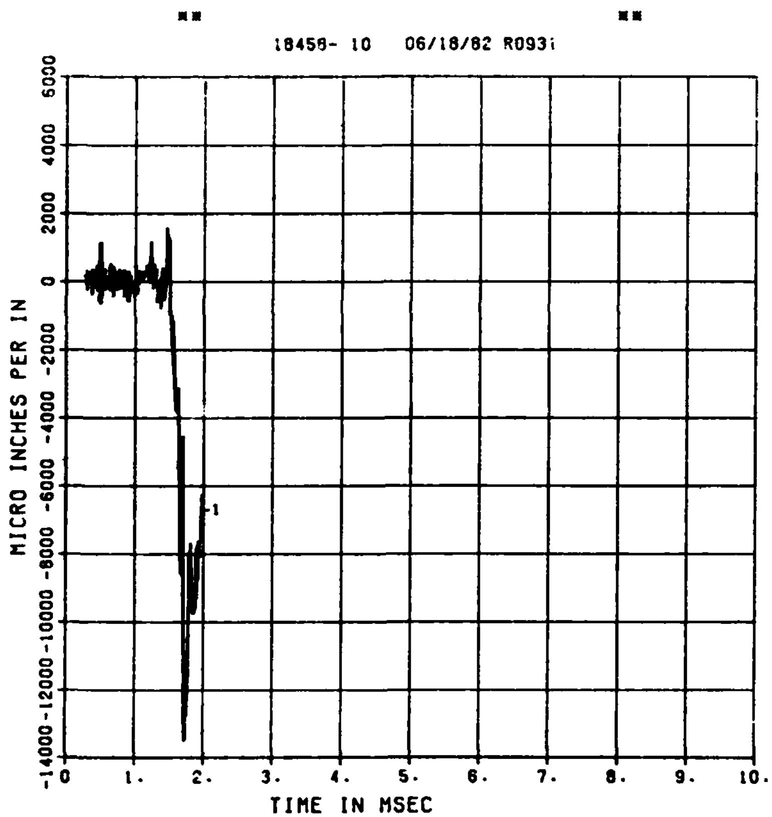

DYN SH II TEST 2
BP1
200000. HZ CAL= 20825.

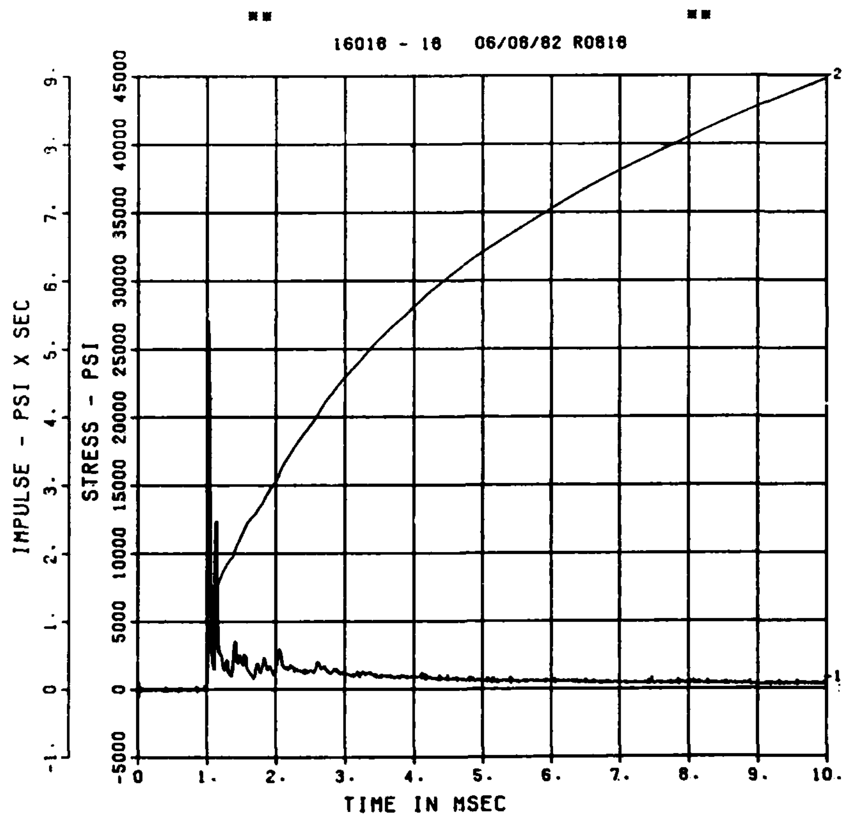

** PEAK VALUE IS 30 % OVER CALIBRATION **

DYN SH II TEST 2
BP1
200000. HZ CAL= 20825.

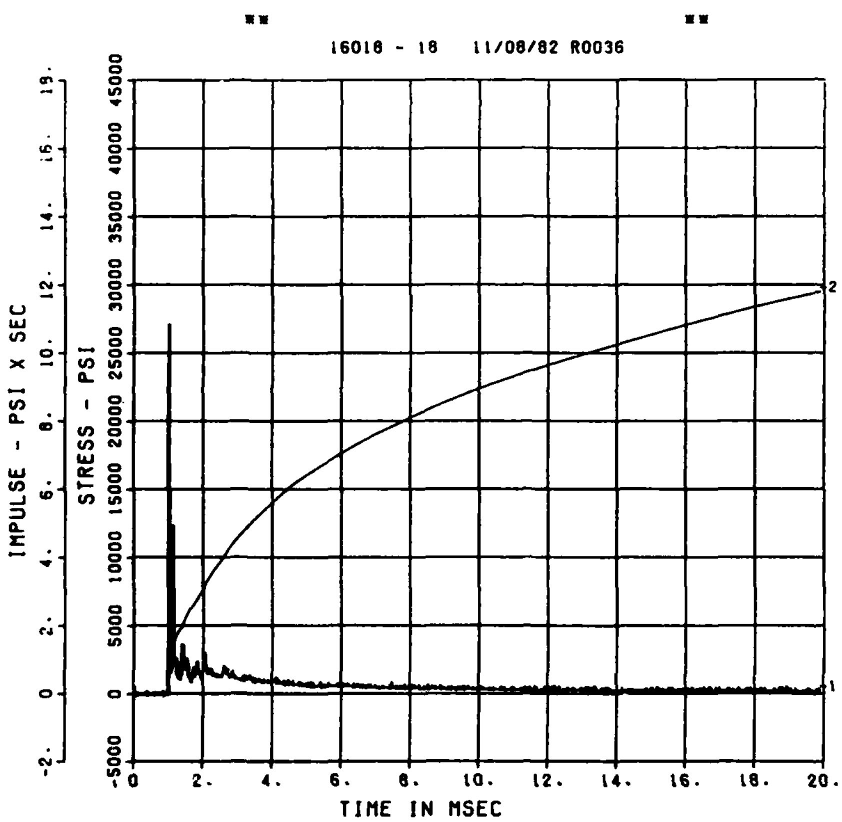

** PEAK VALUE IS 30 % OVER CALIBRATION **

DYN SH II TEST 2
BP2
200000. HZ CAL= 20155.
LP4/0 70% CUTOFF= 9000. HZ

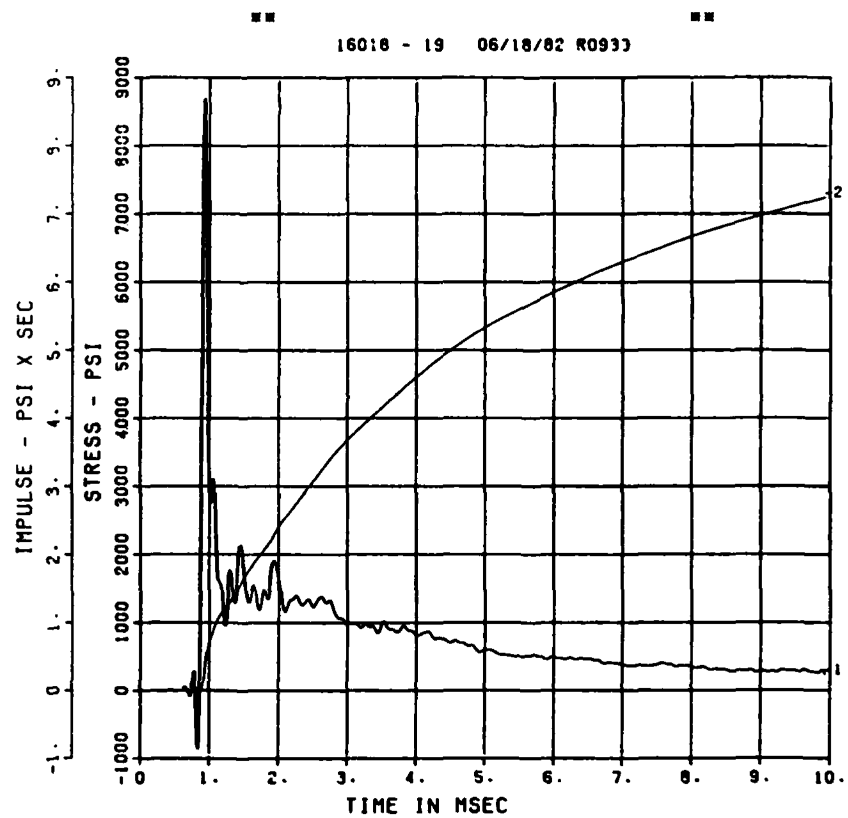

DYN SH II TEST 2
BP2
200000. HZ CAL= 20155.
LP4/0 70% CUTOFF= 9000. HZ

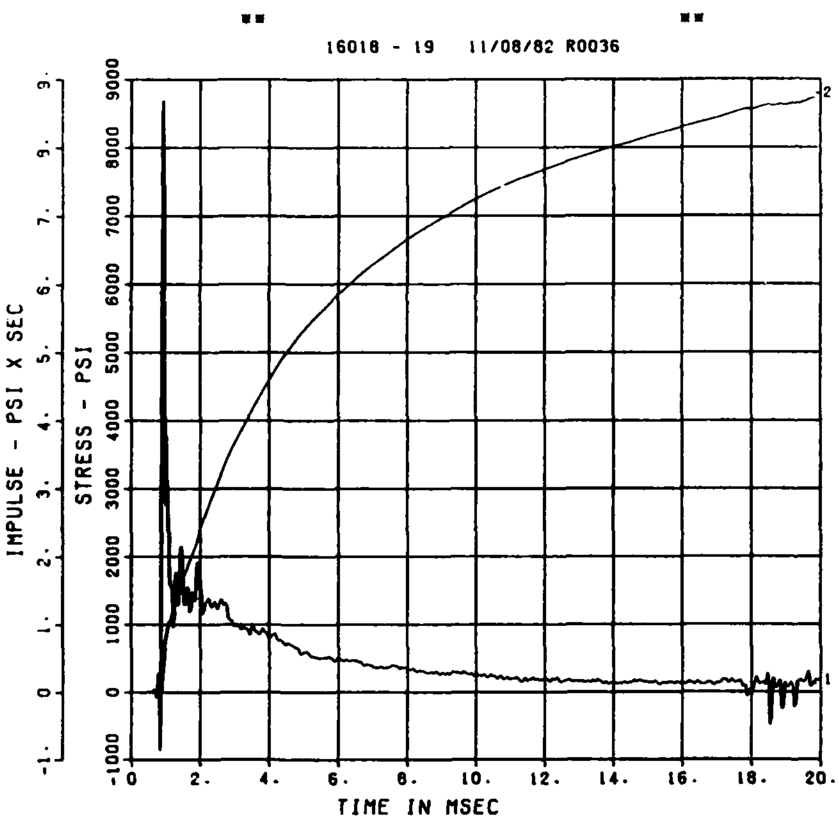

DYN SH II TEST 2
BP3
200000. HZ CAL= 20568.

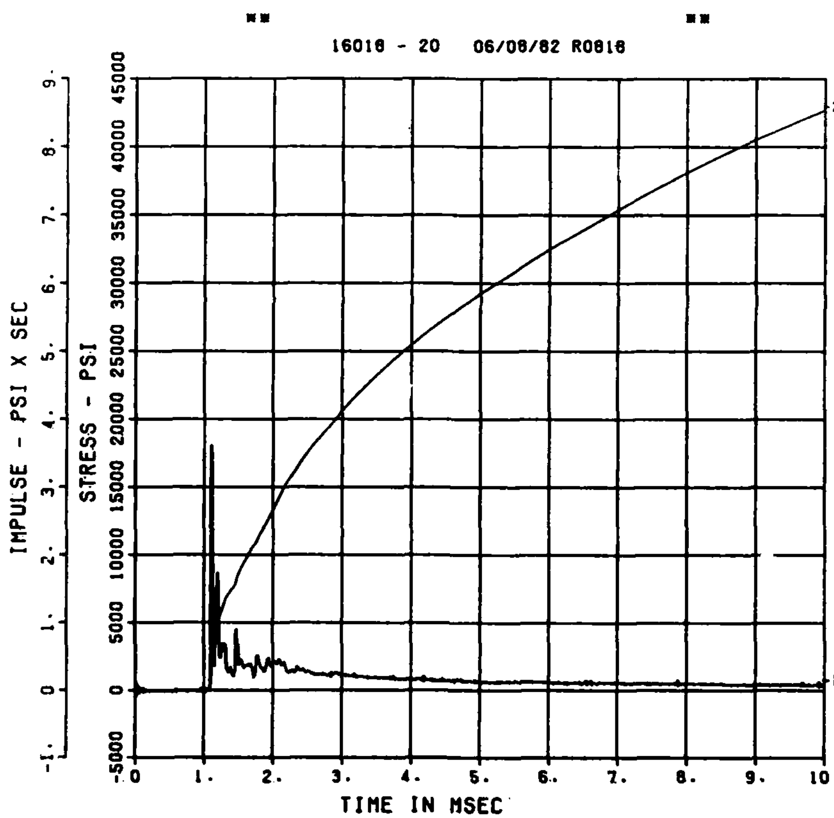

DYN SH II TEST 2
BP3
200000. HZ CAL= 20568.

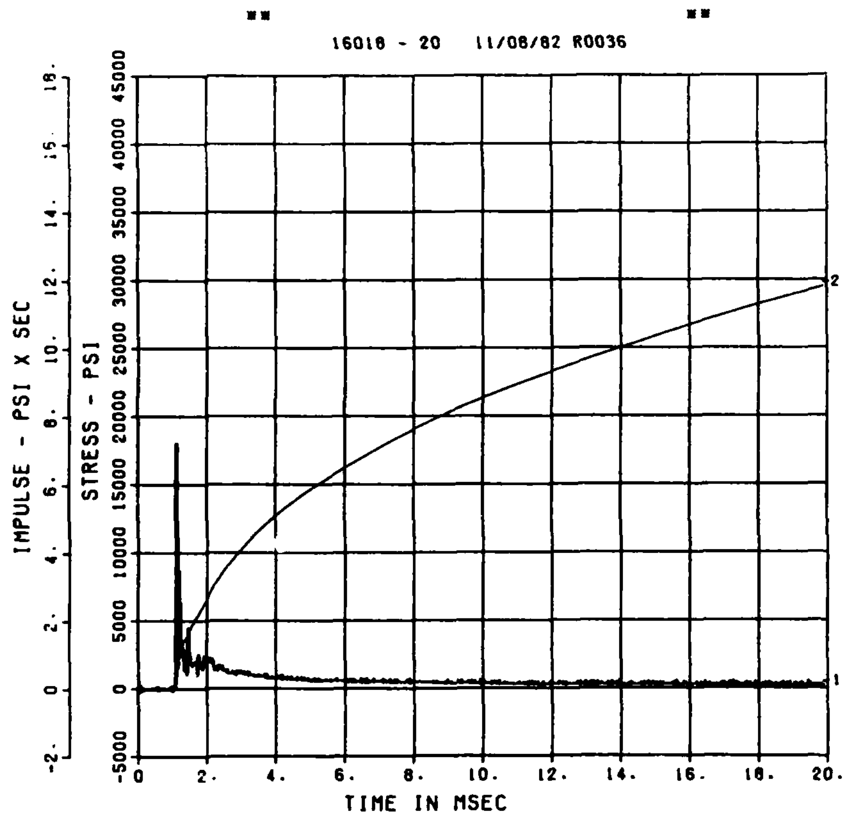

DYN SH II TEST 2
BP4
200000. HZ CAL= 24163.

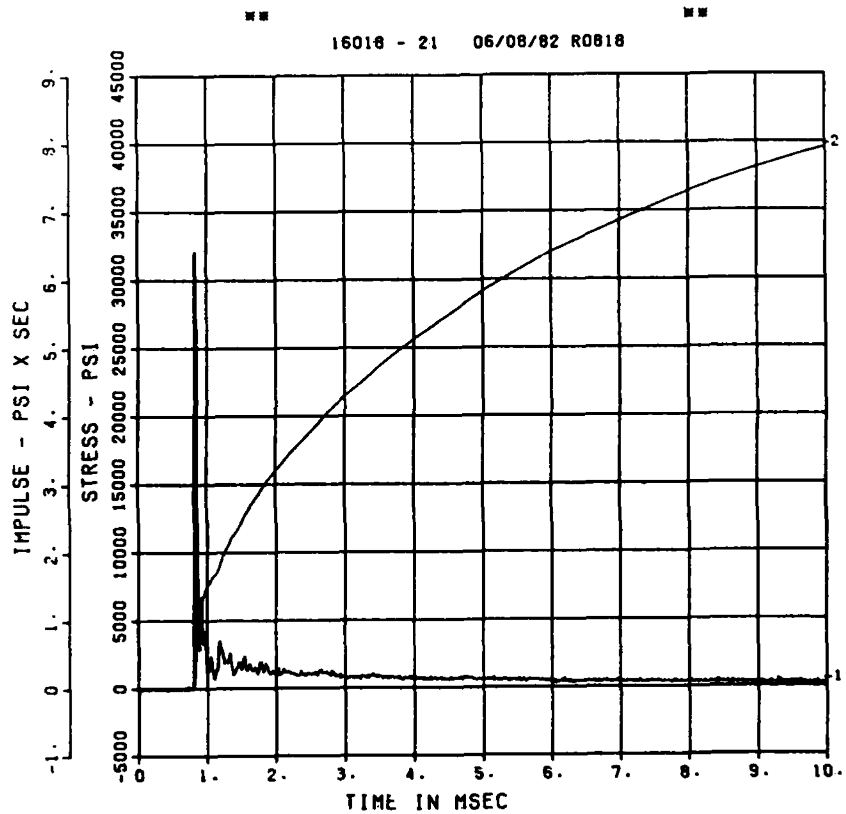

** PEAK VALUE IS 33 % OVER CALIBRATION **

DYN SH II TEST 2
BP4
200000. HZ CAL= 24163.

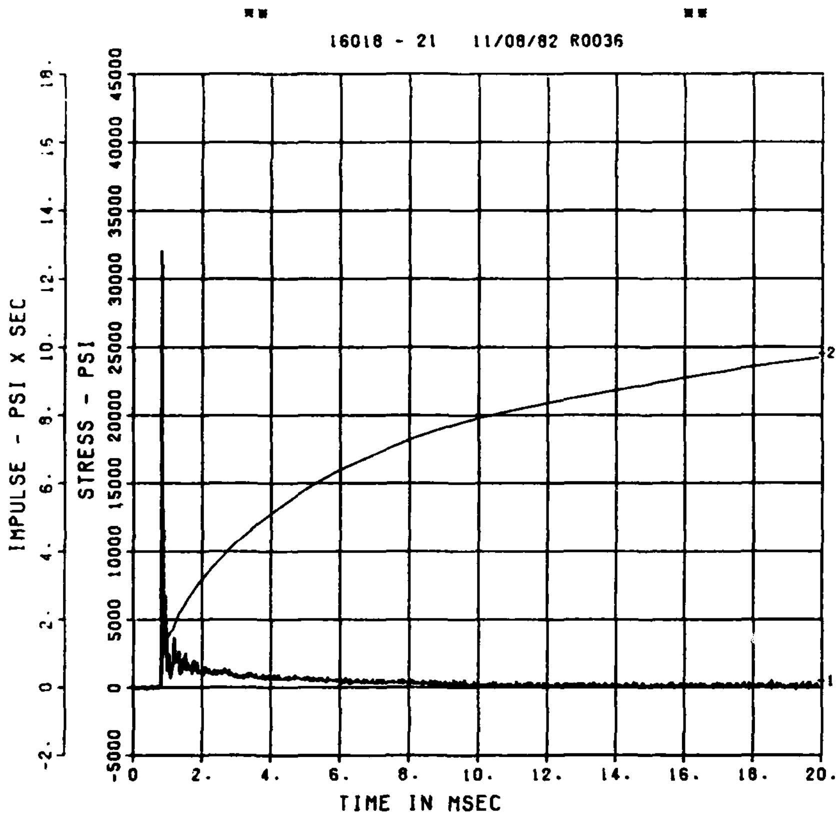

** PEAK VALUE IS 33 % OVER CALIBRATION **

DYN SH II TEST 2
IF1
200000. HZ CAL= 8640.
LP4/0 70% CUTOFF= 9000. HZ

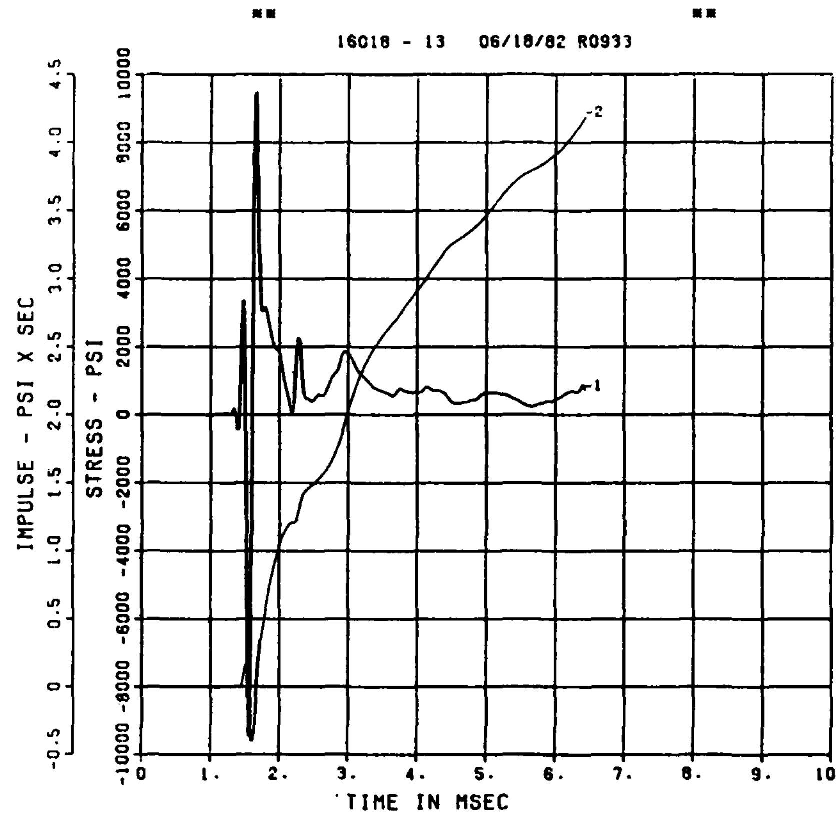

** PEAK VALUE IS 10 % OVER CALIBRATION **

DYN SH II TEST 2
IF3
200000. HZ CAL= 8975.

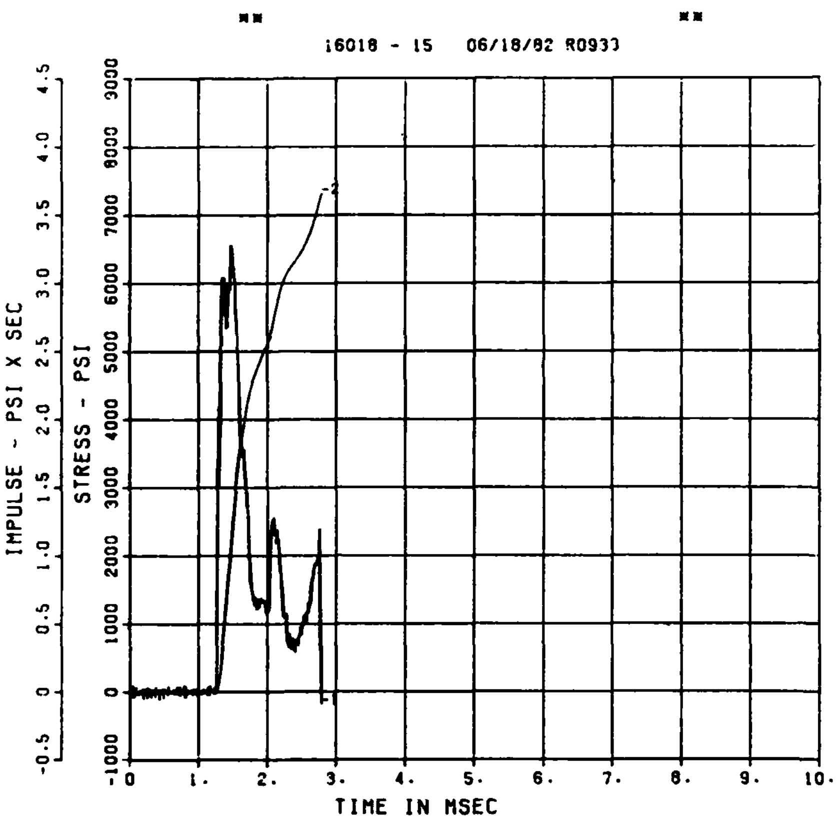

DYN SH II TEST 2
IF4
200000. HZ CAL= 6152.

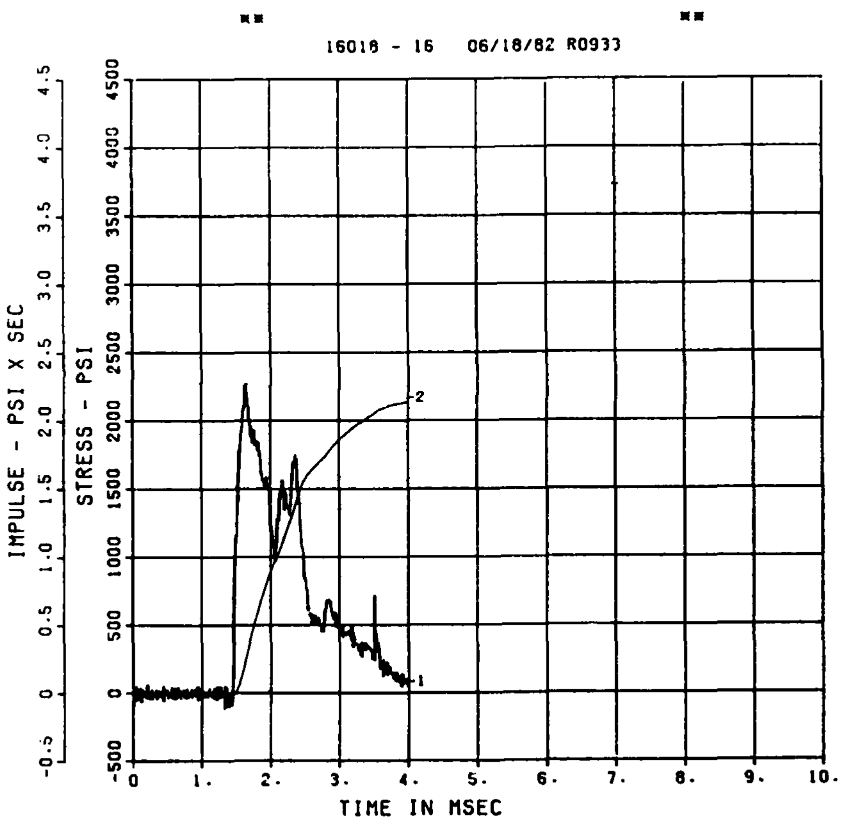

DYN SH II TEST 2
IF5
200000. HZ CAL= 11417.

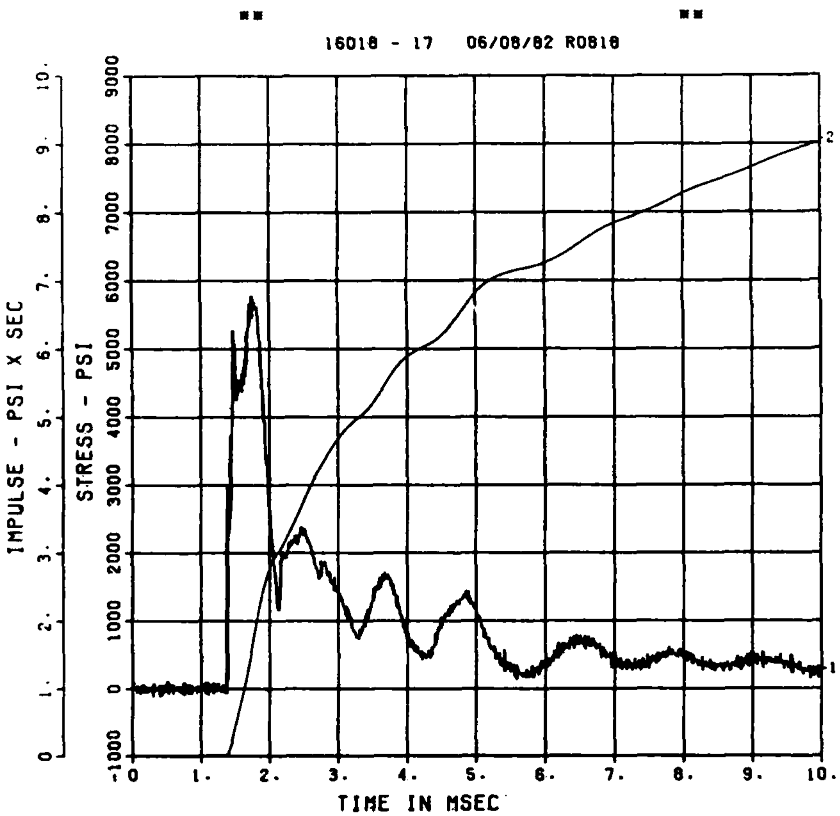

DYN SH II TEST 2
SE1
200000. HZ CAL= 10594.
LP4/0 70% CUTOFF= 9000. HZ

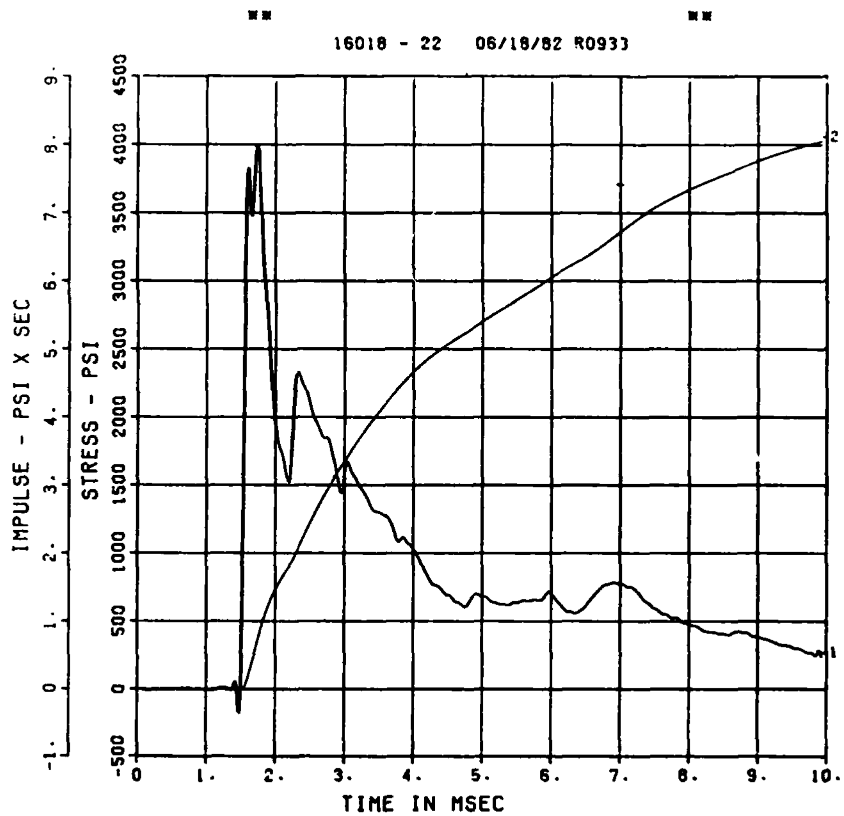

DYN SH II TEST 2
SE2
200000. HZ CAL= 10851.

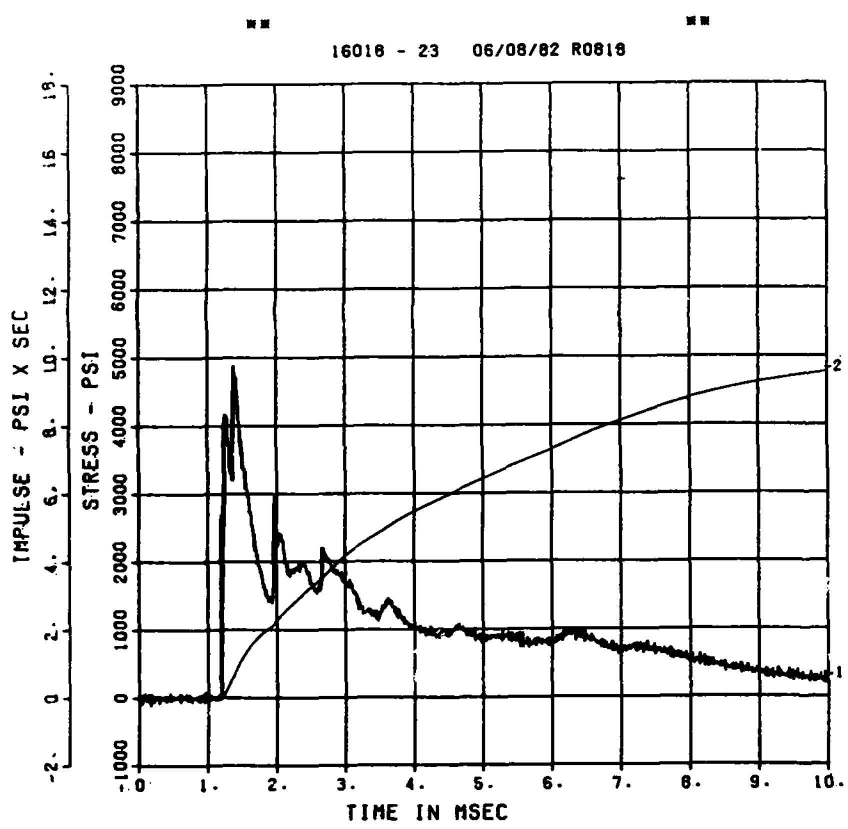

DYN SH II TEST 2
E01
200000. HZ CAL= 21625.

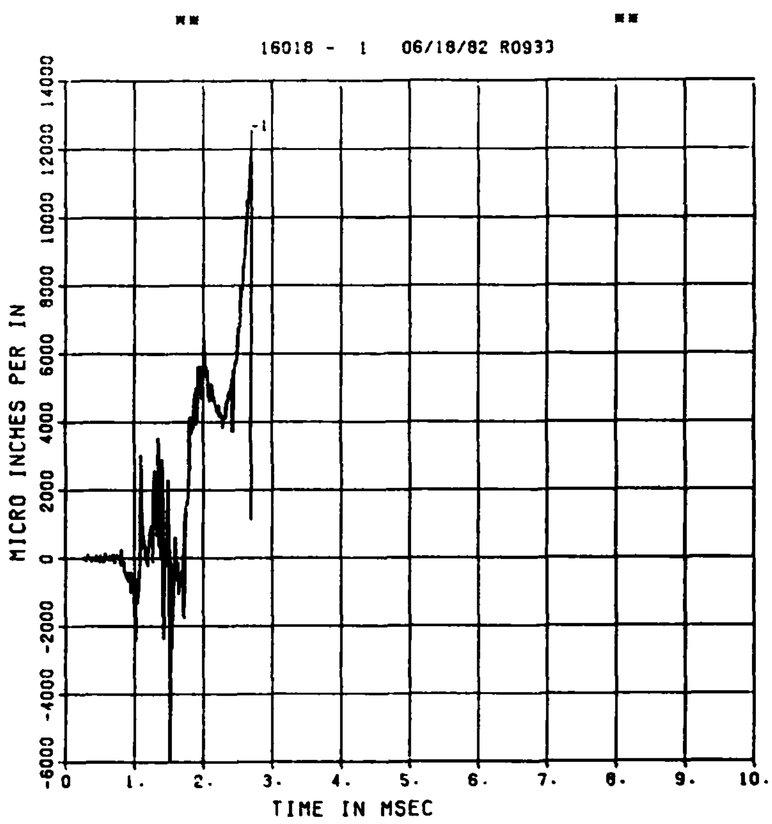

DYN SH II TEST 2
EI1
200000. HZ CAL= 21625.

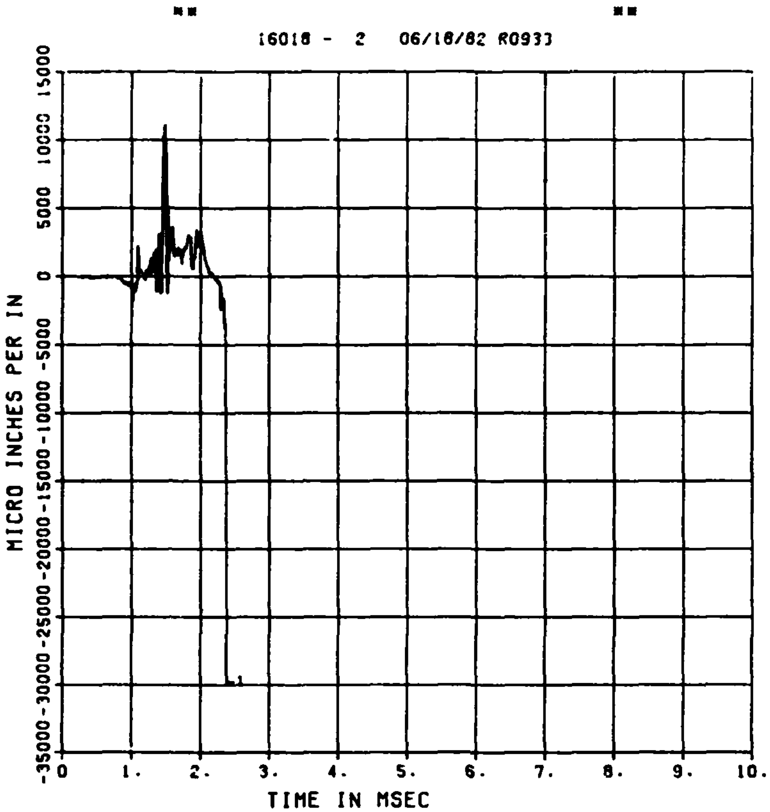

** PEAK VALUE IS 39 % OVER CALIBRATION **

DYN SH II TEST 2
E02
200000. HZ CAL= 14581.
LP4/0 70% CUTOFF= 9000. HZ

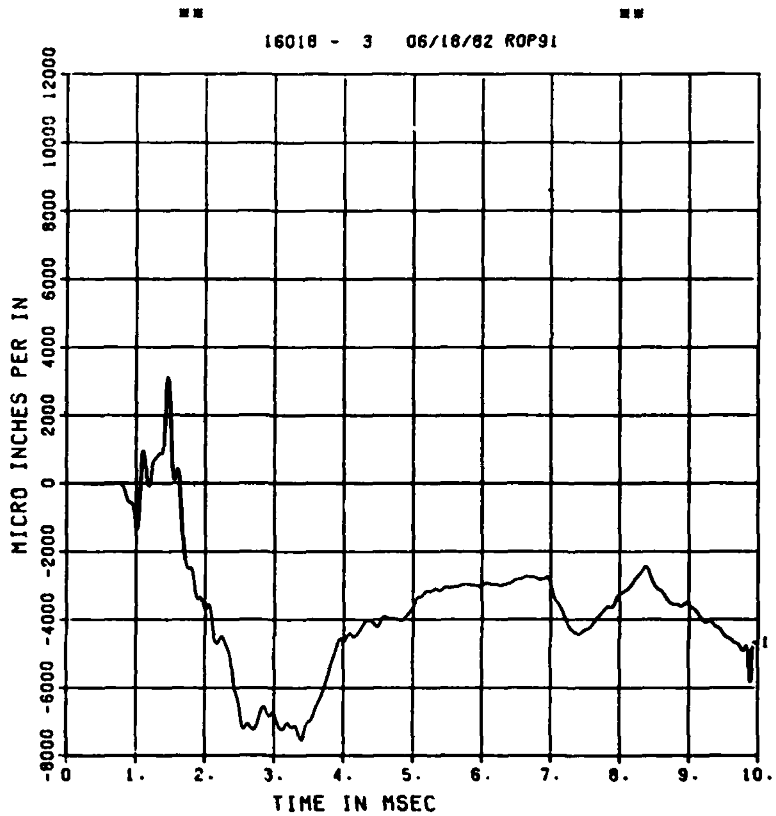

DYN SH II TEST 2
EI2
200000. HZ CAL= 14581.
LP4/0 70% CUTOFF= 9000. HZ

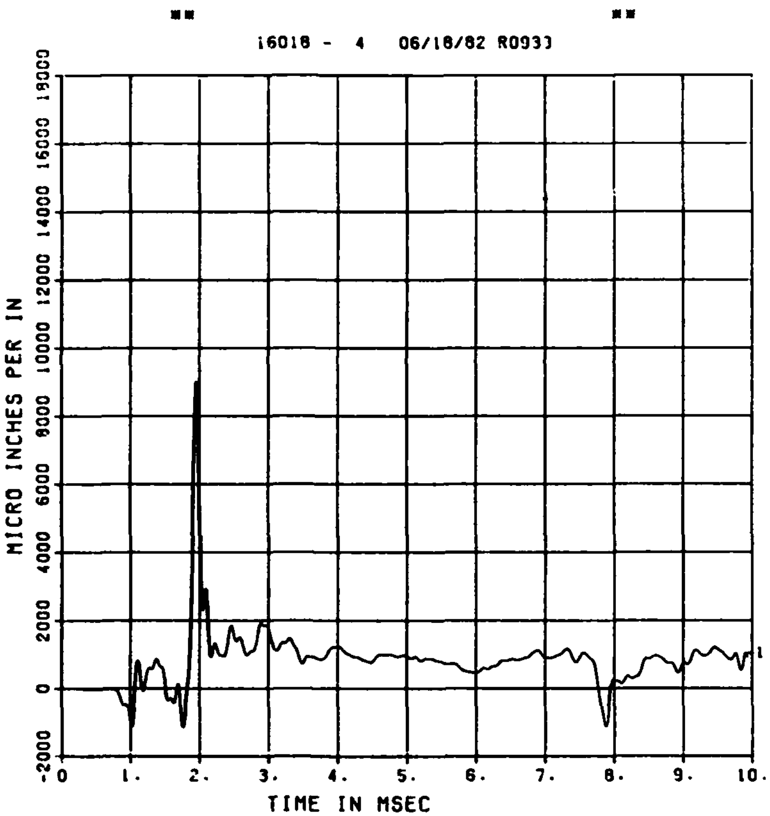

DYN SH II TEST 2
E03
200000. HZ CAL= 21625.
LP4/0 70% CUTOFF= 9000. HZ

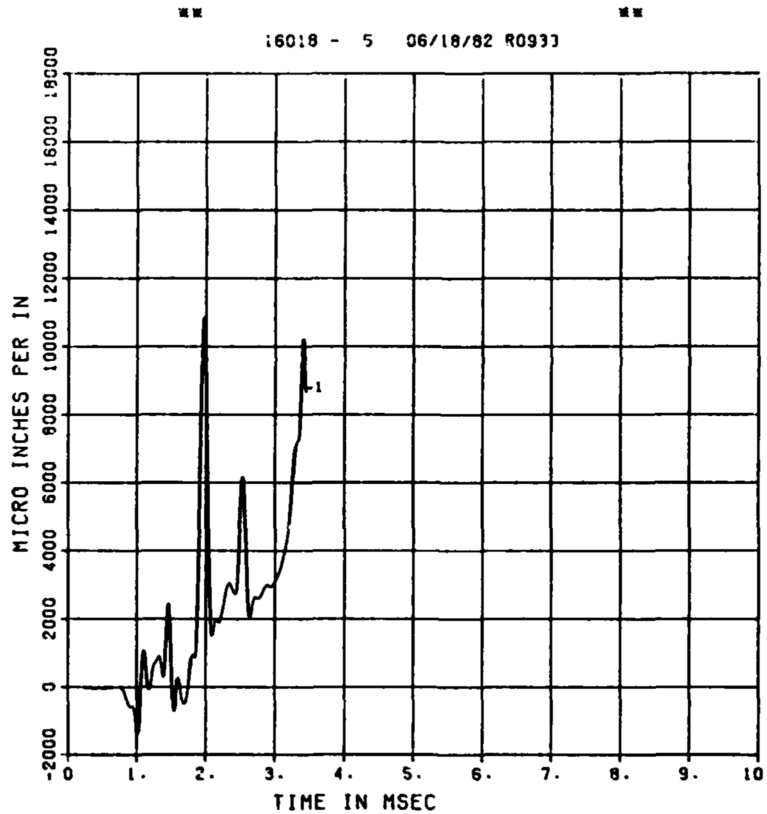

DYN SH II TEST 2
EI3
200000. HZ CAL= 21625.
LP4/0 70% CUTOFF= 9000. HZ

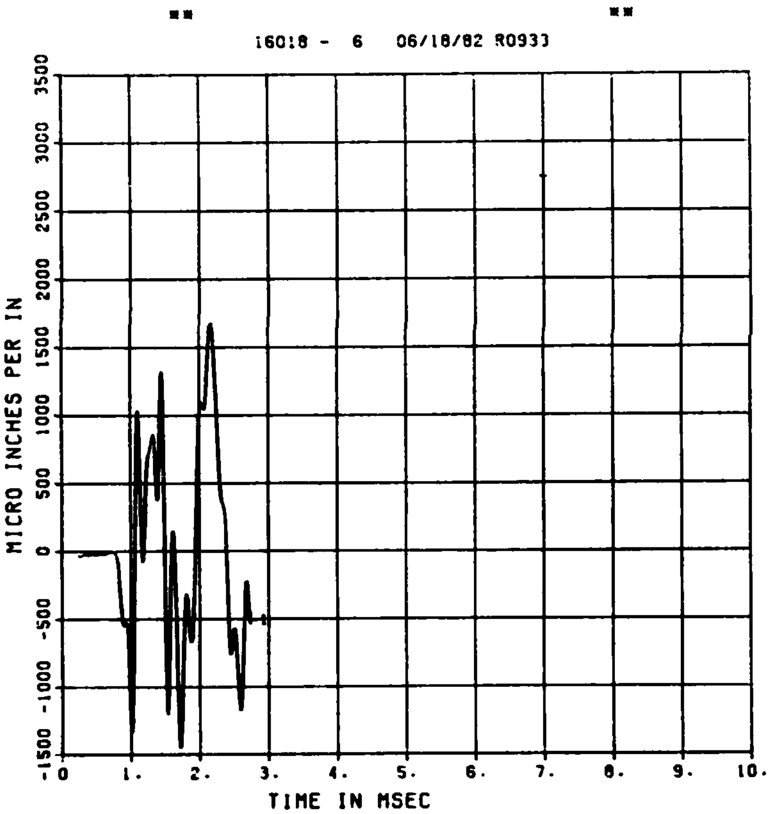

DYN SH II TEST 2
E04
200000. HZ CAL= 21625.

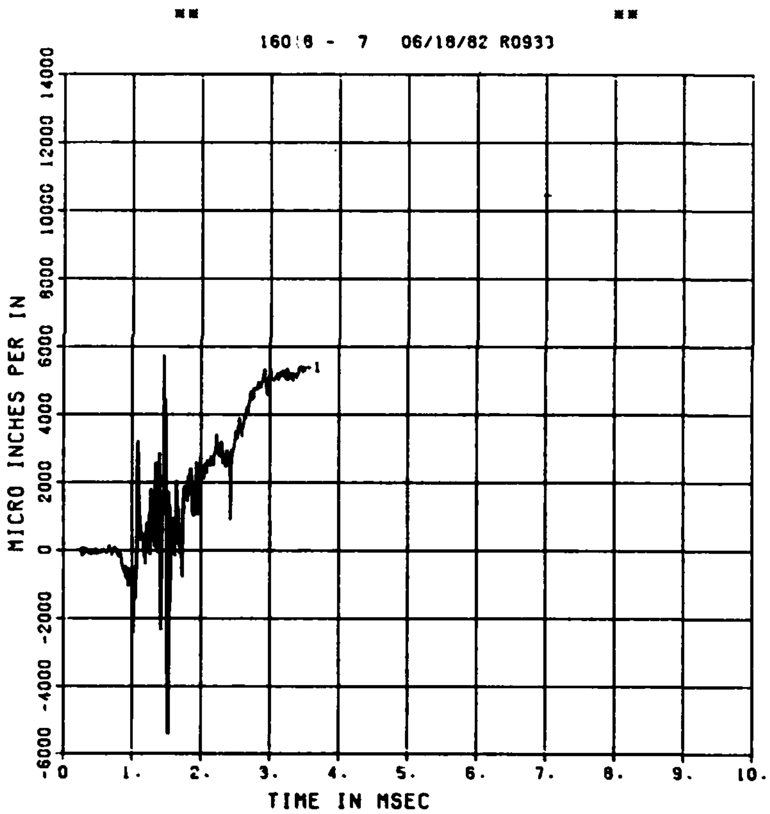

** PEAK VALUE IS 92 % UNDER CALIBRATION **

DYN SH II TEST 2
EI4
200000. HZ CAL= 21625.
LP4/0 70% CUTOFF= 9000. HZ

** **

16018 - 8 06/18/82 R0933

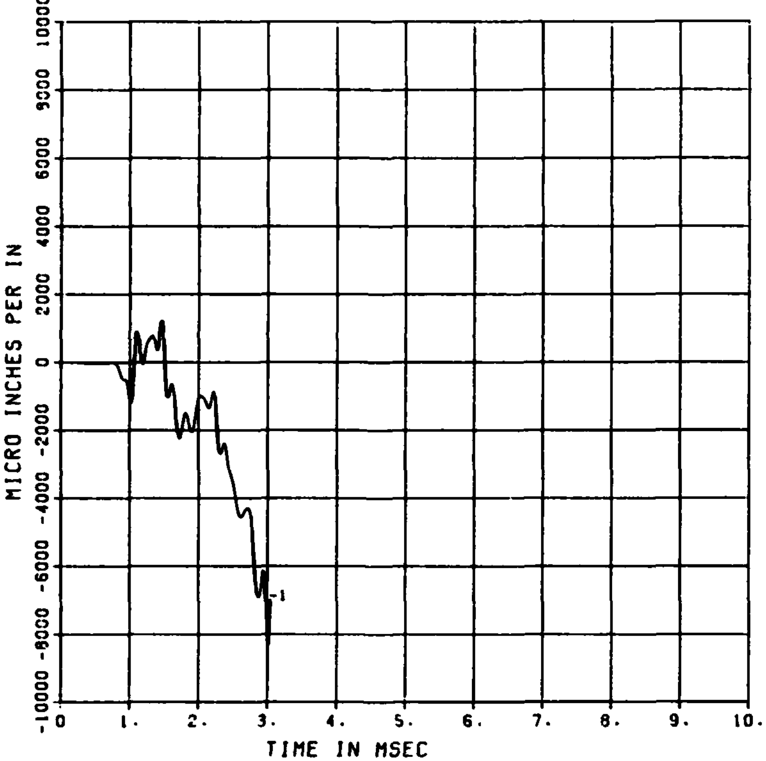

DYN SH II TEST 2
E05
200000. HZ CAL= 21625.
LP4/0 70% CUTOFF= 9000. HZ

** **

16018 - 9 06/18/82 R0933

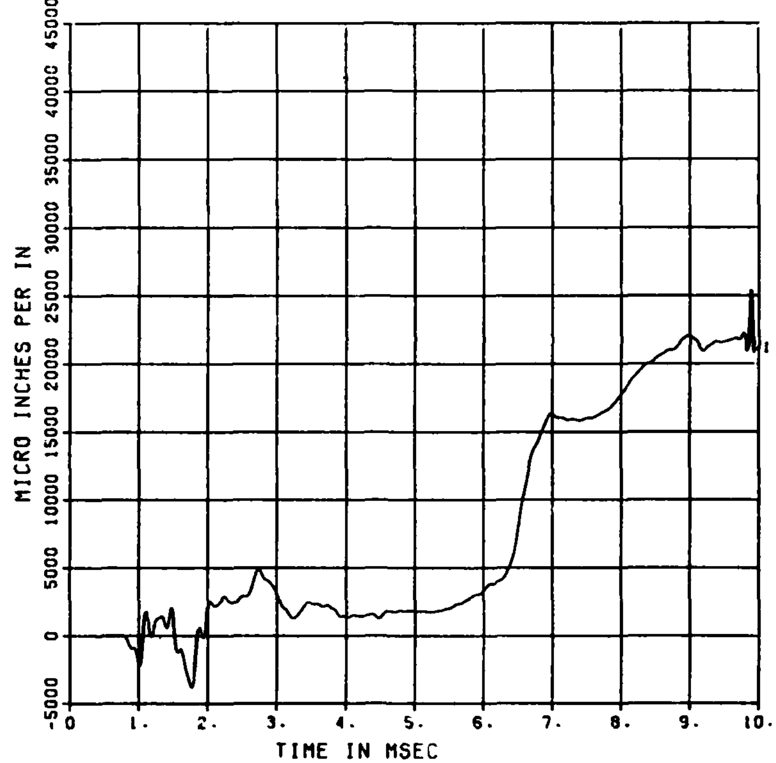

** PEAK VALUE IS 18 % OVER CALIBRATION **

DYN SH II TEST 2
EI5
200000. HZ CAL= 43705.
LP4/0 70% CUTOFF= 9000. HZ

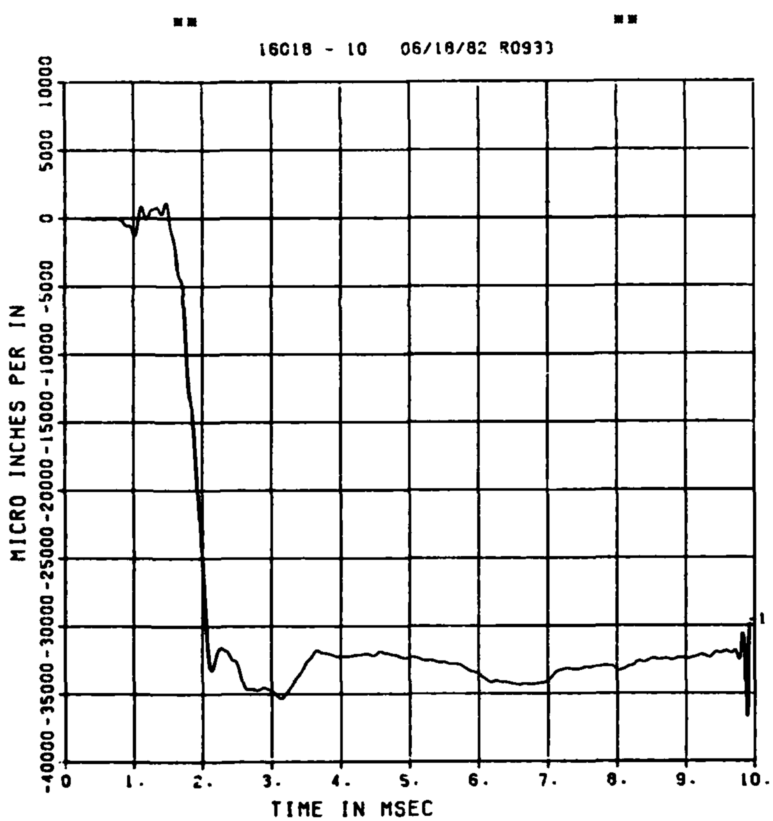

DYN SH II TEST 2
E06
200000. HZ CAL= 21625.
LP4/0 70% CUTOFF= 9000. HZ

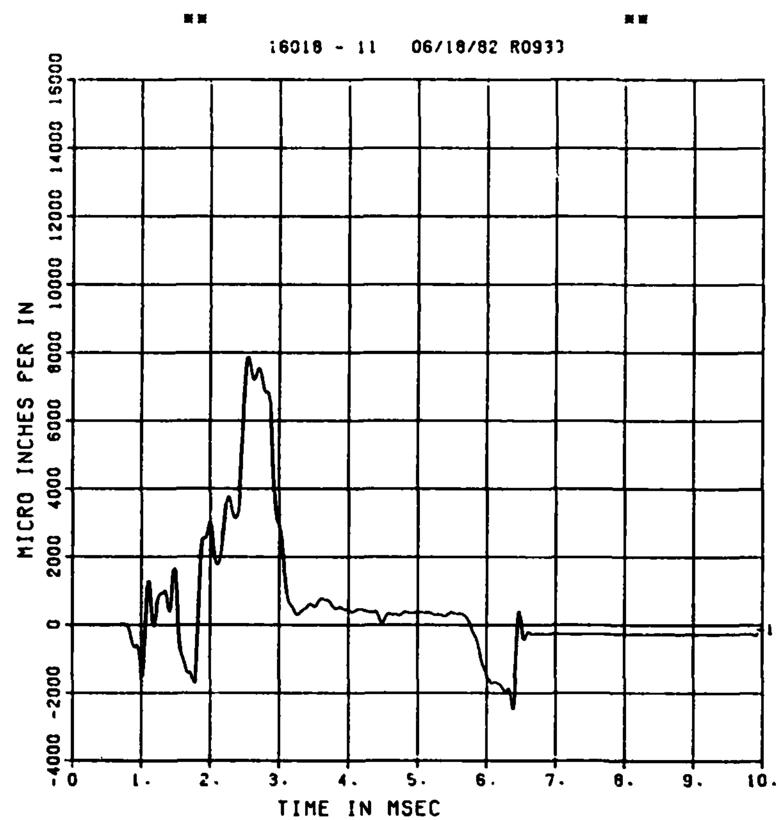

DYN SH II TEST 2
EI6
200000. HZ CAL= 43705.

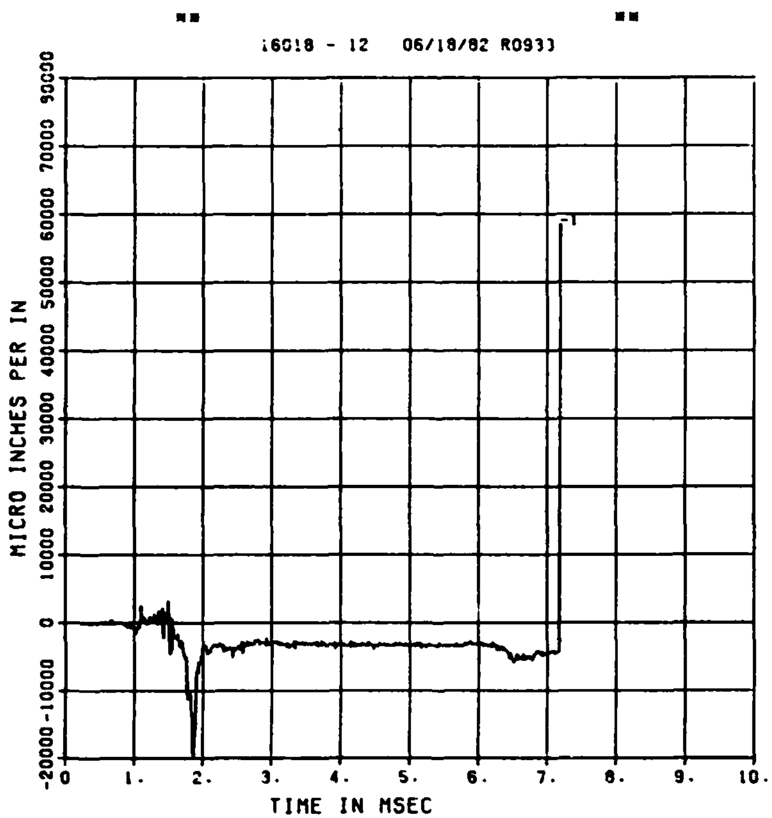

** PEAK VALUE IS 34 % OVER CALIBRATION **

DYN SH II TEST 3
BP1
200000. HZ CAL= 20825.

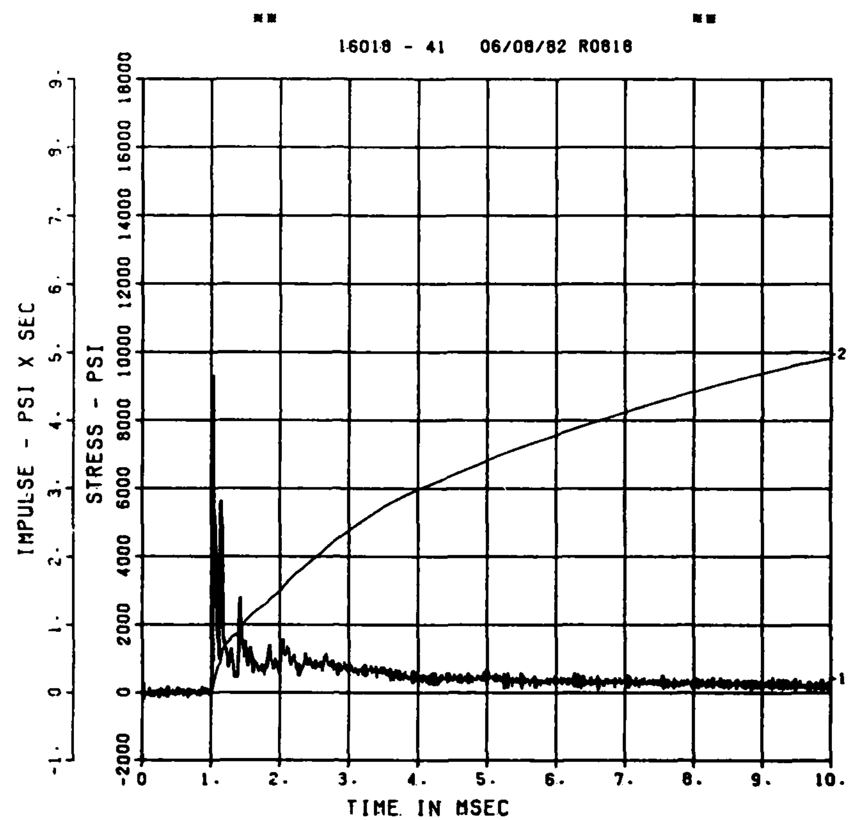

DYN SH II TEST 3
BP1
200000. HZ CAL= 20825.

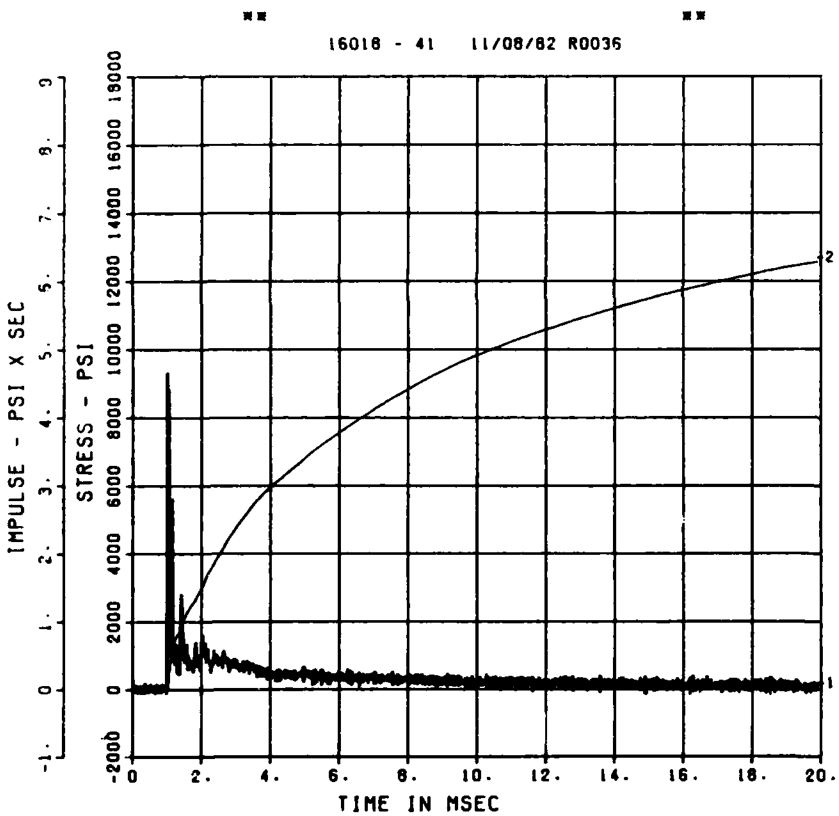

DYN SH II TEST 3
BP2
200000. HZ CAL= 20155.

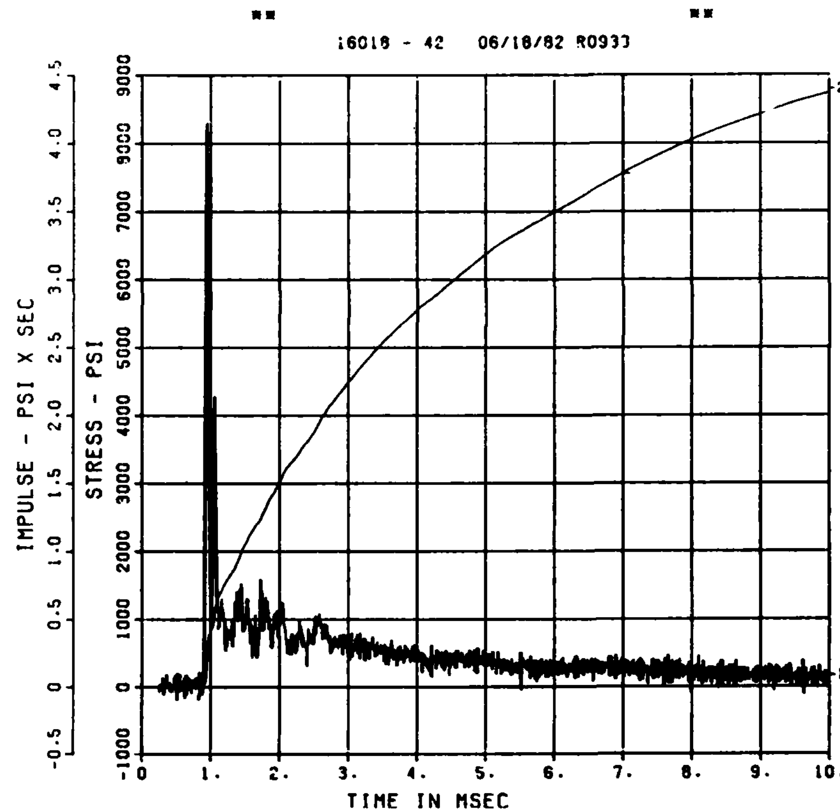

DYN SH II TEST 3
BP2
200000. HZ CAL= 20155.

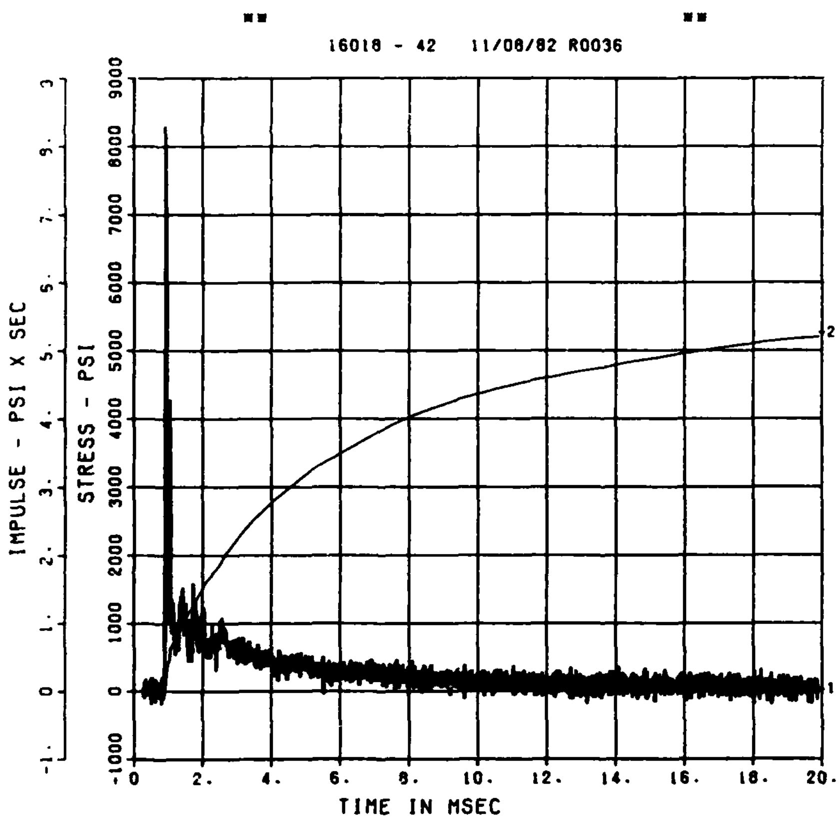

DYN SH II TEST 3
BP3
200000. HZ CAL= 20568.

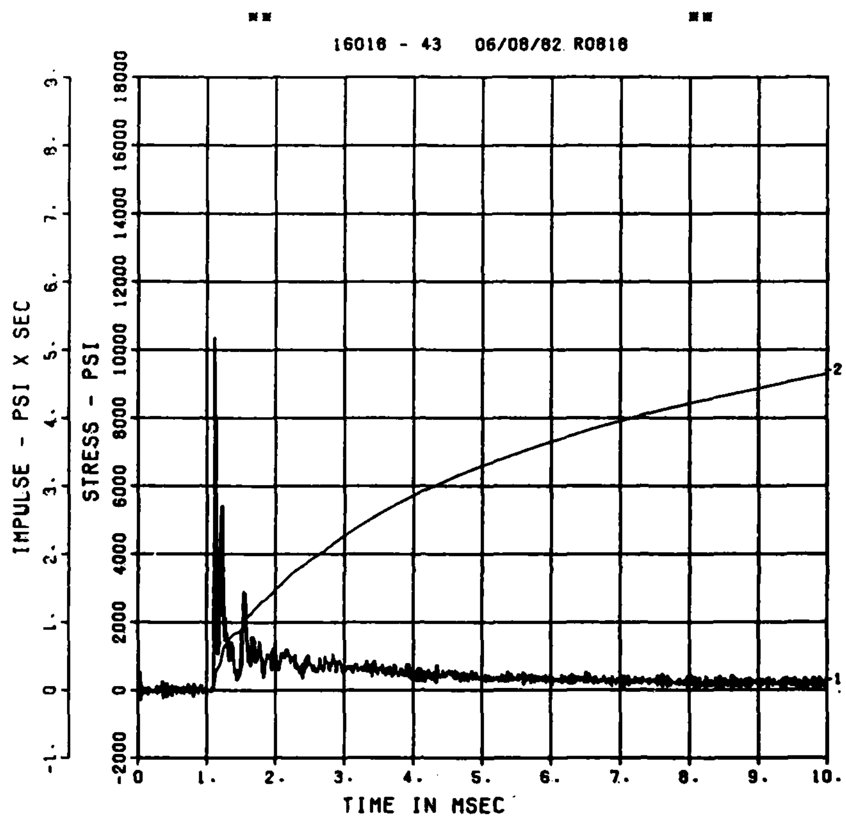

DYN SH II TEST 3
BP3
200000. HZ CAL= 20568.

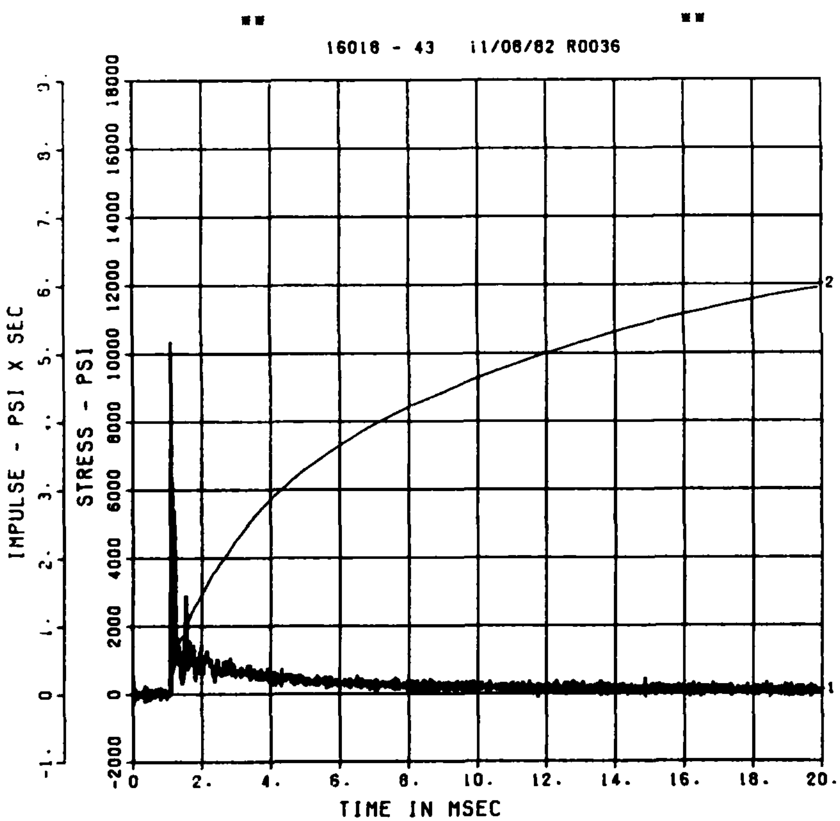

DYN SH II TEST 3
BP4
200000. HZ CAL= 24163.
LP4/0 70% CUTOFF= 9000. HZ

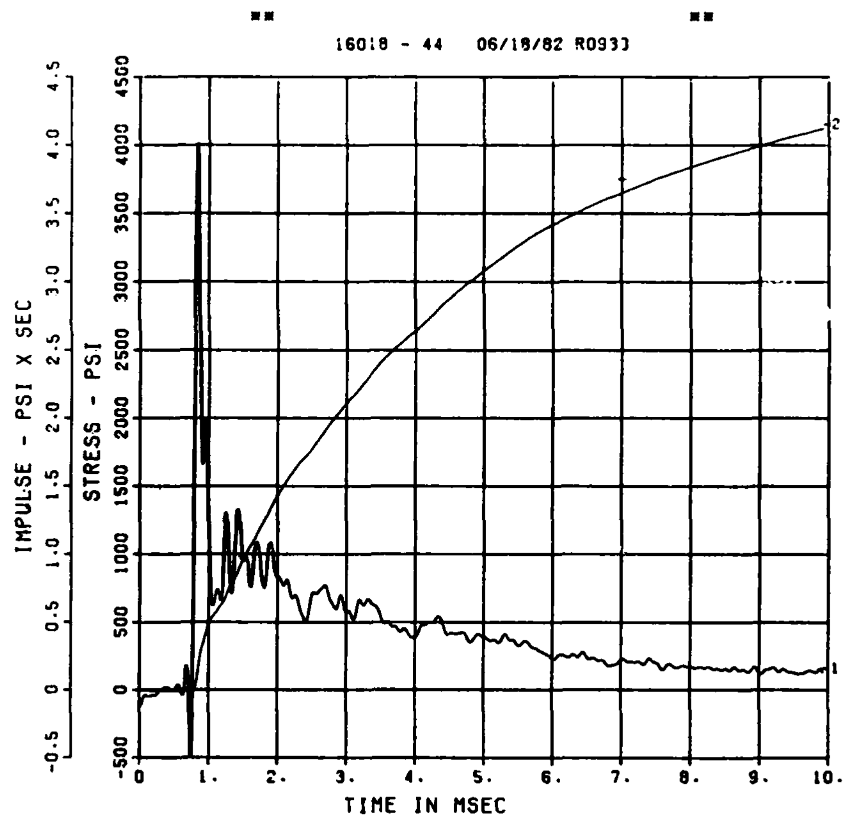

** PEAK VALUE IS 83 % UNDER CALIBRATION **

DYN SH II TEST 3
BP4
200000. HZ CAL= 24163.
LP4/0 70% CUTOFF= 9000. HZ

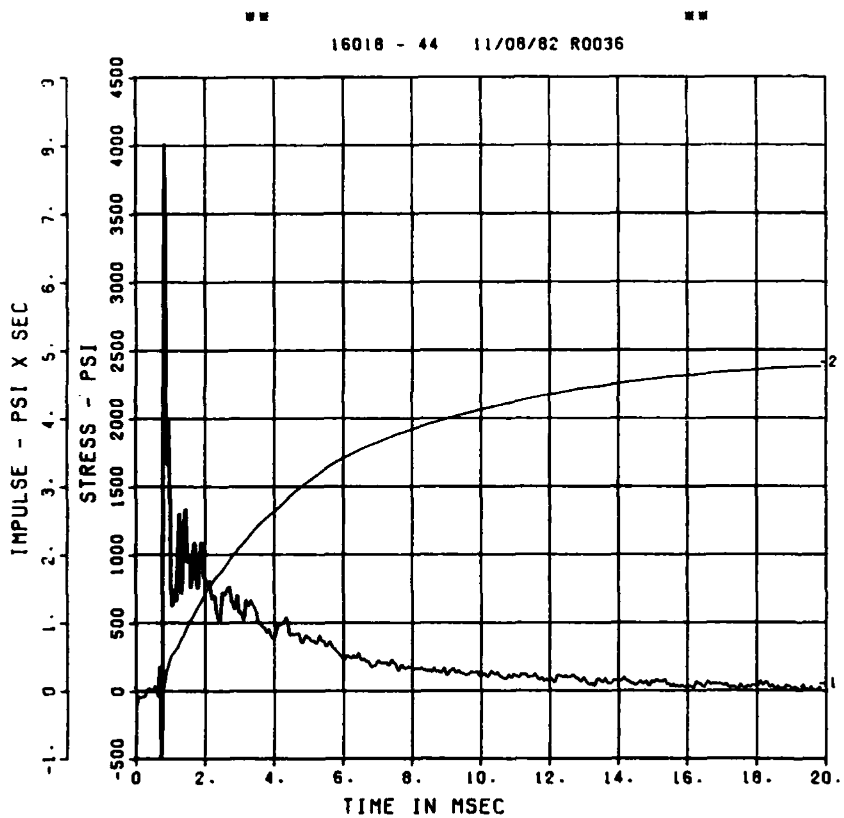

** PEAK VALUE IS 83 % UNDER CALIBRATION **

DYN SH II TEST 3
IF1
200000. HZ CAL= 8604.
LP4/0 70% CUTOFF= 9000. HZ

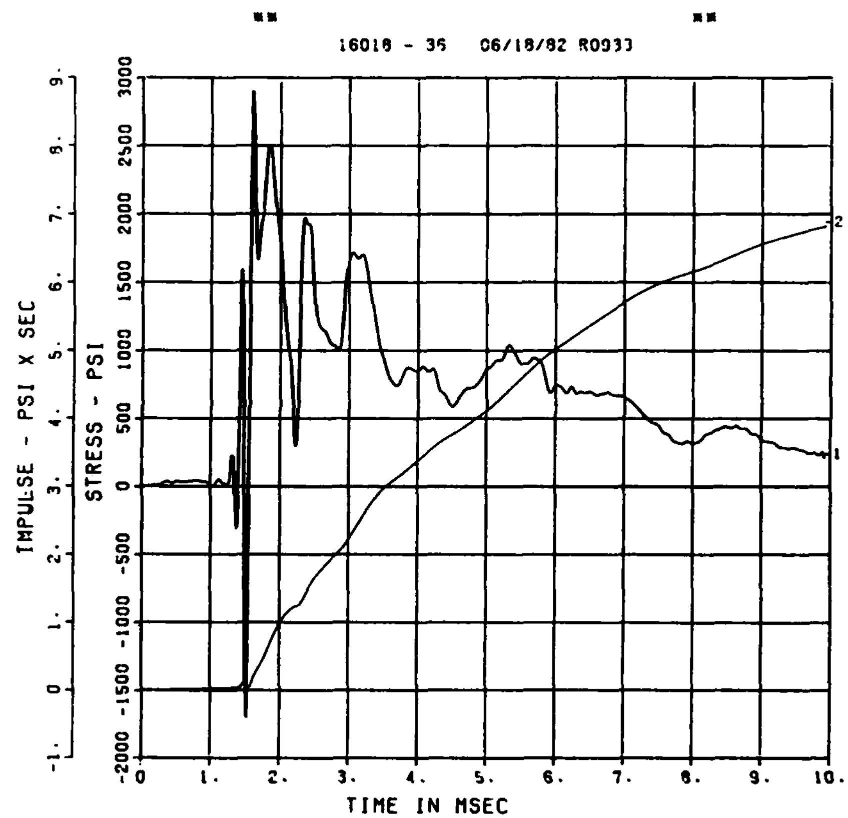

DYN SH II TEST 3
IF2
200000. HZ CAL= 8947.
LP4/O 70% CUTOFF= 9000. HZ

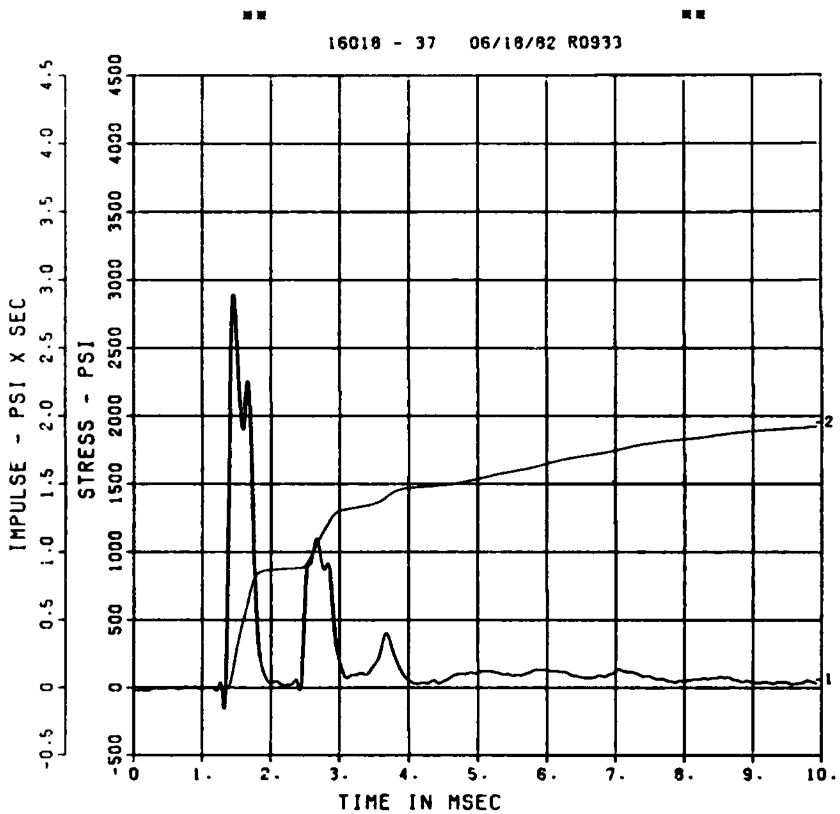

DYN SH II TEST 3
IF3
200000. HZ CAL= 8487.
LP4/O 70% CUTOFF= 9000. HZ

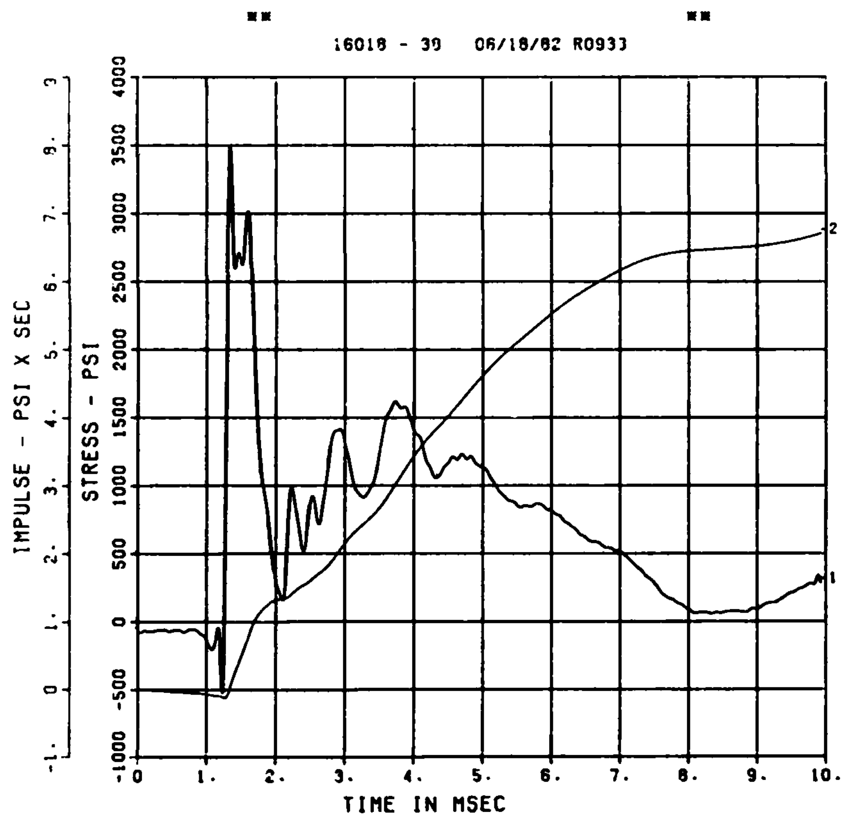

DYN SH II TEST 3
IF4
200000. HZ CAL= 6152.

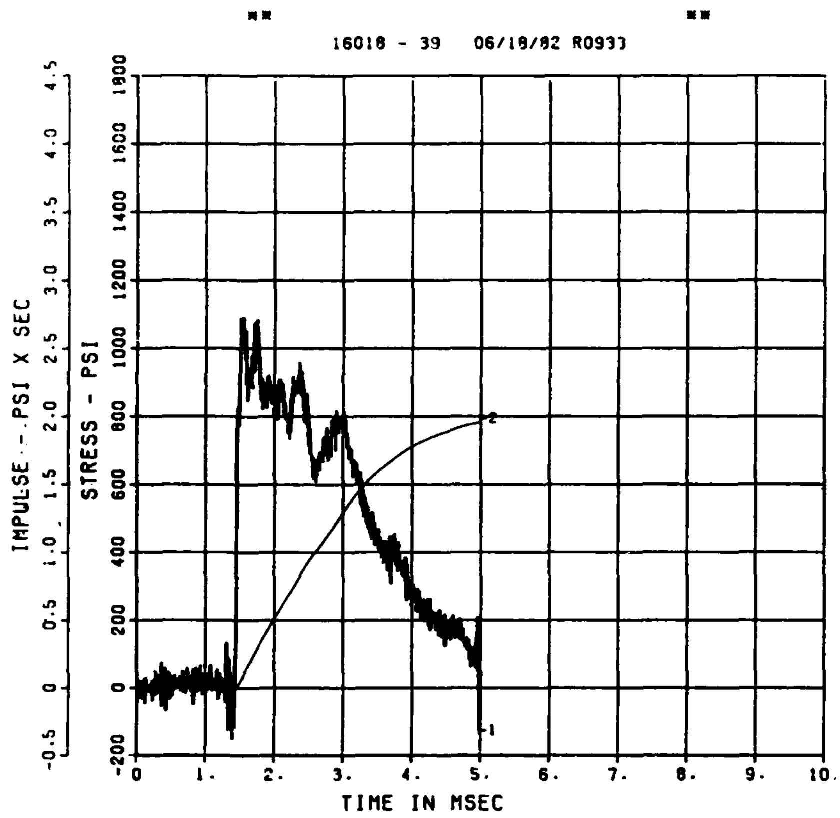

** PEAK VALUE IS 82 % UNDER CALIBRATION **

DYN SH II TEST 3
IF5
200000. HZ CAL= 11417.
LP4/0 70% CUTOFF= 9000. HZ

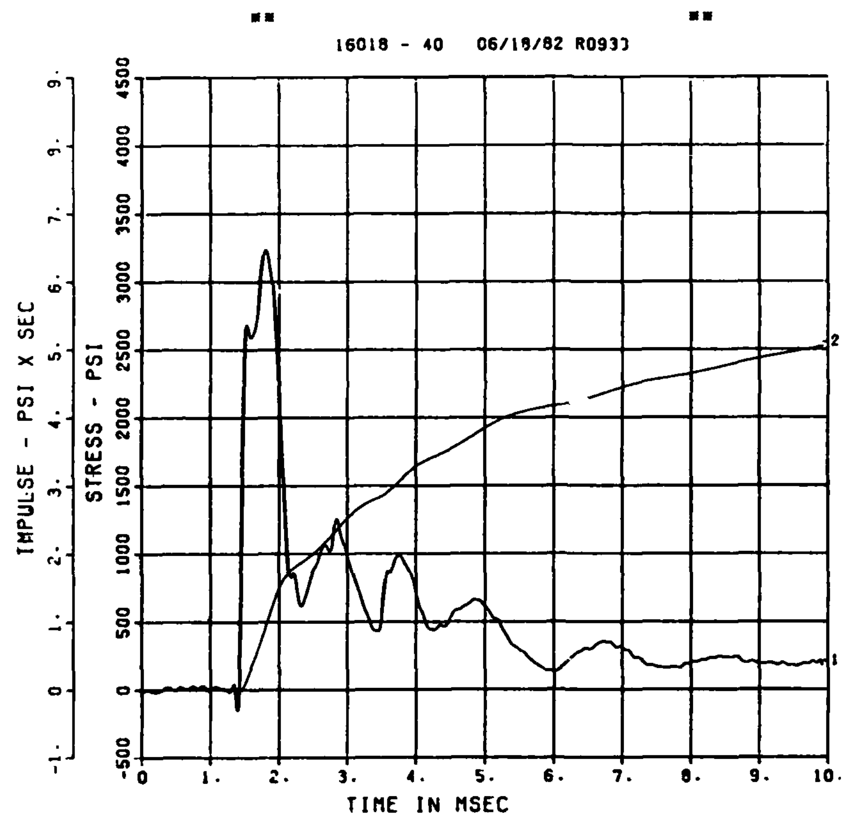

DYN SH II TEST 3
SE1
200000. HZ CAL= 10594.
LP4/0 70% CUTOFF= 9000. HZ

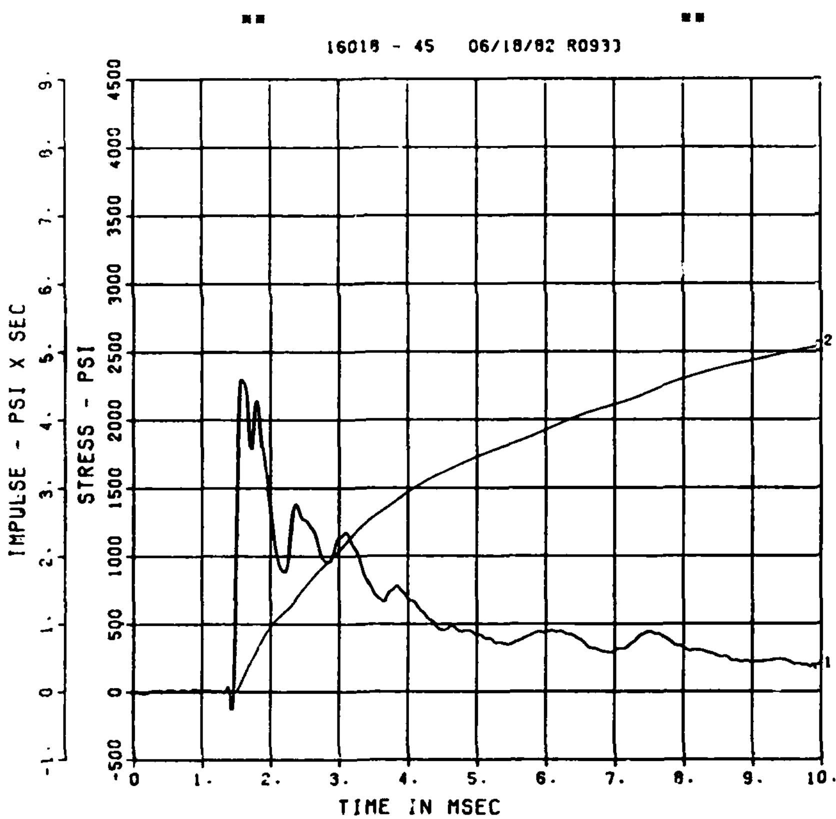

DYN SH II TEST 3
SE2
200000. HZ CAL= 10851.
LP4/0 70% CUTOFF= 9000. HZ

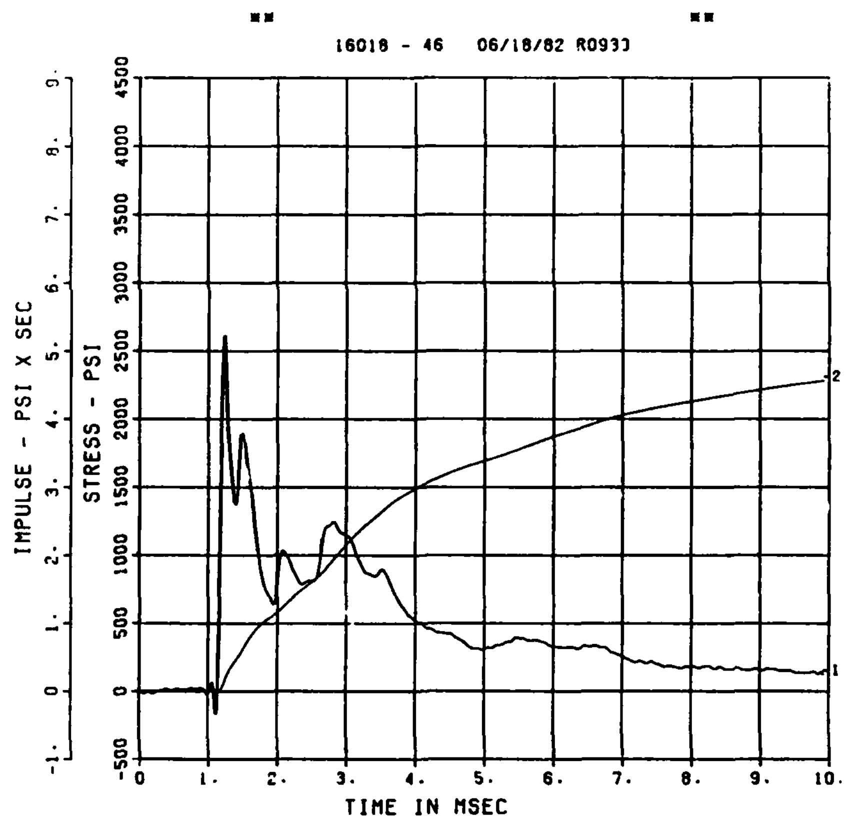

DYN SH II TEST 3
E01
200000. HZ CAL= 21625.

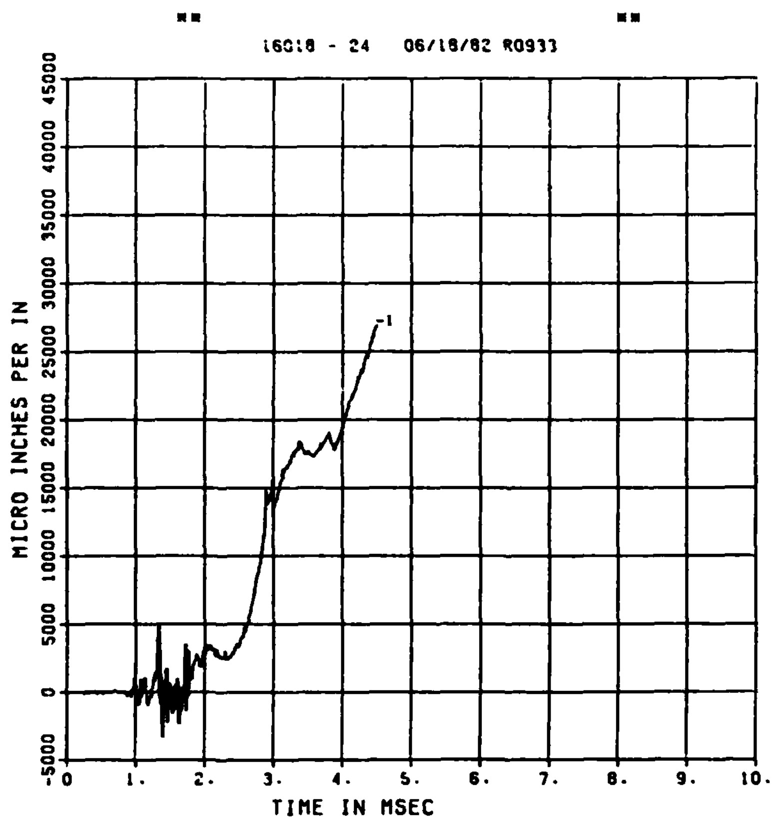

** PEAK VALUE IS 25 % OVER CALIBRATION **

DYN SH II TEST 3
EI1
200000. HZ CAL= 21625.

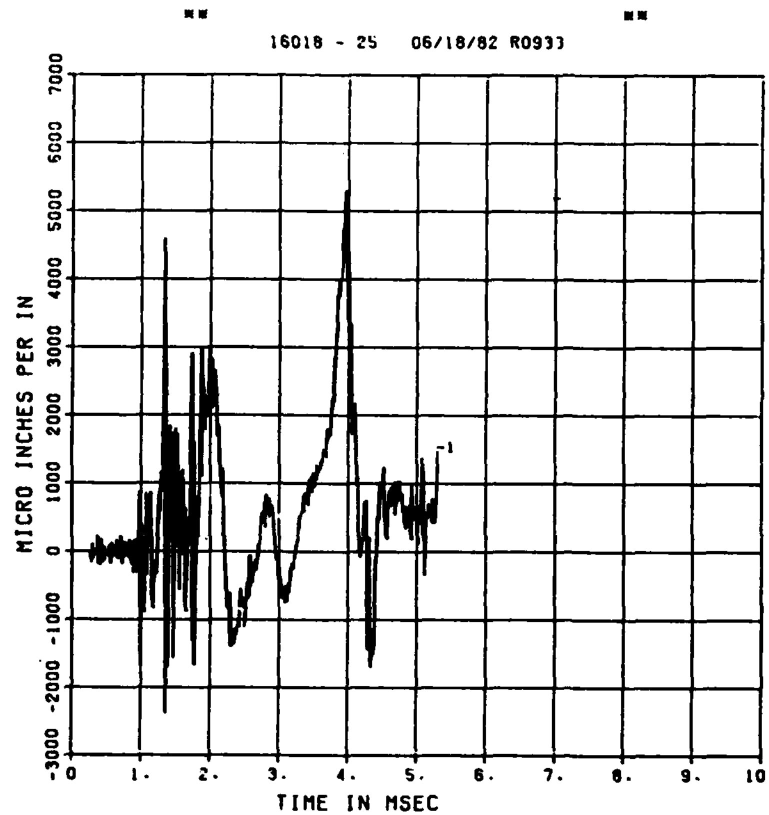

DYN SH II TEST 3
E02
200000. HZ CAL= 14581.
LP4/O 70% CUTOFF= 9000. HZ

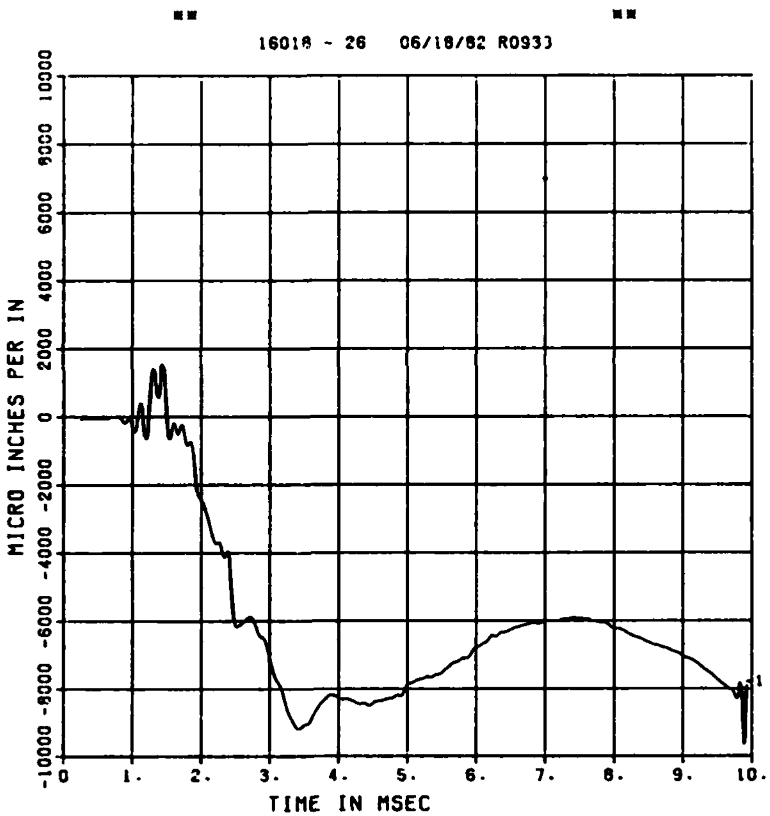

DYN SH II TEST 3
EI2
200000. HZ CAL= 14581.

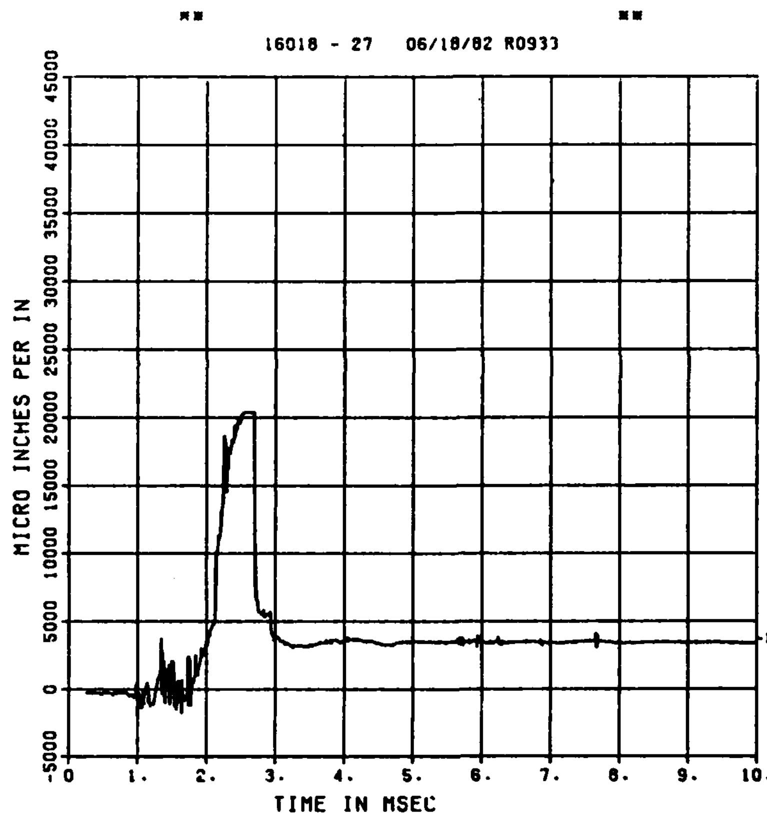

** PEAK VALUE IS 40 % OVER CALIBRATION **

DYN SH II TEST 3
E03
200000. HZ CAL= 21625.

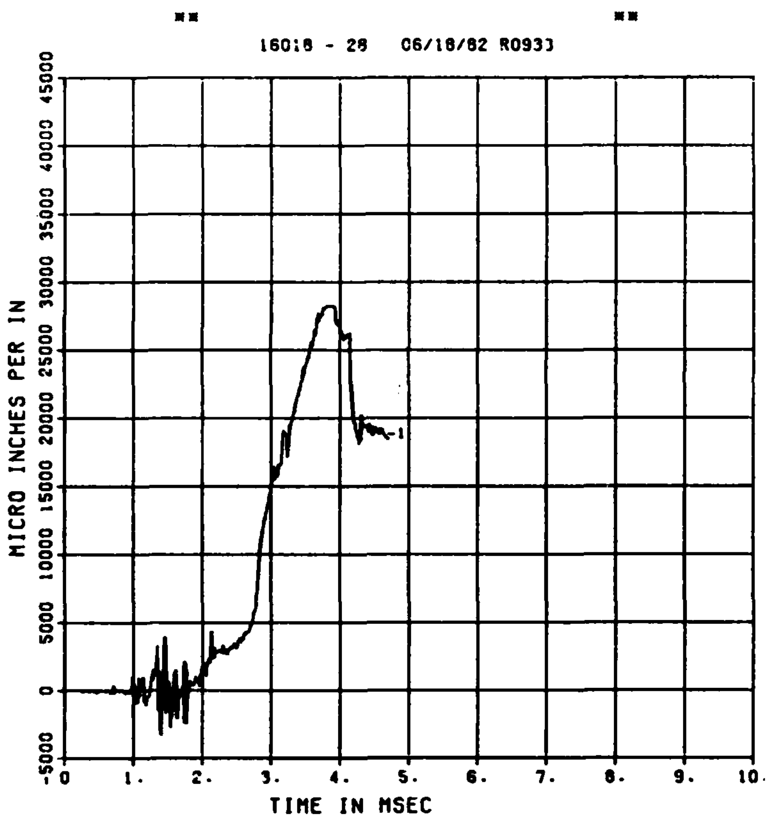

** PEAK VALUE IS 31 % OVER CALIBRATION **

DYN SH II TEST 3
EI3
200000. HZ CAL= 21625.

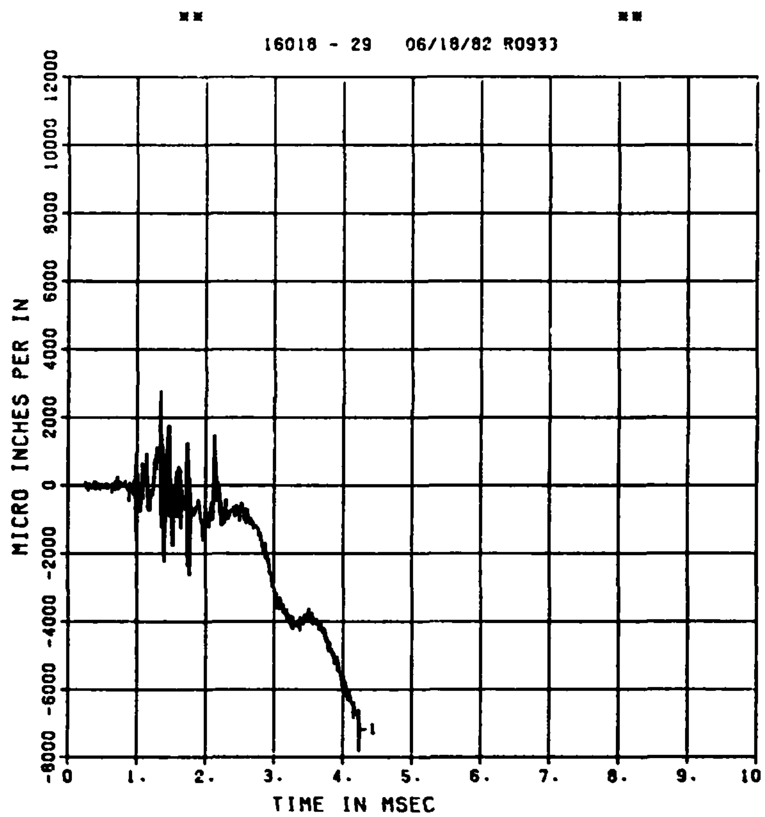

DYN SH II TEST 3
E04
200000. HZ CAL= 21625.

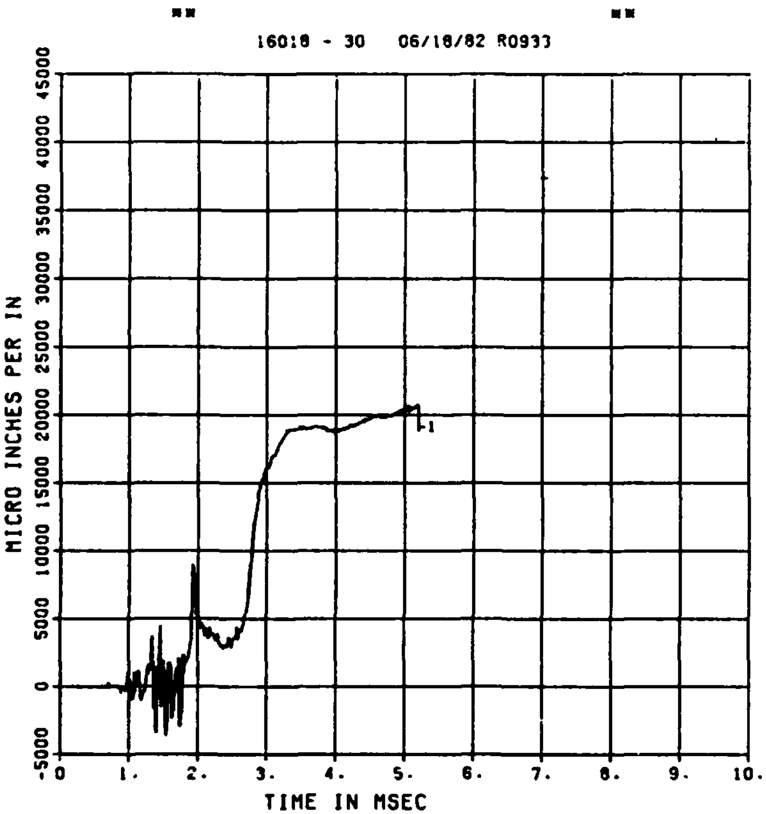

DYN SH II TEST 3
EI4
200000. HZ CAL= 21625.

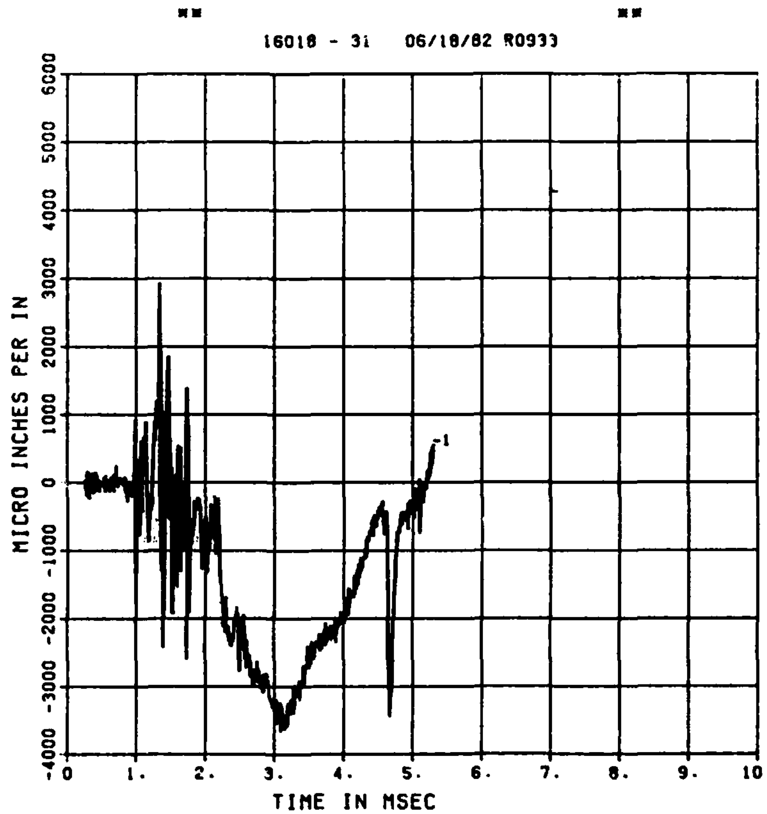

** PEAK VALUE IS 83 % UNDER CALIBRATION **

DYN SH II TEST 3
E05
200000. HZ CAL= 21625.
LP4/0 70% CUTOFF= 9000. HZ

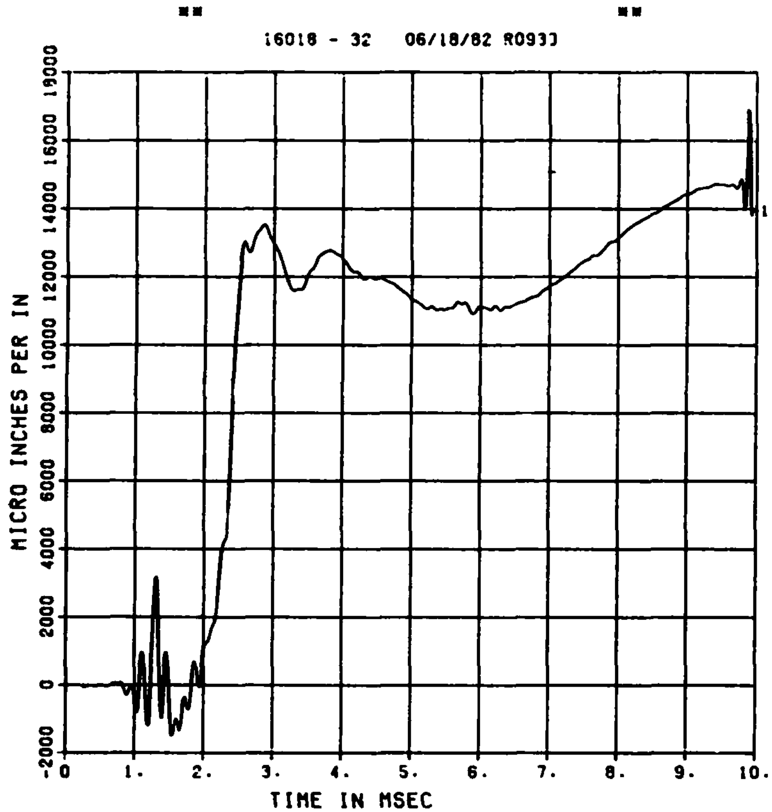

DYN SH II TEST 3
EI5
200000. HZ CAL= 43705.
LP4/0 70% CUTOFF= 9000. HZ

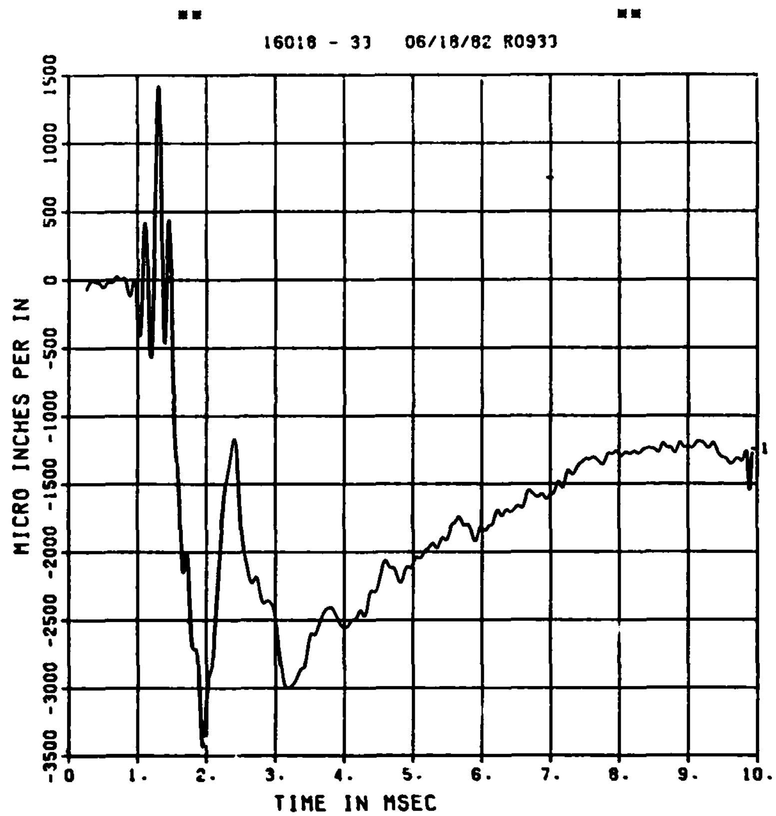

** PEAK VALUE IS 92 % UNDER CALIBRATION **

DYN SH II TEST 3
E06
200000. HZ CAL= 21625.

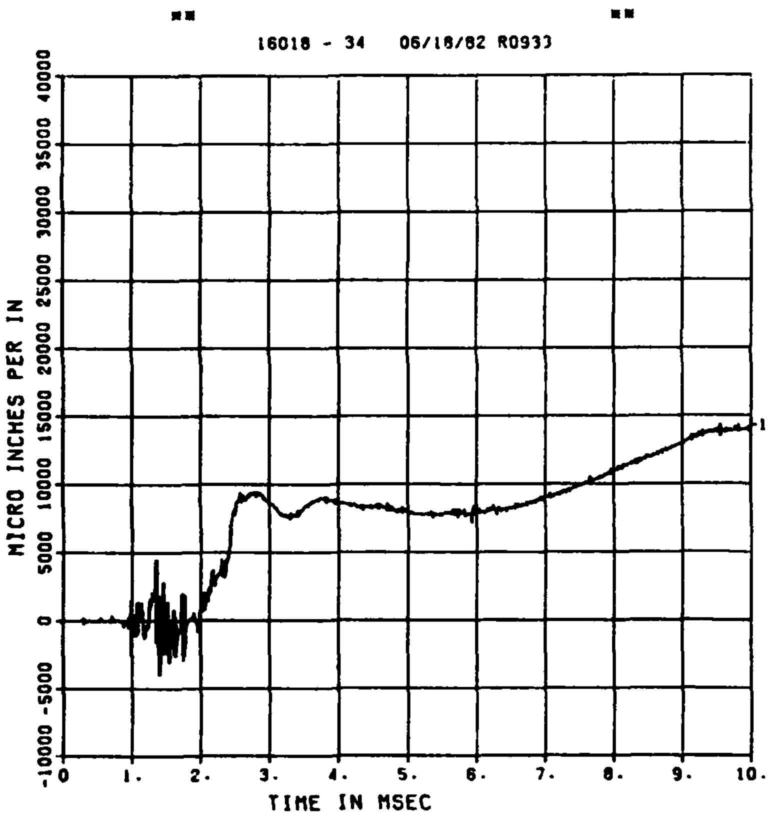

DYN SH II TEST 3
EI6
200000. HZ CAL= 43705.
LP4/0 70% CUTOFF= 9000. HZ

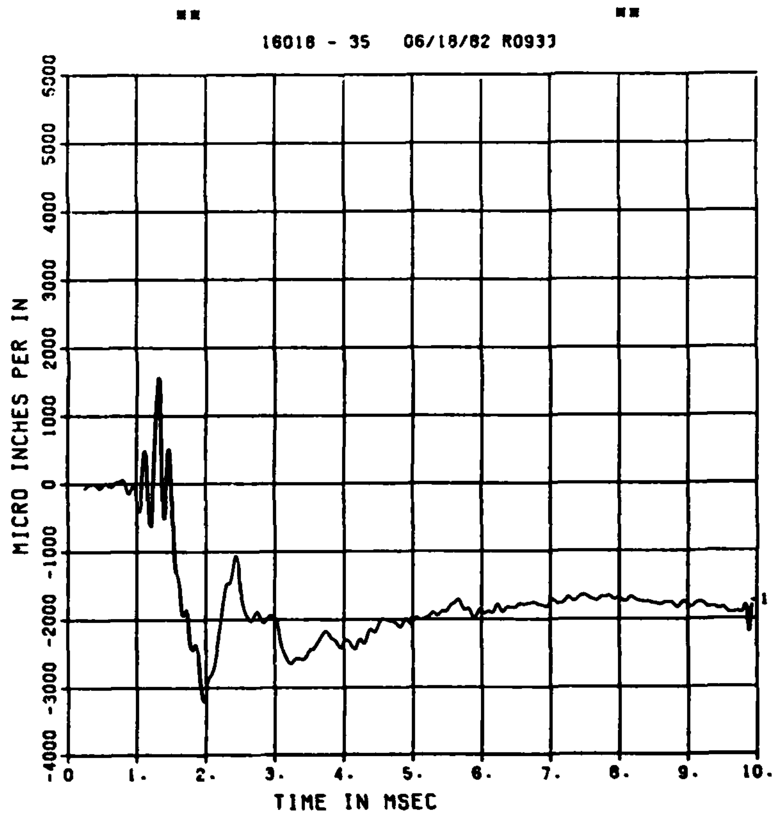

** PEAK VALUE IS 93 % UNDER CALIBRATION **

DYN SH II TEST 4
BP1
200000. HZ CAL= 29975.

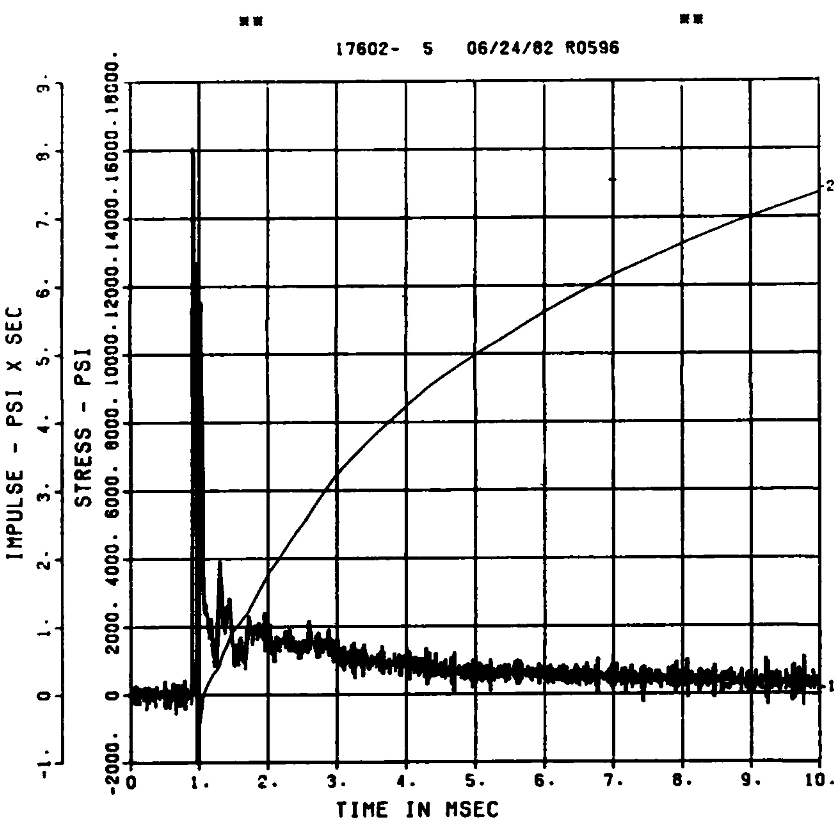

** PEAK VALUE IS 43 % OVER CALIBRATION **

DYN SH II TEST 4
BP1
200000. HZ CAL= 29975.

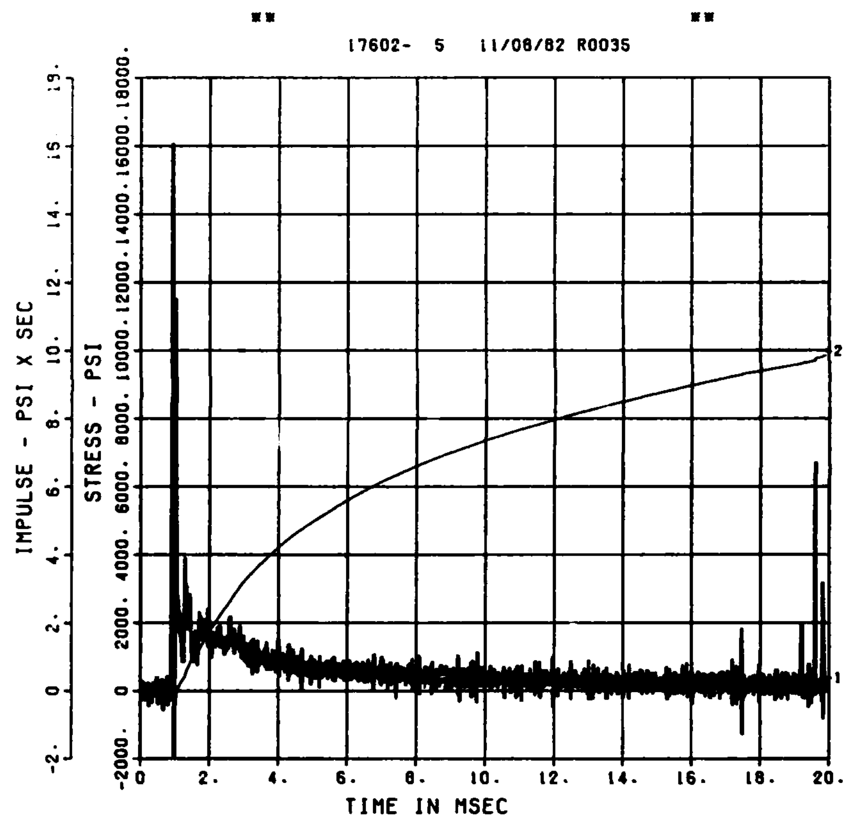

** PEAK VALUE IS 43 % OVER CALIBRATION **

DYN SH II TEST 4
BP2
200000. HZ CAL= 28883.

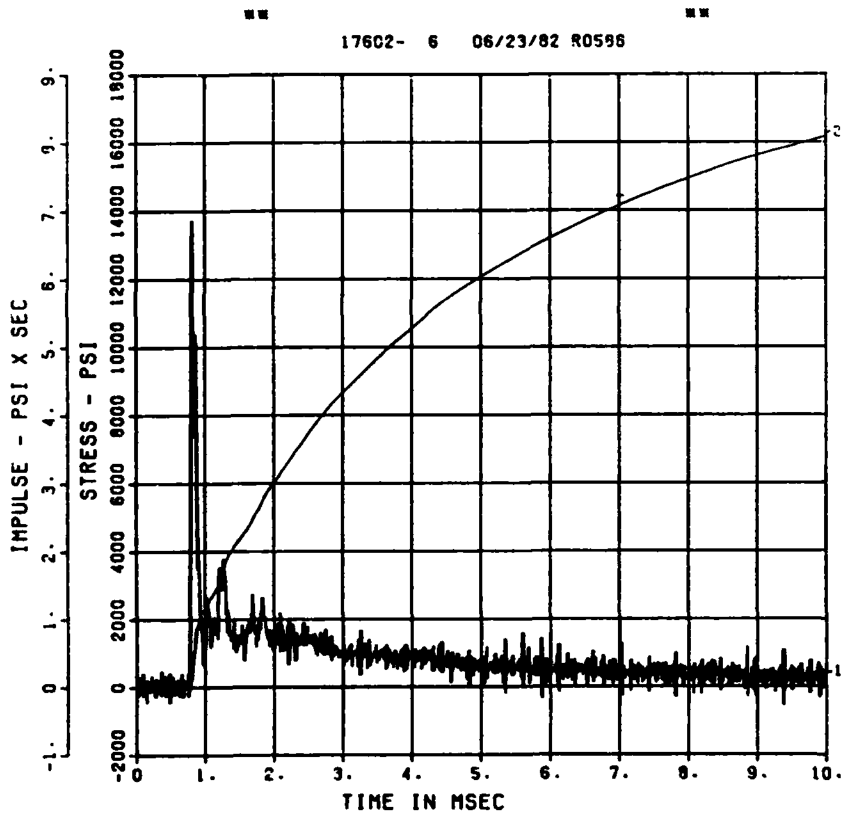

DYN SH II TEST 4
BP2
200000. HZ CAL= 28883.

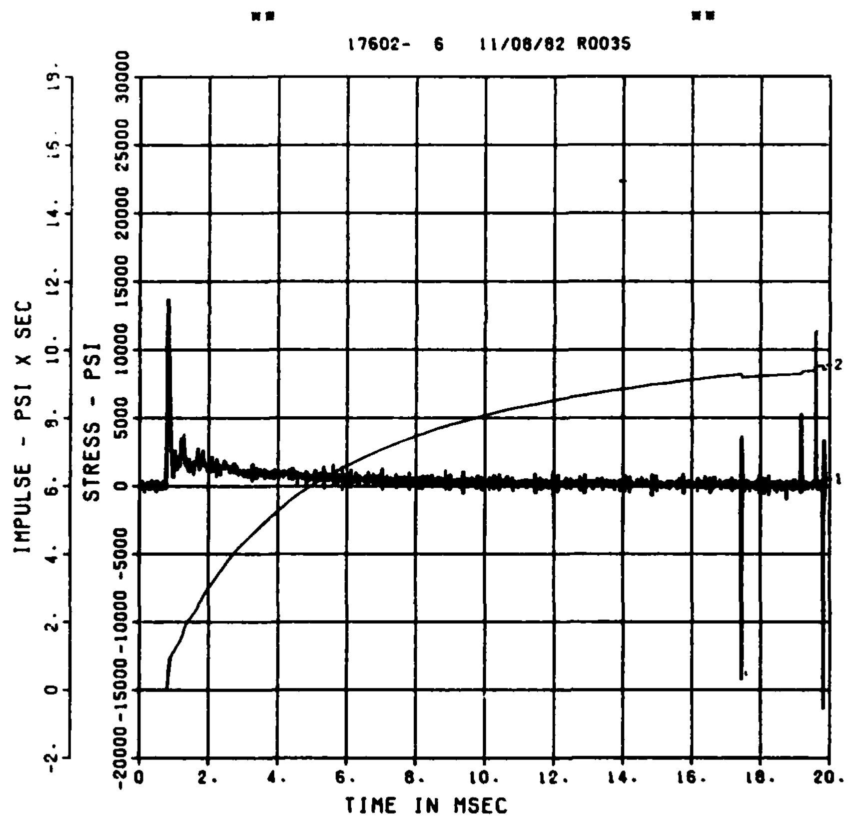

DYN SH II TEST 4
BP3
200000. HZ CAL= 29424.

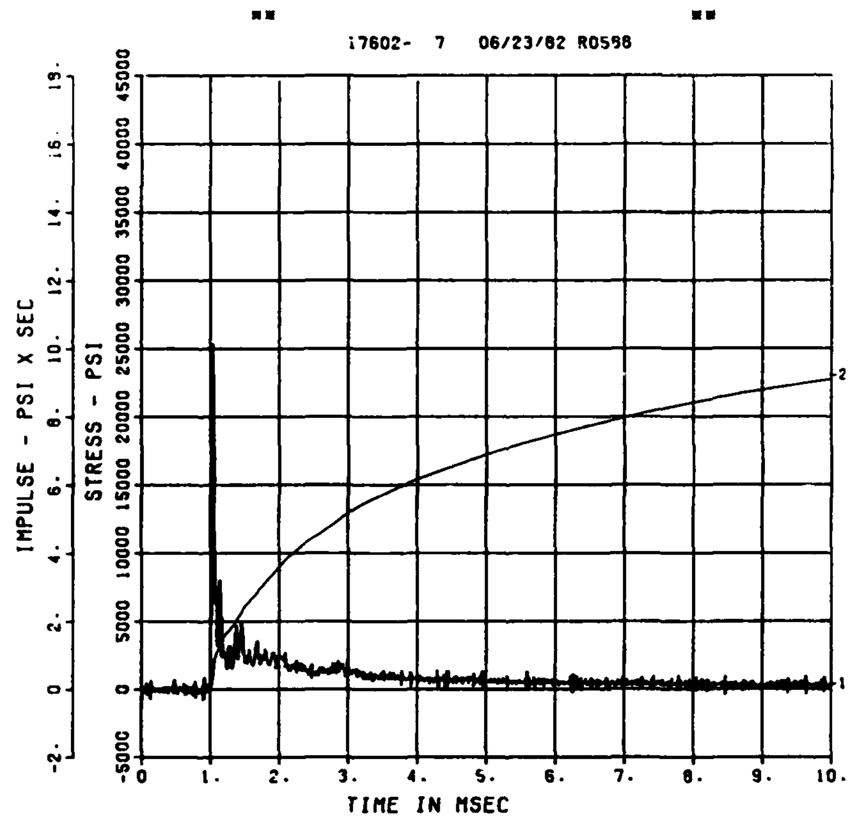

DYN SH II TEST 4
BP3
200000. HZ CAL= 29424.

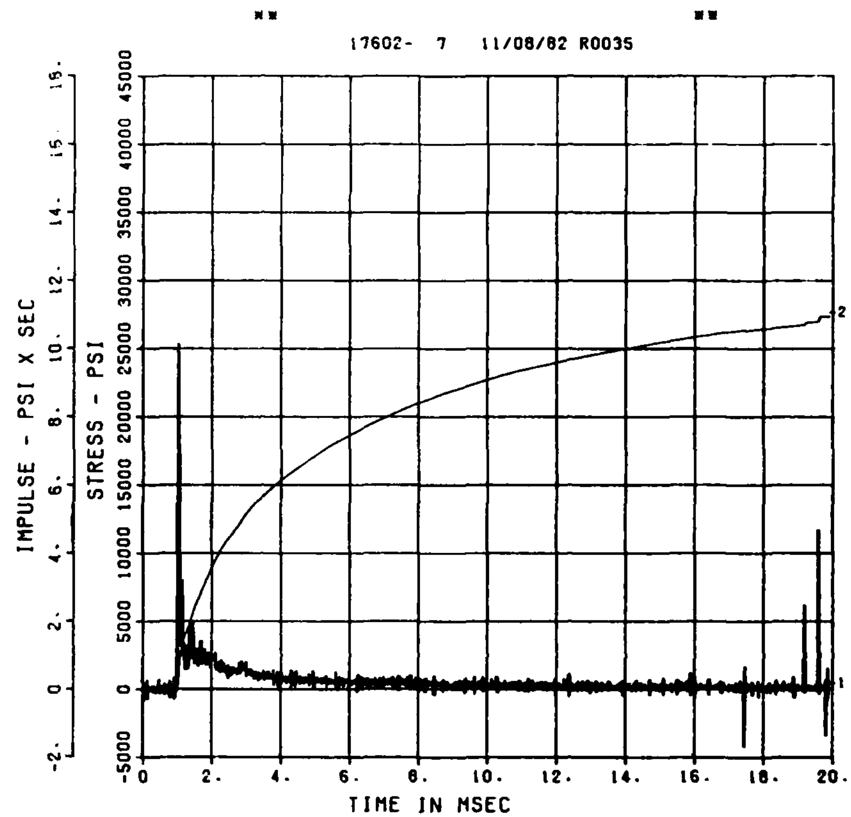

DYN SH II TEST 4
BP4
200000. HZ CAL= 23632.

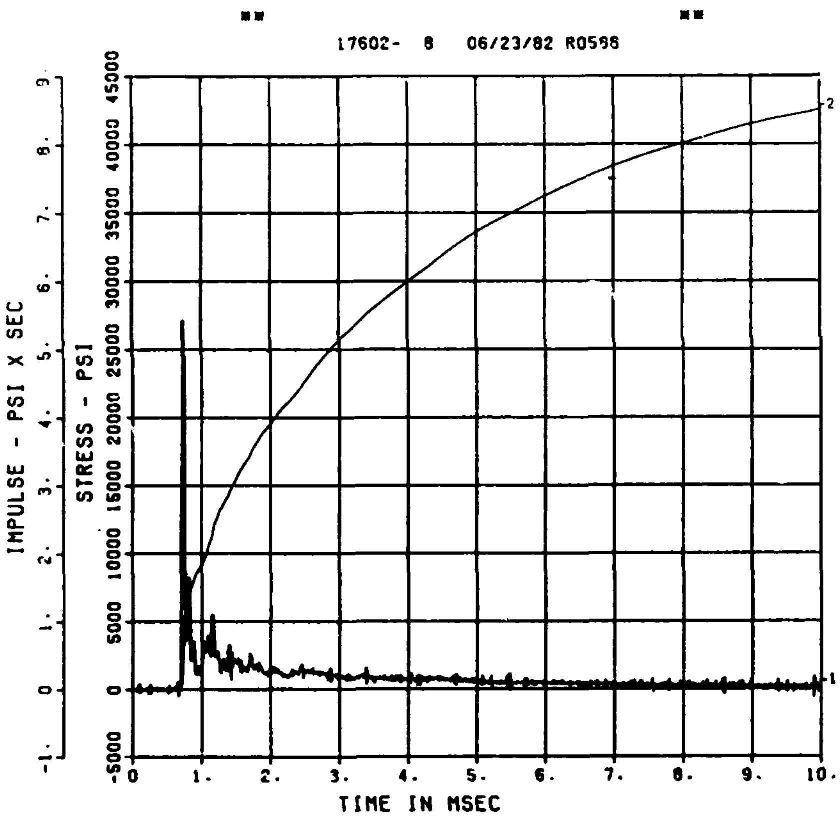

** PEAK VALUE IS 15 % OVER CALIBRATION **

DYN SH II TEST 4
BP4
200000. HZ CAL= 23632.

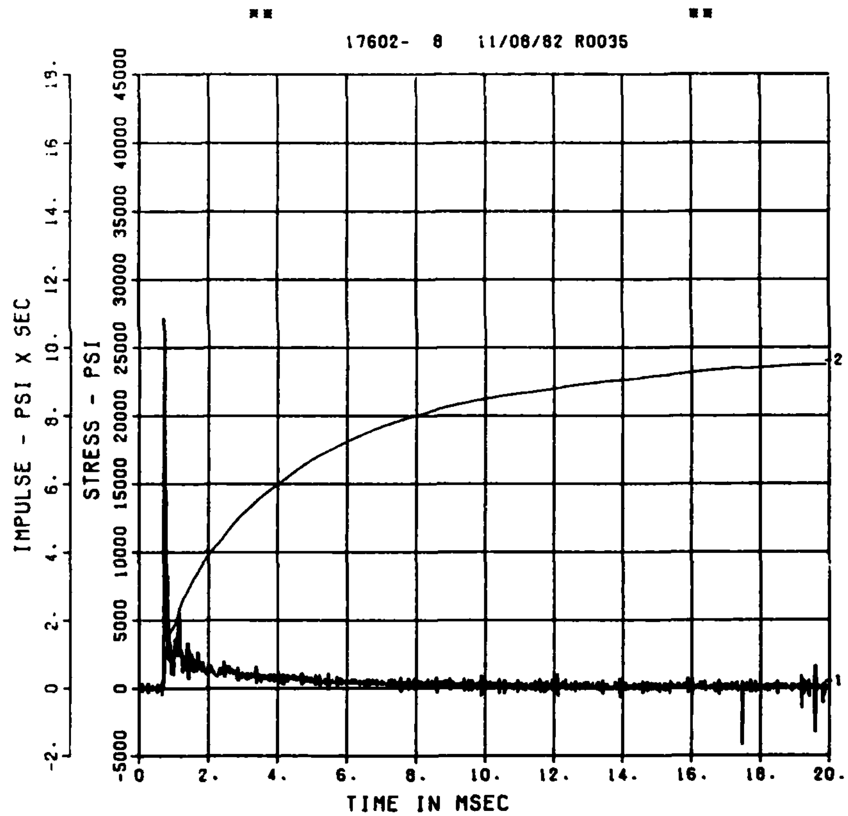

** PEAK VALUE IS 15 % OVER CALIBRATION **

DYN SH II TEST 4
IF1
200000. HZ CAL= 11815.

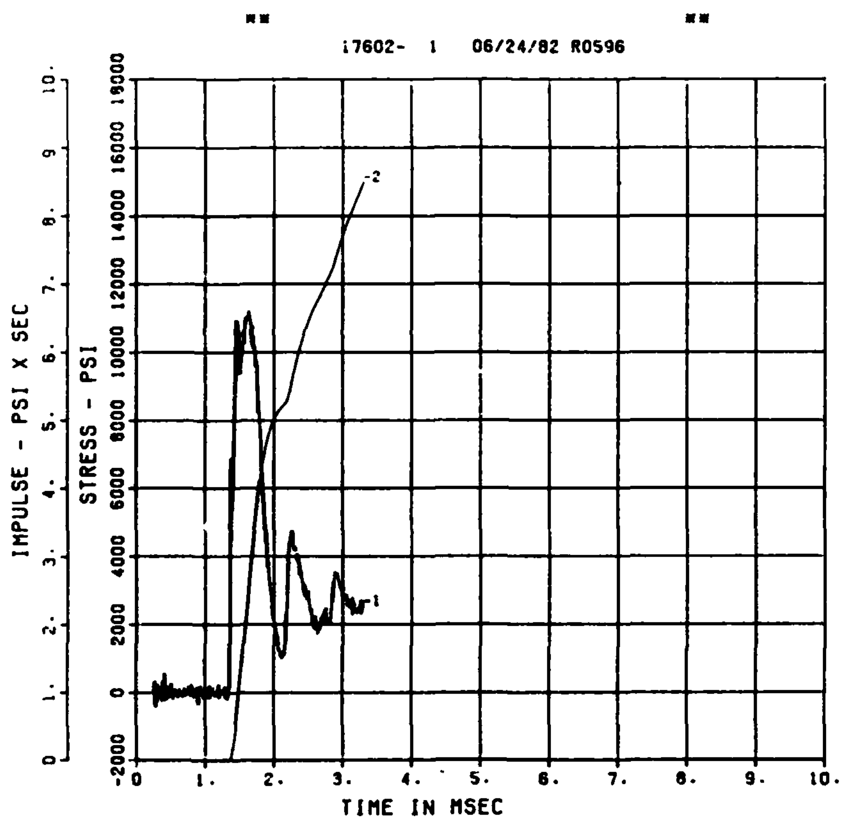

DYN SH II TEST 4
IF2
200000. HZ CAL= 11728.

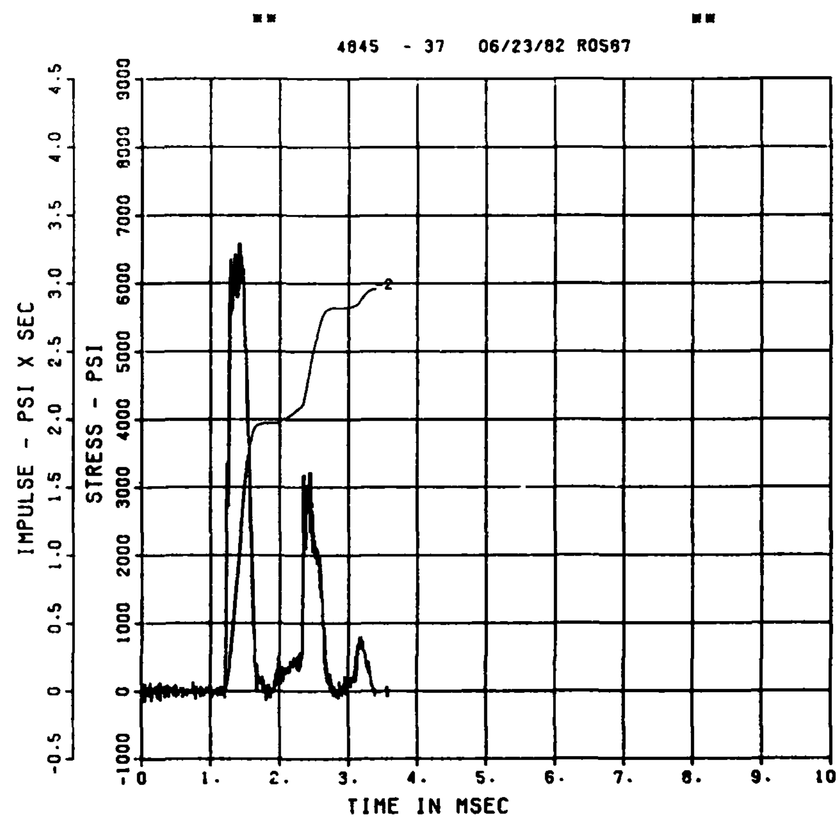

DYN SH II TEST 4
IF3
200000. HZ CAL= 11519.

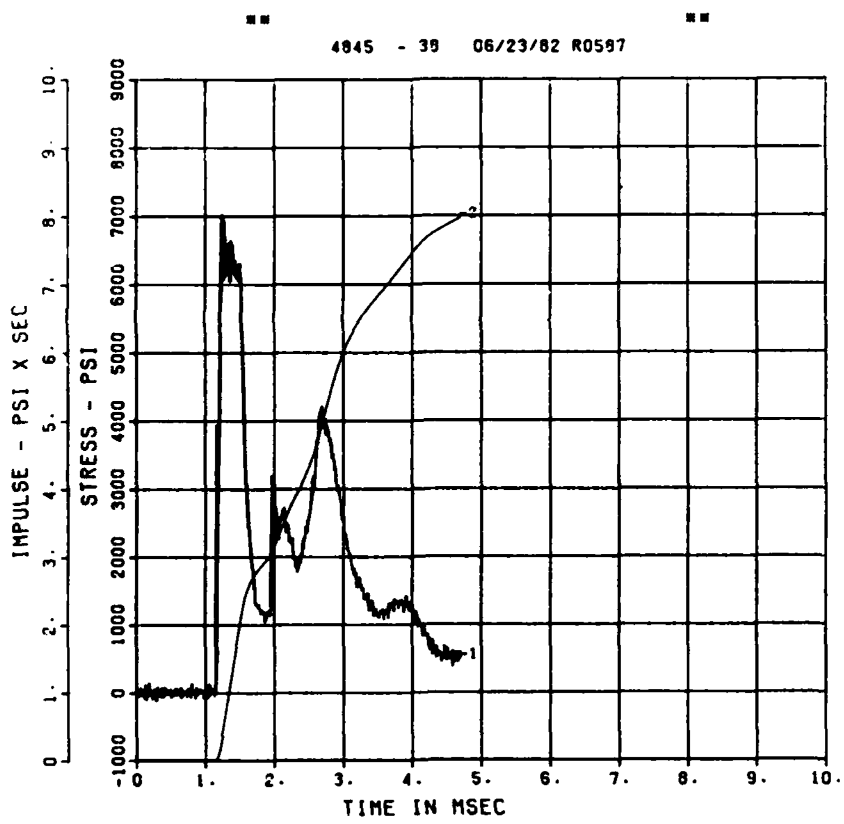

DYN SH II TEST 4
IF4
200000. HZ CAL= 6100.

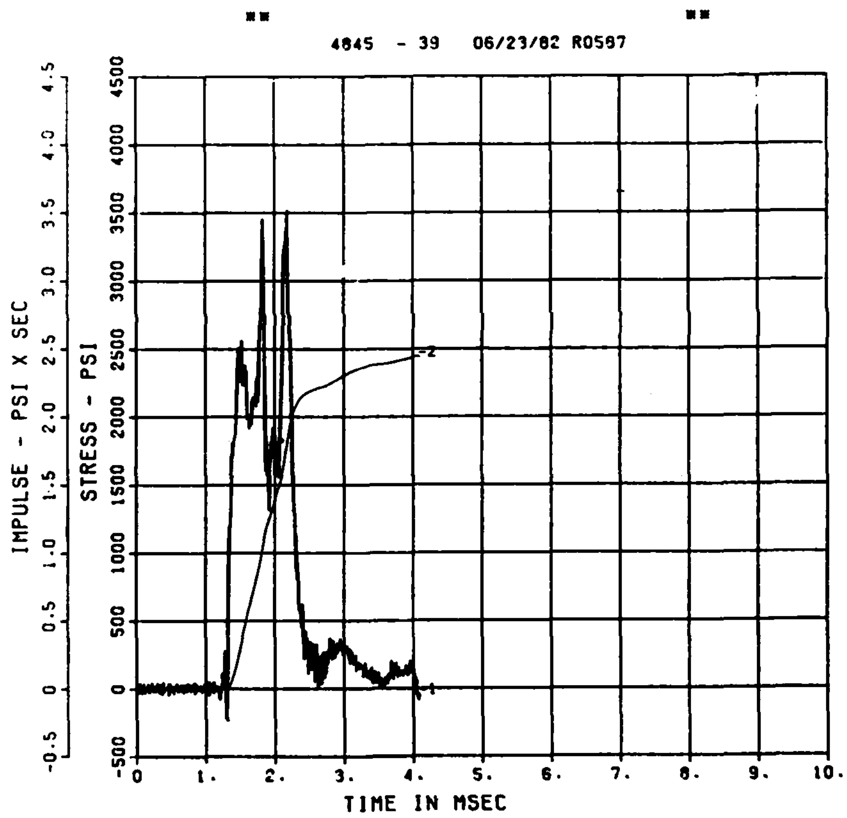

DYN SH II TEST 4
IF5
200000. HZ CAL= 11319.

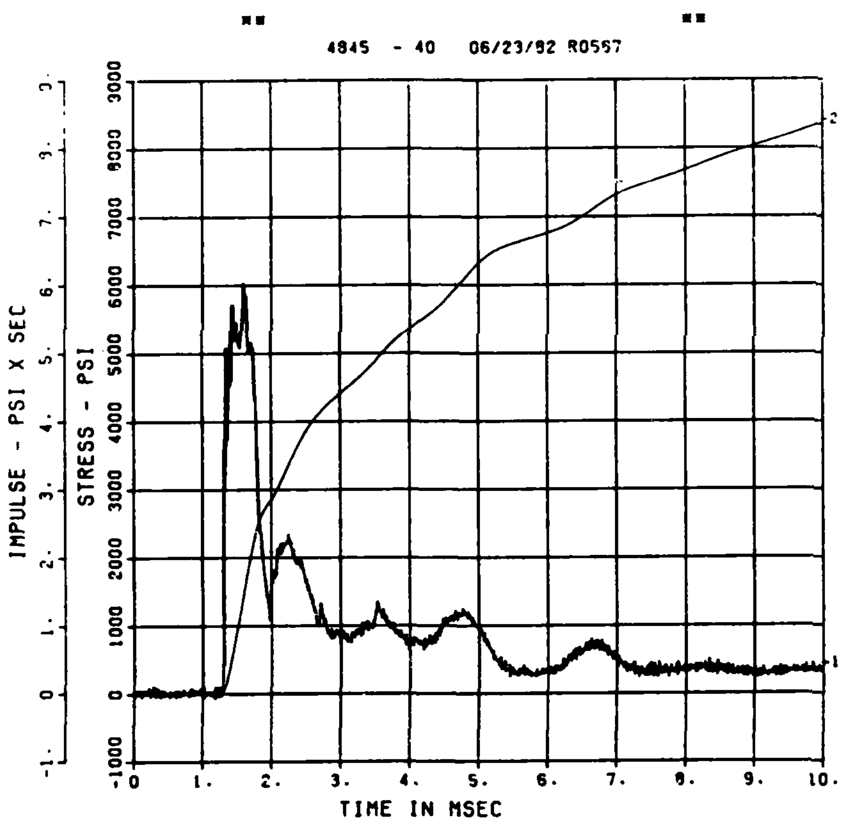

DYN SH II TEST 4
SE1
200000. HZ CAL= 12466.
LP4/0 70% CUTOFF= 9000. HZ

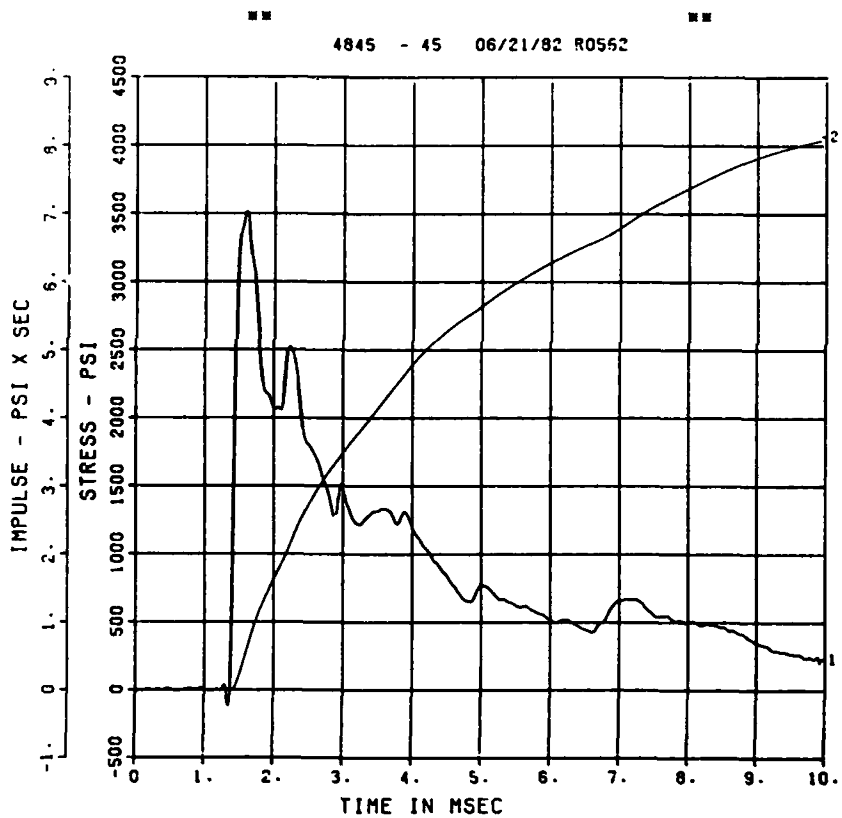

DYN SH II TEST 4
SE2
200000. HZ CAL= 10235.

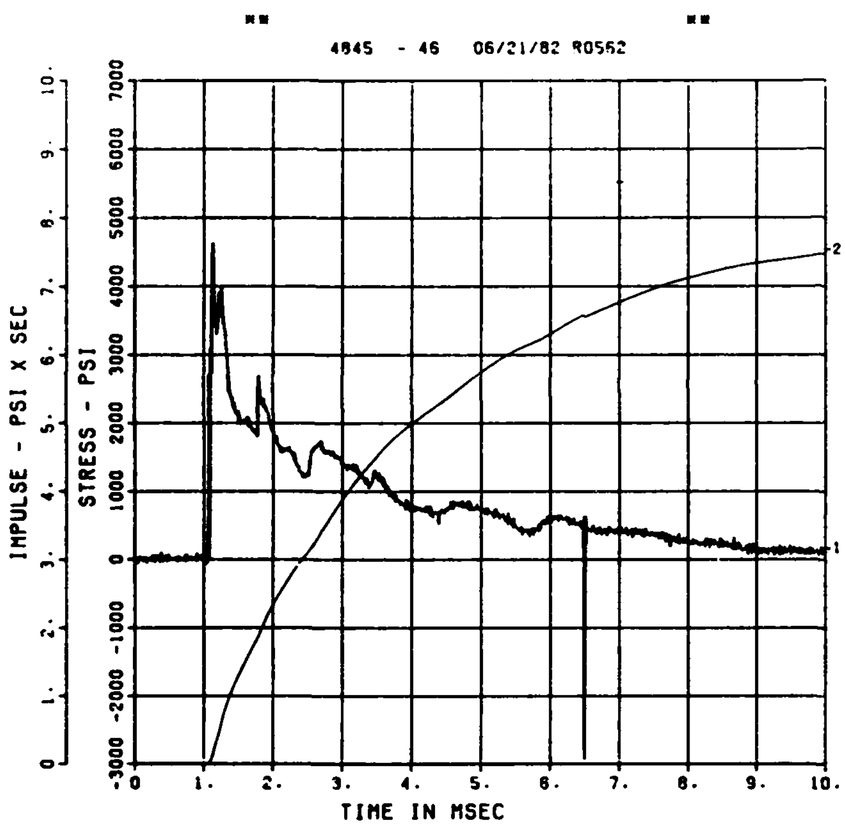

DYN SH II TEST 4
E01
200000. HZ CAL= 29214.

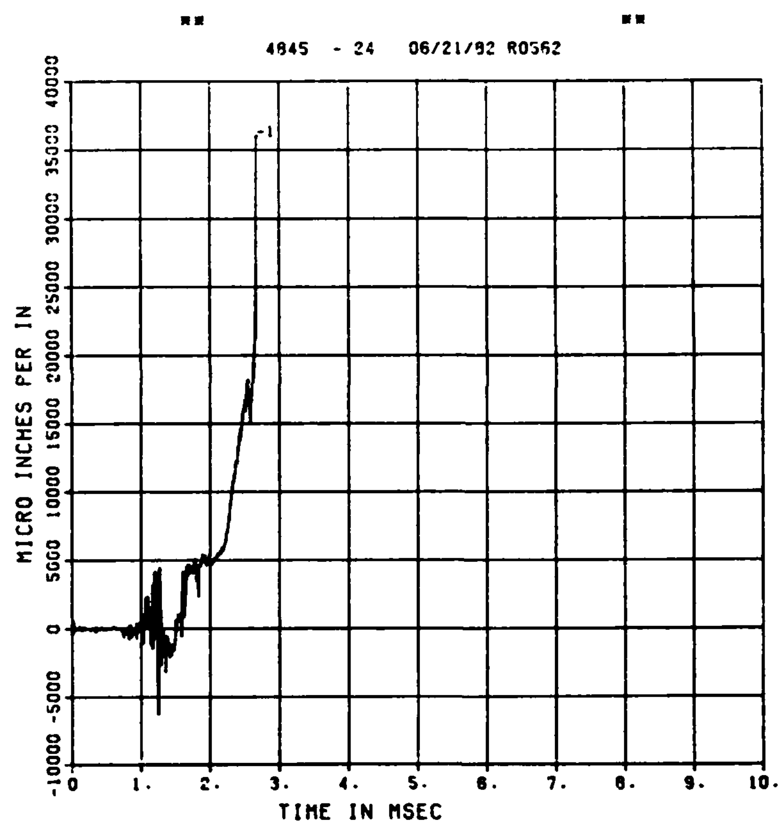

** PEAK VALUE IS 24 % OVER CALIBRATION **

DYN SH II TEST 4
EI1
200000. HZ CAL= 29214.
LP4/0 70% CUTOFF= 9000. HZ

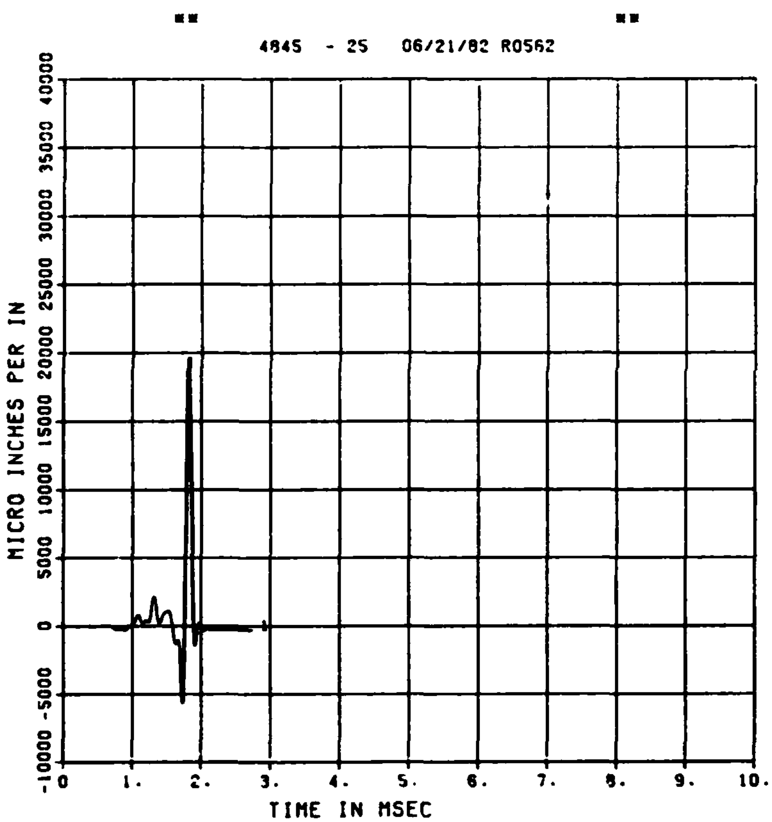

DYN SH II TEST 4
E02
200000. HZ CAL= 29214.

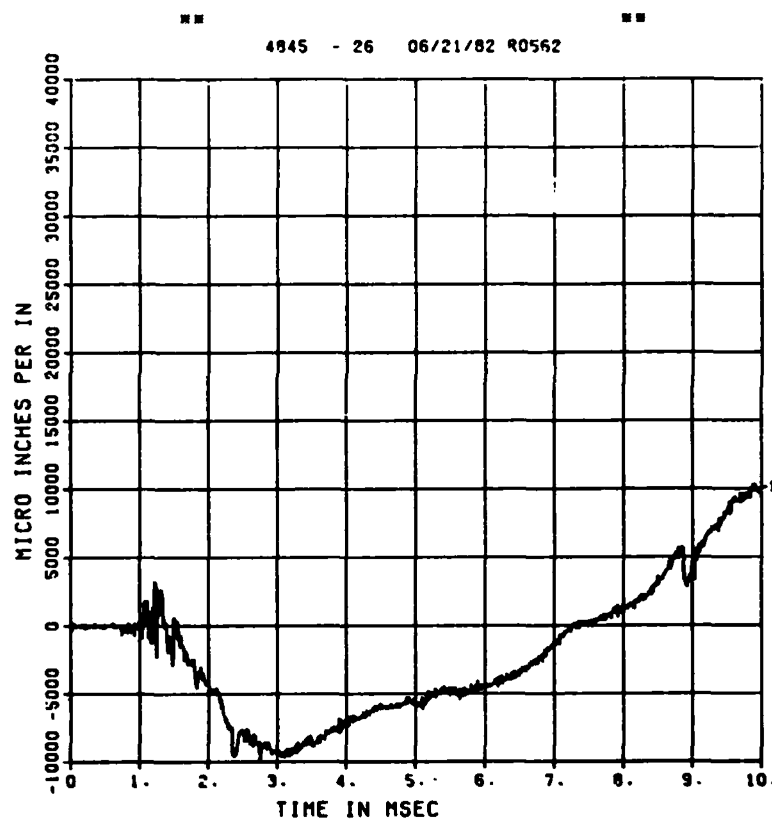

DYN SH II TEST 4
EI2
200000. HZ CAL= 29214.

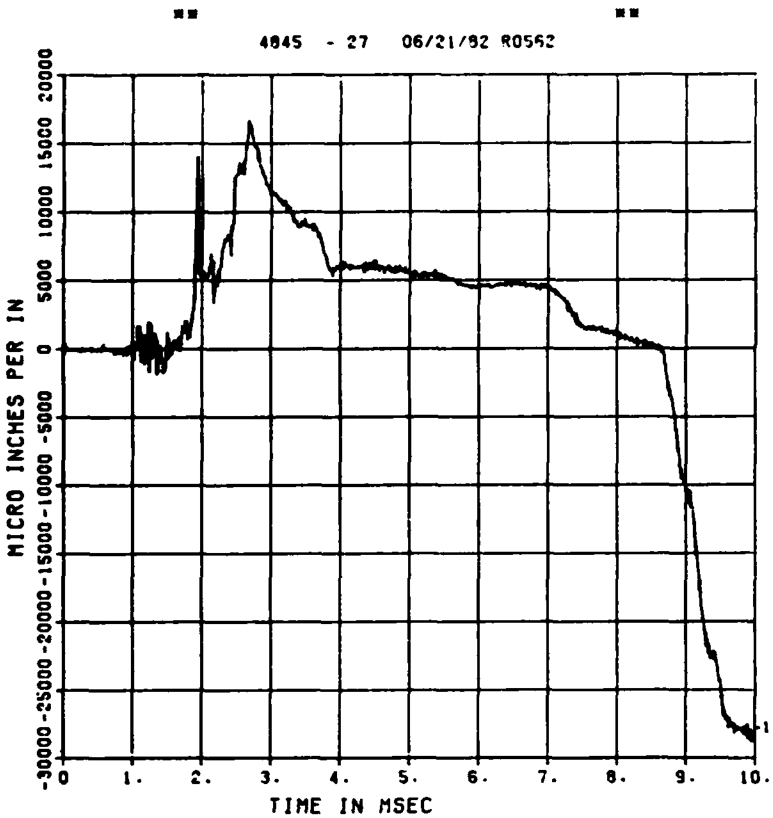

DYN SH II TEST 4
E03
200000. HZ CAL= 29214.

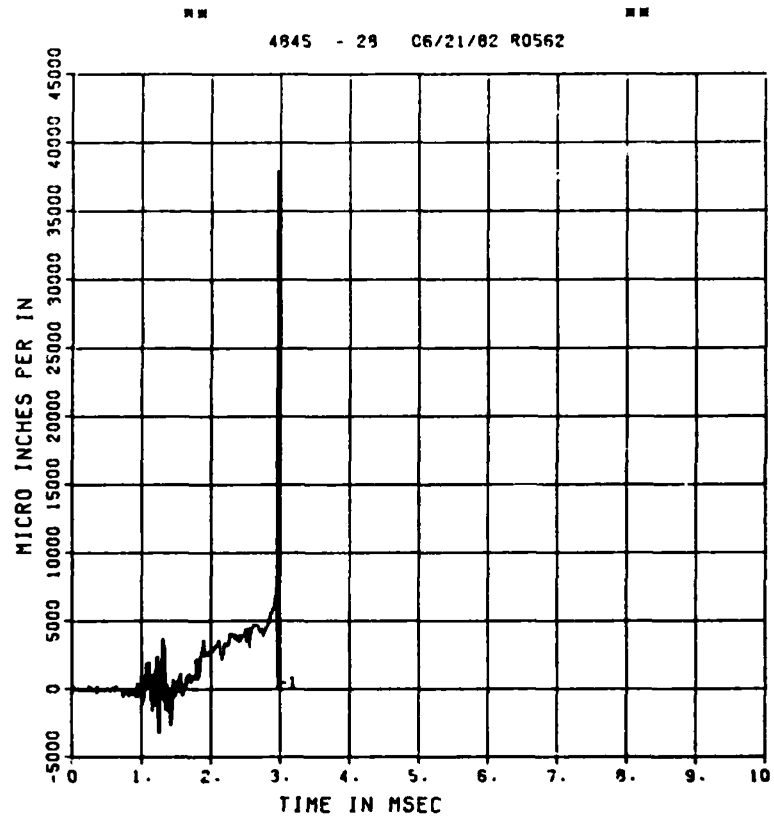

** PEAK VALUE IS 30 % OVER CALIBRATION **

DYN SH II TEST 4
E13
200000. HZ CAL= 29214.

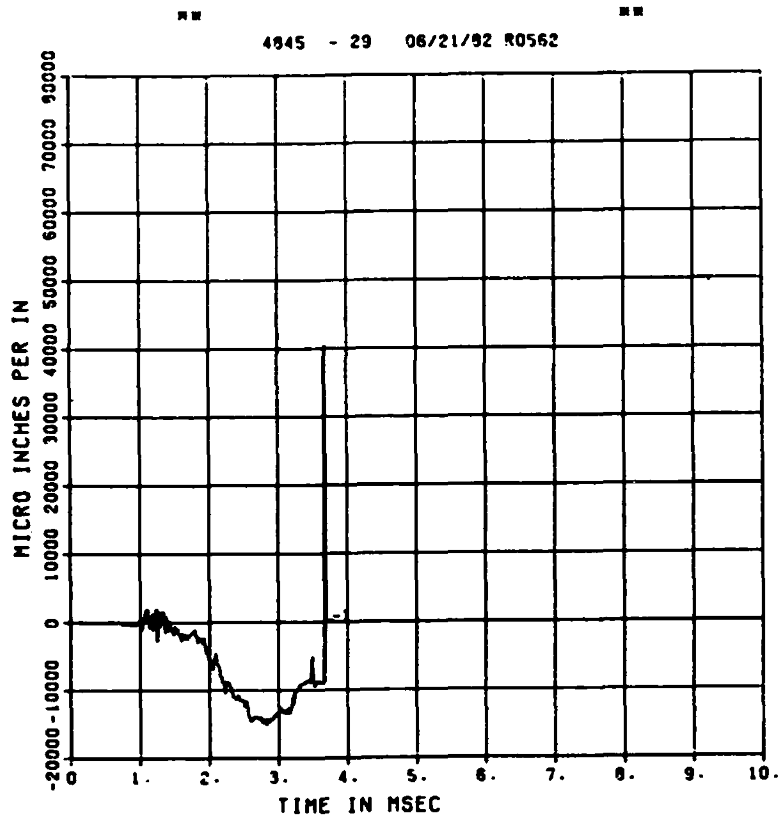

** PEAK VALUE IS 39 % OVER CALIBRATION **

DYN SH II TEST 4
E04
200000. HZ CAL= 29214.

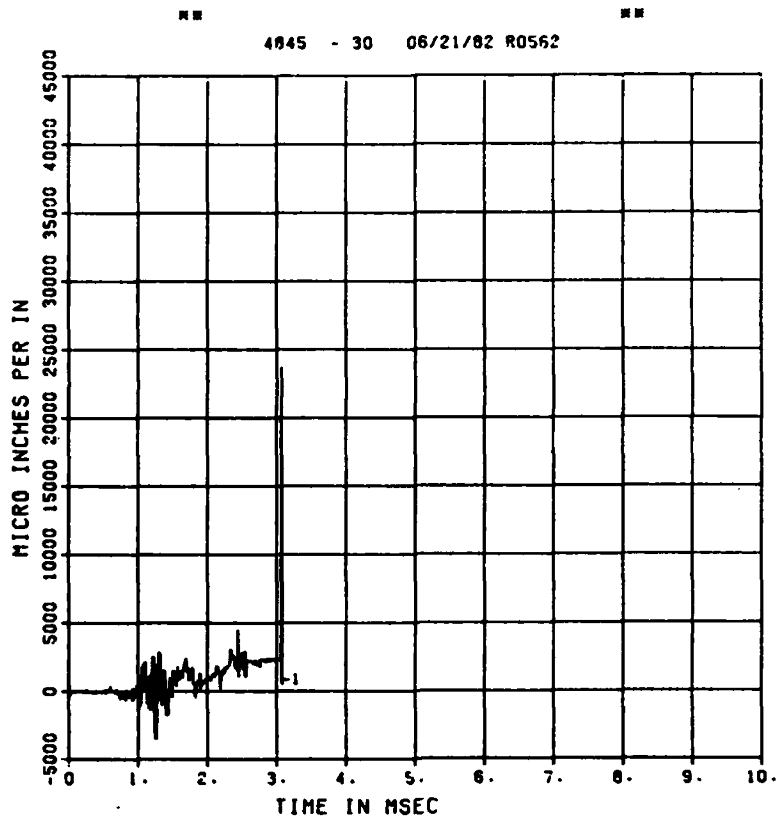

DYN SH II TEST 4
EI4
200000. HZ CAL= 40135.

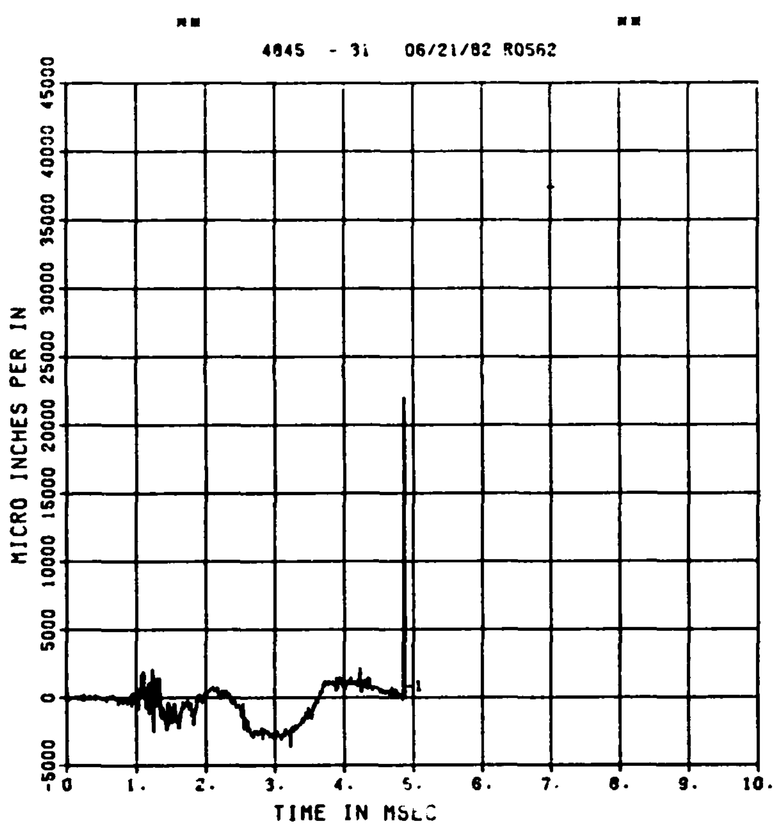

DYN SH II TEST 4
E05
200000. HZ CAL= 40135.

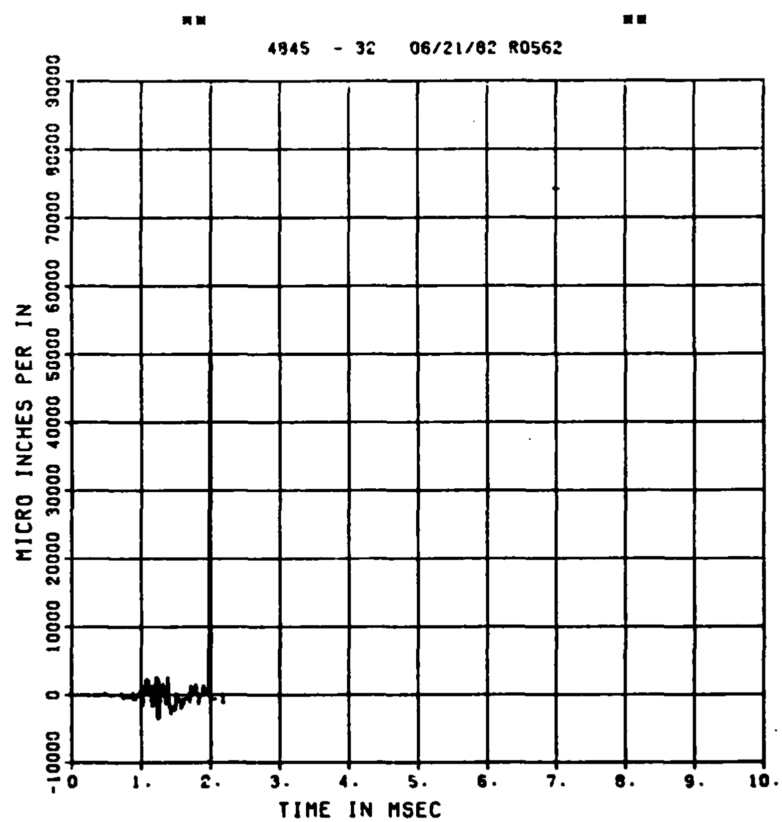

** PEAK VALUE IS 25 % OVER CALIBRATION **

DYN SH II TEST 4
EI5
200000. HZ CAL= 40135.

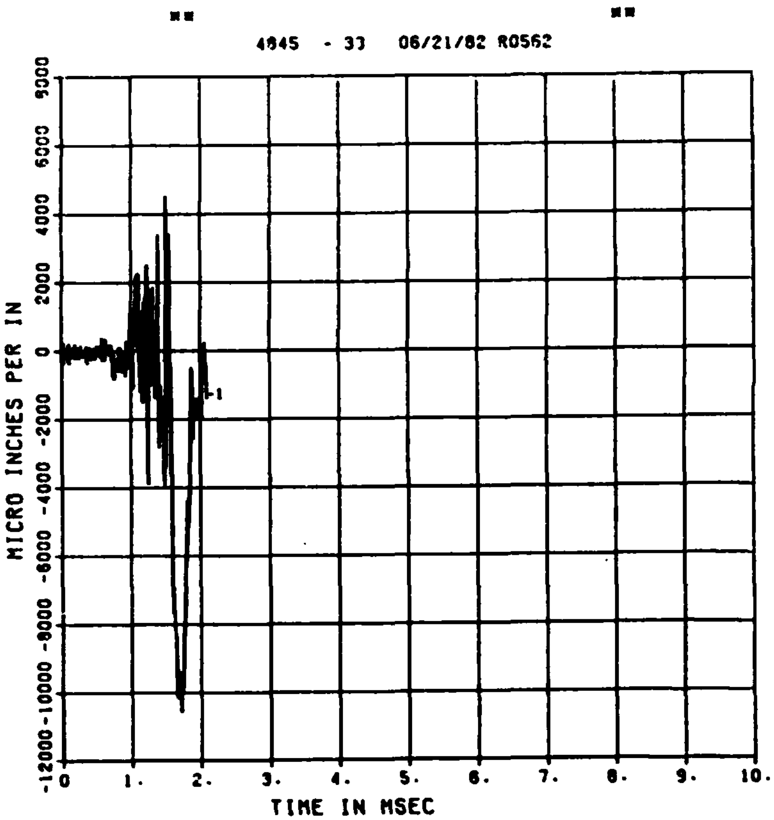

DYN SH II TEST 4
E06
200000. HZ CAL= 40135.

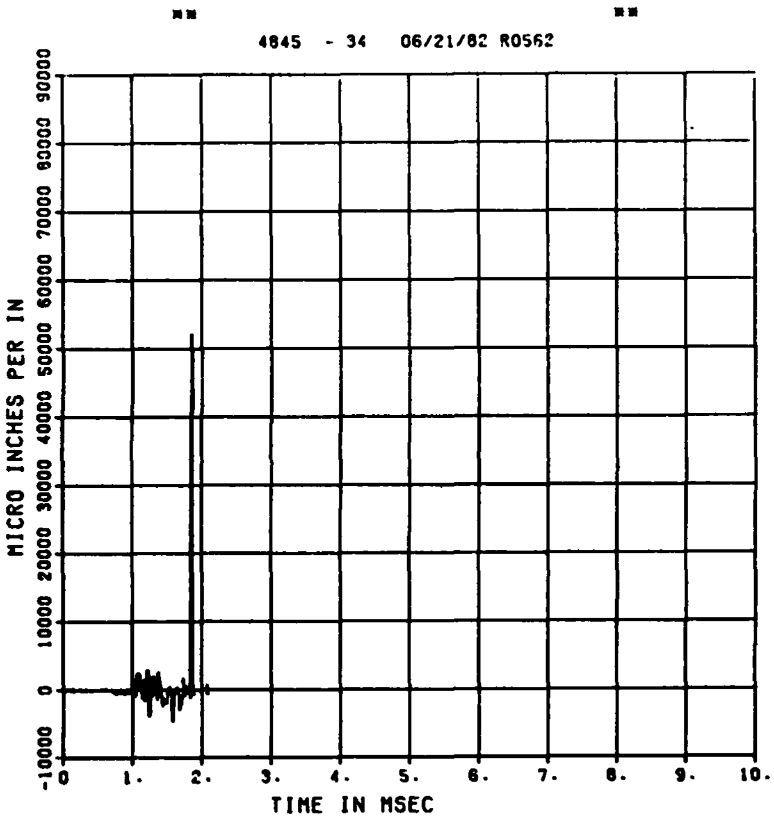

** PEAK VALUE IS 30 % OVER CALIBRATION **

DYN SH II TEST 4
EI6
200000. HZ CAL= 40135.

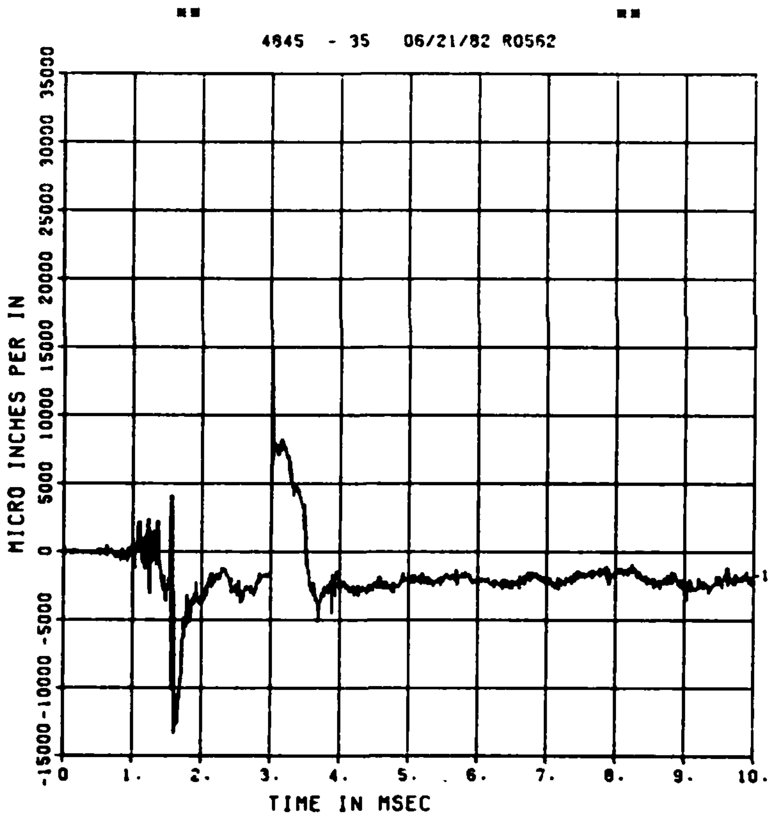

DYN SH II TEST 5
BP1
200000. HZ CAL= 20825.

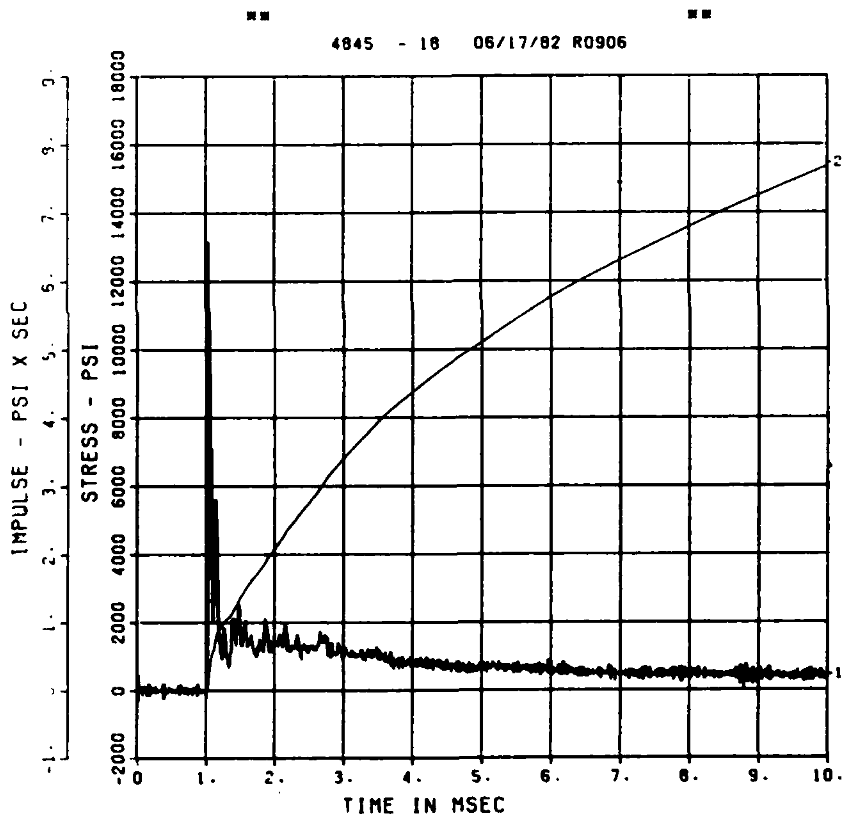

DYN SH II TEST 5
BP1
200000. HZ CAL= 20825.

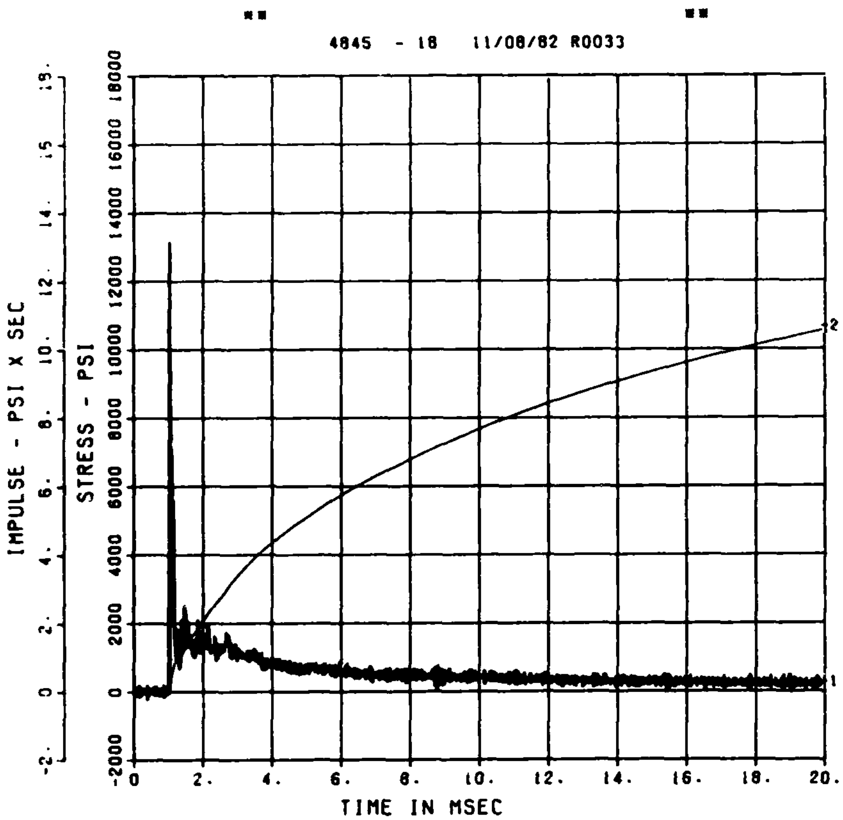

DYN SH II TEST 5
BP2
200000. HZ CAL= 20155.

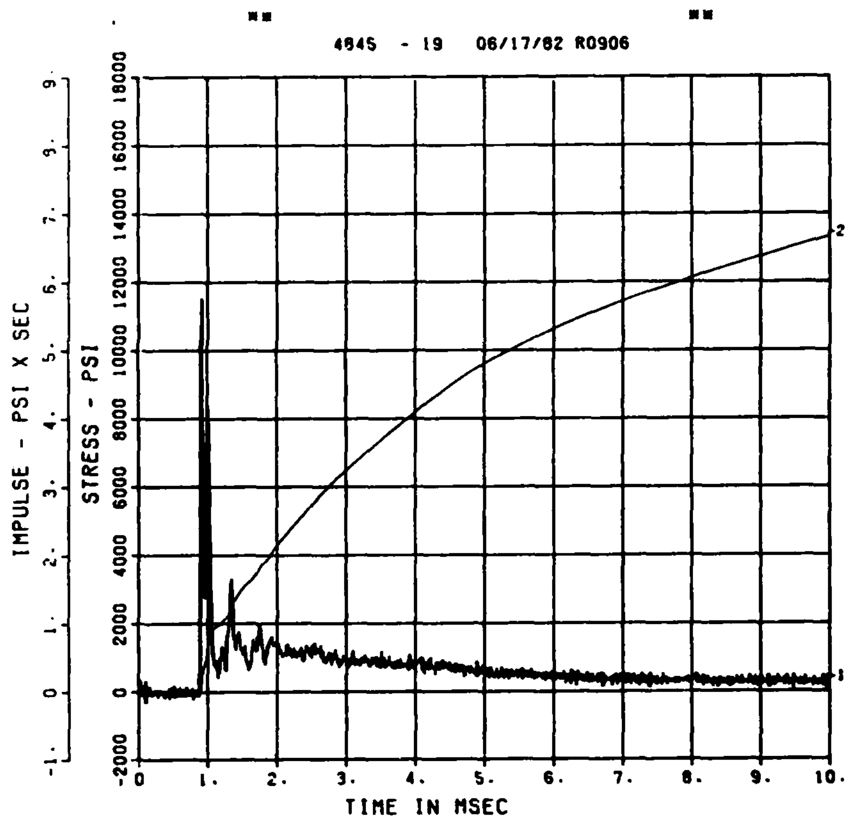

DYN SH II TEST 5
BP2
200000. HZ CAL= 20155.

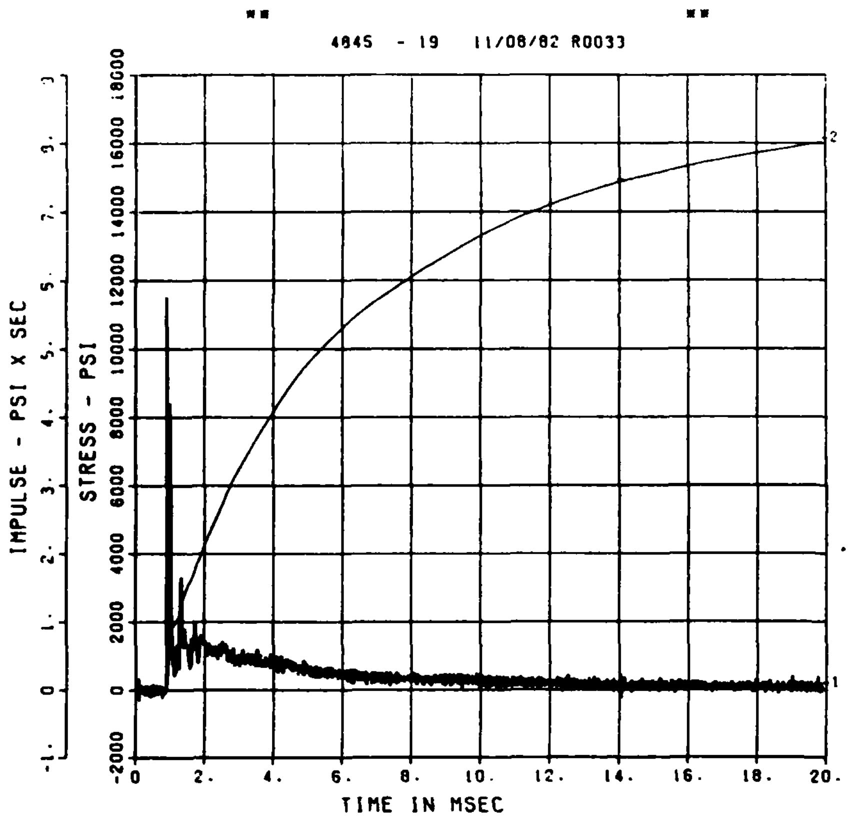

DYN SH II TEST 5
BP4
200000. HZ CAL= 20532.

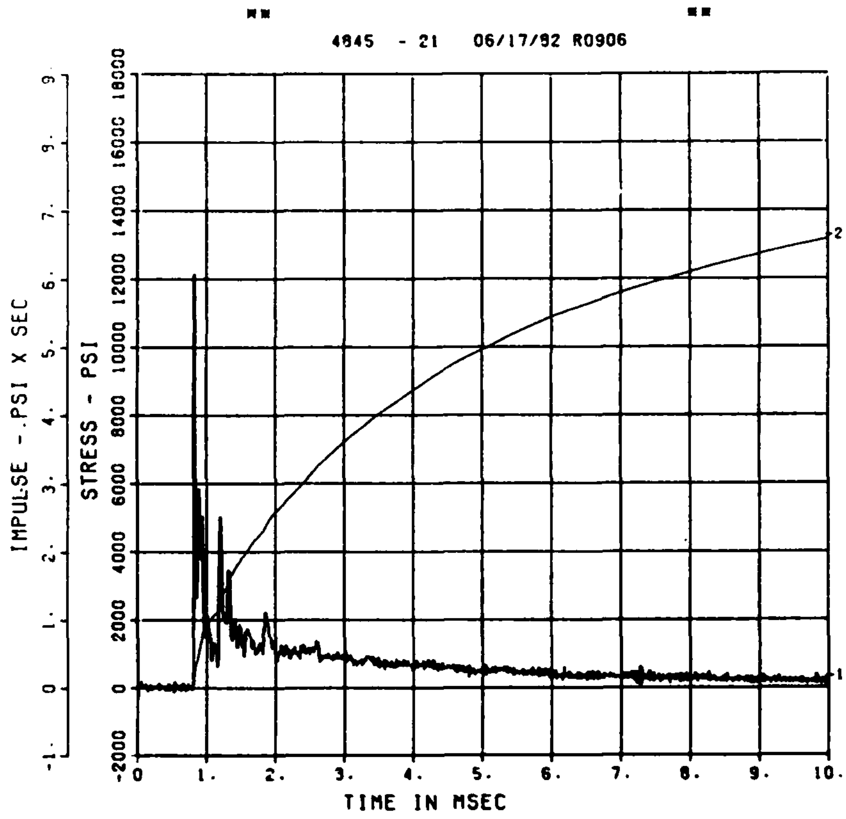

DYN SH II TEST 5
BP4
200000. HZ CAL= 20532.

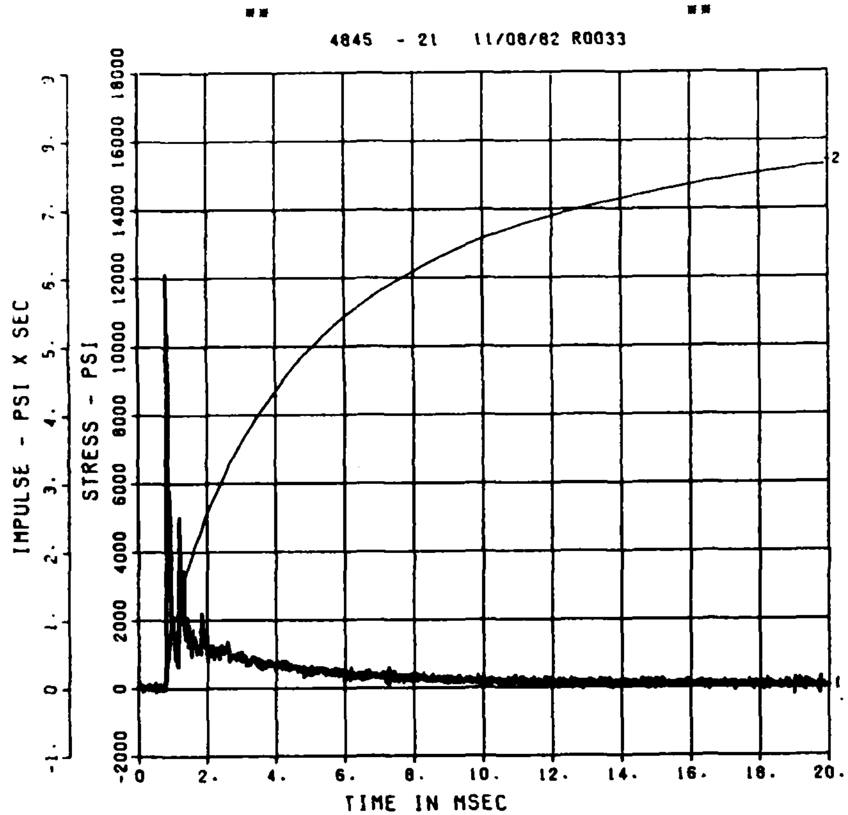

DYN SH II TEST 5
IF1
200000. HZ CAL= 8705.

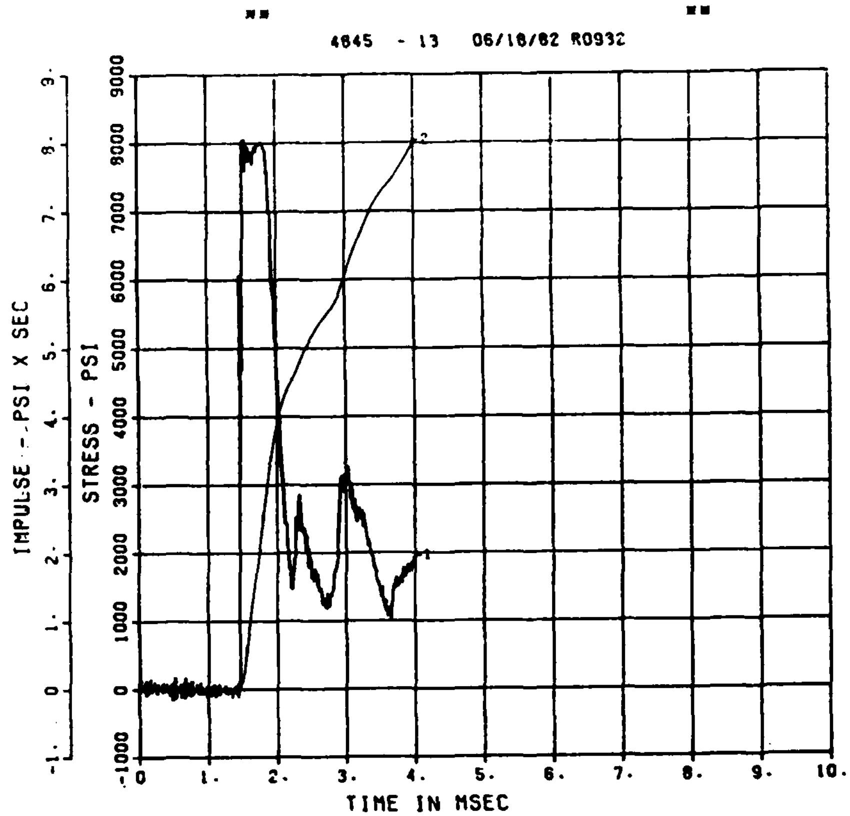

DYN SH II TEST 5
IF2
200000. HZ CAL= 7930.

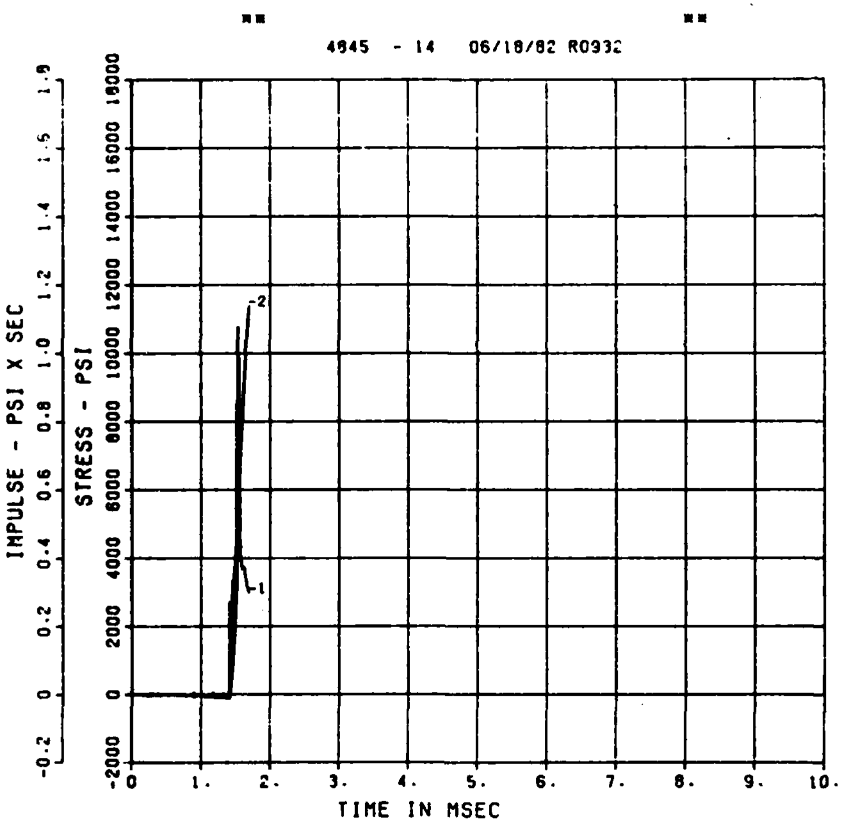

** PEAK VALUE IS 36 % OVER CALIBRATION **

DYN SH II TEST 5
IF3
200000. HZ CAL= 8487.

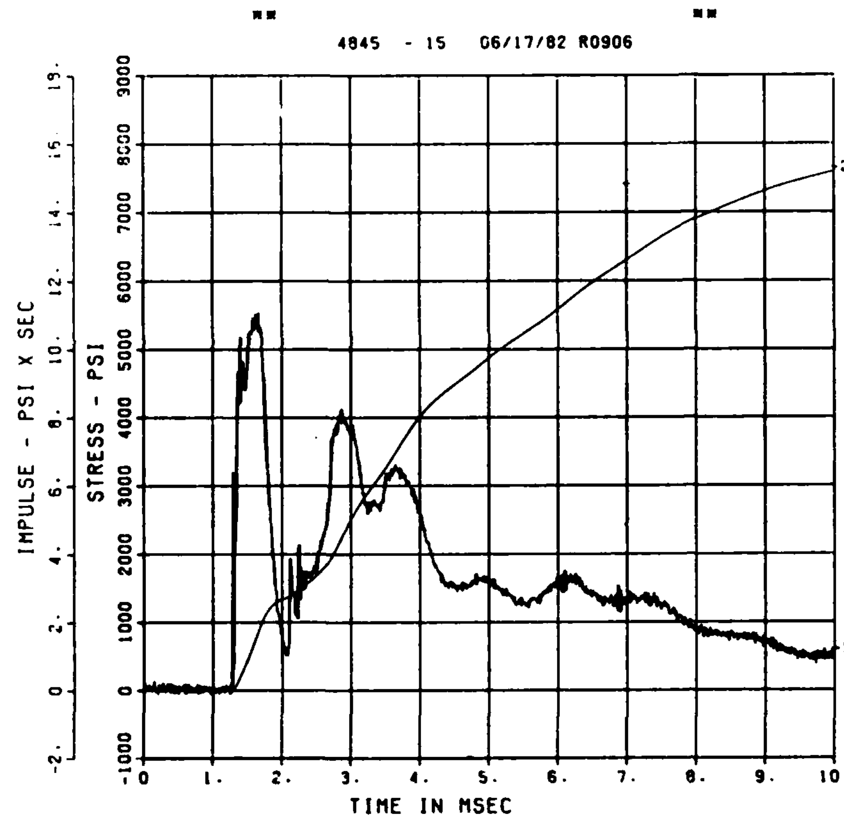

DYN SH II TEST 5
IF4
200000. HZ CAL= 4157.

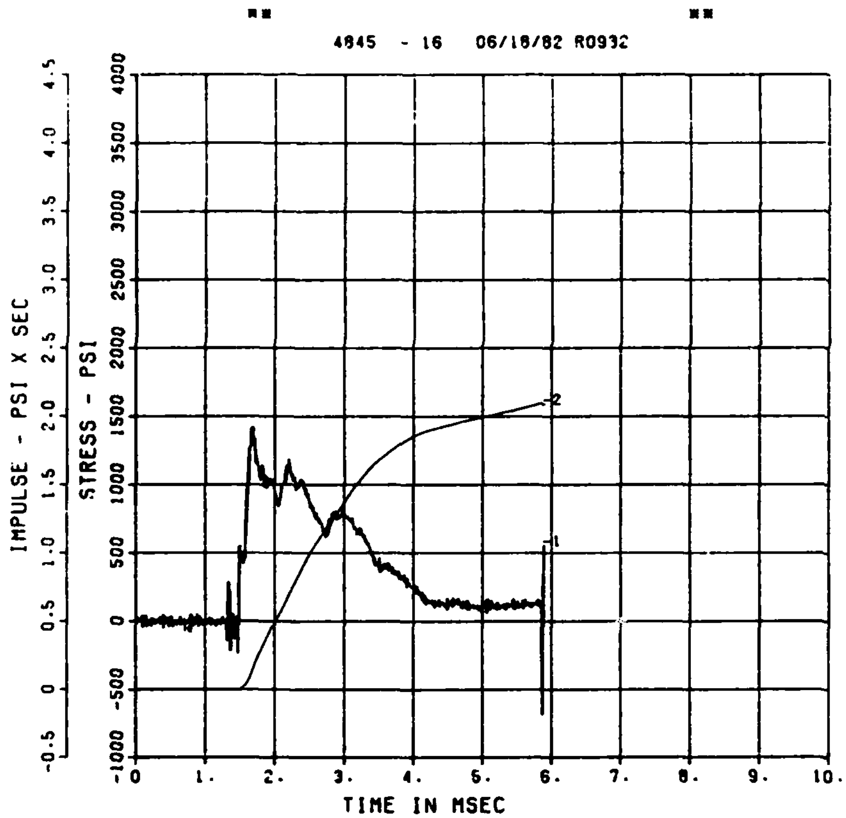

DYN SH II TEST 5
IF5
200000. HZ CAL= 8339.

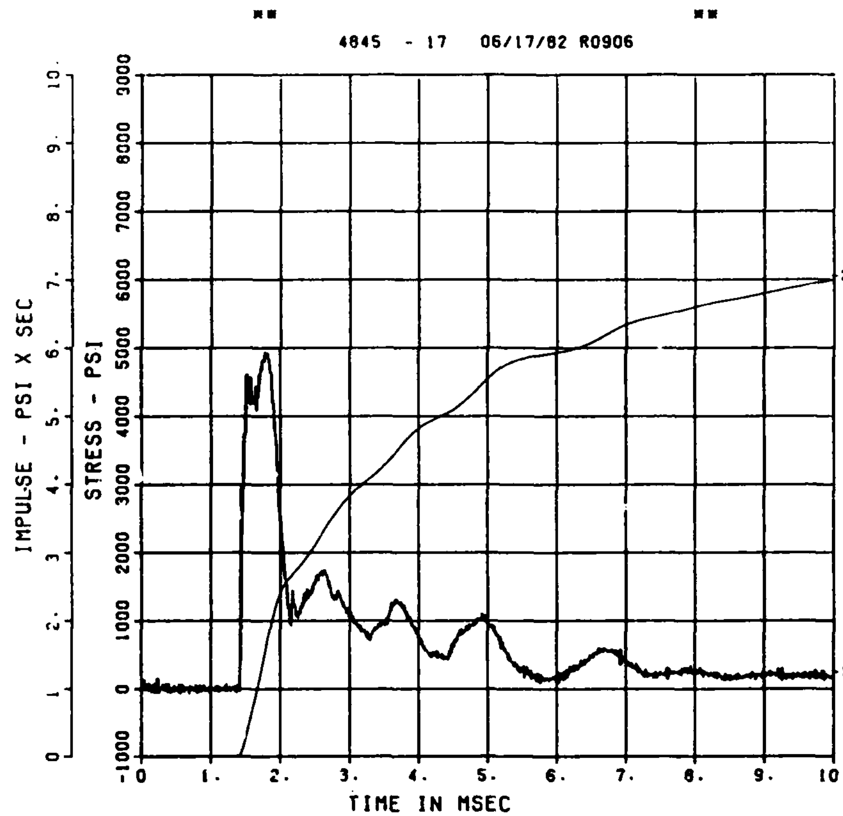

DYN SH II TEST 5
SE1
200000. HZ CAL= 9087.
LP4/0 70% CUTOFF= 9000. HZ

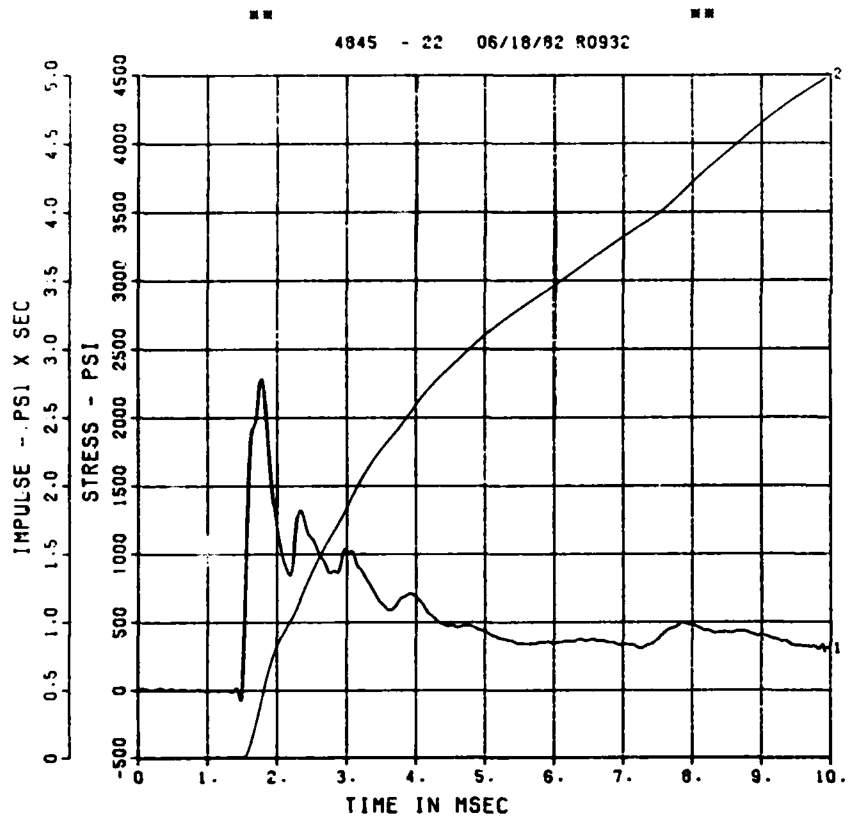

DYN SH II TEST 5
SE2
200000. HZ CAL= 8202.
LP4/0 70% CUTOFF= 9000. HZ

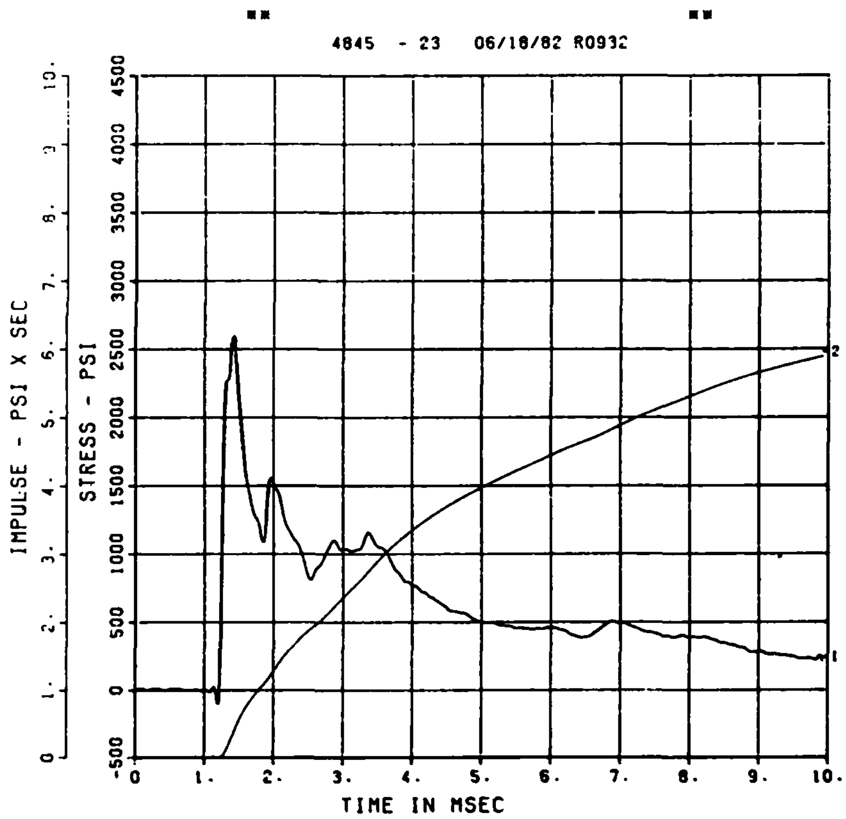

DYN SH II TEST 5
E01
200000. HZ CAL= 43705.

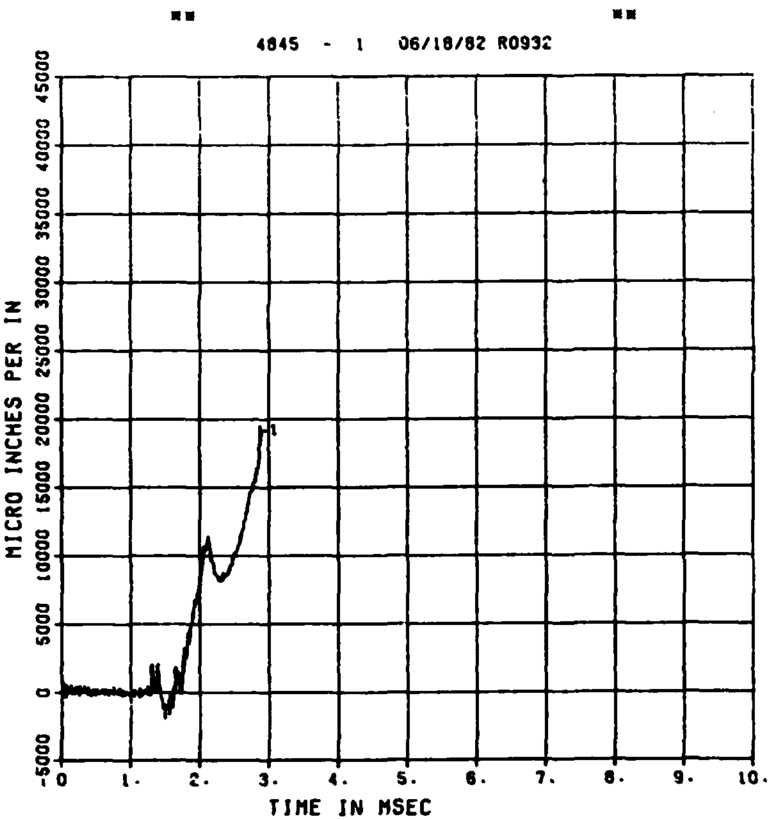

DYN SH II TEST 5
EI1
200000. HZ CAL= 21625.

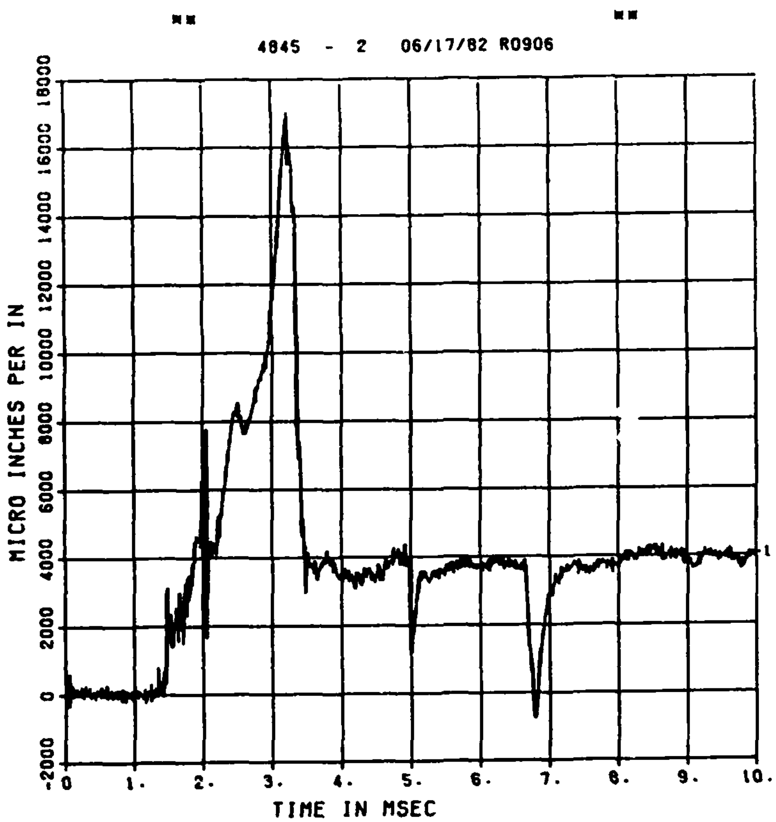

DYN SH II TEST 5
EO2
200000. HZ CAL= 43705.

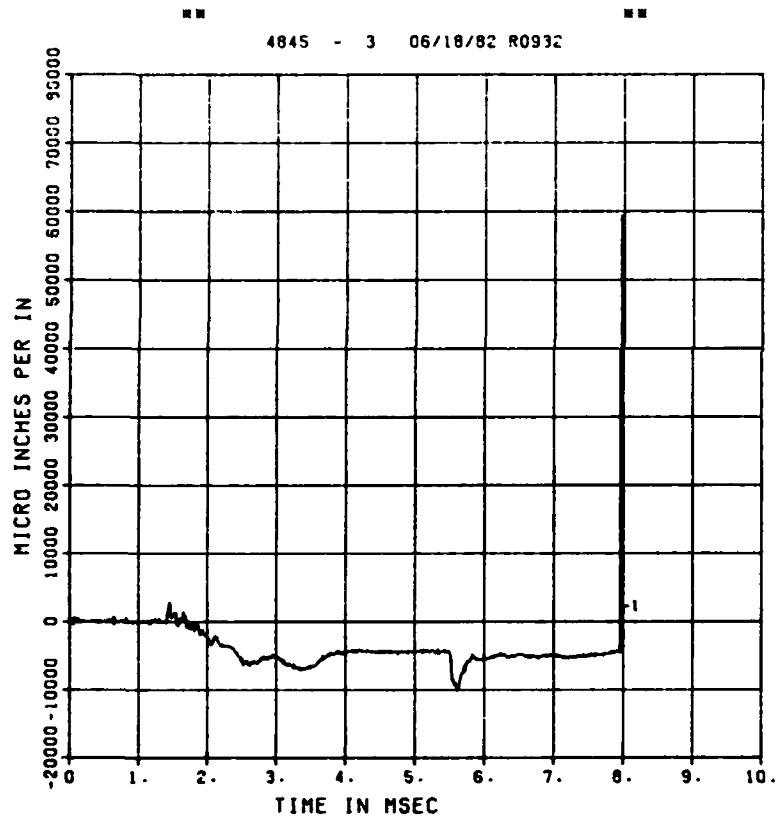

** PEAK VALUE IS 36 % OVER CALIBRATION **

DYN SH II TEST 5
EI2
200000. HZ CAL= 21625.

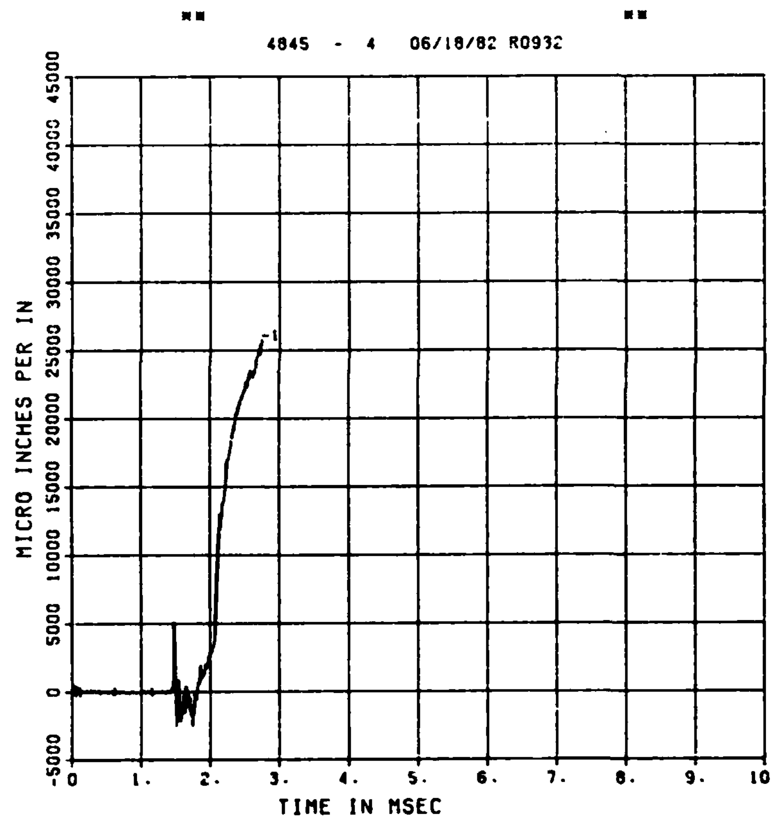

** PEAK VALUE IS 19 % OVER CALIBRATION **

DYN SH II TEST 5
E03
200000. HZ CAL= 43705.

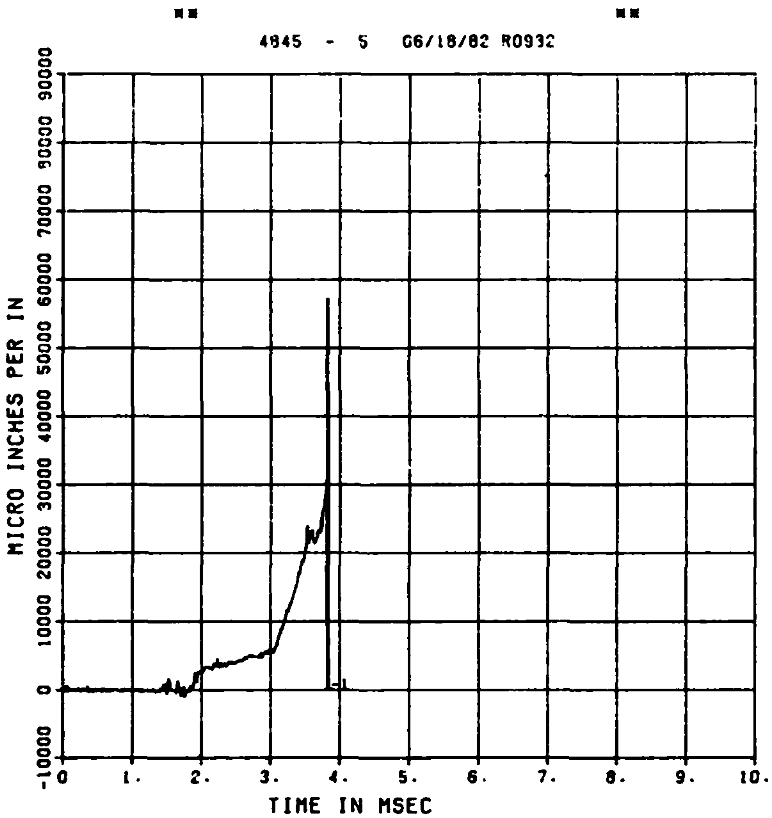

** PEAK VALUE IS 31 % OVER CALIBRATION **

DYN SH II TEST 5
E13
200000. HZ CAL= 21625.

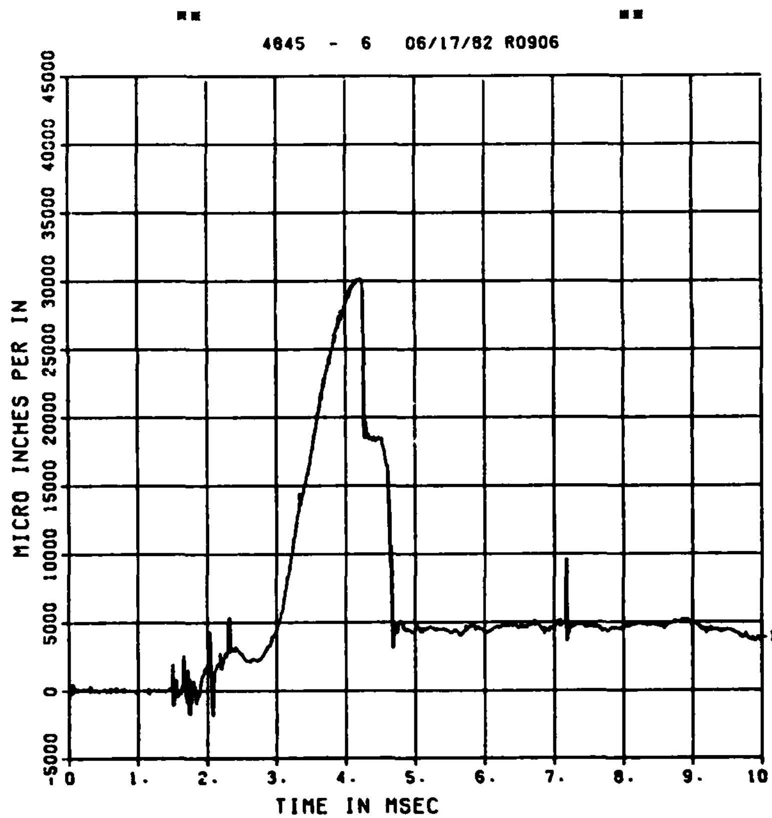

** PEAK VALUE IS 39 % OVER CALIBRATION **

DYN SH II TEST 5
E04
200000. HZ CAL= 30452.

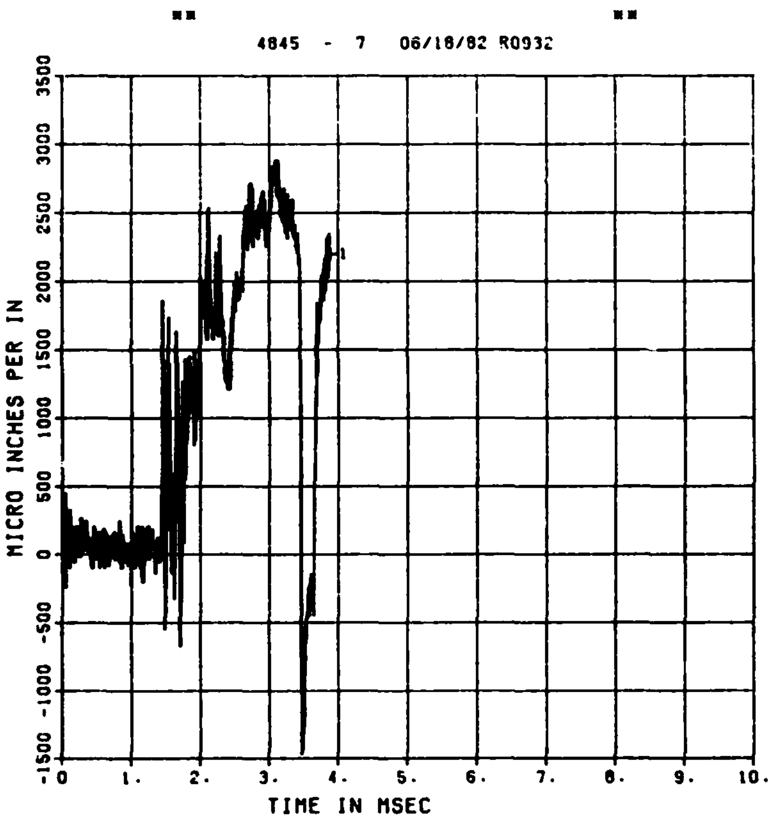

** PEAK VALUE IS 91 % UNDER CALIBRATION **

DYN SH II TEST 5
EI4
200000. HZ CAL= 21625.
LP4/0 70% CUTOFF= 9000. HZ

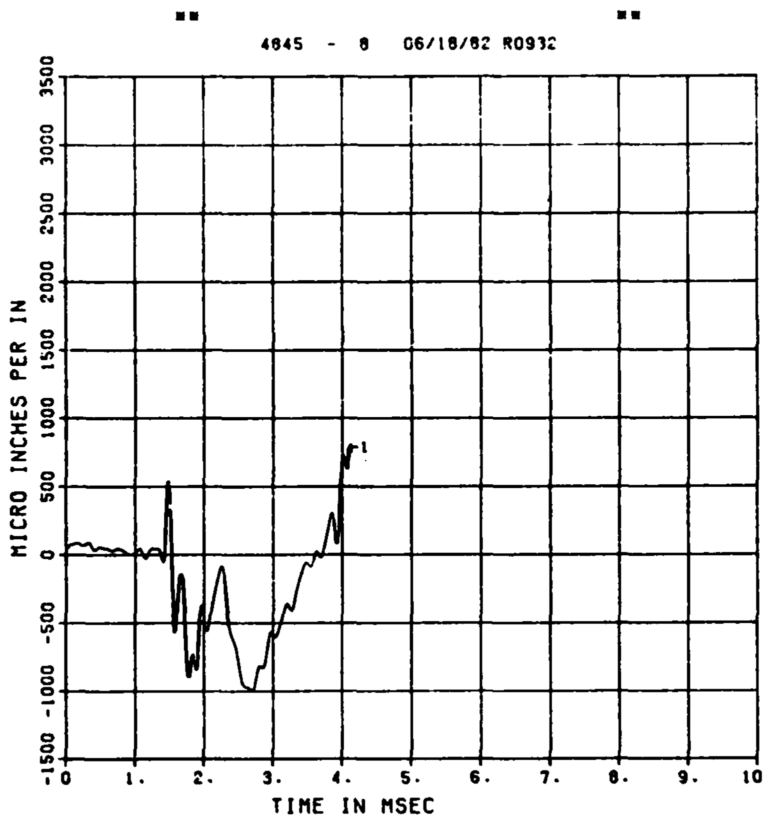

** PEAK VALUE IS 95 % UNDER CALIBRATION **

DYN SH II TEST 5
E05
200000. HZ CAL= 30452.

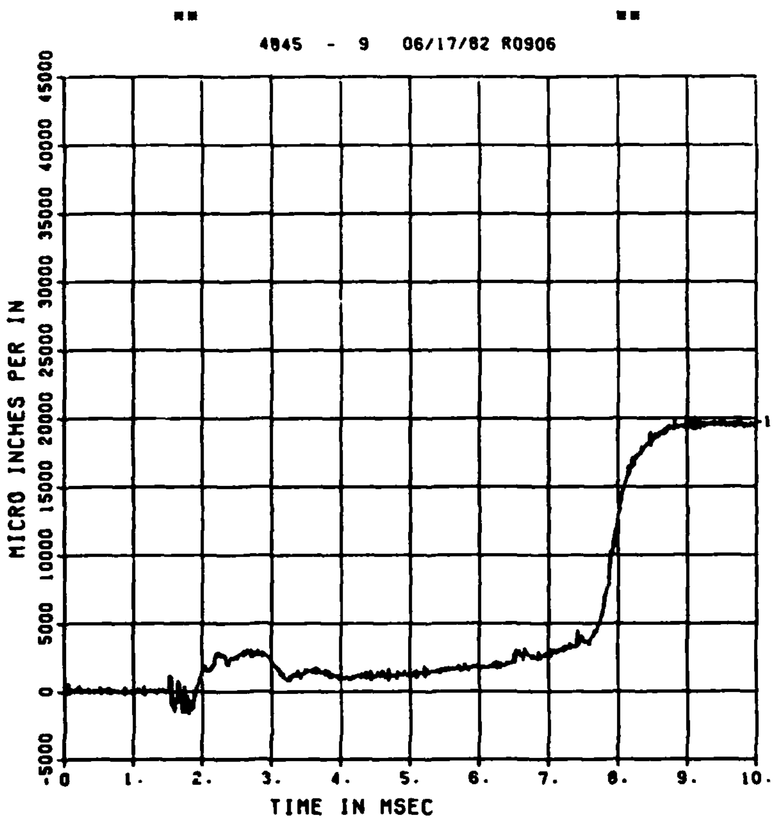

DYN SH II TEST 5
EI5
200000. HZ CAL= 21625.

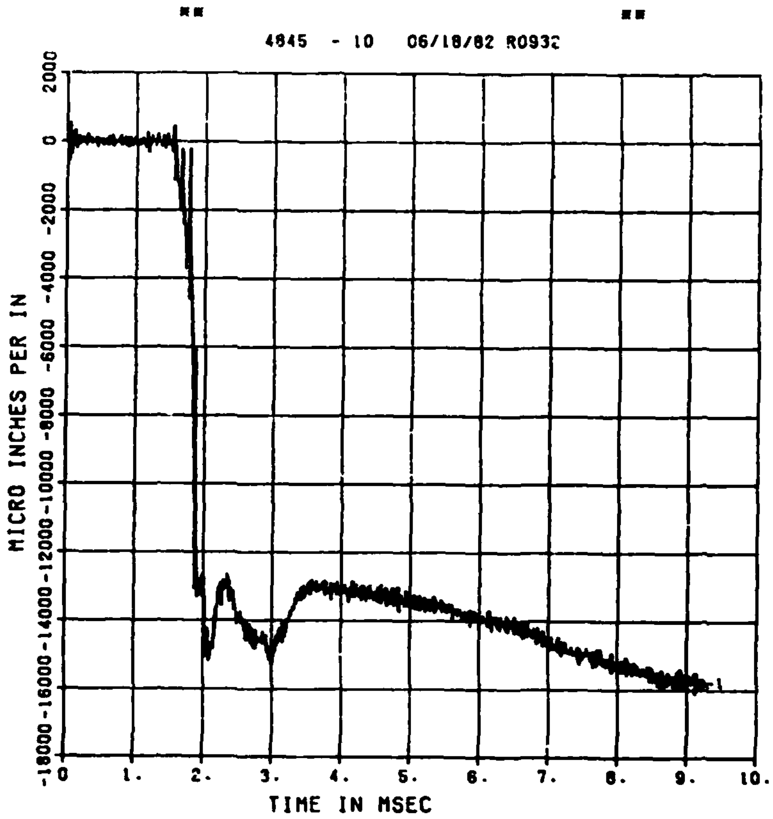

DYN SH II TEST 5
E06
200000. HZ CAL= 30452.

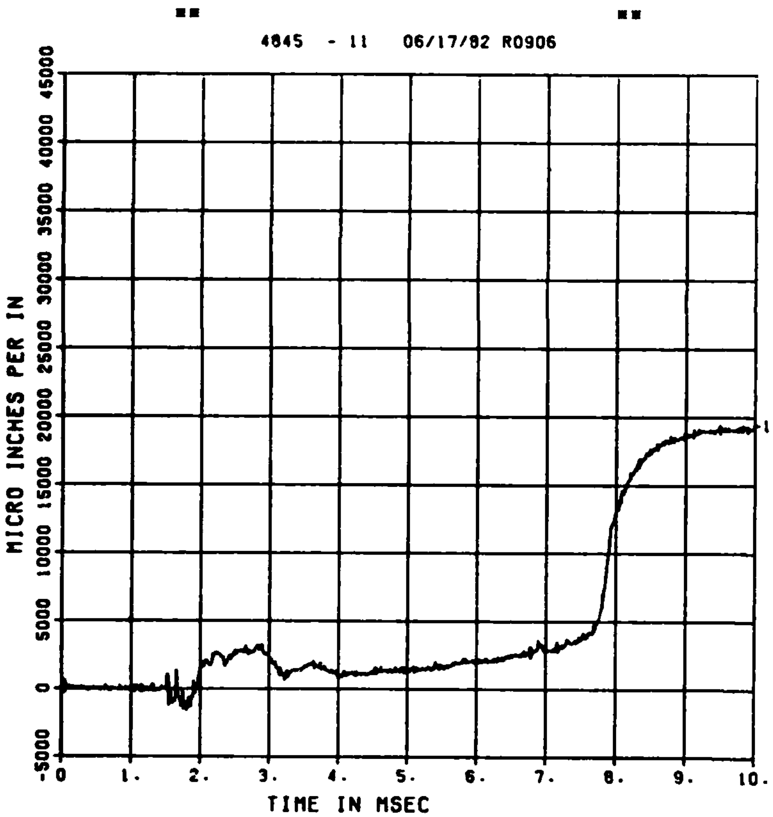

DYN SH II TEST 5
EI6
200000. HZ CAL= 21625.

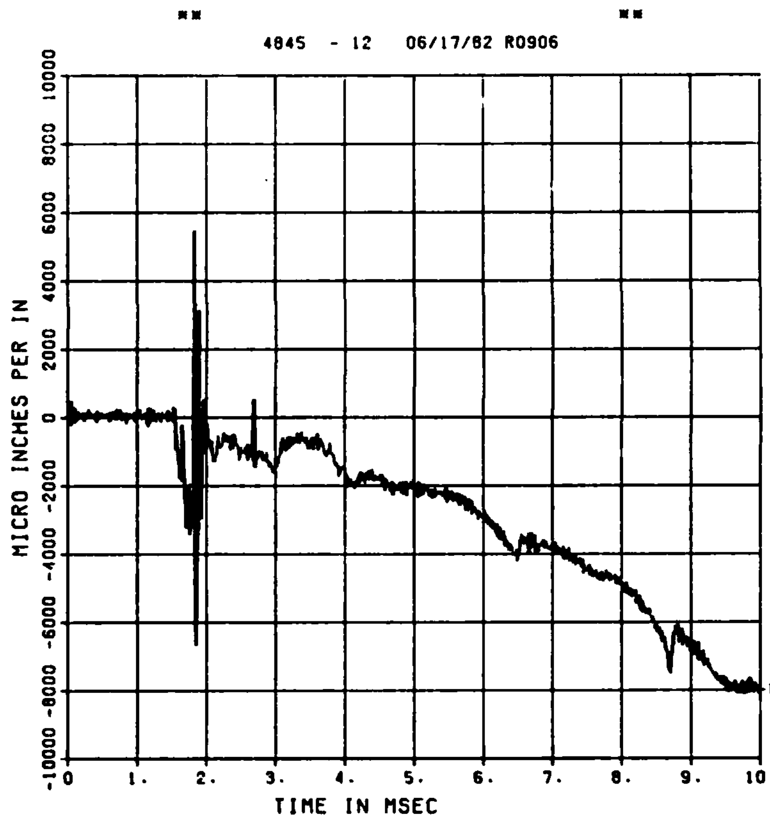

DYN SH II TEST 6
BP1
200000. HZ CAL= 20825.

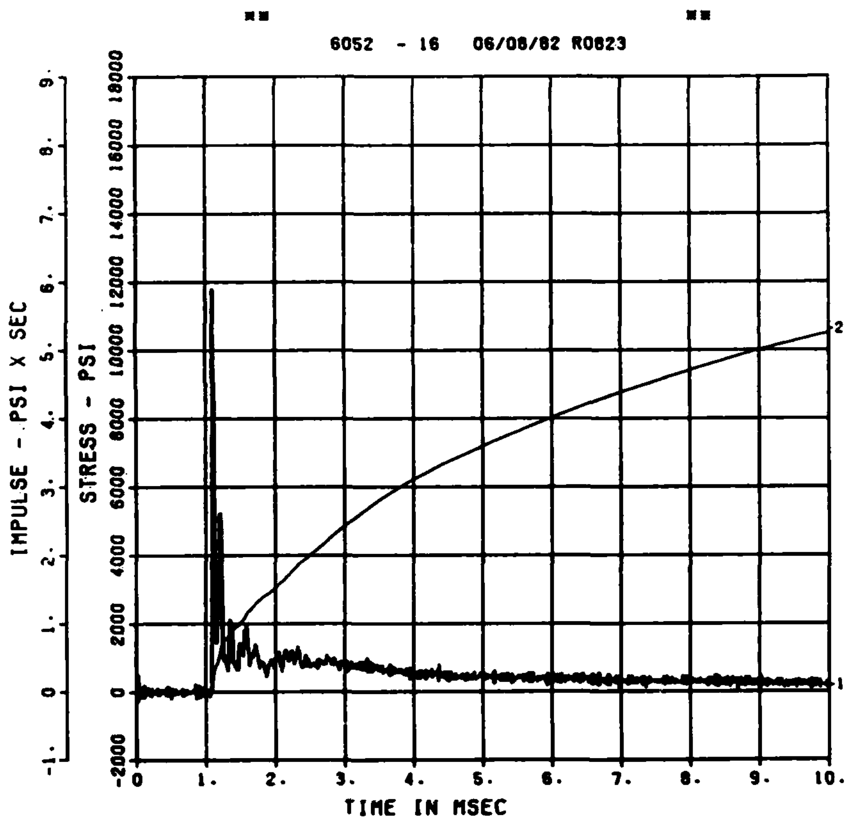

DYN SH II TEST 6
BP1
200000. HZ CAL= 20825.

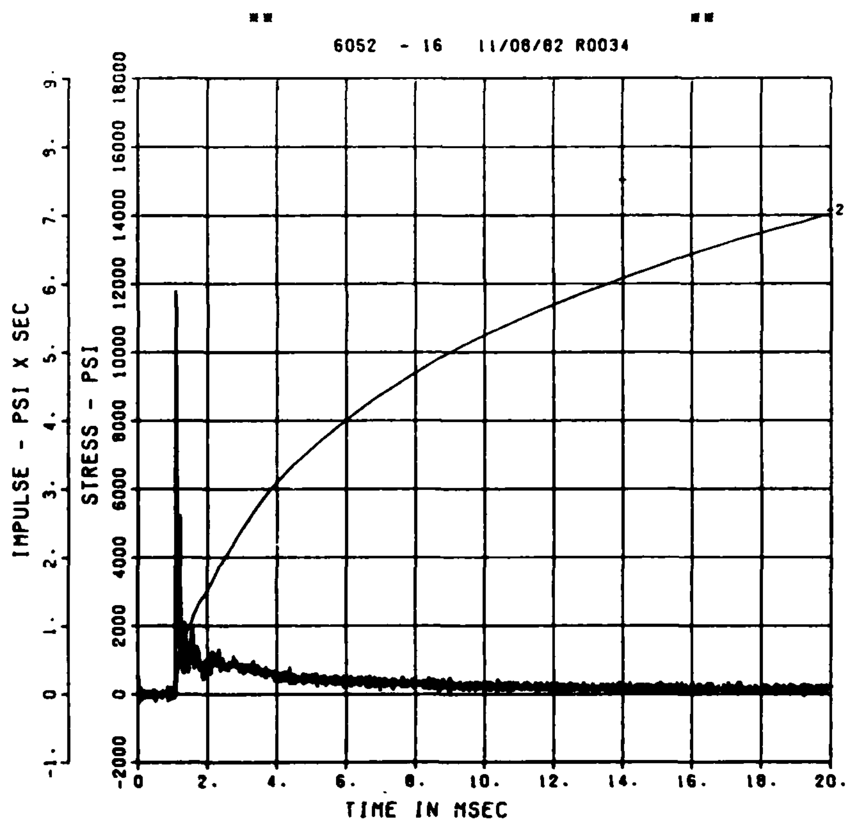

DYN SH II TEST 6
BP2
200000. HZ CAL= 20155.
LP4/0 70% CUTOFF= 9000. HZ

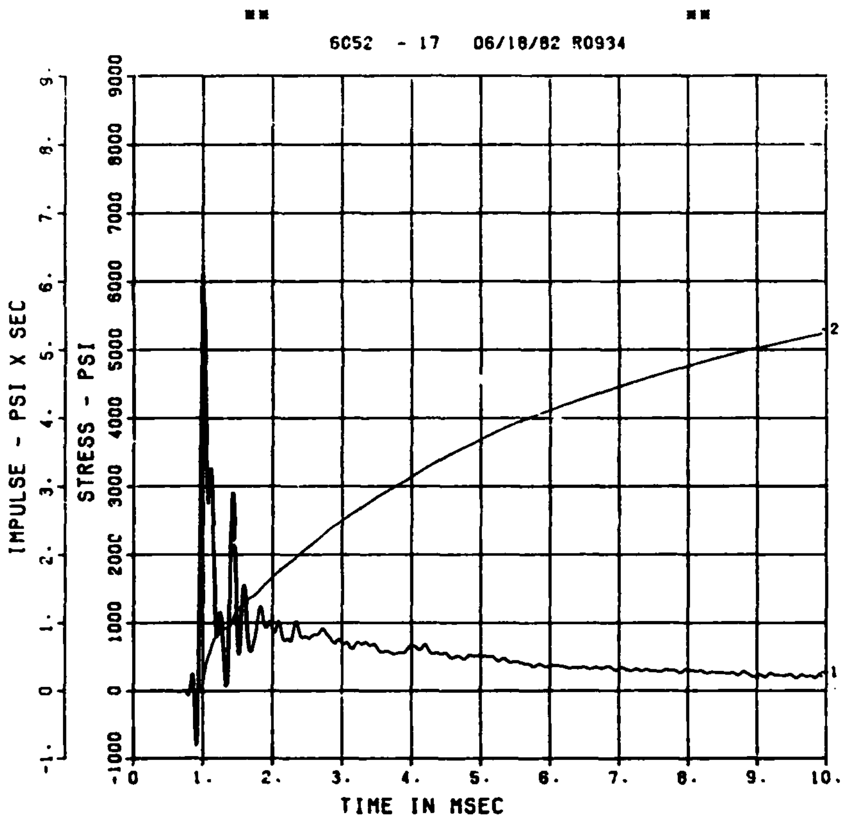

DYN SH II TEST 6
BP2
200000. HZ CAL= 20155.
LP4/0 70% CUTOFF= 9000. HZ

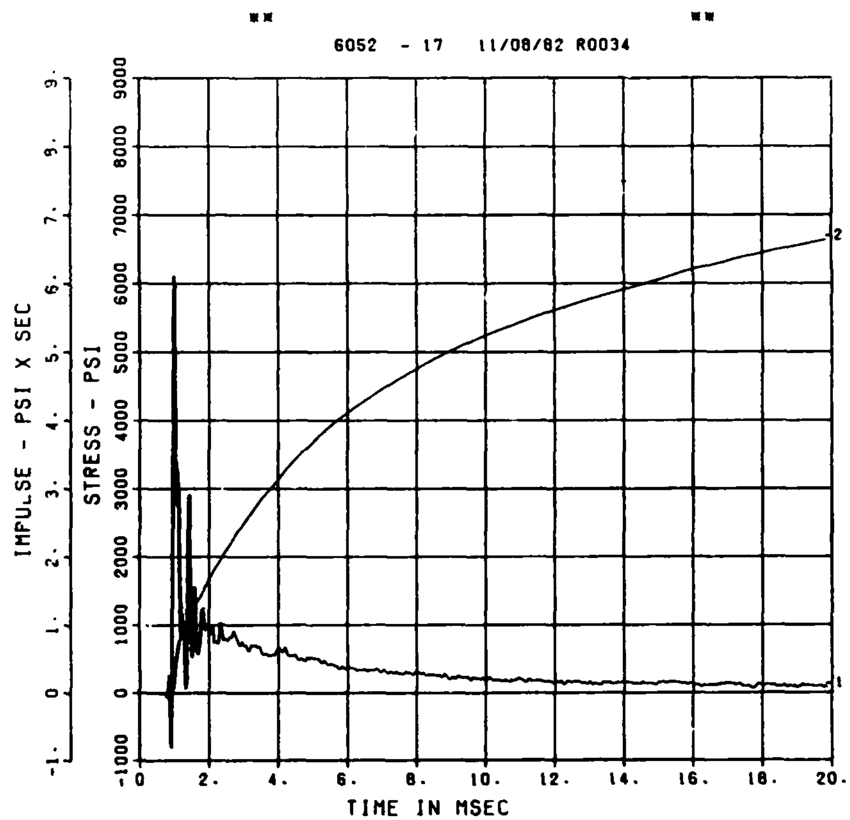

DYN SH II TEST 6
BP4
200000. HZ CAL= 16292.

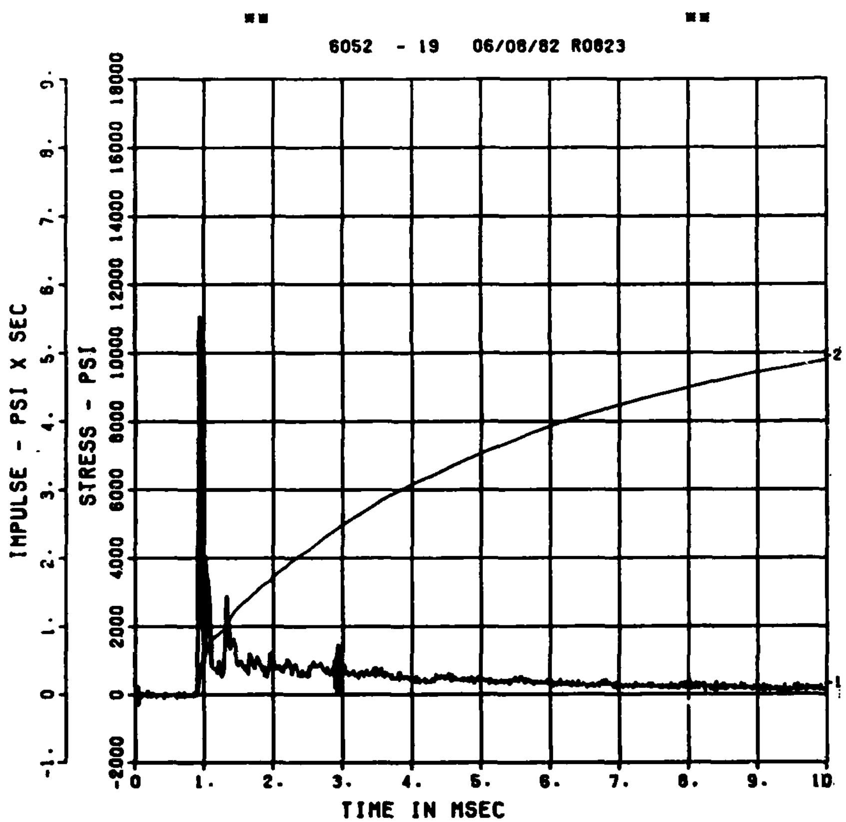

DYN SH II TEST 6
BP4
200000. HZ CAL= 16292.

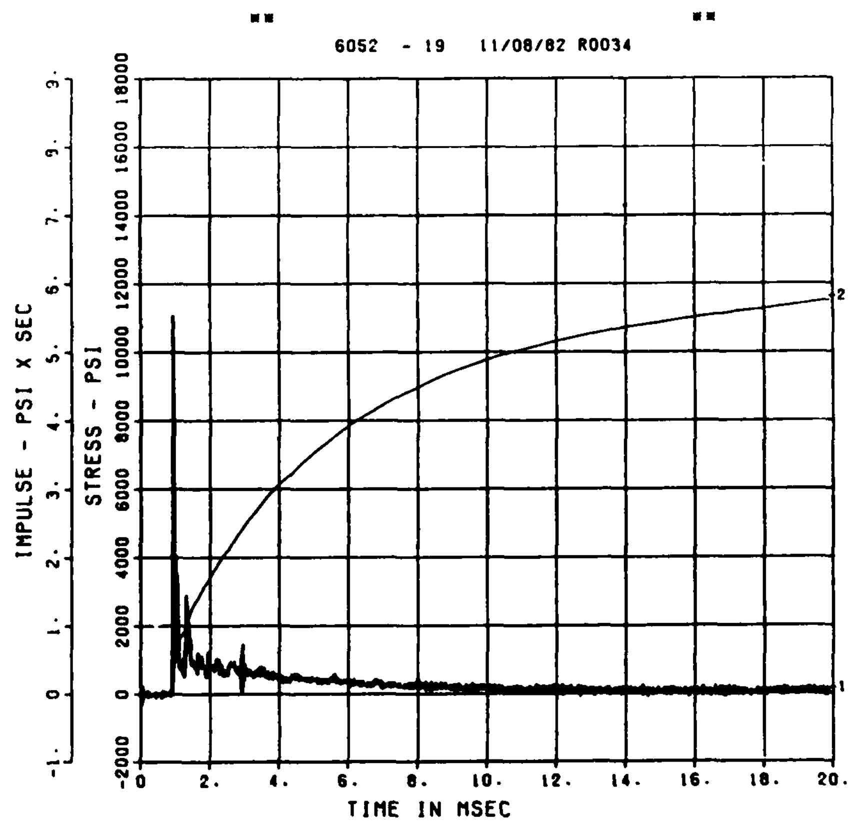

DYN SH II TEST 6
IF1
200000. HZ CAL= 6152.

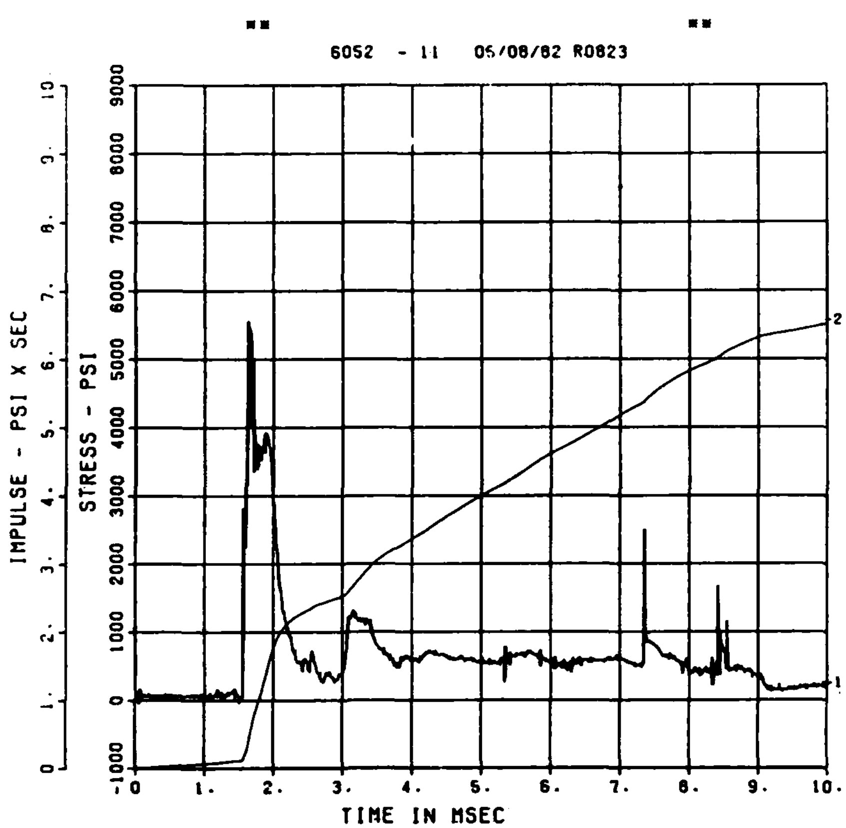

DYN SH II TEST 6
IF2
200000. HZ CAL= 6238.

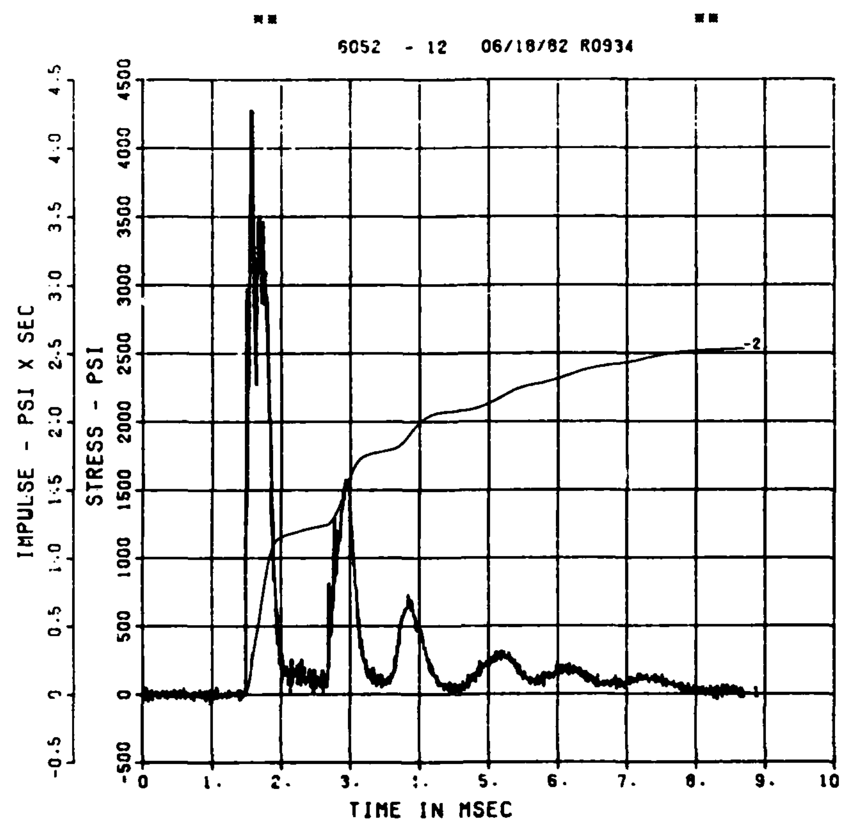

DYN SH II TEST 6
IF3
200000. HZ CAL= 6043.

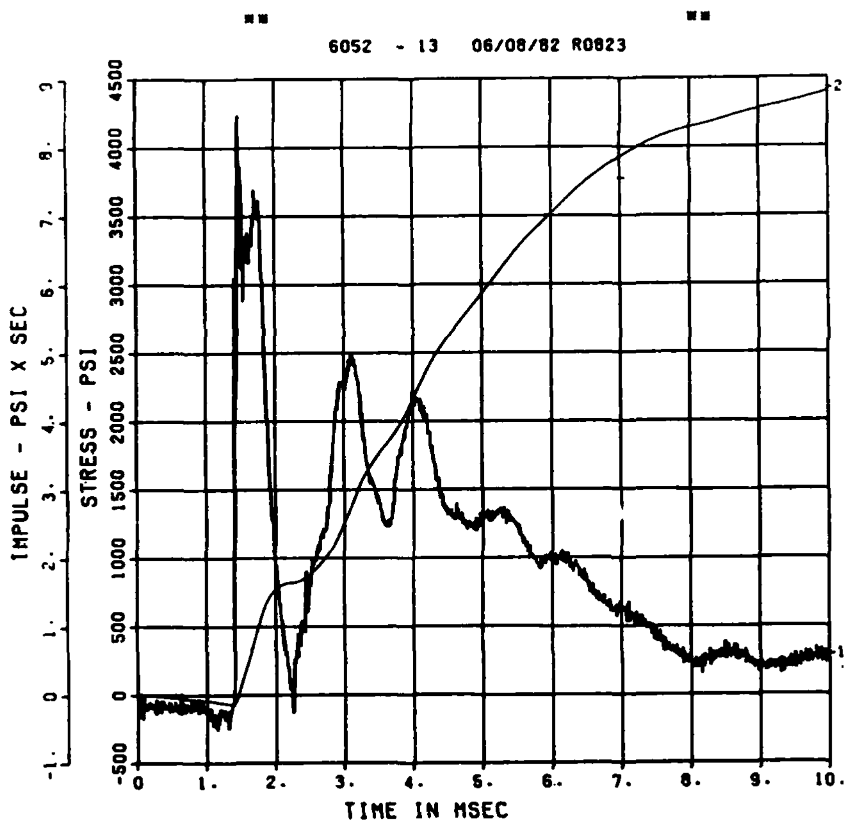

DYN SH II TEST 6
IF4
200000. HZ CAL= 4157.

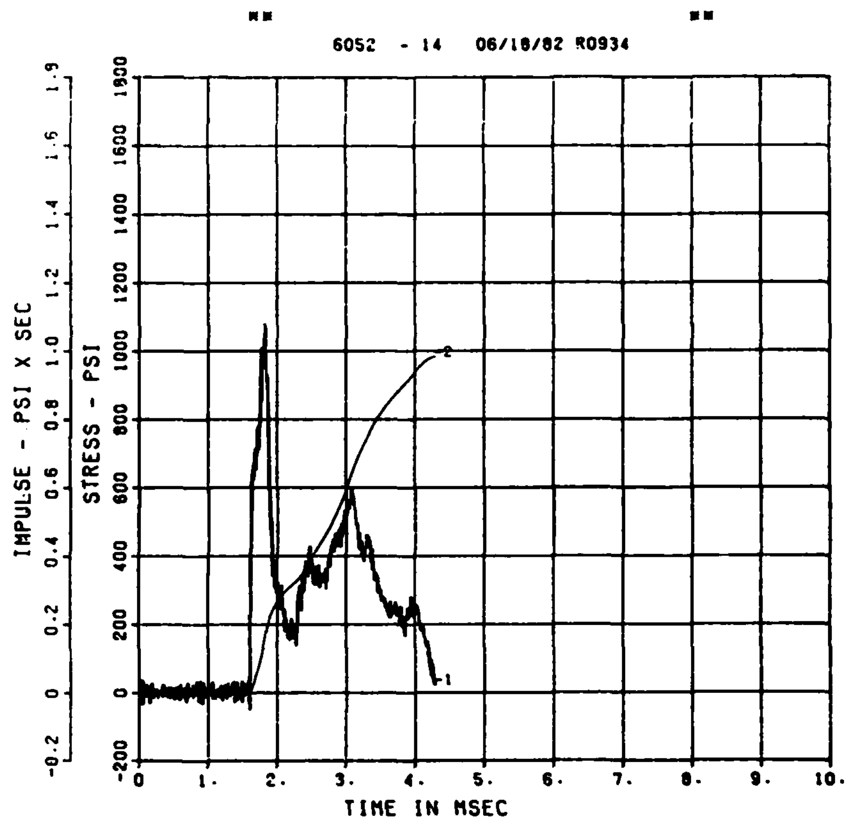

DYN SH II TEST 6
IF5
200000. HZ CAL= 5938.

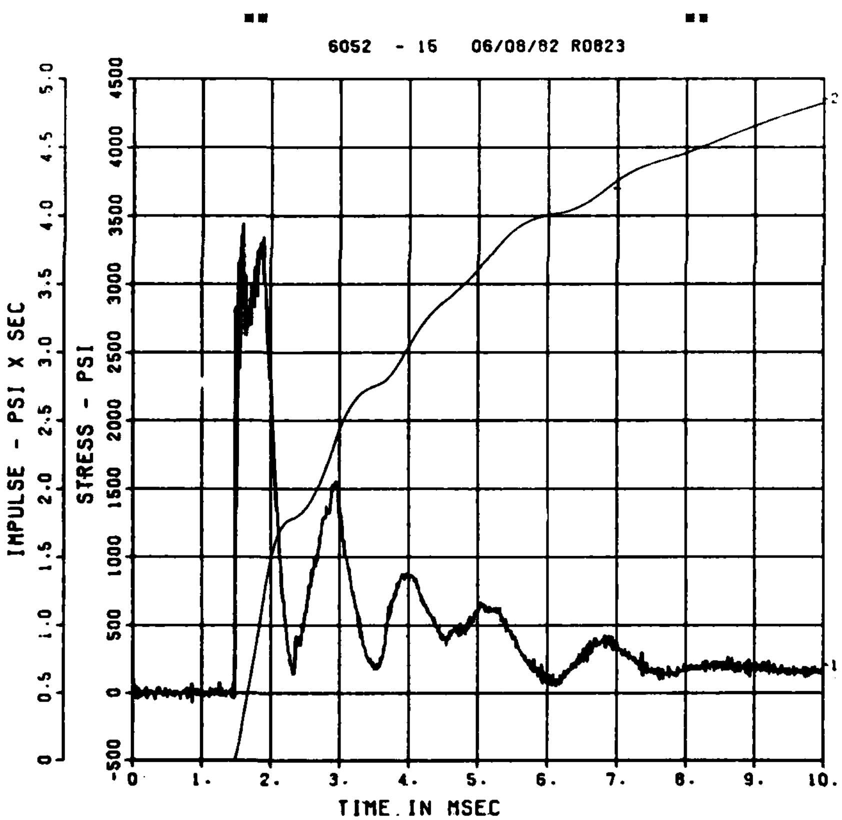

DYN SH II TEST 6
SE1
200000. HZ CAL= 5570.

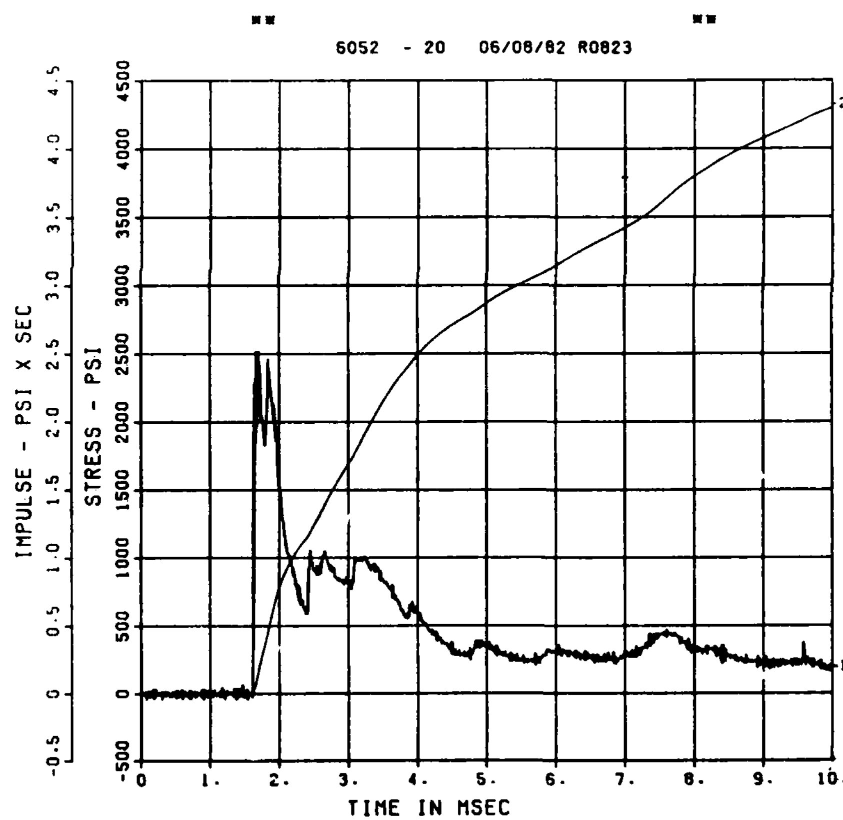

DYN SH II TEST 6
E01
200000. HZ CAL= 30452

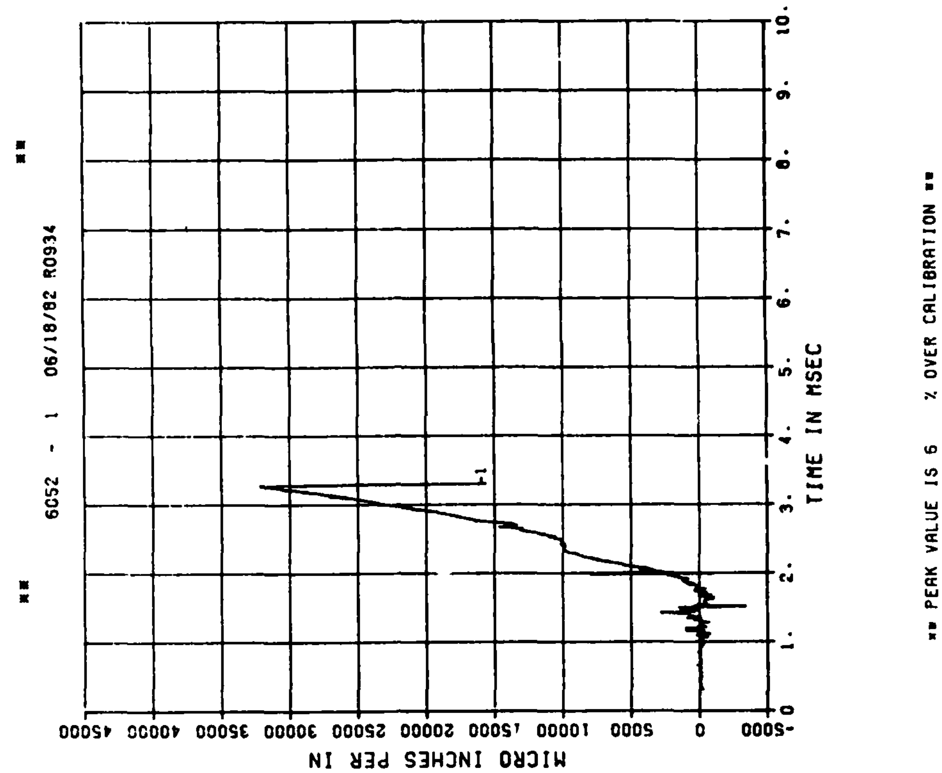

DYN SH II TEST 6
SE2
200000. HZ CAL= 5705.

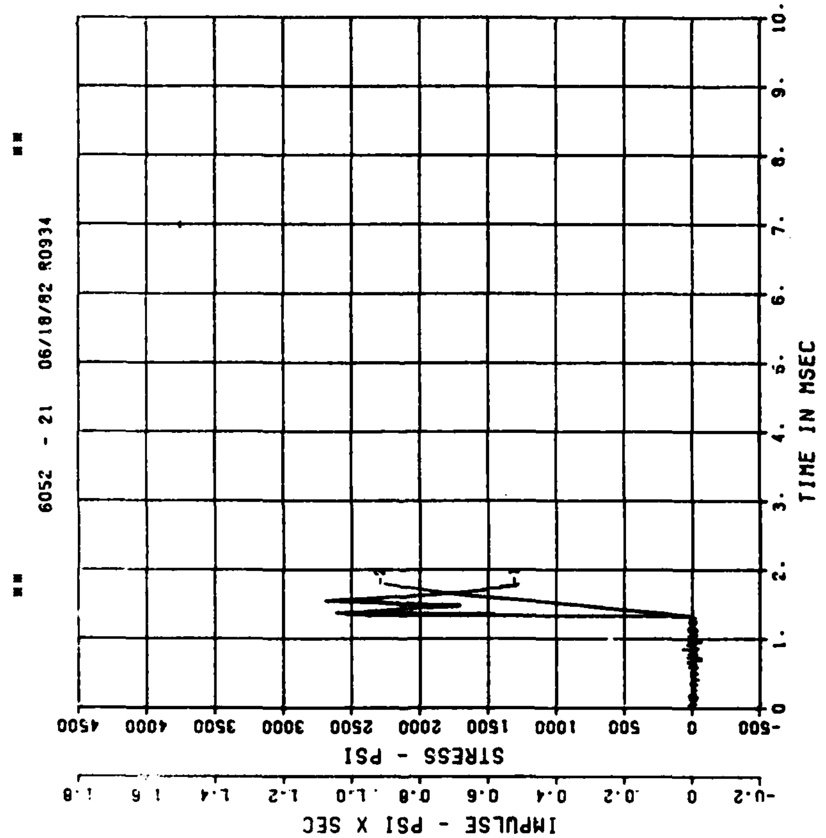

DYN SH II TEST 6
EI1
200000. HZ CAL= 21625.

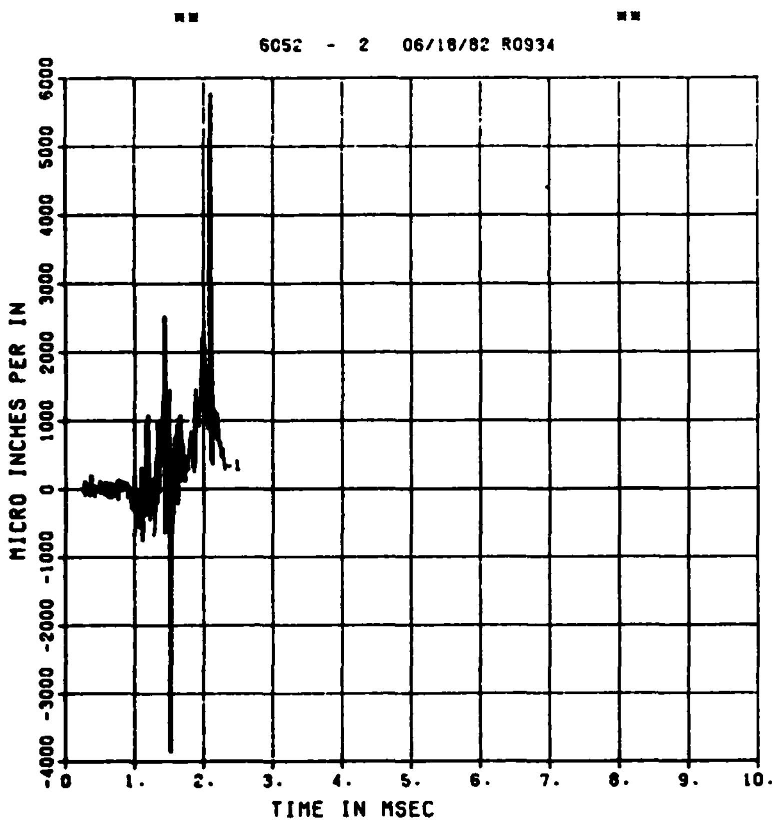

DYN SH II TEST 6
EI2
200000. HZ CAL= 30452.

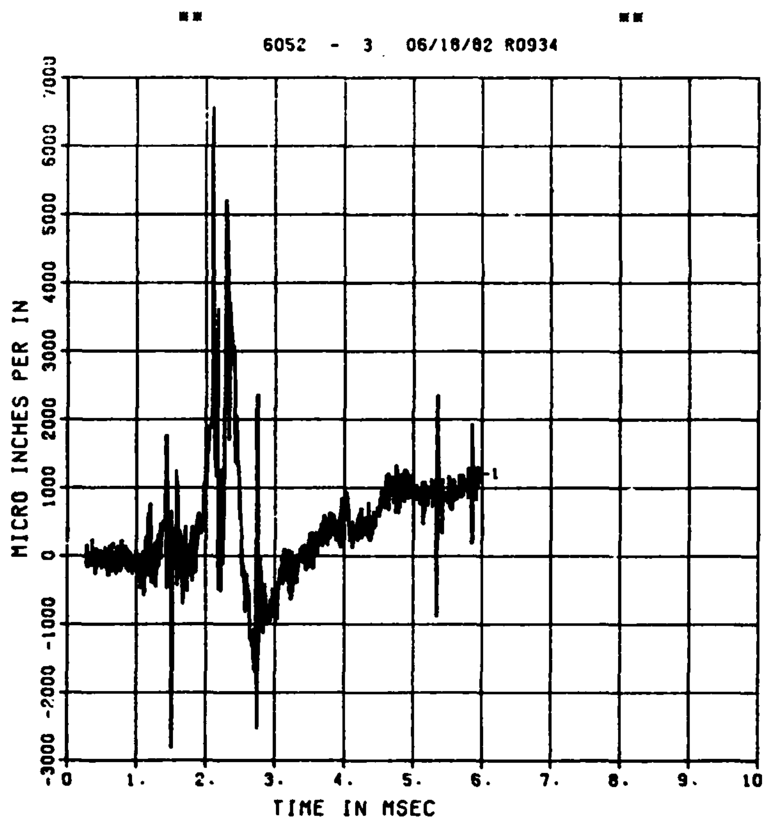

DYN SH II TEST 6
E03
200000. HZ CAL= 30452.

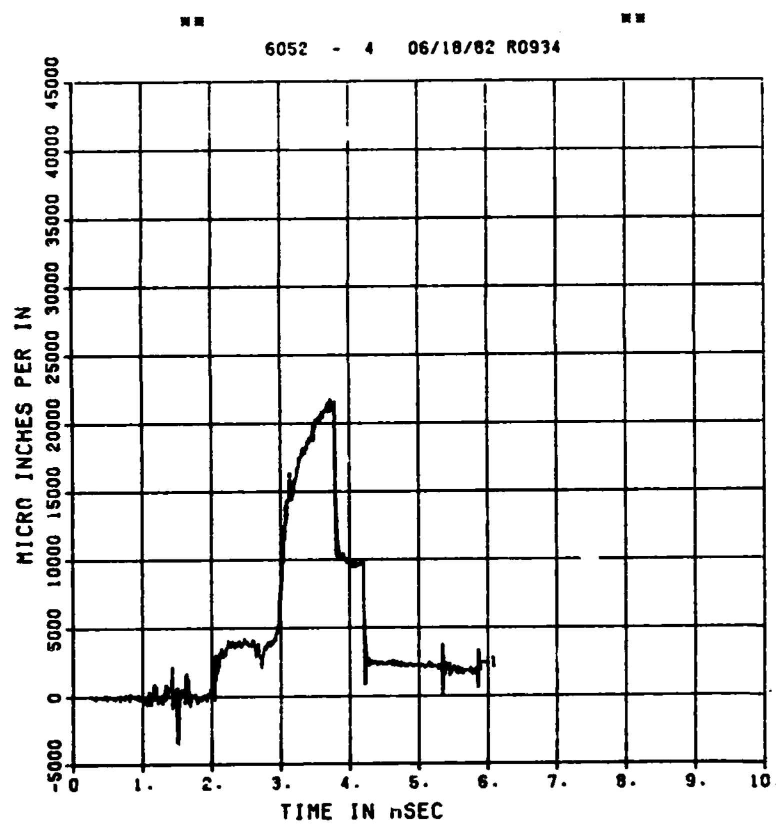

DYN SH II TEST 6
EI3
200000. HZ CAL= 21625.

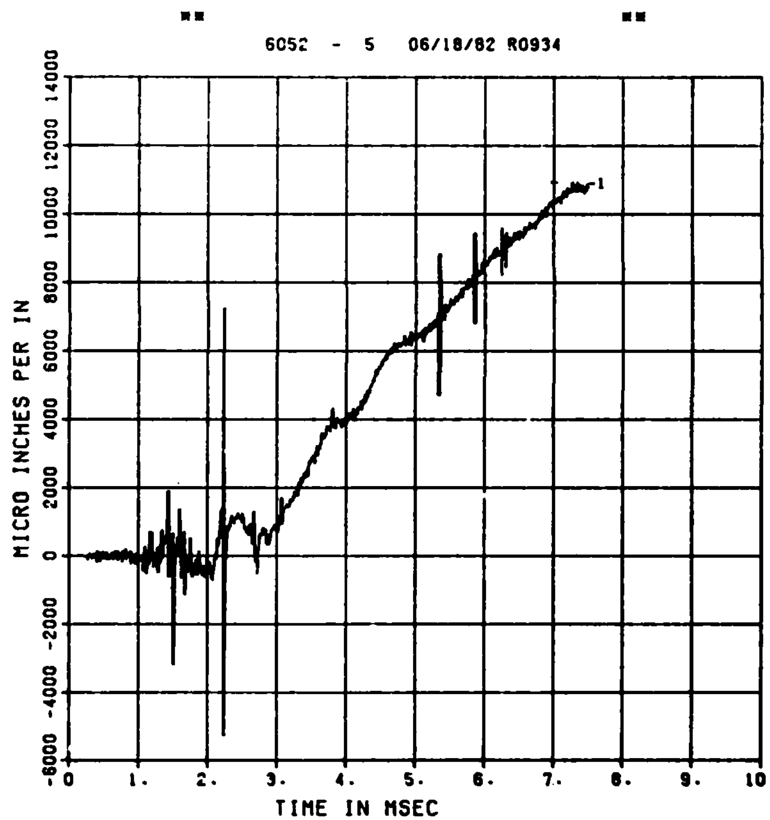

DYN SH II TEST 6
E04
200000. HZ CAL= 21625.

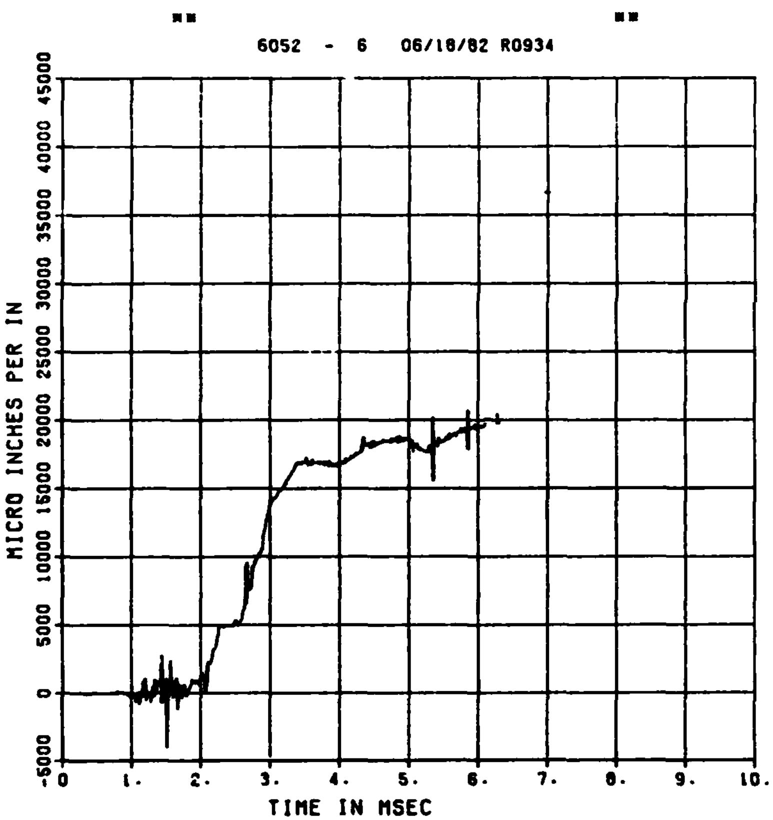

DYN SH II TEST 6
EI4
200000. HZ CAL= 14581.
LP4/0 70% CUTOFF= 9000. HZ

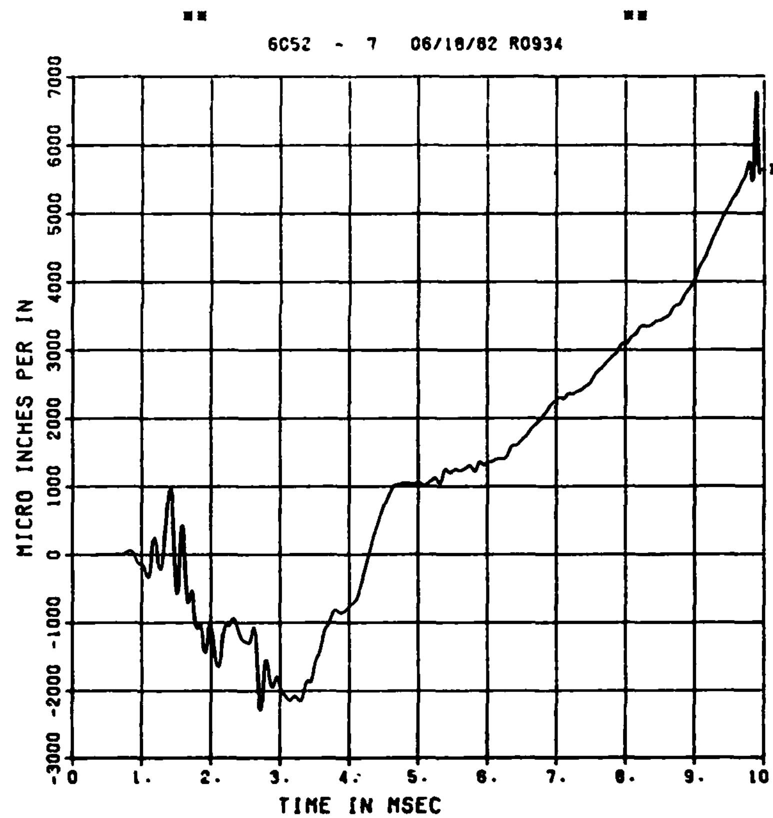

DYN SH II TEST 6
E05
200000. HZ CAL= 21625.

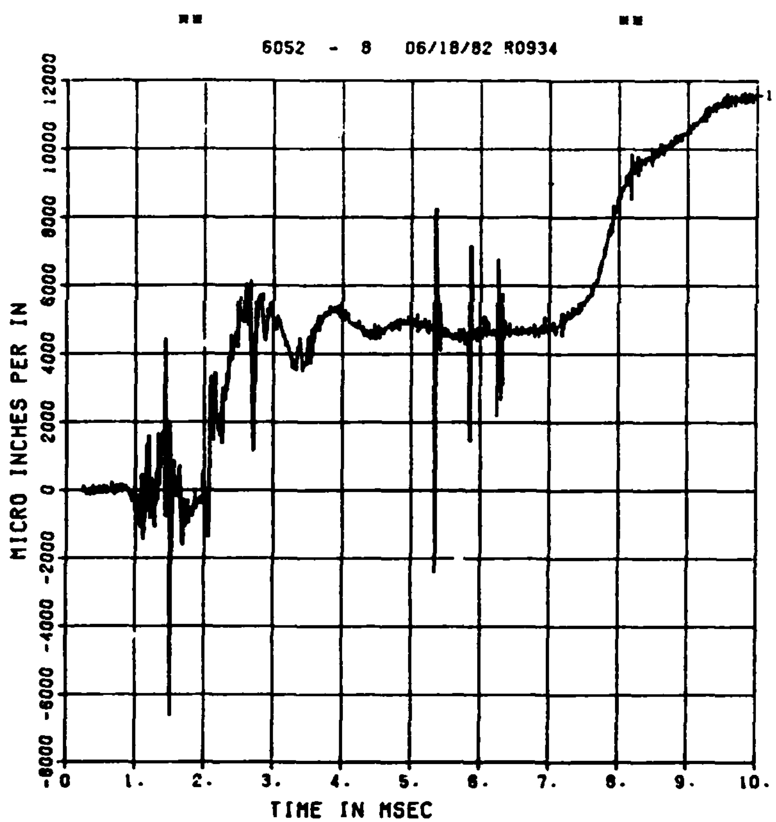

DYN SH II TEST 6
E06
200000. HZ CAL= 21625.

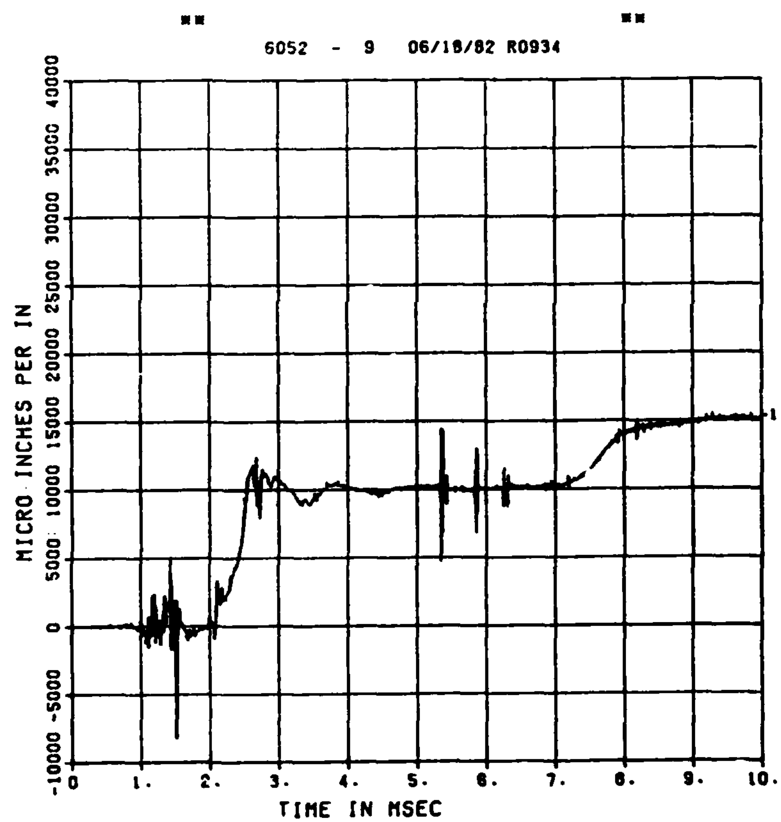

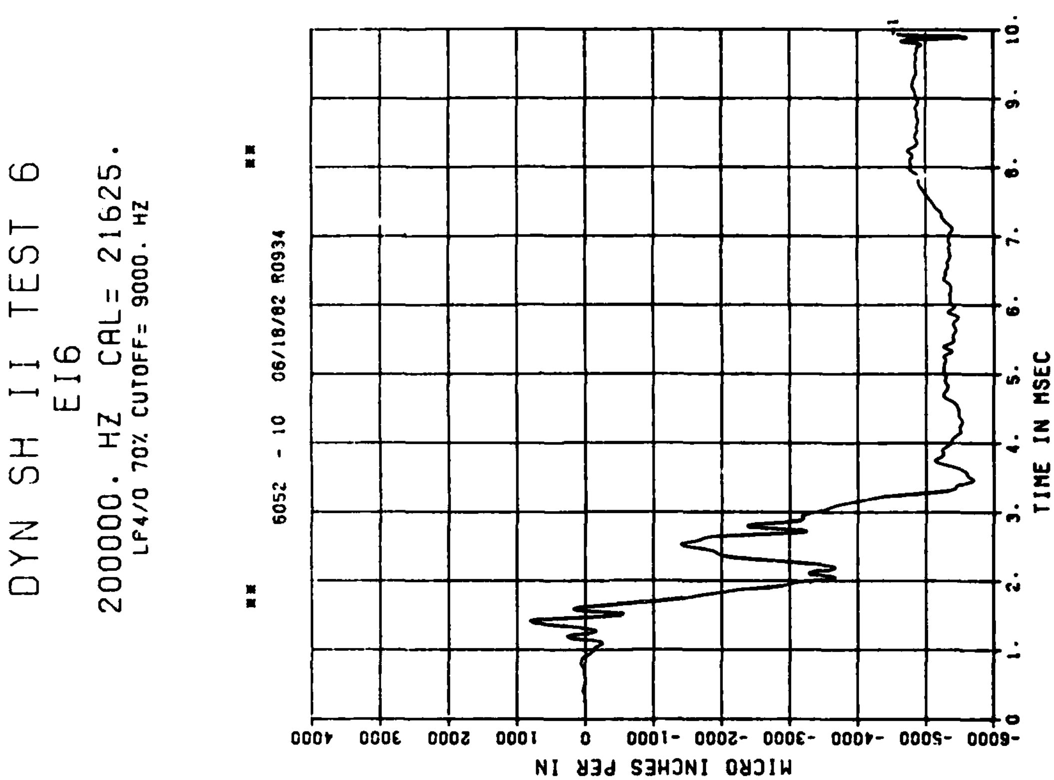

DYN SH II TEST 6
EI6
200000. HZ CAL= 21625.
LF4/O 70% CUTOFF= 9000. HZ
6052 - 10 06/18/82 R0934
MICRO INCHES PER IN
TIME IN MSEC